HAL open science

Cosmology with the Laser Interferometer Space Antenna

Pierre Auclair, David Bacon, Tessa Baker, Tiago Barreiro, Nicola Bartolo, Enis Belgacem, Nicola Bellomo, Ido Ben-Dayan, Daniele Bertacca, Marc Besancon, et al.

To cite this version:

Pierre Auclair, David Bacon, Tessa Baker, Tiago Barreiro, Nicola Bartolo, et al.. Cosmology with the Laser Interferometer Space Antenna. Living Rev.Rel., 2023, 26 (1), pp.5. 10.1007/s41114-023-00045-2 . hal-03669190

HAL Id: hal-03669190

https://hal.science/hal-03669190

Submitted on 15 Feb 2024

HAL is a multi-disciplinary open access archive for the deposit and dissemination of scientific research documents, whether they are published or not. The documents may come from teaching and research institutions in France or abroad, or from public or private research centers.

L'archive ouverte pluridisciplinaire **HAL**, est destinée au dépôt et à la diffusion de documents scientifiques de niveau recherche, publiés ou non, émanant des établissements d'enseignement et de recherche français ou étrangers, des laboratoires publics ou privés.

Distributed under a Creative Commons Attribution 4.0 International License

Living Reviews in Relativity (2023) 26:5
https://doi.org/10.1007/s41114-023-00045-2

WHITE PAPER

Cosmology with the Laser Interferometer Space Antenna

Pierre Auclair · David Bacon · Tessa Baker · Tiago Barreiro · Nicola Bartolo · Enis Belgacem et al. ***[full author details at the end of the article]***

Received: 19 April 2022 / Accepted: 13 June 2023 / Published online: 28 August 2023
© The Author(s) 2023

Abstract
The Laser Interferometer Space Antenna (LISA) has two scientific objectives of cosmological focus: to probe the expansion rate of the universe, and to understand stochastic gravitational-wave backgrounds and their implications for early universe and particle physics, from the MeV to the Planck scale. However, the range of potential cosmological applications of gravitational-wave observations extends well beyond these two objectives. This publication presents a summary of the state of the art in LISA cosmology, theory and methods, and identifies new opportunities to use gravitational-wave observations by LISA to probe the universe.

Keywords Laser Interferometer Space Antenna (LISA) · Cosmology

Acronyms

BAO	Baryon acoustic oscillations
BBH	Binary black hole
BBN	Big bang nucleosynthesis
BBO	Big Bang Observer
BH	Black hole
BNS	Binary neutron star
BSM	Beyond the standard model of particle physics
CE	Cosmic Explorer
CP	Charge parity
CMB	Cosmic microwave background
CPL	Chevalier–Polarski–Linder
DECIGO	DECihertz Interferometer Gravitational wave Observatory
DE	Dark energy
DES	Dark Energy Survey
DESI	Dark Energy Spectroscopic Instrument
EDM	Electric dipole moment

Extended author information available on the last page of the article

E-ELT	European-Extremely Large Telescope
EFT	Effective field theory
EM	Electromagnetic
EMRI	Extreme mass ratio inspiral
EoS	Equation of state
ET	Einstein Telescope
EWPT	Electroweak phase transition
FLRW	Friedmann–Lemaître–Robertson–Walker
FOPT	First-order phase transition
GB	Galactic binary
GW	Gravitational wave
GR	General relativity
IMBBH	Intermediate-mass binary black hole
IMS	Interferometry metrology system
IR	Infrared
KAGRA	Kamioka Gravitational-Wave Detector
KiDS	Kilo-Degree Survey
ΛCDM	Cosmological constant plus cold dark matter
LIGO	Laser Interferometer Gravitational-Wave Observatory
LISA	Laser Interferometer Space Antenna
LSS	Large scale structure
MBBH	Massive binary black hole
MBH	Massive black hole
MCMC	Markov Chain Monte Carlo
MHD	Magnetohydrodynamic
NG	Nambu Goto
PBH	Primordial black hole
PISN	Pair-instability supernova
PLS	Power law sensitivity
ppE	Parameterized post-Einsteinian
PTA	Pulsar timing array
RD	Radiation domination
QCD	Quantum chromodynamics
SGWB	Stochastic gravitational-wave background
SKA	Square Kilometer Array
SM	Standard model of particle physics
SNR	Signal-to-noise ratio
SOBH	Stellar-origin black hole
SOBBH	Stellar-origin binary black hole
TDI	Time domain interferometry
UV	Ultraviolet

Contents

1 Introduction 4
2 Tests of cosmic expansion and acceleration with standard sirens 6
2.1 Introduction 8
2.2 Standard sirens 9
2.2.1 Bright sirens: MBBHs with electromagnetic counterpart 10
2.2.2 Dark sirens: SOBBH, EMRIs, IMBBHs 12
2.2.3 Systematic uncertainties on standard sirens 14
2.3 Constraints on ΛCDM 16
2.3.1 H_0 tension and standard sirens 16
2.3.2 LISA forecast for H_0 17
2.3.3 ΛCDM beyond H_0 19
2.3.4 Tests of ΛCDM at high-redshift 20
2.4 Probing dark energy 21
2.4.1 Equation of state of dark energy: w_0 and w_a 22
2.4.2 Alternative dark energy models 23
2.5 Synergy with other cosmological measurements 24
2.5.1 Integration with standard electromagnetic observations 24
2.5.2 Complementarity with other gravitational-wave observatories 26
2.6 Cross-correlation and interaction with large scale structure 27
2.6.1 Cross-correlations with resolved events 27
2.6.2 Cross-correlations with the stochastic gravitational-wave background 29
2.6.3 Large-scale structure effects on gravitational-wave luminosity distance estimates 31
3 Gravitational lensing of gravitational-wave signals 32
3.1 Introduction 32
3.2 Weak lensing 33
3.2.1 As a source of noise and bias for standard sirens 34
3.2.2 As a probe complementary to standard sirens 34
3.3 Strong lensing 35
3.4 Wave effects 37
3.4.1 Identification of lensed signals 38
3.4.2 Reconstruction of large scale structure and lens properties 38
4 Constraints on modified gravity theories 39
4.1 Models and theories 39
4.2 General expression for modified cosmological gravitational-wave propagation 41
4.2.1 Modified cosmological gravitational-wave propagation 41
4.2.2 The damping term (standard sirens) 43
4.2.3 The gravitational-wave speed 43
4.2.4 Dispersion 45
4.2.5 Interaction terms and gravitational-wave oscillations 45
4.2.6 Polarisation effects, gravitational-wave lensing and triple systems 46
4.2.7 Relation to ppE framework 46
4.3 Open problems 47
5 Stochastic gravitational-wave background as a probe of the early universe 48
5.1 Introduction 48
5.1.1 What is a stochastic gravitational-wave background? 48
5.1.2 How do we characterize a stochastic gravitational-wave background? 50
5.1.3 Current constraints by other observations 51
5.2 Generation mechanisms 53
5.2.1 Cosmological 53
5.2.2 Astrophysical 55
5.3 Characteristics of the stochastic gravitational-wave background 56

5.3.1 Frequency profile of the stochastic gravitational-wave background 56
5.3.2 Anisotropies and propagation effects 57
5.3.3 Polarisations 59
5.3.4 Non-Gaussianity 60
6 First-order phase transitions 61
6.1 Introduction 61
6.2 Determination of the relevant parameters 62
6.3 GW sources 64
6.4 Discovery prospects beyond the standard model 67
6.4.1 First-order phase transitions in the LISA window 69
6.4.2 Connection with baryogenesis 71
6.5 LISA complementarity to other experimental tests 73
7 Cosmic strings 75
7.1 Introduction 76
7.2 Network modelling 78
7.2.1 Model 1 78
7.2.2 Model 2 80
7.2.3 Model 3 81
7.2.4 Field theory 82
7.3 Computation of the gravitational-wave spectrum from loops 83
7.3.1 Method I 84
7.3.2 Method II 85
7.3.3 Templates for the stochastic gravitational-wave background generated by cosmic string loops 87
7.4 LISA detection prospects 89
7.4.1 Anisotropies in the stochastic gravitational-wave background 91
7.5 Extended and alternative considerations 93
7.5.1 Long strings 94
7.5.2 Agnostic approach to loop size 96
7.5.3 Global strings 97
7.5.4 Cosmic superstrings 99
7.5.5 Metastable strings 100
8 Inflation 102
8.1 Introduction 102
8.2 Gravitational waves sourced by additional fields during inflation 104
8.2.1 Axion-gauge field inflation 105
8.2.2 Non-minimally coupled (spinning) fields 107
8.2.3 Models that produce peaks in the power spectrum of scalar perturbations 109
8.3 Small-scale primordial features 111
8.4 Effective field theory of broken space-reparametrisations 114
8.5 UV complete models of $R\alpha R^2$ model 116
8.6 Preheating 118
8.7 Summary of distinctive gravitational-wave observables from inflation 120
8.7.1 Chirality 122
8.7.2 Frequency profile 122
8.7.3 Anisotropies 123
8.7.4 Cross-correlations 125
9 Tests of non-standard pre-Big-Bang nucleosynthesis cosmology via the SGWB 126
9.1 Introduction 126
9.2 Non-standard expansion histories 128
9.2.1 Inflation 128
9.2.2 Phase transitions 130
9.2.3 Cosmic strings 132
9.3 SGWB in quantum gravity 134
10 Primordial black holes 138

10.1 Introduction ... 140
10.2 Formation scenarios ... 142
10.2.1 Origin of curvature fluctuations ... 143
10.2.2 Standard theory of primordial black holes formation from Gaussian curvature fluctuations ... 145
10.2.3 Beyond Gaussianity ... 147
10.2.4 The threshold for primordial black holes and the impact of thermal history 147
10.3 Stochastic gravitational-wave background sourced at second order by curvature fluctuations ... 149
10.4 Resolved sources and stochastic gravitational-wave backgrounds from primordial black holes binaries and hyperbolic encounters ... 151
10.4.1 Binary formation channels and merger rates ... 153
10.4.2 Gravitational-wave chirps from primordial black holes binaries ... 155
10.4.3 Stochastic gravitational-wave background ... 156
10.4.4 Bursts from hyperbolic encounters ... 157
10.5 Massive black hole seeds from primordial black holes at high redshift ... 159
11 Tools/pipelines for the analysis of transient signal data in cosmology ... 160
11.1 Tools for testing the cosmic expansion with standard sirens ... 160
11.1.1 Bright sirens ... 160
11.1.2 Dark sirens ... 161
11.2 Tools for gravitational-wave lensing ... 163
11.3 Tools for testing modified gravity ... 164
11.4 Tools for PBHs ... 165
12 Tools/pipelines for the analysis of stochastic gravitational-wave background data ... 167
12.1 Noise modelling ... 168
12.2 Expected astrophysical foregrounds ... 169
12.3 Spectral shape reconstruction: existing tools and future developments ... 171
12.4 Anisotropy reconstruction ... 173
12.4.1 LISA response function ... 175
12.4.2 Cosmic dipole ... 176
12.5 Gravitational-wave map making with LISA ... 178
12.6 Global fit ... 180
References ... 186

1 Introduction

Contributors: R. Caldwell, G. Nardini.

The Laser Interferometer Space Antenna (LISA) (Amaro-Seoane et al. 2017) is a planned space-borne gravitational-wave (GW) detector that will open a new frontier on astrophysics and cosmology in the mHz frequency band. This European Space Agency-led mission includes participation by ESA member countries and significant contributions from NASA and space agencies of other countries. Phase A work is on track for mission adoption in mid 2020s, and is compatible with a launch in the mid 2030s.

LISA will consist of a trio of satellites, located at the vertices of an equilateral triangle, in an Earth-trailing heliocentric orbit. The 2.5-million km distances between the satellites will be monitored using precision laser interferometry to detect passing GWs. Here we consider a nominal mission of six years with a duty cycle of around 75%, although we understand that the instruments will be engineered to a specification that will enable a possible extension.

LISA will be sensitive to GWs from a wide array of sources (Amaro-Seoane et al. 2017). A primary target will be the inspiral and merger of massive binary black holes (MBBHs), ranging in masses 10^4–$10^7\,M_\odot$, at redshifts out to $z \sim 10$. A significant foreground signal will be the many galactic white dwarf binaries, each effectively a monotone source.

By the time LISA flies, the state of GW observation will have evolved. The extended Advanced Laser Interferometer Gravitational Wave Observatory (LIGO), Advanced Virgo, and Kamioka Gravitational Wave Detector (KAGRA) family of ground-based GW detectors will have begun implementing third-generation technology demonstration upgrades. The network of pulsar-timing radio telescopes will have grown to include the Square Kilometer Array (SKA). Yet, LISA will be different from its predecessors. The size of the detector will enable access to a completely fresh part of the GW spectrum, leading to observations of new astrophysical sources as well as a new window on primordial stochastic gravitational-wave backgrounds (SGWBs). Many sources will produce overlapping signals, owing to the improved sensitivity. Extracting individual sources and events, and discriminating from an unresolved hum, will be part of the challenge.

According to the mission proposal (Amaro-Seoane et al. 2017), LISA has two main scientific objectives of purely cosmological bearing. The first is to probe the expansion rate of the universe, with specific requirements to measure the dimensionless Hubble parameter by means of GW observations alone, and further to constrain cosmological parameters through joint GW and electromagnetic (EM) observations. The second such objective is to understand SGWBs and their implications for early universe and particle physics. This will entail the characterisation of the astrophysical SGWB, and subsequently a measurement or bound on the amplitude and spectral shape of a cosmological SGWB. There are further scientific imperatives to use LISA to explore the fundamental nature of gravity and to search for unforeseen sources with relevance for cosmology. There is a wealth of cosmological information that may be extracted from LISA observations.

We start with Sects. 2 and 3 on standard sirens and weak gravitational lensing; these are "sure bets" for LISA, based on our current understanding of source populations. These sections are directly related to LISA science objective SO6 "probe the rate of the expansion universe" (LISA Science Study Team 2018). They also identify new opportunities to derive cosmological information from GW astrophysical sources, in connection with LISA science objectives SO1, SO2, SO3 and SO4, which are devoted to understanding the galactic and extragalactic astrophysical source populations (LISA Science Study Team 2018). We follow with sections on more exploratory topics, which are potentially profound and revolutionary. Sect. 4 discusses the constraints on modified gravity theories that may be achieved through measurement of GW sources at cosmological distances. Results on this research subject are aligned with LISA science objectives SO5 "explore the fundamental nature of gravity and black holes" as well as the aforementioned SO6. Section 5 introduces the theoretical foundations, observables, and conventions relevant for subsequent sections. Sections 6, 7 and 8 describe predictions of SGWBs sourced by first-order phase transitions, cosmic strings, and inflationary processes.

Section 9 explores how these diverse SGWB signals convey unique information on the expansion rate of the universe at redshift $\sim$ 1000 or higher. These latter four sections touch on topics that are crucial for LISA science objective SO7 "understand SGWB and their implications". Inflation not only leads to a SGWB but also to density perturbations which may give rise to the formation of primordial black holes (PBHs), which is the subject of Sect. 10. Finally, Sects. 11 and 12 present existing or planned tools and methods to analyse the GW signals discussed in the previous sections. Such tools and methods potentially constitute key deliverables for SO1-SO7 as well as LISA science objective SO8 "search for GW bursts and unforeseen sources".

We emphasize that the analyses presented in these final sections need to take into account the superposition between cosmological and astrophysical sources, so that the identification of a potential cosmological contribution necessarily involves modeling of the astrophysical signal. While we briefly discuss the current status of these analyses, we acknowledge that the further development of the astrophysical modeling is by itself a crucial line of reasearch that, while impacting the cosmological searches, goes well beyond what is described in the present document. More in general, certain topics of cosmological interest are intentionally omitted from this document: dark matter particles, some tests of general relativity (GR), waveform uncertainties, astrophysical backgrounds, and the astrophysics of discrete sources such as MBBHs. These and related topics are covered by the Living Reviews maintained by the LISA Astrophysics (Amaro-Seoane et al. 2023), Data Challenge (LISA Data Challenge Working Group n.d.), Fundamental Physics (Arun et al. 2022) and Waveform Working Groups (LISA Waveform Working Group n.d.). Such reviews complement the picture presented herein, by the Cosmology Working Group. The goal of all these documents is to both identify LISA science objectives and corresponding work packages, and to alert the scientific community about novel research opportunities, or potential gaps. The tests of general relativity of Sect. 4 and PBH science of Sect. 10 are exemplary cases of why these Living Reviews are needed. The original LISA proposal (Amaro-Seoane et al. 2017) makes no mention of these science investigations. But in recent years, as the subjects have evolved, a set of new science objectives have been proposed to cover them. The possibility that similar situations arise again justifies the effort and interest for living reviews that report on the thrilling, blooming, and fast-evolving LISA science.

2 Tests of cosmic expansion and acceleration with standard sirens

Section coordinators: J.M. Ezquiaga, A. Raccanelli, N. Tamanini. Contributors: D. Bacon, T. Baker, T. Barreiro, E. Belgacem, N. Bellomo, D. Bertacca, C. Caprini, C. Carbone, R. Caldwell, H-Y. Chen, G. Congedo, M. Crisostomi, G. Cusin, C. Dalang, W. Del Pozzo, J.M. Ezquiaga, N. Frusciante, J. García-Bellido, D. Holz, D. Laghi, L. Lombriser, M. Maggiore, M. Mancarella, A. Mangiagli, S. Mukherjee, A. Raccanelli, A. Ricciardone, O. Sergijenko, L. Speri, N. Tamanini, G. Tasinato, M. Volonteri, M. Zumalacarregui.

2.1 Introduction

Broadly speaking, to learn about the universe and its cosmic expansion we need to measure distances and times. GW astronomy offers a unique perspective in this matter, since the signal emitted by a compact binary coalescence is well predicted by GR. Namely, the amplitude of the GW is inversely proportional to its luminosity distance and it only depends on the masses and orbital inclination of the binary system source. Since cosmological propagation at the background level (namely, excluding the effect of perturbations over the Friedmann–Lemaître–Robertson–Walker (FLRW) geometry) only changes the overall strain amplitude, one can use the frequency evolution of the GW to unveil the masses of the compact binary and the relative amplitude of the two GW polarisations to estimate the orbital inclination, obtaining thus a direct and absolute measurement of the luminosity distance. However, GW signals alone do not provide a way to relate the time (of merger, for example) in the observer frame to the one in the source frame. To access this information, one needs an independent determination of the redshift of the source. In such a case the GW signal from compact binary coalescence can be considered a standard siren (Schutz 1986), namely a cosmological event for which a distance measurement and complementary redshift information are both available. For example, the binary neutron star (BNS) merger GW170817, observed by the Advanced LIGO and Advanced Virgo detectors jointly with several EM facilities which spotted associated EM emissions, has already been used as a proof-of-principles, low-redshift measurement of H_0 (Abbott et al. 2017a). On the other hand, massive black holes (MBHs) seen by LISA with an EM counterpart could be used to map the cosmic expansion up to high redshift (Holz and Hughes 2005; Tamanini et al. 2016; Tamanini 2017; Belgacem et al. 2019c).

In this section we will present the different standard sirens that LISA will detect and the information about the cosmological model that they will provide. The section is organized as follows. We begin by describing the concept of standard siren in Sect. 2.2, detailing the expected LISA bright and dark sirens. We then consider the constraints that could be placed in the standard cosmological constant plus cold dark matter (ΛCDM) cosmological model in Sect. 2.3. Subsequently, we explore LISA capabilities to probe different dark energy (DE) models in Sect. 2.4. Next, we show the synergies of LISA with other EM and GW observatories in Sect. 2.5. Finally, we describe the benefit of cross-correlating LISA data with large-scale structure surveys in Sect. 2.6.

2.2 Standard sirens

GW signals from compact binary coalescences are natural cosmic rulers because of the inverse dependence of the strain with the GW luminosity distance, $h \propto 1/D_L^{\mathrm{GW}}$. In GR and over a Friedman–Lemaître–Robertson–Walker (FLRW) background, the GW luminosity distance is equal to the one of EM radiation and given by

$$D_L^{\rm GW} = \frac{c}{H_0}\frac{(1+z)}{\sqrt{|\Omega_k|}}\,\mathrm{sinn}\left[H_0\int_0^z \frac{\sqrt{|\Omega_k|}}{H(z')}dz'\right], \tag{1}$$

where $\mathrm{sinn}(x) = \sin(x), x, \sinh(x)$ for a positive, zero and negative spatial curvature respectively. Assuming a ΛCDM cosmology, the Hubble parameter is a function of the matter content Ω_m, the curvature Ω_k and the amount of DE Ω_Λ (radiation at present time is negligible)

$$H(z) = H_0\sqrt{\Omega_m(1+z)^3 + \Omega_k(1+z)^2 + \Omega_\Lambda}. \tag{2}$$

LISA will attempt to measure H_0, Ω_m, Ω_k and Ω_Λ using sirens.

GW observations themselves, however, do not provide direct information about the redshift. Therefore, in order to be able to probe the cosmological evolution we need additional input. In the case in which the redshift of the GW source is directly obtained from an EM counterpart, we will refer to the source as a *bright siren*. A beautiful example of this kind of multi-messenger event was the LIGO/Virgo event GW170817 (Abbott et al. 2017d), which provided the first standard siren measurement of H_0 (Abbott et al. 2017a) (see Abbott et al. 2021c for an update on the measurement of H_0 from standard sirens). As we present in Sect. 2.2.1, LISA will be sensitive to very different bright sirens, but the concept remains the same. On the other hand, when the redshift information is obtained from an analysis that does not include EM counterparts, we will refer to the GW sources as *dark sirens*. In Sect. 2.2.2 we will present different dark siren classes that LISA will detect and which can be used to obtain cosmological information by cross-matching the sources with galaxy catalogues and looking for correlated features in the mass distribution.

Modern analyses of standard sirens are based on Bayesian inference. We refer the reader to Sect. 11.1 for a glimpse at the actual statistical tools LISA will use and a detailed discussion of their associated systematic uncertainties. In what follows we focus mostly on the different GW sources and their potential as standard sirens. LISA will detect three types of potential standard siren populations: MBBHs at $1 \lesssim z \lesssim 8$, extreme mass ratio inspirals (EMRIs) at $0.1 \lesssim z \lesssim 1$ and SOBBHs at $z \lesssim 0.1$. An example of the expected Hubble diagrams from these three different standard sirens populations can be found in Fig. 1. The details regarding each of these populations will be presented in the following.

2.2.1 Bright sirens: MBBHs with electromagnetic counterpart

LISA will detect the coalescence of MBBHs up to redshift $z \simeq 15$–20. However, the mass and redshift distributions of the events are still uncertain. Currently, our knowledge of MBHs is limited to cases where either an active galactic nucleus is present or to quiescent MBHs in nearby galaxies (Kormendy and Ho 2013; Graham 2016; Greene et al. 2020). The population of MBBHs accessible by LISA might be considerably different from our current expectations. Several groups have attempted to address this question with hydrodynamics simulations (Salcido et al. 2016; Katz et al. 2020; Volonteri et al. 2020) or semianalytic formation models (Volonteri et al.

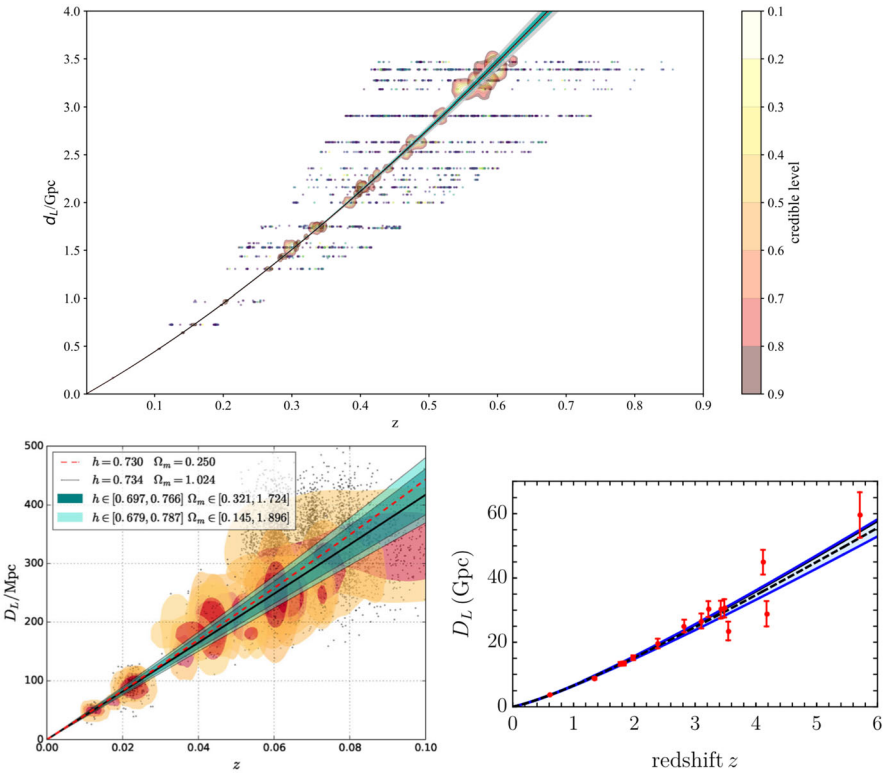

Fig. 1 Examples of LISA standard siren data sets at different redshift ranges. Data from low-redshift dark sirens, defined by SOBBHs, are reported in the bottom-left plot. Data at intermediate redshifts correspond to EMRIs and are reported in the top plot. High-redshift data are provided by standard sirens from MBBHs and are reported in the bottom-right plot. Note how SOBBHs and EMRIs, being dark sirens, can only provide broad likelihood regions in the Hubble diagram, while MBBHs, being bright sirens, provide precise data points thanks to the unique redshift association coming from the EM counterpart identification. Images reproduced with permission from [top] Laghi et al. (2021), [bottom left] Del Pozzo et al. (2018), and [bottom right] Speri et al. (2021), copyright by the author(s)

2003; Barausse et al. 2020; Ricarte and Natarajan 2018; Trinca et al. 2022; Valiante et al. 2018). While the former are able to handle more naturally hydrodynamical, thermodynamical, and dynamical processes, the latter are computationally efficient and can be used to explore a larger parameter space.

Two main sources of uncertainties affect the expected redshift and mass distribution of merging MBBHs: black hole seeding and delay time prescription (Klein et al. 2016). If MBHs grow from the remnants of metal-poor population-III stars, the population of MBBHs accessible by LISA is expected to peak at the total mass $M_{tot} \simeq 10^3\, M_\odot$. However if MBHs arise from the monolithic collapse of gas in protogalaxies, the mass distribution is expected to range from $10^4\, M_\odot$ up to few $10^7\, M_\odot$. We note that additional formation mechanisms have been proposed and that they would further modulate the distribution of merging MBHs. Moreover, delay times, between the merger of two galaxies and the merger of their central MBHs,

shape the redshift distribution, with short delays leading to more mergers at higher redshift. Further uncertainties arise from the gas inflow to the halo centre, its efficiency and the geometry of accretion. Even if LISA will be able to distinguish different formation scenarios (Sesana et al. 2011), the aforementioned uncertainties reflect in a broad interval for the number of events detected and their distributions (e.g. mass, mass ratio, spins, redshift).

Combining these uncertainties, LISA should be able to detect between a few and several tens of MBBH events per year (Klein et al. 2016). Multiple-body interactions among a MBH binary and one or more intruder MBHs, arising naturally from the hierarchical galaxy formation process, might still produce $\simeq 10-20$ events per year (Bonetti et al. 2019).

LISA will also provide exquisite accuracy on MBBH parameters. For the search of a possible EM counterpart, the sky position accuracy is of paramount importance. Taking into account the full inspiral-merger-ringdown GW signal, MBBHs from few $10^5\,M_\odot$ to few $10^6\,M_\odot$ can be localised within $0.4\,\mathrm{deg}^2$ up to $z \simeq 3$ (Mangiagli et al. 2020), but with high accuracy obtained only at merger. For these sources the posterior on the sky position is expected to be Gaussian; however, for more massive and distant sources, the recovered sky position is expected to present multimodalities (Marsat et al. 2021). For heavy systems with total mass $\mathrm{M_{tot}} > 10^7\,M_\odot$ the ringdown portion of the signal might carry most of the information for the source localisation (Baibhav et al. 2020). For cosmology applications, also the estimate on the luminosity distance plays a fundamental role: due to the typical large signal-to-noise ratio (SNR) value for these sources, LISA should be able to constrain the luminosity distance to better than 10% for most of the events at $z<3$ (Tamanini et al. 2016).

If MBBHs evolve in gas-rich environment, EM radiation might be produced by the accretion of gas onto the MBHs close to or after merger. The orbital motion of the binary is expected to open a cavity in the circumbinary disk. Hydrodynamical simulations show that minidisks generally form around each BH from the stream of gas from the circumbinary disk (Farris et al. 2015; Tang et al. 2018).

This leads to pre-merger EM emission across all wavelengths (D'Ascoli et al. 2018), which can be identified if the pre-merger sky localisation is good (Dal Canton et al. 2019). In the optical band, the Vera C. Rubin Observatory (formerly known as Legacy Survey of Space and Time) (Abell et al. 2009) will reach a magnitude limit of 24.5 in 30 s of pointing over a field of view of $\simeq 10\,\mathrm{deg}^2$. This survey speed enables the Vera C. Rubin Observatory to cover a sky area of $\simeq 100\,\mathrm{deg}^2$ allowing for possible pre-merger EM detection, though the number of detected counterparts is expected to be low (Tamanini et al. 2016). At or after merger, several transients have been proposed, from spectral changes and brightening (Schnittman and Krolik 2008; Rossi et al. 2010) to jets (Palenzuela et al. 2010; Khan et al. 2018; Yuan et al. 2021). In X-ray, Athena (Nandra et al. 2013), with a field of view of $0.4\,\mathrm{deg}^2$ and a limiting flux of $\approx 3 \times 10^{-16}\mathrm{erg\ cm^{-2}\ s^{-1}}$ in 100 ks, will be optimal to search for possible post-merger signatures. Similarly, in radio, SKA (Dewdney et al. 2009) will observe the launch of putative post-merger radio jets with an initial field of view of $1\,\mathrm{deg}^2$.

A counterpart detection strategy has been proposed (Tamanini et al. 2016) consisting in first localising the source in the radio with the SKA, and subsequently

to proceed to a redshift determination of the host galaxy in the optical with the Extremely Large Telescope.[1] This strategy is more promising than direct optical identification with the Vera C. Rubin Observatory. Depending on the seed and dynamical evolution models, LISA will detect between $\simeq 10$ and $\simeq 25$ MBBH events with EM counterpart during a mission assumed to be of five year (Tamanini et al. 2016). These estimates are however affected by several astrophysical uncertainties that have as yet not been properly characterised. It is, however, robust to expect that MBBH bright sirens will all be detected at relatively high redshift: one study finds standard sirens distributions peaking at around $z \sim 2-3$ and extending up to $z \sim 8$ (Tamanini et al. 2016; Tamanini 2017). Therefore, MBBH bright sirens will be of great relevance to test the ΛCDM model, and possible deviations from it, in a redshift range so far scarcely probed by EM observations. In Sects. 2.3 and 2.4 we review the cosmological constraints that LISA will be able to impose both at low and high redshift.

2.2.2 Dark sirens: SOBBH, EMRIs, IMBBHs

In addition to observing the EM counterpart of individual events, there are other methods that one can employ to obtain information about the redshift of the GW source. The most common and widely-used among these methods relies on statistical matching the inferred position of the GW source with a catalogue of galaxies with known redshift (see Abbott et al. 2021c for the application of this method to the Advanced LIGO-Advanced Virgo-KAGRA data). GW events for which an EM counterpart cannot be identified, but which can still be used to extract cosmological information statistically, are usually referred to as dark standard sirens. In this section we outline how dark sirens are treated by correlating galaxy catalogues with the localisation of the source, *statistical dark sirens*, and using properties of their mass distribution, *spectral sirens*. Generally speaking, dark standard sirens have the advantage to be applicable to all kind of GW sources for which a distance measurement can be retrieved (not exclusively those emitting EM counterpart signals), although a large number of them are necessary to achieve precise measurements through solid statistics.

In the absence of an EM counterpart, redshift information can be extracted by putting a prior on potential hosts from a galaxy catalogue, assuming that galaxies are good tracers of binary black hole (BBH) mergers. In order to do that (see more details on statistical methods in Sect. 11.1.2), one associates the GW event with every galaxy within the 3D localisation error of the event, assigning to each of them a certain probability of being the true host galaxy of the GW event. In this way, by stacking together the information gathered from several dark sirens, one can statistically infer the true values of the cosmological parameters. For this method to be effective, one requires a large number of events to combine statistics or a very small localisation volume. Errors in the luminosity distance scale with the SNR, $\Delta D_L/D_L \sim 1/\rho$, while the localisation depends also on the duration of the source, since LISA orbital modulation can be used to help disentangle the location in the sky. One complication

[1] https://elt.eso.org/.

is given by the fact that galaxy catalogues are in general not complete, especially at high redshift. This requires one to include information on the missing galaxies within the catalogue, and the catalogue prior must be supplemented by a suitable "completion" term (Chen et al. 2018; Fishbach et al. 2019; Gray et al. 2020; Finke et al. 2021) (again see Sect. 11.1.2 for more details). This aspect will remain a limiting factor until catalogues with very large completeness are available. The availability of complete galaxy catalogues, small GW localisation regions and accurate redshift determination—including characterisation of the uncertainty due to peculiar velocities for low-redshift binaries (Howlett and Davis 2020; Mukherjee et al. 2021c; Nicolaou et al. 2020)—will be crucial in order for the statistical method to give competitive constraints on cosmological parameters. At the time when LISA will be taking data, galaxy catalogues will be available from a plethora of current and future experiments, providing observations of different types of galaxies, with varying number density and sky coverage, over different redshift ranges. In particular, the completed observations from Euclid and Dark Energy Spectroscopic Instrument (DESI), with the addition of redshift-deep catalogues from the Subaru Prime Focus Spectrograph project and the Roman Space Telescope, should be available before LISA is launched. Additionally, the Vera C. Rubin Observatory should have observed hundreds of millions of galaxies, and deep and wide catalogues should be available from SPHEREx. Finally, on time-scales comparable with LISA, the full SKA2 and the ATLAS satellite should provide extremely deep and full-sky catalogues of the sky. Moreover, there are plans to build a next-generation billion-galaxies survey as a successor of DESI. These future surveys are expected to provide well-complete galaxy catalogs up to $z = 1$ and possibly beyond.

Stellar-origin black holes (SOBHs) are guaranteed dark sirens for LISA. From the observations with current LIGO/Virgo detectors (Abbott et al. 2021e), we know that there is a population of BBHs with masses between $\sim 5\,M_\odot$ and $\sim 50\,M_\odot$ that LISA will see in their early inspiral. Some of those events will be subsequently detected by ground-based detectors becoming in this way "multi-band" events (see Sect. 2.5.2). SOBBHs with good enough localisation can be used as dark sirens (Kyutoku and Seto 2017; Del Pozzo et al. 2018). Because of their low masses, cosmologically useful SOBHs could only be seen by LISA up to $z \sim 0.1$, probing essentially the local expansion rate H_0. In practice, only those events with better than 20% accuracy in the luminosity distance and with a typical sky-localisation error better than $\sim 1\text{deg}^2$ will be useful as dark sirens. According to current forecasts, LISA could detect $\sim$ 10–100 dark sirens (Del Pozzo et al. 2018), though uncertainties on the LISA noise level at the high-frequency end of its band (Amaro-Seoane et al. 2017), on the detection threshold (Moore et al. 2019) and merger rate of these systems (Abbott et al. 2021e), might well invalidate the most optimistic expectations. In Sects. 2.3 and 2.4 we will review the cosmological constraints that LISA can impose with SOBBHs as dark sirens.

LISA will also be able to use EMRIs as statistical dark sirens. They will in fact be detected at cosmological distances, possibly in high numbers, though the rates are so far extremely uncertain. EMRIs detected by LISA are expected to be broadly peaked around $0.5 < z < 2$, potentially reaching $z \sim 4$ (Babak et al. 2017). A recent

investigation showed that events up to $z \sim 0.7$ can safely be used to estimate H_0 (Laghi et al. 2021), provided they can be detected with high SNR. These events can reach relative uncertainties on $\Delta D_L/D_L$ below 0.05 and typical sky-localisation errors less than 1 deg^2, representing the best well-localised events suited for a statistical approach on the inference of the GW redshift, comparable to, if not better than, what future third-generation ground-based detectors can achieve (Iacovelli et al. 2022). As we will see in Sects. 2.3 and 2.4, according to the analysis of Laghi et al. (2021), LISA will be able to use from a few to several tens of EMRIs to extract useful cosmological information.

Redshift information on a GW source can also be obtained in a statistical way performing a population analysis when there are distinctive features in the source mass distribution. This is simply because GW observatories are only sensitive to the redshifted or detector frame masses, which directly relate to the source masses via

$$m_z = (1 + z)m. \tag{3}$$

Therefore, if the mass distribution presents a known feature, e.g. a peak or a drop, at a reference scale which is invariant under cosmic evolution, by observing this feature in the GW events at different luminosity distance bins one can infer their redshift, becoming spectral sirens. If such a feature exists, this would be a very convenient probe of the cosmic expansion because it only requires GW data. In case of a time evolution of the reference mass scale, using the full mass distribution helps calibrating against astrophysical uncertainty (Ezquiaga and Holz 2022).

A good example of such features occurs in the mass spectrum of SOBBHs. This is because as stars become more massive, a runaway process induced by electron-positron pair production known as pair-instability supernova (PISN) is triggered (Barkat et al. 1967; Fowler and Hoyle 1964; Heger and Woosley 2002; Fryer et al. 2001; Heger et al. 2003; Belczynski et al. 2016). These PISN result in complete disruption of the stars, preventing the formation of remnant BHs and thus inducing a gap in the mass spectrum starting at around $50\,M_\odot$. Nonetheless, for sufficiently massive stars the PISN process is insufficient to prevent direct collapse, and a population of BBHs with masses larger than $\sim 120\,M_\odot$ could arise. Therefore, the theory of PISN predicts a gap in the BBH mass spectrum with two edges that act as reference scales.[2] While the lower edge of the gap lies within the main sensitivity of present LIGO/Virgo detectors and could lead to precise measurements of $H(z)$ (Farr et al. 2019; Ezquiaga and Holz 2022), LISA will be more sensitive to the upper edge if a population of "far side" binaries in fact exists (Ezquiaga and Holz 2021). These alternative methodologies are currently under development and will need to be further investigated in the future, especially in the framework of GW cosmology with LISA.

Finally, we mention another effect that in principle allows one to access the redshift information directly from the GW signal alone. The variation of the background expansion of the universe during the time of observation of the binary induces an effectively -4 post-Newtonian term in the waveform phase, whose

amplitude directly depends on the redshift and on the value of the Hubble parameter both at the source and at the observer (Seto et al. 2001; Nishizawa et al. 2012). Unfortunately, redshift perturbations due to the inhomogeneous distribution of matter between the source and the observer also depend on time, and therefore also contribute to the extra terms in the phase (Bonvin et al. 2017). Among these, the time-varying peculiar velocity of the GW source centre of mass may dominate the signal, effectively preventing the extraction of the redshift information from the amplitude of the dephasing—but possibly allowing a measurement of the binary's peculiar acceleration (Tamanini et al. 2020; Inayoshi et al. 2017).

2.2.3 Systematic uncertainties on standard sirens

Bright and dark sirens will suffer from some common systematic uncertainties. The measurements of the binary luminosity distances are affected by the detector calibration uncertainty (Karki et al. 2016; Chen et al. 2021a) and the accuracy of the waveform models (see Abbott et al. 2019b for discussions in the context of LIGO/Virgo observations). Accurate waveforms will be particularly needed for the high SNR sources that LISA will detect. Moreover, high redshift sources will be affected by weak lensing uncertainties (Holz and Linder 2005; Hirata et al. 2010; Cusin and Tamanini 2021) (see Sect. 3 for more details). In addition, the parameter estimation of the luminosity distance will be subject to degeneracies with the orbital plane inclination and other parameters, though for long duration signals or when higher harmonics are measured (Baibhav et al. 2020), this degeneracy can be broken. In general, these parameter degeneracies will lead to larger statistical errors but not systematic biases. Finally, our understanding of the possible observational selection effect (Chen 2020) as well as the astrophysical rate evolution (see e.g. Fig. 12 of Finke et al. (2021) for an application to LIGO-Virgo data) are critical to the accuracy of standard siren analysis as well. Not many investigations have so far assessed the systematic uncertainties affecting standard siren measurements with LISA. A thorough exploration of all these effects, needed to consolidate our confidence on LISA cosmological observations, will be necessary in the future.

2.3 Constraints on ΛCDM

In this subsection we present how well LISA will be able to constrain the cosmological parameters of the standard ΛCDM model, by using different classes of standard sirens as presented in Sect. 2.2. We first focus on the Hubble constant H_0 and consider constraints on additional parameters afterwards. We conclude the subsection with a discussion on consistency tests of ΛCDM at high-redshift with LISA MBBH standard sirens.

[2] Recent analyses have shown however that both the lower end of the gap (Farmer et al. 2019) and its width (Farmer et al. 2020) are robust against ambient factors and nuclear reaction rates.

2.3.1 H_0 tension and standard sirens

The standard model of cosmology is extremely successful and allows one to describe the universe from the time of BBN to the present time of cosmic acceleration. Remarkably, it contains only six parameters, one of which, the present-day *Hubble constant* H_0 describes the expansion rate of the universe. At small redshifts, it relates the luminosity distance and the redshift of a source such that $D_L(z \ll 1) = cz/H_0$. Consistency of the model requires the inferred value of H_0 to be independent of the probe and any deviations should be seen as a sign of unaccounted for systematics or more excitingly, new physics.

In recent years, two sets of values for H_0 have emerged from so-called *early* or *late* measurements of H_0 depending on the origin of the calibration. As the error bars shrink, it becomes increasingly clear that the two values are in tension, reaching 4–5σ disagreements (Verde et al. 2019). The most precise measurement of H_0 from the early universe comes from the cosmic microwave background (CMB) (at recombination redshift $z \sim 1100$) with an inferred value of $H_0 = 67.4 \pm 0.5$ km s^{-1} Mpc^{-1} at 68% C.L. assuming a flat ΛCDM cosmology (Aghanim et al. 2020). In this case the H_0 value is inferred from the angle upon which the scale associated to the horizon at the last scattering surface is projected, which is obtained from the measurement of the density fluctuations. Compatible values of H_0 are obtained also from the Atacama Cosmology Telescope and WMAP5 for which $H_0 = 67.6 \pm 1.1$ km s^{-1} Mpc^{-1} at 68% C.L. (Aiola et al. 2020) and from the joint analysis of Dark Energy Survey (DES) clustering and weak lensing data with baryon acoustic oscillations (BAO) and big bang nucleosynthesis (BBN), $H_0 = 67.2^{+1.2}_{-1.0}$ km s^{-1} Mpc^{-1} at 60% confidence (Abbott et al. 2018c).

In contrast, several teams have measured a significantly higher value of H_0 in the local universe with redshifts $z \leq 1$ in a model independent fashion. For example, the SH0ES team used Cepheid calibrated supernovae type Ia to measure $H_0 = 74.03 \pm 1.42$ km s^{-1} Mpc^{-1} (Riess et al. 2019) (see also recent updates, Riess et al. 2022). The H0LiCOW collaboration used strong lensing time delays of background quasars to infer $H_0 = 73.3^{+1.7}_{-1.8}$ km s^{-1} Mpc^{-1} (Wong et al. 2020). The Megamaser Cosmology project used very long baseline interferometric observations of water masers in Keplerian orbits around MBHs to measure $H_0 = 73.9 \pm 3.0$ km s^{-1} Mpc^{-1} (Pesce et al. 2020). The Carnegie-Chicago Hubble Program collaboration used tip of the red giant branch measurements in the large Magellanic cloud to calibrate 18 supernovae type Ia, instead of Cepheids, and found a slightly lower $H_0 = 69.8 \pm 2.6$ km s^{-1} Mpc^{-1} (Freedman et al. 2019).

GWs offer an independent test of the tension using bright or dark sirens as described in Sect. 2.2.1 and Sect. 2.2.2. The LIGO-Virgo collaboration used the first bright siren, namely GW170817, to infer $H_0 = 70^{+12}_{-8}$km s^{-1} Mpc^{-1} at 1σ (Abbott et al. 2017a), which lies somewhat in between the early and late universe values but with a worse precision if compared to current EM results. Furthermore, current dark siren measurements reached an inferred value of $H_0 = 75^{+25}_{-22}$ km s^{-1} Mpc^{-1} at 1σ (Fishbach et al. 2019; Finke et al. 2021; Abbott et al. 2021a). The rather large error bars are expected to shrink as $1/\sqrt{N}$, where N indicates the number of well-localized

events. Percent-level precision on H_0 is expected in the 2020s with BNS mergers detected by Advanced LIGO-Virgo and their EM counterpart observations (Nissanke et al. 2013; Chen et al. 2018). Bright sirens in the era of the third generation of ground-based GW detectors could further constrain other cosmological parameters, such as Ω_m and w_0 (Sathyaprakash et al. 2010; Zhao et al. 2011; Cai and Yang 2017; Jin et al. 2020; Chen et al. 2021a) and usher us into the era of precise GW cosmology.

LISA will offer an alternative and complementary probe of ΛCDM which might as well provide useful information on the Hubble tension. In the following, we explore the potential of LISA to probe H_0 and beyond.

2.3.2 LISA forecast for H_0

LISA will be able to contribute measurements of H_0 coming from different classes of standard siren sources (see Sect. 2.2). For the time being, the literature has described only measurements coming from individual classes of sources. A complete analysis combining the constraining power of different LISA GW sources is still missing.

By considering SOBBHs, and by cross-matching with simulated galaxy catalogues, Kyutoku and Seto (2016), Del Pozzo et al. (2018) found that constraints on H_0 can reach the few % level. In particular, in the study presented in Del Pozzo et al. (2018), several different instrumental configurations for LISA were investigated, as well as several coalescence rate models within the range allowed by the LIGO-Virgo observations from O1. This analysis also had Ω_m as a free parameter, although due to the low-redshift of the sources results are not informative. The SOBBHs entering the analysis were selected to have SNR > 8, a cosmological redshift < 0.1 and an uncertainty on the luminosity distance smaller than 20%. No other selection criteria were applied. With the aforementioned selections, the number of SOBBHs considered ranged from a pessimistic case of 7, yielding an accuracy on H_0 of 7% to a most optimistic case of 259, yielding an accuracy of 1%, see left panel in Fig. 2.

A similar analysis can be done also with EMRIs. A first investigation (MacLeod and Hogan 2008) pointed out that $\sim$20 EMRIs detected at $z \sim 0.5$ could be enough to constrain H_0 at the 1% level. The analysis provided in MacLeod and Hogan (2008) employed however a simplified approach to estimate cosmological forecasts with LISA, and moreover assumed the more optimistic mission design considered at the time. A recent, more detailed analysis has been performed with LISA EMRIs (Laghi et al. 2021). Using only the most informative, high-SNR (> 100) EMRIs up to redshift $z \leq 0.7$, cross-matching with the galaxy catalogue obtained from the simulated sky of Henriques et al. (2013), it is shown that constraints at the few % can be forecast for H_0. An analysis of three different EMRI population models taken from Babak et al. (2017), representing a pessimistic, a fiducial, and an optimistic scenario, points out that in a 4-year LISA mission lifetime constraints are expected to be at 3.6%, 2.5%, and 1.6% (68% CL), respectively, while in case of a 10-year mission H_0 can be constrained at the 2.6%, 1.5%, and 1.1% accuracy (68% CL). The different accuracy in the various scenarios reflects the different number of useful EMRIs available in each model, which in case of 10 years of observation and after the SNR

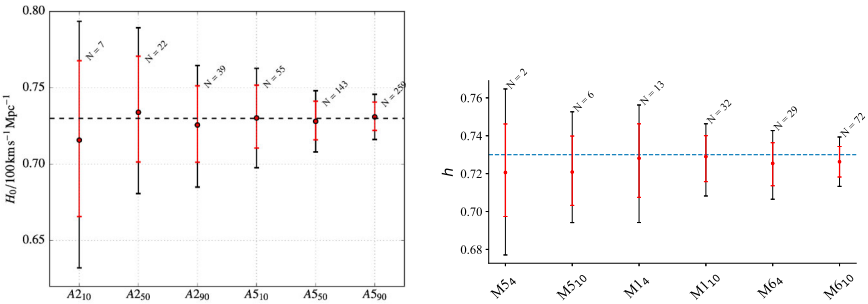

Fig. 2 Left panel: 90% (black) and 68% (red) credible intervals for H_0/km s^{-1} Mpc^{-1} for each of the LISA configurations considered in Del Pozzo et al. (2018). The credible regions are averaged over the galaxy hosts realisations. Right panel: 90% (black) and 68% (red) percentiles, together with the median (red dot) of h for the pessimistic, fiducial, and optimistic EMRI models (M5, M1, M6, respectively) and for two different LISA observational scenario (4 and 10 years). Here $h = H_0/(100\,\mathrm{km\,s^{-1}Mpc^{-1}})$ and the blue dashed horizontal line denotes the true cosmology (set at $h = 0.73$ in Del Pozzo et al. 2018; Laghi et al. 2021). For each data point, we also report the average number N of EMRIs considered in the analysis. Images reproduced with permission from [left] Del Pozzo et al. (2018) and [right] Laghi et al. (2021), copyright by the author(s)

selection, ranges from $\sim$5 (in the worst scenario), passing to $\sim$30 (in the fiducial scenario), up to $\sim$70 (optimistic scenario), see right panel in Fig. 2.

Finally the last standard siren class that LISA can employ to constrain H_0 are MBBHs. Although these events are expected to be detected at high-redshift ($z > 1$), by assuming ΛCDM one can set bounds on H_0, i.e. on the cosmic evolution at low-redshift. By simulating different populations of MBBH mergers, performing (simple) parameter estimations over the expected GW signal, and by simulating the emission and detection of possible EM counterparts, recent works showed that constraints at the few % level can be imposed on H_0 (Tamanini et al. 2016; Tamanini 2017; Belgacem et al. 2019c). These studies predict around four useful standard sirens with observed EM counterpart, per year. Their redshift distribution peaks between redshift 2 and 4, with tails up to $z \simeq 8$. The dominant contribution on the distance uncertainty of these events is not the LISA measurement error, but rather the systematic effect due to week lensing which dominates at high-z providing an estimated average uncertainty of up to 5-10% (Hirata et al. 2010; Cusin and Tamanini 2021). Nevertheless even if LISA will detect only a few MBBH standard sirens, the fact that these will be at high redshift, with relatively precise distance determination, and of course with the single redshift value identified with the EM counterpart, will allow for interesting constraints on H_0 at the few percent level (Tamanini et al. 2016; Tamanini 2017; Belgacem et al. 2019c). This is comparable with what is expected for low-redshift, more numerous LISA dark sirens such as SOBBHs and EMRIs. As we will show below, MBBHs will however be more interesting for cosmological analyses beyond the simple measurement of H_0.

The joint-inference on H_0 resulting from the combination of the analyses described above for SOBBHs, EMRIs and MBBHs, is expected to provide interesting constraints, possibly reaching the 1% level, or better. Such a combined investigation however has not yet been performed and will be the focus of future

studies. Note also that a further class of standard sirens for LISA could be provided by intermediate-mass binary black holes (IMBBHs), ranging from $\mathcal{O}(100)$ to $\mathcal{O}(1000)$ solar masses. Although recent LIGO/Virgo observations may point towards the existence of this class of BBHs (Abbott et al. 2020b), their merger rate and population properties are completely unknown at the moment (Toubiana et al. 2021), making current LISA forecasts too uncertain to be seriously considered. Given their high-mass and redshift range, IMBBHs could nevertheless well represent the best class of LISA dark sirens if they can be detected in high numbers. Moreover the association with possible EM counterparts, which for these systems are being realistically considered (Graham et al. 2020), could well turn the LISA IMBBH detections that merge within the LIGO/Virgo band in a relatively short time, into useful multi-band bright sirens with a great potential to yield precise cosmological measurements (Muttoni et al. 2022).

By surveying the considerations made above, we can expect LISA to deliver constraints on H_0 at the few percent level or better, similarly to what ground-based detectors may produce on comparable timescales (Chen et al. 2021a). The robustness of these constraints against uncertainties in the overall analysis, including for example calibration and waveform modelling issues, will be something to carefully assess in the future. In any case, a precise and accurate measurement of H_0 with LISA will provide useful insights on the Hubble tension, should the tension still persist. On the other hand, a further independent and complementary measurement of H_0 will help strengthen our confidence in the value of the Hubble constant, especially if hints of physics beyond ΛCDM appear.

2.3.3 ΛCDM beyond H_0

The relatively high-redshift reach for some of the standard sirens sources detected by LISA, will allow the inference on cosmological parameters beyond H_0. In particular MBBHs will be extremely useful to test the cosmic expansion at high-redshift ($z \lesssim 8$) while EMRIs could be useful for cosmological applications up to $z \sim 1$, or more generally up to the redshift at which we will be able to employ fairly complete galaxy catalogues.

As shown in Tamanini et al. (2016), Tamanini (2017), MBBH mergers with an identified EM counterpart could be used by LISA to infer the values of Ω_m and Ω_k, albeit with large uncertainties. Assuming ΛCDM, constraints on Ω_m are forecast to reach the $\sim 10\%$ level (68% C.L.) only in the most optimistic scenarios (Tamanini et al. 2016; Belgacem et al. 2019c; Spergel et al. 2015), while allowing for spatial curvature degrades these estimates for Ω_m to $\sim 25\%$ and yields a measurement of Ω_k at similar precision (Tamanini et al. 2016). Needless to say these results will certainly not be competitive with EM observations, but will at least provide an independent and complementary measurement.

Similarly, EMRIs will be able to provide information on Ω_m only in the most optimistic scenarios. In fact recent estimates (Laghi et al. 2021) indicate that using the loudest $\mathcal{O}(70)$ events, as predicted in an optimistic population scenario, it is possible to get constraints with $\sim 20\%$ accuracy (68%CL) on Ω_m when jointly inferred with H_0. Even though this result is not expected to compete with current and

future EM observations (Amendola et al. 2018b; Scolnic et al. 2018), it is somehow not surprising since the EMRIs used in Laghi et al. (2021) are distributed up to $z \lesssim 0.7$. Future analysis, possibly including a larger number of events, thus including low-SNR events which are typically coming from high redshifts, are expected to give more informative results on cosmological parameters beyond H_0.

Preliminary investigations of the full ΛCDM cosmological model where the curvature term Ω_k is not fixed to 0, seem to indicate that, even for moderate redshift sources such as the loudest EMRIs (SNR > 100) at $z \lesssim 0.7$, LISA will provide some simultaneous constraints on all cosmological parameters. In the fiducial scenario of Laghi et al. (2021), Ω_k can be constrained with an accuracy of $\sim 30\%$, while Ω_m can be constrained with an accuracy of $\sim 55\%$, while retaining an accuracy on H_0 of $\sim 2\%$ (all 68% CL) (Laghi 2021). These results will need to be further investigated in the future, however they are suggestive that a possible simultaneous inference of different cosmological parameters with LISA standard sirens will indeed be possible. In particular the full LISA cosmological analysis with results obtained from the combination of all classes of LISA standard sirens, namely SOBBHs, EMRIs and MBBHs, should substantially increase the accuracy of the estimates on Ω_m and Ω_k above, thanks especially to the combination of cosmological datasets from different redshift ranges which might break some of the degeneracy between the cosmological parameters. A future combined investigation will thus be needed to thoroughly assess the ability of LISA to constrain parameters beyond H_0.

2.3.4 Tests of ΛCDM at high-redshift

The most interesting class of LISA standard sirens are MBBHs, not only because they are expected to produce detectable EM counterparts (bright sirens) but also because they will be detected at high redshift and thus can be employed to test the cosmic expansion at early epochs largely unexplored by current EM cosmological surveys. As we will show in Sect. 2.4 and in Sect. 4, MBBHs will have the potential to test different cosmological models alternative to ΛCDM. Here we briefly mention how well LISA can test ΛCDM itself at high z, taking into account possible general deviations (to be discussed shortly) and by comparing with EM probes at similar redshifts. Note also that in analogy to EM distance observations, LISA MBBHs can as well be employed to probe the fundamental assumptions of ΛCDM, e.g. the cosmological principle (Cai et al. 2018).

Let us first of all recall how well MBBHs can test ΛCDM. As shown in the previous section, in the most optimistic cases Ω_m can be tested at the $\sim 10\%$ level, which reflects the fact that at $z \gtrsim 1$ the universe is expected to be matter dominated and thus to provide information mainly on Ω_m. Any deviation from the standard matter-dominated evolution at redshift $1 \lesssim z \lesssim 4$ however will be constrained by LISA, at a level not attained by current EM observations.

To put in context the potential of LISA we can compare its constraining power with other EM measurements of the cosmic expansion at high z. LISA will in fact provide independent and complementary data which will not only deliver useful and accurate information on deviations from ΛCDM but will also be used to check and cross-validate EM measurements, expected to be sparse and inaccurate at such high-

redshift. As a clear example, LISA can successfully compete with quasar cosmological observations at $z \sim 2$ and above (Speri et al. 2021). Current quasar distance measurements indicate possible issues in the Hubble diagram at $z \gtrsim 2$, where deviations from ΛCDM have already been claimed (Risaliti and Lusso 2019) (see also Velten and Gomes 2020; Yang et al. 2020b; Banerjee et al. 2021). To understand if such apparent deviations are due to systematic effects or are indeed due to new physics beyond ΛCDM, complementary measurements at the same redshift range will be needed. As shown in Speri et al. (2021), four MBBH standard sirens detected by LISA are on average enough to unequivocally confirm or rule out the apparent deviation claimed in Risaliti and Lusso (2019), and thus to reveal if indeed this is due to systematics in the quasar Hubble diagram or to new physics. Standard siren observations will play a crucial role to test deviations from the ΛCDM.

GW observations provide a more reliable distance luminosity measurement than other EM observations, such as quasars. Standard sirens rely in fact on fundamental predictions of GR and not on phenomenological relations between observed quantities. Although the quasar Hubble diagram will become more precise and accurate in the time between now and when LISA will fly, for example with observations by the eROSITA (Merloni et al. 2012) and Euclid (Amendola et al. 2018b; Barnett et al. 2019) missions, intrinsic systematics on the quasar cosmological measurement might still be unresolved. LISA will thus provide a unique complementary test of the cosmic expansion at $z \gtrsim 2$, which not only will yield accurate measurement of deviations from ΛCDM but it will also be used to cross-validate any results obtained by other EM observations at the same redshift range, notably with quasars.

2.4 Probing dark energy

This subsection discusses how LISA can probe the fundamental nature of DE through GW standard sirens. Here only simple alternative DE models are considered, and in particular we assume that the underlying gravitational theory remains GR. Models of DE based on modification of GR are discussed in details in Sect. 4.

2.4.1 Equation of state of dark energy: w_0 and w_a

Deviations from the standard cosmological model include the presence of a DE fluid with effective equation of state (EoS) given by: $p_{\rm DE} = w_{\rm DE}(a)\rho_{\rm DE}$, where $p_{\rm DE}$ and $\rho_{\rm DE}$ are the effective pressure and density of the DE fluid respectively. Although the functional dependence of $w_{\rm DE}(a)$ may be very non-trivial (see e.g. self-accelerating cosmologies), for practical purposes we consider here only a simple phenomenological parametrization introduced by Chevalier-Polarski-Linder (CPL) (Chevallier and Polarski 2001; Linder 2003):

$$w_{\rm DE}(a) = w_0 + w_a(1-a), \tag{4}$$

where w_0 and w_a are constants and indicate, respectively, the value and the time

derivative of $w_{\rm DE}$ today. We refer to Sect. 4 about modified gravity for more complicated, model dependent forms.

In all the scenarios studied by Belgacem et al. (2019c) (which depend on the BH seeds and on the assumptions about the error on redshift), the GW sources considered are expected not to contribute relevantly to improve the knowledge on w_0, with respect to what is already known from current cosmological observations. More precisely, the 1σ error Δw_0 only goes from $\Delta w_0 = 0.045$ (using CMB, type Ia supernovae and BAO data) to $\Delta w_0 = 0.044$ adding MBBH standard sirens to the datasets, even in the best scenario where LISA alone can only reach a 20% relative 1σ uncertainty on w_0 (Tamanini 2017). It is important to remark, however, that these outcomes are based on a mission duration of 4 years and sources are limited to MBBHs with EM counterparts. Significant improvements are expected by extending the data taking time or by combining with information from other sources, notably EMRIs.

Indeed, recent investigations (Laghi et al. 2021) suggest that EMRIs will deliver constraints on w_0 of the order of $\sim 10\%$, when inferred simultaneously with w_a. When assuming prior knowledge of H_0 and Ω_m, constraints on w_0 are estimated at the $\sim 7\%$ level in a realistic EMRI scenario, reaching $\sim 5\%$ in the best case (all 90% C.L.). These results are better than what expected with dark sirens analysis for 3 G ground-based detectors (Belgacem et al. 2018b), and compatible with what they can achieve with bright sirens (Belgacem et al. 2019b). While relevant information on w_0 can be obtained with moderately low-redshift events, w_a is expected to be measurable only with higher-redshift events, which in the joint cosmological inference of w_0 and w_a of Laghi et al. (2021) are not considered, and thus no relevant measurement of w_a is obtained.

Although from these estimates it seems that LISA standard sirens will not be competitive with future EM observations, we stress that they will anyway provide independent and complementary measurements which will increase our confidence on any insight on the nature of DE. This is strikingly important for modified gravity models of DE, where GWs can indeed provide orthogonal information with respect to EM observations; see Sect. 4.

2.4.2 Alternative dark energy models

The CPL phenomenological parametrization discussed in the previous subsection constitutes only a simple approach for detecting deviations from the ΛCDM. The theoretical description of DE may require more sophisticated models. Here, we briefly discuss such a possibility focusing on scenarios that change the background cosmological expansion with respect to ΛCDM. We assume the standard evolution equation for GWs. Possible modifications to GW propagation through cosmological spacetimes—motivated by modified graviton dispersion relations, or non-minimal couplings of the dark-energy sector with curvature—are described in Sect. 4.

Models for DE can include quite a large number of parameters, leading to rich dynamics for the DE sector as a function of redshift. Some investigations aim to dynamically explain the puzzling small value for the present-day acceleration rate, leading to a time-dependent evolution of the DE density. These include quintessence

scenarios (Wetterich 1988; Zlatev et al. 1999), which can be generalised to kinetically-driven (Armendariz-Picon et al. 2000) and kinetic-braiding models (Deffayet et al. 2010) without modifying the propagation properties of GWs. Other scenarios aim to alleviate the coincidence problem relating DE with DM at intermediate redshifts, for example in the DE-DM interacting models (Wetterich 1995; Amendola 2000), or in Chaplygin gas cosmology (Kamenshchik et al. 2001). More exotic possibilities include holographic DE, associating the present-day acceleration of the universe with the size of the particle horizon (Li 2004). See e.g. Copeland et al. (2006b), Li et al. (2011), Ishak (2019), Huterer and Shafer (2018) for reviews, including analysis of cosmological implications and observational prospects of DE scenarios. A recent resurgence of interest on DE model building, based on the previous approaches, has been motivated by the H_0 tension discussed in Sect. 2.3.1; see Di Valentino et al. (2021) for a review. Among many examples, such tension can be alleviated in scenarios with DM-DE interactions or with features at small or intermediate redshifts (Di Valentino et al. 2017, 2016; Keeley et al. 2019; Raveri 2020), in ranges that might be probed with GW sirens. See e.g. Knox and Millea (2020) for a comprehensive discussion on this topic, including comparison between theoretical ideas and existing cosmological constraints.

These theoretical models suggest that distinctive DE effects can occur at different redshifts, from very small to relatively large values of z. The capability of LISA to probe cosmological expansion in a large range of redshifts, as discussed in the previous sections, provides invaluable opportunities for building independent cosmological tests (see Sect. 2.3.4) and thus to probe different DE scenarios, in a complementary way with respect to EM probes. A clear example is given by the investigations of Cai et al. (2017), Caprini and Tamanini (2016) where LISA forecasts for testing cosmological models allowing for DE-DM interactions or for early DE have been produced using MBBH as bright sirens. Similar analyses using LISA dark sirens are still missing in the literature and will constitute material for future explorations. By considering the results obtained with both SOBBHs and EMRIs for standard cosmological models (see Sect. 2.3), it would be very interesting to further develop these studies by designing an efficient, unified method to reconstruct the redshift dependence of DE with GWs, similar for example to what already done with EM observations; see e.g. Sahni and Starobinsky (2006). Assumptions going beyond the linear CPL parameterisation discussed in the previous section might be better suited to test specific alternative scenarios, or for improving the DE reconstruction in a wider redshift interval, e.g. through polynomial fitting (Alam et al. 2003). Alternatively, methods based on a principal component analysis of a binned parametrization of the signal as a function of redshift, as proposed in Huterer and Starkman (2003), might be adapted and applied to GW observations with LISA.

Besides the alternative DE models already considered in the literature, there are plenty of others that can still be tested by LISA and for which detailed analyses will be needed in the forthcoming years in order to understand how well LISA will constrain them and thus to better assess and expand the science case of the mission. We conclude by mentioning again that the nature of DE can be further investigated if this is connected to an underlying gravitational theory beyond GR. In this case new

observational signatures might appear, giving rise to a richer phenomenology and to more promising LISA results. Such models and analyses will be discussed in Sect. 4 in the context of modified theories of gravity (Baker et al. 2021).

2.5 Synergy with other cosmological measurements

GW observations by LISA will provide a wealth of cosmological information as we have seen in the previous sections. But LISA will not be alone in the quest of understanding the cosmic history. It is thus of great importance to assess how LISA could complement with other facilities. In what comes next, we discuss LISA synergies with EM observatories and other GW detectors.

2.5.1 Integration with standard electromagnetic observations

To date, most studies constraining cosmological parameters with GWs have focused on the Hubble parameter, see Sect. 2.3.2. This is because the cosmological information in GW amplitudes is primarily held in the luminosity distance of the source, D_L, which for low redshifts ($z \ll 1$) can be approximated to $D_L \simeq cz/H_0$. The majority of LISA sources will exist at higher redshifts where this approximation breaks down. Instead the full expression for the luminosity distance must be used (see Eq. (1)) and so GW amplitudes in principle have sensitivity to further cosmological parameters traditionally measured electromagnetically, such as the fractional densities Ω_m and Ω_Λ, and the DE EoS parameters w_0 and w_a, see Sects. 2.3.3 and 2.4.

A key outstanding question is whether specific combinations of EM and GW probes have the ability to improve constraints on these parameters and break degeneracies between them. Details about the galaxy surveys co-temporal with LISA are not available at present, but as a conservative approach we can consider 'Stage IV' experiments planned over the next decade, such as DESI, Euclid, the Vera C. Rubin Observatory, and the Roman Space Telescope (Aghamousa et al. 2016; Laureijs et al. 2011; Schmidt et al. 2020; Spergel et al. 2015). The corresponding CMB data will come from the LiteBIRD mission (Hazumi et al. 2012). Direct cross-correlation of GW sources with galaxy catalogues will be considered in Sect. 2.6. Here we focus instead on probe combination, though we note that there is a lack of comprehensive studies on this topic in the current literature.

One advantage leveraged by Stage IV galaxy surveys is the ability to combine multiple probes from the same instrument. Most commonly the main probes are shear power spectra from galaxy weak lensing, BAO measurements from galaxy clustering, supernovae, and, additionally, strong gravitational lenses in some analyses. As examples of the expected constraints, Zhan and Tyson (2018) provides forecasts for standard cosmological parameters using weak lensing, BAO and supernovae data from the Vera C. Rubin Observatory, combined with current Planck CMB data. The resulting 68% confidence intervals on $\{w_0, w_a\}$ and $\omega_m = \Omega_m h^2$ are $\{7.05 \times 10^{-2}, 1.86 \times 10^{-1}\}$ and 7.73×10^{-4} respectively, with h being the normalised Hubble parameter. Similar results are expected from the Euclid space

mission, which should yield 68% confidence intervals around $\{3 \times 10^{-2}, 1.3 \times 10^{-1}\}$ for $\{w_0, w_a\}$. Comparing these values to the forecasts using LISA EMRI detections presented in Laghi et al. (2021), it seems unlikely that LISA will be able to offer competitive constraints on Ω_m. However, in mildly optimistic scenarios they may offer moderate constraints on the DE parameters, with (Laghi et al. 2021) forecasting 95% confidence intervals on $\{w_0, w_a\}$ of approximately $\{6.5 \times 10^{-2}, 6.5 \times 10^{-1}\}$ for a four-year LISA mission and optimistic MBH population models.

An alternative strategy is to find probe combinations where GW data can break degeneracies existing between EM probes. One such example is put forwards in Qi et al. (2021), which determines forecasts for the combination BNS data from the DECihertz Interferometer Gravitational wave Observatory (DECIGO) with measurements of redshift drift (the Sandage–Loeb effect, Loeb 1998) from the SKA and the European-Extremely Large Telescope (E-ELT). Redshift drift measurements use high-resolution spectroscopy of the HI emission line (SKA) or Lyman-α absorption lines in quasar spectra (E-ELT) over long time frames (10 years+) to directly measure tiny shifts the line frequencies. Although experimentally challenging, this constitutes a *direct* measurement of $H(z)$, as opposed to the integrated effect of $H(z)$ probed by luminosity distances; see Eq. (1).

GWs can likewise offer a direct measurement of $H(z)$ through the dipole of the luminosity distance. Equation (1) gives the luminosity distance-redshift relation in a perfectly homogeneous and isotropic universe; in fact small corrections to this are induced by gravitational lensing and peculiar velocities. As shown in Bonvin et al. (2006a), Bonvin et al. (2006b) for the EM case (see e.g. Nishizawa et al. 2011 for the GW case), the peculiar motion of our Galaxy with respect to the CMB frame induces a dipole mode in the luminosity distances. This dipole moment is given by

$$D_L^{(1)}(z) = \frac{|\mathbf{v_0}|\,(1+z)^2}{H(z)}, \tag{5}$$

where $\mathbf{v_0}$ is the dipole anisotropy in the CMB, estimated to be approximately 369.1 ± 0.9 km/s. Combining measurements of this dipole from DECIGO BNS sources with the redshift drift measurements above, Qi et al. (2021) finds substantial breaking of degeneracies in the $H_0 - \Omega_m$ plane, leading to 1-σ bounds on $\{H_0, \Omega_m\}$ of $\{0.78\,\mathrm{km\,s^{-1}Mpc^{-1}}, 0.006\}$, competitive with current bounds. Mild improvements on the constant DE EoS were also obtained ($\sigma_{w_0} \sim 0.03$), though no meaningful constraint on w_a was possible. Further analyses are needed to properly understand if such method can equally be applied to LISA.

On cosmological scales, a bias prescription is used to model how GW events trace the large-scale DM distribution. Analogously to galaxy bias, the GW bias is modelled as scale-independent on large scales. Using the parameterisation $b_{\mathrm{GW}}(z) = b^0_{\mathrm{GW}}\,(1+z)^{\alpha}$, Mukherjee et al. (2021d) finds the parameters b^0_{GW} and α to be uncorrelated with H_0 and Ω_m for a ΛCDM model ($w_0 = -1$ fixed). This suggests cautious optimism that combined GW and EM constraints on cosmological parameters should not be strongly sensitive to the GW bias prescription.

2.5.2 Complementarity with other gravitational-wave observatories

In addition to the synergies with other cosmological surveys, LISA will also build new synergies with other GW detectors. In particular, LISA will be able to detect the early inspiral phase of compact binary coalescences that later merge within the frequency bands of Earth-based interferometers. Some example signals are displayed in the left panel of Fig. 3. Because the same signal is detected across different frequencies, these events are known as multi-band. Different populations of BBHs could become multi-band sources. Most notably, the SOBBHs that current LIGO/Virgo detectors are observing could have been seen if LISA was online a few years before these detections (Sesana 2016). Nonetheless, LISA high frequency sensitivity limits their number (Moore et al. 2019). If present in nature, IMBBHs would be more promising candidates (Amaro-Seoane and Santamaria 2010; Jani et al. 2019; Sedda et al. 2020), and possibly yield interesting cosmological results (Muttoni et al. 2022). There is however a limit to their masses, because if they are too heavy they will merge before reaching the frequencies of ground-based detectors. (This limitation could be removed with a deci-Hertz observatory (Sedda et al. 2020).)

The right panel of Fig. 3 displays the *fraction of multi-band events*, defined as the subset of LISA detections merging within 10 years and being detected by a ground-based instrument (Ezquiaga and Holz 2021). For concreteness we consider Advanced LIGO (aLIGO), its possible upgrade (A+), Voyager and the third-generation detectors Cosmic Explorer (CE) and Einstein Telescope (ET). Interestingly, the multi-band fraction peaks where the upper end of the PISN mass gap is expected to be found, implying that far-side binaries could be promising multi-band sources (Ezquiaga and Holz 2021). As noted in Gerosa et al. (2019), for $M_{\rm tot} \lesssim 100\,M_\odot$, there is no difference for the multi-band ratio between 2 G and 3 G detectors because the fraction is limited by LISA high-frequency range. On the contrary, for $M_{\rm tot} > 200\,M_\odot$ the difference among ground-based detectors are sizeable and depends mostly on their low frequency sensitivity.

Besides individual sources, LISA and ground-based detectors could share SGWBs. For example the background of unresolved SOBBHs could be within the

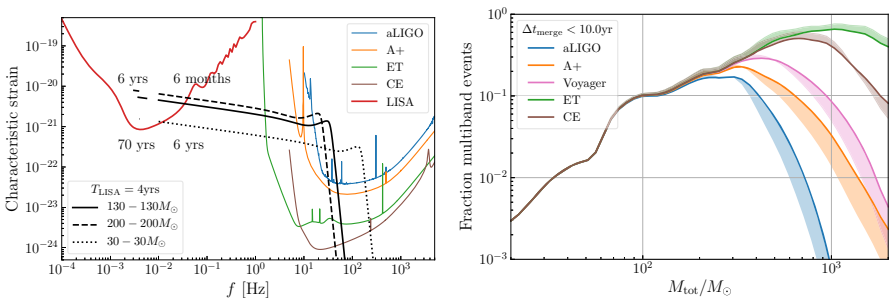

Fig. 3 On the left, GW signals as seen by LISA and different ground-based detectors. The times indicate the time to merge which depends on the initial frequency. On the right, fraction of total events observed by LISA and that will merge within 10 years, being detected by a ground-based detector. Image [right panel] reproduced with permission from Ezquiaga and Holz (2021), copyright by AAS

reach of LISA detectability (Sesana 2016). Similarly, binaries above the PISN gap could leave an additional background (Mangiagli et al. 2019).

Finally, LISA could also complement other space-based detectors. In particular, there are several proposals such as Taiji (Ruan et al. 2020a) and TianQin Wang et al. (2020a) that could potentially fly at the same time as LISA. These additional detectors would help improve the cosmological inference (Wang et al. 2022a, b; Baral et al. 2020; Zhao et al. 2020). Moreover, any further detector in the deci-Hertz frequency band would be an excellent addition to LISA science (Sedda et al. 2020).

Altogether, LISA and the other GW observatories will all contribute to a standard siren measurement of $H(z)$ across a broad redshift range.

2.6 Cross-correlation and interaction with large scale structure

GW maps of resolved events or SGWB can be cross-correlated with other large-scale-structure (LSS) tracers to perform a variety of astrophysical and cosmological measurements. Here we focus on the use of the SGWB measurements while technicalities about this signal are postponed to Sec. 5.

2.6.1 Cross-correlations with resolved events

The analysis of the cross-correlations between galaxy surveys and resolved GW events from compact object mergers has a rich scientific potential (Laguna et al. 2010). From binary mergers with an EM counterpart, such an analysis can constrain DE and modified gravity models (Camera and Nishizawa 2013). A similar analysis for sources as the first ones detected by LIGO/Virgo, yields constraints on the distance-redshift relation, the Hubble constant and other cosmological parameters (Oguri 2016). PBH scenarios as well as different astrophysical models can also be tested (Raccanelli et al. 2016; Raccanelli 2017; Scelfo et al. 2018, 2020).

The cross-correlation of the resolved GW sources with galaxies is a further promising avenue. It enables the measurement of the redshift of the GW sources that do not have EM counterpart. This technique makes it possible to measure the value of Hubble constant, the matter density, the DE EoS and its redshift evolution from the GW sources. Along with probing the expansion history of the universe, it also provides evidence on the relation between the GW sources and DM distribution through the redshift-dependent galaxy bias parameter $b(z)$ (Oguri 2016; Raccanelli et al. 2016; Scelfo et al. 2018; Mukherjee and Wandelt 2018; Mukherjee et al. 2021d).

The observable considered for such studies is the (3D) angular power spectrum:

$$C_\ell^{\mathrm{GW,LSS}}(z_1, z_2) = \frac{2}{\pi} \int dk k^2 P(k)\, \Psi_\ell^{\mathrm{GW}}(k) \Psi_\ell^{\mathrm{LSS}}(k). \tag{6}$$

The two $\Psi_\ell^X(z)$ kernels encapsulate the physical processes in place:

$$\Psi_\ell^X(k) = \int N^X(z) b^X(z) D(z) W(z) \Delta_\ell^X(k,z)\, dz, \tag{7}$$

where X stands for either GW or LSS when considering one or the other observable, and $W(z)$ are the observational window functions related to the experiment specifications. The $\Delta_\ell(k,z)$ terms are the observed overdensities including effects from the intrinsic clustering, velocity effects (redshift-space distortions and Doppler), lensing and gravitational potentials, respectively, and they include information on galaxy clustering, gravity, and of course cosmological and astrophysical parameters:

$$\Delta_\ell(k,z) = \Delta_\ell^{\rm den}(k,z) + \Delta_\ell^{\rm vel}(k,z) + \Delta_\ell^{\rm len}(k,z) + \Delta_\ell^{\rm gr}(k,z)\,; \tag{8}$$

for the complete expression of those terms, see e.g. Bonvin and Durrer (2011), Scelfo et al. (2018). In particular, this correlation can constrain DE and modified gravity models (Camera and Nishizawa 2013; Raccanelli 2017). In this case, the modifications due to different models of gravity and DE enter in the Ψ_ℓ kernels, and the advantage of using the GW-LSS cross-correlation comes from the complementarity with other measurements as well as the potentially higher redshift range for the GW bin.

The fact that GW events trace the LSS allows us to also test and constrain astrophysical models (Scelfo et al. 2020; Libanore et al. 2021). In this case, the change in the model C_ℓ will be in the merger rate, the redshift distribution and the bias of the compact objects' hosts.

Merging of BHs that are the endpoint of stellar evolution happens almost exclusively in galaxies that had sufficient star formation, and therefore in halos with a relatively large galaxy bias ($b_g > 1$). Conversely, PBHs preferentially merge in lower biased objects, and thus have a lower cross-correlation with luminous galaxies (Bird et al. 2016). Therefore, the cross-correlation of GW maps with galaxies, which can measure the bias of the BBH hosts, provides information on the abundance of PBHs (Raccanelli et al. 2016; Scelfo et al. 2018) (for more details on PBHs, see Sect. 10).

Further correlations contain other useful information. The tomographic shear maps and the number density distribution of GW sources, combined with shear-shear and GW-GW auto-correlations, also constrain the cosmological parameters (Osato 2018), though these require a large number of GW detections which LISA is not expected to observe. Nevertheless thanks to GW-LSS cross-correlations with LISA and future galaxy survey data, the detection of GW weak lensing seems viable (Mukherjee et al. 2020b). The cross-correlation between GW weak-lensing and CMB-lensing might also allow to test fundamental predictions of GR (Mukherjee et al. 2020a).

2.6.2 Cross-correlations with the stochastic gravitational-wave background

A complementary study to the cross-correlation between GW resolved sources and LSS is the cross-correlation with the astrophysical SGWB. There are at least two astrophysical backgrounds that LISA will detect: one contribution generated by the galactic binary (GB) mergers, which is expected to dominate at low frequencies (up

to $\sim 10^{-3}$ Hz), and one coming from extragalactic BBH inspirals, expected to be relevant at larger frequencies ($\sim 10^{-3}$–10^{-2} Hz). Several phenomena in the early universe also source a stochastic signal whose strength is poorly predicted (see Sect. 5 and subsequent sections). The SGWB is then expected to be a combination of an astrophysical and a cosmological component, and a priori any of the two can dominate the SGWB signal in the LISA band. In order to be sensitive to both of them, it is of fundamental importance to find ways to disentangle the two signals. The spectral shape of each contribution is a standard tool to try to disentangle the components, however, due to the richness of sources expected in the LISA band, it is worth finding other ways to characterise the SGWB contributions. A promising approach consists in cross-correlating the SGWB with matter distribution at late times. Since, as we will see, the GW energy density depends on cosmological perturbations (besides astrophysical dependencies), it correlates with other cosmological probes. Some analyses and forecasts of the cross-correlation signals between GW observatories and future galaxy surveys, as e.g. Euclid and SKA, are presented in Contaldi (2017), Cusin et al. (2017), Cusin et al. (2018b), Cusin et al. (2018a), Jenkins et al. (2019a), Jenkins and Sakellariadou (2018), Jenkins et al. (2018), Cusin et al. (2019b), Cusin et al. (2020), Jenkins and Sakellariadou (2019), Jenkins et al. (2019b), Bertacca et al. (2020), Pitrou et al. (2020), Mukherjee and Silk (2020), Alonso et al. (2020b). These cross-correlations not only can be useful to disentangle the origin of the SGWB, but represent completely new observables to infer cosmological information. For instance, along with the spatial fluctuation of the astrophysical SGWB, its temporal fluctuation provides a measurement of the high redshift merger rate of the astrophysical sources contributing to the SGWB (Mukherjee and Silk 2020).

As for the case of resolved events, the observable quantity is the angular cross power spectrum, between the galaxies overdensity and the energy density of the astrophysical SGWB, hereafter labelled AGWB:

$$C_\ell^{\mathrm{AGWB}\times\mathrm{LSS}} = \frac{2}{\pi}\int k^2 dk P_\zeta(k)\Delta_\ell^{\mathrm{AGWB}}(k)\Delta_\ell^{\mathrm{LSS}}(k), \tag{9}$$

where $P_\zeta(k) = A_s\left(k/k_{\mathrm{pivot}}\right)^{n_s-1}$ is the scale-invariant curvature power spectrum, with A_s and n_s the amplitude and tilt respectively, while k_{pivot} is the pivot scale. The two transfer functions, $\Delta_\ell^{\mathrm{AGWB}}(k)$ and $\Delta_\ell^{\mathrm{LSS}}(k)$, contain astrophysical and cosmological information (see the previous section). The astrophysical information can be included focusing on the anisotropies of the astrophysical SGWB energy density. The total GW energy density per logarithmic frequency f_{o} and solid angle Ω_o along the line-of-sight $\mathbf{n}$ of a SGWB is (Cusin et al. 2017; Bertacca et al. 2020)

$$\Omega_{\mathrm{GW}}^{\mathrm{TOT}}(f_{\mathrm{o}},\mathbf{n}) = \frac{f_{\mathrm{o}}}{\rho_{\mathrm{c}}}\frac{\mathrm{d}\rho_{\mathrm{GW}}^{\mathrm{tot}}}{\mathrm{d}f_{\mathrm{o}}\mathrm{d}\Omega_{\mathrm{o}}}\,. \tag{10}$$

It contains both a background (monopole) contribution in the observed frame $\bar{\Omega}_{\mathrm{GW}}(f_o)$, which is homogeneous and isotropic, and a direction-dependent contribution $\Omega_{\mathrm{GW}}(f_{\mathrm{o}},\mathbf{n})$. Starting from these, we can define the total relative fluctuation

as $\Delta^{\rm TOT}_{\rm AGWB}(f_o,\hat{\mathbf{n}}) = \left(\Omega^{\rm TOT}_{\rm AGWB} - \bar{\Omega}^{\rm TOT}_{\rm AGWB}\right)/\bar{\Omega}^{\rm TOT}_{\rm AGWB}$. The contributions to the astrophysical SGWB energy density fluctuation are computed in Contaldi (2017), Cusin et al. (2017), Cusin et al. (2018b), Cusin et al. (2018a), Cusin et al. (2019a), Jenkins et al. (2019a), Jenkins and Sakellariadou (2018), Cusin et al. (2019b), Cusin et al. (2020), Jenkins and Sakellariadou (2019), Jenkins et al. (2019b), Bertacca et al. (2020), Pitrou et al. (2020), Alonso et al. (2020b). Here, following Bertacca et al. (2020), we report its expression in the Poisson gauge

$$\begin{aligned}\Delta\Omega_{\rm AGWB}(f_o,\hat{\mathbf{n}},\theta) = \sum_{[i]}\int dz\, W(z)\,\mathcal{F}^{[i]}(f_o,z,\theta)\Bigg\{ & b^{[i]}D \\ & + \left(b^{[i]}_{\rm evo} - 2 - \frac{\mathcal{H}'}{\mathcal{H}^2}\right)\hat{\mathbf{n}}\cdot\mathbf{V} - \frac{1}{\mathcal{H}}\partial_{\parallel}(\hat{\mathbf{n}}\cdot\mathbf{V}) - (b^{[i]}_{\rm evo} - 3)\mathcal{H}V \\ & + \left(3 - b^{[i]}_{\rm evo} + \frac{\mathcal{H}'}{\mathcal{H}^2}\right)\Psi + \frac{1}{\mathcal{H}}\Phi' + \left(2 - b^{[i]}_{\rm evo} + \frac{\mathcal{H}'}{\mathcal{H}^2}\right)\int_0^{\chi(z)} d\tilde{\chi}(\Phi' + \Psi') \\ & + \left(b^{[i]}_{\rm evo} - 2 - \frac{\mathcal{H}'}{\mathcal{H}^2}\right)\left(\Psi_o - \mathcal{H}_0\int_0^{\tau_0} d\tau \frac{\Psi(\tau)}{1+z(\tau)}\bigg|_o - (\hat{\mathbf{n}}\cdot\mathbf{V})_o\right)\Bigg\},\end{aligned} \tag{11}$$

where the *density*, *velocity*, *gravity* and *observer* terms, in the first, second, third and fourth line, respectively contain all the cosmological information. On the other hand, the function $\mathcal{F}^{[i]}(f_o,z,\theta)$ contains all the astrophysical dependencies: e.g. the mass and spin distribution of the binary, the emitted GW energy spectrum, the clustering properties of GW events and the details of the GW detectors. The functions $b^{[i]}(z,\theta)$ and $b^{[i]}_{\rm evo}(z,\theta)$ are the bias and the evolution bias of the i-th type of GW source, which specify the clustering properties of GW sources and characterise the formation of sources.

The cross-correlation analysis of the astrophysical SGWB (from sources at all redshifts along the line of sight) with galaxy number counts at a given redshift leads to a tomographic reconstruction of the redshift distribution of the sources (Cusin et al. 2018a; Mukherjee and Silk 2020; Cañas Herrera et al. 2020; Alonso et al. 2020b; Cusin et al. 2019b; Yang et al. 2020a). Subtleties about the noise and other characteristics of the detector play an important role, so that cross-checks on the detector performances are possible by means of this analysis (Bertacca et al. 2020; Alonso et al. 2020b). Overall, the cross-correlation analysis shows that the combination of galaxy surveys with the astrophysical SGWB can be a powerful probe for GW physics and multi-messenger cosmology.

2.6.3 Large-scale structure effects on gravitational-wave luminosity distance estimates

Here we discuss the effect of cosmological perturbations and inhomogeneities on estimates of the luminosity distance of compact object binary mergers through GWs.

It is important to account for such effects on GW propagation to obtain robust measurements for precision cosmography.

The main attempts to investigate perturbation effects on GWs involve the integrated Sachs–Wolfe effect (Laguna et al. 2010), peculiar velocities or accelerations (Kocsis et al. 2006; Bonvin et al. 2017; Tamanini et al. 2020; Mukherjee et al. 2021c; Nicolaou et al. 2020), lensing (Pyne et al. 1996; Wang et al. 1996; Takahashi and Nakamura 2003; Sathyaprakash et al. 2010; Dai et al. 2017; Takahashi 2017; Baker and Trodden 2017; Dai and Venumadhav 2017; Haris et al. 2018; Dai et al. 2018; Oguri 2018; Contigiani 2020; Ezquiaga and Zumalacárregui 2020; Ezquiaga et al. 2020b) and environmental effects (Barausse et al. 2014). Coherent peculiar velocity of the binaries at low redshift and weak gravitational lensing by intervening inhomogeneities can affect the identification of the hosts' redshift. This introduces changes of typically a few percent (but occasionally much larger) in the flux, while not significantly affecting the redshift, and thus provides a source of noise in the $D_L(z) - z$ relation (Sathyaprakash et al. 2010; Hirata et al. 2010). Using the local wave zone approximation to define the tetrads at source position (Maggiore 2007), the corrections to the luminosity distance read (Bonvin et al. 2017; Bertacca et al. 2018)[3]

$$\begin{aligned}\frac{\Delta D_L}{\bar{D}_L} = &\left(1 - \frac{1}{\mathcal{H}\bar{\chi}}\right) v_{\parallel} - \int_0^{\bar{\chi}} d\tilde{\chi}\, \frac{(\bar{\chi} - \tilde{\chi})}{\tilde{\chi}\bar{\chi}}\, \triangle_{\Omega}\Phi + \\ &+ \frac{1}{\mathcal{H}\bar{\chi}}\Phi - 2\left(1 - \frac{1}{\mathcal{H}\bar{\chi}}\right)\int_0^{\bar{\chi}} d\tilde{\chi}\, \Phi' - 2\Phi + \frac{2}{\bar{\chi}}\int_0^{\bar{\chi}} d\tilde{\chi}\, \Phi,\end{aligned} \tag{12}$$

where prime denotes the derivative with respect to η and $\mathcal{H} = a'/a$, $\triangle_{\Omega} \equiv \bar{\chi}^2 \bar{\nabla}_{\perp}^2 = \bar{\chi}^2(\bar{\nabla}^2 - \bar{\partial}_{\parallel}^2 - 2\bar{\chi}^{-1}\bar{\partial}_{\parallel}) = (\cot\partial_{\theta} + \partial_{\theta}^2 + \partial_{\varphi}/\sin^2\theta)$. We can recognise in Eq. (12) the presence of a velocity term (the first term), followed by a lensing contribution, and the final four terms account for the Sachs–Wolfe, Integrated Sachs–Wolfe, volume and Shapiro time-delay effects.

The additional D_L uncertainty due to the inclusion of perturbations is expected to peak at low-z due to velocity contributions; however, velocity effects rapidly decrease and lensing takes over (Bertacca et al. 2018). Those results indicate that the amplitude of the corrections could be important for future interferometers such as LISA.

In presence of DE or modifications of gravity, the GW luminosity distance might differ from the EM signals also for large-scale fluctuations (Garoffolo et al. 2020; Dalang et al. 2020; Jana et al. 2021; Dalang et al. 2021). In particular, linearised fluctuations of the GW luminosity distance contain contributions directly proportional to the clustering of the DE field (Garoffolo et al. 2020, 2021) and by combining luminosity distance measurements from GW and supernovae sources, it is possible to uncover field inhomogeneities detecting them directly. see e.g. Van Den Broeck et al. (2010) for an analysis of weak lensing effects in the measurement of the DE EoS with LISA.

[3] For simplicity, we have dropped all contributions evaluated at the observer, assuming concordance background model, and work in Poisson Gauge.

3 Gravitational lensing of gravitational-wave signals

Section coordinators: D. Bacon, M. Zumalacarregui. Contributors: D. Bacon, G. Congedo, G. Cusin, J.M. Ezquiaga, S. Mukherjee, M. Zumalacarregui.

3.1 Introduction

Similarly to EM radiation, GWs feel the gravitational potential of both massive objects and also the LSS while traveling across the universe. This opens the possibility of both probing the distribution of structure in the cosmos and the fundamentals of the underlying gravitational interactions. LISA will offer a unique perspective since it will detect high-redshift GWs in a lower frequency band compared to ground-based detectors, increasing the lensing probabilities and the detectability of diffraction effects.

GW lensing phenomena are characterized by two properties: the convergence κ[4] (governing whether there is weak or strong gravitational lensing) and a dimensionless frequency w (governing whether wave optics or geometric optics is relevant). The convergence, κ, is defined as the integral along the line of sight of the redshift-weighted second derivative of the Newtonian potential. Depending on the strength of the gravitational potential, two gravitational lensing regimes exist: weak ($\kappa \ll 1$) or strong ($\kappa \simeq 1$). In the first case, the main observable effect is magnification or demagnification of the observed flux (or equivalently a change in the inferred luminosity distance). In the second case the effect can be both a magnification/demagnification and also production of multiple signals with a time delay that is a function of the lens properties. We will examine both regimes in Sects. 3.2 and 3.3 below.

The low frequency and phase coherence of GWs allows the observation of wave effects. It is convenient to define the dimensionless frequency

$$w = 8\pi G M_L f = 4\pi \left(\frac{M_L}{10^8 M_\odot}\right)\left(\frac{f}{\mathrm{mHz}}\right), \tag{13}$$

as well as a magnification factor $F(w) = h(w)_{\mathrm{lensed}}/h(w)_{\mathrm{unlensed}}$, where M_L is the redshifted lens mass. GW lensing is accurately described by geometric optics only if $w \gg 1$ (more precisely, $w\Delta\tilde{t}_j \gg 1$ for all images). Then, the amplification factor (the ratio between the lensed and unlensed waveform) is a sum over multiple images j:

$$F(w) = \sum_j |\mu_j|^{1/2} \exp(iw\Delta\tilde{t}_j - i\pi n_j), \tag{14}$$

where μ_j is the magnification, $\Delta\tilde{t}_j$ is the time delay (in units of $4GM_L$) evaluated on the j-th image position. Here n_j is the Morse phase of the image, respectively 0, 1/2, 1 for minima, saddle point and maxima of the time delay function (Schneider et al.

[4] Because GW sources are effectively point-like, no image distortions are observable and shear influences GW observations only through its effect on the magnification. This is very different from lensing of galaxies, where shear distortions are directly observable.

1992; Takahashi and Nakamura 2003). These image types are also known as type I, II and III respectively.

For low (w considerably less than 1) or intermediate ($w \sim 1$) frequencies it is necessary to consider the wave optics regime, where the amplification factor is

$$F(w) = \frac{w}{2\pi i} \int dx^2 \exp(iw\Delta\tilde{t}(\vec{x}, \vec{b})), \tag{15}$$

where the time delay $\Delta\tilde{t}(\vec{x}, \vec{b})$ is now a function of the (normalized) lens plane coordinate $\vec{x}$ and source location $\vec{b}$. (see Takahashi and Nakamura 2003 for details). The low frequency limit $w \ll 1$ corresponds to $F \sim 1$, or no magnification. This can be understood as a wave not being sensitive to an object whose effective size is smaller than its wavelength. The high frequency limit corresponds to the geometric optics result Eq. (14), as can be obtained from a Gaussian expansion around the images, which correspond to the extrema of the time delay $\delta\tilde{t}$ (sub-dominant corrections to geometric optics can be computed (Takahashi 2004)). We will discuss wave effects in gravitational lensing and LISA opportunities in Sect. 3.4.

3.2 Weak lensing

The first regime that GWs will undergo is weak lensing. Because of the relatively deep observations LISA will be able to achieve (median $z \sim 2$, reaching out much deeper depending on source types) most of the observed events (if not all) will be subjected to lensing by the large scale structure. In recent years weak lensing has become one of the primary tools in cosmology to study the distribution of DM and the nature of DE (through the evolution with redshift). Galaxy lensing surveys such as KiDS (Heymans et al. 2021) and DES (Troxel et al. 2018) are now providing tighter constraints on cosmological parameters, such as geometry parameters (H_0, Ω_m, and Ω_Λ) and matter clustering parameters (σ_8 and n_S) to a few percent level. Soon Euclid (Blanchard et al. 2020) and the Vera C. Rubin Observatory (Abell et al. 2009) will further constrain those parameters, extending the analysis to DE (w_0 and w_a) and various models beyond ΛCDM, down to the percent level. Most likely, the study of systematic errors affecting those measurements will be the topic of the next decade or so. GWs have the potential to revolutionize the field with virtually bias-free measurements of the luminosity distance. In fact, LISA will give us the first deep luminosity distance measurements that will be both accurate (as this relies on assuming GR is the correct theory) and also precise with typical errors up to a few percent depending on source type and position in the sky. At the same time, the typical root-mean-squared error due to lensing is 0.02 for $z < 1$ and ramping up quite rapidly with redshift (Cusin and Tamanini 2021). This will be a source of unwanted bias and extra noise in the Hubble diagram inference, which must be accounted for in the analysis. However, if modelling of the lensing is introduced, then this systematic error can become a new piece of useful information. For these reasons LISA will also establish the groundwork for planned second generation space-based detectors.

3.2.1 As a source of noise and bias for standard sirens

Magnified sources are easier to detect than de-magnified sources. This simple fact biases the distribution of lensing magnifications of an observed source sample. Lensing selection effects are often neglected when estimating the lensing-induced uncertainty on the cosmological distance measurement from high-redshift GW sources. However, when selection effects are included, flux conservation is no longer enforced, and the mean of the magnification distribution is shifted from 1 for sufficiently high-redshift sources. This introduces an irreducible (multiplicative) bias on the distance reconstruction, independent of the sample size. in Cusin and Tamanini (2021) the effect of selection bias on a population of MBBHs is examined, for different scenarios of MBH formation. It is shown that, while the effect of the bias on the distance estimator for sources with an EM counterpart is typically below the variance threshold, it becomes relevant for high redshift sources when the statistics of detectable events is large (e.g. when MBHs form at high redshift from remnants of Population III stars), and it should be taken into account in population studies.

3.2.2 As a probe complementary to standard sirens

Thanks to the variety and large number of sources, LISA will be able to probe a wide range of redshifts with sufficient statistical significance to constrain cosmological parameters. LISA will be able to measure luminosity distances to within a few percent with optimistic estimates pushing this limit down to one percent. Hence, weak lensing by the LSS will be expected to dominate the error budget of any luminosity distance measure for most sources with EM counterparts (e.g. MBBHs), whose median redshift is ~ 2 (Caprini and Tamanini 2016). This has to be taken into account in geometric analyses, such as the luminosity distance-redshift relationship as illustrated in the previous sections. Here we explore an avenue to extract additional cosmological information: it is well known that the weak lensing signal for background objects is correlated with foreground large scale structure. Foreground over- (under-) densities will magnify (demagnify) the observed luminosity distance to background sources by a small factor. This can be expressed in terms of the convergence via

$$D'_L = (1 - \kappa) D_L, \tag{16}$$

where D_L is the (unknown) unlensed distance, κ is the projected 2D convergence, and D'_L is the (observed) lensed distance. The observed luminosity distance now incorporates information about the convergence field, which in turn is cosmology dependent. In fact its power spectrum has cosmological information imprinted into it that can be extracted from data. It was long ago speculated that this signal could be exploited if large enough statistics (very high number densities and very precise distance measurements) were available in the future with second generation space detectors such as BBO (Cutler and Holz 2009). This approach was then applied to third-generation ground based detectors and deci-Hz space detectors to prove that the method would in principle be applicable to DE and modified gravity in a

tomographic analysis (Camera and Nishizawa 2013). More recently, it was shown that a joint analysis of lensing and distance-redshift on a combined dataset of LISA and third generation ground detectors would allow us to jointly constrain geometry parameters (such as H_0 and density) and clustering parameters (σ_8 and n_s) at the same time with percent precision (ΛCDM with curvature, nominal distance errors, and nominal number density) (Congedo and Taylor 2019; Mpetha et al. 2023). This is because a geometry probe such as distance-redshift can act as a strong prior to break degeneracies that are usually present in lensing. LISA will have good enough statistics to prove that such analysis is indeed possible, bringing in independent constraints on additional cosmological parameters such as σ_8. LISA will be able to perform a combined analysis of this type with other third-generation ground-based detectors such as ET, as well as proposed space-borne detectors operating in other bands (One such proposal is a deci-Hz detector currently under evaluation by ESA (Baker et al. 2021)). In this way LISA will provide an independent measurement of weak lensing, and expand the field of statistical cosmology to GWs in the mHz range.

3.3 Strong lensing

The probability that a GW is lensed depends on the redshift of the source and the distribution of lenses. The merger rate at high redshift depends on the astrophysical formation channels which can affect the event rate of well detected events and the sub-threshold lensed events observed by LIGO/Virgo (Mukherjee et al. 2021a) or, in future, by CE and ET (Piórkowska et al. 2013; Biesiada et al. 2014; Ding et al. 2015). One of the robust ways to predict the lensing event rate is by using the detection or an upper bound on the amplitude of the SGWB (Mukherjee et al. 2021b; Buscicchio et al. 2020). For high-redshift GWs, the intervening matter between the source and the observer magnifies the GW signal, thereby introducing a systematic error in the luminosity distance determination. Correcting for this weak lensing effect is relevant when inferring cosmological parameters from GW standard sirens (Hughes and Holz 2003; Hirata et al. 2010); see Sect. 3.2. But a fraction of these GW events pass close enough to the lens so that lensing produces multiple images of the same event. LISA could detect a few strongly-lensed massive BBH during its mission (Sereno et al. 2010). The detection of multiple lensing events could provide new means for cosmography with LISA (Sereno et al. 2011). Owing to its better sky localization and parameter estimation, LISA may be less susceptible to strong lensing false alarms (unlensed events that mimic lensing due to coincidental overlap of parameters) compared to the LIGO/Virgo detector network.

In the strong lensing regime the time delay between the images increases linearly with the mass of the lens, reaching delays of months for a $10^{12}\,M_\odot$ galaxy lens. Each of the lensed images has a different magnification, but they also acquire a fixed phase shift depending on how many times the image has crossed a lens caustic (Schneider et al. 1992); recall the $i\pi n_j$ term in Eq. (14). The origin of this phase shift can be also understood from the folding of the wavefront, which in strong-lensing configurations

produces a phase of the waveform associated with the properties of the lensing potential (Schneider et al. 1992; Dai and Venumadhav 2017).

In the case of minima of the lensing potential (type I images), there is no phase shift and the lensed waveform reproduces exactly (modulo magnification) the shape of the emitted signal. For maxima (type III), there is an overall change of the sign, $e^{-i\pi} = -1$, but the morphology of the signal remains intact. However, for saddle points (type II), the associated phase shift can distort the waveform, since the frequency-independent phase shift will introduce a frequency-dependent time delay that will differentially transform the GW signal (Ezquiaga et al. 2021). For non-precessing, quasi-circular orbits of equal mass binaries the emitted GWs are dominated by a single quadrupole radiation mode (22). In that case, the lensing phase shift accounts for a $\pi/4$ shift of the coalescence phase (Dai and Venumadhav 2017; Ezquiaga et al. 2021). Nonetheless, whenever higher modes, precession or eccentricity are relevant, the lensed waveform is modified so that it does not conform with expectation from (unlensed) templates in GR (Ezquiaga et al. 2021). This sets up the possibility that type II images near the detection threshold might be missed with standard template bank searches, but also offers the opportunity of identifying strongly lensed events with a single type II image if the SNR is high enough. Explorations of the capabilities of third generation ground-based detectors to identify type II images are performed in Wang et al. (2021b).

Precise measurement of the phase of long duration signals by LISA could be key in distinguishing different types of lensed images (Ezquiaga et al. 2021). The observation of very high SNR MBBHs and sources with very asymmetric masses, such as IMRIs and EMRIs, could give LISA a unique opportunity to identify strongly lensed events, even when detecting a single image, i.e. one term in Eq. (14), if the other images are received outside of the observing window or are too faint to be recovered.

Another very strong lensing effect can exist for LISA MBBH sources. If we observe these in EM during the inspiral, we expect self-lensing flares to occur when the two BHs are aligned with the line-of-sight (to within about an Einstein radius). In a recent pair of papers (Davelaar and Haiman 2022a, b), a binary emission model was ray-traced, and a distinct feature was found in the light curve imprinted by the BH shadow from the lensed BH. A dip occurs in the lightcurve when the foreground BH lenses the shadowed part of the background BH. This could make it possible to extract BH shadows that are spatially unresolvable by high-resolution very-long baseline interferometry. These shadows are another probe of the metric around the MBH.

3.4 Wave effects

GWs can be emitted at low frequencies ($w \lesssim 1$), allowing the observation of wave diffractive phenomena. For typical LISA sources, wave optics as in Eq. (15) needs to be considered for lenses with masses $M_L \sim 10^6 - 10^9\, M_\odot$, cf. Eq. (13). In contrast, wave effects in gravitational lensing are not observed for EM sources, due to the

finite size of these sources and their high EM frequencies ($w \gg 1$), cf. Figs. 12, 13 of Oguri (2019).

Wave effects produce a frequency-dependent amplification factor F. At very low frequencies $w \ll 1$ no magnification occurs, $F \sim 1$, as a wave is not affected by an object smaller than its wavelength. As the frequency increases, an oscillatory pattern emerges, caused by the superposition of different images. This pattern persists for GWs even in the geometric optics limit $w \gg 1$ through the exponents in Eq. (14). We do not see this pattern for optical EM sources due to incoherent emission and lack of time resolution. Note that diffraction prevents the magnification for GWs from diverging, even for perfectly aligned, symmetric lenses with normalized impact parameter $|\vec{b}|/R_E \to 0$. An inspiralling binary sweeps through a range of frequencies before coalescence; a gravitational lens imprints the frequency-dependent amplification factor into the waveform. These effects are shown in Fig. 4.

Several studies address the detectability of wave effects by LISA. Sereno et al. (2010) estimates that a handful of strongly lensed events ($\lesssim 5$) will be observed in a 5 year mission. Because the lensing probabilities are dominated by galactic halos with $M_L \sim 10^{12}\, M_\odot$, wave effects are likely to be unimportant for most strongly lensed LISA sources. However, frequency-dependent diffraction effects in the weak lensing regime may be detectable for a small fraction of sources: (Gao et al. 2022) find that $0.1-1.6\%$ of LISA's MBBH with total mass $10^5-10^{6.5}\, M_\odot$ and redshift $4-10$ may present detectable wave-optics. LISA provides new opportunities to observe these frequency-dependent effects and use them to probe the large-scale structure of the universe at the scale of sub-halos.

Wave effects can help identify GW signals (or groups of them) as lensed events and characterize gravitational lenses. We discuss both possibilities below.

3.4.1 Identification of lensed signals

Diffraction-induced features in the gravitational waveform could be used to identify the event as lensed. The main target for ground detectors is the first diffraction peak, appearing at low frequencies (Dai et al. 2018). These diffraction effects can be

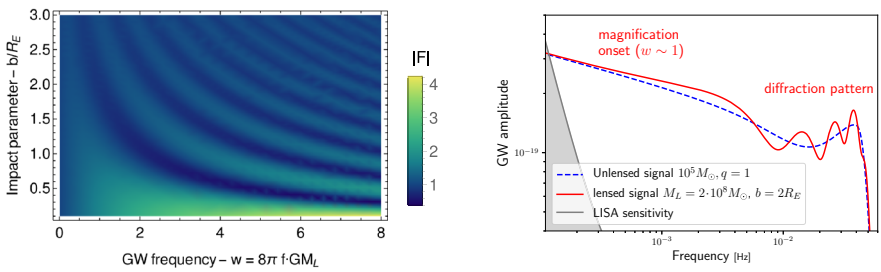

Fig. 4 GW lensing and wave effects. Left panel: Amplification $|F(w)|$ caused by a point lens in the wave optics regime. Low frequency signals $w \ll 1$ undergo no magnification. An oscillatory pattern emerges at higher frequencies. Right panel: Imprint of strong lensing on a MBBH source, as observed by LISA. The frequency dependence (onset of magnification, diffraction pattern) carries information about the gravitational lens

detected even for impact parameters comparable to the Einstein radius $b \gtrsim R_E$, for which there is only one image in the geometric optics limit. Orbital parameters are expected to have some degeneracies with diffraction, but it is in principle possible to distinguish them. Spin precession creates a modulation that affects the amplitude more than the phase (while diffraction affects both equally). Orbital eccentricity can be distinguished by higher harmonics in GWs, which are not induced by gravitational lensing.

Wave effects may produce systematic errors in different analyses. Diffraction-induced distortions make the GW phase appear to arrive earlier than an unlensed EM signal (Takahashi 2017; Morita and Soda 2019), although this is only an apparent superluminality (Suyama 2020; Ezquiaga et al. 2020b). This effect has to be taken into account (Ezquiaga et al. 2020b) when, for example, inferring constraints on the speed of gravity from the possible pre-merger modulated EM brightness of a MBB (Haiman 2017).

The interplay between wave optics and gravitational polarizations may provide alternative means to characterize lensed GWs. This has been investigated using low-frequency corrections to geometric optics. These corrections cause the polarization plane defined in geometric optics to become blurred due to diffraction effects, which leads to the rise of apparent vector and scalar polarization modes (Cusin and Lagos 2020). Moreover, GWs in curved space propagate on different geodesics depending on their circular polarization (an effect known as the gravitational spin hall effect) (Yamamoto 2018; Andersson et al. 2021). These effects might provide means to characterize lensed GWs. As they are suppressed by factors of the GW frequency, these phenomena are more important for LISA than for ground-based detectors.

3.4.2 Reconstruction of large scale structure and lens properties

GW diffraction is sensitive to the power spectrum of matter density fluctuations on very small physical scales (Oguri and Takahashi 2020). Ground detectors are sensitive to this power spectrum at wavenumbers where baryonic effects are smallest, $k \sim 10^6 h\mathrm{Mpc}^{-1}$ for $f \sim 0.1 - 1\mathrm{Hz}$. Individual high SNR sources at high redshift, such as LISA observed MBBHs, may be sensitive to frequency-dependent modulations of the GW phase and amplitude (SNR $\gtrsim 500$ at mHz frequency, $z_S \sim 3$, cf. Fig. 12 of Oguri and Takahashi (2020)). Lensing induced diffraction can be enhanced substantially in non-standard scenarios that affect the small-scale power spectrum (e.g. PBHs).

Wave effects can then improve the chances of detection and provide additional information about the lens. Inspiralling binaries detectable by LISA sweep through a range of frequencies that might include the onset of diffraction for $w \sim 1$ and/or the characteristic diffraction pattern for $w > 1$; see Eq. (13). For the case of LISA MBBHs lensed by point masses and singular isothermal spheres, diffraction allows for a determination of lens mass and source position at the level of 10% to $\sim 0.1\%$ for $M_L \lesssim 10^7 M_\odot$ and $M_L \gtrsim 10^8 M_\odot$ for SNR ~ 1000 (Takahashi and Nakamura 2003). Point lenses can be identified for large impact parameters $b/R_E \sim \mathcal{O}(10)$ (rather than ~ 1), increasing significantly the likelihood of detection $\propto b^2$.

Diffraction is also sensitive to cuspy (or singular) matter distributions, producing an image with magnification $\mu \sim (GMf)^{\alpha-3}$ for a profile with central density $\rho \sim r^{-\alpha}$ $(0 < \alpha \leq 2)$ (Takahashi 2004). Frequency-dependent wave effects can be used to individually detect DM subhalos with $M \lesssim 10^7 M_\odot$ and even measure their mass profiles, although LISA might not provide enough events with sufficiently high SNR (Choi et al. 2021).

Investigations of microlensing (the effect of small-scale structure, such as stars, on the images produced by a large lens) have focused on LIGO-Virgo sources. Microlenses have masses such that wave diffraction effects are important at LISA frequencies, and would normally not leave an observable imprint (magnification ~ 1). However, they can be observed if they are present in regions of high magnification of the macrolens, such as caustics (Diego et al. 2019). Nevertheless, in most situations the macrolens model will be a sufficient description (Cheung et al. 2021). GW microlensing is also sensitive to the stellar mass function, particularly in regions of high magnification (Mishra et al. 2021).

4 Constraints on modified gravity theories

Section coordinator: D. Vernieri. Contributors: T. Baker, E. Belgacem, G. Calcagni, M. Crisostomi, N. Frusciante, K. Koyama, L. Lombriser, M. Maggiore, S. Mukherjee, M. Sakellariadou, I. D. Saltas, D. Vernieri, F. Vernizzi, M. Zumalacarregui.

4.1 Models and theories

GW astronomy offers a new window to test gravity complementing cosmological and astrophysical tests. GWs detectors can allow to measure the cosmological expansion, thus providing independent measurements of both the equation of state of dark energy and Hubble parameter. In particular, in the latter case, it can be used to help resolving the Hubble tension. Furthermore there are keys features in the propagation of GWs in theories beyond GR, such as the modification in the friction term, difference in the speed of propagation, additional polarizations, etc, which will provide unique ways for testing signatures of new physics beyond GR.

To test GR using the propagation of GWs, it is useful to compare it to other models that predict observational deviations. The simplest case that one can consider is the presence of an additional scalar interaction, e.g. a so-called scalar-tensor theory of gravity. Over the years, increasingly more general theories devoid of Ostrogradsky instabilities (Ostrogradksi 1850) have been introduced with the aim to account for the most general modification in this setup. The advent of the Galileon field theory (Nicolis et al. 2009) quickly led to its covariant generalization (Deffayet et al. 2011) and so to the reappraisal of the Horndeski theory (Horndeski 1974), i.e. the most general scalar-tensor theory with second order field equations. Relaxing this last assumption in a suitable way, has resulted in the beyond-Horndeski (Zumalacárregui and García-Bellido 2014) or Gleyzes–Langlois–Piazza–Vernizzi model (Gleyzes et al. 2015a, b), and subsequently degenerate higher-order scalar-tensor theories (Langlois and Noui 2016; Crisostomi et al. 2016; Ben Achour et al. 2016).

At low energy, those relevant for cosmology, the Lagrangian of these theories schematically reads (Pirtskhalava et al. 2015)

$$\mathcal{L} = \sum_{n=0}^{\infty}\sum_{m=0}^{3} c_{n,m}(\phi)\Lambda_2^4\left(\frac{(\partial\phi)^2}{\Lambda_2^4}\right)^n\left(\frac{\Box\phi}{\Lambda_3^3}\right)^m + \cdots, \tag{17}$$

where $c_{n,m}(\phi)$ are dimensionless coefficients that depend mildly on ϕ, Λ_2 corresponds to the spontaneous Lorentz breaking scale, Λ_3 is related to the ultraviolet (UV) cut-off of these scalar-field theories while the ellipses refer to suitable gravitational terms necessary to keep the equations of motion of the propagating degrees of freedom of second order. Higher derivative terms with $m > 0$ have been introduced in cosmology to explain the accelerated expansion without a cosmological constant and simultaneously pass Solar System tests (Luty et al. 2003; Nicolis et al. 2009) using the so-called Vainshtein screening mechanism (Vainshtein 1972; Babichev and Deffayet 2013). In this case, the two scales must be chosen as $\Lambda_2 \sim (M_{\rm Pl}H_0)^{1/2}$ and $\Lambda_3 \sim (M_{\rm Pl}H_0^2)^{1/3}$, where $M_{\rm Pl}$ is the Planck mass and H_0 the value of the current Hubble constant.

The above models represent low energy effective field theory (EFT) whose cut-off scale can be chosen according to the certain type of phenomenology they aim to describe, e.g. DE. An alternative path to follow is to work out cosmological phenomena in a top-down way (Calcagni 2020) starting from a fundamental theory of gravitational and matter interactions, such as quantum gravity.

Quantum gravity is a generic name applied to any theory where the gravitational interaction is consistent with the laws of quantum mechanics. Exploring the cosmological implications of these theories is important to assess how LISA can contribute to our knowledge of fundamental physics.

The corrections to cosmological dynamics and evolution of the universe arising in quantum-gravity scenarios are expected to be very small since they dominate at Planck scales $\ell_{\rm Pl}$ or high curvature, compared to horizon scales $H_0^{-1} \sim 10^{60}\ell_{\rm Pl}$ or low curvature. However, this may hold true for perturbative curvature corrections to GR, while other mechanisms may enhance deviations from classical gravity either by inflation of metric fluctuations to cosmic scales at early times or by non-perturbative cumulative effects on the propagation of GWs. The former mechanism will be explored in Sect. 9.3, while the latter will be developed in this section in parallel with the other models. In particular, the dimension of spacetime in quantum gravity changes with the scale probed and this can affect both the dispersion relation of GWs and the luminosity distance of GW astrophysical sources (Calcagni et al. 2019a, b).

Quantum effects can also manifest themselves as non-local terms in the quantum effective action, and these can affect the long-distance dynamics of the theory. In particular, assuming a non-local term that corresponds to a dynamical generation of a mass for the conformal mode leads to a predictive model that passes all current cosmological constraints (Maggiore 2014; Belgacem et al. 2018c, 2020) and predicts modified GW propagation. In this model the effect can be quite large, leading, at the redshifts accessible to LISA, to deviations from GR that can be as large as 80% (Belgacem et al. 2019a, 2020).

The gravitational interaction can be modified by considering a Lagrangian constructed with a general function of the scalar associated with non-metricity Q, i.e. $f(Q)$ (Nester and Yo 1999; Beltrán Jiménez et al. 2020b; Bajardi et al. 2020). In this theory at least two additional scalar modes are introduced with respect to GR. The equivalent of GR is obtained when the Lagrangian coincides with the non-metricity scalar (Beltrán Jiménez et al. 2019). The $f(Q)$ theory modifies the propagation equation of GWs due to an additional scale-independent friction term which is related to a time-dependent effective Planck mass (Beltrán Jiménez et al. 2018). As a consequence, the GW luminosity distance, $D_L^{\rm GW}$, differs from the standard EM luminosity distance, $D_L^{\rm em}$ (Frusciante 2021). For a specific model it has been shown (Frusciante 2021) that at the redshifts relevant for LISA, the deviations with respect to the standard cosmological model can be relevant depending on the value of the free parameter and that GW detectors such as LISA show a strong power in constraining it.

4.2 General expression for modified cosmological gravitational-wave propagation

4.2.1 Modified cosmological gravitational-wave propagation

The GW propagation over cosmological distances for generalised theories of gravity and other extensions of ΛCDM can be parametrised by the wave equation (Saltas et al. 2014; Gleyzes et al. 2015c; Lombriser and Taylor 2016; Nishizawa 2018; Belgacem et al. 2018a; Ezquiaga and Zumalacárregui 2018; Lombriser 2018; Belgacem et al. 2019c)

$$h_A'' + 2[1-\delta(\eta,k)]\mathcal{H}\,h_A' + \left[c_T^2(\eta,k)\,k^2 + m_T^2(\eta,k)\right]h_A \;=\; \Pi_A, \tag{18}$$

where the primes indicate derivatives with respect to conformal time η. Here, we assume that the GW propagates far away from the source in the form of a plane wave. The modified friction (δ), speed (c_T^2), mass (m_T^2) and the source (Π_A) are in general assumed to be functions of both time and wave-number k.[5] Furthermore, parity-violating theories could also introduce a dependence of these quantities on the polarization index A.

As regards the friction term, within theories beyond GR next to the standard Hubble friction, one may encounter an extra contribution described through δ. The latter can for instance parametrise an effective Planck mass evolution rate or the impact of extra dimensions, or the effect of other modifications of GR at the cosmological scale. The wave propagation may further be modified by a deviation in its speed $c_{\rm T}$ and the mass of the graviton m_T. Finally, in standard GR the source term is due to the anisotropic stress tensor (a typical mechanism that can generate it is neutrino free streaming, see e.g. Section 19.5.3 of Maggiore (2018)), and in modified gravity can in general get further contributions (as is the case for instance in bimetric theories (Hassan and Rosen 2012)). In several modified gravity theories, the only

[5] The function δ is also indicated with other names in the literature, such as ν and α_M, related to δ by $\nu = \alpha_M = -2\delta$. Here we follow the notation of Belgacem et al. (2019c).

modification is in the friction term and is wavenumber-independent, so that Eq. (18) reads

$$h_A'' + 2\mathcal{H}[1 - \delta(\eta)]h_A' + k^2 h_A = 0. \tag{19}$$

In that case, the effect of the modification is such that, from the measurement of the waveform of the inspiral of a coalescing binary, we do not get the standard luminosity distance obtained from EM signals (that, in this context, we will denote by $D_L^{\rm em}$), but rather a GW luminosity distance, $D_L^{\rm GW} := 1/h_A$ defined as the inverse of the strain amplitude, up to a constant coefficient. In the case of Eq. (19), this quantity is related to $D_L^{\rm em}$ by (Belgacem et al. 2018a)

$$D_L^{\rm GW}(z) = D_L^{\rm em}(z) \exp\left[-\int_0^z \frac{dz'}{1+z'}\,\delta(z')\right]. \tag{20}$$

For the purpose of comparison with the data, it is convenient to have a simple parametrization of this effect in terms of a few parameters, rather than a full function of redshift (similarly to the (w_0, w_a) parametrization of the DE EoS). In practice, just as for the DE EoS, a parametrization is useful only if it is quite economical, with at most two parameters, otherwise it will be difficult to extract them from the data. For modified GW propagation, a convenient choice is (Belgacem et al. 2018b)

$$\frac{D_L^{\rm GW}(z)}{D_L^{\rm em}(z)} = \Xi_0 + \frac{1-\Xi_0}{(1+z)^n}, \tag{21}$$

which depends on the two parameters (Ξ_0, n). This parametrization reproduces the fact that, as $z \to 0$, the ratio $D_L^{\rm GW}/D_L^{\rm em}$ must go to one since as the redshift of the source goes to zero, there can be no effect from modified propagation. In the opposite limit of large redshifts, in Eq. (21) $D_L^{\rm GW}/D_L^{\rm em}$ goes to a constant value Ξ_0. This reproduces what happens in typical DE models, where deviations from GR only appear in the recent cosmological epoch, so that $\delta(z)$ goes to zero at large redshift and $D_L^{\rm GW}(z)/D_L^{\rm em}(z)$ saturates to a constant. Equation (21) indeed fits the explicit results from a large class of modified gravity models (Belgacem et al. 2019c). The modification in the luminosity distance shown in Eq. (21) can be tested from observations by combining with EM observational probes such as the BAO and CMB. By combining the BAO angular scale $\theta_{BAO}(z)$ with the measured luminosity distance from the GW sources and the sound horizon scale from CMB r_s, one can write a unique relation to measure the parameters Ξ_0 and n (Mukherjee et al. 2021e):

$$D_L^{GW}(z)\theta_{BAO}(z) = \left[\Xi_0 + \frac{1-\Xi_0}{(1+z)^n}\right](1+z)r_s. \tag{22}$$

If GR is the correct theory of gravity, the above equation indicates that the product of $\theta_{BAO}(z)$ and $D_L^{GW}(z)$ should scale as $(1+z)r_s$ as a function of redshift. Otherwise, it will exhibit a departure from $(1+z)r_s$ which can be explored to reconstruct the parameters Ξ_0 and n for both bright and dark standard sirens as a function of redshift (Mukherjee et al. 2021e).

The (Ξ_0, n) parametrization is the one in terms of which have been written explicit codes and Markov Chain Monte Carlo (MCMC), in order to assess the sensitivity of LISA to modified GW propagation, including the degeneracies of Ξ_0 with other parameters such as w_0, see below. Other two-parameter parametrizations can be found in Belgacem et al. (2019c), Calcagni et al. (2019b).

4.2.2 The damping term (standard sirens)

Late-time constraints on the modified damping term have been forecasted in Lombriser and Taylor (2016), Belgacem et al. (2018a), Amendola et al. (2018a), Belgacem et al. (2019c), Baker and Harrison (2021), Mukherjee et al. (2021e), Frusciante (2021) based on standard siren tests (Schutz 1986; Holz and Hughes 2005), and early-time modifications can be constrained by CMB B-modes (Amendola et al. 2014). However, the dark sirens detected by LIGO and Virgo already impose some actual limits on Ξ_0 (Arai and Nishizawa 2018; Belgacem et al. 2018b; Lagos et al. 2019; Finke et al. 2021). The modified friction term can also be constrained with GW data only analyzing the mass distribution of compact binaries (Ezquiaga 2021), similarly to the methods developed to bound H_0 and other cosmological parameters (Farr et al. 2019; Ezquiaga and Holz 2021; Mastrogiovanni et al. 2021). So far there has not been much exploration of a possible frequency dependence of δ. (See, however, Belgacem et al. (2019c) for forecasts on oscillations in the GW amplitude.)

In specific models of modified gravity, the parameters effecting the GW luminosity distance also impact EM observables. For the Horndeski family of theories, constraints of this type can be found in Alonso et al. (2017), Spurio Mancini et al. (2019), Bonilla et al. (2020), Allahyari et al. (2022), and the combination of EM+GW constraints in Noller and Nicola (2019), Baker and Harrison (2021).

In certain theories GWs can decay via interactions. This effect is induced by non-linear couplings from $m = 2$ in Eq. (17), as the spontaneous violation of Lorentz symmetry allows GWs to decay into two scalar excitations perturbatively (Creminelli et al. 2018) or with resonant enhancement (Creminelli et al. 2019) for which, importantly, LISA will probe a different and complementary region of the parameter space already constrained by LIGO/Virgo.

4.2.3 The gravitational-wave speed

The GW speed c_T is constrained by a variety of measurements. The detection of ultra high energy cosmic rays implies a strong constraint on gravitational Cherenkov radiation from subluminal propagation of the waves, as otherwise the radiation would decay away at a rate proportional to the square of their energy $\mathcal{O}(10^{11}\ \text{GeV})$ before reaching us (Moore and Nelson 2001; Caves 1980; Kimura and Yamamoto 2012). For galactic $\mathcal{O}(10\ \text{kpc})$ or cosmological $\mathcal{O}(1\ \text{Gpc})$ origin, the relative deviation in c_T is constrained to be smaller than $\mathcal{O}(10^{-15})$ or $\mathcal{O}(10^{-19})$, respectively. This bound, however, only applies for subluminal propagation, redshifts of $z \lesssim 0.1$, and modifications in the high-energy regime.

Another constraint on c_T at the subpercent level can be inferred from the energy loss in binary pulsar systems (Beltran Jimenez et al. 2016; Brax et al. 2016). Constraints on c_{T} have also been discussed as forecasts for potential arrival time comparisons with nearby supernovae emissions (Nishizawa and Nakamura 2014; Saltas et al. 2014; Lombriser and Taylor 2016; Brax et al. 2016), which are however very rare, for LISA eclipsing binary systems (Bettoni et al. 2017), or the weak bounds that can be inferred without counterpart emissions from BBH mergers (Cornish et al. 2017), from the comparison of the GW arrival times between the terrestrial detectors (Blas et al. 2016), or the CMB B-mode power spectrum (Raveri et al. 2015) for early-time modifications. A stringent and prominent direct constraint on deviations of $c_T/c = 1$ of $\lesssim \mathcal{O}(10^{-15})$ was obtained from the arrival times of the GWs from the LIGO/Virgo event GW170817 (Abbott et al. 2017d, c) and its EM counterparts. As anticipated, the measurement left a strong impact across a wide range of cosmic acceleration models (Lombriser and Taylor 2016; McManus et al. 2016; Lombriser and Lima 2017; Creminelli and Vernizzi 2017; Sakstein and Jain 2017; Ezquiaga and Zumalacárregui 2017; Baker et al. 2017). This can be observed from Eq. (17): for $\dot{\phi}^2 \sim \Lambda_2^4$ and $H\dot{\phi} \sim \Lambda_3^3$, a c_T very close to c implies a fine tuning of the coefficients $c_{n,2}$ and $c_{n,3}$ for all n.

Importantly, however, the constraint only applies to low redshifts of $z \lesssim 0.01$ and the LIGO/Virgo frequency range (Battye et al. 2018; de Rham and Melville 2018). In particular, it was argued that UV completion terms for modified gravity theories naturally recover a luminal speed of gravity in the high-energy limit tested by GW170817 while allowing deviations at lower energies relevant to modifications that could drive cosmic acceleration (de Rham and Melville 2018). LISA will provide a threefold improvement over a GW170817-like bound. With the detection of GWs from massive BBHs up to $z \sim 10$ and their EM counterparts c_T will be tested across much larger distances, tightening the current constraint. Additionally, a more robust measurement of arrival-time delays can be achieved (Mangiagli et al. 2020; Haiman 2017; Tang et al. 2018). Furthermore, LISA tests the frequency range below the expected UV transition of modified gravity models (de Rham and Melville 2018). Besides providing a new test of GR at different energy scales, a measurement of the speed of GWs with LISA is thus of particular relevance to cosmic acceleration models. Another way to relax the constraints on c_T is by considering larger values of Λ_3 or smaller values of $\dot{\phi}^2$. For instance, it was noted that by raising Λ_3 in Eq. (17) by three orders of magnitudes is enough to agree with most of the constraints discussed in this section (Noller et al. 2020). Although this means that cosmological effects of these theories become irrelevant, their consequences could become manifest in compact astrophysical objects, potentially probed by LISA.

4.2.4 Dispersion

An energy E dependent GW velocity is also introduced with non-vanishing graviton mass $m_g = \mu h/c^2 \neq 0$, where the group velocity becomes $(v_g/c) \simeq 1 - (m_g c^2/E)^2$. The combination of current LIGO/Virgo sources yields a constraint of $m_g \leq 1.76 \times$

10^{-32} GeV$/c^2$ (Abbott et al. 2021f). More distant and more massive sources are generally more effective in constraining the dispersion relation and the lower energy range of LISA will be favourable for tightening the bounds on m_g. Currently, the strongest bound on the mass of the graviton with $m_g \leq 7 \times 10^{-41}$ GeV$/c^2$ is inferred from weak gravitational lensing (Choudhury et al. 2004).

Frequency dependent modifications in the velocity term of Eq. (18) can also more generally be parametrised with the group velocity $(v_g/c) \simeq 1 + (\alpha - 1)A_\alpha E^{\alpha-2} + \mathcal{O}(A_\alpha^2)$, where α and A_α may parametrise quantum-gravity effects, extra dimensions, or Lorentz invariance violations (Mirshekari et al. 2012). The parametrisation recovers for instance the effect of a massive graviton for $\alpha = 0$ with $A_0 = m_g^2 c^4$. In quantum gravity, the parameter α depends on the dimension of spacetime and of momentum space (Calcagni et al. 2019b).

4.2.5 Interaction terms and gravitational-wave oscillations

Finally, the presence of a source term $\Pi \neq 0$ further modifies the GW amplitude with an oscillatory correction of order $\Pi\gamma_{ij}/(Hk)$ (Nishizawa 2018). This effective source term appears naturally in theories with multiple tensor fields. These tensor fields could have a fundamental origin like in bigravity (de Rham et al. 2011; Hassan and Rosen 2012) or they could be an effective field arising from a combination of multiple vector fields as in Yang-Mills (Cervero and Jacobs 1978; Galtsov and Volkov 1991; Darian and Kunzle 1997), Abelian multi gauge fields in a gaugid configuration (Piazza et al. 2017) and multi Proca fields (Armendariz-Picon 2004; Hull et al. 2015; Allys et al. 2016; Beltran Jimenez and Heisenberg 2017). (see Beltrán Jiménez et al. 2020a for a survey of the theory landscape.) The induced GW oscillations have been studied in concrete examples such as (Max et al. 2017, 2018) and gauge field DE (Caldwell et al. 2016; Caldwell and Devulder 2019). The presence of additional tensor modes can leave an imprint in the luminosity distance, introduce waveform modulations and chiral effects (Beltrán Jiménez et al. 2020a).

The effect of GW oscillations on the luminosity distance can be constrained with LISA standard sirens (Belgacem et al. 2019c) (see Sec. 3.3). In the coherent regime, GW oscillations appear as frequency dependent modulations of the waveform and can thus be tested without the need of redshift information, cf. Fig. 11 in Belgacem et al. (2019c). GW oscillations in bigravity depend on a mixing angle (defining the interaction between the two spin-2 fields) and are suppressed by the graviton mass as $\tilde{m}_g^2/f^2$. The lower frequency range and high SNR will allow LISA to improve constraints on m_g to $m_g \lesssim 2 \cdot 10^{-25}$eV, an improvement by 3 orders of magnitude with respect to current LVK bounds ($m_g \lesssim 10^{-22}$) eV (Max et al. 2017).

4.2.6 Polarisation effects, gravitational-wave lensing and triple systems

GW propagation beyond GR can lead to effects on standard $(+, \times)$ or novel GW polarizations (e.g. scalar and vector waves). Due to Lorentz symmetry and parity, on the homogeneous FLRW background $h_\times, h_+$ interacts only with additional tensor

polarizations, either fundamental (bigravity, multigravity) or composite (multiple vector fields), leading to the effects discussed in Sect. 4.2.5. Theories including parity-violating interactions can lead to propagation effects on left/right polarized GWs (Alexander et al. 2008; Okounkova et al. 2022).

Interactions between standard and novel polarizations in parity-preserving theories occur beyond the homogeneous background, leading to new phenomena in GW lensing beyond GR (Ezquiaga and Zumalacárregui 2020). Locally, the propagating field is a superposition of the $+, \times$ and novel polarizations, known as propagation eigenstates. Propagation eigenstates evolve independently with a well defined speed that can depend on the position and direction. In general, each propagation eigenstate has a different speed, leading to birefringence (polarization dependent arrival time and deflection angles). Birefringence causes very distinct effects when the (total) time delay between different polarizations is shorter than the duration of the signal in the observable band. Long signals at high redshift (e.g. MBBHs) will allow LISA to probe birefringence in ways complementary to ground detectors.

GW lensing beyond GR can be particularly powerful in configurations in which the source and the lens are in close proximity. Interesting targets for LISA are stellar mass binaries in the vicinity of a MBH (a scenario suggested by the possible EM counterpart to GW190521, Graham et al. 2020). GW birefringence effects can be strongly enhanced by the strong gravity, potentially allowing tests of Horndeski theories at even higher precision than GW170817 (cf. Sect. 4.2.3 and Fig. 16 in Ezquiaga and Zumalacárregui 2020). GW emission by a binary near a MBH can be affected by the scalar hair of the central body (Brax et al. 2020). A stellar-mass binary orbiting a MBH undergoes a characteristic Doppler shift and (possibly) a strong lensing pattern that can be used to identify the triple system (Toubiana et al. 2021). Those systems can excite the quasi-normal modes of the central BH during the inspiral, with stellar-mass binaries detected by LISA sensitive to central masses $M \sim 10^6\, M_\odot$ (Cardoso et al. 2021). These configurations will allow LISA to perform novel tests of GR, either through the confirmation of the triple-nature of the system or by direct detection of quasi-normal modes.

4.2.7 Relation to ppE framework

The modifications in Eq. (18) can also be cast into the parameterized post-Einsteinian (ppE) framework (Yunes and Pretorius 2009), introduced to parametrise the effects of GR departures in the dynamical strong-field regime on the gravitational waveforms from the binary coalescence of compact objects,

$$h(f) = \left(1 + \sum_j \alpha_j u^j\right) e^{i \sum_k \beta_k u^k} h_{\mathrm{GR}}(f), \tag{23}$$

where $u \equiv (\pi \mathcal{M} f)^{1/3}$ with chirp mass $\mathcal{M}$ and frequency f. The GR waveform $h_{\mathrm{GR}}(f)$ is reproduced for vanishing α_j and β_k. The series in α_j can be expressed as an integral over δ whereas the series in β_k may be expressed as an integral involving c_T and m_T (Nishizawa 2018). In the ppE subclass of the generalised inspiral-merger-ringdown

waveform model $h(f) = e^{i\delta\Phi_{\rm gIMR}} h_{\rm GR}(f)$ (Li et al. 2012) (see e.g. (Nishizawa 2018) for the deatils of this parameterization) the modification is hence independent of δ. The above parametrization has been further extended to include parity violating effects and then used to put constraints on parity violation in gravity by using the LIGO/Virgo O1/O2 catalog (Yamada and Tanaka 2020).

4.3 Open problems

An interesting open problem is the mixture of propagation and source effects for extended theories of gravity and the role of screening mechanisms. A post-Newtonian expansion for the source emission in screened regimes can be performed using a scaling relation (McManus et al. 2017; Renevey et al. 2020). For some GR extensions the relevant modification in v are in fact determined by the screened environments of emitter and observer rather than the cosmological background whereas for c_T screening effects may safely be neglected.

In addition to the effects on the propagation of GWs, modified gravity theories can also affect the generation of GWs. Shift-symmetric scalar-tensor theories are particularly suited for describing DE since they mediate a long range (massless) interaction. However, in these theories, there is a no-hair theorem that proves that the only BH solution is locally isometric to Schwarzschild (Hui and Nicolis 2013; Creminelli et al. 2020a). One way to avoid the no-hair theorem is to consider a time dependent scalar field solution and a number of hairy BH solutions have been found in Horndeski, beyond-Horndeski as well as degenerate higher-order scalar-tensor theories (Babichev et al. 2016). Another possibility for hairy BH solutions is to involve the coupling with the Gauss–Bonnet invariant (Sotiriou and Zhou 2014). A no-hair theorem also exists for neutron stars (Barausse and Yagi 2015; Lehébel et al. 2017). Again the time dependence of the scalar field can evade this no-hair theorem (Sakstein et al. 2017; Ogawa et al. 2020). It is still an open question whether these hairy solutions can be formed dynamically and how they modify the generation of GWs such as BH ringdown (Noller et al. 2020). We note that even if modified gravity theories predict the same BH solutions in static environments, this is not necessarily the case in dynamical situations, and also their perturbations are different in different theories (Barausse and Sotiriou 2008; Tattersall et al. 2018).

An interesting possibility to evade such no-hair theorems, at least for neutron stars, is to allow for a conformal coupling with matter. The conformal coupling breaks the shift symmetry, but so long as this is Planck suppressed, this breaking will be soft. In this case non-trivial solutions featuring screening exist (Babichev et al. 2009) and, most importantly, pass the test of non-linear numerical evolution (ter Haar et al. 2021).

These modified gravity theories admit the existence of scalar GWs. A detection of scalar GWs is a smoking gun for the deviation from general relativity (Scharre and Will 2002). Screening mechanisms are expected to suppress the generation of scalar GWs (Dar et al. 2019), however, very recently, numerical relativity simulations have been performed, which point at a partial breakdown of the screening in BH collapse (ter Haar et al. 2021; Bezares et al. 2021) and in the late inspiral and merger of BNSs

(Bezares et al. 2022). In more detail, stellar collapse seems (quite surprisingly) to produce a very low frequency signal potentially detectable by LISA, while waveforms from BNSs seem to deviate from their GR counterparts at the quadrupole (but not dipole) multipole order.

Finally, there are various theoretical constraints on modified gravity models considered in this section. A notable one is the decay of GWs into scalar field perturbations (Creminelli et al. 2018, 2019). This is due to the low strong-coupling scale of the theory, which is close to the energy scale probed by LIGO/Virgo. Other constraints can be placed in terms with $m = 1$ and $m = 2$ in Eq. (17), and come from avoiding instabilities in the scalar field sector that can be induced by passing GWs (Creminelli et al. 2020b). If new states are present at a scale parametrically below the cut-off, the theory is of no use for the GWs predictions at LIGO/Virgo (de Rham and Melville 2018). LISA will detect GWs at much lower frequencies and will play an essential role in constraining these theories.

5 Stochastic gravitational-wave background as a probe of the early universe

Section coordinator: S. Kuroyanagi. Contributors: N. Bartolo, C. Caprini, G. Cusin, D.G. Figueroa, S. Kuroyanagi, M. Peloso, S. Renaux-Petel, A. Ricciardone.

5.1 Introduction

The SGWB contains information on the GW events that occurred across the whole history of the universe. Its measurement has an immense value for cosmology. It gives access to stages of the early universe that cannot be directly probed by either EM or neutrino observations. The universe before the CMB epoch was indeed not transparent to photons, and neutrinos produced in the very early universe are too weak to be detected at current or forthcoming experiments. We now introduce some key concepts about the SGWB and its observables, while we focus on the physics of its cosmological sources in the subsequent sections.

5.1.1 What is a stochastic gravitational-wave background?

Early universe phenomena that emit GWs typically lead to the production of a background of GWs of stochastic nature. This means that the tensor perturbation $h_{ij}(\mathbf{x}, t)$ that defines the background is a random variable with different realisations everywhere in space. SGWBs can therefore be characterised only at a statistical level, by means of ensemble averages. As there is only one observable universe, what is customary in cosmology is to invoke the *ergodic* hypothesis, stating that either spatial or temporal averages are equivalent to an ensemble average of the underlying statistical distribution. In other words, we interpret that, by observing today a large region of the universe (or for this matter a given region for long enough time), we have access to many realisations of the system. This holds under two conditions: 1) if the universe is almost homogeneous and isotropic at the time of the GW production,

so that the initial condition for the generation of GWs is the same (in a statistical sense) everywhere; 2) if the GW source respects causality. Under these circumstances, the properties of SGWBs from the early universe can be studied by means of the ergodic hypothesis.

Due to causality, a cosmological GW source acting at a given time in the early universe cannot produce a signal correlated at length and time scales larger than the cosmological horizon at the moment of GW generation. If we denote with a subscript p the time of production, the (physical) correlation scale of the emitted GWs must satisfy $\ell_p \leq H_p^{-1}$.[6] Equivalently, the GW signal cannot be correlated at time scales larger than $\Delta t_p \leq H_p^{-1}$. At the present time we have access to much larger length and time scales than today's redshifted scale associated with H_p^{-1}, so a SGWB signal in our detectors is perceived as the superposition of many signals uncorrelated in time and space. The number of independent signals in a given region today can be actually counted, knowing the evolution of the universe and the details of the GW generation mechanism.

We note that the above arguments remain valid also for causal sources continuously emitting GWs over a long period, say during several Hubble times. The paradigmatic example of this is the case of a cosmic string network, which emits GWs continuously, all the way from the moment of the phase transition that created it, till today. The SGWB signal in this case is mostly dominated (at least in the Nambu Goto (NG) approach to strings, see Sect. 7) by the superposition of the GWs emitted by sub-horizon string loops. This GW signal is perceived today as a background formed by the superposition of many GW emissions at different times of cosmic history, and from many different regions. Therefore the observation of this signal today cannot be resolved beyond its stochastic nature, exactly for the same reasons discussed above. The main difference in fact between a continuously sourced background and one arising from a source localised in time, is rather that the former extends over a long frequency range, precisely because its source has been emitting during many Hubble times.

In the case of inflation, the above arguments do not apply, as the causal horizon grows exponentially during the inflationary phase. Yet, it is well known that inflation produces a SGWB, as we discuss in Sects. 8 and 9. The inflationary background of GWs is actually considered to be stochastic because of the intrinsic quantum nature of the generating process. In particular, this background originates during inflation due to the quantum vacuum fluctuations of tensor metric perturbations, which become a random variable. The tensors become effectively classical during the inflationary accelerated expansion as their wavelengths are exponentially stretched to super-Hubble scales, where they acquire very large occupation numbers. (See the discussion e.g. in Caprini and Figueroa (2018).) This transition after Hubble-crossing renders the tensor perturbation a stochastic variable. When the tensor perturbations re-enter the Hubble radius during cosmic evolution after inflation, they form a GW signal that is intrinsically stochastic.

[6] Let us note that we have used the inverse Hubble rate H_p^{-1} as the cosmological horizon, as that is a good approximation for most of the cosmological evolution of the universe, except during inflation.

Finally, let us notice that the superposition of astrophysical GWs also forms a SGWB, which will act as a foreground for cosmological SGWBs. We will briefly review possible astrophysical background contributions expected in the mHz band in Sect. 5.2.2.

5.1.2 How do we characterize a stochastic gravitational-wave background?

Since we speak about random tensor variables, the Fourier modes $h_r(\mathbf{k}, t)$ are also considered to be random variables. For statistically homogeneous and isotropic, unpolarised and Gaussian GW backgrounds, we define the tensor amplitude power spectrum as

$$\langle h_r(\mathbf{k}, t)\, h_p^*(\mathbf{q}, t)\rangle = \frac{8\pi^5}{k^3}\, \delta^{(3)}(\mathbf{k} - \mathbf{q})\, \delta_{rp}\, h_c^2(k, t), \tag{24}$$

with h_c a dimensionless real function, depending only on the time t and the comoving wave-number $k = |\mathbf{k}|$. The previous factor $8\pi^5$ has been chosen so that we can write

$$\langle h_{ij}(\mathbf{x}, t)\, h_{ij}(\mathbf{x}, t)\rangle = 2 \int_0^{+\infty} \frac{dk}{k}\, h_c^2(k, t), \tag{25}$$

with the factor 2 in the RHS as a convention motivated by the fact that the LHS involves the contribution from two independent polarisations. It is then clear that $h_c(k, t)$ represents the characteristic tensor amplitude per logarithmic wave-number interval and per polarisation state, at a given time t. It is common to denote the combination $\frac{h_c(k,t)^2}{2} \equiv P_h(k, t)$ as power spectrum. This last quantity is used in Secs. 8 and 9.

Another relevant quantity to characterise a SGWB is the spectrum of GW energy density per logarithmic wave-number interval, $d\rho_{\rm GW}/d\log k$, defined as

$$\rho_{\rm GW} = \frac{\langle \dot{h}_{ij}(\mathbf{x}, t)\, \dot{h}_{ij}(\mathbf{x}, t)\rangle}{32\pi G} = \frac{\langle h'_{ij}(\mathbf{x}, \eta)\, h'_{ij}(\mathbf{x}, \eta)\rangle}{32\pi G\, a^2(\eta)} = \int_0^{+\infty} \frac{dk}{k}\, \frac{d\rho_{\rm GW}}{d\log k}, \tag{26}$$

where in the second equality we have converted the derivatives with respect to the physical time t into derivatives with respect to the conformal time η. An expression for the GW energy density power spectrum $d\rho_{\rm GW}/d\log k$ valid for free waves inside the Hubble radius, can be found using the simple relation ${h'_c}^2(k, \eta) \simeq k^2\, h_c^2(k, \eta)$, where the prime symbol ($'$) represents the derivative with respect to the conformal time, and ${h'_c}^2(k, \eta)$ characterises the expectation value $\langle h'_{ij}(\mathbf{x}, \eta)\, h'_{ij}(\mathbf{x}, \eta)\rangle = 2 \int_0^{+\infty} \frac{dk}{k}\, {h'_c}^2(k, \eta)$. Using this, we arrive at (Caprini and Figueroa 2018)

$$\frac{d\rho_{\rm GW}}{d\log k} = \frac{k^2\, h_c^2(k, \eta)}{16\pi G\, a^2(\eta)}. \tag{27}$$

As $h_c(k, \eta) \propto 1/a(\eta)$ for sub-Hubble modes, the GW energy density is diluted as

radiation with the expansion of the universe, $\rho_{\rm GW} \propto a^{-4}$, as expected for massless degrees of freedom.

Finally, in order to connect the above expressions with experimental observables, we need to re-express the GW spectra today in terms of the present-day physical frequency, $f = k/(2\pi a_0)$, associated with the comoving wave-number k. In order to do this, we first write the characteristic tensor amplitude per logarithmic frequency interval today as $h_c(f) = h_c(k, t_0)$. We then define the one-sided spectral density of a SGWB as

$$S_h(f) = \frac{h_c^2(f)}{2f}, \tag{28}$$

which has dimensions Hz^{-1}. The reason to define this quantity is that it is directly comparable to the noise in a detector, parametrised by $S_n(f)$. On the other hand, it is convenient to normalise the spectrum of the GW energy density per logarithmic frequency interval like

$$\Omega_{\rm GW}(f) = \frac{1}{\rho_c}\frac{d\rho_{\rm GW}}{d\log f}, \tag{29}$$

where $\rho_c = 3H^2/(8\pi G)$ is the critical energy density at time t. The quantity traditionally considered by cosmologists is then

$$\Omega_{\rm GW}^{(0)}(f) = \frac{4\pi^2}{3H_0^2} f^3 S_h(f), \tag{30}$$

which corresponds to the normalised energy density spectrum today. In terms of the dimensionless amplitude $h_c = \sqrt{2f\,S_h}$, we can also write the following relations

$$S_h(f) = 7.98 \times 10^{-37} \left(\frac{\mathrm{Hz}}{f}\right)^3 h^2\,\Omega_{\rm GW}(f)\,\frac{1}{\mathrm{Hz}}, \tag{31}$$

$$h_c(f) = 1.26 \times 10^{-18} \left(\frac{\mathrm{Hz}}{f}\right) \sqrt{h^2\,\Omega_{\rm GW}(f)}. \tag{32}$$

5.1.3 Current constraints by other observations

There are several ways to place constraints on the SGWB energy density. We briefly review different types of observations which provide constraints on the SGWB at different frequencies.

BBN places a bound on a primordial (i.e. prior to BBN) SGWB as the latter contributes to the total energy density of extra relativistic species and affects the expansion rate of the universe during BBN. In order not to spoil BBN by changing the resulting light-element abundances, the energy density of the SGWB should satisfy (Caprini and Figueroa 2018; Allen 1996)

$$\int d(\ln f)\Omega_{\rm GW}(f)h^2 \leq 5.6\times 10^{-6}\left(N_{\rm eff}^{\rm (upper)} - 3.046\right), \tag{33}$$

where $N_{\rm eff}^{\rm (upper)}$ is the upper bound on the effective number of relativistic degrees of freedom $N_{\rm eff}$. Applying the 2σ upper limit for $N_{\rm eff}$ from BBN (obtained by observations of ^{4}He and D) as $N_{\rm eff}^{\rm (upper)} = 3.41$ (Cyburt et al. 2016), we obtain $\Omega_{\rm GW}h^2 < 2.3\times 10^{-6}$ for a logarithmic frequency bin. This constraint is valid for GWs generated before the BBN epoch $T \sim 1$ MeV.

The CMB is also a powerful tool to constrain the primordial SGWB. CMB anisotropies on large scales, both in temperature and in polarisation (E and B modes), can be induced by the tensor metric perturbations. Non-detection of such anisotropies provides a bound on the tensor-to-scalar ratio r and the current best bound is given by the combined Planck and BICEP2/Keck data up to 2018: $r < 0.036$ at $k = 0.05{\rm Mpc}^{-1}$ (Akrami et al. 2020; Ade et al. 2018; Tristram et al. 2021; Ade et al. 2021), which corresponds to $\Omega_{\rm GW}h^2 < 1.5\times 10^{-16}$ at $f = 7.7\times 10^{-17}$ Hz. On small scales $f > 10^{-15}$ Hz, GW modes are well inside the cosmological horizon and behave like massless neutrinos, contributing to $N_{\rm eff}$, thus affecting the growth of density perturbations as well as the expansion rate at recombination (Smith et al. 2006; Sendra and Smith 2012; Clarke et al. 2020). The updated constraint from the temperature anisotropy is $\Omega_{\rm GW}h^2 < 1.7\times 10^{-6}$ for adiabatic initial conditions and $\Omega_{\rm GW}h^2 < 2.9\times 10^{-7}$ for homogeneous (non-adiabatic) initial conditions at the 95% confidence level (Clarke et al. 2020). In the case of adiabatic initial conditions, GW perturbations evolve in the same way as neutrino perturbations. Most known sources of a SGWB produce an unperturbed background and we should impose homogeneous initial conditions, which assume no initial density perturbation.

Ground-based interferometer experiments, which have sensitivity to the frequency range of $10 - 100$Hz, are rapidly improving the upper limit on a SGWB. The latest constraint by the O3 run of LIGO/Virgo gives $\Omega_{\rm GW} < 5.8\times 10^{-9}$ (with $h = 0.679$) at the 95% confidence level for a flat (frequency-independent) SGWB (Abbott et al. 2021g). The limit is obtained by combining data from the earlier O1 and O2 runs and 99% of the sensitivity comes from the frequency band $20 - 76.6$ Hz.

Pulsar timing arrays probe low-frequency GWs at a frequency range of 10^{-9} and 10^{-6} Hz. Millisecond pulsars are known to have an extremely stable pulse frequency. GWs affect the pulse propagation and change the pulse times of arrival, thus their presence can be tested by regularly monitoring pulse frequencies. Radio telescope projects, such as NANOGrav (Alam et al. 2021), EPTA (Desvignes et al. 2016), and PPTA (Kerr et al. 2020), have been updating the upper limit on the GW amplitude, and recently reported the possible detection of a SGWB (Arzoumanian et al. 2020; Chen et al. 2021b; Goncharov et al. 2021). The strain amplitude for a $f^{-2/3}$ power-law spectrum inferred by the two experiments has central value at $h_c = 1.92\times 10^{-15}$ and $h_c = 2.95\times 10^{-15}$ at $f = 1\,{\rm yr}^{-1}$, respectively, which correspond to $\Omega_{\rm GW}h^2 \simeq 2\text{–}5\times 10^{-9}$ at $f = 3.2\times 10^{-8}$ Hz. A confirmation of quadrupolar spatial correlations in the signal is needed to establish the detection.

A SGWB at μHz frequencies can in principle be observed in binary pulsars as well as in Earth–Moon-like or Earth–Satellites-like systems. The binary system's orbits indeed exhibit resonant interactions with the SGWB in some regimes. Current estimates show that such binaries permit to rule out the existence of a SGWB with $\Omega_{\rm GW} \gtrsim 6 \times 10^{-6}$ at frequencies $f \sim 1$ μHz, with improvement to $\Omega_{\rm GW} \gtrsim 5 \times 10^{-9}$ by late 2030s (Blas and Jenkins 2022a, b).

5.2 Generation mechanisms

5.2.1 Cosmological

Among the targets of the LISA mission there is the cosmological SGWB, which includes different sources active in the early universe. Such a background is characterised by the spectral energy density $\Omega_{\rm GW}(f)$ defined in Eq. (29) and by some peculiar features, which will be described in next sections, that can be useful in the process of characterisation and disentanglement from the astrophysical background, like chirality, non-Gaussianity, anisotropies and so on. A very well known example of a cosmological SGWB is the irreducible GW background due to quantum vacuum tensor fluctuations produced during inflation, which spans a large range of frequencies with an almost scale-invariant spectrum. For the simplest realisation of inflation, it has an amplitude that is too small to be detected by LISA. Besides this, there are several primordial mechanisms which can lead to a non-flat cosmological-SGWB frequency profile at the scales probed by GW interferometers (from 10^{-5} to 10^{2} Hz): from models where the inflaton is coupled with extra (gauge) fields (Sect. 8.2) (Barnaby and Peloso 2011; Cook and Sorbo 2012; Sorbo 2011; Barnaby et al. 2012; Dimastrogiovanni et al. 2017; Peloso et al. 2016; Domcke et al. 2016) to models with features in the scalar power spectrum (Sect. 8.3) (Flauger et al. 2010; Braglia et al. 2020; Fumagalli et al. 2021a), models where spacetime symmetries are broken during inflation (Sect. 8.4) (Endlich et al. 2014; Koh et al. 2013; Cannone et al. 2015a, b; Bartolo et al. 2016a; Ricciardone and Tasinato 2017; Bartolo et al. 2016a; Cannone et al. 2015b; Akhshik et al. 2014; Akhshik 2015), or scenarios where non-attractor phases characterise the universe evolution (Leach et al. 2001; Namjoo et al. 2013; Mylova et al. 2018). GWs sourced by second-order scalar fluctuations (Sect. 10.3) can further be associated with PBH formation (Sect. 10). These models are characterised by an amplitude which, still respecting the CMB bounds, have a large amplitude and a peculiar frequency shape which may enable detection by LISA. A dedicated analysis for the potential of the LISA space-based interferometer to detect the SGWB produced from different inflationary models has been performed in Bartolo et al. (2016b). This analysis has shown how LISA will be able to probe inflationary scenarios, in a complementary way to CMB experiments. Besides these, there are some post-inflationary mechanisms which can also generate GWs with a large amplitude at LISA scales: for instance several setups beyond the standard model of particle physics (BSM) exhibit a first-order phase transition (FOPT) around the TeV energy scale that peaks in the LISA frequency window (see Sect. 6). A dedicated analysis for the detection of a cosmological SGWB from

FOPTs have been done in Caprini et al. (2016), Caprini et al. (2020). Also cosmic defects can generate a cosmological SGWB which crosses the frequency window of the LISA detector. More precisely the GW signal from cosmic defects can be detected if the energy of the phase transition that created the defects is at the right scale (see Sect. 7). A recent analysis to probe the ability of LISA to measure this background, considering leading models of the string networks has been done in Auclair et al. (2020). In the most optimistic case, LISA might be able to probe cosmic strings with tensions $G\mu \gtrsim \mathcal{O}(10^{-17})$. It has been recently pointed out (Boileau et al. 2022) that, depending on different assumptions on the astrophysical background and the galactic foreground, LISA will be able to probe cosmic strings with tensions $G\mu \gtrsim \mathcal{O}(10^{-16} - 10^{-15})$.

The detection of any of these SGWBs from the early universe, would allow us to test high energy scales beyond the reach of particle colliders, like the Large Hadron Collider (LHC).

In Fig. 5 we collect GW cosmological signals expected to peak in the LISA frequency band and we compare them with the sensitivity of present and future GW detectors. To this end we use the PLS curves (Thrane and Romano 2013) designed to graphically assess the ability of a given detector to probe SGWBs: a power-law frequency spectrum crossing these curves is detected, provided it is not masked by a greater foreground.

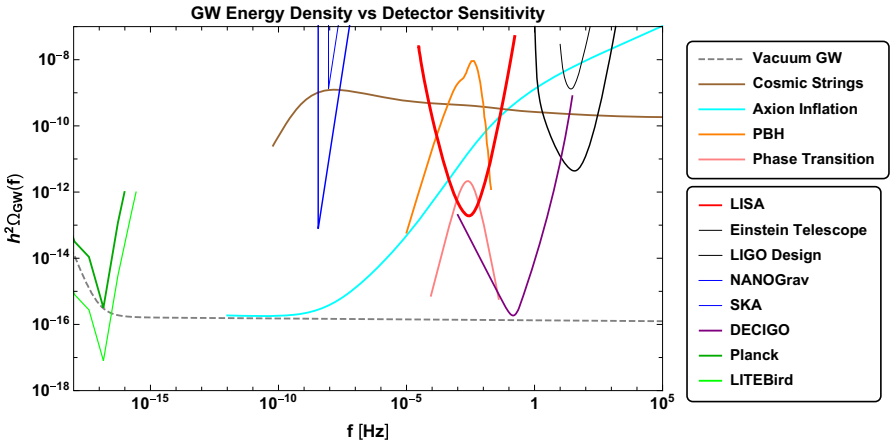

Fig. 5 SGWB energy density $h^2\Omega_{\rm GW}$ for different cosmological sources compared to the sensitivity of different GW detectors. As cosmological signals we have the vacuum GW contribution coming from inflation (grey dashed line) with $r = 0.044$ and $n_T = -r/8$, the signal expected in axion inflation models (cyan), the signal generated by cosmic string networks with $G\mu = 10^{-10}$ (brown), the signal generated by a FOPT with $v_w = 0.9$, $\alpha = 0.1$, $\beta/H_* = 50$, $g_* = 100$, $T_* = 200$GeV (pink) and the signal generated at second-order by the formation mechanism of PBHs with $f_{PBH} = 1$, $\sigma = 0.5$, $k_* = k_{\rm LISA}$ (orange). For GW detectors we report the sensitivity of Planck (darker green), LITEBird (green), EPTA (blue), SKA (darker blue), LISA (red), DECIGO (purple), LIGO Design (black) and ET (darker black)

5.2.2 Astrophysical

The astrophysical SGWB results from the incoherent superposition of signals emitted by numerous unresolved astrophysical sources from the onset of stellar activity until today. As any other background of radiation, the astrophysical SGWB is quantifiable through its isotropic energy density level and through the spatial angular power spectrum encoding its anisotropy. Many different astrophysical sources contribute to the astrophysical SGWB, including SOBBHs and BNSs (Abbott et al. 2016a; Regimbau et al. 2017; Mandic et al. 2016; Dvorkin et al. 2016a; Nakazato et al. 2016; Dvorkin et al. 2016b; Evangelista and Araujo 2014), merging MBBHs (Kelley et al. 2017), rotating neutron stars (Surace et al. 2016; Talukder et al. 2014; Lasky et al. 2013), stellar core collapse (Crocker et al. 2017, 2015) and population III binaries (Kowalska et al. 2012). The astrophysical information that can be extracted from the intensity and polarisation maps of the astrophysical SGWB, are the collective properties of a given population of astrophysical sources (redshift and mass distribution, local properties of galactic environment,...).

The astrophysical SGWB from BBHs is expected to be dominant in the LISA band (Dvorkin et al. 2016a) and below, and may become a source of confusion noise for other sources and cosmological background emissions. Observations with LISA will allow for the study of some aspects of BBH populations that are difficult to observe with ground-based interferometers. For example, at the mHz frequencies accessible to LISA, some of the binaries may not be fully circularised, and their residual eccentricities may provide an indication to their formation channel. In particular, binaries formed through dynamical processes in dense stellar clusters can have measurable eccentricities. These can be constrained for the subset of resolved merger, and in addition the distribution of eccentricities of the entire population may also affect the resulting astrophysical SGWB.

The detection of the BNS merger by the LIGO/Virgo network (Abbott et al. 2017d, e, 2020a) and the estimated rate of mergers in the local universe of $R = 13 - 1900\ \mathrm{Gpc}^{-3}\ \mathrm{yr}^{-1}$ (Abbott et al. 2023) led to the conclusion that in the Hz band these sources may have a comparable contribution to the astrophysical SGWB relative to BBHs (Abbott et al. 2018b, 2021g). We may therefore expect that their contribution to the anisotropies of the astrophysical SGWB will also be important also for LISA. While it will be difficult to disentangle the relative contributions of BBHs and BNSs to the overall astrophysical SGWB, especially in view of the large modelling uncertainty in the BNS merger rates (Chruslinska et al. 2018; Giacobbo and Mapelli 2019), it is interesting to note that their host galaxies are expected to have different properties. In the isolated BH formation scenario discussed e.g. in Cusin et al. (2019b), BH masses are heavily influenced by the metallicity of their progenitor stars. Specifically, metal-poor stars retain most of their mass throughout their evolution and collapse to form heavier BHs. As a consequence, these BHs form preferentially in high-redshift and/or low-mass galaxies (Lamberts et al. 2016; Cao et al. 2018; Mapelli et al. 2018; Artale et al. 2019). In contrast, NSs can also form in metal-rich environments. In view of the different clustering properties of the host galaxy populations, BBHs and BNSs can in principle give rise to very different

anisotropic components of the astrophysical SGWB (Cusin et al. 2019b). Note that, to put this into practice, we need to understand better the time delays between formation and merger, which can change the host galaxy property if delays are long.

Finally, LISA will also allow one to study the astrophysical SGWB from other types of sources such as close white dwarf binaries (see e.g. Vecchio 2002), which may also produce anisotropies in the galactic plane (Ungarelli and Vecchio 2001; Kudoh and Taruya 2005). We refer the reader to Amaro-Seoane et al. (2023) for an in-depth discussion on the astrophysical populations leading to this and the aforementioned astrophysical SGWBs.

5.3 Characteristics of the stochastic gravitational-wave background

5.3.1 Frequency profile of the stochastic gravitational-wave background

As described above, there are many different mechanisms to generate a SGWB both of cosmological and astrophysical origin. The question that arises is, how to determine the origin of the SGWB, once it is detected. Identifying the SGWB source is a challenging but crucial task, essential to extract physical information from the SGWB detection. One of the most useful properties at this aim is the spectral shape of the SGWB. More specifically, one aims at reconstructing $\Omega_{\rm GW}$ as a function of frequency, since the frequency profile of the SGWB depends on the generation mechanisms, thus providing a way to disentangle different SGWB sources. For example, the SGWB formed by the superposition of extragalactic BBHs and BNSs has a characteristic frequency profile of $\Omega_{\rm GW} \propto f^{2/3}$, reflecting the frequency dependence of the inspiral phase of each event, thus enabling us to infer the origin. Also, see Kuroyanagi et al. (2018) for a list of astrophysical and cosmological sources, and examples of their frequency profiles. Reconstructing the frequency profile in detail also allows to explore the possibility that several sourcing components contribute to the SGWB within the same frequency band, leading to a complicated spectral shape arising from their superposition.

While the spectral shape of the primordial signal depends very much on the detail of the source properties, some fairly general considerations on the expected frequency profile of the cosmological SGWB are still possible, based essentially on causality (Caprini et al. 2009a). Sources active on a (conformal) time-scale $\Delta t \lesssim \mathcal{H}_p^{-1}$, where $\mathcal{H}_p^{-1}$ denotes the Hubble time when the source starts operating (we assume here that this occurs during the radiation dominated era), typically lead to peaked SGWB signals in terms of the variable $\Omega_{\rm GW}(k)$. On (comoving) wavenumbers $k \lesssim 1/\Delta t$, in fact, the SGWB source is expected to be uncorrelated both in time and in space, since $k \lesssim 1/\Delta t \sim v/L < 1/L$ for v and L the typical speed and size of the anisotropic stresses. These latter are the part of the source energy momentum tensor leading to the GW generation. Since $\Omega_{\rm GW}(k)$ is the GW energy density per logarithmic wave-number, white-noise anisotropic stresses (flat in k) lead to $\Omega_{\rm GW}(k)$ increasing as k^3. This increase is expected to change at around $k_p \sim 1/\Delta t \sim v/L$, and the subsequent behaviour depends on the detail of the time and space structure of the source (Caprini et al. 2009a). The SGWB spectrum either peaks around k_p, and

decreases for $k > k_p$ with a slope depending on the source characteristics; or it takes a shallower, but positive slope, in which case the peak occurs at a higher wavenumber. This latter can correspond to an inverse length L^{-1}, though other time and length scales can also be relevant and show up in the $\Omega_{\rm GW}(k)$ spectrum: for example, the characteristic *time*-scale over which the source is coherent $\tau < \Delta t$ (as opposed to the source duration Δt), or different *length*-scales, relevant in the space distribution of the anisotropic stresses, other than L.

Notable peaks in the spectrum are then expected for SGWB sources characterised by a finite, short duration $\Delta t \lesssim \mathcal{H}_p^{-1}$. In particular, one example of sources giving rise to peaked spectra that are relevant for LISA (since they are typically peaking in the LISA band), are FOPTs related to the electroweak symmetry breaking, as described in Sect. 6. On the other hand, for generation mechanisms that turn on at a given time $\mathcal{H}_p^{-1}$ in the radiation era, but continue to source GWs throughout the universe evolution $\Delta t \gg \mathcal{H}_p^{-1}$, the region of k^3 increase is less and less relevant, being pushed towards the horizon today. One expects a wide frequency region over which the signal features a slower increase with k or, in some cases, is constant. The most noteworthy example for LISA is the SGWB produced by topological defects in the scaling regime, such as a NG cosmic strings network, which is exactly scale-invariant in the LISA band for wide regions of the model parameter space (see e.g. Figueroa et al. 2013 and the discussion in Sect. 7).

Another almost scale-invariant SGWB is the one generated by slow roll inflation. This constitutes, however, an exception with respect to the cases described above. The SGWB is in fact generated as the tensor perturbations reenter the horizon during the radiation and matter eras, and therefore the spectral shape does not depend on the causal evolution properties of some source anisotropic stresses, but on the amplification of vacuum tensor perturbations during inflation. In some scenarios in which the inflaton is coupled to an external field, the SGWB is indeed produced by the field anisotropic stresses, and one can obtain blue-tilted spectra whose tilt depends on the model. GWs actively generated at second order in perturbation theory from large scalar fluctuations could also have peculiar features depending on the inflaton dynamics. The scenarios pertaining to these categories that are relevant for LISA are presented in detail elsewhere in this paper (cf. Sects. 8, 10.4, 10.3, and for a review see Caprini and Figueroa (2018) and references therein).

5.3.2 Anisotropies and propagation effects

Angular anisotropies in the energy density of the SGWB can be an efficient way to characterise its physical origin and properties. They provide a further tool to help in disentangling a SGWB of cosmological origin from an astrophysical one, besides the exploitation of their different frequency dependence. Angular anisotropies can be imprinted both at the epoch of the SGWB generation and at later times, during its propagation across cosmological perturbations. As such the anisotropies in the SGWB can provide a new way to characterise and distinguish various generation mechanisms of primordial SGWB and they allow one to probe the evolution of cosmological perturbations. Because the universe is transparent to GWs for sub-

Planckian energies, the case of a cosmological SGWB represents a privileged observable to probe the physics of the early universe, and its anisotropies can preserve the memory of the initial conditions of the universe right after inflation.

We are interested in anisotropies and inhomogeneities in the energy density of the SGWB, therefore we allow the monopole Eq. (30) to be dependent on space and direction of observation

$$\Omega_{\rm GW} = \frac{1}{4\pi}\int d^2\hat{n}\,\omega_{\rm GW}(\eta, \vec{x}, q, \hat{n}), \tag{34}$$

thus defining the energy density contrast as

$$\delta_{\rm GW} \equiv \frac{\delta\omega_{\rm GW}(\eta, \vec{x}, q, \hat{n})}{\bar{\omega}_{\rm GW}(\eta, q)} = \frac{\omega_{\rm GW}(\eta, \vec{x}, q, \hat{n}) - \bar{\Omega}_{\rm GW}(q, \eta)}{\bar{\Omega}_{\rm GW}(q, \eta)}\,, \tag{35}$$

where $q = 2\pi f$. Various approaches have been adopted to compute the angular anisotropies and their statistics (such as the angular power spectrum) both for the cosmological and astrophysical SGWB (Alba and Maldacena 2016; Contaldi 2017; Geller et al. 2018; Bartolo et al. 2019a, 2020b; Cusin et al. 2017, 2018b, 2019a; Pitrou et al. 2020; Bertacca et al. 2020; Cusin et al. 2018a; Jenkins et al. 2018, 2019a; Cusin et al. 2019b, 2020; Bartolo et al. 2020a; Valbusa Dall'Armi et al. 2021). A way to compute the SGWB anisotropies is to adopt a Boltzmann equation approach, similarly to CMB anisotropies (Contaldi 2017; Bartolo et al. 2019a, 2020b; Cusin et al. 2019a; Pitrou et al. 2020). In such an approach one considers the generation of high-frequency GW modes and their propagation across a background of lower frequency (large-scale) cosmological perturbations (which can be either scalar or tensor in nature). As for CMB photons, therefore, the propagating GWs become the cosmological carrier of the underlying cosmic inhomogeneities. Such an approach allows one to put in evidence at least two distinguishing features for a cosmological SGWB (Bartolo et al. 2019a, 2020b): first the anisotropies imprinted at the production epoch can be characterised by a strong frequency dependent contribution; secondly, if primordial non-Gaussianity are present in the background large-scale cosmological perturbations, then they will be left imprinted into the SGWB anisotropies. The bispectrum of the angular anisotropies of $\delta_{\rm GW}$ turns out therefore to be a new probe of primordial non-Gaussianity, potentially measurable at interferometers, beyond the CMB and large-scale structure measurements (Bartolo et al. 2019a, 2020b). For these reasons, besides the information they provide for a SGWB from inflation, anisotropies can be a new probe for a whole series of phenomena. They can be produced at the epoch of generation of GWs from a phase transition (Geller et al. 2018; Kumar et al. 2021), and they can characterise also the SGWB which is unavoidably produced by second-order curvature perturbations in PBH formation scenarios (Bartolo et al. 2020a). Specific imprints in the SGWB anisotropies can be also generated by decoupled relativistic particles in the early universe, thus reinforcing the SGWB as a new window into the particle physics content of the universe (Valbusa Dall'Armi et al. 2021).

For a SGWB of astrophysical origin, the analytic derivation of energy density anisotropies can be found in Contaldi (2017), Cusin et al. (2017), Cusin et al.

(2018b), Cusin et al. (2019a), Pitrou et al. (2020), Bertacca et al. (2020). When adopting a Bolzmann-like description, one needs to add an emissivity term to the Vlasov equation for the graviton distribution function, accounting for the generation process at galactic scales (Cusin et al. 2019a; Pitrou et al. 2020). For extragalactic background components, the primary contribution to the energy density anisotropy comes from clustering (sources are embedded in the cosmic web), while a secondary source of anisotropy is due to line of sight effects (e.g. lensing, kinematic and volume distortion effects). Predictions for the energy density angular power spectrum have been presented in Cusin et al. (2018a), Jenkins et al. (2018), Jenkins et al. (2019a), Cusin et al. (2019b), Cusin et al. (2020), Bertacca et al. (2020) in the Hz band and in Cusin et al. (2020) in the mHz band. Anisotropies are typically suppressed by a factor 10^{-1}–10^{-2} with respect to the monopole, the range of variability depending on the underlying astrophysical model for star formation and collapse, and the angular power spectrum scales as ℓ^{-1} on large scales. Different physical choices for the process of BH collapse and mass distribution lead to differences up to 50% on the angular power spectrum in the mHz band, non degenerate with a global scaling (Cusin et al. 2020). With LISA it may be possible to constrain the dipole and quadrupole components of the angular power spectrum, for sufficiently high SNR detection (i.e. sufficiently high monopole) (Alonso et al. 2020a; Contaldi et al. 2020).

As shown in Sect. 2.6, where we have described how to compute the angular cross-spectrum between GW and other cosmological probes, the study of the cross-correlation of the SGWB energy density fluctuation with the LSS (e.g. galaxy distribution) is an interesting subject to examine to distinguish the origin (cosmological versus astrophysical) of a given background component. Unlike a cosmological SGWB, the extragalactic astrophysical background is expected to be highly correlated with the large-scale structure (see e.g. Cusin et al. 2017, 2018b, a; Jenkins et al. 2019a; Jenkins and Sakellariadou 2018; Jenkins et al. 2018; Cusin et al. 2019b, 2020; Jenkins and Sakellariadou 2019; Jenkins et al. 2019b; Bertacca et al. 2020; Pitrou et al. 2020; Mukherjee and Silk 2020; Alonso et al. 2020b; Adshead et al. 2021; Ricciardone et al. 2021; Braglia and Kuroyanagi 2021; Valbusa Dall'Armi et al. 2022). Ways to exploit this feature are discussed in Sect. 3.

5.3.3 Polarisations

As any background of radiation, a SGWB is fully characterised in terms of Stokes parameters, intensity (proportional to the background energy density), and Q, U, V parameters describing polarisation. Classical diffusion of GW radiation from massive objects can generate a net polarisation out of an unpolarised flux, playing a role analogue to Thomson scattering for CMB photons (Cusin et al. 2019a). The amount of polarisation that can be generated depends on the GW frequency, and it is more effective for large wavelength modes, for which wave effects are expected to be more important in an astrophysical context. An order of magnitude estimate of the effect gives that, in the mHz band, the net amount of polarisation generated by diffusion is suppressed by several orders of magnitude with respect to anisotropies in the intensity (Cusin et al. 2019a). As polarisation cannot be effectively generated during

propagation and astrophysical background components are expected to be statistically unpolarised at emission, the detection of a highly polarised background component is a smoking gun of its cosmological origin.

As we review in Sect. 8.7.1, several inflationary mechanisms have been proposed that could produce a net circularly polarised SWGB, which is characterised by Stokes V parameter. A net chiral polarisation can be measured with a network of ground-based (Seto and Taruya 2007, 2008; Crowder et al. 2013; Smith and Caldwell 2017) or space-based (Orlando et al. 2021) interferometers.[7]

The measurement is more problematic in the case of a single planar instrument such as LISA. In this case, a left-handed GW with wave-vector $\vec{k}$ produces the same effects as a left-handed GW with wave-vector $\vec{k}_p$, where $\vec{k}_p$ has been obtained from $\vec{k}$ with a reflection on the plane of the detector. Therefore a difference between the two polarisations cannot be detected in the case of an isotropic SGWB.

A net polarisation can however be detected also by a planar instrument if the SGWB is not isotropic. As discussed in the previous subsection, It is natural to expect that a SGWB of cosmological origin has a dominant monopole component, with large-scale anisotropies of magnitude comparable to that of the CMB ones. This statement is, however, frame-dependent, and the most natural expectation is that the SGWB is isotropic in the CMB rest-frame. As seen in the CMB, the motion of the Solar System in this frame, with a velocity $v \simeq 10^{-3}$, produces a dipole anisotropy, with an amplitude suppressed by a factor v with respect to that of the monopole. Seto (2006), Domcke et al. (2020b) studied how the dipole signal might allow one to measure a net chirality with LISA. This can be done through the cross-correlation between the A and E channels, which vanishes both in the case of isotropic and of unpolarised SGWB. As estimated in Domcke et al. (2020b), the SNR associated with this measurement is

$$\mathrm{SNR} \simeq \frac{v}{10^{-3}} \left| \frac{\sum_\lambda \lambda\, \Omega_{\mathrm{GW}}^{\lambda} h^2}{1.4 \cdot 10^{-11}} \right| \sqrt{\frac{T}{3\ \mathrm{years}}}, \tag{36}$$

where $\lambda = \pm 1$ refers to the right and left chirality, respectively, and where T is the observation time.

5.3.4 Non-Gaussianity

There are two types of non-Gaussianity discussed in the context of GW observations. One is the non-Gaussianity of inhomogeneities, which is defined in position or momentum space (see e.g. Sect. 8.7.3). GWs generated at sub-horizon scales cannot produce correlation across the horizon due to causality, thus the SGWB is Gaussian. Non-Gaussianity typically appears in GWs generated in the context of inflation, which could produce non-trivial spatial correlations stretched over the horizon (see Sects. 8 and 10.2.3). See Bartolo et al. (2019a, 2020b) for a detailed derivation of the non-Gaussianity expected in the SGWB, which is simply generated by the evolution

[7] The detection of a circularly polarised SWGB at CMB scales was studied in Gluscevic and Kamionkowski (2010), Smith and Caldwell (2017), Gerbino et al. (2016), Thorne et al. (2018).

through the background large-scale underlying inhomogeneities, similarly to what happens for CMB photons. This is computed through the angular bispectra (i.e. the three point function) of the graviton energy density.

The other type of non-Gaussianity is the one in the time signal (sometimes referred to as a SGWB in the "popcorn" or "shot noise" regime), which could be a useful statistical measure for a SGWB formed by overlapped short-duration events, such as the astrophysical background. If GW events are not frequent enough to overlap in time, the observed strain has a non-Gaussian distribution. Among the cosmological sources, the SGWB from cosmic strings could show this non-Gaussian feature (Regimbau et al. 2012) (see Method II in Sect. 7.3). For non-Gaussianity of astrophysical sources, see Sect. 12.2.

6 First-order phase transitions

Section coordinators: J. Kozaczuk, M. Lewicki. Contributors: M. Besancon, C. Caprini, D. Croon, D. Cutting, G. Dorsch, O. Gould, R. Jinno, T. Konstandin, J. Kozaczuk, M. Lewicki, E. Madge, G. Nardini, J.M. No, A. Roper Pol, P. Schwaller, G. Servant, P. Simakachorn.

6.1 Introduction

Cosmological FOPTs are one of the most attractive sources of GWs in the early universe (Witten 1984; Hogan 1986). A FOPT can occur when the Higgs or any other scalar fields are trapped in a metastable vacuum in the early universe. As the universe cools down, thermal or quantum fluctuations drive the field over or through the potential barrier, resulting in bubbles of the stable phase nucleating in the sea of metastable phase. These bubbles then expand and collide with each other to complete the transition. The collision of the bubbles and the fluid motion around them produce a SGWB. Since the generated GWs propagate to the present nearly without interaction, they maintain information about the processes that produced them at the time of generation. Their detection may therefore reveal some of the properties of the high-energy universe.

In the standard model of particle physics (SM) there are in principle two phase transitions, at two energy scales: the scale of the electroweak gauge symmetry breaking, and that of the chiral symmetry breaking in quantum chromodynamics (QCD). Given the coupling constants and the mass of the Higgs boson in the SM, it is known that the electroweak symmetry breaking is a crossover (Kajantie et al. 1996b; Csikor et al. 1999). Moreover, at almost zero quark chemical potential, the QCD phase transition cannot be first-order (Stephanov 2006). However, FOPTs are predicted in a number of extensions of the SM aimed at addressing open questions such as the origin of the observed baryon asymmetry (Kuzmin et al. 1985; Rubakov and Shaposhnikov 1996), the nature of DM, and the hierarchy problem.

The millhertz-band GWs that LISA will measure are in the best frequency band to explore FOPTs occurring between the electroweak and the multi-TeV scales. Therefore, it is important to understand how FOPTs source GWs, how such

transitions arise from microphysics, and consequently to appreciate the implications that the detection of GWs from FOPTs has for particle physics. We provide an up-to-date understanding on these topics in the following.

6.2 Determination of the relevant parameters

The main features of the SGWB spectrum can be determined from knowledge of four parameters related to the FOPT: the temperature T_* of the plasma when the bubbles percolate, the transition strength α, the inverse duration of the phase transition β, and the wall velocity v_w. These macroscopic parameters crucially depend on the underlying microscopic model, linking particle physics and cosmology. We dedicate this section to a discussion of how to compute the parameters entering the SGWB spectrum from the underlying microphysics.

The temperature at which the FOPT occurs is determined by the interplay between the nucleation of bubbles of the true-vacuum phase and the expansion of the universe. The nucleation rate per unit volume is given by $\Gamma = A(t)\exp[-S_c(t)]$, where S_c is the critical bubble action. For thermally-induced nucleation, we have $A \sim T^4$ and $S_c = S_3/T$ with S_3 being the three-dimensional Euclidean action of the $O(3)$ symmetric bounce solution.[8] The onset of the FOPT then occurs at the nucleation temperature T_n, at which on average one bubble is nucleated per horizon volume. It is roughly given by the temperature at which $S_c \sim 140$. The characteristic temperature for GW production is however the temperature T_* at which the bubbles percolate, when approximately one third of the comoving volume has transitioned to the true vacuum. For moderately strong transitions, these temperatures are typically sufficiently close to take $T_* \sim T_n$. More precise formulas for the determination of the nucleation and percolation temperatures in from the critical action can be found in Caprini et al. (2020).

The transition strength parameter α describes the amount of energy released as a fraction of the radiation energy $\rho_{\rm rad}$. Different definitions are used throughout the literature, corresponding to different ways of mapping the particle physics model to the bag EoS commonly used for determining the efficiency of converting the released energy into bulk motion of the fluid (Espinosa et al. 2010). A simple but reasonably accurate definition of α in terms of a given particle particle physics model is obtained from the difference of the trace θ of the energy-momentum tensor between the phases,

$$\alpha = \frac{\Delta\theta}{\rho_{\rm rad}}, \qquad \Delta\theta = \Delta V(T) - \frac{T}{4}\frac{\partial \Delta V(T)}{\partial T}, \tag{37}$$

where $V(T)$ is the thermal effective potential. See Giese et al. (2020, 2021) for a comparison of other conventions regarding the transition strength as well as generalisations beyond the bag model. The efficiency factors for the conversion of the energy released in the transition into bulk motion can then be calculated from the transition strength α and the wall velocity (Espinosa et al. 2010; Giese et al. 2021).

[8] For quantum tunnelling, $S_c = S_4$ is the Euclidean action of the $O(4)$ symmetric bounce in four dimensions.

The calculation of the thermal effective potential, starting from an underlying particle physics model, is itself a nontrivial task. Due to the infrared (IR) sensitivity of bosonic fields at high temperature, perturbation theory must be re-summed. As a consequence, the effective expansion parameter increases $g^2 \to g$ (or even $g^2 \to \sqrt{g}$), and the expansion converges more slowly. Typical one-loop calculations utilise daisy re-summation (Parwani 1992; Arnold and Espinosa 1993) to include the leading $\mathcal{O}(g^2)$ and $\mathcal{O}(g^3)$ contributions to the potential, while methods to include still higher order contributions have been developed (Parwani 1992; Arnold and Espinosa 1993; Farakos et al. 1994; Braaten and Nieto 1995; Kajantie et al. 1996a, 2003; Croon et al. 2021; Ekstedt and Löfgren 2020; Gould 2021; Ekstedt et al. 2023). In addition to the slow convergence of the perturbative expansion, there are true IR divergences at $\mathcal{O}(g^6)$ (four-loop order) which re-summation does not resolve (Linde 1980), underlying the importance of nonperturbative calculations (Gould et al. 2019; Kainulainen et al. 2019; Niemi et al. 2021; Halverson et al. 2021; Huang et al. 2021).

The bubble nucleation rate can be expanded around the percolation time t_* as

$$\Gamma \sim T^4 e^{-S_3/T} = \Gamma_* e^{-\beta(t-t_*)}, \tag{38}$$

and adiabaticity of the expansion of the universe yields $dT/dt = -TH$, so

$$\frac{\beta}{H_*} = T_* \frac{d(S_3/T)}{dT}\bigg|_{T_*}. \tag{39}$$

This parameter determines whether the transition will complete mostly by the expansion of a few nucleated bubbles or by the nucleation of new bubbles everywhere in space. Indeed, the larger β/H_* is, the faster the nucleation rate increases in time, the more bubbles will nucleate inside a Hubble horizon before the completion of the phase transition, and the smaller will their radii be when they collide, since there had not been much time for them to expand before meeting a neighbour. Thus one can expect an inverse relation between β and the amplitude of the GW spectrum. Moreover, β enters in the determination of the SGWB peak frequency. Note that, for very strong transitions, the definition above may become inappropriate and should be reformulated (Huber and Konstandin 2008b; Jinno et al. 2017).

As with α, the calculation of the bubble nucleation rate, Γ, is affected by the IR sensitivity of bosonic fields at high temperatures. The spatial inhomogeneity of bubbles, as well as the time dependence of their creation, raises additional challenges. While much effort has gone into overcoming these challenges (Gleiser et al. 1993; Bodeker et al. 1994; Berges et al. 1997; Surig 1998; Strumia and Tetradis 1999; Moore and Rummukainen 2001; Garbrecht and Millington 2015; Gould and Hirvonen 2021), the theoretical uncertainties present in calculations of the bubble nucleation rate are less well understood than those for the effective potential.

The determination of the wall velocity from first principles is a much more daunting task. The passage of the wall perturbs the equilibrium of particles in the plasma, so that the temperature, velocity and chemical potential of each species are different from the background. The distribution function of each species can be written as $f_i = f_i^{\mathrm{eq}} + \delta f_i$,

and the perturbations can be calculated by solving the corresponding Boltzmann equation (Moore and Prokopec 1995; Konstandin et al. 2014),

$$(p^{\mu}\partial_{\mu} + K_{\mu}\partial_{p_{\mu}})f + C[f] = 0, \tag{40}$$

where K_{μ} is (related to) the force term felt by the particles due to the passage of the bubble, and $C[f]$ are collision terms that must be computed from the microphysics of the model under consideration, taking into account the mutual interactions of particles present in the plasma at the electroweak phase transition (EWPT); see e.g. Moore and Prokopec (1995), Kozaczuk (2015). The Higgs equation reads (Konstandin et al. 2014)

$$\Box\phi + \frac{dV(\phi, T)}{d\phi} + \sum_i \frac{dm_i^2}{d\phi}\int \frac{d^3p}{(2\pi)^3 2E_p}\delta f_i = 0, \tag{41}$$

and the term with fluid perturbations δf_i acts as a friction countering the bubble expansion. From this equation one obtains the wall velocity and the wall width, typically by using an ansatz for the Higgs profile

$$\phi(z) = \frac{\phi_0}{2}\left[1 - \tanh\left(\frac{z}{L_w}\right)\right] \tag{42}$$

and solving for the width L_w and the velocity v_w. Although the wall velocity has been computed from first principles for a few models, such as in SUSY extensions (John and Schmidt 2001; Kozaczuk et al. 2015), Higgs plus singlet setups (Kozaczuk 2015; Lewicki et al. 2022) and two Higgs doublet models (Dorsch et al. 2017), the determination of v_w as a function of the parameters of the underlying theory remains an open issue for most of the interesting models discussed in the literature. Crucially, the collision terms appearing in the Boltzmann equation (40) have been calculated only for a few models, such as the SM (Moore and Prokopec 1995) and singlet extensions (Kozaczuk 2015), and even then are known only at a leading-log approximation. For most models, additional collision terms involving interactions of new particles among themselves and with the SM sector have not yet been computed. Altogether, it is fair to say that our current tools allow only for an estimate of the wall velocity, and there is still a large room for improvement on this front.[9]

6.3 GW sources

A FOPT in the early universe occurs when at least one scalar field gets trapped at the symmetric metastable vacuum. As the universe cools down, the scalar field tunnels through or thermally fluctuates over the barrier into the lower-energy vacuum, and at a certain temperature bubbles in the broken phase start to nucleate in the sea of the symmetric phase. The latent heat released in the transition drives these bubbles to

[9] In this respect, a promising alternative direction is the use of a string theory-inspired method (Maldacena 1998) known as gauge/string duality, or holography. The power of this tool is that it allows for a first-principle determination of out-of-equilibrium observables in a four-dimensional quantum field theory. It was used in (Bea et al. 2021b; Bigazzi et al. 2021; Bea et al. 2022) to compute the bubble wall velocity in a family of strongly-interacting, four-dimensional gauge theories.

expand further, and the transition completes when these bubbles collide and merge with each other. During bubble expansion, the latent heat is converted into the energy of the bubble wall and the thermal and kinetic motion of the surrounding plasma. However, due to spherical symmetry of the bubbles, no GWs are generated during this expansion period. It is only when the bubbles collide, at the end of the FOPT, that GWs are produced from the kinetic energy of the scalar field and the fluid. Since there are numerous independent collision regions today within the typical resolution of GW detectors, the resulting spectrum is stochastic.

The amount of GWs generated during a cosmological FOPT is quantified by the fractional energy density of these waves in the universe, $\rho_{\rm GW}$, compared to the critical energy density, $\rho_c \equiv 3H^2/(8\pi G)$, where H is the Hubble constant. One can rephrase the GW density parameter in Eq. (29) as

$$\Omega_{\rm GW} \equiv \frac{1}{\rho_c}\frac{d\rho_{\rm GW}}{d\ln k}. \tag{43}$$

For a stochastic source, the spectrum is proportional to the two-point correlation of the metric perturbations $\langle \dot{h}(\mathbf{k},t)\dot{h}(\mathbf{k}',t)\rangle \equiv (2\pi)^3\delta^{(3)}(\mathbf{k}-\mathbf{k}')P_{\dot{h}}(k)$, as

$$\Omega_{\rm GW} = \frac{k^3}{24\pi^2 H^2}P_{\dot{h}}(k). \tag{44}$$

Since sufficiently distant regions could not have exchanged information with one another during the FOPT, the correlation function for low $|\mathbf{k}|$ corresponds to white noise, i.e. $P_{\dot{h}}(\mathbf{k},t) \sim$ constant, and the spectrum grows as k^3. This growth cannot continue forever, so this pattern must eventually be broken and the spectrum must decrease at some point, for the total energy in GWs must be finite. Therefore, the SGWB spectrum must contain a peak. A typical shape is illustrated in Fig. 6 created using data from PTPlot version 1.0.1.[10]

There are three main sources of GWs from bubble collisions: (i) the kinetic energy of the scalar field along the bubble walls, (ii) coherent motion of the plasma generated by the bubble expansion, also known as "sound waves", and (iii) turbulent motion of this fluid, typically expected to occur at late times after the fluid develops vortical motion. The total contribution to GW energy from FOPTs in the early universe is therefore the sum

$$\Omega_{\rm GW} = \Omega_{\rm GW}^{\rm (coll)} + \Omega_{\rm GW}^{\rm (sw)} + \Omega_{\rm GW}^{\rm (turb)}. \tag{45}$$

How these three contributions arise in principle depends on the detail of the model. However, as discussed in the previous section, it is known that a few parameters determined from microphysics are enough to discuss cosmological consequences: transition strength α, nucleation speed β, wall velocity v_w, and the transition temperature T_*. These parameters determine the fluid profile of the expanding bubbles

[10] Since the release of PTPlot version 1.0.0 there have been several modifications of PTPlot. This includes taking into account the recent erratum from Hindmarsh et al. (2017a) which led to the amplitude of the GW signal being overestimated by a factor of 10. For a more complete list of changes in version 1.0.1, see ptplot.org.

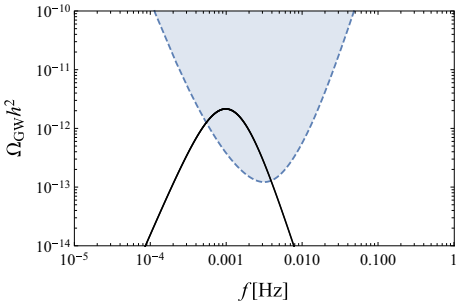

Fig. 6 An example of the GW power spectrum from a FOPT, along with the LISA power-law-sensitivity (PLS) curve of SNR = 10. The model parameters used in this example are $v_w = 0.9$, $\alpha = 0.1$, $\beta/H_* = 50$, $T_* = 200$ GeV, $g_* = 100$

and the energy budget of the transition (Espinosa et al. 2010; Wang et al. 2021a; Giese et al. 2020).

The transition dynamics can vary dramatically for different α. In typical transitions, in which α is moderate, the friction on the wall balances against the pressure from the released energy before bubbles collide, and as a result the walls approach a constant terminal velocity. In this case most of the energy released in the transition is transferred to the surrounding plasma, and only a negligible fraction remains in the scalar field. Macroscopically the energy transferred to the plasma can be classified into heat and bulk kinetic motion of the fluid. The bulk motion takes the form of compression waves, or sound waves. As long as the linearity of the fluid equation holds, i.e. the kinetic energy in play is sufficiently low, sound waves from different bubbles continue to propagate even long after the transition completes, and they overlap to create random velocity field with typical length scale of the sound shell $l_{\rm shell}$. This phenomenon is found in numerical simulations (Hindmarsh et al. 2014, 2015, 2017a), and (Hindmarsh 2018; Hindmarsh and Hijazi 2019) provide a corresponding analytic model based on the picture of an ensemble of overlapping shells. Interestingly, the velocity field sources GWs at the constant scale $l_{\rm shell}$ even well after the completion of the transition (provided that the transition is not too strong). Therefore, it works as an efficient source of GW production. The resulting GW spectrum $\Omega_{\rm GW}^{(\rm sw)}$ contains two important characteristic scales of the bubble size and the fluid shell thickness. A hybrid scheme to calculate the GW spectrum from this phenomena has been proposed recently (Jinno et al. 2021).

The sound waves are expected to decay through the formation of non-linearities in the flow, after which the fluid enters a turbulent phase. The non-linearities develop on a time scale $\tau_{\rm sh}$, which is inversely proportional to the kinetic energy in the fluid. It has been shown that, even for weak transitions, $\tau_{\rm sh}$ is typically smaller than a Hubble time (Ellis et al. 2020b), with $\tau_{\rm sh}$ becoming smaller as α increases. The decay of sound waves produced during a FOPT and the subsequent development of a turbulent flow has not been studied so far using direct numerical simulations and remains a major source of uncertainty when determining the GW spectrum. This holds in particular for strongly FOPTs, when the fluid kinetic energy is expected to be high, and the contribution of kinetic turbulence to the SGWB signal is expected to be relevant. Within the sound wave regime, typically the larger the transition strength the greater the production of GWs. FOPTs with smaller β which produce fewer,

larger bubbles are also preferred. For a detailed discussion on the dependence of the SGWB spectrum from sound waves on α and β (see Caprini et al. 2020).

For deflagrations with $\alpha \sim \mathcal{O}(0.1)$ the sound shell picture breaks down (Cutting et al. 2020). In such transitions, substantial vorticity can be generated during the initial collision of sound shells and bubbles. Furthermore, hot high pressure regions of the metastable phase can form during the transition. These hot regions suppress further bubble nucleation and decrease the wall velocity at the initial stage of the transition (Konstandin and No 2011; Mégevand and Ramírez 2018), while they form droplets at the later stage, extending the duration of the transition and suppressing the production of kinetic energy. Both the generation of vorticity and the formation of droplets can modify the GW spectrum, either by speeding up the decay of sound waves or by reducing the fluid kinetic energy and thus GW spectrum amplitude. Further study is required in this regime to map out the production of vorticity and study the evolution of flows with mixed modes, as well as to find the suppression of kinetic energy from droplets in a wide range of parameter space. It is however worth noting that the wall velocity still needs to be computed as a function of parameter space for many BSM models. It is therefore unclear if there are many realistic models that would give rise to the strong transitions with subsonic wall velocities which would be affected by these results.

Another interesting scenario is extremely strong transitions, in which $\alpha \gg 1$ is realized (Randall and Servant 2007; Espinosa et al. 2008; Konstandin and Servant 2011a; Hambye and Strumia 2013; Jaeckel et al. 2016; Jinno and Takimoto 2017b; Marzola et al. 2017; Iso et al. 2017; Chiang and Senaha 2017; von Harling and Servant 2018; Bruggisser et al. 2018a, b; Hambye et al. 2018; Baldes and Garcia-Cely 2019; Hashino et al. 2019; Prokopec et al. 2019; Brdar et al. 2019b; Marzo et al. 2019; Breitbach et al. 2019; Baratella et al. 2019; Fairbairn et al. 2019) but the bubble walls still reach a terminal velocity because of the higher-order friction terms on the wall (Bodeker and Moore 2017; Höche et al. 2021). In this case the relevant hydrodynamical solution is strong detonation. While the dominant GW source comes from fluid kinetic motion, we must note several things: first, the onset of turbulence is earlier in this type of model (Ellis et al. 2020b); second, the overlap of sound shells, which is one of the requirements for the linear growth of the GW spectrum, may be somewhat delayed (Jinno et al. 2019b). Finally, in typical models there exists a maximum α for which transitions complete. Above this, vacuum energy dominates and the metastable state begins to inflate, prohibiting the percolation of the bubbles of the true vacuum (Ellis et al. 2019b).[11]

When α exceeds a certain threshold, or simply in vacuum transitions, the bubble walls continue to accelerate until they collide ("run away"). While recent studies of the next-leading friction terms on bubble walls (Bodeker and Moore 2017; Höche et al. 2021) suggest that the parameter space for runaway is much smaller than previously thought (Bodeker and Moore 2009), such behaviour can still occur in extremely strong transitions (Ellis et al. 2019c, 2020c). In this case the only

[11] In cases where the phase transition through thermal bubble nucleation fails other mechanisms such as vacuum fluctuations (Lewicki et al. 2021) or spinodal instability (Bea et al. 2021a) can lead to completion of the transition which would have a very different phenomenology and clearly distinguishable GW spectra.

contribution is from the bubble wall $\Omega_{\rm GW}^{\rm (coll)}$. The expanding and colliding bubble walls are highly relativistic and much thinner compared to the typical bubble size. This observation motivates the so-called envelope approximation (Kosowsky et al. 1992; Kosowsky and Turner 1993), in which the shear stress is approximated to be localised in an infinitesimally thin shell at the bubble wall and disappears upon collision (Huber and Konstandin 2008a; Jinno and Takimoto 2017a). However, recent studies revealed that for runaway and vacuum transitions the collided region of intersecting bubbles has a rich structure and cannot be neglected (Weir 2016; Cutting et al. 2018, 2021; Jinno et al. 2019a). The GW spectrum that takes collided regions into account has been actively studied numerically for two bubble (Lewicki and Vaskonen 2020a, b) and many bubble collisions (Cutting et al. 2018, 2021) as well as (semi)-analytically (Jinno and Takimoto 2019; Konstandin 2018). One of the implications is that, while the peak of the spectrum does not grow in amplitude after collisions as occurs for sound waves, the spectrum may have a growing structure towards the IR, which enhances the detection prospect by LISA.

In addition to the aforementioned sources, magnetic fields could be present prior to or generated during a thermal FOPT. In the presence of a magnetic field, the turbulent motion of the primordial plasma would become dynamically coupled to the magnetic field, leading to MHD turbulence Brandenburg et al. (2017), Brandenburg et al. (1996), Christensson et al. (2001). Moreover, the hydrodynamic turbulent motion induced by the expansion of the bubbles arises in an ionised plasma, and this fact in itself can lead to MHD turbulence. The dynamical coupling between the velocity and the magnetic field plays an important role in determining the shape of the GW signal. The latter is affected by the presence of the magnetic field both through the aforementioned dynamical coupling, and because the magnetic anisotropic stresses produce GWs on their own, as studied in early analytic works (Deryagin et al. 1986; Kosowsky et al. 2002; Caprini and Durrer 2006; Gogoberidze et al. 2007; Caprini et al. 2009b). So far, the hydrodynamical simulations of thermal FOPTs have neglected magnetic fields. The early analytic works on the subject require one to make assumptions on the temporal correlation functions of the turbulence velocity and the magnetic field, which strongly affect the SGWB spectral shape (Caprini et al. 2009a). Previous analytical works were extended with updated modelling of the MHD turbulence in Niksa et al. (2018). Numerical simulations avoid resorting to analytical modelling of the MHD turbulence evolution, since they compute directly the solution to MHD equations (Roper Pol et al. 2020; Kahniashvili et al. 2021). Recent numerical simulations and previous analytic estimates agree on the shape of the GW spectrum at high frequencies, scaling as $f^{-8/3}$. However, the dynamical evolution of the magnetic field during the GW production can affect this slope (Roper Pol et al. 2020). At intermediate frequencies, the numerical simulations of Roper Pol et al. (2020) predict a spectrum $\Omega_{\rm GW}(f) \propto f$, that eventually is expected to turn to f^3 at frequencies in the super-horizon range, due to causality (Caprini et al. 2009a). $\Omega_{\rm GW}(f)$ evaluated from the numerical simulations grows as f^3 at early times, shifting to a linear increase $\propto f$ as the time progresses and GWs are building up. The detail of the transition from f to f^3 is an active topic of research. Combining numerical simulations with our theoretical understanding of the MHD turbulence

dynamics will help to obtain an accurate prediction of the spectral shape of the SGWB produced by MHD turbulence in the future. As is the case for other sources, the SGWB by MHD turbulence also depends on the parameters of the FOPT. The strength of the FOPT and the size of the bubbles can be related to the kinetic energy density, and to the characteristic scale of turbulence, respectively.

This picture can get more complicated in the case of magnetic field production during the FOPT, and it would require an appropriate treatment of the magnetic field in both the false and true vacuum regions, which are dynamically converting through the bubble-driven FOPT. During the FOPT, inhomogeneities of the Higgs field give rise to the production of magnetic fields (Vachaspati 1991; Ahonen and Enqvist 1998; Stevens et al. 2008; Vachaspati 2021; Zhang et al. 2019; Yang and Bian 2022).[12] The previous mechanism does not require CP violations, however these are expected in relation to baryogenesis through spontaneous lepton number symmetry breaking at a FOPT (Cohen et al. 1991). This parity violation leads to the production of helical magnetic fields (Vachaspati 1991; Cornwall 1997; Vachaspati 2021; García-Bellido et al. 2003). Such parity-violating turbulent sources lead to the production of circularly polarised GWs, studied analytically in Kahniashvili et al. (2005), Kahniashvili et al. (2008), Kisslinger and Kahniashvili (2015), Ellis et al. (2020a), and computed numerically in Kahniashvili et al. (2021). Further studies are required in this direction for a clear understanding of the GW and the polarisation signals produced from MHD turbulence as a function of the FOPT parameters, and a computation of turbulence in the plasma from first principles.

6.4 Discovery prospects beyond the standard model

GWs are a unique probe of the physics of the early universe. Unlike photons, gravitons were not in thermal equilibrium at early times, and may therefore directly encode information about events long before the time of last scattering. The characteristic broken power-law spectrum from a FOPT peaks at a frequency which can be related to a temperature and a time in the early universe via its redshift. Figure 7 shows this relation using the frequency peak of the acoustic spectrum, described in Caprini et al. (2020). It is seen that for appropriate fiducial values, a FOPT at the electroweak scale temperature, $T \sim 10^2$ GeV, sources a SGWB spectrum peaking at frequencies to which LISA has its best sensitivity (Grojean and Servant 2007; Caprini et al. 2016, 2019). The sensitivity to weak scale physics implies an opportunity to study FOPTs of several different kinds. In particular, several proposals for FOPTs that supply the out-of-equilibrium circumstance for baryogenesis are anchored to the weak scale. However, LISA is also sensitive to energy scales much beyond the electroweak scale: for exceptionally strong FOPTs the peak can fall outside the LISA sensitivity region but the tail of the signal still has a high SNR. In this case, FOPTs even at the MeV or PeV scale can be detected. This feature opens up potential complementary access in other experiments, as will be described in the next section.

[12] Current studies consider vacuum FOPTs. The extension to a thermal FOPT is not straightforward, and it requires further analysis.

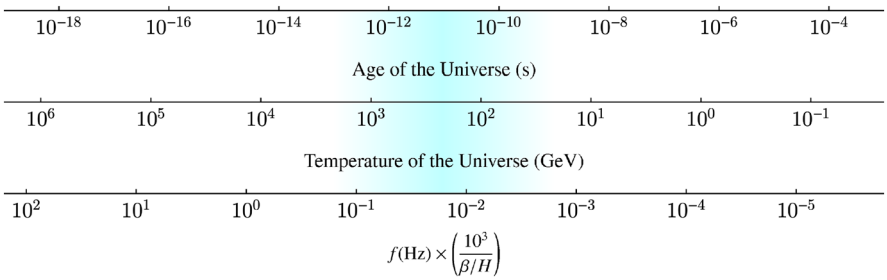

Fig. 7 LISA sensitivity to the SGWB frequency peak of FOPTs in the early universe. Here the fiducial values $v_w = 1$ and $g = 106$ are used to relate the frequency peak of the acoustic spectrum (Caprini et al. 2020) to a time and temperature in the early universe, as a function of the transition rate parameter β/H

6.4.1 First-order phase transitions in the LISA window

FOPTs are studied in the context of a variety of models, which can be divided into two main categories: the spontaneous breaking of a gauge symmetry, and confinement due to the strong coupling of a gauge symmetry (and the related chiral symmetry breaking). The EWPT, which is particularly interesting in light of electroweak baryogenesis (see Sect. 6.4.2), is an example of the former. The transition temperature associated with electroweak symmetry breaking implies that the peak frequency of the GW spectrum falls within the LISA sensitivity window, as seen in Fig. 7. As is well known, the EWPT is a crossover transition in the SM. Therefore, new physics is required to induce a FOPT that can produce a SGWB. FOPTs can be studied in a model-independent effective-field-theory approach, adding non-renormalisable operators to the Higgs potential. These analyses show that for the EWPT to be sufficiently strongly first-order, the cut-off scale must be rather low, below the TeV scale (Zhang 1993; Grojean et al. 2005; Delaunay et al. 2008; Chala et al. 2018), therefore studies of the EWPT in SM extensions generically require the introduction of at least one new degree of freedom at the $\mathcal{O}(100)$ GeV scale.

A weak-scale hidden sector featuring the spontaneous breaking of a gauge symmetry could also lead to a SGWB in the LISA window. An observable amplitude of the signal implies a significant fraction of the radiative degrees of freedom must have participated, hinting at a connection with DM (Schwaller 2015; Jaeckel et al. 2016; Croon et al. 2018; Bertone et al. 2020). The spectral form of such a signal is unlikely to give away much of its origin, though it can be related to particle spectra in specific models (Croon et al. 2018). Complementary search strategies may be applied if such a spectrum is detected—more about this in Sect. 6.5.

Confining gauge theories are thought to feature a FOPT if the confined degrees of freedom either only include the gauge fields themselves, or if confinement implies the breaking of a chiral symmetry $\mathrm{SU}(N_f) \times \mathrm{SU}(N_f)$ and the number of chiral fermions (dynamical at the transition temperature) exceeds $N_f \geq 3$. The foundation for this insight dates back to an argument based on the linear sigma model (Pisarski and Wilczek 1984) and has since been supported in part by lattice simulations

(Iwasaki et al. 1996). Studying the phenomenology of the transition is challenging, as effective theories either apply to the low-temperature (confined) phase and the high-temperature free phase. Moreover, an important role is played by the instantons of the strongly coupled theory. Initial explorations based on the linear sigma model indicate stronger SGWB are found for gapped spectra (Croon et al. 2019b). However, the predictions depend on the chiral symmetry breaking model used (Helmboldt et al. 2019).

Another alternative is solitosynthesis, a FOPT resulting from the growth of non-topological solitons stabilised by a conserved global charge (Griest and Kolb 1989). Unlike phase transitions resulting from the nucleation of critical bubbles, stable sub-critical populations of such solitons—Q-balls—exist, and accumulate charge until they reach a critical size and grow. This slow process may imply supercooled transitions still complete (Kusenko 1997; Croon et al. 2020). This scenario typically relies on the existence of a global symmetry under which the universe is asymmetrically charged. It has therefore been studied in the context of supersymmetry (Kusenko 1997; Postma 2002; Pearce 2012) and asymmetric DM (Huang and Li 2017; Croon et al. 2020).

As described in the previous section, the SGWB due to a cosmological FOPT can be described in terms of a small number of thermal parameters: characteristic temperature, bubble wall velocity, latent heat and a dynamical parameter such as a nucleation rate. These thermal parameters then predict a spectrum with a shape in most cases primarily defined by just two parameters: the peak frequency and peak amplitude. Therefore, the SGWB-inverse problem typically features degeneracies. However, resolution of the full spectrum and in particular the peak gives a unique picture of a crucial stage of the early universe, and may play an important role in answering some of the most fundamental questions. Further resolution of the underlying BSM physics can also be accomplished through complementary experimental observation.

6.4.2 Connection with baryogenesis

An (electroweak) FOPT may also be responsible for the generation of the observed baryon asymmetry. This provides an appealing connection between baryogenesis and the direct probe of the electroweak epoch in the early universe through GWs especially since the corresponding signals would peak in the LISA band. At such a first order EWPT, satisfying simultaneously the three Sakharov conditions for baryogenesis (baryon number violation, CP violation and a departure from thermal equilibrium) becomes possible: baryon number is not an exact symmetry of the SM, violated via non-perturbative processes involving gauge and Higgs fields.[13] In the presence of CP violation, these processes are biased towards producing more baryons than anti-baryons, and because the FOPT introduces a departure from thermal equilibrium, the reverse mechanism is suppressed, ensuring that the generated asymmetry is not washed-out and remains to the present day.

Among these *electroweak baryogenesis* mechanisms, those most widely studied are *non-local* ones, involving charge transport (see Morrissey and Ramsey-Musolf 2012; Konstandin 2013 for reviews): CP violation in the scatterings of plasma

particles with the phase transition boundary yields an excess of fermion handedness, which diffuses into the electroweak symmetric phase and is there converted to a baryonic excess via SM baryon number violating processes known as *sphalerons*; the expansion of the FOPT bubbles then leads the net baryonic excess inside the bubble, where the asymmetry is frozen-out up to the present day. This last condition depends on the sphaleron rate inside the bubble, $\Gamma_{\rm sph} \sim e^{-Esph/T}$ (with $E_{\rm sph}$ the sphaleron energy). Sufficient suppression of $\Gamma_{\rm sph}$ for successful baryogenesis (i.e. $\Gamma_{\rm sph}$ much smaller than the Hubble expansion rate) yields the condition of a strong EWPT, $v/T \gtrsim 1$, where v is the electroweak vacuum expectation value after the phase transition.

Up to very recently it has been assumed that these electroweak baryogenesis scenarios, as they rely on diffusion of particles in the plasma, were not effective for fast moving bubble walls (i.e. faster than the speed of sound of the plasma, with the bubbles consequently expanding as detonations). On the other hand, GWs are more favourably produced by stronger transitions resulting in faster bubble walls. This seemed to put a tension between the generation of a sizeable GW background from the FOPT (e.g. large enough to be observable by LISA) and successful baryogenesis. However, recent works (Cline and Kainulainen 2020; Laurent and Cline 2020; Dorsch et al. 2021) indicate that while diffusion is not as efficient for supersonic bubble walls, it still allows for successful electroweak baryogenesis. It has also been shown that the production of a large GW signal can be made compatible with electroweak baryogenesis for bubbles expanding as subsonic deflagrations (Dorsch et al. 2017), yet in this case the plasma friction against the moving wall must be large enough that even quite strong transitions remain subsonic, which requires the presence of sub-TeV particles with relatively large coupling to the Higgs—a tightly constrained scenario by now.

The strongest bound on non-local electroweak baryogenesis comes from the non-observation of an electric dipole moment (EDM) of the electron by highly precise experiments (Andreev et al. 2018). The additional sources of CP violation required by these transport mechanisms typically impact the electron EDM already at 2-loop order via Barr-Zee diagrams (Engel et al. 2013)—two orders above the SM CP violation contribution, which manifests itself only when all three families of quarks are involved, thus affecting EDMs at 4-loop only, being therefore highly suppressed and unconstrained by EDMs. Whether electroweak baryogenesis is still viable under such tight bounds remains to be investigated. There are, however, models in which it might be possible to avoid those constraints. One possible example involves coupling the CP violation to a vacuum expectation value of an additional scalar field which vanishes after the transition rendering the model safe from EDM constraints (Espinosa et al. 2012; Cline and Kainulainen 2013; Vaskonen 2017; Huang et al. 2018; Cline et al. 2021). Alternatively, CP violation can be secluded in a dark sector, and communicated to the visible sector in a way that the corresponding EDM contribution is suppressed or absent (Cline et al. 2017; Carena et al. 2019, 2020). Yet

[13] More precisely, the baryonic current J_B^μ is anomalous, and the anomaly $\partial_\mu J_B^\mu = (N_c g^2)/(32\pi^2) F^{\mu\nu}\widetilde{F}_{\mu\nu}$ allows for the creation of baryons through the dynamics of the non-abelian gauge fields.

another way is to increase the temperature of the EWPT from symmetry non-restoration phenomena (Baldes and Servant 2018; Glioti et al. 2019; Matsedonskyi and Servant 2020; Biekötter et al. 2021; Carena et al. 2021). The observable effect is a GW peak position shifted towards higher frequencies.

Finally, there are also *local baryogenesis* mechanisms where baryon production and CP violation occur at the same point in space, involving non-trivial gauge and Higgs field dynamics (Tranberg 2011; Konstandin and Servant 2011b). However, these mechanisms are highly inefficient at electroweak scale temperatures (Lue et al. 1997), although they can still be relevant in more exotic scenarios of very supercooled FOPTs. The main advantage of such cold electroweak baryogenesis mechanisms is their ability to generate the observed baryon asymmetry with just the SM CP violation from the Cabibbo-Kobayashi-Maskawa matrix (Tranberg 2011), or from the strong CP phase (Servant 2014), thus avoiding the tight bounds from EDMs (Andreev et al. 2018). Since the thermal plasma is very diluted at the end of the transition due to the supercooling, the GWs are sourced mainly by the kinetic energy of the bubbles.

6.5 LISA complementarity to other experimental tests

The potential of LISA to explore FOPT is complementary to other experimental tests such as searches for beyond SM physics at colliders, tests from flavour physics including neutrinos physics and B mesons physics or searches for signals from the dark sector. LISA detection of SGWB from FOPTs can not only explore the electroweak energy scale but could explore higher energy scales which could be inaccessible to present and future colliders. The other GW observatories available at the time that LISA flies, can also strengthen and complement the LISA findings.

Figure 8 sketches the FOPT energy scales that LISA can probe with SNR >10 as well as its complementarity with other GW observatories expected in the early 2040s. The figure also displays the parameter region ruled out by current BBN, pulsar timing array (PTA) and LIGO/Virgo data.[14]

The EWPT in the SM is a second order phase transition. However, there is a wealth of BSM scenarios in which the EWPT is of the first order leading to sizeable SGWB signals. Without claiming to be exhaustive, one can for example mention the extension of the scalar sector of the SM with extra singlet(s) (Craig et al. 2013; Profumo et al. 2015; Craig et al. 2016; Hashino et al. 2017; Beniwal et al. 2017; Kang et al. 2018; Matsui 2018; Alves et al. 2018; Beniwal et al. 2019; Ahriche et al. 2019; Chala et al. 2019; Chiang and Lu 2020; Alves et al. 2020, 2021; Shajiee and Tofighi 2019; Morais et al. 2020; Morais and Pasechnik 2020) (although some could come without collider traces, Ashoorioon and Konstandin 2009), some having been discussed in the context of LIGO (Balazs et al. 2017), or doublet(s) (Fromme et al. 2006; Dorsch et al. 2013, 2014; Laine et al. 2017; Wang et al. 2020b; Zhou and Bian 2022) (see also Fujikura et al. 2018 for an example from twin Higgs models),

[14] The figure assumes that the SGWB hints arising in the present PTA analyses, are not of primordial origin. The energy scales detectable by LISA result broader than in Fig. 7 since scenarios with the SGWB frequency outside the LISA band can still fulfil the SNR >10 requirement; see Figueroa et al. (2018), Megias et al. (2020) for details.

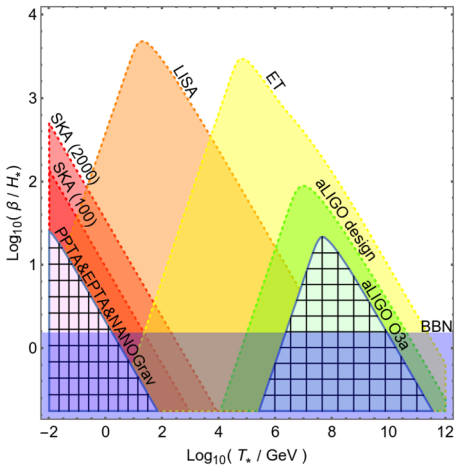

Fig. 8 The parameter reach of present and future GW observational network for phase transitions in a runaway-like regime with $v_w \simeq 1$ and $\alpha \gg 1$. In each shaded area the corresponding experiment (see labels) detects the FOPT signal with SNR >10. The region labelled BBN, PTA and aLIGO O3 are ruled out. Image adapted from Figueroa et al. (2018), Megias et al. (2020)

composite Higgs models (Chala et al. 2016; Bruggisser et al. 2018b; De Curtis et al. 2019; Bian et al. 2019; Xie et al. 2020), so-called fermionic extensions of the SM involving for example $SU(2)_L$ doublet and/or two $SU(2)_L$ singlet vector-like leptons strongly coupled to the Higgs boson (Angelescu and Huang 2019) or the various supersymmetric extensions of the SM (Davies et al. 1996; Apreda et al. 2002; Huber and Konstandin 2008b; Huang et al. 2015; Kozaczuk et al. 2015; Huber et al. 2016; Demidov et al. 2018).

There is also a wealth of theoretical BSM setups in which a FOPT can occur at a higher energy scale than the EW energy scale. These setups for example encompass extensions of the scalar sector (Jinno et al. 2016; Alanne et al. 2020; Baldes and Servant 2018), classical conformal approaches (Brdar et al. 2019b) or nearly conformally invariant field theories in which the generation of neutrino masses is linked to spontaneous scale symmetry breaking (Agashe et al. 2020), gauge extensions of the SM such as models including $U(1)_{B-L}$ (Madge and Schwaller 2019; Ellis et al. 2019c; Hasegawa et al. 2019; Dev et al. 2019; Bian et al. 2020; Ellis et al. 2019a, 2020c), left-right symmetries (Brdar et al. 2019a; Fornal 2021) or even mbigger symmetries (Huang and Zhang 2019), grand unified theories, non-supersymmetric (Croon et al. 2019a; Huang et al. 2020; Buchmüller et al. 2020a; Corianò et al. 2020; Okada et al. 2021) or supersymmetric (Haba and Yamada 2020), extra-dimension models and in particular the one including warped spacetimes (Randall and Sundrum 1999; Goldberger and Wise 1999; Rattazzi and Zaffaroni 2001; Creminelli et al. 2002; Garriga and Pomarol 2003; Randall and Servant 2007; Nardini et al. 2007; Konstandin et al. 2010; Konstandin and Servant 2011a; Bunk et al. 2018; Megías et al. 2018a, b) (often coming together with a stabilisation mechanism such as the Goldberger–Wise mechanism (Goldberger and Wise 1999) and holographic duals of the Composite Higgs models mentioned above) or gauge-Higgs unification approaches (Adachi et al. 2020).

Many of these BSM models are being explored at current particle colliders such as the LHC. Searches performed at the LHC experiments such as ATLAS and CMS

using the data from Run1 and Run2 did not find any evidence for BSM signals and have allowed one to put constraints on masses and couplings of their corresponding predicted new particles.

These BSM models could possibly be further explored at future colliders such as the high-luminosity phase of the LHC or the Future Circular Collider,[15] either by direct detection of new particles or due to their impact on precision measurements of many observables, such as masses and couplings in the different SM sectors (scalar, gauge or fermionic). Still, most models have parameter space corners which will remain inaccessible to present and near-future colliders, but whose early universe dynamics results in GWs detectable by LISA. Figure 9 illustrates this complementarity in a singlet extension, showing the values of α and β/H_* for different parameter points and their prospective detection by LISA and HL-LHC.

Another exciting possibility of complementary observations comes from astrophysics and more specifically gamma ray observations. These are connected with intergalactic magnetic fields, as the latter would lead to pair production $\gamma + \mathbf{B} \to e^+e^-$ followed by scattering of the charged particles off the magnetic field: $e^\pm + \mathbf{B} \to e^\pm + \gamma$, to produce a secondary γ. This process leads to a dilution of the spectra observed from distant blazars, which recently enabled a lower bound on the magnitude of intergalactic magnetic fields (Tavecchio et al. 2010; Ando and Kusenko 2010; Neronov and Vovk 2010; Essey et al. 2011; Chen et al. 2015; Ackermann et al. 2018). Due to the lack of astrophysical processes to account for magnetic fields in intergalactic voids, explanations through a primordial origin have been put forward. One possibility is inflationary magnetogenesis (Turner and Widrow 1988; Ratra 1992; Martin and Yokoyama 2008; Kobayashi 2014) although it has been pointed out recently that models where magnetic fields are produced before the EWPT generically lead to problems with baryon isocurvature constraints (Kamada et al. 2021). Another interesting possibility involves a FOPT (Vachaspati 1991; Sigl et al. 1997; Tevzadze et al. 2012). While there are many differences between the magnetic fields produced by both scenarios, notably involving the uncertainty of their evolution after the transition (Durrer and Neronov 2013), the magnetic field is governed by the same basic parameters as the GW signal. In particular this means that the transition in question has to be strong enough to produce a magnetic field amplitude above the known lower bounds. This, of course, leads to a certain correlation between the two possible signals, and it was found that the parameter space predicting a GW signal observable by LISA can also facilitate generation of a magnetic field strong enough to explain the observed diffusion of the blazar spectra for some models predicting a first order EWPT (Ellis et al. 2019a). Moreover, the presence of helicity in the magnetic fields produced at a FOPT plays a crucial role on its dynamical evolution, playing a crucial role in the resulting restrictions on the strength of the FOPT (Brandenburg et al. 2017, 2019), as well as providing circularly polarised SGWB. Such polarisation can also be measured by LISA providing a distinct signal of this scenario (Ellis et al. 2020a; Domcke et al. 2020b).[16]

[15] Although many of them can be elusive to collider physics (Addazi et al. 2019).

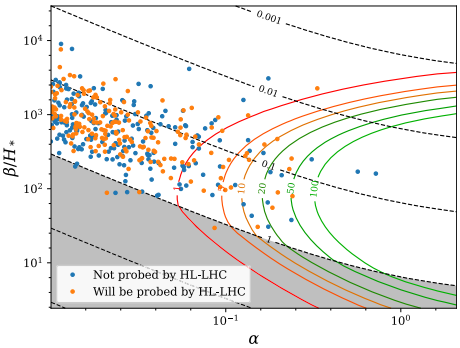

Fig. 9 Typical values of α and β/H_* for the general singlet model, superimposed with LISA SNR curves for $T_* = 50$ GeV (solid lines). The models in blue (orange) are unlikely (likely) to be probed by the high-luminosity LHC. The dotted straight lines are the contours of the fluid turnover time quantifying the effect of turbulence. In the grey shaded region the decay of sound waves into turbulence is less important than the Hubble damping and the SNR curve reflects this effect. Image reproduced with permission from Caprini et al. (2020), copyright by IOP/SISSA

7 Cosmic strings

Section coordinators: M. Lewicki, L. Sousa. Contributors: P. Auclair, J.J. Blanco-Pillado, C-F. Chang, Y. Cui, D.G. Figueroa, A. Jenkins, S. Kuroyanagi, M. Lewicki, M. Sakellariadou, K. Schmitz, L. Sousa, D. Steer, J. Wachter.

7.1 Introduction

Cosmic defects are stable energy configurations that can be formed in early universe phase transitions, usually due to a spontaneous symmetry-breaking process driven by some scalar field(s) acquiring a non-zero expectation value within a (topologically non-trivial) vacuum manifold. If the symmetry broken is global, all non-constant field configurations produce energy-momentum, and are loosely referred to as *global defects*. When the broken symmetry is gauged, we speak of *local defects* instead. Here we will focus on cosmic strings, which correspond to stable one-dimensional defect solutions of field theories (Nielsen and Olesen 1973), independently of whether they are global or gauge. Alternatively, cosmic strings can also be identified with cosmologically stretched fundamental strings from String Theory, formed e.g. at the end of brane inflation (Dvali and Vilenkin 2004; Copeland et al. 2004).

The energy per unit length of a string is $\mu \sim \eta^2$, with η a characteristic energy scale. The string tension, at least for the simplest cases, is typically of order μ. In the case of topological strings, η represents the energy scale of the phase transition. A network of strings formed in the early universe emits GWs throughout most of the history of the universe, generating a SGWB from the superposition of many

[16] Other proposed measures for detecting magnetic helicity in voids involve exploring the twisting of photon paths coming from multiple blazar sources (Vachaspati 2021; Tashiro and Vachaspati 2015; Kahniashvili and Vachaspati 2006).

uncorrelated emissions. Here we forecast the constraints that LISA may put on the dimensionless combination

$$G\mu \sim 10^{-6}\left(\frac{\eta}{10^{16}\ \mathrm{GeV}}\right)^2, \tag{46}$$

where $G = 1/M_p^2$ is Newton's constant, and $M_p = 1.22 \times 10^{19}$ GeV the Planck mass. We note that various potential observational signatures of cosmic string networks, other than GW emission, have been discussed in the literature. These include anisotropies in the CMB (Ade et al. 2014; Charnock et al. 2016; Lizarraga et al. 2016; Ringeval 2010), lensing events (Vilenkin 1984; Bloomfield and Chernoff 2014), and cosmic ray emission (Brandenberger 1987; Srednicki and Theisen 1987; Bhattacharjee et al. 1992; Damour and Vilenkin 1997; Wichoski et al. 2002; Peloso and Sorbo 2003; Sabancilar 2010; Vachaspati 2010; Long et al. 2014). (see Hindmarsh and Kibble 1995; Vilenkin and Shellard 2000; Sakellariadou 2007; Vachaspati et al. 2015 for a review.) Currently, CMB data from the Planck Satellite (Ade et al. 2014) imply $G\mu < 10^{-7}$ for NG, Abelian-Higgs, and semi-local strings. The most stringent bounds, however, come from searches for the SGWB, with PTA constraining $G\mu$ for NG strings to be $G\mu \lesssim 10^{-11}$ (Blanco-Pillado et al. 2018a; Ringeval and Suyama 2017), and LIGO-Virgo observations constraining it to be as low as $G\mu < 2 \times 10^{-14}$, depending on the string network model (Abbott et al. 2019c, 2018a). As we will show, LISA will be sensitive to string tensions with $G\mu \gtrsim 10^{-17}$ for NG strings, improving current upper bounds by ~ 10 orders of magnitude relative to CMB constraints, by ~ 6 orders of magnitude relative to current PTA constraints, and even by ~ 3 orders of magnitude relative to future constraints from next generation of PTA experiments. One important caveat is that these predictions do not include the impact the astrophysical background of GWs. Boileau et al. (2022) shows that, depending on different assumptions on the galactic and extragalactic astrophysical foregrounds, the forecast sensitivity of LISA should be reduced to roughly $G\mu \gtrsim \mathcal{O}(10^{-16} - 10^{-15})$. There is ongoing work in the consortium aimed at providing a refined pipeline for cosmic strings and sharpening these predictions.

As the characteristic width $\delta \sim 1/\eta$ of a cosmic string is much smaller than the size of the horizon, in the following we mainly assume that strings are well described by the NG action, which is the leading-order approximation when the curvature scale of the strings is much larger than their thickness. We refer to such strings as NG strings (we focus on string networks without junctions). Cosmic string networks are expected to reach an attractor solution known as *scaling*, for which the energy density of the network remains a fixed fraction of the background energy density in the universe. When strings within the network collide, they intercommute (i.e. "exchange partners") and reconnect after the collision (technically speaking this corresponds to an intercommutation probability $\mathcal{P} = 1$, which we mainly assume, though we will also comment briefly on the case $\mathcal{P} < 1$). As a result, loops are formed whenever a string self-intersects or two curved strings collide. Sub-horizon sized loops decouple from the cosmological evolution and oscillate under their own tension, emitting GWs in this process. The relativistic nature of the strings typically

leads them to form *cusps*, corresponding to points on the string momentarily moving at the speed of light (Turok 1984). Furthermore, intersections of strings will also generate discontinuities in their tangent vector known as *kinks*. Cusps and kinks generate GW burst emissions (Damour and Vilenkin 2000, 2001), which add up all throughout cosmic history to form a SGWB.

Besides sub-horizon loops, the network also contains long strings that that stretch across a Hubble volume. These are either infinite or super-horizon loops, and they are also expected to emit GWs. However, the dominant contribution is generically produced by the superposition of radiation from many sub-horizon loops along each line of sight.

Cosmic string networks are expected to create one of the largest SGWB of cosmological origin known. In the following we analyse the ability of LISA to probe the SGWB emitted by a network of cosmic strings, considering leading models of the string networks as described in the literature. The prospects for detection or, alternatively, for setting up new stringent constraints on string parameters, are very encouraging.

7.2 Network modelling

The SGWB generated by cosmic string networks in a given frequency f has, at the present time, contributions from all the loops created throughout the history of the universe that have emitted GWs that have a frequency f today. The number density $\mathsf{n}(l, t)$ of non-self-intersecting, sub-horizon, cosmic string loops of invariant length l at any cosmic time t is then the crucial ingredient in this computation. In this section, we review the models for the loop number density that have been proposed in the literature.

7.2.1 Model 1

We start by considering an analytical approach—originally developed in Kibble (1985) and later extended in Caldwell and Allen (1992), DePies and Hogan (2007), Sanidas et al. (2012), Sousa and Avelino (2013)—which is based on two assumptions. The first assumption is that the production of loops is the dominant energy-loss mechanism in the evolution of the long string network. In this case, as we shall see, the loop production function $f(l, t)\, dl$—which gives us the number density of loops of lengths between l and $l + dl$ produced per unit time and per unit volume—is determined by the large-scale evolution of the long string network. Here, we shall use the approach introduced in Sousa and Avelino (2013) and use the Velocity-dependent One-Scale model (Martins and Shellard 1996, 2002) to describe its evolution. This model provides an analytical description of the evolution of the characteristic length $L \equiv (\mu/\rho_\infty)^{1/2}$—where ρ_∞ is the energy density of the long string network—and of the root-mean-squared velocity $\bar{v}$ of the network (Martins and Shellard 1996, 2002):

$$\frac{d\bar{v}}{dt} = \left(1 - \bar{v}^2\right)\left[\frac{k(\bar{v})}{L} - 2H\bar{v}\right], \tag{47}$$

$$\frac{dL}{dt} = \left(1 + \bar{v}^2\right)HL + \frac{\tilde{c}}{2}\bar{v}, \tag{48}$$

with

$$k(\bar{v}) = \frac{2\sqrt{2}}{\pi}\left(1 - \bar{v}^2\right)\left(1 + 2\sqrt{2}\bar{v}^3\right)\frac{1 - 8\bar{v}^6}{1 + 8\bar{v}^6}. \tag{49}$$

The curvature parameter $k(\bar{v})$ accounts (to some extent) for the effects of small-scale structure (Martins and Shellard 2002).

Here, $\tilde{c}$ is a phenomenological parameter that quantifies the efficiency of the loop-chopping mechanism, that may be calibrated with simulations (for NG strings, $\tilde{c} = 0.23 \pm 0.04$ fits both radiation and matter era simulations (Martins and Shellard 2002)). Using Eq. (48), we find that the energy lost as a result of loop production is given by

$$\left.\frac{d\rho_\infty}{dt}\right|_{\text{loops}} = \tilde{c}\bar{v}\frac{\rho_\infty}{L} = \mu\int_0^\infty lf(l,t)dl, \tag{50}$$

and determines the normalisation of loop production function.

The second assumption of this model (which will be somewhat relaxed later) is that all the loops are created with a length l that is a fixed fraction of the characteristic length of the long string network: $l = \alpha_L L$, where $\alpha_L < 1$ is a (constant) free-parameter of the model. We then have

$$f(l,t) = \left(\frac{\mathcal{F}}{f_r}\right)\frac{\tilde{c}}{l}\frac{\bar{v}}{L^3}\delta(l - \alpha_L L), \tag{51}$$

where $\bar{v}$ and L are given by Eqs. (47) and (48). Here the normalisation of $f(l, t)$ is determined using Eq. (51), except for the correction factor f_r and $\mathcal{F}$. The first factor, $f_r \sim \sqrt{2}$, is introduced to account for the energy lost as a result of the redshifting of the peculiar velocities of loops (Vilenkin and Shellard 2000). Also, since in general we do not expect all loops to be created with exactly the same size but to follow a distribution of lengths, a second factor $\mathcal{F}$ is included to account for the effect of the spread of the distribution (see Sanidas et al. 2012; Sousa et al. 2020 for a detailed analysis of this effect.) For NG strings, $\mathcal{F}$ is estimated to be $\mathcal{O}(0.1)$ (Blanco-Pillado et al. 2014).

Note that Eq. (51) is valid throughout any cosmological era, even during the radiation-to-matter and matter-to-dark-energy transitions (in which the network is not in a linear scaling regime). As a result, it allows us to compute $f(l, t)$ through cosmic history in a realistic cosmological background (Sousa and Avelino 2013). The number density of loops $\mathsf{n}(l,t)$ at all times may then be found by solving

$$\mathsf{n}(l,t) = \int_{t_i}^{t} dt' f(l',t') \left(\frac{a(t')}{a(t)}\right)^3 , \tag{52}$$

while accounting for the decrease in the length of loops caused by the emission of GWs $l = l' + \Gamma G\mu\,(t' - t)$ (where Γ is a dimensionless constant characterising GW emission efficiency—that we define more precisely in Sect. 7.3—, l is the length of a loop created at a time t' with a length l' at a later time $t > t'$).

The loop-size parameter α_L may either be calibrated with numerical simulations (as we shall do in Sect. 7.4), but may be also be treated as a free parameter of the model to explore a wider variety of scenarios (as in Sect. 7.5.4). Although α_L is the natural parameter of this model, we will express our results in terms of $\alpha = \alpha_L \xi_r$ (where ξ_r is the value of L/t in the radiation era) in order to ease comparison with other loop distribution models.

7.2.2 Model 2

The second model we consider is a loop number density distribution, $\mathsf{n}(l,t)$, extracted from large scale numerical simulations of the string networks (Blanco-Pillado et al. 2014). These number densities were first obtained from the integration of the loop production function $f(l, t)$ of non-self-intersecting loops computed directly from the simulation. Recently, these loop number densities were also determined directly from simulations without the intermediate use of a loop production function (Blanco-Pillado and Olum 2020). Both approaches produce the same result.

In the following we give the resulting distributions for three types of loops: those created in the radiation era, emitting GWs in the radiation era; those created in the radiation era, emitting GWs in the matter era; and those created in the matter era, emitting GWs in the matter era.

With $\Omega_{\rm rad}$ the fraction of the critical density in radiation, and understanding the redshift z to be a function of time, we can write

$$\mathsf{n}_{\rm r,r}(l,t) = \frac{0.18}{t^{3/2}(1+\Gamma G\mu t)^{5/2}}\,\Theta(0.1 - l/t)\,, \tag{53a}$$

$$\mathsf{n}_{\rm r,m}(l,t) = \frac{0.18(2\sqrt{\Omega_{\rm rad}})^{3/2}(1+z)^3}{(l+\Gamma G\mu t)^{5/2}}\,\Theta(0.09\,t_{\rm eq}/t - \Gamma G\mu - l/t)\,, \tag{53b}$$

$$\mathsf{n}_{\rm m,m}(l,t) = \frac{0.27 - 0.45(l/t)^{0.31}}{t^2(l+\Gamma G\mu t)^2}\,\Theta(0.18 - l/t)\,, \tag{53c}$$

where $\Theta(x)$ is the Heaviside step function, and the subscript "r,m" indicates "loops produced in the (r)adiation era, emitting in the (m)atter era", and so on. For Eqs. (53a) and (53c), the cutoffs are due to the maximum size of loop which can be produced in these eras. For Eq. (53b), there is an additional term in the cutoff which models the decay due to GW emission; that is, a loop formed in the radiation era must have some minimum size in order to survive into the matter era. Equation (53)

contains all the information necessary to compute the SGWB due to decaying loops, as outlined in Sect. 7.3.

Analysis of Eq. (53c), in comparison to Eqs. (53a) and (53b), shows it to be negligible for $G\mu \lesssim 10^{-10}$ and thus for cosmic string tensions of interest to LISA. The cosmic string generated SGWB potentially to be observed by LISA will be for radiation-era loops, integrated up to the present. Of particular interest are radiation-era loops emitting in the matter era; these loops contribute to a "bump" in the SGWB spectrum which may, depending on $G\mu$, fall within the LISA band (see Sect. 7.4). For this particular reason, but also more broadly, it is important to understand how gravitational backreaction affects the evolution of loops. At present, the decay of loops into GWs is accounted for by $\Gamma G\mu$ terms, but this does not take into account potential changes to the loop population due to, e.g. loop fragmentation as a result of backreacted trajectories. While current theoretical studies (Blanco-Pillado et al. 2018b, 2019b), and numerical studies of simple models (Robbins and Olum 2019), suggest that the change to loop trajectories will be small, it is important to keep in mind that no current, simulation-inferred network model incorporates gravitational backreaction directly.

7.2.3 Model 3

The third model we consider is based on the analytical studies of the small-scale structure and the correlation functions of individual infinite strings (Dubath et al. 2008; Polchinski and Rocha 2007, 2006). This analysis predicts a power-law loop production function in terms of scaling units, whose slope is parametrised by a parameter χ linked to the fractal dimension of the strings. The production of cosmic string loops is suppressed by gravitational back-reaction, on scales below

$$\gamma_c = \Upsilon (G\mu)^{1+2\chi}, \tag{54}$$

in which $\Upsilon = \mathcal{O}(20)$. The characteristics of the loop production function were later inferred from measurements of the loop number density in large-scale simulations of NG strings (Ringeval et al. 2007; Lorenz et al. 2010).[17] The numerically inferred loop-production function is then extended from large scales down to the gravitational back-reaction scale, resulting in an extra population of small loops.

The loop number density of Model 3 can be approximated by the following expressions

[17] Note that the relationship between the loop number density and the loop production function is not always one-to-one, see Auclair et al. (2019) for a review.

$$t^4 \mathsf{n}_{\mathrm{r,r}}(l,t) = \begin{cases} \dfrac{0.08}{(\gamma + \Gamma G\mu)^{3-2\chi_{\mathrm{r}}}} & \text{if } \Gamma G\mu < \gamma \\ \dfrac{0.08(1/2 - 2\chi_{\mathrm{r}})}{(2-2\chi_{\mathrm{r}})\Gamma G\mu \gamma^{2-2\chi_{\mathrm{r}}}} & \text{if } \gamma_{\mathrm{c}} < \gamma < \Gamma G\mu \\ \dfrac{0.08(1/2 - 2\chi_{\mathrm{r}})}{(2-2\chi_{\mathrm{r}})\Gamma G\mu \gamma_c^{2-2\chi_{\mathrm{r}}}} & \text{if } \gamma < \gamma_{\mathrm{c}} \end{cases} \tag{55}$$

$$t^4 \mathsf{n}_{\mathrm{m,m}}(l,t) = \begin{cases} \dfrac{0.015}{(\gamma + \Gamma G\mu)^{3-2\chi_{\mathrm{m}}}} & \text{if } \Gamma G\mu < \gamma \\ \dfrac{0.015(1 - 2\chi_{\mathrm{m}})}{(2-2\chi_{\mathrm{m}})\Gamma G\mu \gamma^{2-2\chi_{\mathrm{m}}}} & \text{if } \gamma_{\mathrm{c}} < \gamma < \Gamma_{\mathrm{d}} G\mu \\ \dfrac{0.015(1 - 2\chi_{\mathrm{m}})}{(2-2\chi_{\mathrm{m}})\Gamma G\mu \gamma_c^{2-2\chi_{\mathrm{m}}}} & \text{if } \gamma < \gamma_{\mathrm{c}} \end{cases} \tag{56}$$

$$t^4 \mathsf{n}_{\mathrm{r,m}}(l,t) = \left(\frac{t}{t_{\mathrm{eq}}}\right)^4 \left(\frac{1+z}{1+z_{\mathrm{eq}}}\right)^3 t_{\mathrm{eq}}^4 \mathsf{n}_{\mathrm{rad}}^{(3)} \left[\frac{\gamma t + \Gamma_{\mathrm{d}} G\mu (t - t_{\mathrm{eq}})}{t_{\mathrm{eq}}}\right] \tag{57}$$

in which $(\chi_{\mathrm{r}}, \chi_{\mathrm{m}}) = (0.2, 0.295)$. This extra population of small loops dominates the SBGW in the high frequency spectrum as discussed in Abbott et al. (2018a), Auclair et al. (2020), Abbott et al. (2021b) and hence can lead to very different constraints on $G\mu$ to that of the two above-mentioned models. The energy density of these small loops is very large and the question of energy balance, in the context of the one-scale model, has been raised in Blanco-Pillado et al. (2019a).

7.2.4 Field theory

The above modellings are all based on NG strings, which are infinitely thin. Cosmic strings appear however naturally as solitonic solutions of classical field theory models (Nielsen and Olesen 1973), so in principle they can decay not only by GW radiation but also directly into excitations of their elementary constituents. For example, it has been observed with numerical simulations that global (axionic) strings decay into the massless Goldstone modes present in the vacuum of the theory (Davis and Shellard 1989). For local strings with no long-range interactions, the excitations in the vacuum are however massive, and hence are naturally expected to be suppressed for long wavelengths comparable to the length of the strings (Martins et al. 2004; Olum and Blanco-Pillado 2000, 1999). Furthermore, recent simulations of individual loops in the Abelian-Higgs model (Matsunami et al. 2019) report that extrapolating their results to large loop sizes, the GW emission should be expected to dominate over particle emission for loops larger than a certain critical length scale.

In contrast, large-scale field theory simulations of Abelian-Higgs strings (Vincent et al. 1998; Hindmarsh et al. 2009; Daverio et al. 2016; Hindmarsh et al. 2017b) observe that the network of long strings reaches a scaling regime, thanks to energy loss into classical radiation of the scalar and gauge fields involved. As a consequence of this, sub-horizon loops formed during the network evolution decay very promptly.

This intriguing discrepancy has been under debate for over twenty years, but the origin of this radiation is not currently understood.

The similarities and differences between field theory and NG simulations of string networks can then be summarised as follows: the infinite strings are rather similar in curvature radius and length density, but loops decay into field modes in the field theory simulations. In field theory simulations, the string energy density goes into radiated modes of the fields, which do not belong to the string network anymore. As a consequence, the string loops decay within a Hubble time, and hence do not continue to contribute as a source of GWs. In the NG picture, this channel does not exist, and instead the energy of the infinite strings goes into loops, which then decay via GWs. Our analysis in the following is mostly based on the NG classical evolution of strings. We assume, as supported by NG simulations, that loops are formed throughout cosmic history, and they decay into GWs. Our discussion about the ability of LISA to measure a GW background from cosmic strings is therefore based on this fundamental assumption.

7.3 Computation of the gravitational-wave spectrum from loops

The incoherent superposition of GWs emitted from oscillating cosmic string loops leads to a SGWB. The calculation of the SGWB from the cosmic string networks have been widely studied in the literature (Vachaspati and Vilenkin 1985; Blanco-Pillado et al. 2014; Blanco-Pillado and Olum 2017; Blanco-Pillado et al. 2018a; Ringeval and Suyama 2017; Vilenkin 1981; Hogan and Rees 1984; Accetta and Krauss 1989; Bennett and Bouchet 1991; Caldwell and Allen 1992; Siemens et al. 2007; DePies and Hogan 2007; Olmez et al. 2010; Sanidas et al. 2012, 2013; Binetruy et al. 2012; Kuroyanagi et al. 2012, 2013; Sousa and Avelino 2013, 2014; Cui et al. 2019; Chang and Cui 2020; Jenkins and Sakellariadou 2018; Gouttenoire et al. 2020a). The generic form of a GW spectrum in logarithmic intervals of frequency, introduced in Eq. (29), also applies to the case with cosmic strings. For the cosmic string application, Eq. (29) is implemented by integrating over the GW emission from all the loops throughout cosmic history that contribute to a certain frequency.[18] In the following subsections, we review two methods of calculating SGWB from string loops that have been developed in the literature along with recent updates. There are ingredients that are common to both approaches. The first ingredient is $\mathsf{n}(l,t)$, the number density of non-self-intersecting, sub-horizon, cosmic string loops of invariant length l at cosmic time t, As shown in Sect. 7.2, $\mathsf{n}(l,t)$ can be estimated by analytical or simulation-based methods. Another characteristic function is the gravitational loop power spectrum $P_{\rm GW}(f,l)$, which may be determined as an average based on simulations, or approximated by focusing on the analytical high-frequency behaviour of particular events on the strings, e.g. cusps and kinks.

[18] We neglect the GW contribution from long (horizon-spanning) strings as being subdominant to the GW contribution from loops for NG strings. See Buchmüller et al. (2013), Matsui and Kuroyanagi (2019).

7.3.1 Method I

The first method to calculate $\Omega_{\rm GW}(t_0,f)$ (Vachaspati and Vilenkin 1985; Blanco-Pillado et al. 2014; Blanco-Pillado and Olum 2017; Blanco-Pillado et al. 2018a; Caldwell and Allen 1992; Siemens et al. 2007; DePies and Hogan 2007; Olmez et al. 2010; Kuroyanagi et al. 2012, 2013; Sousa and Avelino 2013; Cui et al. 2019) assumes that $P_{\rm GW}(f,l)$ takes the form of

$$P_{\rm GW}(f,l) = G\mu^2 l P(fl), \tag{58}$$

where $P(f, l)$ is an averaged function that can be computed from an ensemble of loops of length l (but of different shapes) based on simulations.

Integrating all emissions throughout the history of the universe and taking into account the redshift effects, the GW energy density for a particular frequency f as measured today is

$$\frac{d\rho_{\rm GW}}{df}(t_0,f) = G\mu^2 \int_0^{t_0} dt \left(\frac{a(t)}{a_0}\right)^4 \int_0^{\infty} dl\, l\, \mathsf{n}(l,t) P\left(\frac{a_0}{a(t)} fl\right). \tag{59}$$

The GW radiation power of an isolated loop of length l can be computed using the standard formulae in the weak gravity regime (Vachaspati and Vilenkin 1985; Vilenkin and Vachaspati 1987; Garfinkle and Vachaspati 1987). As a simple approximation, we assume that the loops evolve in flat space in a periodic manner, and thus emit GW at discrete frequencies

$$\omega_n = 2\pi n/T, \tag{60}$$

where $T = l/2$ is the oscillation period, and the harmonic modes $n = 1, 2, \ldots$. As a consequence, we replace $P(fl)$ by P_n, a discrete function of the harmonic mode number. For an individual loop, a simple (monochromatic) power spectrum can be obtained assuming the emission is dominated by specific events (e.g. cusps, kinks) (Vachaspati and Vilenkin 1985; Burden 1985; Garfinkle and Vachaspati 1987; Binetruy et al. 2009)

$$P_n = \frac{\Gamma}{\zeta(q)} n^{-q}, \tag{61}$$

where $\zeta(q)$ is Riemann zeta function and $\Gamma = \sum_{n=1}^{\infty} P_n$ is the total power of emission, which is found to be highly peaked around $\Gamma \sim 50$ (Blanco-Pillado et al. 2015, 2014; Blanco-Pillado and Olum 2017; Wachter and Olum 2017; Blanco-Pillado et al. 2018b; Chernoff et al. 2019; Blanco-Pillado et al. 2019b). The power law parameter q is 4/3, 5/3, or 2 for GW emissions dominated by cusps, kinks, or kink-kink collisions, respectively.[19] With this method, the GW energy density today can be calculated by summing over loop harmonic modes (Blanco-Pillado and Olum 2017; Blanco-Pillado et al. 2014).

[19] We should keep in mind that the these simple power laws may not be a good approximation at low n. In this case, the entire loop's structure becomes important.

$$\frac{d\rho_{\rm GW}}{df}(t_0,f) = G\mu^2 \sum_{n=1}^{\infty} C_n(f) P_n, \tag{62}$$

where

$$C_n(f) = \frac{2n}{f^2} \int_0^{\infty} \frac{dz}{H(z)(1+z)^4} \mathsf{n}\left(\frac{2n}{(1+z)f}, t(z)\right). \tag{63}$$

Note that in practice, only a finite number of modes need to be included in calculations, but the necessary number of modes to ensure a good convergence for a reliable result depends on the background cosmology. For standard cosmology $\Omega_{\rm GW}(t_0,f)$ converges by summing over $10^3 - 10^5$ modes (depending on the value of q) (Sanidas et al. 2012). However, recent studies (Cui et al. 2020; Gouttenoire et al. 2020a; Blasi et al. 2020) demonstrated that more than 10^5 modes may be necessary to ensure a convergence to the correct power law at high frequency. For instance, in the presence of an early matter dominated era, summing over a small number of modes gives f^{-1} at high f while an $f^{-1/3}$ relation emerges with higher modes included.

7.3.2 Method II

The second method analytically estimates $P_{\rm GW}(f,l)$ based on unresolved burst events on the strings (Ringeval and Suyama 2017; Abbott et al. 2018a; Siemens et al. 2007; DePies and Hogan 2007; Kuroyanagi et al. 2012, 2013; Jenkins and Sakellariadou 2018; Auclair et al. 2020). The cosmic string GW emission may be dominated by cusps, kinks, or kink-kink collisions. The contribution to the SGWB from unresolved bursts is given by

$$\frac{d\rho_{\rm GW}}{df}(t_0,f) = f^2 \int_{z_{\rm min}}^{\infty} dz \int_0^{\infty} dl\, h^2(l,z,f) \frac{d^2R(z,l)}{dzdl}, \tag{64}$$

where $\frac{d^2R(z,l)}{dzdl}$ denotes the burst rate per unit loop length l and per unit redshift z which is proportional to $\mathsf{n}(l,t)$. $z_{\rm min}$ will be defined shortly. The amplitude $h(l, z, f)$ is the Fourier transform of the waveform of the bursts (Siemens et al. 2007; Damour and Vilenkin 2000, 2001; Binetruy et al. 2009) and reads

$$h(l,z,f) = A_q(l,z) f^{-q}, \tag{65}$$

with

$$A_q(l,z) = g_1^{(q)} \frac{G\mu H_0 l^{2-q}}{(1+z)^{q-1}\varphi_r(z)}, \quad \varphi_r(z) \equiv H_0 \int_0^z \frac{dz'}{H(z')} dz. \tag{66}$$

Again the power q is equal to 4/3, 5/3 and 2 for cusps, kinks and kink-kink collisions, respectively. The calibration constant $g_1^{(q)}$ accounts for loop geometry effects on different bursts. Since the cusps and kinks radiate non-isotropically, the above

waveform is only valid for directions near the cusp or kink direction. A cutoff angle $\theta_{\rm cutoff}$ is thus introduced to account for the geometric beaming effect:

$$\theta_{\rm cutoff}(l,z,f) = \left(\frac{1}{g_2 f(1+z)l}\right)^{1/3}, \tag{67}$$

with $g_2 = \frac{\sqrt{3}}{4}$. The burst rate is then given by (Damour and Vilenkin 2000, 2001; Olmez et al. 2010)

$$\frac{d^2R(z,l)}{dzdl} = 2\frac{4\pi\varphi_r^2(z)}{(1+z)^3 H(z) H_0^2}\left(\frac{\mathsf{n}(l,t(z))}{l(1+z)}\right)\Delta(l,z,f)\,, \tag{68}$$

where the quantity

$$\Delta(l,z,f) \simeq \left(\frac{\theta_{\rm cutoff}(l,z,f)}{2}\right)^{3(2-q)} \Theta(1-\theta_{\rm cutoff}(l,z,f)), \tag{69}$$

represents the fraction of observable bursts (Olmez et al. 2010).

Earlier burst events that cannot be resolved at a GW detector thereby contribute to a SGWB. Integrating over z and l, the spectrum due to a given type of burst is

$$\Omega_{\rm GW}(f) = \frac{\left(g_1^{(q)}\right)^2 g_2^{q-2}}{2^{4-3q}}\frac{N_q}{3}\frac{(G\mu)^2}{H_0^2}(2\pi f)^3 \int_0^\infty dx \int_{z_{\rm min}(x,f)}^\infty dz \frac{(ft(x))^{-2-q}}{(1+z)^{4+q}} x^{1-q}\frac{\mathsf{n}(x)}{H(z)}, \tag{70}$$

where $x \equiv l/t$, $z_{\rm min}$ is the solution to $\theta_{\rm cutoff}(l, z_{\rm min}, f) = 1$, and $N_q \sim \mathcal{O}(1)$ is the average number of bursts per oscillation in a loop (Ringeval and Suyama 2017; Jenkins and Sakellariadou 2018; Abbott et al. 2018a). An alternative calculation of $\Omega_{\rm GW}(f)$ by integrating over z, h is shown in Cui et al. (2020).

More recent bursts of large amplitude could be resolved individually and thus detected as transient events by GW detectors, which is a different type of signal relative to a SGWB. If a burst is to be resolved in a given frequency band f, it must produce a strain greater than the experimental sensitivity $h > h_{\rm exp}$ with rate less than f. The rate of such events is (Siemens et al. 2006; Auclair et al. 2020)

$$R_{\rm exp}(f) = \int_0^{z_*} dz \int_{\max(h_{\rm min},h_{\rm exp})}^{h_{\rm max}} dh\, \frac{d^2R}{dz\,dh}(h,z,f), \tag{71}$$

where z_* enforces the rate condition and is given by

$$f = \int_0^{z_*} dz \int_{h_{\rm min}}^{h_{\rm max}} dh\, \frac{d^2R}{dz\,dh}(h,z,f). \tag{72}$$

For a given cosmic string model, the SGWB channel is usually more sensitive than individual bursts, providing stronger constraints on parameters such as $G\mu$ (Abbott et al. 2018a). Nevertheless in certain motivated scenarios, such as string formation

before or during inflation, a SGWB could be suppressed and burst events would become the leading channel for discovery (Cui et al. 2020).

In addition to the Gaussian SGWB and the resolvable burst events as discussed above, an unresolved string signal from a set of infrequent bursts at low redshift $z \ll 1$ emits a distinct non-Gaussian and non-continuous popcorn-like signal. This effect is negligible on the current pulsar timing limit $G\mu < 10^{-11}$Regimbau et al. (2012), Olmez et al. (2010), and has no effect on the SGWB that is emitted from a large loop size $\alpha \sim 0.1$ (Blanco-Pillado and Olum 2017; Siemens et al. 2007; Olmez et al. 2010; Binetruy et al. 2012). However, if the burst occurs in our neighbourhood with strong amplitude, then GW detectors may be able to identify the signal (Chernoff and Tye 2018; Helfer et al. 2019). Such a coherent signal may provide a complementary detection mechanism: cosmic strings may generate a non-negligible amount of GW memory (Aurrekoetxea et al. 2020) that would not be captured by SGWB probes (Jenkins and Sakellariadou 2021).

7.3.3 Templates for the stochastic gravitational-wave background generated by cosmic string loops

Models 1 and 2 An analytical approximation for the contribution of each of three loop populations—loops that decay in the radiation era, radiation-era loops that survive into the matter era, and loops created in the matter era—to the SGWB was derived in Sousa et al. (2020). Therein, they found that radiation-era loops give rise to a SGWB of the form

$$\Omega^r_{\rm GW}(f) = \frac{128}{9}\pi A_r \Omega_r \frac{G\mu}{\epsilon_r}\left[\left(\frac{f(1+\epsilon_r)}{B_r\Omega_m/\Omega_r + f}\right)^{3/2} - 1\right], \tag{73}$$

where we have defined $\epsilon_r = \alpha/(\Gamma G\mu)$ and

$$A_i = \frac{\tilde{c}}{\sqrt{2}}\mathcal{F}\frac{v_i}{\xi_i^3} \quad \text{and} \quad B_i = \frac{2H_0\Omega_i^{1/2}}{v_i\Gamma G\mu}, \tag{74}$$

and where the labels $i = r, m$ are used to refer to the values of the corresponding variables in the radiation and matter eras, respectively. In the radiation era, we have $v_r = 1/2$, $\xi_r = 0.271$, $v_r = 0.662$ and $A_r = 5.4\mathcal{F}$. This contribution dominates the high-frequency region of the SGWB spectrum (for $f \gg B_r\Omega_m/\Omega_r$), giving rise to a plateau of amplitude

$$\Omega^{\rm plateau}_{\rm GW} h^2 = \frac{128}{9}\pi A_r \Omega_{\rm rad} h^2 \frac{G\mu}{\epsilon_r}\left[(\epsilon_r+1)^{3/2} - 1\right] \simeq 1.02\times 10^{-2}\frac{G\mu}{\epsilon_r}\left[(\epsilon_r+1)^{3/2} - 1\right]. \tag{75}$$

The contribution of the loops that are created in the radiation era but survive into the matter era is of the form

$$\Omega_{\rm GW}^{rm}(f) = 32\sqrt{3}\pi(\Omega_m\Omega_r)^{3/4}H_0\frac{A_r}{\Gamma}\frac{(\epsilon_r+1)^{3/2}}{f^{1/2}\epsilon_r}\left\{\frac{\left(\frac{\Omega_m}{\Omega_r}\right)^{1/4}}{\left(B_m\left(\frac{\Omega_m}{\Omega_r}\right)^{1/2}+f\right)^{1/2}}\left[2+\frac{f}{B_m\left(\frac{\Omega_m}{\Omega_r}\right)^{1/2}+f}\right]\right.$$
$$\left.-\frac{1}{(B_m+f)^{1/2}}\left[2+\frac{f}{B_m+f}\right]\right\}, \tag{76}$$

and gives rise to a peak in the low-frequency portion of the spectrum (for $f \ll B_r\Omega_m/\Omega_r$).

Matter-era loops also give rise to a peak-like contribution in the same frequency range, albeit with a different shape:

$$\Omega_{\rm GW}^{m}(f) = 54\pi H_0\Omega_m^{3/2}\frac{A_m}{\Gamma}\frac{\epsilon_m+1}{\epsilon_m}\frac{B_m}{f}\left\{\frac{2B_m+f}{B_m(B_m+f)}-\frac{1}{f}\frac{2\epsilon_m+1}{\epsilon_m(\epsilon_m+1)}+\frac{2}{f}\log\left(\frac{\epsilon_m+1}{\epsilon_m}\frac{B_m}{B_m+f}\right)\right\}, \tag{77}$$

where $\epsilon_m = \epsilon_r\xi_m/\xi_r$ and we have $\nu_m = 2/3$, $\xi_m = 0.625$, $\nu_m = 0.583$ and $A_m = 0.39\mathcal{F}$. The shape of the SGWB generated by cosmic string loops in this frequency range is then determined by the interplay between these two contributions. For larger values of α, $\Omega_{\rm GW}^{rm}$ dominates, although its relative importance decreases as α decreases (since $\Omega_{\rm GW}^{rm} \sim \alpha^{1/2}$). So, for small enough α, the contribution of matter-era loops dominates the SGWB spectrum in the low-frequency range.

It was demonstrated in Sousa et al. (2020) that the SGWB is well described by an approximation of the form

$$\Omega_{\rm GW}(f) = \Omega_{\rm GW}^{r}(f) + \Omega_{\rm GW}^{rm}(f) + \Omega_{\rm GW}^{m}(f) \tag{78}$$

for $\alpha \gtrsim \Gamma G\mu$ and $f < 3.5\times10^{10}/(1+\epsilon_r)$ Hz (larger frequencies are outside the sensitivity windows of the current major GW experiments; see however (Sousa et al. 2020) for a description of how to extend these results for larger frequencies). For $\alpha \lesssim \Gamma G\mu$, loops survive significantly less than a Hubble time and decay effectively immediately on cosmological times scales. In this case, no loops produced in the radiation era are expected to survive into the matter era and, as a result, the contribution $\Omega_{\rm GW}^{rm}$ should be switched off. However, for small enough α (i.e. $\alpha \lesssim 0.1\Gamma G\mu$), this approximation further simplifies to (Sousa and Avelino 2014; Sousa et al. 2020)

$$\Omega_{\rm GW}(f) = \frac{64\pi}{3}G\mu\Omega_r A_r + 54\pi\frac{H_0\Omega_m^{3/2}}{\epsilon_m\Gamma}\frac{A_m}{f}\left[1-\frac{B_m}{\epsilon_m}\frac{1}{f}\right]. \tag{79}$$

Note that, since Model 1 may be calibrated to describe Model 2 (Auclair et al. 2020), Eq. (78) can also be used as a template for this model by setting $\mathcal{F} = 0.1$ and $\alpha = 0.1$.[20] Note also that, although these approximations only provide a description of the SGWB generated by the fundamental mode of emission, one may use it to

[20] As discussed in Sect. 7.2.2, for $G\mu \lesssim 10^{-10}$, the contribution from matter-era loops $\Omega_{\rm GW}^{m}$ is negligible and does not need to be included.

construct an analytical approximation up to an arbitrary number of modes of emission n_* for any q using

$$\Omega_{\rm GW}(f,q,n_*) = \sum_{j=1}^{n_*} \frac{j^{-q}}{\mathcal{E}} \Omega_{\rm GW}(f/j), \tag{80}$$

with $\mathcal{E} = \sum_m^{n_*} m^{-q}$ (Fig. 10).

Model 3 A first review of the SGWB of Model 3 was conducted in Ringeval and Suyama (2017), and we present below analytical approximations derived in Auclair et al. (2020). The loop distribution of Model 3 is similar on large scales to the two above-mentioned models, but is also characterised by an extra population of small loops with invariant lengths smaller than $\Gamma G\mu t$. This extra population is treated separated from the rest of the loop distribution resulting in five contributions, i.e. the extra populations of small loops emitting GWs either during the radiation era or the matter era, and the three populations mentioned in the previous section.

The contribution from radiation-era loops is given by

$$\Omega_{\rm GW}^{r} = \frac{64\pi C_r \Omega_r}{3\Gamma(2-2\chi_r)} (\Gamma G\mu)^{2\chi_r} \left(1 + \frac{4H_r(1+z_{\rm eq})}{f\Gamma G\mu}\right)^{2\chi_r - 2}, \tag{81}$$

where $C_r = 0.08$ and $\chi_r = 0.2$. This formula is characterised by a plateau at high frequency. The loops produced during radiation-era that survive during matter era also contribute to the SGWB

$$\begin{aligned}\Omega_{\rm GW}^{rm} = &\frac{54\pi C_r H_m \Omega_m}{\Gamma f (\Gamma G\mu)^{1-2\chi_r}} (1+z_{\rm eq})^{3(2\chi_r-1)/2} \\ &\left[\frac{x^{2-6\chi_r}}{2-6\chi_r} {}_2F_1(3-2\chi_r, 2-6\chi_r; 3-6\chi_r; -\frac{3H_m x}{f\Gamma G\mu})\right]_1^{\sqrt{1+z_{\rm eq}}}.\end{aligned} \tag{82}$$

Matter-era loops give rise to a SGWB given by

$$\begin{aligned}\Omega_{\rm GW}^{m} = &\frac{2\times 3^{2\chi_m} \pi C_m \Omega_m}{H_m^{2-2\chi_m} \Gamma f^{2\chi_m - 2}} (\Gamma G\mu)^2 \\ &\left[\frac{x^{2\chi_m - 4}}{2\chi_m - 4} {}_2F_1(3-2\chi_m, 4-2\chi_m; 5-2\chi_m; -\frac{f\Gamma G\mu}{3H_m x})\right]_1^{\sqrt{1+z_{\rm eq}}},\end{aligned} \tag{83}$$

where $C_m = 0.015$ and $\chi_m = 0.295$, and ${}_2F_1$ is the Gauss hypergeometric function.

The extra population of small loops plays an important role in determining the SGWB, particularly at high frequencies. Due to their small size ($<\Gamma G\mu t$) their contribution is cutoff at low frequencies and their lifetime is too short for them to survive from the radiation-era to the matter-era. The contribution of the extra population of small loops emitting GWs during the radiation era is given by the piece-wise formula

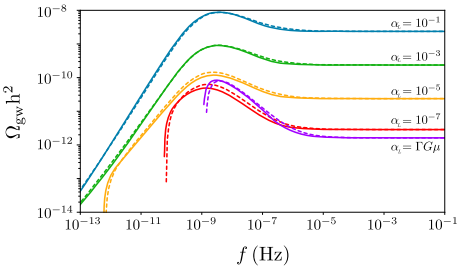

Fig. 10 Analytical approximation to the SGWB generated by cosmic string networks with $G\mu = 10^{-10}$ and different values of α for Model 1. The solid lines represent the approximation to the SGWB in Eq. (78), while the dashed lines correspond to the SGWB obtained numerically. Image reproduced with permission from Sousa et al. (2020)

$$\Omega_{\rm GW}^{r,\rm epsl} = \frac{64\pi C_r \Omega_r (1/2 - 2\chi_r)}{3(1-2\chi_r)(2-2\chi_r)} G\mu \gamma_c^{2\chi_r - 1} \times \begin{cases} 0 & \text{if } f < 4(1+z_{\rm eq}) H_r (\Gamma G\mu)^{-1} \\ \left[4(1+z_{\rm eq})H_r/(\gamma_c f)\right]^{2\chi_r-1} - (\Gamma G\mu/\gamma_c)^{2\chi_r-1} & \text{if } f < 4(1+z_{\rm eq})H_r\gamma_c^{-1} \\ (2-2\chi_r) - 4(1+z_{\rm eq})H_r(1-2\chi_r)/(\gamma_c f) - (\Gamma G\mu/\gamma_c)^{2\chi_r-1} & \text{if } f > 4(1+z_{\rm eq})H_r\gamma_c^{-1} \end{cases} \tag{84}$$

and the contribution of the extra population of small loops emitting GWs during the matter era is given by the piece-wise formula

$$\Omega_{\rm GW}^{m,\rm epsl} = \frac{54\pi C_m H_m \Omega_m (1-2\chi_m)}{(3-2\chi_m)(2-2\chi_m) f} G\mu \gamma_c^{2\chi_m - 2} \left(\frac{3H_m}{\gamma_c f}\right) \times \begin{cases} 0 & \text{if } f < 4H_m (\Gamma G\mu)^{-1} \\ \left[\frac{3H_m}{\gamma_c f}\right]^{2\chi_m-3} \left\{1 - [3H_m/(\Gamma G\mu f)]^{3-2\chi_m}\right\} & \text{if } f < 4H_m\sqrt{1+z_{\rm eq}}(\Gamma G\mu)^{-1} \\ \left[\frac{3H_m}{\gamma_c f}\right]^{2\chi_m-3} \left[1 - (1+z_{\rm eq})^{-(3-2\chi_m)/2}\right] & \text{if } f < 4H_m\gamma_c^{-1} \\ (3-2\chi_m) f\gamma_c/(3H_m) + (2\chi_m - 2) - \left(\frac{f\gamma_c}{3H_m\sqrt{1+z_{\rm eq}}}\right)^{3-2\chi_m} & \text{if } f < 4H_m\sqrt{1+z_{\rm eq}}\gamma_c^{-1} \\ \left[\frac{3H_m}{\gamma_c f}\right]^{-1} (3-2\chi_m)\left[1 - (1+z_{\rm eq})^{-1/2}\right] & \text{if } f > 4H_m\sqrt{1+z_{\rm eq}}\gamma_c^{-1} \end{cases}. \tag{85}$$

Similarly to the previous section, these approximations assume that the GW are emitted by the fundamental mode, ie. by the oscillations of the loop. One can use Eq. (80) to construct predictions with an arbitrary number of modes (Fig. 11).

7.4 LISA detection prospects

Searches by current GW experiments (by LIGO/VIRGO and PTAs) on power spectra of the form $\Omega_{\rm GW}(f) = Af^n$ have provided upper bounds on the amplitude A for different fixed values of the spectral index n (Abbott et al. 2019c; Lentati et al. 2015;

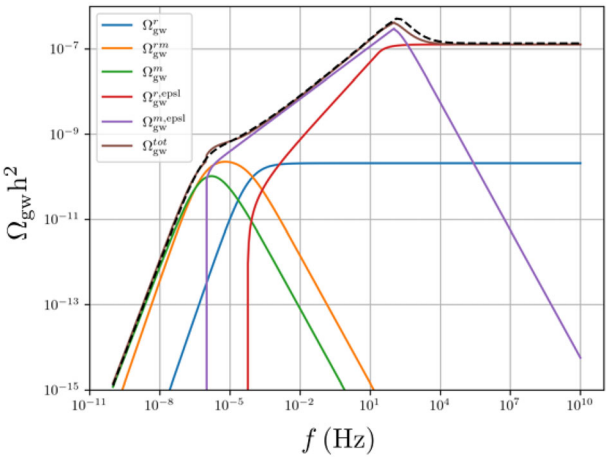

Fig. 11 Figure to demonstrate the validity of the templates for Model III. The dark dashed line is the result from numerical integration with only the fundamental mode and $G(z) = 1$

Arzoumanian et al. 2018). Very recently, the NANOGrav and EPTA collaborations have even reported an excess that might be due to a SGWB signal (Arzoumanian et al. 2020; Chen et al. 2021b), although the origin is still uncertain. As no statistical significant evidence of the expected quadrupolar spatial correlations has been found, the detected signal can still be ascribed to some unknown systematics. More data is needed in order to discern whether this signal is a real SGWB or not, and if it is, whether it is due to BSM scenarios (Ellis and Lewicki 2021; De Luca et al. 2021b; Neronov et al. 2021) or to astrophysics (Sesana 2016).

The PLS curve (Thrane and Romano 2013) is a useful construction that graphically quantifies the ability of a detector to measure a SGWB with a spectrum characterised by a power-law in frequency (the extension to a generic frequency-dependence of the signal is discussed in Sect. 9). Specifically, we use the LISA PLS as introduced by Thrane and Romano (2013), but using the most updated LISA sensitivity curves based on the final configuration of LISA and new knowledge of its noise. (see LISA 2023 for all current LISA documentation.)

Claiming detection of a given SGWB from cosmic string loops (say for a given tension and other fixed string network parameters), can be roughly interpreted as the detection of the signal after 3 years of accumulated data (corresponding to 4 years of LISA operation), with a SNR ≥ 10. Since the shape can be more complicated than a simple power law, a more elaborated analysis following (Caprini et al. 2019; Flauger et al. 2021) is required to assess the SNR for a given detection, see also Karnesis et al. (2020). Here, for the moment, we simply quantify the parameter space compatible with a detection, without quantifying the SNR associated to such a detection. We do not reconstruct such parameter space with appropriate statistical techniques, though such work is already in the pipeline of coming work from the LISA collaboration.

In Figs. 12 and 13, we present numerical results for the SGWB generated by cosmic string loops, in a standard cosmological background. The LISA band is well

suited to set strong constraints on the string tension, thanks to the natural shift of the "bump" in the SGWB to larger frequencies as $G\mu$ decreases. This effect can be clearly seen in these figures, where we show a sequence of SGWB spectra over the LISA PLS, as we vary the string tension. We can find in this way the lowest $G\mu$ for which an intersection between the SGWB spectrum and the PLS still takes place. While the exact bound depends on our choice of model and P_n, in the regime LISA will probe, all three models—Model 2 and Model 3, as well as Model 1 (when calibrated to describe NG simulations by setting $\alpha = 0.1$ and $\mathcal{F} = 0.1$)—predict a string tension bound of $\mathcal{O}(10^{-17})$. We note that the trailing edge of the bump of the SGWB (that scales as $\Omega_{\rm GW} \propto f^{3/2}$) will be the last part of the spectrum to pass through the LISA sensitivity band.

Note also that for string tensions $G\mu > 10^{-16}$, LISA will probe the high-frequency side of the SGWB bump, the particular shape of which depends on how the number of particle degrees of freedom change across the universe history. This is relevant because while the three models predict roughly equal lower bounds for the LISA window, Models 1 and 2 disagree with Model 3 at high frequencies. These discrepant regions will pass through the LISA band and hence, in the event of a detection, we could discern among the different models.

7.4.1 Anisotropies in the stochastic gravitational-wave background

GW sources with an inhomogeneous spatial distribution would lead to anisotropies in the SGWB, in addition to the anisotropies induced by the nature of spacetime along the line of propagation of GWs. The formalism (Jenkins and Sakellariadou 2018) to study anisotropies induced by the distribution of string loops was consequently applied for the string distribution of Models 2 and 3. It has been shown that the

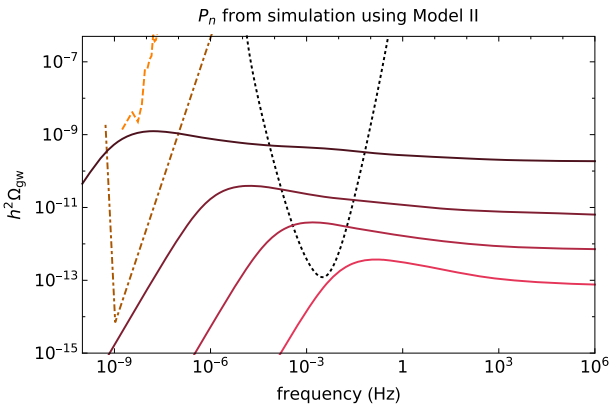

Fig. 12 Solid red curves show cosmic string SGWB curves for a range of $G\mu$ values. From the darkest most high up line to the lightest lowest one these read: $G\mu = 10^{-10}$, $G\mu = 10^{-13}$, $G\mu = 10^{-15}$ and $G\mu = 10^{-17}$. The P_n used in computation of these spectra was inferred from simulations (Blanco-Pillado and Olum 2017), and the loop number density is from Model 2. The dashed orange curve shows the sensitivity of EPTA. The dark orange dash-dotted line shows the projected SKA sensitivity. The dotted black line shows the LISA PLS of SNR = 10

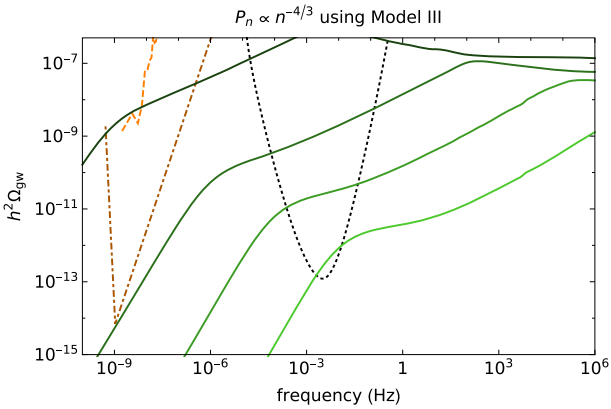

Fig. 13 Identical to Fig. 12, however, $P_n \propto n^{-4/3}$ and using the loop number density from Model 3 (Lorenz et al. 2010)

angular spectrum of the 2-point correlator is relatively insensitive to the particular choice of the string loop model: regardless of the model, the anisotropies are driven by local Poisson fluctuations in the number of loops, and the resulting angular power spectrum is spectrally white (i.e. $C_\ell =$ constant with respect to ℓ) (Jenkins and Sakellariadou 2018).

In Fig. 14 we show the amplitude of the SGWB angular power spectrum for models 2 and 3 as a function of $G\mu$. We also include Model 1 with a small value of the initial loop size α, as this has been studied in the literature as a source of significant anisotropies in the PTA frequency band (Kuroyanagi et al. 2017). We find that, regardless of the loop model and the string tension, the predicted C_ℓ spectrum is unfortunately far too small to be detected with LISA.

7.5 Extended and alternative considerations

In the previous sections we focused on GW signals from cosmic string loops in most conventional scenarios, i.e. NG strings evolving in the standard cosmology background with particle content of the SM. Nevertheless there are well motivated variations encoding new physics that can lead to subtle or dramatic deviations to the standard prediction of string SGWB spectra that we have demonstrated. In this section we review a few representative cases. We will start with the fact that long strings also radiate a SGWB that add up to the previously discussed SGWB from loops. We will also consider cosmic string scenarios with different loop sizes and forecast the parameter space available for exploration with LISA. We will then move on to the possible signals from networks of cosmic strings formed during a global symmetry breaking which as we will see are quite distinct as then particle production and not GW production becomes the dominant emission mode. Next we will turn to cosmic strings emerging from superstring theory and in particular the possibility of smaller reconnection probability they can feature. We finally consider the case of metastable cosmic strings.

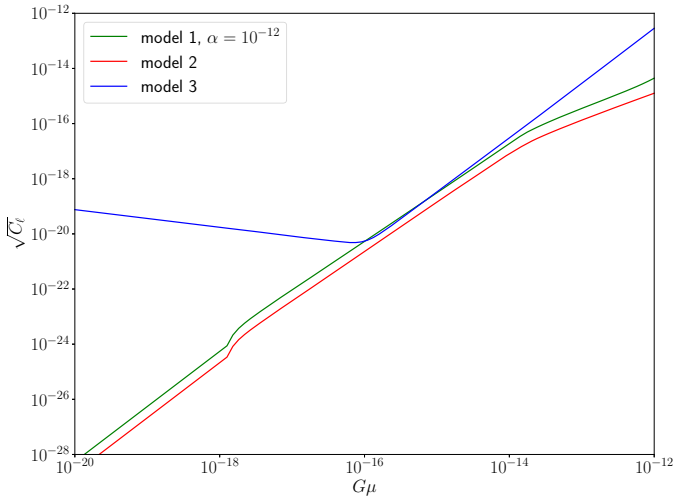

Fig. 14 Amplitude of the SGWB anisotropies for different cosmic string network models, as a function of the string tension. We use a representative LISA-band GW frequency of 1 mHz. Note that the spectra here are not normalised with respect to the monopole, so $\sqrt{C_\ell}$ is proportional to $\Omega_{\rm GW}$. We note that the angular spectrum is constant with respect to ℓ, since the anisotropies are driven by local Poisson fluctuations in the number of loops

Another key aspect is that the general broad band nature of cosmic strings SGWB enables *cosmic archaeology* which would allow us to probe the expansion history prior to BBN as well as new particles beyond the SM that are difficult to access by other means. We will not cover this method here, instead referring the interested reader to Sect. 9 where methods of probing the expansion history are discussed and specifically to its Sect. 9.2.3 dealing with cosmic strings.

7.5.1 Long strings

We have focused so far on the GW emission by sub-horizon size string loops. Long strings, however, either infinite or super-horizon loops, emit also GWs. One contribution to this signal originates due to the relativistic motion of the long strings, as the network energy-momentum tensor adapts itself to maintain scaling during cosmic evolution. As a result, an emission of GWs sourced by the anisotropic stress of the network, takes place around the horizon scale at every moment (Krauss 1992; Jones-Smith et al. 2008; Fenu et al. 2009; Figueroa et al. 2013). This SGWB background is actually expected to be emitted by any scaling network of cosmic defects, independently of the topology and origin of the defects (Figueroa et al. 2013). It represents an *irreducible background* generated by any defect network (that has reached scaling). For NG cosmic string networks, such irreducible background represents however a sub-dominant signal compared to the background emitted from the loops discussed before. In the case of field-theory string networks (for which simulations to date indicate the absence of "stable" loops (Vincent et al. 1998;

Hindmarsh et al. 2009; Daverio et al. 2016; Hindmarsh et al. 2017b, 2021)), it is instead the dominant GW signal emitted by the network.

The energy density spectrum of this irreducible SGWB from long strings is predicted to be scale-invariant for the modes emitted during radiation domination (RD) (Figueroa et al. 2013). The amplitude of the background depends on the fine details of the so called *unequal-time-correlator* of the network's energy-momentum tensor, which can be only accurately obtained from very large scale lattice simulations of defect networks. In the case of global defects, the scale-invariant GW power spectrum has been analytically estimated in Jones-Smith et al. (2008), Fenu et al. (2009). The amplitude of the spectrum plateau for global strings has been recently calibrated in lattice field theory simulations (Figueroa et al. 2020), obtaining

$$h_0^2\Omega_{\rm GW}^{(0)} \simeq 3.13 \cdot 10^{-13} \left(\frac{G\mu}{10^{-6}}\right)^2. \tag{86}$$

Using the latest Planck CMB constraints (Lopez-Eiguren et al. 2017), Figueroa et al. (2020) finds that the amplitude of the plateau satisfies

$$h^2\Omega_{\rm GW}^{(0)} < 9.7 \cdot 10^{-15}, \tag{87}$$

with the number in the right hand side of the inequality corresponding to the amplitude when the CMB bound $10^{12}(G\mu)^2 \leq 0.031$ is saturated. The amplitude in Eq. (87) is larger, for instance, than the maximum amplitude expected (as bounded by current CMB constraints (Ade et al. 2021)) for the quasi-scale invariant GW background in slow-roll inflation (Caprini and Figueroa 2018), $h_0^2\Omega_{\rm GW}^{(\rm inf)} \lesssim 10^{-16}$. It is however, still too small to be observed by LISA, and it is clearly subdominant when compared to the amplitude of the dominant GW signal from the long lived NG loops, which scales as $(G\mu)^{1/2}$.

One can also consider the contribution to the GW spectrum coming from the accumulation of small-scale structure on long strings. These kinks are the product of the multiple intercommutations that infinite strings suffer over the course of their cosmological evolution, and were noticed early on in numerical simulation of cosmic networks (Bennett and Bouchet 1988; Sakellariadou and Vilenkin 1990). The emission of GW from individual infinite strings modulated by kinks has been calculated in Sakellariadou (1990), Hindmarsh (1990). Using these results, one can also compute the spectrum produced by these kinks on a network assuming the simple model in which their characteristic scale is given by αt. At high frequencies one can then estimate that the radiation-era plateau of this contribution should be (Vilenkin and Shellard 2000)

$$h^2\Omega_{\rm GW} \simeq \frac{128\pi^2}{3\xi^2\alpha}\, h^2\Omega_{\rm rad}(G\mu)^2, \tag{88}$$

which, for $\alpha \approx 0.1$ and $\xi_{\rm r} = 0.271$, shows a rough agreement with the value obtained from field theory simulations. On the other hand, recently, Matsui and Kuroyanagi (2019) has calculated the GW spectrum produced by kink-kink collisions on long strings, and found that the amplitude is larger than in previous estimates. This is

because the characteristic scale α turns out to be much smaller than 0.1 according to their semi-analytic estimation of the kink number distribution.

7.5.2 Agnostic approach to loop size

In Sect. 7.4, we have analyzed the detection prospects for NG strings using either Model 1 (calibrated to NG simulations) or simulation-inferred Models 2 and 3. Here, we extend the analysis a bit further, by using Model 1 to study scenarios with different loop sizes. As we have seen in Sect. 7.3.3, although the typical shape of the SGWB spectrum generated by cosmic strings is roughly independent of α, the amplitude of the radiation-era plateau and the characteristics of the peak—its shape, height and broadness—are highly dependent on the size of loops. As a matter of fact, the amplitude of the spectrum generally decreases with decreasing α and, therefore, LISA should, in general, be less sensitive to scenarios in which loops are created with a smaller size.

The $(\alpha, G\mu)$ parameter space available for exploration with LISA—which we plot in Fig. 15—is characterized in Auclair et al. (2020). This analysis finds that LISA should be able to probe about 16 orders of magnitude in loop size and, thus, it will have a good capability to detect string models that deviate from the standard NG scenario. Note, however, that the projected constraints on cosmic string tension are also less stringent as the loop size decreases. Nevertheless, LISA shall be able (conservatively) to probe cosmic string scenarios in which loop production is significant up to tensions

$$G\mu < 8 \times 10^{-12}, \tag{89}$$

independently of loop size (Auclair et al. 2020). This corresponds to an improvement of almost 5 order of magnitude over current equivalent constraints (Sanidas et al.

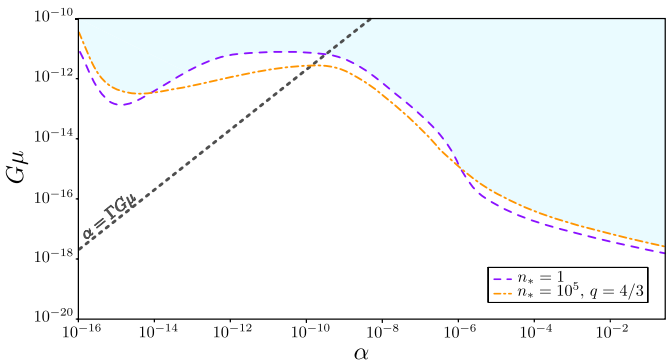

Fig. 15 Projected constraints on $G\mu$ of the LISA mission for cosmic string scenarios characterised by different loop-size parameter α for $n_* = 1$ (dashed line) and $n_* = 10^5$, with $q = 4/3$ (dash-dotted line). The shaded area corresponds to the region of the $(\alpha, G\mu)$ parameter space that will be fully available for exploration with LISA. The dotted line corresponds to scenarios for which $\alpha = \Gamma G\mu$, so that the region above this line corresponds to cosmic string models in which loops are small, while the region bellow corresponds to the large loop regime. Image reproduced with permission from Auclair et al. (2020), copyright by IOP/SISSA

2012) and of more than 2 orders of magnitude over the projected SKA constraints (Sanidas et al. 2013).

7.5.3 Global strings

Global cosmic strings are generically predicted in BSM frameworks with e.g. a post-inflationary global U(1) symmetry breaking which may be associated to axion-like DM. The GW emission from global strings have been less actively studied than that from NG strings, with only few papers having addressed an explicit computation of the SGWB from global/axion strings (see Jones-Smith et al. 2008; Fenu et al. 2009; Giblin et al. 2012; Figueroa et al. 2013; Chang and Cui 2020; Gouttenoire et al. 2020a; Figueroa et al. 2020; Gorghetto et al. 2021). Studying this topic is however particularly timely given the increasing interest in axion DM. In the following we review the semi-analytical approach taken in the recent work (Chang and Cui 2020).

The approach taken in Chang and Cui (2020) systematically follows a similar procedure as for NG strings which is reviewed in Sect. 7.2.1 but there are a few key differences for global strings. First, global strings have a time-dependent string tension (Copeland et al. 1990; Dabholkar and Quashnock 1990; Vilenkin and Shellard 2000)

$$\mu(t) = 2\pi\eta^2 \ln(L/\delta) \equiv 2\pi\eta^2 N, \tag{90}$$

where $L \simeq H^{-1}\xi^{-1}$ is the string correlation length, ξ is the number of long strings per horizon volume, $\delta \simeq 1/\eta$ is the string thickness, and $N \equiv \ln(L/\delta) \simeq \ln(\eta\xi^{-1}t)$ is time-dependent. Once reaching the scaling regime, the long string energy density evolves as

$$\rho_\infty = \xi(t)\frac{\mu(t)}{t^2}, \tag{91}$$

where $\xi(t)$ quickly approaches a constant for NG strings, yet needs to be determined for global strings. In addition, global string loops have an additional significant decay channel, through Goldstone emission. Taking these into account, the evolution equations of a global string network are as follows based on a Velocity-dependent One-Scale model (Martins 2019; Vilenkin and Shellard 2000):

$$\left(2 - \frac{1}{N}\right)\frac{dL}{dt} = 2HL\left(1 + v^2\right) + cv + \sigma\frac{v}{N}, \quad \frac{dv}{dt} = \left(1 - v^2\right)\left[\frac{k}{L} - 2Hv\right], \tag{92}$$

where $k \sim 0.28$ is a momentum parameter, $v \sim 0.57$ is the averaged long string velocity, $c \sim 0.5$ is the loop chopping parameter and $\sigma \sim 5.83$ is the Golstone radiation parameter. These values are obtained (Chang and Cui 2020) from recent simulation results (Gorghetto et al. 2018; Kawasaki et al. 2018; Hindmarsh et al. 2020; Klaer and Moore 2017).

As presented in Eq. (90), reliable numerical simulations of global string networks require a huge scale separation in string length $L \propto 1/H(t)$ and core width δ. Thus the global string simulation is much more challenging. Nevertheless, it has seen rapid

development in recent years (Gorghetto et al. 2018; Kawasaki et al. 2018; Hindmarsh et al. 2020; Klaer and Moore 2017; Buschmann et al. 2020; Figueroa et al. 2020), while uncertainties remain to be resolved with future higher resolution simulations. Due to the lack of dedicated simulation results for global string loop distribution at formation time, a reasonable benchmark inspired by Model 2 for the NG case is considered while the effects of alternative possibilities of loop distribution are discussed in Chang and Cui (2020).

Once formed, a loop oscillates and loses energy by the rate (Vilenkin and Vachaspati 1987; Battye and Shellard 1996, 1994; Vilenkin and Shellard 2000)

$$dE/dt = -\Gamma G\mu^2 - \Gamma_a \eta^2, \tag{93}$$

where the right hand side represents GW and Goldstone radiation in order. Studies show that $\Gamma \simeq 50$ (Vilenkin 1981; Blanco-Pillado et al. 2011, 2014; Blanco-Pillado and Olum 2017), $\Gamma_a \simeq 65$ (Vilenkin and Shellard 2000). Consequently the length of a loop after its formation time t_i would evolve as

$$\ell(t) \simeq \alpha t_i - \Gamma G\mu(t - t_i) - \kappa(t - t_i), \tag{94}$$

where $\kappa \equiv \Gamma_a/(2\pi N)$. The SGWB from global strings can be computed following the similar procedure of computing the SGWB for NG strings while taking into account these distinctions. Figure 16 illustrates the results with varying symmetry breaking scale η, assuming standard cosmic history, with the NG string GW spectra shown in contrast. As can be seen, the global string amplitudes are more sensitive to scale η, i.e. $\Omega_{\rm GW}^{\rm global} \propto \eta^4$ and the NG string $\Omega_{\rm GW}^{\rm NG} \propto \eta$. The spectrum falls off at $f \sim \frac{1}{t_0} \sim 10^{-17}$ Hz due to the last GW emissions, today. Meanwhile, in the late matter domination period, it follows the frequency dependence $\Omega_{\rm GW}^{\rm global}(f) \propto f^{-1/3}$ for summation of higher oscillation normal modes $n \gg 10^5$ as demonstrated in very recent studies (Cui et al. 2020; Blasi et al. 2020). Then, at $f \sim 10^{-8}$ Hz, the logarithmic time dependence of μ made a gradually, logarithmically declining plateau towards high f on the GW spectrum, instead of a large plateau in NG strings in RD period.

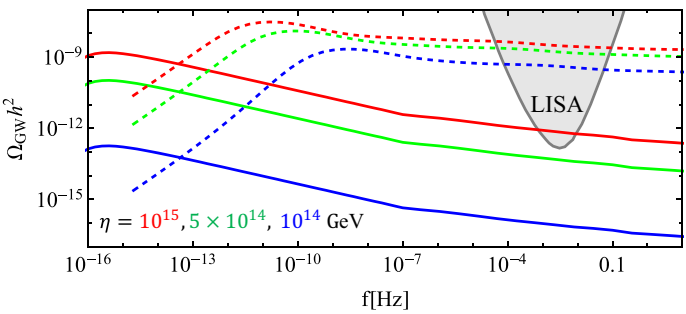

Fig. 16 SGWB spectrum from a global (solid) and gauge (dashed) string network in standard cosmology with loop length parameter $\alpha = 0.1$, and symmetry breaking scale $\eta = 10^{15}, 5\times10^{14}, 10^{14}$ GeV for red, green, blue, respectively. The grey region is the LISA sensitivity

In very recent simulation studies (Saurabh et al. 2020), they have concluded that the global string loop lifetime is of the order the loop initial length $l \sim \alpha t$ which is in a good agreement with the prediction of Eq. (94) by energy conservation. However, the amplitude of the SGWB from large-scale simulations of global string networks from Figueroa et al. (2020), Figueroa et al. (2013), c.f. Eqs. (86) and (87), obtain an amplitude of the SGWB notably smaller than the above semi-analytical prediction. More work is therefore needed, with further investigation and improvements on both global string simulation and analytical analysis, in order to understand the origin of this discrepancy.

7.5.4 Cosmic superstrings

Several brane-inflationary scenarios predict the copious production of cosmic superstrings (see e.g. Copeland et al. 2004; Dvali et al. 2001; Jones et al. 2003): fundamental strings—or F-strings—and 1-dimensional Dirichlet branes—or D-strings—that grow to macroscopic sizes and play the cosmological role of cosmic strings. These cosmic superstrings, as a result of their quantum nature, do not always exchange partners when they collide: strings may simply pass through each other without intercommutation. In other words, the probability of intercommutation $\mathcal{P}$ is —unlike that of ordinary strings (Shellard 1987; Verbiest and Achucarro 2011)— smaller than 1. In fact, it was shown that $10^{-3} \lesssim \mathcal{P} \lesssim 1$ in collisions between F-strings and $10^{-1} \lesssim \mathcal{P} \lesssim 1$ for D-string collisions (Jackson et al. 2005).

Cosmic superstring networks are then expected to lose energy less efficiently and, consequently, to be significantly denser than networks of ordinary cosmic strings and to generate a SGWB with a higher amplitude as a result. As a matter of fact, the loop-chopping parameter—which quantifies the energy that is lost in the form of loops—is expected to be such that $\tilde{c} \propto \mathcal{P}^{\gamma}$, where $\gamma > 0$.[21] For such weakly interacting networks, with $\tilde{c} \ll 1$, the amplitude of the SGWB is expected to roughly scale as (Avelino and Sousa 2012; Sousa and Avelino 2016)

$$\Omega_{\rm GW} \propto \tilde{c}^{-2} \propto \mathcal{P}^{-2\gamma}. \tag{95}$$

The constraints on $G\mu$ derived on the previous sections for $\mathcal{P} = 1$ are then conservative for cosmic superstrings: for $\mathcal{P} < 1$ the bounds should necessarily be tighter.

Note, however, that the length of loops produced by cosmic superstring networks is not known, since the precise number density of loops was not yet measured in simulations.[22] Nevertheless, conservative "α-independent" constraints on cosmic superstring tension—obtained using the radiation-era plateau of the SGWB generated by small loops—can be derived. In fact, LISA will be able to probe cosmic strings up

[21] The exact value of the exponent γ is still a matter of debate—$\gamma = 1/2$ was observed in NG simulations in Minkowski space (Sakellariadou 2005) and $\gamma = 1/3$ in both radiation- and matter-era simulations (Avgoustidis and Shellard 2006)—and, thus, here we discuss the effects of $\mathcal{P}$ (mostly) qualitatively.

[22] There is some evidence that the reduction of the intercommuting probability is more efficient in suppressing the production of large loops than that of small loops (Avgoustidis and Shellard 2006), which seems to indicate that smaller α ($\sim \Gamma G\mu$) may be favoured for these networks.

to a tension of $G\mu \sim 10^{-12}, 10^{-13}, 10^{-14}$, for $\mathcal{P} = 10^{-1}, 10^{-2}, 10^{-3}$ respectively (Auclair et al. 2020).[23]

Note also that there are relevant aspects of cosmic superstring dynamics that were not taken into account when deriving these constraints. In particular, when superstrings of different types collide, they are expected to bind together to create a (heavier) third type of string. This is expected to lead to networks with junctions and a hierarchy of tensions—whose dynamics differ from that of ordinary string networks (Copeland et al. 2004, 2006a, 2007, 2008; Avgoustidis and Shellard 2008; Rajantie et al. 2007; Sakellariadou and Stoica 2008; Avgoustidis and Copeland 2010; Avgoustidis et al. 2015) – and to have an impact on the shape and amplitude of the SGWB (Pourtsidou et al. 2011; Sousa and Avelino 2016). Moreover, there are several other important aspects regarding the GW emission by cosmic superstrings that need to be clarified—most notably the number and strength of the cusps (Elghozi et al. 2014) as well as the possible coupling of superstrings to other fields—before a detailed study of the parameter space available to LISA can be performed.

7.5.5 Metastable strings

Up to this point, the discussion in this section focused on stable cosmic strings, i.e. cosmic superstrings or strings whose stability is protected by the nontrivial vacuum topology in the underlying field theory. However, in certain scenarios, cosmic strings can become metastable, with important implications for the expected signal in GWs. In the following, we will discuss metastable strings in models with an enlarged gauge group at higher energies, as they often arise in the context of grand unified theories. For other models resulting in cosmic strings with a finite lifetime, see e.g. Kamada and Yamada (2015b), Kamada and Yamada (2015a), Bettoni et al. (2019).

Consider a $U(1)$ model giving rise to cosmic strings and its embedding in a gauge group G with symmetry breaking pattern $G \to H' \times U(1) \to H$. The second symmetry breaking step will still produce cosmic strings as before. However, if G and H are such that the vacuum manifold of the broken subgroup G/H is simply connected, these cosmic strings are metastable, i.e. classically stable, but quantum mechanically unstable against the nonperturbative Schwinger production of monopole–antimonopole pairs (Vilenkin 1982; Preskill and Vilenkin 1993; Martin and Vilenkin 1996, 1997). These monopoles are the topological defects associated with the first symmetry breaking step, $G \to H' \times U(1)$. They nucleate along the strings, such that the network breaks apart into individual string segments with a monopole on the one end and an antimonopole on the other end. These dumbbell-like objects (Nambu 1977) keep losing energy via the emission of GWs, until the defect network has fully disappeared. This late-time contribution to the GW spectrum requires further investigation. In the following, we will neglect it and focus on the emission of GWs from string loops prior to their decay.

Models based on the symmetry breaking pattern $G \to H' \times U(1) \to H$ have recently been investigated in Buchmüller et al. (2020a), Buchmüller et al. (2020b),

[23] For larger loop sizes, the strength of the constraints may increase by up to 6 orders of magnitude (Auclair et al. 2020).

Buchmüller (2021). While Buchmüller et al. (2020a), Buchmüller et al. (2020b) consider the breaking chain $SO(10) \to G_{\rm SM} \times U(1)_{B-L} \to G_{\rm SM}$, with $G_{\rm SM}$ denoting the SM gauge group, Buchmüller (2021) studies the breaking of $G = SU(2)_R \times U(1)_{B-L}$ in an extended electroweak sector down to the hypercharge group $H = U(1)_Y$ via $H' = U(1)_R \subset SU(2)_R$. In both cases, $U(1)_{B-L}$ is the Abelian gauge symmetry associated with baryon-minus-lepton number, $B-L$, and both models thus predict the production of a network of metastable cosmic $B-L$ strings.[24]

The lifetime of the collapsing string network is controlled by the monopole–antimonopole nucleation rate per unit length (Leblond et al. 2009) (see also Monin and Voloshin 2008),

$$\Gamma_d = \frac{\mu}{2\pi}\, e^{-\pi\kappa}, \quad \kappa = \frac{m^2}{\mu}, \tag{96}$$

where μ denotes the cosmic string tension and m is the mass of the monopoles nucleating on the string. The parameter κ can, at least in principle, be calculated in terms of the parameters of the grand unified theory model; see Buchmüller (2021) for an example. The string network then decays around a redshift z_d, which can be estimated by equating the decay rate of an average-sized string with the expansion rate (Buchmüller et al. 2020a; Leblond et al. 2009),

$$z_d \simeq 8.4 \left(\Gamma G\mu \frac{\Gamma_d}{H_0^2} \right)^{1/4}. \tag{97}$$

Here, $\Gamma \sim 50$ is defined in Eq. (61) and H_0 is the present-day Hubble parameter. In order to compute the SGWB signal from the collapsing string network, the lower boundary in the redshift integral in Eq. (63) needs to be replaced by z_d. Fixing $G\mu = 2 \times 10^{-7}$, this results in the GW spectra shown in the left panel of Fig. 17. These spectra saturate the CMB bound on $G\mu$ and are close to the sensitivity reach of existing ground-based interferometers; see the right panel of Fig. 17. At high frequencies, the SGWB signal exhibits the usual plateau, while going to lower frequencies, it decays in proportion to $f^{3/2}$. For $\sqrt{\kappa} \lesssim 6$, the string network is only short-lived, such that the signal dies off at frequencies above the LISA band, whereas for $\sqrt{\kappa} \gtrsim 8$, LISA will not be able to distinguish the signal from a standard string signal. In this case LISA will be able to access $G\mu$ values that would otherwise be excluded by PTA measurements. A LISA detection of a standard string signal at $G\mu$ in excess of current PTA bounds would therefore point to metastable strings with $\sqrt{\kappa} \lesssim 8$. In fact, values of $\sqrt{\kappa} \simeq 8$ are probed by existing PTA observations (Buchmüller et al. 2020b). Even larger values of $\sqrt{\kappa}$ can leave an imprint in CMB spectral distortions (Kite et al. 2021). The most interesting value from the perspective of LISA is $\sqrt{\kappa} \sim 7$, which can be easily achieved in realistic models (Buchmüller 2021). For $\sqrt{\kappa} \sim 7$, LISA will see the turnover in the spectrum caused by the collapse of the

[24] Both models also predict the production of a monopole gas during the first symmetry breaking step. These monopoles are, however, diluted by a stage of inflation preceding the production of the metastable string network and are hence irrelevant.

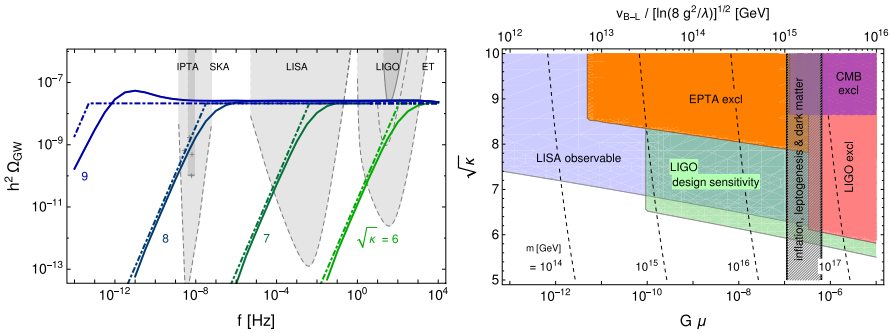

Fig. 17 Left panel: SGWB signals from a metastable string network for $G\mu = 2 \times 10^{-7}$ and $\alpha = 0.1$, for different values of $\sqrt{\kappa}$; see Eq. (96). The solid lines represent the numerical result, the dashed lines show the analytical approximation in terms of a flat plateau at high frequencies and an $f^{3/2}$ rise at low frequencies. Right panel: Existing and future constraints on the metastable string parameter space. The hashed vertical band marks the prediction of the $U(1)_{B-L}$ model in Buchmüller et al. (2020a), where both plots appeared for the first time. Copyright by the author(s)

string network and hence uncover valuable information on new physics close to the energy scale of grand unification.

8 Inflation

Section coordinators: E. Dimastrogiovanni. Contributors: D. Comelli, E. Dimastrogiovanni, M. Fasiello, D.G. Figueroa, J. Fumagalli, L. Iacconi, A. Malhotra, S. Matarrese, A. Mazumdar, L. Pilo, S. Renaux-Petel, A. Ricciardone, R. Rollo, G. Tasinato, V. Vennin, D. Wands, L. Witkowski.

8.1 Introduction

Can LISA detect GWs produced at the time of the big bang? This section aims to investigate such a possibility focusing on cosmic inflation.

Inflation is the leading paradigm for describing the very early phases of cosmic expansion. Furthermore, it offers a mechanism for GW production that can be probed with GW experiments. The inflationary era is a short phase of accelerated expansion believed to have occurred within the first instants of the history of our universe and leading to the hot big bang phase, which characterises the standard cosmological evolution. This framework was initially proposed and developed to solve basic problems within the standard big bang cosmology (Guth 1981; Starobinsky 1980; Linde 1982; Albrecht and Steinhardt 1982). After the original proposal, it was soon realised that inflation comes equipped with a mechanism of particle production, an inevitable consequence of quantum mechanics applied to an accelerating cosmological spacetime. The same mechanism is responsible for generating both the primordial scalar anisotropies (Mukhanov and Chibisov 1981; Hawking 1982; Starobinsky 1982; Guth and Pi 1982; Bardeen et al. 1983) that source the evolution

of cosmic structures at large scales, and a SGWB of primordial GWs (Grishchuk 1974; Starobinsky 1979; Rubakov et al. 1982; Fabbri and Pollock 1983).

The basic setup of GW production during inflation is as follows. Consider the dynamics of spin-2, transverse-traceless fluctuations $h_{ij}(t, \vec{x})$ around a flat FLRW line element

$$ds^2 = -dt^2 + a^2(t)\left[\delta_{ij} + h_{ij}(t, \vec{x})\right] dx^i dx^j, \tag{98}$$

with $a(t)$ being the scale factor. During inflation one typically assumes that the Hubble parameter $H = \dot{a}/a$ is nearly constant, leading to a quasi-exponential expansion. The dynamics of spin-2 fluctuations is obtained by expanding the Einstein-Hilbert action at quadratic order in h_{ij} around the homogeneous FLRW solution above. Cosmological perturbations can be quantized according to the basic rules of quantum field theory (see e.g. Birrell and Davies 1984). Quantum mechanics converts the large gradients characterising the spacetime geometry, associated with the rapid cosmological expansion, into the production of spin-2 quanta whose amplitude, at wavelengths larger than the Hubble horizon H^{-1}, freezes to a nearly scale-invariant value

$$P_h(k) \simeq \frac{2}{\pi^2}\left(\frac{H_{\rm inf}}{M_{\rm Pl}}\right)^2 \left(\frac{k}{k_*}\right)^{n_T}, \tag{99}$$

with k_* a pivot scale, $H_{\rm inf}$ is the inflationary Hubble scale when k_* exited the Hubble radius during inflation and P_h is the dimensionless tensor power spectrum (here $M_{\rm Pl}$ is the reduced Planck mass). In an exact *de Sitter* background, the tensor spectrum would be exactly scale invariant, $n_T = 0$. In slow-roll inflation, however, a small ("slow-roll suppressed") red tilt is developed, $n_T \simeq -2\epsilon$, where $\epsilon \equiv \frac{M_p^2}{2}\left(\frac{1}{V}\frac{dV}{d\phi}\right)^2$ is a slow roll parameter (and V is the potential of the inflaton field ϕ).

After inflation ends, the Hubble scale starts to increase, reaching the size of the wavelength of the fluctuations produced during inflation. The latter re-enter the horizon with a very large occupation number, behaving as classical stochastic variables, and forming a primordial SGWB (see e.g. Caprini and Figueroa 2018; Maggiore 2018 for reviews). A detection of the (as of today undetected) inflationary SGWB would provide key information on the physics of the early universe. Moreover, it would be the first direct experimental evidence of the quantization (see Riotto 2003 for a review and Polarski and Starobinsky 1996 for a discussion on the transition to a semi-classical behaviour) of spin-2 gravitational interactions: the production of GWs is based on quantum mechanical notions applied to cosmology.

The simplest class of inflationary models relies on a single scalar field, the inflaton, characterised by a standard kinetic term and driving the acceleration. In this configuration, the inflaton homogeneous and time-dependent profile rolls slowly down an almost flat potential throughout the inflationary phase (Liddle and Lyth 2000; Baumann 2011). Such scenarios are associated to rather specific predictions in terms of the inflationary SGWB properties. They consist in an almost scale-invariant spectrum, whose amplitude is too small for detection by direct GW experiments such as LISA and whose slope is slightly red-tilted (the amplitude decreases as frequency

increases). At present the most promising path to detection of an inflationary SGWB from standard single-field slow-roll models is through its footprints on the B-mode polarisation of the CMB radiation (see e.g. Kamionkowski and Kovetz 2016 for a review).

There are nevertheless plenty of good reasons to go beyond vanilla models of inflation. Such a step is motivated for example by the need to embed inflationary physics in the broader context of particle physics and especially within quantum theories of gravity. Upon exploring a richer inflationary dynamics, one must also revisit the corresponding predictions of primordial GW properties.

Particularly relevant for this work is the fact that in scenarios beyond single-field slow-roll, the amplitude of the primordial SGWB can be enhanced, and this may well occur in the LISA frequency band. As a result, LISA has the potential and the opportunity to probe our understanding of the early universe and, in particular, of the inflationary phase. In this section we expand on such a possibility. We refer the reader to Bartolo et al. (2016b) for previous work on the topic by the LISA Cosmology Working Group.

We shall consider here the following scenarios:

- When embedding inflation in particle physics and string theory setups (Lyth and Riotto 1999; Baumann and McAllister 2015), several additional fields may enter the game thereby changing the basic predictions of inflation. As we shall see in Sect. 8.2, the presence of extra degrees of freedom brings about the possibility of enhanced cosmological correlators and associated signatures. Of particular interest for us will be the case where such dynamics affects the tensor sector and leads to an amplification of the primordial GW signal. Additional properties of the SGWB that may reveal a multi-field mechanism include chirality, non-Gaussianity, and specific frequency profiles that can help distinguish the primordial signal from its astrophysical counterpart.
- A SGWB with sufficiently large amplitude to allow detection by LISA can be induced at second order in perturbations by a boosted scalar power spectrum. The mechanism leading to such enhancement typically gives rise also to oscillatory features. In Sect. 8.3 we discuss the characteristic oscillatory frequency profiles of the SGWB that can be probed in the LISA frequency ranges. In the process, we discuss novel methods to identify the different signatures associated to a number of inflationary models.
- The inflationary mechanism can be realised in scenarios with alternative spacetime symmetry breaking patterns, in which the background of the fields driving inflation depends also on space coordinates. As we discuss in Sect. 8.4, the dynamics of the corresponding tensor sector are different than in standard scenarios, and can lead to a primordial SGWB signal within reach of LISA.
- Explicit UV completions of inflation motivated by non-local versions of Starobinsky's $R + \alpha R^2$ model are discussed in Sect. 8.5. There we also show how considering such approaches reflects on the properties of the primordial GW spectrum.

- Inflation is an early period of accelerated expansion that must come to end so as to give way to cosmological evolution within the framework of standard big bang cosmology. In the transition phase the inflaton field couples with or decays into SM particles. This process may lead to GW production and to a SGWB spectrum whose properties are investigated in Sect. 8.6.
- All the scenarios mentioned above point to the fact that the primordial SGWB from inflation can be produced by qualitatively distinct mechanisms, all of which are markedly different from astrophysical processes. Section 8.7 aims to put together and investigate the features of the inflationary SGWB—chirality, frequency profile, anisotropies—that can be probed by LISA.

8.2 Gravitational waves sourced by additional fields during inflation

8.2.1 Axion-gauge field inflation

Ubiquitous in particle physics, the existence of axion-like particles driving inflation has received considerable attention (see Pajer and Peloso 2013 for a comprehensive review) starting with the well-known natural inflation proposal (Freese et al. 1990; Adams et al. 1993). The appeal of such a setup relies in part on their approximately shift-symmetric potential protecting the inflaton mass from large corrections. As a result of non-perturbative contributions from gauge field configurations (instantons), the potential acquires the typical cosine profile

$$V(\chi) = \Lambda^4 \left[1 + \cos\left(\frac{\chi}{f_\chi}\right) \right]. \tag{100}$$

The axion-like field χ is driven by a potential at a scale Λ and with decay constant f_χ. In the absence of other fields, a nearly scale-invariant scalar spectral index, as required by CMB observations, leads to a large axion decay parameter $f_\chi \sim M_P$. On the other hand, a number of reasons favour inflationary realisations with a sub-Planckian f_χ: (i) quantum gravity effects are expected to break the shift symmetry, as well as any global symmetry, at the Planck scale through the formation of a (virtual) BH; (ii) in typical string theory constructions one finds $f_\chi < M_P$ (Banks et al. 2003). It follows that a field content allowing for a smaller decay constant whilst preserving the naturalness of the potential, is of interest in this context. Coupling the axion-inflaton with gauge fields is a simple and intriguing possibility. Perhaps the most studied example is that of a Chern–Simons-type coupling

$$\mathcal{L} \supset \frac{\lambda}{4 f_\chi} \chi F \tilde{F}, \tag{101}$$

which preserves the shift symmetry and "dissipates" some of the inflaton kinetic energy into the gauge sector, in so flattening its effective potential without the need to resort to a large f_χ. Several specific axion-gauge fields realisations are found in the literature, employing both Abelian (Anber and Sorbo 2010) and non-Abelian (Adshead and Wyman 2012) gauge modes. Their phenomenology is a rich one, but

we shall focus here mostly on the gravity (i.e. tensor) sector. The Abelian and non-Abelian scenarios share some key features:

• Inspection of the equations of motion for the gauge sector in Eqs. (102) and (103), reveals that the effect of the coupling to the axion-like inflaton depends also on the popularisation of the gauge field, and it is controlled by the parameter $\xi \equiv \lambda\dot{\chi}/(2f_\chi H)$. More specifically, denoting by $A_\pm$ the mode functions of the two circular polarisations of the gauge field, one has (Garretson et al. 1992; Anber and Sorbo 2010; Maleknejad and Sheikh-Jabbari 2011; Adshead and Wyman 2012)

$$\text{Abelian case}: \qquad A''_\pm + \left(k^2 \pm \frac{2k}{\tau}\xi\right)A_\pm = 0\,; \tag{102}$$

$$\text{non-Abelian case}: \quad t''_\pm + \left[k^2 + \frac{2}{\tau^2}\left(m_Q\xi \pm k\tau(m_Q+\xi)\right)\right]t_\pm \simeq 0\,; \tag{103}$$

where τ is conformal time. The quantity t in Eq. (103) is the wave-function associated with the tensor degrees of freedom t_{ia}, stemming from choosing SU(2) as the gauge group (Maleknejad and Sheikh-Jabbari 2013); the parameter m_Q is defined as $m_Q \equiv gQ/H$ where g is the gauge coupling, H the Hubble rate, and Q the background of one of the (three) gauge sector scalar modes. We note the slow roll relation $\xi \simeq m_Q + 1/m_Q$, so that the two parameters that control the production in the Abelian and non-Abelian case coincide in the large ξ limit.

It is intuitively clear then that the effect of the Chern–Simons coupling, driven by ξ, is stronger as one approaches the end of inflation where a large kinetic term $\dot{\chi}$ breaks the slow-roll condition.

• Given that the amplitude of the relevant gauge degrees of freedom is enhanced by the coupling, and that these modes source GWs, the tensor power spectrum is typically blue in these scenarios. This makes them of immediate interest for GW detectors, such as LISA (see e.g. Figs. 18 and 19, respectively for the Abelian and for the non-Abelian cases).

The fact that minimal single-field slow-roll scenarios predict instead a slightly red-tilted GW power spectrum, well below the sensitivity of LISA and possibly of the proposed BBO, is very much relevant here. A detection of a *primordial* GW signal at small scales will strongly point to a multi-field inflation mechanism such as the ones discussed in this and the next subsection (Fig. 20).

• Polarisation-dependent equations of motion and solutions for gauge fields feed directly into a polarisation dependent GW spectrum. If the sourced contribution is comparable or larger than the ever-present vacuum tensor fluctuations the GW spectrum will be a *chiral* one. This is particularly interesting a signature because (i) it is testable with LISA by means of the kinematically induced dipole (Domcke et al. 2020b) and (ii) is rather uniquely associated with a Chern–Simons-type coupling, at least in terms of chirality of primordial origin.

Further characterisation of these inflationary scenarios necessarily includes the study of their scalar sector, especially vis a vis CMB constraints as well as scalar, tensor and mixed higher-point functions. The possibility of large tensor non-Gaussianity (i.e. the GW bispectrum) (Anber and Sorbo 2012; Namba et al. 2016; Agrawal et al. 2018) is

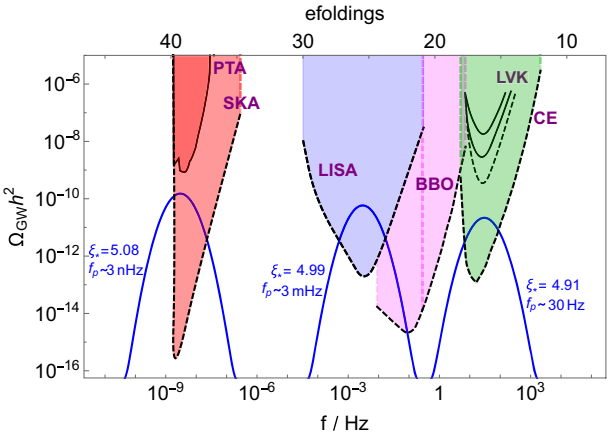

Fig. 18 Axion-Abelian gauge field coupling can produce a large amplitude and varying width GW background depending on the evolution of fields during inflation. One can have a bump/Gaussian peak at scales where the axion rolls fast. The figure shows three examples that are relevant for current and forthcoming/future interferometers, namely PTA (frequencies around 10^{-10}–10^{-7} Hz), LISA (frequencies 10^{-5}–10^{-1} Hz) and Advanced LIGO-Advanced Virgo-KAGRA (around 1-100 Hz). In all those examples, the upper limit of the GW background is set by constraints from enhanced curvature perturbations and PBH bounds. Interestingly, density perturbations peaked at PTA and LISA scales can also generate PBHs which can be phenomenologically relevant and possibly constitute some fraction of DM. Image adapted from García-Bellido et al. (2017), Ünal (2019)

worth mentioning here, with the reminder that its shape function is typically very similar to the so-called equilateral template. As a result, it is best tested at CMB scales (namely by studying the impact on the CMB of modes with wavelength not much smaller than the present horizon), rather than at higher frequencies where propagation effects strongly suppress the signal (Bartolo et al. 2019b). Moreover, models with axions and gauge fields can also produce a SGWB peaked at scales relevant for various GW detectors, Domcke et al. (2016), García-Bellido et al. (2016) including aLIGO/AVirgo/Kagra, LISA and PTAs. They can also produce peaked density perturbations that can seed an abundance of PBHs compatible with that of DM (Bugaev and Klimai 2014; García-Bellido et al. 2016; Domcke et al. 2017; García-Bellido et al. 2017), as we briefly touch upon in Sect. 8.2.3. We shall also point to the intriguing possibility of similar scenarios being responsible for the matter–antimatter asymmetry of the universe (Maleknejad 2014; Caldwell and Devulder 2018).

For the sake of completeness we should also mention some caveats one may extract from recent literature on the subject as well as several emerging new research paths. Coupling the axion with the gauge sector allows for a sub-Planckian dynamics by essentially feeding the axion kinetic energy into the gauge sector. This effect is regulated by the coupling λ. The ensuing flattening of the inflaton effective potential makes for a viable scalar spectral index n_s at large scales. At the same time, the (enhanced) gauge sector also sources GWs. It turns out that the parameter space granting the appropriate n_s may correspond to an overproduction of GWs (Dimastrogiovanni and Peloso 2013).

In addition, the amplified gauge fields also source scalar density perturbations, and it challenging to generate observable GW without overproducing scalar modes (Barnaby and

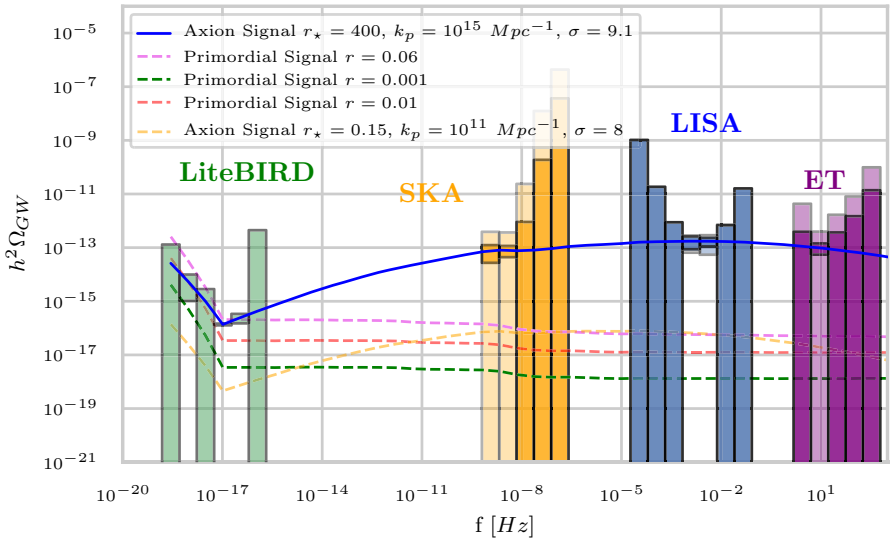

Fig. 19 The GW energy density $\Omega_{\rm GW}$ as a function of frequency sourced by SU(2) axion-gauge field setups (solid blue line and yellow dashed line). A signal outside the reach of certain probes may still be accessed via LISA at small scales (and e.g. LiteBIRD at very large scales). The vertical bars are the expected 1σ error bars estimated with and without the presence of astrophysical foregrounds (light and dark shared areas, respectively). Different colours are used for LiteBIRD (green), SKA (orange), LISA (blue), and ET (purple). Logarithmic binning in wavenumber is employed with $\Delta \ln k = 1.2$. For the sake of comparison, the tensor spectrum predicted in some illustrative single-field slow-roll scenario (dashed lines) are displayed, including their BICEP2/Keck/Planck upper bound $r = 0.06$. The quantity k_p is the pivot scale and the quantity σ in the upper left box is a parameter of the SU(2) model, typically of order 1–10. Image reproduced with permission from Campeti et al. (2021), copyright by IOP/SISSA

Fig. 20 Feynman diagrams for the GW power spectrum. Left panel: The gauge fields A_μ source GW non-linearly in the Abelian case. Right panel: The $SU(2)$ scenario, where gauge tensor degrees of freedom t_{ij} source GWs already at tree level

Peloso 2011; Namba et al. 2016; Papageorgiou et al. 2018, 2019). Several routes have been explored to preserve the intriguing GW phenomenology of these models whilst also satisfying CMB and PBH bounds. One of the most economical choices is to introduce a spectator scalar field (Namba et al. 2016; Dimastrogiovanni et al. 2017; Obata and Soda 2016). This weakens the production of density perturbations and the corresponding scalar sector constraints on the axion-like particle and delivers viable scenarios both in the Abelian and non-Abelian cases. The back-reaction dynamics (Peloso et al. 2016; Maleknejad and Komatsu 2019) as well as the requirements stemming from perturbativity bounds (Ferreira et al. 2016; Peloso et al. 2016; Dimastrogiovanni et al. 2018; Papageorgiou et al. 2018, 2019) have been recently studied for these setups.

The possibility of Schwinger pair production has been explored in the same context as well as the coupling with fermionic fields (Domcke and Mukaida 2018; Mirzagholi et al. 2020b). In the same spirit, it is natural to investigate couplings with SM particles (Ferreira and Notari 2017; Domcke et al. 2020a). Also of note are several successful embeddings of axion gauge fields models within supergravity and string theory constructions (Dall'Agata 2018; McDonough and Alexander 2018; Holland et al. 2020).

8.2.2 Non-minimally coupled (spinning) fields

As a useful approach that is complementary to the one in the previous section, we will briefly expand here on a recently introduced EFT of non-minimally coupled (spinning) fields (Bordin et al. 2018). The presence of multiple fields during inflation is completely natural from the top-down perspective (Baumann and McAllister 2015). The benefit of an effective approach to such dynamics lies in the fact it provides a general, unified, description of the inflationary field content and the ensuing cosmological signatures. It is well-known that the presence of spinning fields makes for a richer phenomenology,[25] one that is certainly worth exploring.

The presence of increasingly demanding unitary constraints as one goes up the spin ladder, typically implies that higher $(s \geq 2)$ spin fields decay within of a few e-folds during inflation, to the detriment of their imprints on early universe observables. This is remedied by coupling the extra spinning content directly to the inflaton: the background breaks de Sitter isometries and weakens the related unitarity constraints, thus allowing for a lighter (more long-lived) particle content. As a result, extra spin-2 fields can for example directly source the GW spectrum providing the leading contribution to the signal (Bordin et al. 2018).

It is instructive to report a few of the leading operators in the Lagrangian coupling an extra spin-2 field σ with the standard tensor modes γ_{ij} and the Goldstone boson π, related to the scalar curvature ζ via $\zeta \sim -H\pi$:

$$\begin{aligned}
\mathcal{S} \supseteq \mathcal{S}^{(2)}_{\text{free}} + \mathcal{S}^{(2)}_{\text{int}} + \mathcal{S}^{(3)}_{\text{int}} &= \int dt\, d^3x\, a^3 \left(L^{(2)}_{\text{free}} + L^{(2)}_{\text{int}} + L^{(3)}_{\text{int}} \right) \\
L^{(2)}_{\text{free}} &= \frac{1}{4} \Big((\dot{\sigma}^{ij})^2 - c_2^2 a^{-2} (\partial_i \sigma^{jk})^2 - \frac{3}{2} (c_0^2 - c_2^2) a^{-2} (\partial_i \sigma^{ij})^2 \\
&\quad - m^2 (\sigma^{ij})^2 \Big) \\
L^{(2)}_{\text{int}} &= -\frac{\rho}{\sqrt{2\epsilon} H} a^{-2} \partial_i \partial_j \pi_c \sigma^{ij} + \frac{1}{2} \rho \dot{\gamma}_{c\,ij} \sigma^{ij} \\
L^{(3)}_{\text{int}} &= -\frac{\rho}{2\epsilon_1 H^2 M_{\text{Pl}}} a^{-2} (\partial_i \pi_c \partial_j \pi_c \dot{\sigma}^{ij} + 2H \partial_i \pi_c \partial_j \pi_c \sigma^{ij}) \\
&\quad - \mu (\sigma^{ij})^3 + \cdots ,
\end{aligned} \tag{104}$$

where c_i is the sound speed for the helicity-i mode of the spin-2 particle σ. The first line of Eq. (104) contains the free quadratic Lagrangian for σ whilst the second and third lines respectively describe the quadratic and cubic mixing of σ with standard

[25] For example, scalar and mixed non-Gaussianities display a characteristic extra angular behaviour in the squeezed limit (Arkani-Hamed and Maldacena 2015). Even more relevant in this context is the fact that extra tensor modes, such as those of spin-2 particles, can directly source GWs.

scalar and tensor modes. In addition to vacuum fluctuations, the GW power spectrum receives a contribution proportional to the quadratic coupling ρ, which may well be the leading one. Upon allowing a time dependent ρ or a time dependent helicity-2 sound speed c_2, it is possible to obtain a blue GW spectrum (Iacconi et al. 2020a, b) and, more in general, one with a non-trivial scale dependence (see Fig. 21). There is a substantial portion of parameter space in this EFT that delivers a GW power spectrum detectable by LISA.

Further, even within bounds ensuring perturbativity control, lack of gradient instabilities, and compliance with CMB bounds, this setup supports large squeezed non-Gaussianities, including the purely tensorial three-point function. It follows that the EFT field content may also be tested by probing GW anisotropies (see Sect. 8.7.3) as well as via cross-correlating the SGWB with the CMB (see Sect. 8.7.4 below).

8.2.3 Models that produce peaks in the power spectrum of scalar perturbations

Primordial density waves in the early radiation-dominated universe interact gravitationally with GWs and therefore generate a SGWB (Mollerach et al. 2004; Ananda et al. 2007; Baumann et al. 2007). As discussed in Sect. 10.3, LISA is sensitive to GWs with frequency f generated from primordial density perturbations with power spectrum $\mathcal{P}_\zeta(f) \approx 10^{-4}$ which re-entered the Hubble-horizon at a temperature $T \approx 10^5 (f/mHz)$ GeV. These density waves can be generated from quantum fluctuations that are swept up by the accelerated expansion during a preceding period of inflation and exit the Hubble-scale N e-folds before the end of inflation. By assuming instantaneous reheating (a finite period of reheating can reduce this number), one obtains

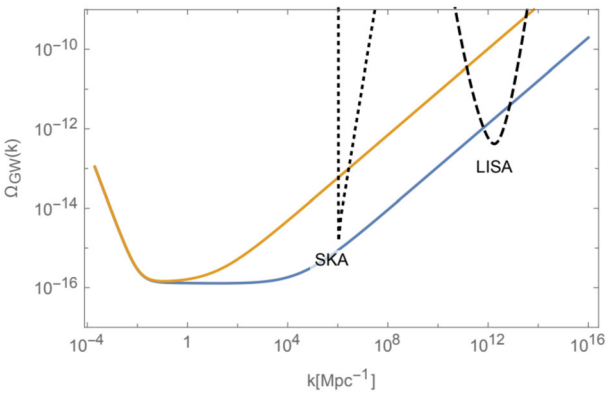

Fig. 21 The GW energy density of the EFT when including the contribution of an extra spin-2 field whose helicity-2 mode has a time-dependent sound speed. The two colours correspond to different values of ρ/H, respectively $(3 \times 10^{-3}, 4 \times 10^{-4})$, supporting a signal within reach for both SKA and LISA, or for LISA only. In generating both lines, the time dependence of the sound speed has been kept constant to $s_2 \equiv \dot{c}_2/(Hc_2) \simeq -0.2$. Image reproduced with permission from Iacconi et al. (2020b)

$$N \approx 22 + \ln\left(\frac{V_*^{1/4}}{10^{15}\,\mathrm{GeV}}\right) - \ln\left(\frac{f}{\mathrm{mHz}}\right), \tag{105}$$

where $N = \int H\,dt$ is the integrated expansion, and V_* is the energy density during inflation.

It is often assumed that the power spectrum of primordial density perturbations from inflation can be described by a power law, $\mathcal{P}_\zeta \propto f^{n-1}$, whose amplitude and spectral index are fixed by observations on CMB scales, where $\mathcal{P}_\zeta \approx 10^{-9}$ and $n < 1$. This is not general (Chluba et al. 2015). However, within slow roll, the deviation from a simple power law (running of the spectral index) is limited (second order in slow-roll parameters) and thus a significant enhancement in the primordial power spectrum on the scales probed by LISA requires the breakdown of the usual slow-roll approximations.

Quantum fluctuations in the fields driving the accelerated expansion naturally generate primordial density fluctuations in the subsequent radiation era, and there may be additional fluctuations from fields that, although subdominant during inflation (so-called spectator fields), affect the subsequent evolution between the end of inflation and the epoch when modes re-enter the Hubble-horizon. The dimensionless density contrast, ζ, can be identified with the perturbation in the local integrated expansion, $\zeta = \delta N$. In the large-scale limit (neglecting spatial gradients) this can be related to the field fluctuations at first order $\zeta = (\partial N/\partial\vec{\Phi}) \cdot \delta\vec{\Phi}$, where $N(\vec{\Phi})$ corresponds to the background expansion as a function of the local field values, $\vec{\Phi}$, during inflation.

For a single inflaton field (or more generally for adiabatic field fluctuations in a multi-field setting (Liddle et al. 1998; Gordon et al. 2000)) $\partial N/\partial\varphi = H/\dot{\varphi}$ while the amplitude of quantum field fluctuations at Hubble exit are given by $\mathcal{P}_{\delta\varphi} \simeq H/2\pi c_s$, where c_s is the sound speed. Given that the Hubble rate at Hubble-exit ($k = aH$) necessarily decreases during inflation, there are essentially two ways to boost the primordial density perturbations in single field models. Either one can decrease the speed of the inflaton, $\dot{\varphi}$ faster than the slow-roll evolution, known as ultra-slow roll (Inoue and Yokoyama 2002; Kinney 2005), or one can rapidly decrease the sound speed, c_s, e.g. due to non-decoupling of massive fields (Achucarro et al. 2011). Ultra-slow roll describes a regime where the potential gradient becomes negligible and the field becomes friction dominated, $\dot{\varphi} \propto e^{-3N}$, which can occur in models with a near-inflection point in the potential. Typically the ultra-slow roll phase is transient, leading to a localised step (Starobinsky 1992; Leach et al. 2001) or broad peak (García-Bellido and Ruiz Morales 2017) in the power spectrum. In some cases the departure from slow-roll may interrupt inflation, before inflation restarts in an ultra-slow roll phase (Roberts et al. 1995; Leach and Liddle 2001; Ragavendra et al. 2021).

If the energy scale of inflation is as low as $V_*^{1/4} \sim 10^6$ GeV then LISA could be sensitive to physical processes that end inflation and reheat the universe. The coherent oscillation of the inflaton (and, possibly, other field) that characterised this stage may lead to resonant amplification of scalar metric perturbations near the Hubble scale at the end of inflation, a phenomenon known as metric preheating

(Nambu and Taruya 1997; Finelli and Brandenberger 1999; Jedamzik et al. 2010; Easther et al. 2011). Density perturbations produced close to the Hubble scale at this stage may become large in models where inflation ends due to an instability, triggering a phase transition. This may be second-order, as in hybrid inflation models (Linde 1994; Copeland et al. 1994), where a tachyonic instability in a second "waterfall" field leads to the rapid growth of quantum fluctuations, or in the geometrical destabilisation of inflation, due to a geometrical instability in a negatively-curved field-space (Renaux-Petel and Turzyński 2016). A FOPT at the end of inflation requires the rapid nucleation of bubbles of a broken symmetry phase, whose collisions both reheat the universe and can generate GWs (Caprini et al. 2016).

More generally fluctuations in fields orthogonal to the instantaneous trajectory in field-space, and hence independent of the adiabatic field fluctuations, can enhance the primordial scalar power spectrum, $\mathcal{P}_\zeta$, after Hubble exit (Wands et al. 2002). Any non-geodesic "turn" in field space during inflation converts isocurvature field perturbations at Hubble-exit into an additional source of curvature perturbations on super-Hubble scales (Gordon et al. 2000; Groot Nibbelink and van Tent 2002; Palma et al. 2020; Fumagalli et al. 2023). In a different mechanism, spectator axion fields might also exhibit a brief phase of fast roll during inflation, generating a localised peak in the power of density perturbations (Namba et al. 2016). Alternatively, the effect of spectator fields may be completely subdominant during inflation but boost the primordial power spectrum after the end of inflation as in the curvaton (Enqvist and Sloth 2002; Lyth and Wands 2002; Moroi and Takahashi 2001) or other modulated reheating (Dvali et al. 2004; Kofman 2003) scenarios. Quite generally we expect otherwise light scalar fields present during inflation to acquire effective masses of order the Hubble scale during inflation (Dine et al. 1995; Baumann and Green 2012), suppressing their fluctuations on large scales, leading to a steep blue tilt, dominating the power spectrum on small scales, as in the axion-like curvaton model (Kawasaki et al. 2013).

8.3 Small-scale primordial features

Embeddings of inflation in high energy theory motivate the exploration of inflationary mechanisms beyond the single-field slow-roll framework. For example, UV completions of inflation in string compactifications typically introduce many new degrees of freedom that ultimately contribute to the inflationary dynamics. Thus, from the UV point of view, single-field slow roll models have the semblance of toy-models that capture the essence of inflation without being fully realistic.

Avenues for going beyond single-field slow-roll are plentiful and, as a result, a large number of models have been constructed. However, instead of proceeding model by model, there is also a more systematic way for going beyond the simplest version of inflation. The idea is to characterise departures from single-field slow-roll in terms of their effect on the scalar power spectrum.

These signatures of a departure from single-field slow-roll have been termed "features" after corresponding characteristic properties of the scalar power spectrum.

See Chen (2010), Chluba et al. (2015), Slosar et al. (2019) for reviews on this topic. Using the language of features, departures from single-field slow-roll inflation can be assigned to one of the two following broad classes[26]:

1. A so-called "sharp feature" is characterised by an oscillation in the scalar power spectrum that is periodic in the wavenumber k. This arises whenever there is some sudden transition during inflation, like e.g. a step in the inflation potential or a sharp turn in the trajectory.
2. A so-called "resonant feature" denotes an oscillation in the scalar power spectrum in $\log(k)$. It arises when some components of the background oscillate with a frequency larger than the Hubble scale, inducing a resonance with the oscillations of the quantum modes of the density perturbations, a typical example being axion monodromy inflation (Silverstein and Westphal 2008; Flauger et al. 2010).

Over the relevant range of scales, the scalar power spectrum corresponding to each class can be written as

$$\text{Sharp:} \quad \mathcal{P}_\zeta(k) = \mathcal{P}_0(k)\Big[1 + A_{\rm lin}\cos\big(\omega_{\rm lin}k + \vartheta_{\rm lin}\big)\Big], \tag{106}$$

$$\text{Resonant:} \quad \mathcal{P}_\zeta(k) = \mathcal{P}_0(k)\Big[1 + A_{\rm log}\cos\big(\omega_{\rm log}\log(k/k_\star) + \vartheta_{\rm log}\big)\Big], \tag{107}$$

with $k_\star$ being some arbitrary reference scale introduced for dimensional reasons. That is, a sharp or resonant feature is described by an oscillation with amplitude $A_{\rm log/lin}$ about an envelope $\mathcal{P}_0(k)$. The precise form on the envelope will depend on the model, but can be taken as sufficiently smooth over the period of oscillations.[27] For sharp features, the frequency $\omega_{\rm lin} \sim 1/k_{\rm f}$, where $k_{\rm f}$ corresponds to the scale that crosses the Hubble radius at the time of the feature. As for resonant ones, one has $\omega_{\rm log} \sim M/H$, where M is the frequency of the background oscillations.

At large scales ($k \lesssim 1\ \text{Mpc}^{-1}$) features are severely constrained by CMB and LSS data, which mandate a nearly scale-invariant power spectrum with amplitude $\mathcal{P}_\zeta \sim 10^{-9}$. In contrast, at small scales ($k \gg 1\ \text{Mpc}^{-1}$), CMB and LSS constraints do not apply and the scalar power spectrum can depart significantly from scale-invariance. This opens the possibility that the feature constitutes the dominant contribution to the scalar power spectrum at small scales.

For such contribution to be sufficiently large to make the SGWB detectable by current or forthcoming interferometers, the scalar power spectrum at the scale of the feature needs to be significantly enhanced compared to its value at CMB scales. Specifically, $\mathcal{P}_\zeta$ should increase from $\sim 10^{-9}$ to $\sim 10^{-4}$ by moving k from the CMB to the LISA momentum scale. GW observatories such as LISA are thus sensitive to

[26] Oscillations of heavy fields act as "primordial standard clocks", leading to feature signals resembling that of a sharp feature at larger scales and of a resonant feature at smaller scales.

[27] In realistic models the amplitude and frequency of the oscillation as well as phase offset can run with the scale k, but if this running is sufficiently "slow", the templates (106) and (107) will still be applicable over a suitable range of scales.

feature models where the scalar power spectrum exhibits a peak at small scales, where the CMB and LSS constraints do not apply, as previously explained in Sect. 8.2.3. This is not an unrealistic expectation: such localised enhancements of the power spectrum occur frequently in inflation models with features. In fact, the mechanism of amplification of scalar fluctuations is often also responsible for producing the oscillatory feature and vice versa, as observed e.g. in Ballesteros et al. (2019), Palma et al. (2020), Fumagalli et al. (2023), Braglia et al. (2020), Fumagalli et al. (2021a), Tasinato (2021), Braglia et al. (2021). GW observatories such as LISA can thus test models of inflation at scales inaccessible to CMB and LSS surveys.

What is interesting for GW astronomy is that features in the scalar power spectrum lead to corresponding features in the frequency profile of the corresponding scalar-induced GWs (Fumagalli et al. 2021a; Braglia et al. 2021; Fumagalli et al. 2021b). Here we focus on the contribution to the SGWB sourced by scalar fluctuations when they re-enter the horizon during RD after inflation, see Sect. 10.3.[28] Remarkably, this inherently nonlinear effect does not lead to oscillations being washed out. One rather finds that a sharp feature leads to a periodic modulation in the spectral shape of the SGWB contribution, while a resonant feature produces a corresponding log-periodic modulation. As a result, over some range of scales the spectral shape of $\Omega_{\rm GW}(k)$ can be matched by the following templates (Fumagalli et al. 2021a; Braglia et al. 2021; Fumagalli et al. 2021b):

$$\text{Sharp:}\quad \Omega_{\rm GW}(k) = \overline{\Omega}_{\rm GW}(k)\left[1 + \mathcal{A}_{\rm lin}\cos\left(\omega_{\rm lin}^{\rm GW} k + \phi_{\rm lin}\right)\right], \tag{108}$$

$$\begin{aligned}\text{Resonant:}\quad \Omega_{\rm GW}(k) = \overline{\Omega}_{\rm GW}(k)\Big[&1 + \mathcal{A}_{\log,1}\cos\left(\omega_{\log}\log(k/k_\star) + \phi_{\log,1}\right)\\ &+ \mathcal{A}_{\log,2}\cos\left(2\omega_{\log}\log(k/k_\star) + \phi_{\log,2}\right)\Big],\end{aligned} \tag{109}$$

with $\omega_{\rm lin}^{\rm GW} = \sqrt{3}\omega_{\rm lin}$. Here, $\overline{\Omega}_{\rm GW}(k)$ refers to the GW fraction with the oscillatory component averaged out.

The above is best illustrated by an example. As has been observed in Palma et al. (2020), Fumagalli et al. (2023), an amplification of scalar fluctuations can be achieved in multi-field inflation when the inflationary trajectory exhibits a strong turn. If the turn is also sufficiently sharp, i.e. it is executed in a short time interval, this leads to a sharp feature. In simple cases the scalar power spectrum can then be computed analytically as (Palma et al. 2020; Fumagalli et al. 2021a)

$$\frac{\mathcal{P}_\zeta(k)}{\mathcal{P}_0} = \frac{e^{2\sqrt{(2-\kappa)\kappa}\,\eta_\perp\delta}}{2(2-\kappa)\kappa} \times \sin^2\left(e^{-\delta/2}\kappa\eta_\perp + \arctan\left(\frac{\kappa}{\sqrt{(2-\kappa)\kappa}}\right)\right), \tag{110}$$

which is valid for $\kappa \leq 2$ and where $\kappa \equiv k/k_\star = k/(k_{\rm f}\eta_\perp)$. Here $\eta_\perp$ quantifies the strength of the turn in terms of the departure from a geodesic, δ is the duration of the turn in units of e-folds and $k_{\rm f}$ is the scale crossing the Hubble radius at the time of the

[28] In addition, there will also be a scalar-induced contribution to the SGWB sourced during inflation. The latter is slow-roll suppressed compared to the post-inflationary contribution and will be ignored in the following, even though it can dominate in selected models, see e.g. Zhou et al. (2020).

sharp turn (see Fumagalli et al. 2021a for generalisations). As can easily be checked, Eq. (110) is indeed of the form of Eq. (106) characteristic of a sharp feature.

In Fig. 22a we plot $\mathcal{P}_\zeta(k)$ in Eq. (110) for two example models and in Fig. 22b the corresponding GW energy density $\Omega_{\rm GW}(k)$. We can then make the following observations, which will not only hold for the model at hand, but will be generic for a sharp feature and can be also generalised to the case of a resonant feature:

- The overall spectral shape $\overline{\Omega}_{\rm GW}(k)$ is determined by the envelope $\mathcal{P}_0(k)$. If this is sufficiently narrowly-peaked, the spectral shape of $\overline{\Omega}_{\rm GW}(k)$ consists of a broad lower peak at lower frequencies and a narrow principal peak at higher frequencies. This is what is observed in Fig. 22b. The principal peak occurs at $k = 2/\sqrt{3}\,k_\star$, where $k_\star$ is the frequency where the envelope $\mathcal{P}_0$ has its maximum, and this can be understood to arise from resonant amplification (Kohri and Terada 2018).
- The oscillatory running of the SGWB induced by the feature is visible as a modulation of $\Omega_{\rm GW}(k)$ on the principal peak, see again Fig. 22b. In the vicinity of the maximum the modulation is well-matched by the template in Eq. (108) for a sharp feature, as can be seen in Fig. 22c where we plot the ratio $\Omega_{\rm GW}(k)/\overline{\Omega}_{\rm GW}(k)$: Especially near the centre of the peak this exhibits a sinusoidal oscillation with near-constant amplitude.
- The modulation in $\Omega_{\rm GW}(k)$ can be understood as a superposition of resonance peaks sourced by the individual maxima of $\mathcal{P}_\zeta(k)$. Labelling the maxima in $\mathcal{P}_\zeta(k)$ by k_i, the resonance analysis predicts a series of peaks in $\Omega_{\rm GW}(k)$ at (Cai et al. 2019c):

$$k_{{\rm max},ij} = \frac{1}{\sqrt{3}}(k_i + k_j), \quad \text{with} \quad k_{{\rm max},ij} > |k_i - k_j|. \tag{111}$$

  Applying this to the sharp and resonant feature case one can show that this predicts the periodic structure recorded in the templates Eqs. (108) and (109) (Fumagalli et al. 2021a, b).
- The amplitude of oscillation in $\Omega_{\rm GW}(k)$ is typically attenuated compared to the amplitude of oscillation in $\mathcal{P}_\zeta(k)$. For example, a sharp feature with $A_{\rm lin} = 1$ leads to a modulated GW spectrum with $\mathcal{A}_{\rm lin} \sim \mathcal{O}(10\%)$ (Fumagalli et al. 2021a; Braglia et al. 2021).
- Consider a feature in the scalar power spectrum with an associated peak at $k_\star = k_{\rm CMB} e^{N_\star}$, with $N_\star$ the number of e-folds after horizon-crossing of the CMB modes. This bump in $\mathcal{P}_\zeta(k)$ will produce a peak in $\Omega_{\rm GW}$ whose frequency $f_{\rm peak}$ is related to $N_\star$ as

$$N_\star \approx \ln\left(\frac{f_{\rm peak}}{\rm Hz}\right) + 37. \tag{112}$$

  For the peak to fall into the frequency range of maximal sensitivity of LISA, $f = 10^{-3}$–10^{-2} Hz, the enhancement and the feature in $\mathcal{P}_\zeta(k)$ has to occur

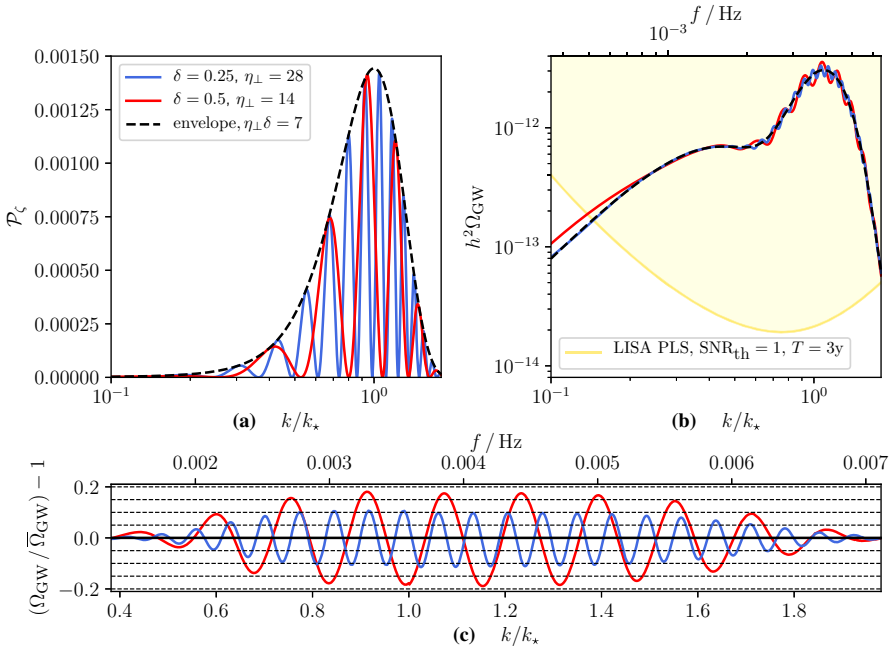

Fig. 22 Scalar power spectrum $\mathcal{P}_\zeta$ (**a**) and the scalar-induced GW energy density $\Omega_{\rm GW}$ (**b**) for two inflation models (see text for details) with a sharp feature and enhanced fluctuations from a strong turn in the inflationary trajectory, together with the PLS for SNR threshold $\mathrm{SNR_{th}} = 1$ and total observation time $T = 3$ years assumed in the analysis of (Fumagalli et al. 2021a). The black dashed line in (**a**) shows the envelope of $\mathcal{P}_\zeta$ and in (**b**) the corresponding GW energy density $\overline{\Omega}_{\rm GW}$. The $\mathcal{O}(1)$-oscillations in $\mathcal{P}_\zeta$ are processed into $\mathcal{O}(10\%)$ modulations on the principal peak of $\Omega_{\rm GW}$. Over the frequency range of the principal peak, the modulations in $\Omega_{\rm GW}$ can be modelled as cosine-oscillations about $\overline{\Omega}_{\rm GW}$, as can be seen in (**c**). To translate $k/k_\star$ into f/ Hz, we considered $N_\star = 31.5$, i.e. the peak in $\mathcal{P}_\zeta$ occurs at wavenumber $k = k_\star$, which is 31.5 e-folds larger than the CMB value. Images adapted from Fumagalli et al. (2021a)

$N_\star \sim 30$–32 e-folds after the generation of the CMB modes, making LISA sensitive to a wide range of models producing features during the later stages of inflation.

We thus find that features in the scalar power spectrum, encoding departures from single-field slow-roll inflation, lead to corresponding features in the scalar-induced contribution to the SGWB. If the feature is associated with a sufficient enhancement of the relevant scalar fluctuations, the resulting contribution to the SGWB is in principle detectable by GW observatories like LISA. As features encode departures from single-field slow-roll without reference to explicit models, this leads to the exciting prospect that SGWB measurements can be used to learn about inflation in a model-independent fashion.

8.4 Effective field theory of broken space-reparametrisations

LISA can shed light also on the symmetries characterising the early universe, and in particular the inflationary period. Standard models of inflation are based on the assumption that the inflaton background field is only time dependent, and this is well described within the EFT of inflation framework (Creminelli and Vernizzi 2017). However within the standard EFT framework, it is hard to produce GWs which have an amplitude large enough to be detected by interferometers. On the other hand, if space-diffeomorphisms are broken during inflation, and so the background field can have a space-dependent vacuum expectation value, then GWs are amplified at small scales becoming a potential target for GW detectors, like LISA. In particular, the breaking of space-diffeomorphism allows the graviton to be massive, since there are no symmetries preventing tensor fluctuations from acquiring a mass during inflation. If this is the case, the graviton is characterised by an action which is the most general one for tensor fluctuations:

$$S_T^{(2)} = \frac{M_P^2}{8} \int d^4x a^2(\eta) \left[h'_{ij} h'^{ij} - (k^2 + a^2(\eta) m_g^2) h_{ij} h^{ij} \right], \tag{113}$$

where $a(\eta)$ is the scale factor and m_g is the graviton mass, which is the distinctive feature of a setup that breaks space-diffeomorphism. Whereas such action can be derived within an EFT framework, there are models which realise such a possibility, like Solid (Endlich et al. 2014) and Supersolid (Koh et al. 2013; Cannone et al. 2015a, b; Bartolo et al. 2016a) inflation. They are described by Lagrangians which contain three (or four) scalar fields, which respect some internal symmetries ensuring the homogeneity and isotropy of the background. Such models can lead to a blue spectrum for tensor modes, as well as to other distinctive properties in the tensor spectrum (Endlich et al. 2014; Ricciardone and Tasinato 2017; Bartolo et al. 2016a; Cannone et al. 2015b; Akhshik et al. 2014; Akhshik 2015). Such an action leads, in the small graviton mass limit ($|m_h/H| \ll 1$), to a tensor primordial power spectrum like

$$\mathcal{P}_h = \frac{2H^2}{\pi^2 M_P^2} \left(\frac{k}{k_*} \right)^{n_T}, \tag{114}$$

with the tensor spectral index equal to

$$n_T = \frac{2}{3} \frac{m_h^2}{H^2}. \tag{115}$$

Notice that a blue spectrum, $n_T > 0$, requires a positive m_h^2. This is the case of interest, since it enhances the tensor spectrum at small scales, and can lead to a signal detectable by LISA. A model-independent analysis of such kind of models, and the possibility to detect the GW signal in the range of frequencies and energy densities probed by LISA has been carried out in Bartolo et al. (2016b).

$$\varphi^0 = \bar{\varphi}(t), \qquad \varphi^a = x^a, \quad a = 1, 2, 3\,; \tag{116}$$

this time 4D diffeomorphisms are completely broken, leaving only a global symmetry as a leftover, where an SO(2) rotation is performed both to the fields and to the spatial coordinates. To allow for a FLRW background solution, the action for the scalar fields dynamics needs to be symmetric under internal rotations and shift transformations

$$\varphi^a \to \mathcal{R}^a_b\,\varphi^b, \qquad \mathcal{R}^t\mathcal{R} = \mathbf{1}, \qquad \varphi^A \to \varphi^A + c^A, \qquad A = 0, 1, 2, 3. \tag{117}$$

In general, the fluctuations around Eq. (117) can be interpreted as the phonons of a supersolid (Son 2005; Celoria et al. 2017), while the special case where only the "spatial" Stueckelberg fields φ^a (with $a = 1, 2, 3$) are present corresponds to a solid (Endlich et al. 2013). Similar models have been proposed as massive deformation of gravity (Ballesteros et al. 2016; Celoria et al. 2018). In the scalar sector there are two propagating degrees of freedom that mix non-trivially both at early and late times and, after exiting the horizon, give rise to non-trivial cross-correlations with distinctive features for primordial non-Gaussianity. One key feature is that the production of GWs during inflation can be enhanced by the cubic interaction of the graviton with phonons (Celoria et al. 2021); the spectral index of the secondary produced GWs is blue-tilted with the amplitude within the LISA sensitivity.

8.5 UV complete models of $R + \alpha R^2$ model

Starobinsky's $R + \alpha R^2$ model of inflation matches the latest CMB data extremely well (Akrami et al. 2020; Starobinsky 1983). Since massless gravity contains only derivative interactions, it invites higher and infinite covariant derivative contributions as well. One particularly attractive model of higher derivative theory of gravity which contains infinite covariant derivatives and generalizes the quadratic curvature theory of gravity has been presented in Biswas et al. (2006), Modesto (2012), Biswas et al. (2012a). It has several cosmological implications, from providing the initial conditions from a non-singular cosmology to modifying the power spectrum for the primordial GWs (Koshelev et al. 2018, 2020). One particular subset of the action has been studied deeply, which generalizes Starobinsky's model and recovers it in the IR limit:

$$S = \int d^4x\sqrt{-g}\left(\frac{M_p^2}{2}R + \frac{\lambda}{2}\left[R\mathcal{F}_1(\Box_s)R + W_{\mu\nu\rho\sigma}\mathcal{F}_2(\Box_s)W^{\mu\nu\rho\sigma}\right]\right). \tag{118}$$

Here $\Box_s = \Box/M_s^2$ with M_s being the scale of non-locality, and λ is a dimensionless parameter useful to control the effect of higher curvature contributions. In the limit $M_s \to \infty$, one recovers the local Starobinsky's model of inflation. The ghost-free condition around an inflationary, i.e. approximate de Sitter background, constrains the gravitational form factors $\mathcal{F}_1$ and $\mathcal{F}_2$ (Biswas et al. 2016, 2017). Noticeably, the scalar power spectrum does not get any modification compared to the local Starobinsky's model of $R + \alpha R^2$ inflation (Starobinsky 1983). However, the

gravitational power spectrum, the tilt and the tensor to scalar ratio r all get modified in an interesting manner (Koshelev et al. 2018, 2020):

$$\begin{aligned} \mathcal{P}_T &= \frac{1}{12\pi^2 \mathcal{F}_1(m^2/M_s^2)}(1-3\epsilon)e^{-2\gamma_T(-\bar{R}/2M_s^2)}|_{k=aH}, \\ n_T &\equiv \frac{d\ln \mathcal{P}_T}{d\ln k}|_{k=aH} \approx -\frac{3}{2N^2} - (\frac{2}{N}+\frac{3}{2N^2})\frac{\bar{R}}{2M_s^2}\gamma_T(-\frac{\bar{R}}{2M_s^2})|_{k=aH}, \\ r &= \frac{12}{N^2}e^{-2\gamma_T(-\bar{R}/2M_s^2)}|_{k=aH}. \end{aligned} \tag{119}$$

The crucial difference here in comparison with the local Starobinsky model is that the tensor power spectrum is scaled by an exponential factor of γ_T evaluated at the pole of the tensor mode $\bar{R}/(6M_s^2)$, where $\bar{R} = 3.7 \times 10^{-8}(55/N_*)^3 M_p^2$ denotes the Ricci scalar evaluated at the pivot scale $k_* = aH$, and N_* denotes the number of e-foldings of inflation corresponding to the pivot scale. Accordingly, also the tensor tilt gets modified. The ghost-free condition demands that γ_T is an entire function (namely, that it can be represented as a power series that converges everywhere in the complex plane) (Biswas et al. 2016, 2017). In the local R^2 model one obtains $r = 12/N^2 = 3(1-n_s)^2$ as it follows from the original computation of scalar and tensor power spectra generated during inflation (Starobinsky 1983). From the CMB data (Ade et al. 2021) we can infer that the constraint $r < 0.036$ implies $\gamma_T > -1.05$ at $N_* = 55$, while there are no constraints on the tilt in the tensor power spectrum, due to lack of data. LISA could be able to test it, although there are indications that at LISA frequencies the nonlocal model is indistinguishable from local Starobinsky inflation (Koshelev et al. 2018; Calcagni and Kuroyanagi 2021) (section 9.3). Additional mechanisms (Bartolo et al. 2016b) or a modification in the theory (e.g., in the form factor) could reopen this opportunity.

8.6 Preheating

Preheating is characterised by non-perturbative particle production mechanisms (Traschen and Brandenberger 1990; Kofman et al. 1994; Shtanov et al. 1995; Kaiser 1996; Khlebnikov and Tkachev 1996; Prokopec and Roos 1997; Kaiser 1997; Kofman et al. 1997; Greene et al. 1997; Kaiser 1998), which typically take place after inflation in many models of particle physics (see Allahverdi et al. 2010; Amin et al. 2014; Lozanov 2019 for reviews). Following the end of inflation, interactions between the inflaton and some other field species—the *preheat field(s)*—can induce an exponential growth of the modes of the preheat field(s) within certain bands of momenta. A paradigmatic example of this is *parametric resonance* (Kofman et al. 1994, 1997; Greene et al. 1997; Figueroa and Torrenti 2017b), though there are other mechanisms (see below). The field gradients created during this stage can generate a sizeable anisotropic stress to source GWs, with the specific details of the resulting GW spectrum depending strongly on the considered scenario (Khlebnikov and Tkachev 1997; Easther and Lim 2006; Easther et al. 2007; García-Bellido and Figueroa 2007; García-Bellido et al. 2008; Dufaux et al. 2007, 2009; Kusenko and

Mazumdar 2008; Kusenko et al. 2009; Fenu et al. 2009; Figueroa et al. 2011). In general, preheating mechanisms are very efficient in transferring a significant fraction of the total energy available from the inflationary sector into the preheat field(s), and as a result, a large amount of GWs are radiated in the process. Furthermore, if the inflaton-preheat field coupling is tuned to certain values, the resulting SGWBs may develop large anisotropies at cosmological scales (Bethke et al. 2013, 2014).

For illustrative purposes, let us consider a standard scenario where the inflaton oscillates around the minimum of its potential after the end of inflation. For example we can consider a power-law potential $V(\phi) = \frac{1}{p}\lambda\mu^{4-p}\phi^p$, with λ a dimensionless coefficient, μ some mass scale, and p an integer index $p \geq 2$. Denoting as $t_\star$ the end of inflation, the inflaton oscillates for $t \gtrsim t_\star$ with a time-dependent frequency $\Omega_{\rm osc} \equiv \omega_\star (t/t_\star)^{1-2/p}$, $\omega_\star \equiv \sqrt{\lambda}\mu^{(2-p/2)}\phi_\star^{(p/2-1)}$, where $\phi_\star \equiv \phi(t_\star)$ (Figueroa and Torrenti 2017b). To be specific, let us also consider a quadratic interaction $g^2\phi^2\chi^2$ between the inflaton ϕ and a the preheat field χ, with g a dimensionless coupling constant. If the *resonance parameter* $q_\star \equiv g^2\phi_\star^2/\omega_\star^2$ is much larger than unity $q_\star \gg 1$, the preheat field is excited through a process of *broad resonance* during the inflaton oscillations, with the amplitude of the resonant modes growing exponentially inside a Bose-sphere of radius $k \lesssim k_\star \sim q_*^{1/4}\omega_\star$. This radiates GWs efficiently within a similar band of momenta. At the end of the process the resulting energy density spectrum of GWs exhibits a peak with amplitude and location (redshifted to frequencies today) given by (Figueroa and Torrenti 2017a)

$$f \simeq 8 \cdot 10^9 \left(\frac{\omega_\star}{\rho_\star^{1/4}}\right) \epsilon_\star^{\frac{1}{4}} q_\star^{\frac{1}{4}+\eta} \text{ Hz}, \tag{120a}$$

$$\Omega_{\rm GW}^0(f) \simeq \mathcal{O}(10^{-9}) \times \epsilon_\star\, \mathcal{C} \frac{\omega_\star^6}{\rho_\star M_p^2}\, q_\star^{-\frac{1}{2}+\delta}, \tag{120b}$$

where $\rho_\star$ is the total energy density at $t = t_\star$, η and δ are parameters that account for non-linearities of the system, and $\mathcal{C}$ is a constant that characterises the strength of the resonance. The factor $\epsilon_\star \equiv (a_\star/a_{\rm RD})^{1-3w}$ parametrises the expansion history between the end of inflation and the onset of RD, assuming an averaged EoS $w \neq 1/3$ during this period (if $w = 1/3$ then $\epsilon_* = 1$). The values for $\mathcal{C}$, η, and δ, can only be determined with classical lattice simulations in a model by model basis.

Leaving aside non-linear effects for simplicity, we observe that the frequency and amplitude of the peak, roughly scale as $f \sim q_\star^{1/4}$ and $\Omega_{\rm GW,0} \sim q_\star^{-1/2}$. This means that in order to shift the peak to observable frequencies, we need to decrease $q_\star$; but in doing so, we further decrease the amplitude of the signal. Using this linear approximation we see that decreasing the peak frequency say by an order of magnitude, implies the reduction of the amplitude of the background by two orders of magnitude. Furthermore, we see that these backgrounds can only be expected down to a minimum frequency, as efficient GW production requires $q_* > 1$ to sustain broad resonance during the field instability, and hence $q_* = 1$ marks a minimum frequency we can think of. Even though such scaling behaviours are modified when

considering corrections due to non-linearities, the logic persists (Figueroa and Torrenti 2017a), and as a result these backgrounds are forced to be peaked at high-frequencies way above those accessible by LISA. To be concrete, considering for instance a quartic potential around the minimum, we obtain $f \simeq (10^7 - 10^8)$ Hz and $\Omega_{\rm GW,0} \simeq (10^{-13} - 10^{-11})$, when assuming the range $q_\star \in (1, 10^4)$.[29] For a quadratic potential around the minimum of the potential, we find instead (assuming $\epsilon_\star = 1$) a frequency $f \simeq (10^8 - 10^9)$ Hz and amplitude $\Omega_{\rm GW,0} \simeq (10^{-12} - 10^{-11})$, when considering a resonance parameter $q_\star \in (10^4, 10^6)$. The conclusion is clear, these backgrounds are completely out of reach of current and (so far) planned direct detection GW experiments.

If the scalar field interactions induce a tachyonic effective mass in the preheat species, GWs can also be strongly produced, e.g. during hybrid preheating (García-Bellido and Figueroa 2007; García-Bellido et al. 2008; Dufaux et al. 2009). In this case, contrary to parametric resonance, the present day frequency and amplitude of the generated SGWB might be tuned to peak at small frequencies, while retaining a large amplitude. This depends on the model parameters, but in general a strong fine-tuning is required for this to happen. A similar circumstance arises in the case of the GWs produced from oscillons produced during hilltop preheating (Antusch et al. 2017, 2018; Amin et al. 2018), which upon similar fine tuning of the potential parameters, can also lead to observable GW backgrounds at low frequencies.

If the field species involved in preheating are of a different nature than just scalar fields, then new channels of GW production open up. For example, GWs can be produced during the out-of-equilibrium excitation of fermions after inflation, both for spin-1/2 (Enqvist et al. 2012; Figueroa and Meriniemi 2013; Figueroa 2014) and spin-3/2 (Benakli et al. 2019) fields. In this case a SGWB with large amplitude is also forced to peak at high frequencies. GWs can also be generated when the preheat fields are (Abelian and non-Abelian) gauge fields. For example gauge fields could be coupled to a charged scalar field via standard gauge covariant derivatives like in Dufaux et al. (2010), Figueroa et al. (2016), Tranberg et al. (2018), or to a pseudo-scalar field through a derivative axial coupling as in Adshead et al. (2018), Adshead et al. (2020a), Adshead et al. (2020b). Preheating can be remarkably efficient in the second case (Adshead et al. 2015; Cuissa and Figueroa 2019), with the energy density produced in GWs possibly reaching up to $\sim 1\%$ of the total energy in the system for the strongest coupling strengths (Adshead et al. 2020a, b). The peak frequency is however also very large in these scenarios as well.

In conclusion, preheating mechanisms are capable of creating very large SGWBs, but these are naturally peaked at very high frequencies, which are typically beyond the LISA window. Some particular models can sustain a sizeable amplitude at LISA frequencies, but only at the expense of a strong fine-tuning of their parameters.

[29] The GW spectrum in the quartic potential case also features additional peaks, see Figueroa and Torrenti (2017a) for more details.

8.7 Summary of distinctive gravitational-wave observables from inflation

In what follows we describe the relevant observables that can be used to break possible degeneracies between the SGWB from inflation, and the one due to other cosmological sources, as well as to astrophysical ones.

8.7.1 Chirality

Although parity violation has so far been observed only in weak interactions, it is important to investigate whether the same phenomenon may occur also in the very early universe, during inflation. In the primordial context, we shall refer to chirality whenever the two polarisations of GWs have different amplitudes, see Sect. 5.

For convenience, one may introduce the parameter $\chi \equiv |P_\gamma^L - P_\gamma^R| / \sum_\lambda P^\lambda$, whose range extends up to $\chi = 1$. Several mechanisms for generating chiral GWs are found in the literature. The common trait to such realisations is the presence of a Chern–Simons-type interaction. In the case of the EM field strength such term reads

$$\mathcal{L} \supset \phi F_{\mu\nu} \tilde{F}^{\mu\nu}, \tag{121}$$

where $\tilde{F}^{\mu\nu}$ is the dual EM field. The reader will recognise the similarities between Eq. (101) and (121). The comparison underscores the fact that the field corresponding to F does not need to be the Standard Model photon, nor an Abelian gauge field. In modified gravity theories, Chern–Simons gravity is obtained by promoting the three dimensional gravitational Chern–Simons term to 4D (Jackiw and Pi 2003; Alexander and Yunes 2009):

$$\mathcal{L} \supset f(\phi) R^\sigma{}_{\mu\nu\rho} \tilde{R}_\sigma^{\ \mu\nu\rho}, \tag{122}$$

where $\tilde{R}$ is the dual Riemann tensor. The matter field ϕ in the last two equations is typically (but not necessarily) identified as the inflaton in models of the early phase acceleration. The parity violation ensuing from Chern–Simons-type coupling in the early universe can be tested across a vast range of scales, from CMB (Lue et al. 1999; Thorne et al. 2018) to interferometers (Crowder et al. 2013; Smith and Caldwell 2017; Domcke et al. 2020b), including LISA. Both types of interactions in Eqs. (121) and (122) have been extensively studied (Anber and Sorbo 2010; Satoh 2010; Crisostomi et al. 2018; Bartolo and Orlando 2017; Bartolo et al. 2019d; Qiao et al. 2020; Bartolo et al. 2021; Bordin and Cabass 2020)), sometimes considered together (Lue et al. 1999; Mirzagholi et al. 2020a), and investigated as emerging from quantum gravity (in the sense of Hořava–Lifshitz theories, Horava 2009) (Takahashi and Soda 2009).

8.7.2 Frequency profile

The single-field slow-roll inflationary paradigm predicts a slightly red-tilted GW spectrum. The tilt of the tensor power spectrum is indeed proportional to the slow-roll parameter, $n_T \simeq -2\epsilon \ll 1$. Such a GW signal is well below the sensitivity of

LISA and could even elude detection from more sensitive instruments, including the proposed BBO. This is the key notion behind the claim that a detection of primordial GWs by LISA would be a smoking gun for an inflationary mechanism that goes beyond the single-field slow-roll scenario. With some interesting exceptions (Mylova et al. 2018) one may go further and state that a primordial signal at LISA scales (and sensitivity) is strongly suggestive of multi-field (or multi-clock) dynamics.

A typical case in point is that of GW sourced by extra fields during inflation. Whenever the sourced contribution goes beyond vacuum fluctuations, the richer multi-field dynamics can give rise to a non-trivial frequency dependence, from a blue GW spectrum to a "bump-like" structure and to oscillatory features mimicking the ones of the scalar power spectrum. For all these examples there exist explicit realisations, as detailed in Sects. 8.2 and 8.3.

In studying the SGWB frequency profile one ought to be aware of the bounds at CMB scales, those set at intermediate scales by PTAs and, perhaps most importantly for LISA, those set at the relatively close frequencies accessed by LIGO/Virgo.

8.7.3 Anisotropies

The angular resolution of the LISA detector might enable a detection of another peculiar feature useful in the SGWB characterisation process: the anisotropy (direction dependence) in the energy density. Such anisotropies contain information about the generation process of GWs and their propagation across cosmic inhomogeneities. Using a Boltzmann equation approach, the contribution coming from the generation mechanism retains a frequency dependence, which is peculiar of the SGWB, and, due to the non-thermal nature of the graviton distribution function at their decoupling time (Bartolo et al. 2019a, 2020b). The contribution arising from the propagation of GWs through large-scale cosmological scalar (and tensor) background perturbations, happens to be larger compared to the same effect for CMB photons. So, in a similar way to CMB photons, the SGWB from e.g. inflation is affected by the Sachs–Wolfe and the Integrated Sachs–Wolfe effects. The former is a gravitational redshift, due to the difference of the gravitational potential at the moment of the SGWB production and today. The latter is due to the variation of the gravitational potential along the line of sight from the SGWB production to its the detection, integrated in time (Bartolo et al. 2019a, 2020b).

It turns out that LISA is sensitive to these effects in the angular power spectrum if the SGWB isotropic energy density is $\Omega_{\rm GW} \gtrsim 10^{-12}$ (Bartolo et al. 2019a, 2020b; Valbusa Dall'Armi et al. 2021). For a representative inflationary model, namely axion inflation (Cook and Sorbo 2012; García-Bellido et al. 2016), it was shown that the predicted SGWB can be within the reach of LISA and exhibits anisotropies with a large frequency dependence, a possible distinctive target for the SGWB detection and characterisation in LISA.

In the remaining part of this subsection we will discuss GW anisotropies that result from squeezed primordial non-Gaussianity. This is yet another case in point for the use of GW anisotropies as a probe of the production mechanism for GWs. Let us briefly describe the genesis of these non-Gaussianity-sourced anisotropies. A

squeezed primordial bispectrum encodes a coupling between two short-wavelength modes and one long-wavelength mode. The effect of the very same coupling is also manifest at the level of the power spectrum of the short-wavelength modes, in the form of a modulation by the long-wavelength mode (Jeong and Kamionkowski 2012; Dai et al. 2013; Brahma et al. 2014; Dimastrogiovanni et al. 2014, 2016). The magnitude and form of this modulation depends on the specific type of interactions (as dictated by the inflationary Lagrangian) and on the nature (e.g. scalar vs. tensor) of the long-wavelength mode. Let us consider the case of a tensor bispectrum:

$$\langle h_{\mathbf{k}_1} h_{\mathbf{k}_2} h_{\mathbf{q}} \rangle = (2\pi)^3 \delta^{(3)}(\mathbf{k}_1 + \mathbf{k}_2 + \mathbf{q}) B^{\mathrm{ttt}}(\mathbf{k}_1, \mathbf{k}_2, \mathbf{q}). \tag{123}$$

In the squeezed limit, $q \ll k_1 \simeq k_2$, and for models preserving statistical isotropy and parity, the long wavelength tensor mode imprints a quadrupolar modulation in the primordial power spectrum of the short-wavelength modes (Dimastrogiovanni et al. 2020):

$$P_h^{\mathrm{mod}}(\mathbf{k}, \mathbf{x}) = P_h(k)[1 + \mathcal{Q}_{\ell m}(\mathbf{k}, \mathbf{x})\, \hat{n}_\ell \hat{n}_m], \tag{124}$$

where $\mathbf{k} = k\hat{n}$ and we have defined

$$\mathcal{Q}_{\ell m}(\mathbf{k}, \mathbf{x}) \equiv \int \frac{d^3 q}{(2\pi)^3} e^{i\mathbf{q}\cdot\mathbf{x}} \sum_{\lambda_3} h_{\ell m}^{\lambda_3}(\mathbf{q}) F_{\mathrm{NL}}^{\mathrm{ttt}}(\mathbf{k}, \mathbf{q}). \tag{125}$$

Here $F_{\mathrm{NL}}^{\mathrm{ttt}}(\mathbf{k}, \mathbf{q})$ is the amplitude of the tensor bispectrum in the squeezed limit, normalised by the product of the power spectra, $P_h(k) \cdot P_h(q)$. The anisotropy in Eq. (124) determines a contribution to the energy density contrast (see Eq. (35) for the definition of δ_{GW}) given by

$$\delta_{\mathrm{GW}}(k, \hat{n}) = \mathcal{Q}_{\ell m}(\mathbf{k}, \mathbf{d})\, \hat{n}_\ell \hat{n}_m, \tag{126}$$

where $\mathbf{d} = -\hat{n}d$, $d \equiv \eta_0 - \eta_{\mathrm{in}}$ being the separation in conformal time between horizon re-entry of the k-mode and the present time.

In a similar way, for inflationary models predicting a long-short mode coupling between scalars and tensors, a long-wavelength scalar fluctuation will modulate the power spectrum of GWs on small scales:

$$P_h^{\mathrm{mod}}(\mathbf{k}, \mathbf{x}) = P_h(k) \left[1 + \int \frac{d^3 q}{(2\pi)^3} e^{i\mathbf{q}\cdot\mathbf{x}}\, \zeta(\mathbf{q}) F_{\mathrm{NL}}^{\mathrm{stt}}(\mathbf{k}, \mathbf{q}) \right]. \tag{127}$$

This generates an anisotropic component for the GW energy density measured at present time, which leads to

$$\delta_{\mathrm{GW}}(k, \hat{n}) = \int \frac{d^3 q}{(2\pi)^3} e^{-id\hat{n}\cdot\mathbf{q}} \zeta(\mathbf{q}) F_{\mathrm{NL}}^{\mathrm{stt}}(\mathbf{k}, \mathbf{q}), \tag{128}$$

with $F_{\mathrm{NL}}^{\mathrm{stt}}(\mathbf{k}, \mathbf{q})$ being the amplitude of the scalar-tensor-tensor bispectrum in the squeezed limit, normalised by $P_\zeta(q) \cdot P_h(k)$.

Primordial non-Gaussianity is one of the most informative probes of field interactions during inflation. Already at the level of the bispectrum (the lowest-order non-Gaussian correlator), a variety of constraints can be placed on inflationary models based on its momentum dependence (a.k.a. shape) and overall amplitude. In particular, bispectra that receive substantial contribution in the *squeezed* momentum configuration are a smoking gun for inflationary dynamics that go beyond the single-field slow-roll realisation. This is due to the fact that, whenever the inflationary dynamics is guided by a single effective degree of freedom, the leading order contribution to the squeezed bispectrum can be removed by a gauge transformation (Maldacena 2003; Tanaka and Urakawa 2011; Pajer et al. 2013). Single-clock models therefore predict a suppressed bispectrum. On the other hand, typical classes of models that can lead to sizeable soft limits for cosmological correlators include multiple fields, excited initial states, or an inflationary background that breaks space diffeomorphism invariance.

While at large (e.g. CMB) scales primordial bispectra can be directly constrained, this is not the case at small scales due to loss of coherence from propagation in the perturbed universe (see e.g. discussion in Sect. 10.3). Anisotropies are therefore a key observable for constraining tensor and mixed non-Gaussianity at interferometer scales.

As an example, in the left panel of Fig. 23 we display the auto-correlation $\langle \delta_{\mathrm{GW},\ell_1 \mathrm{m}_1} \delta_{\mathrm{GW},\ell_2 \mathrm{m}_2} \rangle = \delta_{\ell_1 \ell_2} \delta_{m_1 m_2} \mathcal{C}_{\ell_1}^{\mathrm{GW}}$ arising from anisotropies of the kind described in Eq. (128) (red line). For the sake of comparison, in the same plot we show the auto-correlation for anisotropies imprinted as gravitons travel in the perturbed background after horizon re-entry (blue line) (Alba and Maldacena 2016; Contaldi 2017; Bartolo et al. 2019a, 2020b).

The recent works (Contaldi et al. 2020; Bartolo et al. 2022) study the capability of LISA to access the SGWB anisotropies. See Sect. 12 for more details.

8.7.4 Cross-correlations

Anisotropies such as those just discussed in Sect. 8.7.3 are produced by the effect of long-wavelength (scalar or tensor) perturbations and are therefore correlated with anisotropies in the CMB (Adshead et al. 2021; Malhotra et al. 2021). These cross-correlations provide an additional observable for constraining primordial non-Gaussianity (see right panel of Fig. 23 for an application). As an example, we report in Fig. 24 the error in determining $F_{\mathrm{NL}}^{\mathrm{stt}}$ using a measurement of these cross-correlations. The calculation of the error follows that of Malhotra et al. (2021) and it is adapted here, under that assumption that Taiji and LISA should happen to fly together (Ruan et al. 2020b; Orlando et al. 2021). We see that for the combination $\{r = 0.05, n_T = 0.30\}$ one would be able to detect $F_{\mathrm{NL}}^{\mathrm{stt}}$ of order 10^4 or larger.

For any given inflationary model generating non-trivial scalar-tensor-tensor or tensor-tensor-tensor bispectra in the squeezed limit, the overall level of the GW anisotropies is determined by the specific form of the angular dependence of the bispectra and by the magnitude of the F_{NL} parameters. Typically, there exist minimum values of F_{NL} below which the GW anisotropy map is dominated by noise.

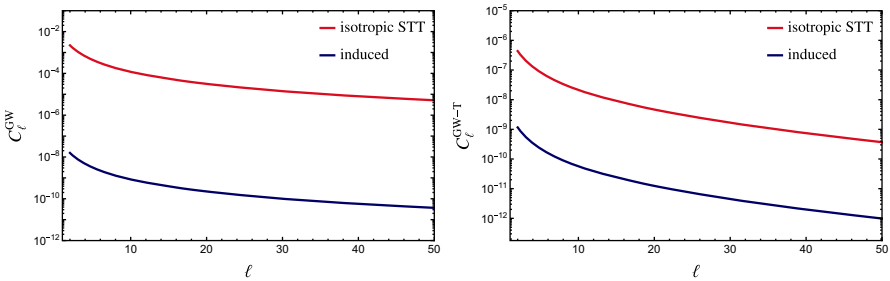

Fig. 23 Left panel: Auto-correlation of GW anisotropies induced by a scalar-tensor-tensor squeezed bispectrum with $F_{\rm NL}^{\rm stt} \sim \mathcal{O}(10^3)$ (red line), and of GW anisotropies arising from propagation through the perturbed background (blue line). Right panel: Cross-correlation of GW anisotropies and CMB temperature anisotropies in the same two cases

Cross-correlations can be particularly helpful in these cases as they have the potential to constrain smaller levels of non-Gaussianity (Malhotra et al. 2021).

9 Tests of non-standard pre-Big-Bang nucleosynthesis cosmology via the SGWB

Section coordinator: G. Calcagni. Contributors: I. Ben-Dayan, G. Calcagni, C-F. Chang, Y. Cui, D.G. Figueroa, S. Kuroyanagi, M. Lewicki, A. Mazumdar, G. Servant, P. Simakachorn.

9.1 Introduction

In the standard model of cosmology, the universe begins with a inflationary epoch that first induces an exponential growth of the universe and then reheats it with a very hot plasma. In the standard picture, it is the energy density of such a plasma that dominates the expansion of the universe until the matter and DE domination final stages. It is however worth remembering that this picture is based on several

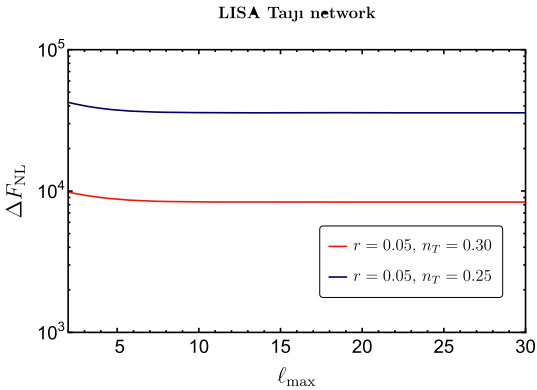

Fig. 24 The expected 1σ error in determing $F_{\rm NL}^{\rm stt}$ with cross-correlations of CMB temperature anisotropies and GW anisotropies, as a function of $\ell_{\rm max}$

theoretical assumptions and has only been tested up to temperatures $T \approx 5\,\mathrm{MeV}$ thanks to data from CMB (Aghanim et al. 2020) and successful predictions of BBN (Cyburt et al. 2016). The period between that temperature and inflation still holds many unknowns (Allahverdi et al. 2020). In this section, we will discuss how detection of a SGWB by LISA would allow us to probe the evolution of the universe during that time. We will begin with the possibility of probing the expansion rate including the number of relativistic degrees of freedom thanks to the SGWB sources discussed in the previous sections and move on to possible departures from GR.

According to the standard inflationary paradigm in GR, scalar and tensor perturbations are generated during an early era of accelerated expansion induced by a slow-rolling phase. In the vanilla inflationary scenario, the primordial tensor spectrum is red-tilted at CMB scales, i.e. its amplitude decreases with frequency. If inflation is followed by the long-lasting RD period, then also the produced SGWB, late-time remnant of the primordial tensor spectrum, turns out to be red-tilted and its amplitude at the mHz—Hz frequencies remains too small to be detected by any present or planned near-future GW detector. However, both deviations from the vanilla inflationary scenario (see Sect. 8) and the usual RD epoch of the standard model of cosmology can enhance the SGWB to amplitudes large enough to reach the LISA sensitivity. In the latter case, for instance, if the expansion rate of the universe between the end of inflation and the onset of RD, is dictated by an effective EoS parameter $w \neq 1/3$, the inflationary SGWB is naturally tilted at high frequencies, for the modes that re-entered the Hubble radius during such non-standard epoch. If the EoS is stiff, i.e. $w > 1/3$, then the tilt is blue, thus enhancing the power of the GW spectrum at large frequencies, and hence making this branch of the spectrum potentially observable with LISA. If, on the contrary, the EoS is $w < 1/3$, then the tilt at high frequencies is red, and hence the spectrum goes below the standard plateau amplitude due to modes crossing during RD.

Any modification of the expansion rate occurring after a FOPT also leaves its imprint on the SGWB produced by that phase transition. The modified redshift results in an overall shift of the entire signal but, more interestingly, characteristic features might also be produced in the signal. This is possible for modes with lengths larger than the horizon size at the time of the transition. If these modes enter the horizon during a time of modified expansion, the typical f^3 slope at low frequencies will be modified allowing us to decode the EoS at that time. However, as this feature is always present significantly below the main amplitude peak of the FOPT SGWB (see Sect. 6), measuring the expansion using this method will always be much more challenging than the initial detection of the spectrum.

Cosmic strings are another possible GW source which would also allow us to probe the expansion history. As a network of strings would continuously produce GWs throughout most of cosmological history (see Sect. 7), also the expansion history is encoded in the resulting spectral shape. This, in fact, includes not only drastic modifications such as periods of non-standard expansion, but also subtler modifications including the number of degrees of freedom contributing to the radiation dominating at early times. As we will see, an accurate observation of a

SGWB from cosmic strings will always give us some information on the expansion rate of the very early universe.

Finally, we will also explore the possibility to test quantum gravity cosmological models via SGWB observations at LISA. After excluding a plethora of models whose SGWB does not reach the instrument's sensitivity curve, we single out two pre-Big-Bang scenarios as candidates that could generate a signal relevant for LISA science.

9.2 Non-standard expansion histories

9.2.1 Inflation

Equation (99) provides the amplitude of the vacuum tensor modes produced at super-horizon scales during inflation. During the expansion history following inflation, the tensor modes re-enter successively back inside the Hubble radius, turning into a proper classical (yet stochastic) background of GWs. Once the modes become sub-Hubble, they start oscillating with a decaying amplitude $h_{ij} \propto 1/a$ (this is independent of the expansion rate (Caprini and Figueroa 2018)), propagating as relativistic degrees of freedom. Since modes with different wavelengths re-enter the Hubble radius at different moments of cosmic evolution, different modes may propagate through different periods of expansion. As a result, modes with very different wavelengths may sustain very different amplitudes with respect to each other, depending on the rate of expansion of the universe at their time of Hubble-crossing. To characterise the spectrum of the SGWB today, we can write the energy density spectrum normalised to the critical density $\rho_{\rm crit} = 3M_{\rm Pl}^2 H^2$, as (Caprini and Figueroa 2018)

$$\Omega_{\rm GW}(t,k) \equiv \frac{1}{\rho_{\rm crit}} \frac{d\rho_{\rm GW}(t,k)}{d\ln k} = \frac{k^2}{12a^2(t)H^2(t)} P_h(t,k), \tag{129}$$

where the power spectrum $P_h(t,k)$ at a generic time t is related to the power $P_h(k)$ generated super-horizon during inflation by a transfer functions,

$$P_h(t,k) \equiv T_h(t,k)P_h(k), \quad T_h(t,k) \simeq \frac{1}{2}\left[\frac{a_k}{a(t)}\right]^2. \tag{130}$$

The transfer function $T_h(t,k)$ depends on the expansion history between the moment $t = t_k$ of horizon re-entry of a given mode k, and a later moment $t > t_k$. Here t_k is implicitly defined from the condition $a_k H_k \equiv k$, with $a_k \equiv a(t_k)$, and $H_k \equiv H(t_k)$. The factor 1/2 is due to the time-average of the rapidly-oscillating sub-horizon wave.

The transfer function today can be evaluated as

$$T_h(k) \simeq \frac{1}{2}\left(\frac{a_k}{a_0}\right)^2 \simeq \frac{1}{2}\mathcal{G}_k \Omega_{\rm rad}^{(0)} \left(\frac{a_0 H_0}{a_k H_k}\right)^2, \quad \mathcal{G}_k \equiv \left(\frac{g_{*,k}}{g_{*,0}}\right)\left(\frac{g_{s,0}}{g_{s,k}}\right)^{4/3}, \tag{131}$$

where g_s and g_* are the relativistic number density of species contributing to the total entropy and energy densities, respectively. Using $\Omega_{\rm rad}^{(0)} \simeq 9 \cdot 10^{-5}$, $g_{s,0} \simeq 3.91$,

$g_{*,0} = 2$, and $g_{s,k} \simeq g_{*,k} \simeq 106.75$, so that $\mathcal{G}_k \simeq 0.65$, we obtain that tensor modes crossing during the RD epoch lead to an energy density spectrum with amplitude

$$\Omega_{\rm GW}^{(0)}\Big|_{\rm inf} \simeq \mathcal{G}_k \frac{\Omega_{\rm rad}^{(0)}}{12\pi^2}\left(\frac{H_{\rm inf}}{m_{\rm Pl}}\right)^2\left(\frac{H_{\rm inf}}{H_{\rm max}}\right)^2\left(\frac{f}{f_{\rm Pl}}\right)^{n_T} \simeq 5\times 10^{-16}\left(\frac{H_{\rm inf}}{H_{\rm max}}\right)^2\left(\frac{f}{f_{\rm Pl}}\right)^{n_T}, \tag{132}$$

with n_T given by the original inflationary tilt. In other words, the RD energy spectrum retains the (quasi-) scale invariant spectral shape of the original inflationary tensors. We note that in evaluating Eq. (132) we have considered for concreteness that $g_{s,k}, g_{*,k}$ equal the SM degrees of freedom before electroweak symmetry breaking, and hence they are independent of k. In reality the number of SM relativistic degrees of freedom change with the scale, but for simplicity in Eq. (132) we considered an identical suppression for all the modes as $\mathcal{G}_k \simeq 0.65$, so that we can provide a single number for the amplitude of this plateau.

If between the end of inflation and the onset of RD there is a period of expansion characterised by an EoS different than that of radiation $w \neq 1/3$, the inflationary GW energy density spectrum develops a tilt within the range of scales corresponding to the modes crossing the Hubble radius during such period. As a result, the (quasi-) scale invariance of the original tensor spectrum is lost. This feature is actually quite interesting from an observational point of view, as we might detect or constrain in this way the post-inflationary expansion history, and hence the properties of the fields driving the expansion between inflation and RD (Giovannini 1998, 1999; Boyle and Steinhardt 2008; Watanabe and Komatsu 2006; Boyle and Buonanno 2008; Kuroyanagi et al. 2009, 2011, 2015; Figueroa and Tanin 2019ab; Gouttenoire et al. 2021a).

In order to understand better the above discussion, let us consider that between the end of inflation and the onset of RD, the expansion rate is dictated by an effective EoS parameter $w \neq 1/3$. In scenarios where the inflaton potential is a monomial, $V(\phi) \propto \phi^p$, the inflaton oscillates around the minimum of such a potential after inflation, so that an effective EoS, averaged over inflaton oscillations, emerges as $w \simeq (p-2)/(p+2)$ (Turner 1983; Lozanov and Amin 2017). For $p<4$ the EoS is in the range $0<w<1/3$. For $p = 2$, the oscillations of a massive free field lead to an energy density redshifting on average (over one oscillation cycle) as $\langle \rho_\phi \rangle_{\rm osc} \propto 1/a^3$, analogous to that of non-relativistic particle species. Thus, an EoS of $w \simeq 0$ emerges in that case. Nothing prevents however the possibility of a stiff dominated stage with EoS $w = w_s$ for $1/3<w_s<1$. Such a case can be actually achieved quite naturally if the kinetic energy of the inflaton dominates after inflation, either through inflaton oscillations (Turner 1983) under a steep potential (e.g. $V(\phi) \propto \phi^p$ with $p > 4$), or simply by an abrupt drop of the inflationary potential at at moment that triggers itself the end of inflation.

Propagating the inflationary tensor modes through the epoch starting immediately after the end of inflation, leads to a GW energy density spectrum today, expressed as a function of present-day frequencies $f = k/(2\pi a_0)$, like (Figueroa and Tanin 2019a)

$$\Omega_{\rm GW}^{(0)}(f) = \Omega_{\rm GW}^{(0)}\Big|_{\rm inf} \times \mathcal{W}(f/f_{\rm RD}) \times \mathcal{C}_w \left(\frac{f}{f_{\rm RD}}\right)^{2\left(\frac{3w-1}{3w+1}\right)} \simeq \Omega_{\rm GW}^{(0)}\Big|_{\rm inf} \times \begin{cases} 1 & , \quad f \ll f_{\rm RD} \\ \mathcal{C}_w \left(\frac{f}{f_{\rm RD}}\right)^{2\left(\frac{3w-1}{3w+1}\right)} & , \quad f \gg f_{\rm RD} \end{cases} \tag{133}$$

with $\mathcal{C}_w$ a numerical prefactor in the range $1 < \mathcal{C}_w < 2^{5/2}/\pi \simeq 1.80$ for $1/3 < w < 1$, and where $f_{\rm RD} \equiv k_{\rm RD}/(2\pi a_0)$ is the frequency corresponding to the horizon scale at the onset of RD, $k_{\rm RD} = a_{\rm RD} H_{\rm RD}$, and $\mathcal{W}(x)$ is a window function connecting the two sides of the spectrum: the high-frequency branch on the one hand, corresponding to modes crossing during the non-standard period ($f \gg f_{\rm RD}$), and the low frequency branch corresponding to modes crossing during RD ($f \ll f_{\rm RD}$). The tilt in Eq. (133) indicates that models with a stiff epoch between the end of inflation and the onset of RD are actually very appealing observationally, as in these scenarios a blue tilt is developed in the GW energy density spectrum at large frequencies, with $0 < n_T < 1$ (Giovannini 1998, 1999; Riazuelo and Uzan 2000; Sahni et al. 2002; Tashiro et al. 2004; Boyle and Buonanno 2008; Giovannini 2008, 2009; Caprini and Figueroa 2018; Bernal and Hajkarim 2019; Figueroa and Tanin 2019a). This potentially opens up the possibility of detection by upcoming direct detection GW experiments, including LISA. The presence of a stiff period is actually well-motivated theoretically in scenarios like Quintessential inflation (Peebles and Vilenkin 1999; Peloso and Rosati 1999; Huey and Lidsey 2001; Majumdar 2001; Dimopoulos and Valle 2002; Wetterich 2014, 2015; Hossain et al. 2014; Rubio and Wetterich 2017), gravitational reheating (Ford 1987; Spokoiny 1993) (with the caveats explained in Figueroa and Tanin (2019b)), the Higgs-reheating scenario (Figueroa and Byrnes 2017) and generalisations (Dimopoulos and Markkanen 2018; Opferkuch et al. 2019). The GW spectrum in these scenarios is controlled by $w, f_{\rm RD}$, and $H_{\rm inf}$, and the parameter space compatible with a detection by various experiments has been recently analysed in Gouttenoire et al. (2021a), Bernal and Hajkarim (2019), Figueroa and Tanin (2019a). In Fig. 25 we can see the form of the spectrum in the left panel (including scale-dependent changes in $\mathcal{G}_k$ due to changes in the number of relativistic species). In the right panel of the same figure we plot the parameter space that LISA can probe. The tilt in Eq. (133) indicates that models with a stiff epoch between the end of inflation and the onset of RD are actually very appealing observationally, as in these scenarios a blue tilt is developed in the GW energy density spectrum at large frequencies, with $0 < n_T < 1$ (Giovannini 1998, 1999; Riazuelo and Uzan 2000; Sahni et al. 2002; Tashiro et al. 2004; Boyle and Buonanno 2008; Giovannini 2008, 2009; Caprini and Figueroa 2018; Bernal and Hajkarim 2019; Figueroa and Tanin 2019a). This potentially opens up the possibility of detection by upcoming direct detection GW experiments, including LISA. The presence of a stiff period is actually well-motivated theoretically in scenarios like Quintessential inflation (Peebles and Vilenkin 1999; Peloso and Rosati 1999; Huey and Lidsey 2001; Majumdar 2001; Dimopoulos and Valle 2002; Wetterich 2014, 2015; Hossain et al. 2014; Rubio and Wetterich 2017), gravitational reheating (Ford 1987; Spokoiny 1993) (with the caveats explained in Figueroa and Tanin

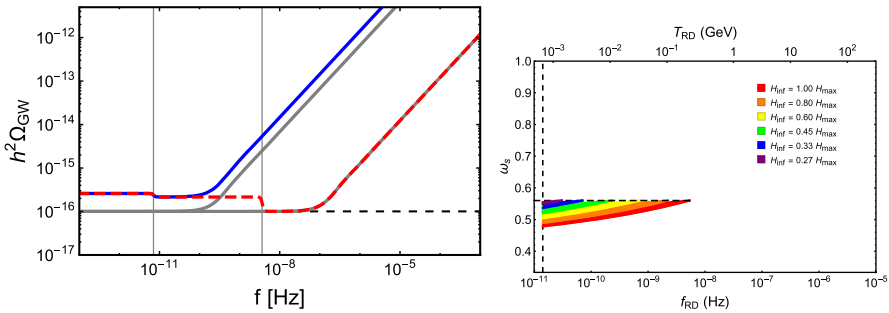

Fig. 25 Left panel: GW energy spectra including changes in the number of relativistic degrees of freedom, depending on whether the transition from stiff domination to RD takes place before (red dashed line) or after (blue solid line) than the QCD phase transition. For comparison we show the corresponding spectra (grey solid line) without correcting for changes in the number of degrees of freedom. Image reproduced with permission from Figueroa and Tanin (2019a), copyright by IOP/SISSA. Right panel: Parameter space region that LISA can probe after removing the region (above the dashed horizontal line) incompatible with the BBN bound on GW backgrounds. Here w_s refers to the EoS for a *stiff* background

(2019b)), the Higgs-reheating scenario (Figueroa and Byrnes 2017) and generalisations (Dimopoulos and Markkanen 2018; Opferkuch et al. 2019). The GW spectrum in these scenarios is controlled by w, $f_{\rm RD}$, and $H_{\rm inf}$, and the parameter space compatible with a detection by various experiments has been recently analysed in Bernal and Hajkarim (2019), Figueroa and Tanin (2019a), Gouttenoire et al. (2021a). In Fig. 25 we can see the form of the spectrum in the left panel (including scale-dependent changes in $\mathcal{G}_k$ due to changes in the number of relativistic species). In the right panel of the same figure we plot the parameter space that LISA can probe.

Consistency with upper bounds on SGWBs, like the BBN and CMB constraints, rules out a significant fraction of the observable parameter space. (See discussion at the end of Sect. 5.1.) This renders for instance this signal as unobservable by Advanced LIGO, independently of the parameter space $\{w, f_{\rm RD}, H_{\rm inf}\}$ (Figueroa and Tanin 2019a). The GW background remains detectable in LISA, but only in a small island of parameter space, see right panel of Fig. 25 corresponding contrived scenarios having a low EoS $0.46 \lesssim w \lesssim 0.56$, a high inflationary scale $H_{\rm inf} \gtrsim 10^{13}$ GeV at the same, and a low transition frequency 10^{-11} Hz$\lesssim f_{\rm RD} \lesssim 3.6 \times 10^{-9}$ Hz (or equivalently a low reheating temperature 1 MeV$\lesssim T_{\rm RD} \lesssim$150 MeV). There exists other bounds beyond those from BBN and CMB on the duration of the stiff era (Gouttenoire et al. 2021a).

A short kination era ($w = 1$) happening much after reheating and inside the radiation era can be realized naturally by rotating-axion dynamics in the early universe (Gouttenoire et al. 2021b; Co et al. 2022; Gouttenoire et al. 2021a). Such kination typically lasts for 2–10 e-foldings and occurs after a matter era such that the inflationary SGWB gets boosted into a peak shape that is highly observable by future planned GW observatories while evading the BBN and CMB constraints in Fig. 25. LISA can probe the striking signature for kination eras happening at 100 GeV–

100 TeV energy scales (Gouttenoire et al. 2021a, b). Interestingly, such GW peaked signature would be a unique probe of axion physics.[30]

If there is an intermediate phase with EoS in the range $0 \leq w < 1/3$, the transfer function of the inflationary GW spectrum in Eq. (133), develops instead a red-tilted high-frequency branch, corresponding to the modes propagating through that phase. If we could detect the (quasi-)scale invariant GW plateau part of the spectrum, the transition to the high-frequency branch due to the non-standard era, could be used to determine the reheating temperature $T_{\rm RD}$ of the universe. This is because the end of the non-standard era also corresponds to the onset of RD, and hence the pivot frequency $f_{\rm RD}$ separating the two branches in the energy density spectrum informs directly about the energy scale at the onset of RD (Nakayama et al. 2008; Kuroyanagi et al. 2009, 2011; D'Eramo and Schmitz 2019). Unfortunately, given the suppression of the amplitude of the plateau, c.f. Eq. (132), the determination of $T_{\rm RD}$ by this method cannot be probed with LISA, and only a futuristic experiment like BBO or DECIGO (Crowder and Cornish 2005; Seto et al. 2001; Sato et al. 2017) might have a chance.

Another interesting opportunity is to look for a signal of particles beyond the SM. When particles becomes non-relativistic as the temperature drops below the mass and decouple from thermal equilibrium, they no longer contribute to the radiation energy density. This can be seen as a change in the values of $g_{*,k}$ and $g_{s,k}$, resulting in a temporary speed-up of the Hubble expansion rate. SM particles induce changes in $g_{*,k}$ and $g_{s,k}$ in the frequency range of $\sim 10^{-12}$ to 10^{-5} Hz (Watanabe and Komatsu 2006), which is beyond the range of LISA sensitivity curve. However, any change due to BSM particles with mass near 100 TeV leave an imprint on the SGWB spectrum at the LISA sensitivity. This effect is not detectable in the case of standard slow-roll inflation, since the amplitude of the SGWB is far below the LISA sensitivity as in Eq. (132), while a strongly blue-tilted primordial spectrum would provide an opportunity to test BSM physics by LISA (Caldwell et al. 2019).

9.2.2 Phase transitions

We discussed the production of GWs in FOPTs in detail in Sect. 6. We will now discuss the impact a period of non-standard evolution would have on these backgrounds. The first most obvious change will come in through modified red-shifting of the spectra from the time of their production until today (Allahverdi et al. 2020; Gouttenoire et al. 2021a). Simply parametrising the non standard evolution through a barotropic parameter w we find for the abundance

[30] Such a peaked GW signature from a kination era induced by a spinning complex scalar field in the context of self-interacting DM was found and studied in Li et al. (2014), Rindler-Daller and Shapiro (2014), Li et al. (2017), Li and Shapiro (2021) where the initial rotation is postulated and the preceeding matter era is a consequence of inflaton oscillations rather than axion dynamics.

$$\Omega_{\mathrm{GW},0} = \left(\frac{a_*}{a_0}\right)^4 \left(\frac{H_*}{H_0}\right)^2 \Omega_{\mathrm{GW},*} = 1.67 \times 10^{-5} h^{-2} \left[\frac{100}{g_s(T_{\mathrm{RD}})}\right]^{\frac{4}{3}} \left[\frac{g_*(T_{\mathrm{RD}})}{100}\right] \left(\frac{H_*}{H_{\mathrm{RD}}}\right)^{2\frac{3w-1}{3w+3}} \Omega_{\mathrm{GW},*}, \tag{134}$$

and for the frequency

$$f_0 = \frac{a_*}{a_0} f_* = \frac{a_{\mathrm{RD}} H_{\mathrm{RD}}}{a_0} \frac{a_* H_*}{a_{\mathrm{RD}} H_{\mathrm{RD}}} \frac{f_*}{H_*} = 1.65 \times 10^{-5}\,\mathrm{Hz} \left(\frac{T_{\mathrm{RD}}}{100\,\mathrm{GeV}}\right) \left(\frac{100}{g_s(T_{\mathrm{RD}})}\right)^{\frac{1}{3}} \left(\frac{g_*(T_{\mathrm{RD}})}{100}\right)^{\frac{1}{2}} \left(\frac{f_*}{H_*}\right) \left(\frac{H_*}{H_{\mathrm{RD}}}\right)^{\frac{3w+1}{3w+3}},$$

where the asterisk ($*$) denotes quantities at the time of the transition, while "RD" refers to the moment when the universe becomes radiation dominated. In a decelerating universe $H_*/H_{\mathrm{RD}} > 1$ and the direction of these modifications depends on the barotropic parameter. In radiation domination, $w = 1/3$, the amplitude does not change as GWs redshift at the same rate as the background. For an expansion dominated by energy density redshifting slower than radiation $w < 1/3$ the amplitude will keep decreasing while in the opposite case of an extra component redshifting faster $w > 1/3$ the abundance would increase looking at only the effect of redshift.

Another crucial modification comes from the conditions at the time of the transition. While typically the GW production is not crucially modified (Barenboim and Park 2016; Guo et al. 2021), the transition is linked to the radiation component and if that is subdominant the GW abundance also needs to be corrected. In terms of the strength of the transition this leads to a simple modification by

$$\alpha \propto \rho_R^{-1} \rightarrow (\rho_{\mathrm{tot}} - \rho_V)^{-1}, \tag{135}$$

where ρ_R is radiation density while ρ_V is the difference between the initial and final state energy densities. Finally ρ_{tot} is the total energy density which in domination of any additional component is of course the dominant contribution.

This modification makes observation of scenarios where the transition occurs during the domination of an extra component rather unlikely. Even in the optimistic case of kination (with $w = 1$) where the redshift of the signal would increase the amplitude from Eq. (135) we get $(\rho_V/\rho_{\mathrm{tot}})^2 \approx (H_*/H_{\mathrm{RD}})^{-4\frac{3w-1}{3w+3}}$ which results in an overall suppression. Due to this, to get any hope of observation we would need the modified expansion to end almost immediately after the transition (Barenboim and Park 2016) despite the fact that the two are governed by completely separate mechanisms. Thus, the most promising models from the observational point of view are the ones in which the transition occurs in standard circumstance, but it is strong enough to itself modify the expansion history, as in this case Eq. (135) does not apply. One example here would be a very strong transition in which the field dominates the total energy density and after the transition as the field oscillates around its minimum it is causing a matter dominated period which will last until the field decays (Ellis et al. 2020c).

All the modifications of the spectrum we discussed up to now, essentially come down to shifts of the entire spectrum that could also be mimicked by simple changes in the parameters of the transition. We now switch to a modification changing the spectral shape which could provide a smoking gun signal for a modified expansion period.

This modification has to do with the fact that at scales larger than the horizon size at the time of the transition the features of our source become irrelevant. The source at this large scale is effectively just white noise and GWs entering the horizon at later time during RD always predict a spectrum proportional to f^3 (Caprini et al. 2009a; Ünal 2019; Cai et al. 2020) at frequencies corresponding to superhorizon scales $f < f_{H_*} = a_* H(a_*)/2\pi$. This behaviour, however, depends on the expansion rate at the time when GWs enter the horizon (Hook et al. 2021). In our relevant example of matter domination, it would create an f^1 plateau in the spectrum for $f_{H_{\rm RD}} < f < f_{H_*}$. The main issue with observation of this feature comes from the fact that the peak of the signal has to do with the characteristic scale of the transition, which is typically much smaller than horizon size such that $f_*/f_{H_*} \propto \beta/H$, which is typically much bigger than one. As a result, this feature will typically appear significantly below the peak and, given that the abundance decreases quickly off peak, it will also have a much smaller abundance. Concerning LISA scales, in Fig. 26, we show several examples of this modification on bubble collision spectra calculated according to Lewicki and Vaskonen (2021) using parameter examples not difficult to realise in classically conformal models (Ellis et al. 2020c). From top to bottom the lines show the decay width of the scalar field $\Gamma_\phi/H = 1$, $\Gamma_\phi/H = 10^{-2}$ and $\Gamma_\phi/H = 10^{-4}$ which results in longer matter-dominated periods and reheating temperatures of $T_{\rm RD} = 10^4$ GeV, $T_{\rm RD} = 10^3$ GeV and $T_{\rm RD} = 10^2$ GeV, respectively. We also stress that departure from standard cosmology that we have just explained, is not the only option leading to relevant chances of the SGWB frequency profile. For instance, the occurrence of an intermediate matter and kination era inside the radiation epoch as

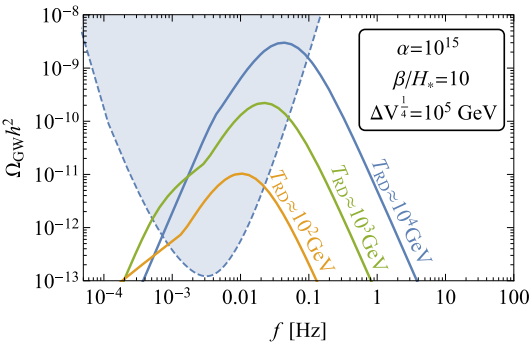

Fig. 26 The lines show the GW spectrum produced in FOPT by bubble collisions for the indicated transition parameters. From top to bottom, the decay width of the scalar field decreases leading to a lengthening period of effectively matter-dominated expansion as the field oscillates around its minimum before finally decaying. The resulting reheating temperatures read $T_{\rm RD} = 10^4$ GeV, $T_{\rm RD} = 10^3$ GeV and $T_{\rm RD} = 10^2$ GeV, respectively

motivated by e.g. early axion dynamics also impacts the low-frequency slope of the SGWB signal (Gouttenoire et al. 2021b).

9.2.3 Cosmic strings

We now turn to the case of GW spectra produced by cosmic strings that we first discussed in Sect. 7. We focus on analytical modelling described in Sect. 7.2.1 with numerical factors set to agree with Model 2 described in Sect. 7.2.2.

These spectra are very convenient laboratories to study the expansion history of the early universe, since in RD they simply produce a flat plateau. Any features beyond that can be linked to modifications of the expansion rate from minor modifications caused by variations in the number of degrees of freedom to simply a different power-law caused by domination of energy density red-shifting differently than radiation (Cui et al. 2018, 2019; Gouttenoire et al. 2020a, b). The feature will appear in the spectrum above at the characteristic frequency $f_{\rm RD}$ corresponding to the temperature $T_{\rm RD}$ at which the expansion begins to follow the standard radiation-dominated picture (with SM number of degrees of freedom) (Cui et al. 2019):

$$f_{\rm RD} = (8.67 \times 10^{-3}\,{\rm Hz}) \left(\frac{T_{\rm RD}}{\rm GeV}\right) \left(\frac{10^{-11}}{G\mu}\right)^{1/2} \left[\frac{g_*^{\rm SM}(T_{\rm RD})}{g_*^{\rm SM}(T_0)}\right]^{\frac{8}{6}} \left[\frac{g_s^{\rm SM}(T_0)}{g_s^{\rm SM}(T_{\rm RD})}\right]^{\frac{7}{6}}, \quad (136)$$

where $G\mu$ is the tension characterising the string network. We stress that, for local strings, the relevant energy scale is not the size of the horizon, in contrast with phase transitions for instance. This is because loops do not suddenly decay after production, in contrast with other cosmological sources of GW. So, for LISA, the cosmic-strings GW spectrum is sensitive to MeV scale, rather than the 100 GeV−TeV scale (Gouttenoire et al. 2020a). In Fig. 27, we show the part of the $(G\mu, T_{\rm RD})$ parameter space in which LISA can probe the spectra at $f_{\rm RD}$ testing the standard cosmological expansion rate.

For global strings, the turning-point frequency turns out to be (Gouttenoire et al. 2020a)

$$f_{\rm RD} = \left(\frac{T_{\rm RD}}{\rm GeV}\right) \left(\frac{0.1}{\alpha}\right) \left[\frac{g_*^{\rm SM}(T_{\rm RD})}{g_*^{\rm SM}(T_0)}\right]^{\frac{1}{4}} \times \begin{cases} 8.9 \times 10^{-7}\,{\rm Hz} & \text{for } 10\,\%, \\ 7.0 \times 10^{-8}\,{\rm Hz} & \text{for } 1\,\%, \end{cases} \quad (137)$$

where α is the loop size with respect to the Hubble horizon and the percentage

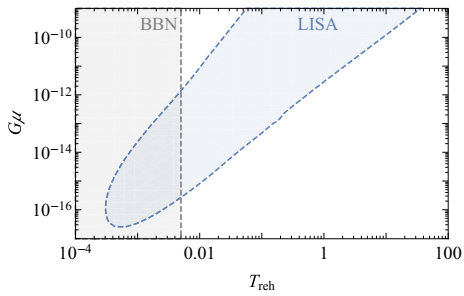

Fig. 27 Range of temperature $T_{\rm RD}$ to which LISA can probe the cosmological expansion rate using a spectrum from a cosmic string network with the indicated string tension $G\mu$. The grey region indicates temperatures where modifications of the expansion rate would already be in tension with BBN

indicates the relative deviation $|(\Omega_{\rm st} - \Omega_{\rm nonst})/\Omega_{\rm st}|$ of the non-standard spectrum with respect to the standard one. Thus, in contrast to local strings,the turning-point frequency is independent of the string tension (cf. Eqs. (136) and (137)).

Coming back to the local-string case, assuming that at earlier times the expansion is governed by a simple EoS with $\rho \propto a^{3(1+w)}$, we can approximate the slope of the spectrum at $f > f_{\rm RD}$ as

$$\Omega_{\rm GW}(f > f_{\rm RD}) \propto \begin{cases} f^{2\frac{3w-1}{3w+1}} & \text{for} \quad w \geq 5/21, \\ f^{-1/3} & \text{for} \quad w < 5/21. \end{cases} \tag{138}$$

We show examples of modified spectra for spectrum from a cosmic string network $G\mu = 10^{-10}$ including early matter domination (with $w = 0$) and kination (with $w = 1$) lasting up until $T_{\rm RD} = 5$ MeV and $T_{\rm RD} = 5$ GeV in Fig. 28. A change in the number of degrees of freedom would instead create a smooth step in the spectrum with the total change in abundance given by (Cui et al. 2019),

$$\Omega_{\rm GW}(f \gg f_{\rm RD}) \simeq \Omega_{\rm GW}^{\rm SM}(f) \left(\frac{g_*^{\rm SM}}{g_*^{\rm SM} + \Delta g_*} \right)^{\frac{1}{3}}, \tag{139}$$

where the SM index denotes quantities computed assuming the number of degrees of freedom as in the SM while Δg_* is the number of new degrees of freedom decoupling at $T_{\rm RD}$. According to this simple formula probing the abundance of the plateau with $\mathcal{O}(1\%)$ accuracy would allow us to discover inclusion of even several new degrees of freedom with larger amounts requiring less accuracy. The range of temperatures we can survey is again given by Fig. 27 although ascertaining the exact accuracy concerning our possible estimation of the number of degrees of freedom in this range would require further scrutiny. It was also shown that measurements of the turning-point frequency in the SGWB from cosmic strings due to a temporary matter era induced by a massive unstable particle can enable to probe unstable particles with

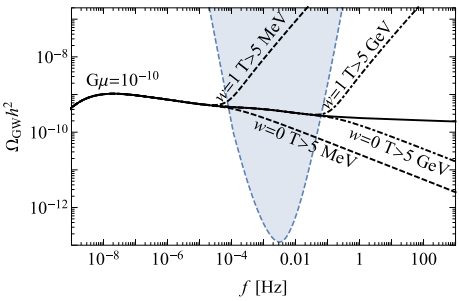

Fig. 28 GW spectrum produced by a cosmic string network with $G\mu = 10^{-10}$ together with spectra produced if that network evolved in an early matter domination period (with $w = 0$) or kination (with $w = 1$) lasting up until $T_{\rm RD} = 5$ MeV and $T_{\rm RD} = 5$ GeV. We note that the blue tilted branches in the figure are only shown for representative purposes, as they violate BBN and CMB constraints [recall discussion at the end of Sect. 5.1], so for a realistic effect compatible with those bounds, a much smaller stiff EoS is required, somehow larger than (but very close to) $w \approx 1/3$

lifetime in the range 10^{-8} to 0.1 s, extending significantly the well-known BBN bound (Gouttenoire et al. 2020b).

In addition to the potential of probing a new EoS and new relativistic degrees of freedom with a SGWB from cosmic strings, (pre-)inflationary dynamics may leave distinctive imprints in GW signals. Although a cosmic string network formed during or before inflation is diluted by inflation, it may come back into horizon at later times and lead to detectable GW signals. In this case, the SGWB typically gets suppressed especially at higher frequencies (Guedes et al. 2018). Nevertheless, well-motivated BSM scenario of an intermediate short inflationary period inside the radiation era can lead to detectable effects. With LISA, intermediate inflation scales in the range 0.1–10^{12} GeV can be probed (Gouttenoire et al. 2020a). Besides, a GW burst signal could be significant and be the leading signal (Cui et al. 2020), in contrast to the conventional cases where the SGWB is the more sensitive means to probe cosmic strings. The dedicated study of the correlated burst and SGWB signals could reveal information about when the strings come back into the horizon as well as related inflationary dynamics.

Non-standard pre-BBN cosmology can significantly distort the vanilla shape of the SGWB from cosmic strings. It can turn it into a peaked shape (Gouttenoire et al. 2020a). Note that a peaked shape can also be generated in standard cosmology in the presence of a particle production cut-off. However, this works only for small string tension and lies outside of LISA. So, a peaked GW spectrum from comic strings is a smoking-gun signature of a non-standard era (less stiff than radiation, i.e. matter or inflationary era). Note that this peak is much broader than the peak from the FOPT SGWB signal and can be distinguished.

9.3 SGWB in quantum gravity

In Sect. 4.1 we saw some modifications to the propagation of GWs of astrophysical origin that could happen in quantum gravity. Here we will concentrate on the potential quantum-gravity effects on primordial SGWBs. (see Addazi et al. 2022 for an overview of the experimental and theoretical constraints on quantum gravity.)

Early-universe models embedded in or inspired by theories of quantum gravity have the potential to leave an observable imprint in the SGWB. In fact, these cosmological scenarios usually predict modifications in the shape of the primordial scalar and tensor spectra, which are generated either from the quantum fluctuations of an inflationary field or by an alternative mechanism. If these modifications include a blue tilt at high frequencies, they could overcome the CMB bounds and still give rise to a primordial SGWB $\Omega_{\rm GW}(f)$ reaching the sensitivity curves of the present or future interferometers.

We can classify early universe models related to quantum gravity according to the tilt of the tensor spectrum, which we call $\mathcal{P}_{\rm t}(f)$ to distinguish the full spectrum from the exact power-law parametrization $\Delta^2_{h,\rm inf}$ in Eq. (99).

This classification is based on the overall trend of the full spectrum. We should note that in some models a positive tensor index $n_T > 0$ at CMB scales does not

imply a blue tilt at higher frequencies. The models are the following (see Calcagni and Kuroyanagi 2021 for a full list of references):

- *Red-tilted tensor spectrum*: the large class of string-cosmology models with flux compactification (not to be confused with the cosmic-strings models discussed above); one semi-classical solution in Wheeler–DeWitt canonical quantum cosmology; loop quantum cosmology, where gravity is quantized canonically using the Ashtekar–Barbero connection. There are three main approaches to describe perturbations in loop quantum cosmology: with a dressed metric, in hybrid quantization and with effective constraints, the latter in turn being characterised by the presence of inverse-volume corrections, holonomy corrections or both. The first two and the third in the presence of inverse-volume corrections predict a red-tilted tensor spectrum.
- *Blue-tilted tensor spectrum*: another semi-classical solution in Wheeler–DeWitt canonical quantum cosmology; loop quantum cosmology in the effective-constraints approach in the presence of holonomy corrections; non-local Starobinsky inflation, a model embedded in non-local quantum gravity where early-universe acceleration is driven by curvature; string-gas cosmology (again, unrelated to cosmic-strings models), where primordial spectra are generated by a thermal bath of strings most of which are wrapped around compact extra dimensions; new ekpyrotic scenario, where the spectra are generated by the collision of branes; Brandenberger–Ho non-commutative inflation, an inflationary stage realised in a geometry which is fuzzy at microscopic scales; multi-fractional inflation, an inflationary era realised in a geometry whose dimension changes with the probed scale; pre-Big-Bang scenario, where the dualities of string theory suggest the existence of a phase prior to the big bang.

Models with red-tilted tensor spectrum do not generate a observable SGWB detectable at ground- or spaced-based interferometers. Regarding models with a blue-tilted spectrum, quantum modifications in Wheeler–DeWitt canonical cosmology are too small to be observable by any of the present or planned interferometers (Calcagni and Kuroyanagi 2021). Loop quantum cosmology in the effective-constraints approach in the presence of holonomy corrections is already ruled out observationally (Bolliet et al. 2016). The tensor spectrum of non-local Starobinsky inflation (see Sect. 8.5) tends asymptotically to the spectrum of local Starobinsky inflation, hence it is unobservable even if the amplitude at interferometer scales is larger than at CMB scales (Calcagni and Kuroyanagi 2021). String-gas cosmology, the new ekpyrotic scenario, Brandenberger–Ho non-commutative inflation and multi-fractional inflation can all reach the sensitivity of DECIGO but, unfortunately, not of LISA (Calcagni and Kuroyanagi 2021).

A model worth further investigation is the *pre-Big-Bang scenario* (Gasperini and Veneziano 1993), where CMB constraints are respected and, at the same time, the amplitude of the SGWB at high frequencies can increase to touch the sensitivity curves of GW experiments, possibly including LISA (Gasperini 2016). In Gasperini (2016), the sensitivity threshold of a six-link, 5 M-km-arm-length configuration was

assumed (Caprini et al. 2016). An updated analysis could determine the parameter space of the model opening an observational window.

While the above model has a singular hypersurface at which perturbations are matched, another non-standard pre-BBN expansion history is realised by bouncing models where the universe slowly contracts (Ben-Dayan 2016; Ben-Dayan and Kupferman 2019; Artymowski et al. 2021), and then expands without a big-bang singularity or inflation (e.g. (Battefeld and Peter 2015; Lehners 2010) for reviews). In conformal time, before the bounce the scale factor goes as $a(\eta) \sim (-\eta)^b$, where $0 < b \ll 1$ for slow contraction. Considering vacuum fluctuations on top of this background metric and using the standard power-law parametrization $P_h \sim f^{n_T}$, the expected SGWB spectral tilt from vacuum fluctuations is $n_{T,\text{vacuum}} \simeq 3 - |2b - 1| \simeq 2 + 2b$, resulting in a blue spectrum (Starobinsky 1979; Boyle et al. 2004; Artymowski et al. 2021) possibly slashing through the LISA sensitivity band. Hence, the SGWB signal is directly probing the geometry of the universe $a(\eta)$ making LISA the natural arena to test alternatives to inflation. As is well known, bouncing models with only one scalar field typically predict vacuum fluctuations generating spectra with $n_{T,\text{vacuum}} = n_{s,\text{vacuum}} - 1 \sim 2$. One still has to make sure that the slow-contracting bouncing models actually generate a viable scalar spectrum in accord with CMB observations, for instance by a curvaton mechanism or some other alternative. Specifically, coupling to gauge fields has been considered with an interaction term $\mathcal{L} \propto I^2(\phi)(F^2 - \gamma F\tilde{F})$, where I is a function of the scalar. As seen in Sect. 8.7.1, gauge fields can provide an additional source of chiral GWs, whose tilt we denote by $n_{T,\text{sourced}}$ and is such that $n_{T,\text{sourced}} = n_{s,\text{sourced}} - 1 \approx -0.04$ in accord with CMB observations, however $r \sim 1/9$ which is above current bounds. Hence, the scalar spectrum needs to be generated by some curvaton or entropic mechanism from a second scalar field. Contrary to the inflationary case in Sect. 8.2.1, the spectral tilt $n_{T,\text{sourced}}$ is constant in the bouncing case (Ben-Dayan 2016; Ben-Dayan and Kupferman 2019). Once CMB observations are determined by a curvaton mechanism, then depending on the parameters of the model the sourced tensor spectrum may be detected by LISA with $0.15 < n_{T,\text{sourced}} < 0.31$ or $0.85 < n_{T,\text{sourced}} < 1.1$. If one wishes to match CMB observations solely with the sourced spectrum, then one open question is carrying out the calculation of the spectra across the bounce and check that the model consistently generates sourced spectra observed at CMB scales and vacuum spectra observed by LISA. This is the opposite to what happens in the inflationary models discussed in Sect. 8.2, where the tensor spectrum observed on CMB scales must be the vacuum one while LISA can only observe the sourced spectrum.

Another model worth exploring in the LISA context might be the non-perturbative gravity and bouncing universe of Biswas et al. (2006), Biswas et al. (2010), Biswas et al. (2012b), where it is possible to explore a pre-Big-Bang phase by modelling it by a string-gas dominated Hagedorn phase (Biswas et al. 2007, 2014). In this non-perturbative extension of Einstein's gravity, there exists a bouncing phase given by the scale factor $a(t) = \cosh \lambda t$ in the presence of radiative matter and a non-zero cosmological constant. Such a solution would also permit a stiff fluid in a Hagedorn phase where the universe is primarily dominated by string winding modes (Biswas

et al. 2007, 2014). Their eventual decay into radiation, and exit from the bounce would yield the standard big-bang cosmology. Primordial perturbations are created during the thermal phase with thermal statistical initial conditions which lead, specifically, to a blue tilt in the tensor power spectrum, while keeping the amplitude of the matter spectrum within the PLANCK observation. The blue tilt in the power spectrum, along with the matter power spectrum, constrains the scale entering in the gravitational sector to be around $10^{-4}\,M_{\rm Pl}$ (Biswas et al. 2014).

In parallel with the observability of these and any other model related to quantum gravity with a blue-tilted SGWB (e.g. Dapor and Liegener 2020), it will be important to assess their theoretical robustness, which we have not discussed here. In general, models directly derived from quantum gravity should yield more rigid predictions and be better falsifiable than those only inspired by quantum-gravity phenomena. A faithful and realistic description of a high-energy, high-curvature generation mechanism would move this sector of GW astronomy beyond the level of *ad hoc* model building towards a mini-program contributing to LISA science, according to the following algorithm:

1. Selection or construction of early-universe models embedded into or inspired by quantum gravity, under the criterion of giving a blue-tilted spectrum $\mathcal{P}_{\rm t}(f)$ of primordial tensor fluctuations.
2. Control of the underlying theoretical steps leading from the fundamental theory to the cosmological model: assumptions, approximations, parameter space, fine tunings.
3. Generation of the SGWB spectrum $\Omega_{\rm GW}(f)$ from the primordial spectrum $\mathcal{P}_{\rm t}(f)$ via transfer functions.
4. Comparison of the theoretical SGWB with the LISA sensitivity curve and constraints on the parameter space of the model. Non-detection of a SGWB can be used to rule out theories or to constrain their parameter space. If it was detected, one could further investigate characteristics of the SGWB such as anisotropies or the local spectral tilt at LISA frequencies to extract information on the underlying physics.

In order to achieve the last goal, we will capitalise on the LISA SGWB search and use some of the pipelines described in Sect. 12.

10 Primordial black holes

Section coordinators: S. Clesse, J. García-Bellido. Contributors: S. Clesse, V. De Luca, J.M. Ezquiaga, G. Franciolini, J. García-Bellido, R. Kumar Jain, S. Kuroyanagi, I. Musco, T. Papanikolaou, M. Peloso, S. Renaux-Petel, A. Riotto, E. Ruiz Morales, M. Scalisi, O. Sergijenko, C. Unal, C. Joana, V. Vennin, D. Wands.

10.1 Introduction

The idea that BHs may have formed in the early universe comes back to the late 1960s with the precursor work of Zel'dovich and Novikov (1967) and to the 1970s

with the works of Hawking (1971), Carr and Hawking (1974), Carr (1975) and of Chapline (1975). Already in Carr and Hawking (1974) and Chapline (1975) it was mentioned that such PBHs could contribute to the suspected DM in the universe or to the seeds of MBHs. The first formation scenarios in the context of inflation were proposed in the 1990s (Dolgov and Silk 1993; Carr et al. 1994; García-Bellido et al. 1996) but these usually led to (evaporating) PBHs of very small mass. In the late 1990s, stellar-mass PBHs have been seriously considered as a DM candidate, following the possible detection (e.g. in the MACHO survey) of several microlensing events towards the Magellanic clouds (Aubourg et al. 1993; Alcock et al. 1997). However, the EROS (Tisserand et al. 2007) and OGLE (Wyrzykowski et al. 2010, 2011a, b; Calchi Novati et al. 2013) surveys later set more stringent limits on the PBH abundance, and at the same time, very stringent constraints from CMB observations were claimed in Ricotti et al. (2008). Figure 29 summarizes the current constraints on the PBH abundance in the idealized limit that all PBHs have the same mass.

Since 2016, the real game-changer that has rekindled the idea that PBHs may exist and constitute from a significant fraction to the totality of the DM (Bird et al. 2016; Clesse and García-Bellido 2017b; Sasaki et al. 2016) has been the first GW detection from a BH merger by Advanced LIGO/Virgo (Abbott et al. 2016b). Nowadays, the importance of the different PBH binary formation channels, the possible abundance of PBHs, and their viable mass function, are subject to an intense activity and are under discussion (for recent reviews, see e.g. Carr and Kuhnel (2020), Carr et al. (2021c)). Furthermore, since PBHs are formed by the collapse of large density perturbations, PBHs are accompanied by a SGWB sourced by these perturbations at second-order. It has been calculated that if BHs detected by LIGO/Virgo have primordial origin, there is an inevitable accompanying SGWB peaking around PTA frequencies (Ando et al. 2018; García-Bellido et al. 2017).[31] In late 2020, NANOGrav has claimed the possible detection of a SGWB at nHz frequencies (Arzoumanian et al. 2020) which, among several options, can be explained as the result of the density perturbations at the origin of stellar-mass PBH formation (De Luca et al. 2021b; Kohri and Terada 2021) (although many other explanations exist. In this context, LISA will search for the GW signatures of PBHs (García-Bellido et al. 2017; Cai et al. 2019a; Bartolo et al. 2019b; Ünal 2019) and will be complementary to ground-based GW detectors (Maggiore et al. 2020; Reitze et al. 2019) and EM probes (Kashlinsky et al. 2019), in order to prove or exclude the existence of PBHs, to evaluate the possible contribution to the DM, to the seeds of MBHs at high redshift, and to distinguish PBHs from SOBHs, on a wide range of mass scales. Any firm detection would open a new window on the physics at play in the very early universe and a possible way to solve various long-standing astrophysical and cosmological puzzles (Clesse and García-Bellido 2018; Carr et al. 2021b).

[31] This SGWB is ineludible in the sense that it does not require any further assumption other than GR and large density perturbations. It is a standard SGWB formed by anisotropic stress which is quadratic order in scalar perturbations.

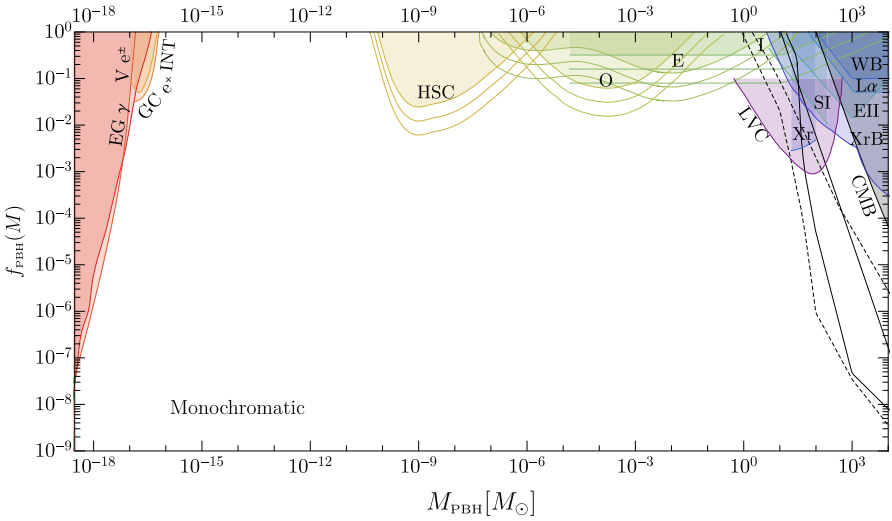

Fig. 29 Most stringent limits on the DM fraction made of PBHs, $f_{\rm PBH}$, coming from the Hawking evaporation producing extragalactic gamma-ray (EGγ), e$^{\pm}$ observations by Voyager 1 (Ve$^{\pm}$), positron annihilations in the Galactic Center (GCe^{+}), gamma-ray observations by INTEGRAL (INT), microlensing searches by Subaru HSC (HSC), MACHO/EROS (E), OGLE (O) and Icarus (I), from CMB limits (CMB), GW observations by LIGO/Virgo (LVC), wide binaires in the galactic halo (WB), the ultra-faint dwarf galaxies Eridanus II (EII) and Segue 1 (S1), X-rays towards the galactic center (XrB) and Lyman-α limits (Lα). For microlensing and CMB limits, the different lines indicate some degree of uncertainties, respectively due to PBH clustering and disk vs. spherical accretion. Microlensing limits only apply to the fraction of PBHs uniformly distributed in galactic halos and are less stringent if a non-negligible fraction $f_{\rm clust}$ of PBHs are in clusters. We show the limits for $f_{\rm clust} = 0, 0.4$ and 0.8. For LVC, the rate suppression of early binaries still allows $f_{\rm PBH} \gtrsim 0.1$. *All these limits apply to monochromatic models* and can be model dependent. Recasting them to realistic PBH models with arbitrary mass functions requires a careful analysis. Image adapted from De Luca et al. (2021b)

This section is organized as follows: after reviewing the principal formation scenarios (Sect. 10.2), we will consider the principal sources of GWs related to PBHs and their detectability with LISA, which are the SGWB generated at second-order by the non-linear cosmological density fluctuations at the origin of PBH formation (Sect. 10.3), the PBH binaries and hyperbolic encounter (Sect. 10.4) which may unveil a possible primordial origin of MBH seeds if they are detected at high redshifts (Sect. 10.5).

10.2 Formation scenarios

Hereafter we first provide a rapid overview of the principal mechanisms that can lead to large curvature fluctuations and PBH formation, which can be related to the early-universe phenomena discussed in Sects. 6, 7 and 8. We then review the general theory of PBH formation from large curvature fluctuations. Finally we discuss some recent developments related to PBH formation, such as non-linear and non-Gaussian effects, thermal history, that are all relevant for the estimation of the curvature

threshold to lead to PBH formation, as well as their possible abundance and mass distribution.

10.2.1 Origin of curvature fluctuations

There exists a broad variety of scenarios leading to large curvature fluctuations and PBH collapse, which can be classified as below. Some scenarios are detailed in the corresponding sections of this white paper.

1. **Single-field inflation:** Slow-roll single field inflation models can produce a power spectrum amplitude of curvature fluctuations on smaller scales larger than the ones probed by CMB and large scale structures observations. The simplest example is to have two subsequent inflationary phases, the second one lasting less than 50 *e*-folds (roughly). Potentials with inflection points (García-Bellido and Ruiz Morales 2017; Germani and Prokopec 2017), like critical Higgs inflation (Ezquiaga et al. 2018), can also lead to a transient enhancement of the primordial power spectrum. More generically, in the slow-roll approximation, any potential leading to a transient reduction of the speed of the inflaton will lead to large curvature fluctuations, eventually leading to PBH formation. Another possibility is to invoke a variation of the sound speed during inflation, see e.g. Özsoy et al. (2018).
2. **Multi-field inflation:** Large curvature fluctuations may also arise in multi-field models, e.g. during the waterfall phase of *hybrid inflation* (Clesse and García-Bellido 2015) or due to *turning trajectories* in the inflationary landscape (Fumagalli et al. 2023). Eventually, the power spectrum will not only exhibit a broad or sharp peak on scales that are relevant for PBHs, but for a sufficiently sharp turn, this is accompanied by oscillatory features that may lead to specific signatures in the PBH population and to oscillatory patterns in the scalar-induced SGWB (Fumagalli et al. 2021a; Braglia et al. 2021; Palma et al. 2020). It is also possible that curvature fluctuations are generated by the tunneling of the inflaton towards a local minimum of the field space (Garriga et al. 2016; Deng and Vilenkin 2017; Kusenko et al. 2020) and the subsequent *bubble collapse*. Another intriguing possibility has been proposed by employing axions and their interaction with the *gauge fields* to enhance primordial density perturbations and producing PBHs (Bugaev and Klimai 2014; Linde et al. 2013; Domcke et al. 2017; García-Bellido et al. 2016, 2017; Özsoy and Lalak 2021; Özsoy 2021). In Natural Inflation (Freese et al. 1990; Adams et al. 1993), the inflaton is a pseudo-scalar particle protected from quantum corrections for super-Planckian excursions via the shift symmetry. Also, theories with UV completion predict a large number of pseudo-scalar particles that could be the inflaton or spectator fields. In this scenario, curvature fluctuations are sourced by enhanced vector modes and can have a non-Gaussian distribution.
3. **Quantum diffusion:** The backreaction of quantum fluctuations during inflation makes the dynamics of the fields stochastic, and allow them to explore wider regions of the inflationary potential. This makes the tails of the distribution functions of primordial density fluctuations much heavier (Vennin and

Starobinsky 2015; Pattison et al. 2017; Ezquiaga et al. 2020a; Figueroa et al. 2021), since they decay exponentially instead of in a Gaussian way, which boosts the production of PBHs afterwards.

4. **Curvaton and stochastic spectator fields:** PBHs could have formed due the existence of a curvaton field, e.g. with a simple modification of the original curvaton scenario (Lyth and Wands 2002). The primordial curvature perturbations on CMB scales are produced by the inflaton, which acts very similarly to the standard single-field scenario, while the curvaton field becomes responsible for perturbations on smaller scales, at the origin of PBH formation. In another scenario (Carr et al. 2021a), a stochastic spectator field experiences quantum fluctuations during inflation making it exploring a wide range of the potential, including its slow-roll part but without having any impact on the inflationary dynamics. In regions where the field acquires a value allowing slow-roll, after inflation but when these are still super-horizon, additional expansion is produced locally, which generates curvature fluctuations that later collapse into PBHs. This model has the advantage that the primordial curvature power spectrum remains at level observed at CMB scales almost everywhere, except in PBH-forming regions.
5. **Preheating:** If inflation is followed by a preheating, when the inflaton oscillates coherently at its ground state and decays to other degrees of freedom, resonant amplification of the quantum field fluctuations take place (Kofman et al. 1994, 1997). These are accompanied with a resonant amplification of curvature fluctuations (Finelli and Brandenberger 1999; Bassett et al. 1999; Jedamzik and Sigl 2000; Bassett and Viniegra 2000), which may collapse and form PBHs (Martin et al. 2020; Auclair and Vennin 2021). The PBHs that form are typically very light and only if reheating completes at very low energy (below the electroweak scale) the formed PBHs would have a relevant mass for the LISA frequency range (for GW radiation from PBH binaries). It is however also possible that these curvature fluctuations source a detectable SGWB at second order (Papanikolaou et al. 2021).
6. **Phase transitions:** The formation of PBHs may have been facilitated in FOPTs (Jedamzik and Niemeyer 1999), in non-equilibrium second order phase transitions (Rubin et al. 2000) and in specific realizations of the QCD transition (Davoudiasl 2019).
7. **Early matter era:** The curvature threshold for the PBH collapse depends on the EoS of the universe. It goes to zero in a matter dominated era, and so it is possible that PBH have formed from standard $\mathcal{O}(10^{-5})$ inflationary curvature fluctuation if the early universes has undergone a transient matter-dominated era. Several mechanisms have been proposed to be at the origin of such early matter era, see e.g. Nayak and Singh (2012), Ballesteros et al. (2020), Green et al. (1997).
8. **Cosmic strings, domain walls:** Topological defects may have lead to the production of PBHs. For instance, cosmic string cusps can collapse gravitationally into PBHs with a mass function that could extend up to stellar masses (Jenkins and Sakellariadou 2020). The collapse of domain walls, e.g. produced

by tunnelling during inflation (Deng et al. 2017; Liu et al. 2020) or in QCD axion models (Ferrer et al. 2019; Ge 2020) is another class of PBH formation scenarios.

9. **Primordial magnetic fields:** It is suspected that the required seeds for extragalactic magnetic fields have an origin in the early universe. These primordial magnetic fields induce an anisotropic stress that can act as a source of large super-Hubble curvature fluctuations, leading to PBH formation with a broad possible range of masses (Saga et al. 2020).

10.2.2 Standard theory of primordial black holes formation from Gaussian curvature fluctuations

If PBHs have been formed due to the collapse of large primordial curvature perturbations, the fraction of the density of the universe made of PBHs at the time of their formation, $\beta_{\rm form}$ (usually defined per unit of logarithmic mass interval), is determined by the probability that the amplitude of a primordial curvature fluctuation, measured in terms of the mass excess of the density contrast δ is above a certain threshold $\delta_{\rm c}$ when the perturbation re-enter the cosmological horizon, corresponding to the Hubble length $1/H$, where H denotes the Hubble parameter. The corresponding PBH mass M is therefore linked to the Hubble horizon mass of the collapsing fluctuation, and so also to its size and its corresponding wavenumber $k_M = aH$ (and a is the scale factor),

$$M = \gamma M_{\rm H} = \left(\frac{3H^2}{8\pi G}\right)\frac{c^3}{H^3} \ , \tag{140}$$

where γ is the ratio between the final PBH mass and the collapsing Horizon mass, which depends on the formation model details (a realistic range is $0.1 \div 1$). This should take into account that, when the perturbation amplitude δ is close enough to the threshold $\delta_{\rm c}$ (i.e. $(\delta - \delta_{\rm c}) \lesssim 10^{-2}$), the mass follows the scaling law of critical collapse:

$$M = \mathcal{K}(\delta - \delta_{\rm c})^{\Gamma} M_{\rm H}, \tag{141}$$

where Γ depends only on the EoS ($\Gamma \simeq 0.36$ in the radiation dominated universe) and $\mathcal{K}$ depends on the shape of the perturbation (typically $1 \div 10$).

If the curvature fluctuations originate from inflation, the PBH mass can be related to the time of Hubble exit of the corresponding scale during inflation, expressed in terms of the number of e-folds before the end of inflation N_* (see e.g. García-Bellido et al. 1996), which gives, in the case of instantaneous reheating,

$$M \sim 4\pi \frac{M_{\rm Pl}^2}{H_{\rm inf}} e^{2N_*}, \tag{142}$$

where $M_{\rm Pl}$ is the reduced Planck mass and $H_{\rm inf}$ is the (almost constant) Hubble rate during inflation.

In most inflationary scenarios, the distribution of primordial curvature fluctuations is Gaussian, or almost Gaussian. Some recent scenarios have proposed more complex

distributions that can be useful to alleviate or reduce the need of a large power spectrum amplitude. These are shortly discussed later and assuming that the curvature fluctuations are described by a Gaussian distribution the fraction of PBHs at formation is then usually given by

$$\beta_{\rm form}(M) = 2\int_{\delta_{\rm c}}^{\infty} \frac{1}{\sqrt{2\pi}\sigma} e^{-\frac{\delta^2}{2\sigma^2}} {\rm d}\delta = 1 - {\rm erf}\left(\frac{\delta_{\rm c}}{\sqrt{2}\sigma}\right) = {\rm erfc}\left(\frac{\delta_{\rm c}}{\sqrt{2}\sigma}\right). \tag{143}$$

This expression however does not take into account that when δ is larger then a certain value $\delta_{\rm max}$ (originally estimated $\delta_{\rm max} \sim 1$ by Bernard Carr in 1975 (Carr 1975)) the perturbation forms a separate closed universe, topologically disconnected. A more accurate version can nevertheless be obtained re-normalizing the previous expression as

$$\beta_{\rm form}(M) = \frac{\displaystyle\int_{\delta_{\rm c}}^{\delta_{\rm max}} \frac{1}{\sqrt{2\pi}\sigma} e^{-\frac{\delta^2}{2\sigma^2}} {\rm d}\delta}{\displaystyle\int_{0}^{\delta_{\rm max}} \frac{1}{\sqrt{2\pi}\sigma} e^{-\frac{\delta^2}{2\sigma^2}} {\rm d}\delta} = 1 - \frac{{\rm erf}\left(\frac{\delta_{\rm c}}{\sqrt{2}\,\sigma}\right)}{{\rm erf}\left(\frac{\delta_{\rm max}}{\sqrt{2}\,\sigma}\right)} = \frac{{\rm erfc}\left(\frac{\delta_{\rm c}}{\sqrt{2}\sigma}\right) - {\rm erfc}\left(\frac{\delta_{\rm max}}{\sqrt{2}\sigma}\right)}{1 - {\rm erfc}\left(\frac{\delta_{\rm max}}{\sqrt{2}\sigma}\right)}. \tag{144}$$

The variance of the field of density perturbations σ, according to the Gaussian distribution of δ used before, is given by

$$\sigma^2 = \langle \delta^2 \rangle = \int_0^{\infty} \frac{{\rm d}k}{k} \mathcal{P}_\delta(k,r) = \frac{16}{81}\int_0^{\infty} \frac{{\rm d}k}{k} (kr)^4 \tilde{W}^2(k,r) T^2(k,r) \mathcal{P}_\zeta(k), \tag{145}$$

where $\mathcal{P}_\delta(k,r)$ and $\mathcal{P}_\zeta(k)$ are the density and the curvature power spectrum, while $\tilde{W}(k,r) = 3(\sin kr - kr\cos kr)/(kr)^3$ is the Fourier transform of the top-hat smoothing function and $T(k,r) = \tilde{W}(k, r/\sqrt{3})$ is the linear transfer function, both computed at the horizon crossing scale. All this shows that a larger power spectrum could increase significantly the fraction of PBHs because the abundance of PBHs is exponentially sensitive to the value of the amplitude.

One can then calculate the contribution of PBHs to the density of the universe today, in terms of the fraction of DM that they represent, given by

$$f_{\rm PBH}(M) \sim 2.4 \times \beta_{\rm form}(M)\sqrt{\frac{M_{\rm eq}}{M}}, \tag{146}$$

where $M_{\rm eq} \simeq 2.8 \times 10^{17} M_\odot$ is the horizon mass at matter-radiation equality, and the numerical factor corresponds to $2 \times (1 + \Omega_b/\Omega_{\rm CDM})$. In this standard scenario, where PBHs form from Gaussian curvature pertubations, one does not expect spatial clustering at formation larger than the one predicted by the Poisson distribution (Ali-Haïmoud 2018; Desjacques and Riotto 2018; Ballesteros et al. 2018; Moradinezhad Dizgah et al. 2019).

10.2.3 Beyond Gaussianity

The above formalism applies to Gaussian perturbations but it can be generalized to non-Gaussian distributions, by replacing the integrand in the left-hand side of Eq. (144) with the appropriate distribution function.

At the perturbative level, even a small amount of local non-Gaussianity (Lyth 2012; Byrnes et al. 2012), or the inevitable non-linear (and hence non-Gaussian) relation between the primordial curvature perturbations and density perturbations can have important effects (Young and Byrnes 2015; Franciolini et al. 2018; De Luca et al. 2019; Young et al. 2019). In the regime of large non-Gaussianity (Linde et al. 2013; García-Bellido et al. 2016; Ünal et al. 2021), the amplitude of the power spectrum can produce same abundance of PBHs even if it is many orders of magnitude smaller with respect to Gaussian case. The existence of non-Gaussianity also influences the amount of SGWB accompanying the PBHs (Nakama et al. 2017; García-Bellido et al. 2017; Cai et al. 2019a; Ünal 2019). The fact that the power spectrum needs to deviate from the quasi scale invariance observed on CMB scales to reach fluctuations allowing PBHs to form also implies that it is natural to expect the non-Gaussianity to be strongly scale dependent too. Moreover, the merger rate of PBHs is strongly impacted by non-Gaussianity (Young and Byrnes 2020; Atal et al. 2020), because non-Gaussianity couples the long and short wavelength primordial density perturbations, leading to initial spatial clustering of the PBHs.

Since PBHs require large fluctuations to form, a perturbative description may not be sufficient. Quantum diffusion of the inflationary fields leads to large deviations from Gaussian statistics on the tails of the distribution functions of primordial density fluctuations (Pattison et al. 2017; Biagetti et al. 2018; Ezquiaga and García-Bellido 2018; Figueroa et al. 2021, 2022), which acquire an exponential (rather than Gaussian) profile (Vennin and Starobinsky 2015; Pattison et al. 2017; Ezquiaga et al. 2020a; Figueroa et al. 2021, 2022). It implies that PBHs can be formed with a much smaller amplitude of the power spectrum than what would be inferred using Gaussian statistics. This cannot be properly taken into account with the usual, perturbative parametrisation of non-Gaussian statistics (such as those based on computing the few first moments of the distribution and the non-linearity parameters $f_{\rm NL}$, $g_{\rm NL}$, etc.), which can only account for polynomial modulations of Gaussian tails, and needs to be described with a non-perturbative approach such as the stochastic-δN formalism (Fujita et al. 2013; Vennin and Starobinsky 2015).

10.2.4 The threshold for primordial black holes and the impact of thermal history

A crucial parameter of the formalism presented above is the critical value δ_c, distinguishing between cosmological perturbations collapsing into PBHs ($\delta > \delta_{\rm c}$) and those ones bouncing back into the surrounding medium ($\delta < \delta_{\rm c}$). This is a fundamental parameter because the resulting PBH abundance is exponentially sensitive to its value. The analysis of the gravitational collapse of curvature perturbations to form PBHs and the appropriate threshold condition has been an active line of research in the past years (Kopp et al. 2011; Harada et al. 2013; Young et al. 2014). It has been estimated using analytical methods (Harada et al. 2013) but

the best approach is to use fully relativistic simulations of PBH formation in spherical symmetry (Musco et al. 2005). Important results having emerged from recent studies are that its exact value is impacted by non-linear and non-Gaussian effects, and that it depends on the radial profile of the overdensity (Musco 2019; Young et al. 2019; De Luca et al. 2019; Kehagias et al. 2019) as well as on the shape of the primordial power spectrum (Yoo et al. 2018; Germani and Musco 2019).

Very recently, a new semi-analytical method tested against simulations in numerical relativity has been proposed in Musco et al. (2021), computing δ_c from the shape of the power spectrum, applied to a few particular cases (power-law spectra, log-normal or Gaussian peak, ...). In the radiation dominated universe the typical range of the threshold lies within $0.4 < \delta_c < 0.6$, with the larger values corresponding to a more peaked shape of the peak of the power spectrum.

On super horizon scales the non-linear amplitude of the curvature profile ζ is important for the formation of PBHs, and the energy density contrast $\delta\rho/\rho_b$, when the universe is radiation dominated, is expressed in terms of ζ as

$$\frac{\delta\rho}{\rho_b} \equiv \frac{\rho(r,t) - \rho_b(t)}{\rho_b(t)} = -\frac{1}{a^2H^2}\frac{8}{9}e^{-5\zeta(r)/2}\nabla^2 e^{\zeta(r)/2}. \tag{147}$$

It can be shown that the amplitude δ is a quadratic function of the curvature profile (see for example (Musco 2019) for more details)

$$\delta = -\frac{2}{3}\zeta'(r_m)[2 + r_m\zeta'(r_m)] = \delta_{\rm G}\left(1 - \frac{3}{8}\delta_{\rm G}\right), \tag{148}$$

where $\delta_{\rm G} \equiv -\frac{4}{3}r_m\zeta'(r_m)$ is the linear component of the amplitude δ. The value of r_m is defined by the location of the peak of the compaction function $\mathcal{C} \equiv 2\Delta M/R$ (where $\Delta M = M - M_b$ is the excess of mass with respect the background) and is given by $\zeta(r_m) + r_m\zeta'(r_m) = 0$. Given the value of $\delta_{\rm c}$ the threshold value of the linear component $\delta_{\rm G}$ is included within $0.5 \lesssim \delta_{\rm c,G} \lesssim 0.9$, and from Eq. (148) we see that $\delta_{\rm max} = 8/3$, corresponding to the maximum value of $\delta_{\rm G}$, above which δ becomes negative, and does not describe a cosmological perturbation of our universe.

The threshold $\delta_{\rm c}$ is also sensitive to the EoS at the time of formation. For example, the QCD phase transition makes the EoS to drop, increasing the production of PBHs of mass $\mathcal{O}(M_\odot)$ (Jedamzik 1997; Byrnes et al. 2018). The reheating at the end of inflation should have filled the universe with radiation. In the absence of extensions beyond the SM, the universe remains dominated by relativistic particles with an energy density decreasing as the fourth power of the temperature as the universe expands. The number of relativistic degrees of freedom remains constant ($g_* = 106.75$) until around 200 GeV, when the temperature of the universe falls to the mass thresholds of SM particles.

The first particle to become non-relativistic is the top quark at $T \simeq m_{\rm t} = 172$ GeV, followed by the Higgs boson at 125 GeV, and the Z and W bosons at 92 and 81 GeV, respectively. These particles become non-relativistic at nearly the same time and this induces a significant drop in the number of relativistic degrees of freedom down to $g_* = 86.75$. There are further changes at the b and c quark and τ-lepton thresholds but these are too small to appear in Fig. 30. Thereafter g_* remains approximately

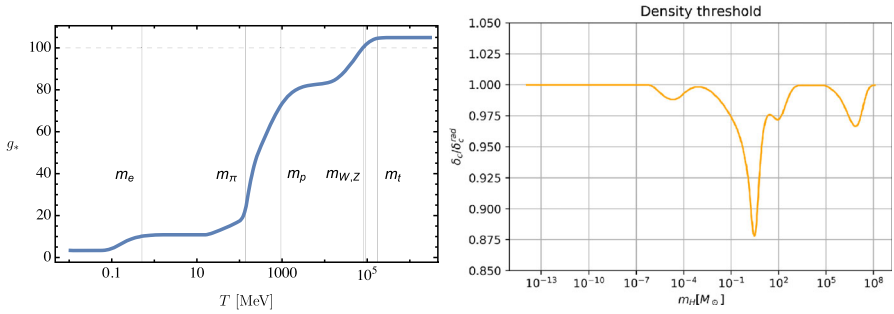

Fig. 30 Left panel: Evolution of the relativistic degrees of freedom g_* as a function of the temperature. The grey vertical lines correspond to the masses of the electron, pion, proton/neutron, W, Z bosons and top quark, respectively. Right panel: Effect of the evolution of g_* on the critical overdensity δ_c leading to PBH formation, as a function of the Hubble horizon mass (related to the PBH mass by $M = \gamma m_H$)

constant until the QCD transition at around 200 MeV, when protons and neutrons condense out of the free light quarks and gluons. The number of relativistic degrees of freedom then falls abruptly to $g_* = 17.25$. A little later the pions become non-relativistic and then the muons, giving $g_* = 10.75$. Thereafter, g_* remains constant until e^+e^- annihilation and neutrino decoupling at around 1 MeV, when it drops to $g_* = 3.36$.

Whenever the number of relativistic degrees of freedom suddenly drops, it changes the effective EoS parameter w. There are thus four periods in the thermal history of the universe when w decreases. After each of these, w resumes its relativistic value of 1/3 but each sudden drop modifies the probability of gravitational collapse of any large curvature fluctuations present at that time, as shown in Fig. 30.

As illustrative examples, we have computed the PBH mass functions for two models with an (almost) scale-invariant power spectrum and two different values of the spectral index, $n_s = 0.97$ (Model 1) and $n_s = 1$ (Model 2). We assumed $\gamma = 0.8$ in both cases. The imprints of the thermal history on the PBH mass function are clearly visible. It is worth noticing that these features rely on known physics and are therefore unavoidable for any PBH model with a wide mass function. The former case corresponds to the scenario proposed in Carr et al. (2021b), Clesse and García-Bellido (2022) and the latter in Byrnes et al. (2018), De Luca et al. (2021b). They can both account for the totality of the DM and somehow explain some LIGO/Virgo GW events, but produce different abundances in the stellar mass range: $f_{\rm PBH}(M_\odot) \approx 0.8$ in the first case, $f_{\rm PBH}(M_\odot) \approx 10^{-4}$ in the second case where the peak lies in the sub-lunar range. We stress that the second example avoids the bounds in the LIGO/Virgo range.

10.3 Stochastic gravitational-wave background sourced at second order by curvature fluctuations

If PBHs are generated by the collapse of large density perturbations, they are unavoidably associated to the emission of induced GWs at second order by the same scalar perturbations due to the intrinsic nonlinear nature of gravity (Acquaviva et al.

2003; Mollerach et al. 2004). The phenomenological implications have been investigated in various contexts also associated to PBHs Ananda et al. (2007), Baumann et al. (2007), Bugaev and Klimai (2010), Saito and Yokoyama (2010), García-Bellido et al. (2017), Ando et al. (2018), Bartolo et al. (2018), Bartolo et al. (2019c), Bartolo et al. (2019b), Clesse et al. (2018), Ünal (2019), Chatterjee and Mazumdar (2018), Wang et al. (2019), Domènech (2020), Domènech et al. (2020), Pi and Sasaki (2020), Ragavendra et al. (2021), Fumagalli et al. (2021a). If the enhancement of the scalar power spectrum responsible for the generation of PBHs occurs around characteristic scales associated with frequencies between 10^{-7} and 10^{-2} Hz, this SGWB becomes detectable by GW experiments like LISA. It is worth emphasizing that contrary to the PBH abundance that is exponentially sensitive to the power spectrum, this SGWB depends on the power spectrum amplitude to the second power. This way, LISA will even be able to exclude the existence of an extremely tiny fraction of DM made of PBHs (even a single PBH in our universe) (Clesse et al. 2018), within a wide mass range.

Figure 31 presents the PBH density fraction at formation $\beta_{\rm form}$ (left panel) and the corresponding PBH mass function $f_{\rm PBH}$ today (right panel) for two models with a power-law power spectrum (see the caption of the Figure for details). The SGWB associated with one of these two models is shown in Fig. 32, where it is confronted with several current or forecasted experimental limits. The SGWB covers a wide frequency range. In the ultra-low frequency range, around nHz, PTA experiments like PPTA (Shannon et al. 2015), NANOGrav (Arzoumanian et al. 2018) and EPTA (Lentati et al. 2015) give the most stringent constraints on the GWs abundance. Future experiments like SKA (Dewdney et al. 2009) (see also Moore et al. 2015) will greatly improve the sensitivity. In the LIGO/Virgo frequency range, an additional constraint has been set by the non-observation of a SGWB after O1-O2 (Abbott et al. 2019c) and O3 runs (Abbott et al. 2021g). All these searches can be translated into a constraint on the amplitude of the comoving curvature perturbation at the

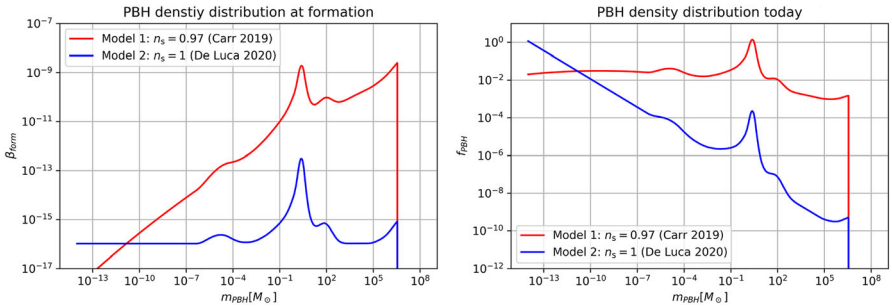

Fig. 31 PBH density fraction at formation $\beta_{\rm form}$ (left panel) and the corresponding PBH mass function $f_{\rm PBH}$ today (right panel), neglecting the effect of PBH growth by accretion and hierarchical mergers, for two models with a power-law power spectrum and including the effects of thermal history: Model 1 from Carr et al. (2021b), Clesse and García-Bellido (2022) with spectral index $n_{\rm s} = 0.97$; Model 2 from De Luca et al. (2021b), Byrnes et al. (2018) with $n_{\rm s} = 1.$ and a cut-off mass of $10^{-14}\,M_\odot$. The transition between the large-scale and small-scale power spectrum is fixed at $k = 10^3{\rm Mpc}^{-1}$. The power spectrum amplitude is normalized such that both models produce an integrated PBH fraction $f_{\rm PBH} = 1$, i.e. PBH constitute the totality of DM. A value of $\gamma = 0.8$ was assumed

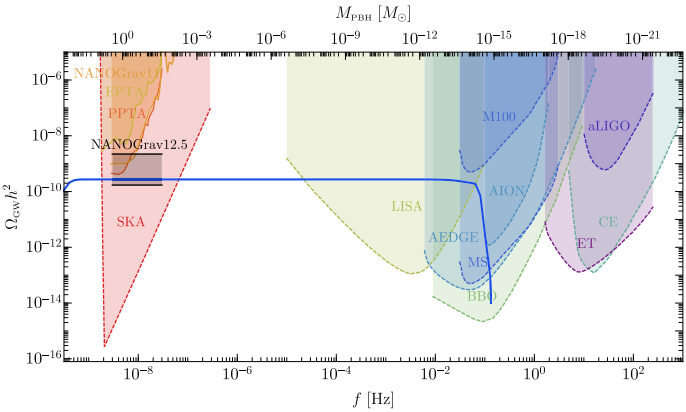

Fig. 32 SGWB sourced at second order by the density perturbations at the origin of PBH formation, for Model 2 of Fig. 31. On top of the plot, we show the PBH mass associated to a given GW frequency as in Eq. (149). The LISA sensitivity (Amaro-Seoane et al. 2017) and the hint for a detection by NANOGrav 12.5 yr (Arzoumanian et al. 2020) are represented, as well as the constraints coming EPTA (Lentati et al. 2015), PPTA (Shannon et al. 2015), NANOGrav 11 yrs (Arzoumanian et al. 2018; Aggarwal et al. 2019) and future sensitivity curves for planned experiments like SKA (Zhao et al. 2013), DECIGO/BBO (Yagi and Seto 2011), CE (Abbott et al. 2017b), ET (Hild et al. 2011), Advanced LIGO + Virgo collaboration (Abbott et al. 2017f), Magis-space (MS) and Magis-100 (M100) (Coleman 2019), AEDGE (El-Neaj et al. 2020) and AION (Badurina et al. 2020). Image reproduced with permission from De Luca et al. (2021b)

corresponding scales (Bugaev and Klimai 2010; Byrnes et al. 2019; Inomata and Nakama 2019; Ünal et al. 2021). Those bounds are also affecting the maximum allowed PBHs fraction of DM with the hypothesis that they originate from the collapse of density perturbations. Detailed studies with the LIGO/Virgo data affecting the mass range $M \in [10^{-20}, 10^{-18}]M_\odot$ are reported in Kapadia et al. (2020), while very tight bounds in the mass range $M \in [10^{-3}, 1]M_\odot$ are obtained in Chen et al. (2020) using the latest NANOGrav data; see also Cai et al. (2019b) where the dependence of the result to non-Gaussianities is also investigated, finding that local non-Gaussianity can for example alleviate the bounds (see Sect. 10.2.3 for details). Finally, the next generation multimessenger experiments, CMB distortion (PIXIE) and PTA-SKA, can test the PBH scenario over solar mass robustly, namely they can conclusively detect or rule out the PBHs over solar-mass and the intriguing proposal that the seeds of the MBHs are formed by PBHs (Ünal et al. 2021) independent of i) statistical properties of perturbations, ii) accretion and merger history and iii) clustering effects.

LISA will be able to provide insights in the intermediate frequencies, and corresponding masses. Since the emission mostly comes when the corresponding scales cross the horizon, one can relate the GWs frequency to the PBHs mass M as (see for example (Saito and Yokoyama 2010; García-Bellido et al. 2017))

$$f \simeq 3\,\mathrm{mHz}\left(\frac{\gamma}{0.2}\right)^{1/2}\left(\frac{M}{10^{-12}M_\odot}\right)^{-1/2}, \tag{149}$$

where the factor γ is capturing the relation between the horizon mass at formation and

the PBH mass after the collapse. Notice that the peak frequencies fall within the LISA sensitivity band for PBH masses around $M \sim \mathcal{O}(10^{-15} \div 10^{-8})\, M_\odot$ and for this mass range, the PBHs can constitute the totality of the DM. Hence, García-Bellido et al. (2017) proposed PBHs in this mass range as DM and further found that density perturbations forming PBHs lead to GWs detectable by LISA. This proposal has been studied in more detail in Cai et al. (2019a), Bartolo et al. (2019b), Bartolo et al. (2019c), Ünal (2019).

The computation of the resulting SGWB spectrum was originally performed in Ananda et al. (2007). We provide here the main result, assuming a generic form for the power spectrum of curvature fluctuation. The current GW abundance can then be obtained as

$$\Omega_{\rm GW}(\eta_0, k) = \frac{a_f^4 \rho_{\rm GW}(\eta_f, k)}{\rho_r(\eta_0)} \Omega_{r,0} = \frac{g_*(\eta_f)}{g_*(\eta_0)} \left(\frac{g_{*S}(\eta_0)}{g_{*S}(\eta_f)} \right)^{4/3} \Omega_{r,0} \Omega_{\rm GW}(\eta_f, k), \tag{150}$$

in terms of the present radiation energy density fraction $\Omega_{r,0}$ if the neutrinos were massless. The crucial quantity is $\Omega_{\rm GW}(\eta_f, k)$, that is the fractional GW energy density for log interval at the emission epoch η_f, related to the critical energy density of a spatially flat universe $\rho_c = 3H^2 M_p^2$. Assuming that the scalar perturbations ζ are Gaussian, it can be calculated as

$$\begin{aligned} \left\langle \rho_{\rm GW}(\eta, \vec{x}) \right\rangle &\equiv \rho_c(\eta) \int d \ln k \; \Omega_{\rm GW}(\eta, k) \\ &= \frac{2\pi^4 M_p^2}{81 \eta^2 a^2} \int \frac{d^3 k_1 d^3 p_1}{(2\pi)^6} \frac{1}{k_1^4} \frac{\left[p_1^2 - (\vec{k}_1 \cdot \vec{p}_1)^2 / k_1^2 \right]^2}{p_1^3 \left| \vec{k}_1 - \vec{p}_1 \right|^3} \\ &\mathcal{P}_\zeta(p_1) \mathcal{P}_\zeta(|\vec{k}_1 - \vec{p}_1|) \left(\mathcal{I}_c^2(\vec{k}_1, \vec{p}_1) + \mathcal{I}_s^2(\vec{k}_1, \vec{p}_1) \right), \end{aligned} \tag{151}$$

where the functions $\mathcal{I}_{c,s}$ are found in Espinosa et al. (2018), Kohri and Terada (2018). The integrals need to be done numerically for general power spectra (see Saito and Yokoyama 2010; Bugaev and Klimai 2010 for analytical calculations in the specific case of a monochromatic or Gaussian curvature spectrum).

For the frequencies of interest, using $f \simeq 8\,\text{mHz}(g_*/10)^{1/4}(T/10^6\text{GeV})$, one can show that the emission of GWs takes place at η_f well before the time at which top quarks start annihilating, above which we can assume a RD universe with constant effective degrees of freedom.

The non-linear coupling with the curvature perturbation naturally leads to an intrinsically non-Gaussian GWs signal imprinted in phase correlations. However, the coherence is washed out by the propagation of the waves in the perturbed universe mainly due to time delay effects originated from the presence of large scale variations of gravitational potential (Bartolo et al. 2018, 2019b, c; Margalit et al. 2020). This is simply a consequence of the central limit theorem applied to a number

$N \sim (k_\star \eta_0)^2 \ggg 1$ of independent lines of sight (Bartolo et al. 2019b), $k_\star$ being the characteristic perturbation wave-number roughly proportional to the the inverse horizon size at GW emission. Possible small deformations smearing the GWs spectrum can also arise from similar effects (Domcke et al. 2020c).

An interesting primordial signal that is potentially observable is related to scenarios where the scalar power spectrum presents oscillations of sufficiently large amplitude, characteristic of large particle production mechanisms, leading to oscillatory $\mathcal{O}(10\%)$ modulations in the frequency profile of the scalar-induced SGWB (Fumagalli et al. 2021a; Braglia et al. 2021), see Sect. 8.3 for details.

10.4 Resolved sources and stochastic gravitational-wave backgrounds from primordial black holes binaries and hyperbolic encounters

PBHs can source GWs in several ways, which will be probed as individual and resolved sources, as a SGWB, or continuous wave signals with LISA. One can distinguish:

- GW chirps from the merging of PBH binaries
- SGWB from PBH binaries
- Continuous GWs from PBH binaries far from the merging time.
- Bursts from close BH-BH interactions

The amplitude of these signals depends on the PBH mass function and the resulting merger rates, which themselves depend on the PBH binary formation channel. Two main channels have been identified: at formation in the early universe and by tidal capture in dense PBH clusters. For each we provide an estimation of the corresponding merger rates. We then compute the expected signals for a few example models. For the purpose of calculating the PBH merging/encounter rates and the resulting GW signatures, we use a general mass distribution $f(m_{\rm PBH})$ that would be specified by the underlying formation model.

10.4.1 Binary formation channels and merger rates

Primordial binaries may have been created before the epoch of matter-radiation equality, when two PBHs formed sufficiently close to each other for their dynamics to be independent of the expansion the universe. If this binary takes a time of the order of the age of the universe to merge, the resulting GWs could be detected. One can estimate the merger rate of such binaries (Kocsis et al. 2018; Raidal et al. 2019) in the simplest scenario where PBHs are not clustered at formation and only contribute to less than about 10% of the DM as

$$\frac{\mathrm{d}R^{\mathrm{prim}}}{\mathrm{d}(\ln m_1)\mathrm{d}(\ln m_2)\mathrm{d}z} = \frac{1.6\times 10^6}{\mathrm{Gpc}^3\,\mathrm{yr}} f_{\mathrm{PBH}}^{\frac{53}{37}} S(m_1, m_2, f_{\mathrm{PBH}}) \left[\frac{t\, m_1 m_2}{t_0 (m_1+m_2)^2}\right]^{-\frac{34}{37}} \left(\frac{m_1+m_2}{M_\odot}\right)^{-\frac{32}{37}} f(m_1) f(m_2) \tag{152}$$

where m_1 and m_2 are the BH masses and S accounts for the suppression factor of the merger rate coming from binary disruption in early universe substructures (Raidal et al. 2019). We use the definition of the PBH mass function $f(m)$ normalised to unity as $\int f(m)\mathrm{d}\ln m = 1$.

Notice that accretion onto PBHs in binaries can be effective for masses above $\mathcal{O}(10)\,M_\odot$ with an impact on the merger rate (De Luca et al. 2020d, c). When $f_{\mathrm{PBH}} \gtrsim 0.1$, N-body simulations (Raidal et al. 2019) have shown that PBH clusters can rapidly form and change the lifetime of PBH binaries, due to their tidal force. However, the fraction of unperturbed binaries at the present time is at least of the order of 10^{-2} for $f_{\mathrm{PBH}} = 1$ (Vaskonen and Veermäe 2020; De Luca et al. 2020a; Jedamzik n.d.). Furthermore, one should also recall that not all the binaries end up inside halos, about 10^{-3} to 10^{-2} remain isolated. For instance, this gives a primordial merger rate still above the inferred LIGO/Virgo rate, even for large PBH abundances.

It is worth mentioning that, as investigated in (De Luca et al. 2021a), an overall PBH abundance of the order $f_{\mathrm{PBH}} \sim 10^{-4}$ would be enough to explain the rate of events in the pair-instability mass gap as inferred by the LIGO/Virgo observations (Abbott et al. 2020b). This result depends on the rate of PBH accretion which is needed to avoid CMB constraints in that relevant mass window (De Luca et al. 2020b). The redshift dependence of the GW source merger rate at high redshift is a key feature which can be explored to distinguish between the astrophysical BHs and PBHs from LIGO/Virgo (Mukherjee and Silk 2021) and CE and ET (Mukherjee et al. 2022). LISA will be able to observe events in that mass window (Kaiser and McWilliams 2021) and thus potentially help in constraining the population properties of events falling in the pair-instability mass gap (see Abbott et al. 2020c and references therein).

Capture in PBH clusters: The second most important PBH binary formation channel is through dynamical capture in dense PBH clusters. Therefore the PBH clustering properties, which are still uncertain and highly model-dependent, mostly determine their overall merger rate. In the absence of additional clustering compared to ΛCDM expectations, one has a rate $R \approx \mathcal{O}(1)\,\mathrm{yr}^{-1}\,\mathrm{Gpc}^{-3}$ for equal-mass binaries (Bird et al. 2016). But in the case of wide mass functions, clustering may be boosted as well as the merger rates, up to the values inferred by LIGO/Virgo if stellar-mass PBHs constitute a significant fraction of the DM. One can encode the clustering uncertainties in a single, rescaling parameter R^{clust} (Vaskonen and Veermäe 2020; De Luca et al. 2020a). Then, the rate distribution can be approximated as (Bird et al. 2016; Clesse and García-Bellido 2017b; Sasaki et al. 2018)

$$\frac{\mathrm{d}R^{\mathrm{capt}}}{\mathrm{d}\ln m_1 \mathrm{d}\ln m_2} \approx \mathrm{Gpc}^{-3} yr^{-1} f_{\mathrm{PBH}} R^{\mathrm{clust}} \frac{(m_1+m_2)^{10/7}}{(m_1 m_2)^{5/7}} f(m_1) f(m_2). \tag{153}$$

One has to notice though that both in the LIGO/Virgo and LISA mass ranges there are various severe constraints on the PBH abundance (Carr et al. 2021c), which are not sensitive to uncertainties on the PBH clustering, e.g. those coming from the CMB anisotropies (Ali-Haïmoud and Kamionkowski 2017; Poulin et al. 2017; Inman and Ali-Haïmoud 2019; Serpico et al. 2020).

10.4.2 Gravitational-wave chirps from primordial black holes binaries

The merger rates expected for the two illustrative PBH models considered here are represented on Fig. 33, for the two binary formation channels detailed in the previous section. From these rates, one can identify three types of GW sources that are relevant for LISA.

Intermediate-mass binaries: The LISA frequency range is ideal to detect IMBBH mergers with mass above $10^3\,M_\odot$. PBHs can produce such merger events with rates of order $\sim 10^{-2}\mathrm{yr}^{-1}\mathrm{Gpc}^{-3}$ for PBHs in clusters, which could therefore be detected by LISA given the expected astrophysical reach for such events, typically above Gpc. The rate of equal-mass primordial binaries roughly goes like $\sim M^{-1}$ for primordial

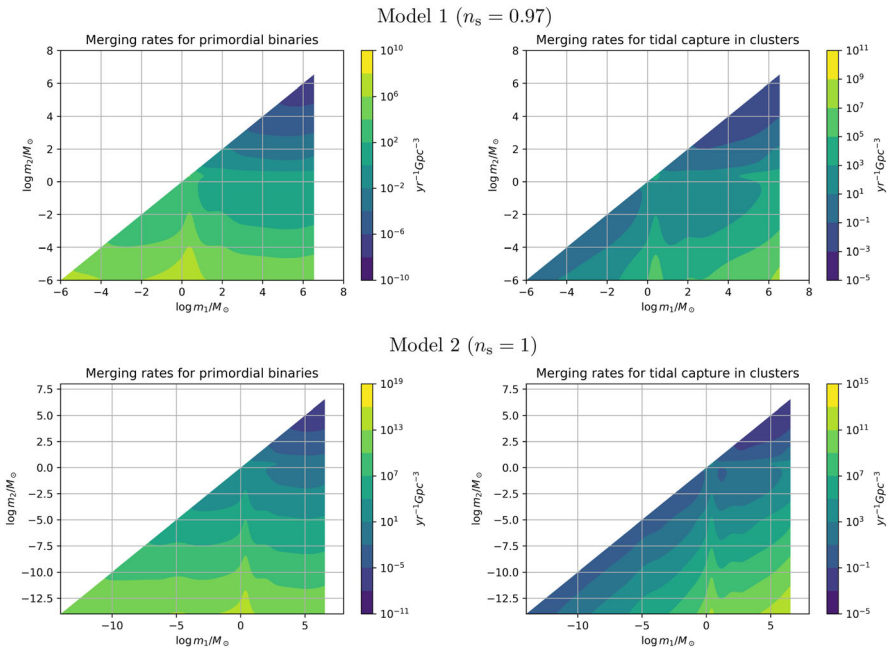

Fig. 33 Expected merger rates of PBH of mass m_1 and m_2 for the Model 1 (top panels) and Model 2 (bottom panels) mass distributions displayed in Fig. 31 due to the binary formation channels "primordial binaries" (left panels) and "tidal capture in halos" (right panels) coming from Eqs. (152) and (153) respectlisaively

binaires and is thus relatively low, while it is constant for binaries in clusters. Merger rates are also much larger for Model 1 than for Model 2, due to a much larger PBH density fraction in this range. It must be pointed out that this fraction is restricted by CMB limits. These are not calculated for such wide-mass distributions of highly clustered PBHs, and so they should not be directly applied to the models.

Extreme mass ratios: Another distinctive feature of PBHs with wide mass distributions is to predict large merger rates of binaries with extreme mass ratios, especially those involving a PBH from the QCD peak, merging with an intermediate mass PBH, as shown in Fig. 33. For Model 1 and tidal capture in clusters, these rates can be larger than $10^3 \mathrm{yr}^{-1}\mathrm{Gpc}^{-3}$. Therefore LISA could detect such extreme mass ratio coalescences, because of the ideal sub-Hertz GW frequency of such mergers and the large merger rates that allow for the compensation of the reduced strain sensitivity of LISA compared to the one of ground-based detectors at higher frequencies.

Continuous waves from galactic binaries: Models with an important PBH fraction at planetary-masses and below typically lead to very high merger rates at low mass, which could allow for the detection of such binaries within our galaxy. This is especially motivated for the Model 2 and for primordial binaries. But in the LISA range, such binaries are still far from the time of merger, when the strain evolution is almost constant over the duration of an observing run. For these kind of signals the continuous wave searches (see e.g. Miller et al. 2021) look promising. The sensitivity of LISA to planetary-mass PBHs using such search techniques is still to be determined.

10.4.3 Stochastic gravitational-wave background

The overlap of GWs from PBH binaries that are close to merger form together a SGWB that could be detected by LISA. The possible spectral shape of this SGWB for the two possible binary formation channels, the constraints coming from observations and their implications for PBH models, have been discussed in the recent literature (Mandic et al. 2016; Clesse and García-Bellido 2017a; Wang et al. 2018; Raidal et al. 2017; Chen et al. 2019; Wang et al. 2019). Hereafter, we review the basic principle and formula to compute this SGWB and present some predictions for particular PBH models.

The amplitude of the SGWB is given by summing up the energy spectrum of each binary system by taking into account the merger rate distribution as well as its possible evolution with redshift. For binary systems with a circular orbit and for a generic PBH mass function leading to merger rates $R(m_1, m_2)$, e.g. given by Eq. (152) for primordial binaries and by Eq. (153) for capture in halos, one gets (Clesse and García-Bellido 2017a)

$$\begin{aligned}\Omega_{\mathrm{GW}}(f) = &\frac{8\pi^{5/3}G^{5/3}}{9H_0^2} f^{2/3} \int_0^{z_{\max}} \mathrm{d}z \, \frac{1}{H(z)(1+z)^{4/3}} \\ &\times \int \mathrm{d}\ln m_1 \int \mathrm{d}\ln m_2 \; R(m_1, m_2, z) \mathcal{M}_c^{5/3}(m_1, m_2)\end{aligned} \tag{154}$$

where $\mathcal{M}_c$ is the chirp mass. The maximum frequency in the observer's frame is

determined by the innermost stable circular orbit which is given by $f_{\rm ISCO} \approx 4.4{\rm kHz}\, M_\odot/((m_1+m_2)(1+z)$. This can be translated to the maximum redshift as $z_{\rm max} = f/f_{\rm ISCO} - 1$.

As an example, we used a peaked mass distribution around $2.5\, M_\odot$ (motivated by the QCD peak) and computed the corresponding SGWB, for binaries formed in halos. This SGWB is clearly detectable by LISA but probably below the sensitivity of LIGO/Virgo. By probing the amplitude and spectral index of this SGWB, LISA would be able to distinguish between different mass functions, different clustering properties, as well as the dominant binary formation channel. Indeed, the lower limit of the frequency range covered by PBH binaries depends on their relative velocity when the binary is formed, which itself depends on the typical cluster mass and radius.

10.4.4 Bursts from hyperbolic encounters

If PBHs are at present grouped in clusters, a fraction of BH encounters will not end up producing bound systems, but a single scattering event. This could happen e.g. when the relative velocity is too high for the capture to be possible. The GW signals from hyperbolic encounters can have frequencies, strain amplitudes and characteristic time durations that create GWs signals that can be detected by LISA. These events would have unique signatures (García-Bellido and Nesseris 2018, 2017) and would provide direct information about the orbital parameters and spatial distribution of these BHs, thereby providing complementary information to inspiral binaries, and strong evidence in favor of the scenario of clustered PBHs (Fig. 34).

The waveforms of the GW emission in hyperbolic encounters are very different from those of the inspiraling binaries, since the majority of the energy is released near the point of closest approach, generating a burst of GWs with a characteristic "tear-drop" shape of the emission in the time-frequency domain (García-Bellido and Nesseris 2018, 2017). The burst has a characteristic peak frequency

$$f_{\rm peak} = 0.32\,{\rm mHz} \times \frac{\beta(e+1)}{(e-1)}\frac{\rm AU}{b}, \tag{155}$$

which corresponds to the maximum GW amplitude and depends only on the impact parameter b, the total mass of the system M and the eccentricity of the hyperbolic orbit $e = \sqrt{1 + b^2 v_0^4/G^2 M^2}$), where v_0 is the asymptotic relative velocity of the encounter and $\beta \equiv v_0/c$. The burst duration can be of the order of a few milliseconds to several hours (depending on the PBH masses and encounter parameters) and bright enough to be detected at distances up to several Gpc. The maximum strain amplitude of the GW burst is given by

$$h_{\rm c}^{\rm max} = 3.24 \times 10^{-23} \frac{R_{\rm S}({\rm km})}{d_{\rm L}({\rm Gpc})} \frac{q\beta^2 g_{\rm max}}{(1+q)^2} \tag{156}$$

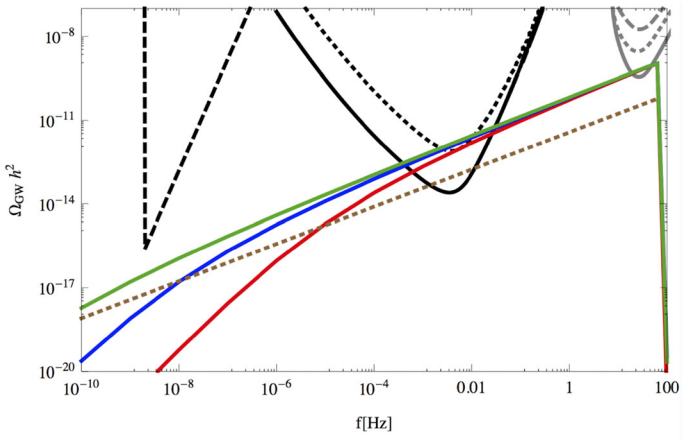

Fig. 34 Example of SGWB expected for PBH binaries formed by tidal capture in clusters, with rates given by Eq. (153) and different virial velocities (2 km/s in green, 20 km/s in blue and 200 km/s in red) and a peaked PBH mass distribution around $30\,M_\odot$. Image reproduced with permission from Clesse and García-Bellido (2017a)

$$P_{max}(e) = 5.96 \times 10^{26} L_\odot \frac{q^2 \beta^{10}}{(1+q)^4} \frac{(e+1)}{(e-1)^5}, \tag{157}$$

where $L_\odot$ is the solar luminosity, R_S is the Schwarzschild radius, $q \equiv m_1/m_2$ is the black hole mass ratio, $m_1 = q m_2 \geq m_2$ and $g_{\max} = 2\sqrt{18(e+1) + 5e^2/(e-1)}$.

GWs detectable by LISA could be generated by close encounters of an intermediate-mass BH and a MBH as expected at the centers of galaxies, as well as from encounters of two MBHs that could occur during galactic collisions at low redshift. In the first case, an intermediate-mass BH of mass $m_2 = 10^3\,M_\odot$ and a MBH of mass $m_1 = 10^6\,M_\odot$, with an impact parameter b = 1AU and velocity $v_0 = 0.05\,c$, gives an eccentricity parameter $e = 1.031$ with event duration of about 440 s. The maximum stress amplitude would be $h_c^{\max} = 1.02 \times 10^{-19}$ at a distance $d_L = 1$ Gpc, with the peak at frequency $f_{peak} = 1.05$ mHz, well within the sensitivity band of LISA [17]. In a hyperbolic encounter between two MBHs of equal mass $m_1 = m_2 = 10^6\,M_\odot$ with impact parameter $b = 10$ AU and relative velocity $v_0 = 0.015c$, the eccentricity is low $e = 1.01$ and the stress amplitude is huge $h_c^{\max} = 2.22 \times 10^{-17}$ at $f_{\rm peak} = 1.51 \times 10^{-4}$Hz, again right in the middle of the LISA observational band. Such a close hyperbolic encounter event would be clearly detectable due to a distinctive "burst" waveform (Morrás et al. 2022) that is very different from the usual "chirp" signatures of BBH. Furthermore, even if a single close hyperbolic encounter event may be difficult to detect, their characteristics can be distinguished population-wise, given their expected rates.

10.5 Massive black hole seeds from primordial black holes at high redshift

It is challenging to explain how MBHs can exist in only partially reionized environments at redshifts $z \gtrsim 7$ (Banados et al. 2018). The first populations of stars or the direct collapse of gas into BHs are two possible astrophysical mechanisms to generate the seeds of these MBHs. But even if one invokes super-Eddington accretion, it is very challenging for these seeds to reach sufficiently large masses to explain observations. PBHs are an alternative explanation to the existence of MBHs since they can provide seeds of intermediate-mass BHs at higher redshift than for the other astrophysical mechanisms (Duechting 2004; Kawasaki et al. 2012; Clesse and García-Bellido 2015; Bernal et al. 2018). The easiest way to distinguish PBH seeds from other candidates is therefore to observe IMBBHs at $z \gtrsim 20$, before star formation.

The astrophysical range of LISA will allow will allow for the observation of IMBBH mergers at redshifts $z > 20$ with a SNR larger than five, for equal-mass mergers and progenitor masses between $10^3\,M_\odot$ and $10^6\,M_\odot$, as shown in Fig. 35. The possible merger rates of PBHs for a broad mass function with the imprints of the thermal history, shown in Fig. 33, can be larger than $\mathcal{O}(1)\mathrm{yr}^{-1}$ for primordial IMBBHs that would be formed in PBH clusters at high redshift. The existence of these clusters is relevant since they would also form in the standard Press–Schechter theory. LISA observations will be complementary to those of Earth-based GW detectors, like CE and ET, which will probe mergers with lower masses, and to future PTA limits from SKA, which will probe eventual mergers of MBHs at similar redshifts.

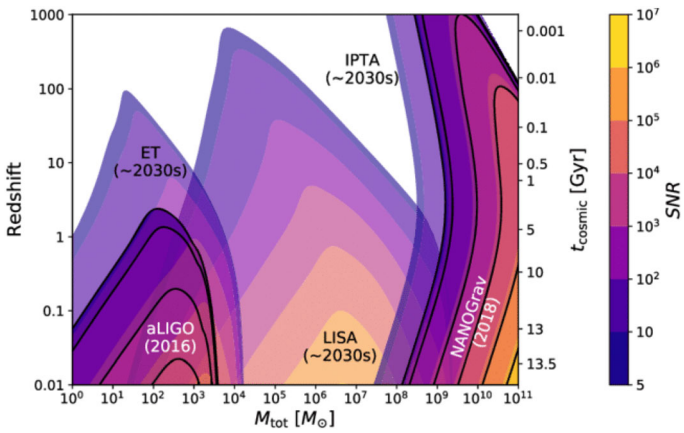

Fig. 35 Redshift range of LISA according to the analysis of Burke-Spolaor et al. (2019) for equal-mass BBH coalescences as a function of the total system mass, and comparison with the range of other detectors and pulsar timing arrays. The color scale represents the expected SNR emerged from the study. Image reproduced with permission from Burke-Spolaor et al. (2019)

11 Tools/pipelines for the analysis of transient signal data in cosmology

Section coordinator: L. Lombriser. Contributors: T. Baker, E. Belgacem, G. Calcagni, S. Clesse, G. Congedo, J.M. Ezquiaga, J. García-Bellido, D. Laghi, L. Lombriser, M. Maggiore, M. Mancarella, A. Raccanelli, M. Sakellariadou, N. Tamanini, M. Zumalacarregui.

This section presents a discussion of the tools available and in need of development for the analysis of the LISA transient signal data, including codes, pipelines, algorithms, and methodologies. While the highlighted tools are of specific relevance to the analysis of LISA data, their application is generally not restricted to that. Sect. 11.1 focuses on standard sirens tests of the cosmic expansion (see Sect. 2). Section 11.2 is devoted to the tools for GW lensing (Sect. 3). Tools for tests of modified gravity (Sect. 4) are presented in Sect. 11.3, and finally Sect. 11.4 discusses the tools for PBHs (see Sect. 10).

11.1 Tools for testing the cosmic expansion with standard sirens

As presented in Sect. 2, GW observations are natural cosmological probes because their amplitude directly traces the luminosity distance as predicted by GR. When additional redshift information is obtained, GW events become standard sirens. Depending on whether the redshift information comes directly from an EM counterpart or from statistical inference, we will refer to them as bright and dark sirens respectively. In both cases, modern GW data analysis techniques are based on Bayesian inference. In the following we describe them independently.

11.1.1 Bright sirens

For bright sirens, the single–event posterior for a set of parameters $\mathcal{H}$ given GW data $\mathcal{D}_{\rm GW}$ and EM-wave data $\mathcal{D}_{\rm EM}$ can be written as (Chen 2020)

$$p(\mathcal{H}|\mathcal{D}_{\rm GW},\mathcal{D}_{\rm EM}) = p(\mathcal{H})\frac{\int p(\mathcal{D}_{\rm GW}|\vec{\Theta})p(\mathcal{D}_{\rm EM}|\vec{\Theta})p_{\rm pop}(\vec{\Theta}|\mathcal{H})d\vec{\Theta}}{\int p_{\rm det}(\vec{\Theta})p_{\rm pop}(\vec{\Theta}|\mathcal{H})d\vec{\Theta}}, \tag{158}$$

where $p(\mathcal{H})$ is the prior probability density on $\mathcal{H}$, and $\vec{\Theta}$ represents all the binary parameters. The set of parameters $\mathcal{H}$ can be expressed in full generality as $\mathcal{H} = \{\mathcal{H}_{\rm cosmo}, \mathcal{H}_{\rm pop}\}$, where $\mathcal{H}_{\rm cosmo} = \{H_0, \Omega_m, \Omega_k, \Omega_\Lambda\}$ are the cosmological parameters and $\mathcal{H}_{\rm pop}$ represent a set of parameters used to model the population such as the mass and spin distribution or the merger rate evolution with redshift. The population prior $p_{\rm pop}(\vec{\Theta}|\mathcal{H})$ is the probability density of binaries with parameters $\vec{\Theta}$ under our assumption of the merger rate density. The detection probability is given by

$$p_{\rm det}(\vec{\Theta}) = \int\limits_{\substack{\mathcal{D}_{\rm GW} > {\rm GW}_{\rm thr} \\ \mathcal{D}_{\rm EM} > {\rm EM}_{\rm thr}}} p(\mathcal{D}_{\rm GW}|\vec{\Theta}) p(\mathcal{D}_{\rm EM}|\vec{\Theta}) d\mathcal{D}_{\rm GW} d\mathcal{D}_{\rm EM}, \tag{159}$$

in which the integration is only carried out over the data above the GW and EM detection thresholds, $\mathrm{GW}_{\rm thr}$ and $\mathrm{EM}_{\rm thr}$, respectively.

GW and EM-wave observations can both introduce systematic uncertainties to the standard siren measurements. The measurements of the host redshifts can suffer from peculiar motions of the hosts (Howlett and Davis 2020; Mukherjee et al. 2021c; Nicolaou et al. 2020). The measurements of the binary luminosity distances are affected by the detector calibration uncertainty (Karki et al. 2016; Sun et al. 2020), lensing (Holz and Linder 2005; Hirata et al. 2010), and the accuracy of the waveforms (Abbott et al. 2019b). In addition, as shown in Eq. (158), our understanding of the possible observational selection effects (Chen 2020) as well as the astrophysical rate evolution (see e.g. Fig. 12 of Finke et al. (2021) for an application to LIGO-Virgo data) are critical to the accuracy of the standard siren as well.

11.1.2 Dark sirens

In the absence of an EM counterpart, one may extract redshift information by putting a prior on potential hosts from a galaxy catalogue.[32] In this case, it is natural to consider the catalogue as a prior and the most convenient choice is to make a change of variables $d_L \mapsto z(d_L, \mathcal{H})$ in Eq. (158), and use the redshift z instead of the luminosity distance $d_L \in \vec{\Theta}$.[33] Denoting $\vec{\Theta} = \{d_L, \hat{\Omega}, \vec{\Theta}'\}$, Eq. (158) reads

$$p(\mathcal{H}|\mathcal{D}_{\rm GW}) = \frac{p(\mathcal{H})}{\alpha(\mathcal{H})} \int dz d\hat{\Omega} d\vec{\Theta}' \, p(\mathcal{D}_{\rm GW}|d_L(z,\mathcal{H}), \hat{\Omega}, \vec{\Theta}') p_{\rm pop}(z, \hat{\Omega}, \vec{\Theta}'|\mathcal{H}), \tag{160}$$

where $\alpha(\mathcal{H}) \equiv \int p_{\rm det}(\vec{\Theta}) p_{\rm pop}(\vec{\Theta}|\mathcal{H}) d\vec{\Theta}$ and we set $p(\mathcal{D}_{\rm EM}|\vec{\Theta}) = 1$, being in the absence of a counterpart. Note that the GW likelihood now carries an explicit dependence on the parameters $\mathcal{H}$. The population prior on redshift and position is expressed as

$$p_{\rm pop}(z, \hat{\Omega}|\mathcal{H}) \propto \sum_i w_i \frac{dV_c}{dz d\Omega}(z, \mathcal{H}) \, p(z_i, \hat{\Omega}_i | z, \hat{\Omega}). \tag{161}$$

In the above equation, $p(z_i, \hat{\Omega}_i|z, \hat{\Omega})$ is the likelihood of the redshift and position of the i-th galaxy in the catalogue, with observed values $z_i, \hat{\Omega}_i$. The angular position can be assumed to be known with very good precision—since the GW likelihood does not vary significantly over the scale of the galaxy location—and the corresponding

[32] This method assumes that the true source is not of primordial origin.

[33] Note that the GW likelihood $p(\mathcal{D}_{\rm GW}|\vec{\Theta})$ is unaffected by this transformation since it is a PDF with respect to the data $\mathcal{D}_{\rm GW}$.

distribution is just a delta function about the observed values; the redshift-dependent part of the likelihood can be instead approximated by a Gaussian centered around the observed redshift z_i and with standard deviation given by the redshift uncertainty.[34] The term $dV_c/dzd\Omega$ is the differential of the comoving volume element V_c, which is a uniform-in-volume prior on the redshift z (Chen et al. 2018; Soares-Santos et al. 2019; Palmese et al. 2020). A more refined choice is to assume a prior that follows the expected evolution with redshift of the rate of GW sources (Gray et al. 2020; Finke et al. 2021). However, since this is not known a priori, this choice also adds more parameters to the analysis. Finally, the factors w_i in Eq. (161) represent the possibility of assigning different weights to the galaxies. Common choices are the B-band luminosity, which traces the star formation rate, or K-band luminosity that traces the total stellar mass.

One has then to deal with the fact that galaxy catalogues are in general not complete. This requires one to include information on the missing galaxies, and the prior in Eq. (161) must be supplemented by a suitable "completion" term (Chen et al. 2018; Fishbach et al. 2019; Gray et al. 2020; Finke et al. 2021), which requires two pieces of information. The first is the knowledge on the "completeness" of the catalogue, that is usually computed by comparing the luminosity distribution in the catalogue to the one given by a Schechter function (Chen et al. 2018; Fishbach et al. 2019; Finke et al. 2021).[35] The second is to specify a "completion" procedure, i.e. to determine how the missing galaxies are spatially distributed. The simplest options can be to distribute them uniformly (Chen et al. 2018; Fishbach et al. 2019), or to assume that the catalogue traces well the actual structures, hence assigning higher weight to the galaxies that are in low completeness regions (Finke et al. 2021), or even assuming that completion is not needed (Soares-Santos et al. 2019; Palmese et al. 2020; Laghi et al. 2021). Eventually, the best choice depends on the galaxy survey, its sky coverage and on the completeness of the catalogue. A more refined procedure is to use the uniform, uninformative distribution in regions of low completeness, while switching to the second option where the galaxy survey traces the actual structures fairly well (Finke et al. 2021). This aspect will become more important as the precision on the localisation increases but will remain a limiting factor until catalogues with very large completeness are available. Since the completeness drops drastically with increasing redshift, this can be limiting for LISA sources at high redshift when using catalogues that have a large sky coverage but limited redshift range. Another option is to use deeper catalogues with limited sky coverage, but this requires to take into account the variation of the completeness with the angular position in the sky (Finke et al. 2021). In any case, the availability of complete galaxy catalogues, accurate determination of the redshifts, and small GW localisation regions will be crucial in order for the statistical method to give competitive constraints on cosmological parameters.

[34] However, the true PDF should be used when available, and this choice can have a non-negligible impact on the result (Palmese et al. 2020).

[35] A slightly different, though comparable, approach is to include the possibility that the true host is not in the catalogue in the formalism (Gray et al. 2020).

Finally, a good understanding and an accurate computation of the selection bias is required (Chen 2020; Finke et al. 2021). This is related to other relevant systematic uncertainties that deserve further investigation, related to our limited knowledge of the population properties of BBHs. In particular, the population prior should encode information on the mass distribution of the system's component and on the rate of BBH formation as a function of redshift. At the moment, very mild constraints exist on both in the case of SOBBH (Fishbach et al. 2018; Abbott et al. 2021e), but their impact—especially of the evolution of the BBH merger rate—can be relevant (Finke et al. 2021).

A public `Python` code implementing the completion procedures described above, as well as calculation of selection effects, is available at https://github.com/CosmoStatGW/DarkSirensStat. The code has been applied to the latest data release from the LIGO-Virgo collaboration for constraining H_0 and modified GW propagation and supports the combination with the GLADE, DES and GWENS galaxy catalogues, but it could easily be be adapted for LISA and other galaxy catalogues.

11.2 Tools for gravitational-wave lensing

GW lensing has attracted considerable attention recently, leading to different groups developing tools to compute amplification factors and lensed waveforms. In order to maximise the science yield of gravitational lensing with LISA, it is important to develop codes to compute amplification factors for general lenses and including wave effects.

`LensingGW` is a publicly available tool for GW lensing in geometric optics. It is a `Python` package designed to compute amplification factors for general lenses, adapted to the needs of GW observations (Pagano et al. 2020). Currently, `LensingGW` operates in the geometric optics regime, using a selective sub-tiling to find microimages, their associated magnifications and time delays, cf. Eq. (14). The code is based on the `lenstronomy` package (Birrer and Amara 2018), allowing it to draw from its library of algorithms and lens models.

It is necessary to develop wave optics codes able to solve Eq. (15). The diffraction integral is highly oscillatory, which makes numerical solutions challenging. Proposed methods to address this problem use the time delay function (Ulmer and Goodman 1995) and Fourier transforms to the frequency domain. Variants of these ideas have been implemented in Diego et al. (2019), Cheung et al. (2021) and others. These codes are not publicly available. An alternative approach employs Picard-Lefschetz theory (Feldbrugge et al. 2023). This is valid only for lensing potentials that are meromorphic functions, which may be used to approximate non-analytic lensing potentials. Finally, corrections to geometric optics rely on higher derivatives of the Fermat potential around images (Takahashi 2004) and could be easily implemented in a geometric optics formalism.

Predictions on GW propagation beyond GR are notoriously complicated. (Ezquiaga and Zumalacárregui 2020) develops a `Python` package to study GW birefringence. The code is able to (1) compute static spherical backgrounds in Horndeski theory; (2) compute the local propagation eigenstates and their speed as a function of position and direction; (3) solve the geodesics in the Born approximation

to compute time delays and deflection angles for each eigenstate; and (4) obtain the waveform, including birefringence. Future tools to study GW lensing should improve by (a) including higher-order corrections in the Wentzel-Kramers-Brillouin (WKB) expansion to compute the amplitude and diffraction effects (or optimally, arrive at a full wave optics expression); (b) include more general theories of gravity; and (c) work with more general backgrounds (for instance, performing GW ray tracing on modified gravity simulations). These codes could be interfaced with a statistical sampler to analyse real or mock data.

11.3 Tools for testing modified gravity

The sensitivity of LISA to modified GW propagation introduced by a frequency independent modification of the damping term was investigated in Belgacem et al. (2019c). A MCMC analysis was conducted on LISA mock catalogues of MBBHs with EM counterparts, where luminosity distances were evaluated according to a fiducial ΛCDM cosmology. As discussed in (Belgacem et al. 2018b, 2019c), in the context of late-time modifications of GR invoked for DE studies, the most relevant parameters affecting GW propagation are the high-redshift ratio of GW to EM luminosity distances Ξ_0, defined in Eq. (21), the DE EoS w_0, the Hubble parameter H_0, and the current matter energy density fraction Ω_m. The exponent n of the parametrisation in Eq. (21) plays a less important role and was fixed to a reference value. In order to reduce the degeneracies among those parameters and assess the potential of LISA for cosmological parameter inference, in addition to LISA mock catalogues, the analysis in Belgacem et al. (2019c) also included further currently available datasets such as CMB measurements from Planck 2015, Type Ia Supernovae (JLA catalog), and a collection of BAO measurements. The likelihood of the LISA mock data given the parameters $\{H_0, \Omega_m, w_0, \Xi_0\}$ was assumed to follow

$$\ln(L(H_0, \Omega_m, w_0, \Xi_0)) = -\frac{1}{2}\sum_{i=1}^{N_s} \frac{\left[d_L^{\mathrm{GW}}(z_i; H_0, \Omega_m, w_0, \Xi_0) - d_i\right]^2}{\sigma_i^2}, \tag{162}$$

where an additive constant in the logarithm of the likelihood from normalization is omitted. Here N_s is the number of mock sources in the catalogue, $d_L^{\mathrm{GW}}(z_i; H_0, \Omega_m, w_0, \Xi_0)$ is the theoretical value of the GW luminosity distance for the i-th source (at redshift z_i), σ_i is the error on luminosity distance taking also into account the error on redshift determination, and d_i is the "measured" value of the luminosity distance of each event contained in the catalogue (obtained by scattering the fiducial ΛCDM prediction with a Gaussian distribution with variance σ_i^2). The MCMC code of Belgacem et al. (2019c) explores the cosmological parameter space, accepting or rejecting sampled points following a Metropolis-Hastings algorithm. The total likelihood used in the algorithm is obtained by multiplying the independent contributions from each of the four datasets employed, namely from CMB, Type Ia supernovae, BAO, and LISA. The cosmological evolution, both at the level of the background and perturbations, is computed using the `CLASS` Boltzmann code. The modified version of `CLASS`, implementing the GW luminosity distance parametrisation in Eq. (21), is available at https://github.com/enisbelgacem/class_public. The

MCMC code is built on `MontePython` with the inclusion of the LISA mock source catalogues and the likelihood from Eq. (162), which uses the modified `CLASS` version. The code is available at https://github.com/enisbelgacem/montepython_public.

In addition to the test of the model-independent parameters $\{\Xi_0, n\}$, similar analyses have been carried out using the modified luminosity distances of specific gravity models, e.g. Horndeski gravity (Lombriser and Taylor 2016; Baker and Harrison 2021) or $f(\mathcal{Q})$ gravity (Frusciante 2021). These make use of the modified Boltzmann codes `hi_CLASS` (Zumalacárregui et al. 2017; Bellini et al. 2020) and `EFTCAMB` (Hu et al. 2014; Raveri et al. 2014), respectively. A wrapper to interface `hi_CLASS` with the MCMC code `Cosmosis` (Zuntz et al. 2015) is available at https://github.com/itrharrison/hi_class.

Current tools are predominantly specialised to probing the effects of frequency-independent modifications of the GW propagation, although frequency-dependent effects have been studied in the context of GW oscillations in bigravity (Belgacem et al. 2019c), where the associated numerical tools have however not been made publicly available yet. The desire for UV-completion of modified gravity theories, whilst maintaining IR phenomenology, also motivates frequency-dependent modifications of the GW propagation equation (de Rham and Melville 2018). Such modifications could be detectable in the LISA band whilst being suppressed to irrelevant levels in the band of ground-based detectors ($\sim$10–1000 Hz). Their basic phenomenology corresponds to a frequency-dependent GW luminosity distance or a frequency-dependent GW propagation speed.

To study the detectability of these effects, one must first construct a motivated and manageable parameterisation for the frequency and redshift dependence of $c_T(f,z)$ and $\delta(f,z)$ that appear in Eq. (19). One then needs to solve for the amplitude and phase evolution of the waveform under this parameterisation, up to some appropriate post-Newtonian order. A Fisher forecast code, ideally calibrated against a smaller, more rigorous (but computationally expensive) MCMC forecast, can analyse the ability of LISA to constrain the frequency-dependent modifications to c_T and $d_{\rm GW}$. The parameterisation must be carefully chosen to minimise degeneracies between the MG and standard source parameters. The creation of these tools is in progress (Baker et al. 2022).

Finally, we note that sources of anisotropic stress in the universe act as source terms on the right-hand side of Eq. (19). Neutrinos are one such example, although their effects on GW propagation in the late-time universe are expected to be extremely small. However, their effects on GWs travelling through the early universe may be more significant. Analytical tools for solving GW evolution in the presence of neutrino anisotropic stress are presented in Wren et al. (2017) and could likely be adapted for a generic imperfect fluid with anisotropic stress.

11.4 Tools for PBHs

The recent developments in the field of PBHs have revealed a rather rich phenomenology, e.g. related to PBH formation with a broad variety of primordial power spectra and new classes of models relying on non-trivial modifications of the

statistical distribution of curvature fluctuations; related to the history of PBH clustering, accretion and mergings, etc. The computations of GW observables therefore need to become more accurate and have to take into account model dependencies and various astrophysical uncertainties. It becomes increasingly difficult to integrate all the recent development in new analyses. Therefore, there is need in the community for an advanced numerical tool that progressively integrates all these recent developments at various levels (theoretical models, PBH formation, clustering, accretion, merging rates, SGWBs) in a unified and modular manner. This is the main objective of an ongoing project of the LISA Cosmology Working Group that is developing the `PrimBholes` toolbox for the computation of model-dependent gravitational observables that are relevant for LISA and other GW experiments. The `PrimBholes` toolbox is currently under development and will be made publicly available soon along with both a code companion paper and a review paper on PBHs.

The different computations performed with `PrimBholes` and the possible options and effects that will be implemented for selection are the following:

1. For the primordial curvature fluctuations this will include (a) several phenomenological models of power spectra (power-law, log-normal, Gaussian, broken power-law, etc.); (b) Gaussian and non-Gaussian perturbations with a generic distribution function and some specific realisations; and (c) generic power spectra and/or distribution functions imported from a file provided by the user.
2. The SGWB from second-order perturbations will be calculated for general as well a number of specific shapes of the primordial power spectrum.
3. The computation of the PBH formation and density distribution $\beta(m_{\rm PBH})$ at formation will be performed following (a) the standard formalism of Sect. 10.2.2 and (b) an advanced method and algorithm presented in Musco et al. (2021) accounting for non-linear effects and the shape of the primordial power spectrum. This will include (c) effects of the evolution of the EoS through the thermal history of the universe and (d) a *reversed* method to rescale the amplitude of primordial curvature fluctuations in order to get a fixed value of $f_{\rm PBH}$.
4. To obtain the late-time PBH mass function $f(m_{\rm PBH})$, `PrimBholes` will rely on the standard formalism and include additional effects from accretion and hierarchical mergers.
5. The distribution of merging rates $R(m_1, m_2)$ will be computed for (a) primordial binaries, accounting for the effects from the formation of early clusters due to the Poisson noise, from matter inhomogeneities and from nearby BHs, and (b) for tidal capture in clusters, accounting for different clustering histories and halo mass functions. This will include (c) the dependence on the redshift of the merging rates.
6. Finally, `PrimBholes` will include the spin distribution, based on (De Luca et al. 2019; 7) the rate of hyperbolic encounters, based on (García-Bellido and Nesseris 2018); and (8) the SGWB from primordial binaries, for the two aforementioned formation channels.

`PrimBholes` will also provide plotting modules that will facilitate the production and exportation of key figures. Examples are given in Figs. 31 and 33.

In a first step, the `PrimBholes` code will focus on the computation of GW observables without including a likelihood module for LISA. However, it will be made modular so that it can be used in combination with other codes such as the LISA analysis code for the SGWBs or the Botzmann code `CLASS` (Blas et al. 2011). Later, likelihood modules for the `MontePython` code (Brinckmann and Lesgourgues 2019) could be included for the computation of the various astrophysical and cosmological limits on the PBH abundance.

12 Tools/pipelines for the analysis of stochastic gravitational-wave background data

Section coordinators: N. Karnesis, M. Peloso, M. Pieroni. Contributors: N. Bartolo, G. Boileau, N. Christensen, C. Contaldi, V. Desjacques, R. Flauger, N. Karnesis, V. Mandic, S. Mataresse, M. Peloso, M. Pieroni, A. Renzini, A. Ricciardone, J. Romano, M. Sakellariadou, L. Sorbo, J. Torrado.

The SGWB to be measured by LISA consists mainly of the confusion noise created by the overlapping signals from unresolved astrophysical events, and possibly of a cosmological component due to one or more physical mechanisms taking place at different stages of the late or early universe (e.g. the mechanisms discussed in Secs. 8, 7 and 6). LISA will open a completely new window into the parameter space of each of these phenomena and has the potential to produce new discoveries about the physics of the early universe through the characterisation of this primordial SGWB component. A careful characterisation of the total background is also necessary to aid the detection and identification of individual events. In this section, we discuss the features of each contribution to the background signal, the instrumental noise, and the different tools we need to develop to separate and characterise all of of them.

We start with Sect. 12.1 which summarises the main characteristics of the noise in LISA. We comment on existing noise models, the assumptions on which they are built, and on possible improvements. In Sect. 12.2 we discuss foregrounds (i.e. astrophysical sources of a SGWB) by describing the possible sources and the characteristics and main properties of the different signals. In Sect. 12.3 we then focus on frequency shape reconstruction methods i.e. methods which aim at recovering the spectral profile of an unknown SGWB. We proceed by discussing anisotropy reconstruction i.e. recovering the angular structure hidden in the signal. For this topic both theoretical and data oriented approaches are covered in Sect. 12.4 and in Sect. 12.5 respectively. Finally, in Sect. 12.6 we frame the different topics touched in this section in the big picture of the so called *global fit* problem. For all of these points the discussion covers both existing techniques and possible further developments.

12.1 Noise modelling

The instrumental noise in LISA is expected to be non-stationary, and at the same time we expect noise transients that cause the statistical properties of the noise to depart from Gaussianity. At a first approximation we can assume that the short noise transients (i.e. glitches) will be modelled, identified, and removed from the data streams (Robson and Cornish 2019). However, slow variations of the noise, like for example the slow decrease of the acceleration noise of the test-masses due to outgassing (Armano et al. 2018), are due to known effects that can be properly modelled and considered in the analysis. We can tackle those problems by adopting a piecewise analysis, where we can consider that each data segment can be assumed as stationary and Gaussian. In order to eliminate the dominant noise sources (i.e. fluctuations of the laser central frequency and displacements of the of the optical benches), LISA will employ time domain interferometry (TDI) techniques (Tinto and Armstrong 1999; Estabrook et al. 2000; Tinto et al. 2002; Armstrong et al. 2003; Tinto et al. 2004; Tinto and Dhurandhar 2021; Vallisneri et al. 2021). In the simplified scenario considered in most of the literature (Bartolo et al. 2019a; Caprini et al. 2019; Contaldi et al. 2020; Smith et al. 2019; Pieroni and Barausse 2020; Flauger et al. 2021; Orlando et al. 2021) the residual noise for each arm link has two main components: the "acceleration" and the "interferometric" noise components. The acceleration component is associated with the random force noise acting on the test masses inside each of the three satellites, due for example to local environmental disturbances, and it dominates the low frequency part of the LISA band. The interferometric noise is directly connected to the interferometry metrology system (IMS). It describes the random readout noise of the optical system (mostly due to shot noise), and dominates the spectrum at high frequencies. For the 1.5 TDI variables (Bayle et al. 2019; Babak et al. 2021), one can follow the recipe of Flauger et al. (2021) and construct a likelihood based on the $\{ X, Y, Z \}$ TDI channels. In principle, analogous procedures can be defined for any kind of TDI variable combination. In order to remove noise correlations between different channels, it is customary to introduce an alternative TDI basis, typically dubbed the *AET* basis, which diagonalises the noise matrix. The total noise spectra for both *XYZ* and *AET* basis are shown in the right panel of Fig. 36. On the other hand, the left panel of Fig. 36 shows the acceleration and IMS noise power spectra.

Naturally, searching for SGWB signals requires a sufficient knowledge of the noise spectral shape, and it is possible that a simplified model such as the two-parameter model described above might not suffice for the signal search. Any instrument calibration mismatch will impact the joint fit of the noise and signal parameters, which may jeopardise our abilities to measure the underlying SGWB spectrum. Therefore, a possible solution to this problem would be to incorporate the calibration of the instrument in the analysis, by allowing a flexible model of the noise spectral shape. The development of methods (and of corresponding tools) which do not explicitly depend on analytical parameterisation for the noise spectra, will be an interesting research line to be explored over the years before the launch of LISA.

Another important aspect for searching for SGWB signals is assessing the quality of the data before they reach the designated pipelines. The use of signal subtraction,

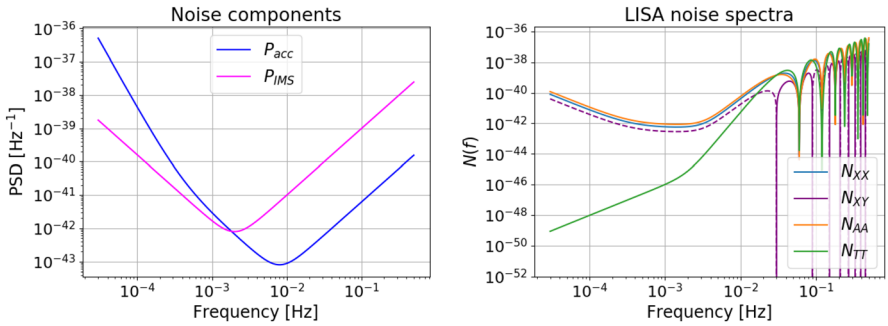

Fig. 36 Left panel: IMS and acceleration noise power spectra expressed in the simplified scenario where all test-mass and laser noises are equal for all space-crafts. Right panel: LISA noise spectra in the *XYZ* and *AET* basis as given in e.g. in Flauger et al. (2021). Images reproduced with permission from Flauger et al. (2021), copyright by IOP/SISSA

if implemented for LISA data, could result in imperfect subtraction and hence residuals, which in turn would affect the statistical properties of the noise (Thrane 2013; Romano and Cornish 2017; Smith and Thrane 2018; Ginat et al. 2020). The impact of theses residuals on the search for SGWBs with LISA is yet to be investigated. A better framing of this problem in the broader picture of the global fit problem for LISA is presented in Sect. 12.6.

12.2 Expected astrophysical foregrounds

Due to the richness of the sky in the milliHertz band LISA will be sensitive to a wide variety of sources such as MBBHs with masses $\sim 10^4$–$10^7\,M_\odot$, SOBBHs, EMRIs, and GBs. Beyond the resolvable sources, measurements by LISA will also be affected by a huge number of unresolvable events which will sum up incoherently, leading to the generation of a SGWB (Farmer and Phinney 2003; Regimbau and Hughes 2009; Regimbau 2011; Lamberts et al. 2019). At least two SGWB components are guaranteed to be present in the LISA band: a contribution due to signals originating from compact GBs is expected to dominate the LISA band at low frequencies (up to $\sim 10^{-3}$ Hz), and a contribution from extragalactic BBH mergers is expected to be present at slightly larger frequencies ($\sim 10^{-3} - 10^{-2}$ Hz). A plot of the impact of these signals as described in Flauger et al. (2021) on data measured in in the self correlations of the *A* and *T* channels (denoted by *AA* and *TT*, respectively; we note that the self correltion *EE* is identical to *AA*) is shown in Fig. 37. While the latter is expected to be isotropic and stationary, the GB contribution is expected to be anisotropic (since the binaries mostly lie on the galactic plane). Moreover, as discussed in Adams and Cornish (2014), due to the yearly rotation of the satellite constellation, this signal is expected to present a yearly modulation. Both these features are thus expected to be, at least partially, present in the total SGWB measured by LISA.

The characteristics of the GBs, i.e. being almost monochromatic, and the majority of them being located in our galactic neighbourhood, will allow us to build reliable

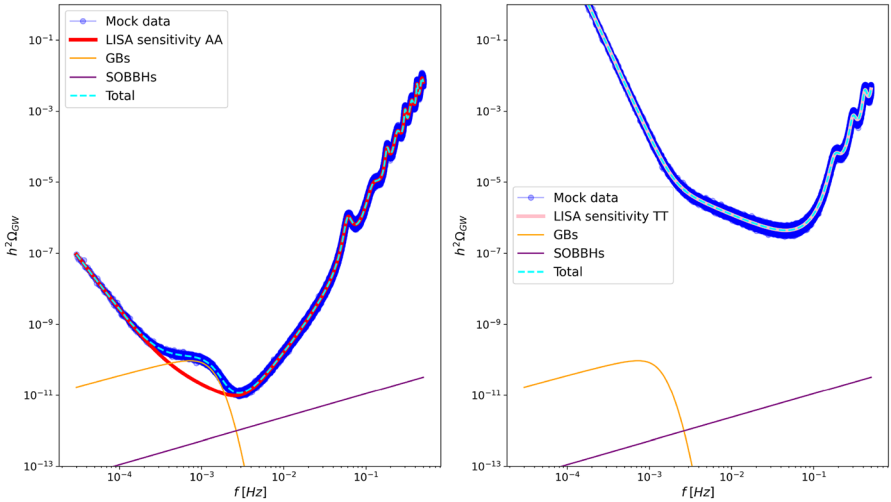

Fig. 37 Theoretical models for the LISA sensitivity in the self-correlation of the *A* and *T* TDI data channels (*AA* and *TT*, respectively) and for the SGWBs due to GBs and SOBBHs as specified in Flauger et al. (2021). Mock data for the sum of all these theoretical templates are shown for reference

models for their residual foreground noise contribution (Crowder and Cornish 2007; Sachdev et al. 2020). The same applies to the case of the isotropic signal due to SOBBH events, where the spectral model of the residual confusion noise will be constructed based on the priors from ground observations (Abbott et al. 2021d)[36] and the actual measurements with LISA.

There is a possibility to measure a foreground signal component due to EMRIs (Barack and Cutler 2005), but a more detailed study on this type of source is needed in order to make robust predictions on their expected level. A generic method to make a first-level characterisation of the stochastic signals originating from compact binaries populations is studied in Karnesis et al. (2021).

The classical central-limit theorem is violated when the single source variance is infinite, which is the case of e.g. astrophysical backgrounds produced by compact mergers. As a consequence, the convergence to a Gaussian distribution can be much slower depending on the event rates (which determines the average number of sources overlapping in the detector frequency band(s)) and the properties of the source distribution (Ginat et al. 2020). If the sources are a spatial Poisson process, the resulting (non-Gaussian) distribution of the observed strain can be predicted (both in the time and frequency domains) using the techniques outlined in Ginat et al. (2020). This approach can be extended to include the subtraction of bright sources, which (partly) gaussianises the signal (Timpano et al. 2006), and to furnish predictions for the distribution of the background of unresolved binary mergers. Quantifying deviations from Gaussianity is necessary to optimise searches for this confusion

[36] This can be done by generating catalogues of events with the estimated population properties as measured by Earth-based detectors (Dvorkin et al. 2016b; Babak et al. 2023). Further investigation is needed to assess the potential uncertainties that arise from extrapolating the population properties as measured by Earth-based detectors to predictions in the LISA band.

background (Thrane 2013; Smith and Thrane 2018) and backgrounds of cosmological origin (Bartolo et al. 2019a), and for their shape reconstruction.

Models for the residual foreground contributions can be provided when attempting a frequency shape reconstruction (see Sect. 12.3), so that the reconstructed spectrum can be expected to consist of contributions from unknown, possibly cosmological sources. The energy spectrum of the foreground due to unresolved GBs can be modelled by a broken power law. Indeed, at sufficiently large frequencies the number of sources decreases, which produces a break in the $\alpha = 2/3$ power law behaviour (where α is the spectral index in $h^2\Omega_{\rm GX} \propto f^{\alpha}$). On the other hand, the foreground due to SOBBHs and BNSs is expected to be a power law with slope $\alpha = 2/3$. Studies of SOBBH and BNS populations, such as (Périgois et al. 2021), predict $\Omega_{\rm GW}(25\ {\rm Hz}) \simeq 4.97 \times 10^{-9} - 2.58 \times 10^{-8}$. Ground detectors (Abbott et al. 2021g) set an upper limit for this foreground at $\Omega_{2/3}(f_{ref} = 25\ \ {\rm Hz}) \lesssim 5.8 \times 10^{-9}$. Clearly, these residual foreground models must account for the right amount of statistical uncertainty, or we risk overestimating the significance of a detection or of a spectral shape reconstruction. This includes, at descending levels in the Bayesian hierarchy, the possibility of different population models being used (mass or spin distribution, merger rate at different redshifts, etc), the uncertainty on the parameters of a given population when inferred from resolved events by LIGO/Virgo and LISA, and the possibility of residuals being left by the imperfect subtraction of these resolved events, either because of a sub-optimal SNR that leads to imperfect characterisation of the waveform to be subtracted, or to the very waveform not representing the actual events with perfect accuracy. Beyond these problems, as discussed in the previous paragraph, the statistical properties of the SGWBs of astrophysical origin (either before and after the removal of loud sources) may be dominated by strong non-Gaussianities which have to be appropriately modelled. A careful study is thus required to asses the impact of each of these sources of statistical uncertainty. A computational pipeline that, for each component of the residual confusion noise, can take a number of resolved events with their associated parameter uncertainties, and assuming a Bayesian-hierarchical population model (or family of them), can generate a probability distribution for each component of the foreground confusion noise needs to be developed. The final result would, of course, rely on theoretical and/or observational uncertainties on the statistical properties of the populations in the parameter regions where the binaries cannot be individually resolved. However, the integrated contribution from all these unresolved sources would substantially affect the foreground (e.g. the SOBBH binaries at redshift $z \approx 2$ impact the SOBBH LISA foreground (Babak et al. 2023)). Improvements in our understanding of the LISA astrophysical populations (Amaro-Seoane et al. 2023) will thus be crucial to strengthen this kind of pipeline. Preliminary work on similar pipelines has been developed for current- and next-generation ground-based detectors (Sachdev et al. 2020; Périgois et al. 2021; Abbott et al. 2021g; Callister et al. 2020), but a comprehensive study is needed in the framework of LISA.

12.3 Spectral shape reconstruction: existing tools and future developments

The richness of sources in the LISA frequency band requires the development of techniques and tools to disentangle the different contributions. These may include both a residual background of unresolved astrophysical sources (see Sect. 12.2), a stochastic cosmological component sourced by topological defects, phase transitions, or inflationary mechanisms, among others. Different cosmological sources are expected to produce SGWBs of characteristic frequency shapes (Bartolo et al. 2016b; Caprini et al. 2016, 2020; Auclair et al. 2020). The reconstruction of the spectral shape of the SGWBs, regardless of its origin, is expected to play a special role in the separation of its different components. The correct estimation of the SGWB and its associated uncertainty is also essential for the characterisation and subtraction of resolved events, for which this background plays the role of an additional noise component, together with the instrumental noise.

Most of the SGWB detectability studies and ground-based searches have so far only focused on power-law templates (Thrane and Romano 2013; Adams and Cornish 2014; Lentati et al. 2015; Arzoumanian et al. 2018; Abbott et al. 2019c) (and a few on more complicated, but fixed templates (Kuroyanagi et al. 2018; Barish et al. 2021)). In the context of preparations for the LISA mission, some recent works (Karnesis et al. 2020; Caprini et al. 2019; Pieroni and Barausse 2020; Flauger et al. 2021) have attempted an agnostic template-free frequency shape reconstruction. One such reconstruction can take into account more complicated scenarios where the overall signal can be the superposition of several unknown signals, and can be extremely useful both for the disentanglement of the GW sources and for the constraining power that they have on astrophysical and cosmological parameters of the underlying theories (see previous sections). An example of reconstruction obtained with the method of Caprini et al. (2019), Flauger et al. (2021) in the presence of the foreground due to GBs is shown in Fig. 38.

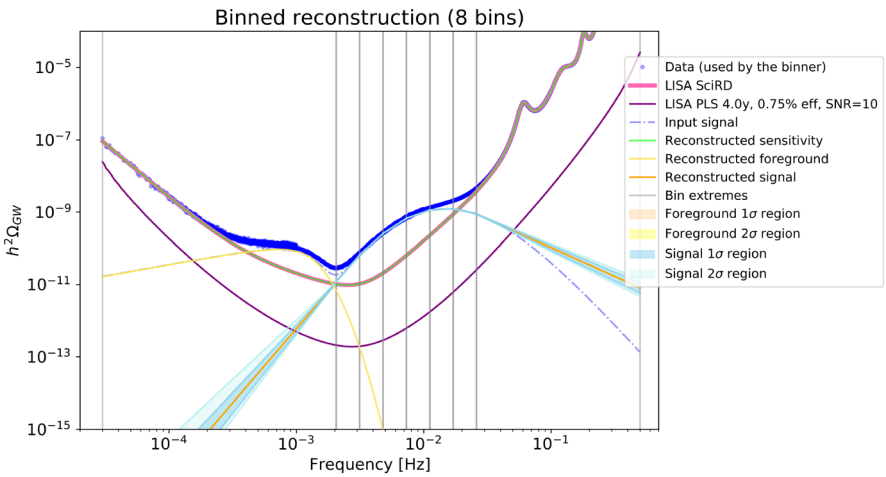

Fig. 38 Reconstruction of a broken power law signal in presence of GB foreground. Image reproduced with permission from Flauger et al. (2021)

In Karnesis et al. (2020), Caprini et al. (2019), Flauger et al. (2021), under the assumption of stationary, Gaussian, and isotropic signals, TDI data is processed into a set of frequency bins whose amplitudes are jointly estimated in the presence of noise. In the state-of-the art iteration (Flauger et al. 2021), the number of bins is dynamically chosen using Bayesian criteria, and in each of the bins, together with the signal amplitude, a power-law tilt is also considered, leading to a more accurate reconstruction with fewer bins. On the other hand, the procedure employed in Pieroni and Barausse (2020) first expresses the signal as a linear combination of an arbitrarily dense basis of Gaussians and then selects the components associated with large eigenvalues of the Fisher information matrix. While technically different, this strategy follows the same philosophical approach set by Karnesis et al. (2020), Caprini et al. (2019), Flauger et al. (2021) and offers an interesting alternative to the methods developed therein. For example, in Karnesis et al. (2020), after proper assumptions about the Gaussianity of the instrument noise, one can construct a posterior distribution for the level of the excess of spectral power, caused by an unmodelled SGWB signal at each frequency of the analysis.

All of the methods discussed in this section are focused on spectral shape reconstruction at the power spectrum level only. While in the most general set up this could be performed by only assuming the noise to be Gaussian, the techniques described here all assume (at the likelihood level) approximate Gaussianity of the SGWB as well. As long as the SNR per frequency mode is small, this is a good approximation but should be revisited for a bright signal. As discussed in Sect. 12.2 the assumption of Gaussianity can be violated for SGWBs of astrophysical origin. On the other hand, for SGWBs of cosmological origin any intrinsic non-Gaussianity in the metric perturbations is expected to be washed out by propagation effects (Bartolo et al. 2019b, c; Margalit et al. 2020). Notice however that, as pointed out in Bartolo et al. (2020b), non-Gaussianities in the energy density of the SGWB could be non-zero. For a better discussion of propagation effects see Sect. 5.3.2. If the backgrounds are expected to be significantly non-Gaussian, spectral shape reconstruction methods based on the observed strain distributions will have to be modified accordingly.

It is also worth mentioning that all the methods discussed in this section are applied to time-averaged data. While it could be difficult to induce any intrinsic time modulation in SGWBs of either cosmological or astrophysical origin, the motion of the detector with respect to the SGWB source frame is expected to naturally induce a yearly modulation in the amplitude of SGWB. While for isotropic SGWBs the effect is expected to be very small (of order of the velocity of the detector in units of the speed of light), for intrinsically anisotropic SGWBs (as for unresolved GBs) this effect could become sizeable (Adams and Cornish 2014). In order to model these effects it would be necessary to modify the existing pipelines to keep track (both at the generation and at the data analysis level) of the measurement time associated with each data segment. Such a modification in the existing tools would simultaneously improve their suitability to be applied to real data and possibly their capability of disentangling the different components contributing to the SGWB.

The methods discussed in this section do not consider possible angular structure in the signal. While techniques for reconstruction of anisotropies are more extensively

discussed in the next section, it is worth mentioning that for most SGWB sources different angular structure is expected to be associated with different spectra (namely, with a different frequency-dependence). As a consequence, by simultaneously tackling the frequency shape and the angular reconstruction it could be possible to break degeneracies between different components contributing to the observed signal. This could potentially lead to a significant improvement of the existing component separation techniques. For this reason embedding this possible method in the present pipelines may be an interesting possibility for future developments.

We conclude this section by commenting on the impact of foregrounds on the minimal SGWB intensity that would yield a detectable signal and allow us to attempt reconstruction. While detection thresholds are clearly model dependent, i.e. different amplitudes and SNRs are required in order to make quantitative statements for different SGWB shapes, some studies (see Sect. 12.6 for details) have already demonstrated the possibility of performing component separation with LISA. This implies that SGWB reconstruction can typically be performed even in the presence of foregrounds. However, it is worth mentioning that a crucial ingredient for component separation is the absence of degeneracies between the foregrounds and other SGWB components. Otherwise, unless this degeneracy is broken by the prior knowledge on the foreground parameters, the detection of the SGWB originating from cosmological sources could be negatively affected.

12.4 Anisotropy reconstruction

The intensity of astrophysical and cosmological SGWBs are in general anisotropic. These anisotropies could allow one to differentiate between these two backgrounds. They can be generated both at the moment of the GW production and by the GW propagation in the perturbed universe. In the case of the cosmological SGWB the anisotropies contain information about the primordial generation mechanism and moreover they can be a new probe of the primordial non-Gaussianity of the large-scale cosmological perturbations (Bartolo et al. 2019a, 2020a, b). In the case of the astrophysical SGWB they contain information about the angular distribution of the sources and astrophysical properties, and they can be used as a tracer of large-scale structure; in both cases they also allow one to test the particle physics content of the universe (Valbusa Dall'Armi et al. 2021). The LIGO/Virgo collaboration has already produced upper limits on the SGWB anisotropy in the 20–500 Hz band (Abbott et al. 2019a). The poor angular resolution of second-generation ground-based interferometers will probably not allow for the detection of the anisotropies of the SGWB, however future third-generation ground-based experiments like ET and CE will be sensitive to such a signal especially if it is characterised by a large monopole amplitude. For future space missions, like LISA, DECIGO, and BBO, prospects for reconstruction and measurement of the anisotropies in the SGWB, both astrophysical and cosmological, have been explored in the literature (see e.g. Giampieri and Polnarev 1997; Allen and Ottewill 1997; Cornish 2001; Seto 2004; Kudoh and Taruya 2005; Kudoh et al. 2006). An updated analysis for LISA, using the most up-to-date specifications, is ongoing (Bartolo et al. 2022), and in the next sections we report some main results. While in this section we discuss anisotropy reconstruction

from a more theoretical point of view, in Sect. 12.5 we present data analysis techniques to tackle this problem.

12.4.1 LISA response function

The reconstruction of an isotropic SGWB has been studied for instance in Flauger et al. (2021), combining measurements in the A,E,T channels. This computation can be readily extended to an anisotropic SGWB. Details of this extension can be found in Bartolo et al. (2022). Here we simply report the main result.

For a Gaussian SGWB, the object of our study is the two point correlation function of the GW signal. From the standard decomposition

$$h_{ab}(\mathbf{x},\, t) = \int_{-\infty}^{+\infty} df \int d\Omega_{\hat{k}}\, \mathrm{e}^{2\pi i f\left(t-\hat{k}\cdot\mathbf{x}\right)} \sum_{\lambda} \tilde{h}_{\lambda}\left(f,\, \hat{k}\right) e^{\lambda}_{ab}\left(\hat{k}\right), \tag{163}$$

where, for definiteness, λ denotes the GW polarisation in the chiral basis. We are interested in the intensity of an unpolarised signal, for which

$$\left\langle \tilde{h}_{\lambda}\left(f,\, \hat{k}\right) \tilde{h}_{\lambda'}\left(f',\, \hat{k}'\right) \right\rangle = \frac{1}{4\pi}\, \delta(f+f')\delta^{(2)}\left(\hat{k}-\hat{k}'\right)\, \delta_{\lambda,-\lambda'}\, I\left(f,\, \hat{k}\right). \tag{164}$$

We further decompose

$$I\left(f,\, \hat{k}\right) \equiv \sum_{\ell m} \tilde{I}_{\ell m}(f)\, \tilde{Y}_{\ell m}\left(\hat{k}\right), \tag{165}$$

where $\tilde{Y}_{\ell m}\left(\hat{k}\right) \equiv \sqrt{4\pi}\, Y_{\ell m}\left(\hat{k}\right)$, are rescaled spherical harmonics, normalised so that $\tilde{Y}_{00} = 1$. In this way the isotropic case corresponds to $I\left(f,\, \hat{k}\right) = \tilde{I}_{00}(f)$.

The multipole coefficients $\tilde{I}_{\ell m}$ of the intensity are related to those of the fractional density by (Bartolo et al. 2022)

$$\tilde{I}_{\ell m}(f) = \frac{1}{\sqrt{4\pi}}\, \frac{3H_0^2}{4\pi^2}\, \frac{\Omega_{\mathrm{GW}}(f)}{f^3}\, \delta_{\mathrm{GW},\ell \mathrm{m}}, \tag{166}$$

where the latter are defined from

$$\frac{\omega_{\mathrm{GW}}\left(f,\, \hat{k}\right) - \Omega_{\mathrm{GW}}(f)}{\Omega_{\mathrm{GW}}(f)} \equiv \sum_{\ell m} \delta_{\mathrm{GW},\ell \mathrm{m}}(f)\, Y_{\ell m}\left(\hat{k}\right), \tag{167}$$

with $\omega_{\mathrm{GW}}\left(f,\, \hat{k}\right)$ being the fractional energy density before angular integration,

$$\Omega_{\mathrm{GW}}(f) = \int d^2\hat{k}\, \omega_{\mathrm{GW}}\left(f,\, \hat{k}\right)/4\pi. \tag{168}$$

In Eq. (166), H_0 is the present value of the Hubble rate.

For definiteness, we consider a statistically isotropic signal, so that the unbiased estimators $\hat{\delta}_{\mathrm{GW},\ell\mathrm{m}}$ for coefficients of the decomposition $\delta_{\mathrm{GW},\ell\mathrm{m}}$, have expectation value[37]

$$\left\langle \delta_{\mathrm{GW},\ell\mathrm{m}}\, \delta^*_{\mathrm{GW},\ell'\mathrm{m}'} \right\rangle = C_\ell^{\mathrm{GW}}\, \delta_{\ell\ell'}\, \delta_{mm'}. \tag{169}$$

The expectation value of the SNR can be then expressed as the sum $\langle \mathrm{SNR} \rangle \equiv \sqrt{\sum_\ell \langle \mathrm{SNR}_\ell^2 \rangle}$ over multipoles. Each term is formally of the type

$$\langle \mathrm{SNR}_\ell^2 \rangle = T_{\mathrm{obs}} \int_0^\infty df \left[\frac{\sqrt{C_\ell^{\mathrm{GW}}}\, \Omega_{\mathrm{GW}}(f) h^2}{\Omega^\ell_{\mathrm{GW,n}}(f)\, h^2} \right]^2, \tag{170}$$

where T_{obs} is the observation time, and $\Omega^\ell_{\mathrm{GW,n}}(f)\, h^2$ denotes the LISA sensitivity to the $\ell-$th multipole. The sensitivity to the first few multipoles are shown in Fig. 39. The mathematical form of the sensitivity, and its derivation, are given in Bartolo et al. (2022).

12.4.2 Cosmic dipole

One would expect that LISA sensitivity degrades as the multipole order increases. While this is generally true, as can be also seen from Fig. 39, due to the symmetries of the system, LISA turns out to be more sensitive to the quadrupole than to the dipole. Nevertheless, once the isotropic component of the SGWB is detected, a naturally expected value of the amplitude and the direction of the dipole will be determined by the velocity of the Earth with respect to the cosmic rest frame, providing a first target for the detection of SGWB anisotropies.

There are only two correlators sensitive to the dipole, namely the one between the A and the T channel, and the one between the E and the T channel. Remarkably, moreover, these AT and ET correlators vanish for the SGWB monopole. The SNR for the dipole induced by the Earth's motion with speed β with respect to the cosmic rest frame is given, in the noise dominated regime, by the formula

$$\mathrm{SNR}^2_{A/ET} = 6\,\beta^2 \left(\frac{3\, H_0^2\, \Omega_{\mathrm{GW}}}{4\pi^2} \right)^2 \int_0^{T_{\mathrm{obs}}} dt \int \frac{df}{f^6} \sum_{J=A,E} \frac{\left(\mathcal{R}^{JT}_{\ell=1}\, \hat{n}(t) \cdot \hat{\beta} \right)^2}{N_J\, N_T}, \tag{171}$$

where N_J is the noise in mode J (see the right panel of Fig. 36) and $\mathcal{R}^{AT}_{\ell=1} = \mathcal{R}^{ET}_{\ell=1}$ measures the amplitude of the $\ell = 1$ mode of the angular response (see Bartolo et al. 2022), evaluating to $\sim 10^{-2}$ for $f = 0.1$ Hz and to $\sim 10^{-3}$ for $f = 0.01$ Hz. Also, $\hat{\beta}$

[37] Notice that the brackets in Eq. (164) denote an ensemble average. Since we have a single realisation of the observable universe, an estimator $\hat{C}_\ell^{\mathrm{GW}}$ for C_ℓ^{GW} is typically built by averaging the measured value of $\delta_{\mathrm{GW},\ell\mathrm{m}}\, \delta^*_{\mathrm{GW},\ell'\mathrm{m}'}$ over the different m indices.

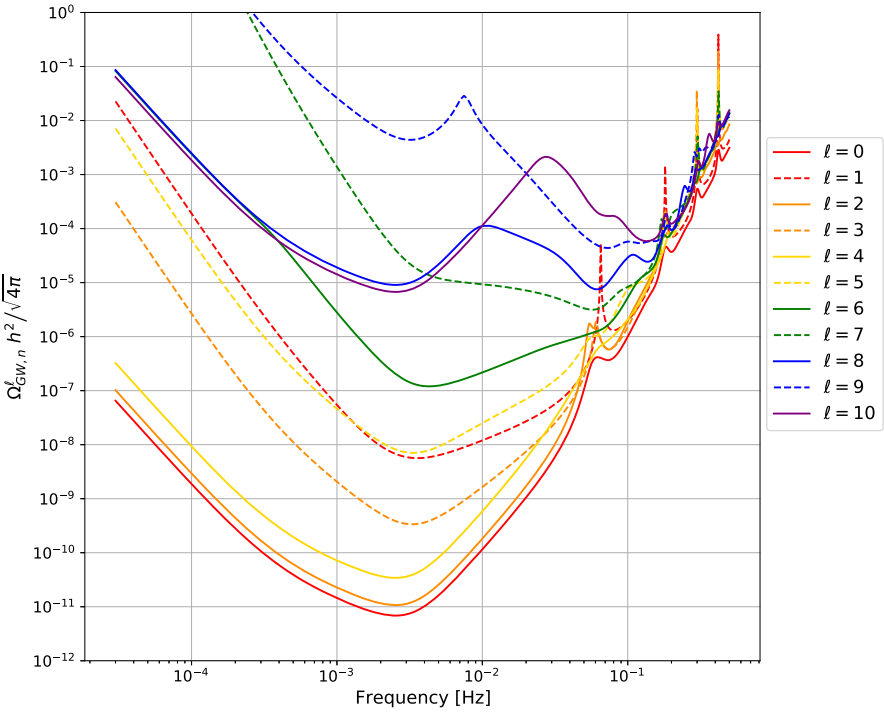

Fig. 39 LISA Sensitivity (170) to various multipoles of the SGWB. Image reproduced with permission from Bartolo et al. (2022)

is the direction of the dipole, whereas $\hat{n}(t)$ is the unit normal to the LISA configuration, whose direction changes over the course of the year.

Assuming a flat energy spectrum in the LISA band, the SNR takes the approximate value

$$\mathrm{SNR} \simeq 0.5 \times \left(\frac{\beta}{10^{-3}}\right)\left(\frac{\Omega_{\mathrm{GW}}}{6 \times 10^{-8}}\right)\sqrt{\frac{T_{\mathrm{obs}}}{1\ \mathrm{year}}}, \tag{172}$$

where β is normalised to its value with respect to the CMB rest frame, and Ω_{GW} is normalised to its upper bound from LIGO/Virgo (Abbott et al. 2019c). While Eq. (172) suggests a small SNR already for a SGWB that saturates the current constraint, it is important to note that the bound (Abbott et al. 2019c) holds at LIGO/Virgo frequencies, and there is no reason for the SGWB spectrum to be flat all the way to LISA frequencies.

Remarkably, due to the higher sensitivity to the quadrupole, LISA will have comparable sensitivity to the dipole and to the quadruple induced by the motion of the Solar System with respect to the cosmic rest frame, despite the fact that the quadrupole has an amplitude that is a factor of $\beta \approx 10^{-3}$ smaller than the dipole.

It is also worth pointing out that LISA will be much more sensitive to the dipole if the SGWB contains a chiral component. In this case, in fact, the AE correlator is not vanishing, leading to a SNR (Domcke et al. 2020b)

$$\mathrm{SNR} \simeq 10^3\, \delta\chi \left(\frac{\beta}{10^{-3}}\right) \left(\frac{\Omega_{\mathrm{GW}}}{6 \times 10^{-8}}\right) \sqrt{\frac{T_{\mathrm{obs}}}{1\ \mathrm{year}}}, \tag{173}$$

where $0 \leq \delta\chi \leq 1$ measures the degree of chirality of the SGWB, see Sect. 8.7.1.

12.5 Gravitational-wave map making with LISA

An available mapping algorithm tailored to the LISA detector is based on an optimal quadratic estimator (Contaldi et al. 2020). The mapper takes advantage of the time-dependent sky response of the LISA constellation to scan the sky over a long observation times. It reconstructs full-sky stochastic signals and their anisotropies. A prime example of anisotropic SGWB signal in the LISA band is the statistical signal from unresolved white dwarf GBs. This signal is expected to trace out the distribution of white dwarfs in the Milky Way. Beyond this, the astrophysical SGWB from extragalactic stellar mass compact binaries is also expected to have some degree of angular anisotropy, as do many of the cosmological backgrounds reviewed in this paper. More details on anisotropic SGWB sources potentially detectable by LISA may be found in Bartolo et al. (2022).

The sky response used assumes equal arms and heliocentric circular orbits, which are considered to be good approximations until full, time-dependent flight solutions become available after launch. These are the same assumptions made throughout Sect. 12.4.1. The frequency transfer function included in the response induces a frequency dependence in the sky modulation, as may be seen in Fig. 40. This drives the effective angular resolution as a function of frequency sensitivity and determines the resolution of final maps. The map-making can be based on a broad-band integration of frequencies or the integration can be split into narrower frequency bands (Contaldi et al. 2020).

The estimator is based on the assumption that the signal and noise components in the timestream data are Gaussian and maximises the standard Gaussian likelihood. This approach is similar to optimal map-making steps in CMB analysis (see e.g. Bond et al. 1998). In this case, the likelihood for the data is parametrised by the sky-signal covariance as function of direction. The maximum-likelihood solution for the

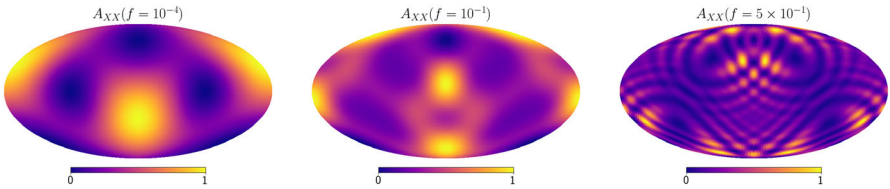

Fig. 40 Normalised auto-correlated response of TDI channel X at time $t = 0$ in the Solar System barycentre reference frame, at frequencies $f = 10^{-4}$ Hz, $f = 10^{-1}$ Hz, $f = 5 \times 10^{-1}$ Hz from left to right respectively. Estimates based on (Contaldi et al. 2020)

covariance (signal intensity) is obtained using a quadratic, iterative estimator which effectively inverts the time-integrated projection of the sky-signal onto the data. A noise model is added to the total covariance in the likelihood. The algorithm is tailored to and applied in the pixel domain but it can also be applied in the spherical harmonic domain. The two choices differ in the use of regularisation methods that need to be applied to the ill-conditioned problem.

In practice, the data are segmented into short-duration frames, throughout which the sky response of the detector is considered to be constant. The time-frame length is a key element in the analysis: it sets the lower limit of frequency space probed, while also setting the maximum pixelisation scale to ensure a smooth transition on the sky, frame by frame. The covariance of the signal is initially estimated by subtracting the noise model from the data covariance, and is then noise-weighted over frequencies and projected onto the sky via the response operator to obtain a map. This operation is performed over all time-segments and subsequently averaged. The pixel-pixel Fisher matrix relative to the measurement is similarly calculated and inverted, using singular-value-decomposition techniques to regularise the inversion. The inverse Fisher matrix is then applied to the sky-and-noise weighted data to extract the optimal map solution. This is performed iteratively, until convergence require ments are satisfied.

Figure 41 shows the ℓ-mode transfer function T_ℓ for sky-map reconstruction presented in Contaldi et al. (2020) in the case of very high SNR injections. This shows the effective angular resolution of LISA at different frequency pivot points. This is calculated by combining sets of 50 simulations for each frequency window examined. Each simulation consists of the injection and reconstruction of an $\ell^2 C_\ell$-flat Gaussian realisation for the sky GW intensity. The procedure works under the assumption that the frequency and directional dependence can be separated:

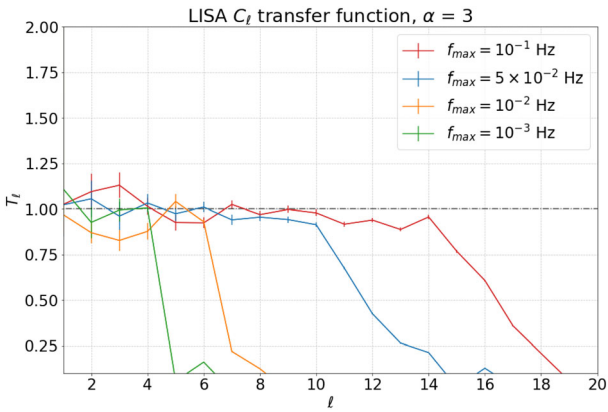

Fig. 41 Transfer functions T_ℓ for the average reconstructed C_ℓs obtained with different frequency cutoffs $f_{\max}$, drawn from Contaldi et al. (2020). Each simulation set consists of 50 maps, each a different realisation of the same C_ℓ input (dashed grey baseline). There appears to be a clear one-to-one relation between the resolution $\ell_{\max}$ of the instrument and the frequency cutoff

$$\Omega_{\rm GW}(f,\mathbf{n}) = \Omega(f)\mathcal{P}(\mathbf{n}). \tag{174}$$

For simplicity, the spectral dependence of the signal is taken to be a simple power law, with spectral index $\alpha = 3$. The transfer function is defined as $T_\ell = C_\ell^{\rm out}/C_\ell^{\rm in}$. In this extremely high signal scenario, the solution converges after a single iteration. As shown in Fig. 41, the higher angular modes are well preserved when allowing the reconstructor to integrate up to higher frequencies, where there is finer structure in the response pattern, whereas they are aliased into lower modes when integrating over lower frequencies only. In the best case scenario of a strong signal at high frequencies, the map-maker can recover anisotropies up to scales of $\ell_{\rm max} \sim 15$. The reconstruction of a simplified model for the GB background is also tested; it is found that even though the signal has a relatively high SNR, it peaks above the noise around 10^{-3} Hz and hence may be recovered at best at $\ell_{\rm max} \sim 5$.

The estimator currently assumes a fixed instrumental noise model, however it is possible to include independent noise estimates for each time segment. A possible extension of this method would fit for both signal and noise components simultaneously. The current noise model employed in the mapping pipeline is the one presented in Sect. 12.1. It is also possible to extend the estimator to include different spectral shapes for the signal, beyond a simple power law, or alternatively solve for maps in narrow frequency bands to attempt a model-independent directional search. Furthermore, it is important to note that the Fisher matrix is highly singular and requires heavy conditioning before inversion; this is a delicate process which may bias the outcome of the mapping, and further investigation is required to assess its impact. The implications of the inversion for certain high and low SNR stationary SGWB signals are discussed in Contaldi et al. (2020).

Going a step further, a recently developed Bayesian formalism (Banagiri et al. 2021) allows for simultaneous estimation of the frequency and directional content of a SGWB with LISA.[38] One again starts with the assumption in Eq. (174), where a frequency dependence of choice could be inserted, for example a simple power law (as for example in Adams and Cornish 2010, 2014; Caprini et al. 2019; Flauger et al. 2021), while the angular dependence can be decomposed with respect to a basis on the sphere, such as spherical harmonics.

One can then divide LISA data into segments of duration $T_{\rm seg}$ and compute the Fourier transforms of the LISA TDI channels in each segment (in either the X-Y-Z or A-E-T configuration). It is then straightforward to define the likelihood function

$$\mathcal{L}(\tilde{d}|N_p, N_a, \alpha, \Omega_\alpha, \{b_{l,m}\}) = \prod_{t,f} \frac{1}{2\pi T_{\rm seg}|C(t,f)|} \times \exp\left(-\frac{2\,\tilde{d}^*_{t,f}\,C(t,f)^{-1}\,\tilde{d}_{t,f}}{T_{\rm seg}}\right), \tag{175}$$

where $\tilde{d}_{t,f} = [\tilde{d}_X(t,f), \tilde{d}_Y(t,f), \tilde{d}_Z(t,f)]$ is the array of data in the Fourier domain for the three LISA channels (in the time segment t and at frequency f), and $C(t, f)$ is the 3×3 covariance matrix for the three channels. The covariance matrix can be modelled to include both instrumental noise (here described by position and

[38] The code for this analysis pipeline can be found at https://github.com/sharanbngr/blip.

acceleration noise parameters N_p and N_a), as well as the astrophysical and cosmological contributions to the GWB. In this example, we use the amplitude Ω_α and spectral index α to describe the frequency dependence of the astrophysical/cosmological contributions, and the $b_{l,m}$, coefficients of the decomposition onto spherical harmonics, to describe the directional dependence. Using this likelihood in Bayesian parameter estimation, with suitable choices for prior distributions on the free parameters, allows for the recovery of the free parameters. In particular, the recovery of simulated noise and a cosmological background up to $l = 2$ is achievable (Banagiri et al. 2021). The same technique can be applied to study the galactic foreground due to white dwarf binaries, as shown in Fig. 42. Of course, additional model complexity could be added to this method: for example a more complex instrument noise model, or frequency dependence of $b_{l,m}$ coefficients, or polarisation dependence of the cosmological model.

12.6 Global fit

One of the main data analysis challenges that LISA will face is to disentangle the various sources that overlap in time and in frequency. To tackle this problem, the LISA Consortium will employ a *global fit* scheme (Teukolsky and Vallisneri 2019; Littenberg et al. 2020) for detecting, separating and eventually identifying/classifying many overlapping signals of astrophysical and hopefully early-universe origin. Different strategies could be employed to tackle this compelling task. A fully consistent Bayesian framework, ideally the most accurate approach to this problem, would perform a simultaneous fit of all resolvable sources and SGWBs. From a computational point of view this would be extremely difficult due to very high dimensionality of the parameter space that would need to be explored.

A possible approach (for a first step in this direction see Karnesis et al. 2021) would alternate between a step in which, given some current estimation of co-added background noise (instrumental noise, astrophysical confusion noise and a possible stochastic cosmological component), resolved events are detected, characterised and subtracted from the data streams, and a step in which the resulting "residual" data is used to update the knowledge on this background noise. In this step the residual is treated as a component which simultaneously models instrumental noise as well as the expected confusion noise inferred from the current catalogues of resolved sources (see Sect. 12.2), and a free-form SGWB spectrum (see Sect. 12.3). The advantage of this approach is that the dimensionality of the parameter inference problem at each of these steps is significantly lower (since technically we are performing conditional—or Gibbs—sampling at each step) and could be easily dealt with using standard techniques. Hereafter we discuss the state of the art on integrating SGWB detection, characterisation and component separation into a LISA *global fit* pipeline, and the further developments which are crucial for LISA to match its scientific goals regarding this problem.

The detection of an astrophysical SGWB with an accurate modelling, in the presence of the instrumental noise has been established in e.g. Christensen (1997), Adams and Cornish (2010), Meyers et al. (2020). In what concerns the simultaneous

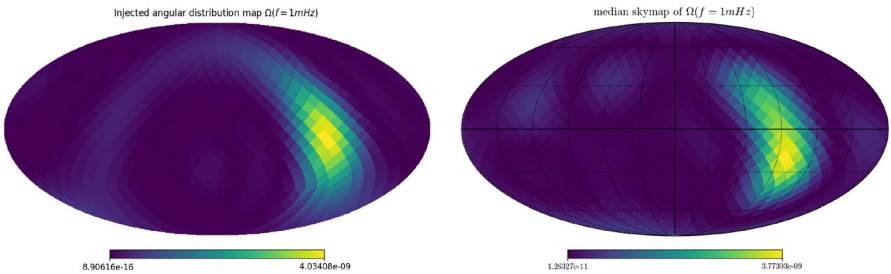

Fig. 42 Simulation (left) and recovery (right) of the white dwarf GB foreground energy density in GWs at 1 mHz, using one year of data in the Solar System barycentric frame. The bright spot in the map corresponds to the galactic central bulge. Image reproduced with permission from Banagiri et al. (2021)

estimation of a cosmological component and one or more astrophysical confusion backgrounds, a number of approaches have been explored. We anticipate that their conclusions must be considered as preliminary since they all rely on some simplifying assumptions on the noise modelling, response functions and contamination from resolved-event misreconstructions, among others. Properly addressing these aspects is one of the main priorities in the forthcoming years.

Flauger et al. (2021) demonstrates the capability of LISA to separate between general astrophysical templates and a free-form cosmological component of sufficient intensity. In this work the three LISA TDI channels are fully exploited, using the *AET* basis (Hogan and Bender 2001; Adams and Cornish 2010), in particular the ability of the closed-path *T* channel to place strong, independent constraints on the instrumental noise, using the noise model of Sect. 12.1. The proposed pipeline determines an optimal binning for the reconstruction of the cosmological signal using maximum likelihood estimation. This binning is then used in a fully Bayesian pipeline implemented in the Cosmological sampling framework Cobaya (Torrado and Lewis 2021), to jointly estimate the parameters of the noise model, the amplitude of an astrophysical foreground template, and the free-form binned cosmological component. Using the Monte Carlo Nested Sampler PolyChord (Handley et al. 2015), it turns out that a sufficiently high-SNR broken-power-law signal can be efficiently reconstructed in the presence of either a power-law model for extragalactic binaries consistent with LIGO/Virgo observations (Abbott et al. 2019c), or a foreground of GBs modelled as in Robson et al. (2019). On the contrary, SGWBs with SNR $\lesssim 10$ such as flat signal with $\Omega_{\rm GW} \lesssim 10^{-13}$ are likely to escape the LISA searches.

Another step in this direction is taken in Boileau et al. (2021a) and Boileau et al. (2021b) which progressively increase the complexity of the foreground. The analyses adopt a Bayesian strategy based on an Adaptive MCMC algorithm (Christensen and Meyer 1998; Cornish and Littenberg 2007) analysing the *A*, *E* and *T* channels given by the LISA model of Smith et al. (2019). The Adaptive MCMC results are independently confirmed by an analysis from the Fisher information matrix. Also with these analyses, it turns out that the LISA *T* channel helps to efficiently estimate the LISA noise parameters and to thus measure the SGWB in the *A* and *E* channels. Ultimately, it comes out that LISA can detect (power-law) cosmological backgrounds

in the presence of astrophysical foregrounds. In particular, given the expected LISA noise and the astrophysical foreground consistent with LIGO/Virgo observations, it is possible to observe a flat power-law SGWB with amplitude larger than $\Omega_{\mathrm{GW,Cosmo}} \approx (1-10) \times 10^{-13}$ after 4 years of LISA observations (Boileau et al. 2021a). Boileau et al. (2021b) makes this lower bound more robust by adding the foreground due to GBs simulated with the binary catalogues of Lamberts et al. (2019). The study takes into account that the GB foreground measured by LISA has a yearly modulation (see Fig. 43). It implements a Bayesian analysis for each week in the year, and the corresponding variation of the LISA pattern antenna. Based on this analysis, the reconstruction of the amplitude of a flat SGWB has uncertainties below 50% when $\Omega_{\mathrm{GW,Cosmo}} \gtrsim 8 \times 10^{-13}$ (see Fig. 44).

Similar efforts is carried out in the context of ground-based experiments. Martinovic et al. (2021) explores a method for the simultaneous estimation of astrophysical and cosmological SGWBs in the frequency band of current and future terrestrial interferometers. As an example, the detection of cosmological signals with GW fractional energy density 4.5×10^{-13} at 25 Hz, for cosmic strings, and 2.2×10^{-13}, for a broken power-law model of an early universe phase transition, turns out to be possible in the presence of astrophysical confusion noise from compact binary coalescences, assuming a detector network containing CE and ET. In these approaches, reasonable levels of individual source subtraction are always assumed (Cutler and Harms 2006; Harms et al. 2008; Sharma and Harms 2020; Sachdev et al. 2020), given that future detector networks should be sensitive enough

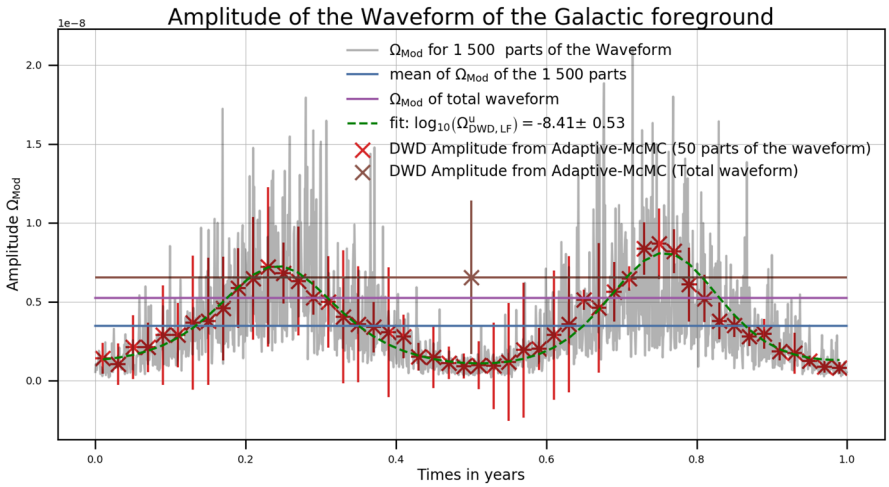

Fig. 43 Measurement of the orbital modulation of the white dwarf binary foreground. In grey: 1500 estimates of $\Omega_{\mathrm{Mod},i} = \frac{4\pi^2}{3H_0}\left(\frac{c}{2\pi L}\right)^2 A_i^2$ (A_i amplitude of the characteristic strain). In red: 50 MCMC results with 8 parameters (2 parameters for BBHs, 4 parameters for white dwarf binaries, 2 parameters for the LISA noise). In green, fit to the 50 MCMC run results to estimate the modulation from the LISA antenna pattern amplitude at 3 mHz. Modulation model: $\Omega_{\mathrm{Mod},i} = \Omega^{u}_{\mathrm{DWD,LF}}\left(F^2_{+,i} + F^2_{\times,i}\right)$. Image reproduced with permission from Boileau et al. (2021b)

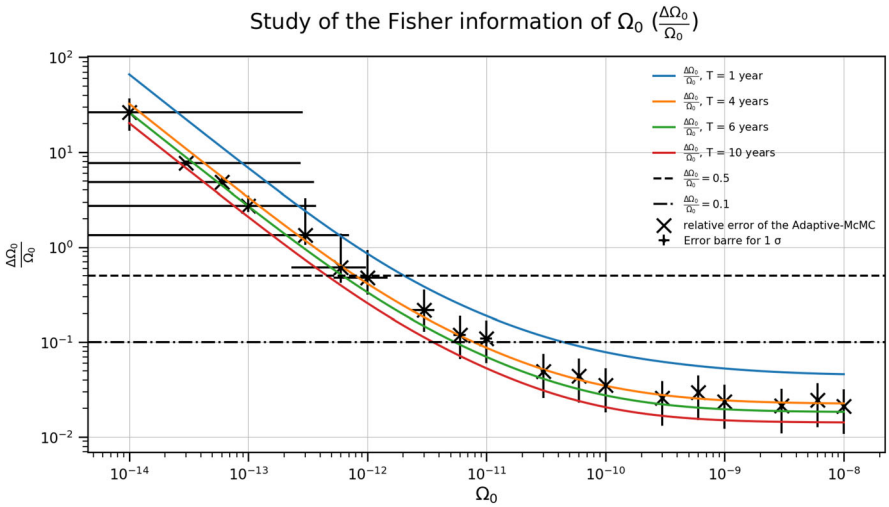

Fig. 44 Cosmological amplitude uncertainty estimates from the Fisher Information study denoted by solid lines and from the MCMC by crosses. The upper horizontal dashed line represents the error level 50%. Image reproduced with permission from Boileau et al. (2021b)

to accurately resolve a large fraction of the compact binary mergers in the visible universe.

Biscoveanu et al. (2020) explores an alternative method to source subtraction. It proposes a Bayesian framework for simultaneously measuring individual compact binary mergers and a confusion foreground of these sources, together with a cosmological background. This method, in which the parameters of individual events are approximately marginalised-over, takes into account the non-Gaussian nature of the astrophysical signal (see Sect. 12.2), increasing the sensitivity to the Gaussian cosmological background. The capability of the method is demonstrated with a combination of an astrophysical foreground of merging BBHs and a cosmological background with a power-law spectrum.

The methods of both Martinovic et al. (2021) and Biscoveanu et al. (2020) could be adapted for the space-based detector LISA. In doing so, one should keep in mind that the corresponding spectral separation study for LISA would be more involved due to the nature of the TDI and the necessity to simultaneously estimate the LISA noise. A successful contribution separation will give us valuable information on the one hand about merger rates and population models and the astrophysics of exotic objects, and on the other about phenomenology in early universe models. This is indeed a research line that should be incentivated over the next years.

Acknowledgements This work is partly supported by: A.G. Leventis Foundation; Academy of Finland Grants 328958 and 345070; Alexander S. Onassis Foundation, Scholarship ID: FZO 059-1/2018-2019; Amaldi Research Center funded by the MIUR program "Dipartimento di Eccellenza" (CUP: B81I18001170001); ASI Grants No. 2016-24-H.0 and No. 2016-24-H.1-2018; Atracción de Talento Grant 2019-T1/TIC-15784; Atracción de Talento contract no. 2019-T1/TIC-13177 granted by the Comunidad de Madrid; Ayuda 'Beatriz Galindo Senior' by the Spanish 'Ministerio de Universidades', Grant BG20/00228; Basque Government Grant (IT-979-16); Belgian Francqui Foundation; Centre national

d'Etudes spatiales; Ben Gurion University Kreitman Fellowship, and the Israel Academy of Sciences and Humanities (IASH) & Council for Higher Education (CHE) Excellence Fellowship Program for International Postdoctoral Researchers; Centro de Excelencia Severo Ochoa Program SEV-2016-0597; CERCA program of the Generalitat de Catalunya; Cluster of Excellence "Precision Physics, Fundamental Interactions, and Structure of Matter" (PRISMA+ EXC 2118/1); Comunidad de Madrid, Contrato de Atracción de Talento 2017-T1/TIC-5520; Czech Science Foundation GAČR, Grant No. 21-16583M; Delta ITP consortium; Department of Energy under Grant No. DE-SC0008541, DE-SC0009919 and DE-SC0019195; Deutsche Forschungsgemeinschaft (DFG), Project ID 438947057; Deutsche Forschungsgemeinschaft under Germany's Excellence Strategy - EXC 2121 Quantum Universe - 390833306; European Structural and Investment Funds and the Czech Ministry of Education, Youth and Sports (Project CoGraDS - CZ.02.1.01/0.0/0.0/15 003/0000437); European Union's H2020 ERC Consolidator Grant "GRavity from Astrophysical to Microscopic Scales" (Grant No. GRAMS-815673); European Union's H2020 ERC, Starting Grant Agreement No. DarkGRA-757480; European Union's Horizon 2020 programme under the Marie Sklodowska-Curie Grant Agreement 860881 (ITN HIDDeN); European Union's Horizon 2020 Research and Innovation Programme Grant No. 796961, "AxiBAU" (K.S.); European Union's Horizon 2020 Research Council grant 724659 MassiveCosmo ERC-2016-COG; FCT through national funds (PTDC/FIS-PAR/31938/2017) and through project "BEYLA – BEYond LAmbda" with Ref. Number PTDC/FIS-AST/0054/2021; FEDER-Fundo Europeu de Desenvolvimento Regional through COMPETE2020 - Programa Operacional Competitividade e Internacionalização (POCI-01-0145-FEDER-031938) and research Grants UIDB/04434/2020 and UIDP/04434/2020; Fondation CFM pour la Recherche in France; Foundation for Education and European Culture in Greece; French ANR project MMUniverse (ANR-19-CE31-0020); FRIA Grant No.1.E.070.19F of the Belgian Fund for Research, F.R.S.-FNRS Fundação para a Ciência e a Tecnologia (FCT) through Contract No. DL 57/2016/CP1364/CT0001; Fundação para a Ciência e a Tecnologia (FCT) through Grants UIDB/04434/2020, UIDP/04434/2020, PTDC/FIS-OUT/29048/2017, CERN/FIS-PAR/0037/2019 and "CosmoTests – Cosmological tests of gravity theories beyond General Relativity" CEECIND/00017/2018; Generalitat Valenciana Grant PROMETEO/2021/083; Grant No. 758792, project GEODESI; Government of Canada through the Department of Innovation, Science and Economic Development and Province of Ontario through the Ministry of Colleges and Universities; Grants-in-Aid for JSPS Overseas Research Fellow (No. 201960698); I+D Grant PID2020-118159GB-C41 of the Spanish Ministry of Science and Innovation; INFN *iniziativa specifica* TEONGRAV; Israel Science Foundation (Grant No. 2562/20); Japan Society for the Promotion of Science (JSPS) KAKENHI Grant Nos. 20H01899 and 20H05853; IFT Centro de Excelencia Severo Ochoa Grant SEV-2; Kavli Foundation and its founder Fred Kavli; Minerva Foundation; Ministerio de Ciencia e Innovacion Grant PID2020-113644GB-I00; NASA Grant 80NSSC19K0318; NASA Hubble Fellowship grants No. HST-HF2-51452.001-A awarded by the Space Telescope Science Institute with NASA contract NAS5-26555; Netherlands Organisation for Science and Research (NWO) Grant Number 680-91-119; new faculty seed start-up grant of the Indian Institute of Science, Bangalore, the Core Research Grant CRG/2018/002200 of the Science and Engineering; NSF Grants PHY-1820675, PHY-2006645 and PHY-2011997; Polish National Science Center Grant 2018/31/D/ST2/02048; Polish National Agency for Academic Exchange within the Polish Returns Programme under Agreement PPN/PPO/2020/1/00013/U/00001; Pró-Reitoria de Pesquisa of Universidade Federal de Minas Gerais (UFMG) under Grant No. 28359; Ramón y Cajal Fellowship contract RYC-2017-23493; Research Project PGC2018-094773-B-C32 [MINECO-FEDER]; Research Project PGC2018-094773-B-C32 [MINECO-FEDER]; ROMFORSK Grant Project. No. 302640; Royal Society Grant URF/R1/180009 and ERC StG 949572: SHADE; Shota Rustaveli National Science Foundation (SRNSF) of Georgia (Grant FR/18-1462); Simons Foundation/SFARI 560536; SNSF Ambizione grant; SNSF professorship Grant (No. 170547); Spanish MINECO's "Centro de Excelencia Severo Ochoa" Programme Grants SEV-2016-0597 and PID2019-110058GB-C22; Spanish Ministry MCIU/AEI/FEDER Grant (PGC2018-094626-B-C21); Spanish Ministry of Science and Innovation (PID2020-115845GB-I00/AEI/10.13039/501100011033); Spanish Proyectos de I+D via Grant PGC2018-096646-A-I00; STFC Consolidated Grant ST/T000732/1; STFC Consolidated Grants ST/P000762/1 and ST/T000791/1; STFC Grant ST/S000550/1; STFC Grant ST/T000813/1; STFC Grants ST/P000762/1 and ST/T000791/1; STFC under the research Grant ST/P000258/1; Swiss National Science Foundation (SNSF), project *The Non-Gaussian Universe and Cosmological Symmetries*, Project Number: 200020-178787; Swiss National Science Foundation Professorship Grants No. 170547 and No. 191957; SwissMap National Center for Competence in Research; "The Dark Universe: A Synergic Multi-messenger Approach" Number 2017X7X85K under the MIUR program PRIN 2017; UK Space Agency; UKSA Flagship Project, Euclid.

Open Access This article is licensed under a Creative Commons Attribution 4.0 International License, which permits use, sharing, adaptation, distribution and reproduction in any medium or format, as long as you give appropriate credit to the original author(s) and the source, provide a link to the Creative Commons licence, and indicate if changes were made. The images or other third party material in this article are included in the article's Creative Commons licence, unless indicated otherwise in a credit line to the material. If material is not included in the article's Creative Commons licence and your intended use is not permitted by statutory regulation or exceeds the permitted use, you will need to obtain permission directly from the copyright holder. To view a copy of this licence, visit http://creativecommons.org/licenses/by/4.0/.

Author Contribution D. Bacon, G. Calcagni, S. Clesse, E. Dimastrogiovanni, J. M. Ezquiaga, J. García-Bellido, N. Karnesis, J. Kozaczuk, S. Kuroyanagi, M. Lewicki, L. Lombriser, M. Peloso, M. Pieroni, A. Raccanelli, L. Sousa, N. Tamanini, D. Vernieri and M. Zumalacárregui: Section coordinators. More details at the beginning of each section. R. Caldwell, G. Nardini, M. Peloso and N. Tamanini: Document coordinators.

References

Abbott BP et al (2016a) GW150914: implications for the stochastic gravitational wave background from binary black holes. Phys Rev Lett 116(13):131102. https://doi.org/10.1103/PhysRevLett.116.131102. arXiv:1602.03847 [gr-qc]

Abbott BP et al (2016b) Observation of gravitational waves from a binary black hole merger. Phys Rev Lett 116(6):061102. https://doi.org/10.1103/PhysRevLett.116.061102. arXiv:1602.03837 [gr-qc]

Abbott BP et al (2017a) A gravitational-wave standard siren measurement of the Hubble constant. Nature 551(7678):85–88. https://doi.org/10.1038/nature24471. arXiv:1710.05835 [astro-ph.CO]

Abbott BP et al (2017b) Exploring the sensitivity of next generation gravitational wave detectors. Class Quantum Grav 34(4):044001. https://doi.org/10.1088/1361-6382/aa51f4. arXiv:1607.08697 [astro-ph.IM]

Abbott BP et al (2017c) Gravitational waves and gamma-rays from a binary neutron star merger: GW170817 and GRB 170817A. Astrophys J Lett 848(2):L13. https://doi.org/10.3847/2041-8213/aa920c. arXiv:1710.05834 [astro-ph.HE]

Abbott BP et al (2017d) GW170817: observation of gravitational waves from a binary neutron star inspiral. Phys Rev Lett 119(16):161101. https://doi.org/10.1103/PhysRevLett.119.161101. arXiv:1710.05832 [gr-qc]

Abbott BP et al (2017e) Multi-messenger observations of a binary neutron star merger. Astrophys J Lett 848(2):L12. https://doi.org/10.3847/2041-8213/aa91c9. arXiv:1710.05833 [astro-ph.HE]

Abbott BP et al (2017f) Upper limits on the stochastic gravitational-wave background from advanced LIGO's first observing run. Phys Rev Lett 118(12):121101. https://doi.org/10.1103/PhysRevLett.118.121101, [Erratum: Phys. Rev. Lett. 119, 029901 (2017)]. arXiv:1612.02029 [gr-qc]

Abbott BP et al (2018a) Constraints on cosmic strings using data from the first Advanced LIGO observing run. Phys Rev D 97(10):102002. https://doi.org/10.1103/PhysRevD.97.102002. arXiv:1712.01168 [gr-qc]

Abbott BP et al (2018b) GW170817: implications for the stochastic gravitational-wave background from compact binary coalescences. Phys Rev Lett 120(9):091101. https://doi.org/10.1103/PhysRevLett.120.091101. arXiv:1710.05837 [gr-qc]

Abbott BP et al (2019a) Directional limits on persistent gravitational waves using data from Advanced LIGO's first two observing runs. Phys Rev D 100(6):062001. https://doi.org/10.1103/PhysRevD.100.062001. arXiv:1903.08844 [gr-qc]

Abbott BP et al (2019b) Properties of the binary neutron star merger GW170817. Phys Rev X 9(1):011001. https://doi.org/10.1103/PhysRevX.9.011001. arXiv:1805.11579 [gr-qc]

Abbott BP et al (2019c) Search for the isotropic stochastic background using data from Advanced LIGO's second observing run. Phys Rev D 100(6):061101. https://doi.org/10.1103/PhysRevD.100.061101. arXiv:1903.02886 [gr-qc]

Abbott BP et al (2020a) GW190425: observation of a compact binary coalescence with total mass $\sim 3.4M_{\odot}$. Astrophys J Lett 892(1):L3. https://doi.org/10.3847/2041-8213/ab75f5. arXiv:2001.01761 [astro-ph.HE]

Abbott BP et al (2021a) A gravitational-wave measurement of the Hubble constant following the second observing run of advanced LIGO and Virgo. Astrophys J 909(2):218. https://doi.org/10.3847/1538-4357/abdcb7. arXiv:1908.06060 [astro-ph.CO]

Abbott R et al (2020b) GW190521: a binary black hole merger with a total mass of $150M_{\odot}$. Phys Rev Lett 125(10):101102. https://doi.org/10.1103/PhysRevLett.125.101102. arXiv:2009.01075 [gr-qc]

Abbott R et al (2020c) Properties and astrophysical implications of the 150 $M_{\odot}$ binary black hole merger GW190521. Astrophys J Lett 900(1):L13. https://doi.org/10.3847/2041-8213/aba493. arXiv:2009.01190 [astro-ph.HE]

Abbott R et al (2021b) Constraints on cosmic strings using data from the third advanced LIGO–Virgo observing run. Phys Rev Lett 126(24):241102. https://doi.org/10.1103/PhysRevLett.126.241102. arXiv:2101.12248 [gr-qc]

Abbott R et al (2021c) Constraints on the cosmic expansion history from GWTC-3. arXiv e-prints arXiv:2111.03604 [astro-ph.CO]

Abbott R et al (2021d) GWTC-2: compact binary coalescences observed by LIGO and Virgo during the first half of the third observing run. Phys Rev X 11:021053. https://doi.org/10.1103/PhysRevX.11.021053. arXiv:2010.14527 [gr-qc]

Abbott R et al (2021e) Population properties of compact objects from the second LIGO–Virgo gravitational-wave transient catalog. Astrophys J Lett 913(1):L7. https://doi.org/10.3847/2041-8213/abe949. arXiv:2010.14533 [astro-ph.HE]

Abbott R et al (2021f) Tests of general relativity with binary black holes from the second LIGO–Virgo gravitational-wave transient catalog. Phys Rev D 103(12):122002. https://doi.org/10.1103/PhysRevD.103.122002. arXiv:2010.14529 [gr-qc]

Abbott R et al (2021g) Upper limits on the isotropic gravitational-wave background from Advanced LIGO and Advanced Virgo's third observing run. Phys Rev D 104(2):022004. https://doi.org/10.1103/PhysRevD.104.022004. arXiv:2101.12130 [gr-qc]

Abbott R et al (2023) Population of merging compact binaries inferred using gravitational waves through GWTC-3. Phys Rev X 13(1):011048. https://doi.org/10.1103/PhysRevX.13.011048. arXiv:2111.03634 [astro-ph.HE]

Abbott TMC et al (2018c) Dark energy survey year 1 results: a precise h0 estimate from DES Y1, BAO, and D/H data. Mon Not R Astron Soc 480(3):3879–3888. https://doi.org/10.1093/mnras/sty1939. arXiv:1711.00403 [astro-ph.CO]

Abell PA et al (2009) LSST science book, version 2.0. arXiv e-prints arXiv:0912.0201 [astro-ph.IM]

Accetta FS, Krauss LM (1989) The stochastic gravitational wave spectrum resulting from cosmic string evolution. Nucl Phys B 319:747–764. https://doi.org/10.1016/0550-3213(89)90628-7

Achucarro A, Gong JO, Hardeman S, Palma GA, Patil SP (2011) Mass hierarchies and non-decoupling in multi-scalar field dynamics. Phys Rev D 84:043502. https://doi.org/10.1103/PhysRevD.84.043502. arXiv:1005.3848 [hep-th]

Ackermann M et al (2018) The search for spatial extension in high-latitude sources detected by the *Fermi* large area telescope. Astrophys J Suppl 237(2):32. https://doi.org/10.3847/1538-4365/aacdf7. arXiv:1804.08035 [astro-ph.HE]

Acquaviva V, Bartolo N, Matarrese S, Riotto A (2003) Second order cosmological perturbations from inflation. Nucl Phys B 667:119–148. https://doi.org/10.1016/S0550-3213(03)00550-9. arXiv:astro-ph/0209156

Adachi Y, Maru N, Maru N (2020) Strong first order electroweak phase transition in Gauge–Higgs unification at finite temperature. Phys Rev D 101(3):036013. https://doi.org/10.1103/PhysRevD.101.036013. arXiv:1911.05963 [hep-ph]

Adams FC, Bond JR, Freese K, Frieman JA, Olinto AV (1993) Natural inflation: particle physics models, power law spectra for large scale structure, and constraints from COBE. Phys Rev D 47:426–455. https://doi.org/10.1103/PhysRevD.47.426. arXiv:hep-ph/9207245

Adams MR, Cornish NJ (2010) Discriminating between a stochastic gravitational wave background and instrument noise. Phys Rev D 82:022002. https://doi.org/10.1103/PhysRevD.82.022002. arXiv:1002.1291 [gr-qc]

Adams MR, Cornish NJ (2014) Detecting a stochastic gravitational wave background in the presence of a galactic foreground and instrument noise. Phys Rev D 89(2):022001. https://doi.org/10.1103/PhysRevD.89.022001. arXiv:1307.4116 [gr-qc]

Addazi A, Marcianò A, Pasechnik R (2019) Probing trans-electroweak first order phase transitions from gravitational waves. Physics 1(1):92–102. https://doi.org/10.3390/physics1010010. arXiv:1811.09074 [hep-ph]

Addazi A et al (2022) Quantum gravity phenomenology at the dawn of the multi-messenger era—a review. Prog Part Nucl Phys 125:103948. https://doi.org/10.1016/j.ppnp.2022.103948. arXiv:2111.05659 [hep-ph]

Ade PAR et al (2014) Planck 2013 results. XXV. Searches for cosmic strings and other topological defects. Astron Astrophys 571:A25. https://doi.org/10.1051/0004-6361/201321621. arXiv:1303.5085 [astro-ph.CO]

Ade PAR et al (2018) BICEP2 / Keck Array x: constraints on primordial gravitational waves using Planck, WMAP, and New BICEP2/Keck observations through the 2015 season. Phys Rev Lett 121:221301. https://doi.org/10.1103/PhysRevLett.121.221301. arXiv:1810.05216 [astro-ph.CO]

Ade PAR et al (2021) Improved constraints on primordial gravitational waves using Planck, WMAP, and BICEP/Keck observations through the 2018 observing season. Phys Rev Lett 127(15):151301. https://doi.org/10.1103/PhysRevLett.127.151301. arXiv:2110.00483 [astro-ph.CO]

Adshead P, Wyman M (2012) Chromo-natural inflation: natural inflation on a steep potential with classical non-Abelian gauge fields. Phys Rev Lett 108:261302. https://doi.org/10.1103/PhysRevLett.108.261302. arXiv:1202.2366 [hep-th]

Adshead P, Giblin JT, Scully TR, Sfakianakis EI (2015) Gauge-preheating and the end of axion inflation. JCAP 12:034. https://doi.org/10.1088/1475-7516/2015/12/034. arXiv:1502.06506 [astro-ph.CO]

Adshead P, Giblin JT, Weiner ZJ (2018) Gravitational waves from gauge preheating. Phys Rev D 98 (4):043525. https://doi.org/10.1103/PhysRevD.98.043525. arXiv:1805.04550 [astro-ph.CO]

Adshead P, Giblin JT, Pieroni M, Weiner ZJ (2020a) Constraining axion inflation with gravitational waves across 29 decades in frequency. Phys Rev Lett 124(17):171301. https://doi.org/10.1103/PhysRevLett.124.171301. arXiv:1909.12843 [astro-ph.CO]

Adshead P, Giblin JT, Pieroni M, Weiner ZJ (2020b) Constraining axion inflation with gravitational waves from preheating. Phys Rev D 101(8):083534. https://doi.org/10.1103/PhysRevD.101.083534. arXiv:1909.12842 [astro-ph.CO]

Adshead P, Afshordi N, Dimastrogiovanni E, Fasiello M, Lim EA, Tasinato G (2021) Multimessenger cosmology: correlating cosmic microwave background and stochastic gravitational wave background measurements. Phys Rev D 103(2):023532. https://doi.org/10.1103/PhysRevD.103.023532. arXiv:2004.06619 [astro-ph.CO]

Agashe K, Du P, Ekhterachian M, Kumar S, Sundrum R (2020) Cosmological phase transition of spontaneous confinement. JHEP 05:086. https://doi.org/10.1007/JHEP05(2020)086. arXiv:1910.06238 [hep-ph]

Aggarwal K et al (2019) The NANOGrav 11-year data set: limits on gravitational waves from individual supermassive black hole binaries. Astrophys J 880:2. https://doi.org/10.3847/1538-4357/ab2236. arXiv:1812.11585 [astro-ph.GA]

Aghamousa A et al (2016) The DESI experiment part I: science,targeting, and survey design. arXiv e-prints arXiv:1611.00036 [astro-ph.IM]

Aghanim N et al (2020) Planck 2018 results. VI. Cosmological parameters. Astron Astrophys 641:A6. https://doi.org/10.1051/0004-6361/201833910, [Erratum: Astron.Astrophys. 652, C4 (2021)]. arXiv:1807.06209 [astro-ph.CO]

Agrawal A, Fujita T, Komatsu E (2018) Large tensor non-Gaussianity from axion-gauge field dynamics. Phys Rev D 97(10):103526. https://doi.org/10.1103/PhysRevD.97.103526. arXiv:1707.03023 [astro-ph.CO]

Ahonen J, Enqvist K (1998) Magnetic field generation in first order phase transition bubble collisions. Phys Rev D 57:664–673. https://doi.org/10.1103/PhysRevD.57.664. arXiv:hep-ph/9704334

Ahriche A, Hashino K, Kanemura S, Nasri S (2019) Gravitational waves from phase transitions in models with charged singlets. Phys Lett B 789:119–126. https://doi.org/10.1016/j.physletb.2018.12.013. arXiv:1809.09883 [hep-ph]

Aiola S et al (2020) The Atacama cosmology telescope: DR4 maps and cosmological parameters. JCAP 12:047. https://doi.org/10.1088/1475-7516/2020/12/047. arXiv:2007.07288 [astro-ph.CO]

Akhshik M (2015) Clustering fossils in solid inflation. JCAP 05:043. https://doi.org/10.1088/1475-7516/2015/05/043. arXiv:1409.3004 [astro-ph.CO]

Akhshik M, Emami R, Firouzjahi H, Wang Y (2014) Statistical anisotropies in gravitational waves in solid inflation. JCAP 09:012. https://doi.org/10.1088/1475-7516/2014/09/012. arXiv:1405.4179 [astro-ph.CO]

Akrami Y et al (2020) Planck 2018 results. X. Constraints on inflation. Astron Astrophys 641:A10. https://doi.org/10.1051/0004-6361/201833887. arXiv:1807.06211 [astro-ph.CO]

Alam MF et al (2021) The NANOGrav 12.5 yr data set: wideband timing of 47 millisecond pulsars. Astrophys J Suppl 252(1):5. https://doi.org/10.3847/1538-4365/abc6a1. arXiv:2005.06495 [astro-ph.HE]

Alam U, Sahni V, Saini TD, Starobinsky AA (2003) Exploring the expanding universe and dark energy using the Statefinder diagnostic. Mon Not R Astron Soc 344:1057. https://doi.org/10.1046/j.1365-8711.2003.06871.x. arXiv:astro-ph/0303009

Alanne T, Hugle T, Platscher M, Schmitz K (2020) A fresh look at the gravitational-wave signal from cosmological phase transitions. JHEP 03:004. https://doi.org/10.1007/JHEP03(2020)004. arXiv:1909.11356 [hep-ph]

Alba V, Maldacena J (2016) Primordial gravity wave background anisotropies. JHEP 03:115. https://doi.org/10.1007/JHEP03(2016)115. arXiv:1512.01531 [hep-th]

Albrecht A, Steinhardt PJ (1982) Cosmology for grand unified theories with radiatively induced symmetry breaking. Phys Rev Lett 48:1220–1223. https://doi.org/10.1103/PhysRevLett.48.1220

Alcock C et al (1997) The MACHO project LMC microlensing results from the first two years and the nature of the galactic dark halo. Astrophys J 486:697–726. https://doi.org/10.1086/304535. arXiv:astro-ph/9606165

Alexander S, Yunes N (2009) Chern–Simons modified general relativity. Phys Rep 480:1–55. https://doi.org/10.1016/j.physrep.2009.07.002. arXiv:0907.2562 [hep-th]

Alexander S, Finn LS, Yunes N (2008) A gravitational-wave probe of effective quantum gravity. Phys Rev D 78:066005. https://doi.org/10.1103/PhysRevD.78.066005. arXiv:0712.2542 [gr-qc]

Ali-Haïmoud Y (2018) Correlation function of high-threshold regions and application to the initial small-scale clustering of primordial black holes. Phys Rev Lett 121(8):081304. https://doi.org/10.1103/PhysRevLett.121.081304. arXiv:1805.05912 [astro-ph.CO]

Ali-Haïmoud Y, Kamionkowski M (2017) Cosmic microwave background limits on accreting primordial black holes. Phys Rev D 95(4):043534. https://doi.org/10.1103/PhysRevD.95.043534. arXiv:1612.05644 [astro-ph.CO]

Allahverdi R, Brandenberger R, Cyr-Racine FY, Mazumdar A (2010) Reheating in inflationary cosmology: theory and applications. Annu Rev Nucl Part Sci 60:27–51. https://doi.org/10.1146/annurev.nucl.012809.104511. arXiv:1001.2600 [hep-th]

Allahverdi R et al (2020) The first three seconds: a review of possible expansion histories of the early universe. arXiv e-prints https://doi.org/10.21105/astro.2006.16182. arXiv:2006.16182 [astro-ph.CO]

Allahyari A, Nunes RC, Mota DF (2022) No slip gravity in light of LISA standard sirens. Mon Not R Astron Soc 514(1):1274–1281. https://doi.org/10.1093/mnras/stac1445. arXiv:2110.07634 [astro-ph.CO]

Allen B (1996) The stochastic gravity wave background: sources and detection. In: Les Houches School of Physics: Astrophysical Sources of Gravitational Radiation, pp 373–417. arXiv:gr-qc/9604033

Allen B, Ottewill AC (1997) Detection of anisotropies in the gravitational wave stochastic background. Phys Rev D 56:545–563. https://doi.org/10.1103/PhysRevD.56.545. arXiv:gr-qc/9607068

Allys E, Peter P, Rodriguez Y (2016) Generalized SU(2) Proca theory. Phys Rev D 94(8):084041. https://doi.org/10.1103/PhysRevD.94.084041. arXiv:1609.05870 [hep-th]

Alonso D, Bellini E, Ferreira PG, Zumalacárregui M (2017) Observational future of cosmological scalar–tensor theories. Phys Rev D 95(6):063502. https://doi.org/10.1103/PhysRevD.95.063502. arXiv:1610.09290 [astro-ph.CO]

Alonso D, Contaldi CR, Cusin G, Ferreira PG, Renzini AI (2020a) Noise angular power spectrum of gravitational wave background experiments. Phys Rev D 101(12):124048. https://doi.org/10.1103/PhysRevD.101.124048. arXiv:2005.03001 [astro-ph.CO]

Alonso D, Cusin G, Ferreira PG, Pitrou C (2020b) Detecting the anisotropic astrophysical gravitational wave background in the presence of shot noise through cross-correlations. Phys Rev D 102(2):023002. https://doi.org/10.1103/PhysRevD.102.023002. arXiv:2002.02888 [astro-ph.CO]

Alves A, Ghosh T, Guo HK, Sinha K (2018) Resonant Di-Higgs production at gravitational wave benchmarks: a collider study using machine learning. JHEP 12:070. https://doi.org/10.1007/JHEP12(2018)070. arXiv:1808.08974 [hep-ph]

Alves A, Gonçalves D, Ghosh T, Guo HK, Sinha K (2020) Di-Higgs production in the 4*b* channel and gravitational wave complementarity. JHEP 03:053. https://doi.org/10.1007/JHEP03(2020)053. arXiv:1909.05268 [hep-ph]

Alves A, Gonçalves D, Ghosh T, Guo HK, Sinha K (2021) Di-Higgs blind spots in gravitational wave signals. Phys Lett B 818:136377. https://doi.org/10.1016/j.physletb.2021.136377. arXiv:2007.15654 [hep-ph]

Amaro-Seoane P, Santamaria L (2010) Detection of IMBHs with ground-based gravitational wave observatories: a biography of a binary of black holes, from birth to death. Astrophys J 722:1197–1206. https://doi.org/10.1088/0004-637X/722/2/1197. arXiv:0910.0254 [astro-ph.CO]

Amaro-Seoane P et al (2017) Laser Interferometer Space Antenna. arXiv e-prints arXiv:1702.00786 [astro-ph.IM]

Amaro-Seoane P et al (2023) Astrophysics with the Laser Interferometer Space Antenna. Living Rev Relativ 26:2. https://doi.org/10.1007/s41114-022-00041-y. arXiv:2203.06016 [gr-qc]

Amendola L (2000) Coupled quintessence. Phys Rev D 62:043511. https://doi.org/10.1103/PhysRevD.62.043511. arXiv:astro-ph/9908023

Amendola L, Ballesteros G, Pettorino V (2014) Effects of modified gravity on B-mode polarization. Phys Rev D 90:043009. https://doi.org/10.1103/PhysRevD.90.043009. arXiv:1405.7004 [astro-ph.CO]

Amendola L, Sawicki I, Kunz M, Saltas ID (2018a) Direct detection of gravitational waves can measure the time variation of the Planck mass. JCAP 08:030. https://doi.org/10.1088/1475-7516/2018/08/030. arXiv:1712.08623 [astro-ph.CO]

Amendola L et al (2018b) Cosmology and fundamental physics with the Euclid satellite. Living Rev Relativ 21:2. https://doi.org/10.1007/s41114-017-0010-3. arXiv:1606.00180 [astro-ph.CO]

Amin MA, Hertzberg MP, Kaiser DI, Karouby J (2014) Nonperturbative dynamics of reheating after inflation: a review. Int J Mod Phys D 24:1530003. https://doi.org/10.1142/S0218271815300037. arXiv:1410.3808 [hep-ph]

Amin MA, Braden J, Copeland EJ, Giblin JT, Solorio C, Weiner ZJ, Zhou SY (2018) Gravitational waves from asymmetric oscillon dynamics? Phys Rev D 98:024040. https://doi.org/10.1103/PhysRevD.98.024040. arXiv:1803.08047 [astro-ph.CO]

Ananda KN, Clarkson C, Wands D (2007) The cosmological gravitational wave background from primordial density perturbations. Phys Rev D 75:123518. https://doi.org/10.1103/PhysRevD.75.123518. arXiv:gr-qc/0612013

Anber MM, Sorbo L (2010) Naturally inflating on steep potentials through electromagnetic dissipation. Phys Rev D 81:043534. https://doi.org/10.1103/PhysRevD.81.043534. arXiv:0908.4089 [hep-th]

Anber MM, Sorbo L (2012) Non-Gaussianities and chiral gravitational waves in natural steep inflation. Phys Rev D 85:123537. https://doi.org/10.1103/PhysRevD.85.123537. arXiv:1203.5849 [astro-ph.CO]

Andersson L, Joudioux J, Oancea MA, Raj A (2021) Propagation of polarized gravitational waves. Phys Rev D 103(4):044053. https://doi.org/10.1103/PhysRevD.103.044053. arXiv:2012.08363 [gr-qc]

Ando K, Inomata K, Kawasaki M, Mukaida K, Yanagida TT (2018) Primordial black holes for the LIGO events in the axionlike curvaton model. Phys Rev D 97(12):123512. https://doi.org/10.1103/PhysRevD.97.123512. arXiv:1711.08956 [astro-ph.CO]

Ando S, Kusenko A (2010) Evidence for gamma-ray halos around active galactic nuclei and the first measurement of intergalactic magnetic fields. Astrophys J Lett 722:L39. https://doi.org/10.1088/2041-8205/722/1/L39. arXiv:1005.1924 [astro-ph.HE]

Andreev V et al (2018) Improved limit on the electric dipole moment of the electron. Nature 562 (7727):355–360. https://doi.org/10.1038/s41586-018-0599-8

Angelescu A, Huang P (2019) Multistep strongly first order phase transitions from new fermions at the TeV scale. Phys Rev D 99(5):055023. https://doi.org/10.1103/PhysRevD.99.055023. arXiv:1812.08293 [hep-ph]

Antusch S, Cefala F, Orani S (2017) Gravitational waves from oscillons after inflation. Phys Rev Lett 118 (1):011303. https://doi.org/10.1103/PhysRevLett.118.011303, [Erratum: Phys. Rev. Lett. 120, 219901 (2018)]. arXiv:1607.01314 [astro-ph.CO]

Antusch S, Cefala F, Orani S (2018) What can we learn from the stochastic gravitational wave background produced by oscillons? JCAP 03:032. https://doi.org/10.1088/1475-7516/2018/03/032. arXiv:1712.03231 [astro-ph.CO]

Apreda R, Maggiore M, Nicolis A, Riotto A (2002) Gravitational waves from electroweak phase transitions. Nucl Phys B 631:342–368. https://doi.org/10.1016/S0550-3213(02)00264-X. arXiv:gr-qc/0107033

Arai S, Nishizawa A (2018) Generalized framework for testing gravity with gravitational-wave propagation. II. Constraints on Horndeski theory. Phys Rev D 97(10):104038. https://doi.org/10.1103/PhysRevD.97.104038. arXiv:1711.03776 [gr-qc]

Arkani-Hamed N, Maldacena J (2015) Cosmological collider physics. arXiv e-prints arXiv:1503.08043 [hep-th]

Armano M et al (2018) Beyond the required LISA free-fall performance: New LISA pathfinder results down to 20 μHz. Phys Rev Lett 120(6):061101. https://doi.org/10.1103/PhysRevLett.120.061101

Armendariz-Picon C (2004) Could dark energy be vector-like? JCAP 07:007. https://doi.org/10.1088/1475-7516/2004/07/007. arXiv:astro-ph/0405267

Armendariz-Picon C, Mukhanov VF, Steinhardt PJ (2000) A dynamical solution to the problem of a small cosmological constant and late time cosmic acceleration. Phys Rev Lett 85:4438–4441. https://doi.org/10.1103/PhysRevLett.85.4438. arXiv:astro-ph/0004134

Armstrong JW, Estabrook FB, Tinto M (2003) Time delay interferometry. Class Quantum Grav 20:S283–S289. https://doi.org/10.1088/0264-9381/20/10/331

Arnold PB, Espinosa O (1993) The effective potential and first order phase transitions: beyond leading-order. Phys Rev D 47:3546. https://doi.org/10.1103/PhysRevD.47.3546, [Erratum: Phys. Rev. D 50, 6662 (1994)]. arXiv:hep-ph/9212235

Artale MC, Mapelli M, Giacobbo N, Sabha NB, Spera M, Santoliquido F, Bressan A (2019) Host galaxies of merging compact objects: mass, star formation rate, metallicity and colours. Mon Not R Astron Soc 487(2):1675–1688. https://doi.org/10.1093/mnras/stz1382. arXiv:1903.00083 [astro-ph.GA]

Artymowski M, Ben-Dayan I, Thattarampilly U (2021) Sourced fluctuations in generic slow contraction. JCAP 06:010. https://doi.org/10.1088/1475-7516/2021/06/010. arXiv:2011.00626 [gr-qc]

Arun KG et al (2022) New horizons for fundamental physics with LISA. Living Rev Relativ 25:4. https://doi.org/10.1007/s41114-022-00036-9. arXiv:2205.01597 [gr-qc]

Arzoumanian Z et al (2018) The NANOGrav 11-year data set: pulsar-timing constraints on the stochastic gravitational-wave background. Astrophys J 859(1):47. https://doi.org/10.3847/1538-4357/aabd3b. arXiv:1801.02617 [astro-ph.HE]

Arzoumanian Z et al (2020) The NANOGrav 12.5 yr data set: search for an isotropic stochastic gravitational-wave background. Astrophys J Lett 905(2):L34. https://doi.org/10.3847/2041-8213/abd401. arXiv:2009.04496 [astro-ph.HE]

Ashoorioon A, Konstandin T (2009) Strong electroweak phase transitions without collider traces. JHEP 07:086. https://doi.org/10.1088/1126-6708/2009/07/086. arXiv:0904.0353 [hep-ph]

Atal V, Sanglas A, Triantafyllou N (2020) LIGO/Virgo black holes and dark matter: the effect of spatial clustering. JCAP 11:036. https://doi.org/10.1088/1475-7516/2020/11/036. arXiv:2007.07212 [astro-ph.CO]

Aubourg E et al (1993) Evidence for gravitational microlensing by dark objects in the galactic halo. Nature 365:623–625. https://doi.org/10.1038/365623a0

Auclair P, Vennin V (2021) Primordial black holes from metric preheating: mass fraction in the excursion-set approach. JCAP 02:038. https://doi.org/10.1088/1475-7516/2021/02/038. arXiv:2011.05633 [astro-ph.CO]

Auclair P, Ringeval C, Sakellariadou M, Steer D (2019) Cosmic string loop production functions. JCAP 06:015. https://doi.org/10.1088/1475-7516/2019/06/015. arXiv:1903.06685 [astro-ph.CO]

Auclair P et al (2020) Probing the gravitational wave background from cosmic strings with LISA. JCAP 04:034. https://doi.org/10.1088/1475-7516/2020/04/034. arXiv:1909.00819 [astro-ph.CO]

Aurrekoetxea JC, Helfer T, Lim EA (2020) Coherent gravitational waveforms and memory from cosmic string loops. Class Quantum Grav 37(20):204001. https://doi.org/10.1088/1361-6382/aba28b. arXiv:2002.05177 [gr-qc]

Avelino PP, Sousa L (2012) Scaling laws for weakly interacting cosmic (super)string and p-brane networks. Phys Rev D 85:083525. https://doi.org/10.1103/PhysRevD.85.083525. arXiv:1202.6298 [astro-ph.CO]

Avgoustidis A, Copeland EJ (2010) The effect of kinematic constraints on multi-tension string network evolution. Phys Rev D 81:063517. https://doi.org/10.1103/PhysRevD.81.063517. arXiv:0912.4004 [hep-ph]

Avgoustidis A, Shellard EPS (2006) Effect of reconnection probability on cosmic (super)string network density. Phys Rev D 73:041301. https://doi.org/10.1103/PhysRevD.73.041301. arXiv:astro-ph/0512582

Avgoustidis A, Shellard EPS (2008) Velocity-dependent models for non-Abelian/entangled string networks. Phys Rev D 78:103510. https://doi.org/10.1103/PhysRevD.78.103510, [Erratum: Phys. Rev. D 80, 129907 (2009)]. arXiv:0705.3395 [astro-ph]

Avgoustidis A, Pourtsidou A, Sakellariadou M (2015) Zipping and unzipping in string networks: dynamics of Y-junctions. Phys Rev D 91(2):025022. https://doi.org/10.1103/PhysRevD.91.025022. arXiv:1411.7959 [hep-th]

Babak S, Gair J, Sesana A, Barausse E, Sopuerta CF, Berry CPL, Berti E, Amaro-Seoane P, Petiteau A, Klein A (2017) Science with the space-based interferometer LISA. V: Extreme mass-ratio inspirals. Phys Rev D 95(10):103012. https://doi.org/10.1103/PhysRevD.95.103012. arXiv:1703.09722 [gr-qc]

Babak S, Petiteau A, Hewitson M (2021) LISA sensitivity and SNR calculations. arXiv e-prints arXiv:2108.01167 [astro-ph.IM]

Babak S, Caprini C, Figueroa DG, Karnesis N, Marcoccia P, Nardini G, Pieroni M, Ricciardone A, Sesana A, Torrado J (2023) Stochastic gravitational wave background from stellar origin binary black holes in LISA. arXiv e-prints arXiv:2304.06368 [astro-ph.CO]

Babichev E, Deffayet C (2013) An introduction to the Vainshtein mechanism. Class Quantum Grav 30:184001. https://doi.org/10.1088/0264-9381/30/18/184001. arXiv:1304.7240 [gr-qc]

Babichev E, Deffayet C, Ziour R (2009) k-Mouflage gravity. Int J Mod Phys D 18:2147–2154. https://doi.org/10.1142/S0218271809016107. arXiv:0905.2943 [hep-th]

Babichev E, Charmousis C, Lehébel A (2016) Black holes and stars in Horndeski theory. Class Quantum Grav 33(15):154002. https://doi.org/10.1088/0264-9381/33/15/154002. arXiv:1604.06402 [gr-qc]

Badurina L et al (2020) AION: an atom interferometer observatory and network. JCAP 05:011. https://doi.org/10.1088/1475-7516/2020/05/011. arXiv:1911.11755 [astro-ph.CO]

Baibhav V, Berti E, Cardoso V (2020) LISA parameter estimation and source localization with higher harmonics of the ringdown. Phys Rev D 101(8):084053. https://doi.org/10.1103/PhysRevD.101.084053. arXiv:2001.10011 [gr-qc]

Bajardi F, Vernieri D, Capozziello S (2020) Bouncing cosmology in f(Q) symmetric teleparallel gravity. Eur Phys J Plus 135(11):912. https://doi.org/10.1140/epjp/s13360-020-00918-3. arXiv:2011.01248 [gr-qc]

Baker J et al (2021) High angular resolution gravitational wave astronomy. Exper Astron 51(3):1441–1470. https://doi.org/10.1007/s10686-021-09712-0. arXiv:1908.11410 [astro-ph.HE]

Baker T, Harrison I (2021) Constraining scalar–tensor modified gravity with gravitational waves and large scale structure surveys. JCAP 01:068. https://doi.org/10.1088/1475-7516/2021/01/068. arXiv:2007.13791 [astro-ph.CO]

Baker T, Trodden M (2017) Multimessenger time delays from lensed gravitational waves. Phys Rev D 95(6):063512. https://doi.org/10.1103/PhysRevD.95.063512. arXiv:1612.02004 [astro-ph.CO]

Baker T, Bellini E, Ferreira PG, Lagos M, Noller J, Sawicki I (2017) Strong constraints on cosmological gravity from GW170817 and GRB 170817A. Phys Rev Lett 119(25):251301. https://doi.org/10.1103/PhysRevLett.119.251301. arXiv:1710.06394 [astro-ph.CO]

Baker T et al (2022) Measuring the propagation speed of gravitational waves with LISA. JCAP 08(08):031. https://doi.org/10.1088/1475-7516/2022/08/031. arXiv:2203.00566 [gr-qc]

Balazs C, Fowlie A, Mazumdar A, White G (2017) Gravitational waves at aLIGO and vacuum stability with a scalar singlet extension of the Standard Model. Phys Rev D 95(4):043505. https://doi.org/10.1103/PhysRevD.95.043505. arXiv:1611.01617 [hep-ph]

Baldes I, Garcia-Cely C (2019) Strong gravitational radiation from a simple dark matter model. JHEP 05:190. https://doi.org/10.1007/JHEP05(2019)190. arXiv:1809.01198 [hep-ph]

Baldes I, Servant G (2018) High scale electroweak phase transition: baryogenesis & symmetry non-restoration. JHEP 10:053. https://doi.org/10.1007/JHEP10(2018)053. arXiv:1807.08770 [hep-ph]

Ballesteros G, Comelli D, Pilo L (2016) Massive and modified gravity as self-gravitating media. Phys Rev D 94(12):124023. https://doi.org/10.1103/PhysRevD.94.124023. arXiv:1603.02956 [hep-th]

Ballesteros G, Serpico PD, Taoso M (2018) On the merger rate of primordial black holes: effects of nearest neighbours distribution and clustering. JCAP 10:043. https://doi.org/10.1088/1475-7516/2018/10/043. arXiv:1807.02084 [astro-ph.CO]

Ballesteros G, Beltran Jimenez J, Pieroni M (2019) Black hole formation from a general quadratic action for inflationary primordial fluctuations. JCAP 06:016. https://doi.org/10.1088/1475-7516/2019/06/016. arXiv:1811.03065 [astro-ph.CO]

Ballesteros G, Rey J, Rompineve F (2020) Detuning primordial black hole dark matter with early matter domination and axion monodromy. JCAP 06:014. https://doi.org/10.1088/1475-7516/2020/06/014. arXiv:1912.01638 [astro-ph.CO]

Banados E et al (2018) An 800-million-solar-mass black hole in a significantly neutral Universe at redshift 7.5. Nature 553(7689):473–476. https://doi.org/10.1038/nature25180. arXiv:1712.01860 [astro-ph.GA]

Banagiri S, Criswell A, Kuan T, Mandic V, Romano JD, Taylor SR (2021) Mapping the gravitational-wave sky with LISA: a Bayesian spherical harmonic approach. Mon Not R Astron Soc 507(4):5451–5462. https://doi.org/10.1093/mnras/stab2479. arXiv:2103.00826 [astro-ph.IM]

Banerjee A, Colgáin EO, Sasaki M, Sheikh-Jabbari MM (2021) Lost in the log-polynomial expansion: comment on arXiv:2101.08278. arXiv e-prints arXiv:2102.02098 [astro-ph.CO]

Banks T, Dine M, Fox PJ, Gorbatov E (2003) On the possibility of large axion decay constants. JCAP 06:001. https://doi.org/10.1088/1475-7516/2003/06/001. arXiv:hep-th/0303252

Barack L, Cutler C (2005) Confusion noise from extreme-mass-ratio inspirals. In: 38th ESLAB symposium and 5th international LISA symposium. arXiv:gr-qc/0502052

Baral P, Roy SK, Pal S (2020) Prospects of probing dark energy with eLISA: Standard versus null diagnostics. Mon Not R Astron Soc 500(3):2896–2907. https://doi.org/10.1093/mnras/staa3346. arXiv:2005.07231 [astro-ph.CO]

Baratella P, Pomarol A, Rompineve F (2019) The supercooled universe. JHEP 03:100. https://doi.org/10.1007/JHEP03(2019)100. arXiv:1812.06996 [hep-ph]

Barausse E, Sotiriou TP (2008) Perturbed Kerr Black Holes can probe deviations from General Relativity. Phys Rev Lett 101:099001. https://doi.org/10.1103/PhysRevLett.101.099001. arXiv:0803.3433 [gr-qc]

Barausse E, Yagi K (2015) Gravitation-wave emission in shift-symmetric Horndeski theories. Phys Rev Lett 115(21):211105. https://doi.org/10.1103/PhysRevLett.115.211105. arXiv:1509.04539 [gr-qc]

Barausse E, Cardoso V, Pani P (2014) Can environmental effects spoil precision gravitational-wave astrophysics? Phys Rev D 89(10):104059. https://doi.org/10.1103/PhysRevD.89.104059. arXiv:1404.7149 [gr-qc]

Barausse E, Dvorkin I, Tremmel M, Volonteri M, Bonetti M (2020) Massive black hole merger rates: the effect of kiloparsec separation wandering and supernova feedback. Astrophys J 904(1):16. https://doi.org/10.3847/1538-4357/abba7f. arXiv:2006.03065 [astro-ph.GA]

Bardeen JM, Steinhardt PJ, Turner MS (1983) Spontaneous creation of almost scale—free density perturbations in an inflationary universe. Phys Rev D 28:679. https://doi.org/10.1103/PhysRevD.28.679

Barenboim G, Park WI (2016) Gravitational waves from first order phase transitions as a probe of an early matter domination era and its inverse problem. Phys Lett B 759:430–438. https://doi.org/10.1016/j.physletb.2016.06.009. arXiv:1605.03781 [astro-ph.CO]

Barish BC, Bird S, Cui Y (2021) Impact of a midband gravitational wave experiment on detectability of cosmological stochastic gravitational wave backgrounds. Phys Rev D 103(12):123541. https://doi.org/10.1103/PhysRevD.103.123541. arXiv:2012.07874 [gr-qc]

Barkat Z, Rakavy G, Sack N (1967) Dynamics of supernova explosion resulting from pair formation. Phys Rev Lett 18:379–381. https://doi.org/10.1103/PhysRevLett.18.379

Barnaby N, Peloso M (2011) Large nongaussianity in axion inflation. Phys Rev Lett 106:181301. https://doi.org/10.1103/PhysRevLett.106.181301. arXiv:1011.1500 [hep-ph]

Barnaby N, Pajer E, Peloso M (2012) Gauge field production in axion inflation: consequences for monodromy, non-Gaussianity in the CMB, and gravitational waves at interferometers. Phys Rev D 85:023525. https://doi.org/10.1103/PhysRevD.85.023525. arXiv:1110.3327 [astro-ph.CO]

Barnett R et al (2019) Euclid preparation - V. Predicted yield of redshift 7 z 9 quasars from the wide survey. Astron Astrophys 631:A85. https://doi.org/10.1051/0004-6361/201936427. arXiv:1908.04310 [astro-ph.GA]

Bartolo N, Orlando G (2017) Parity breaking signatures from a Chern–Simons coupling during inflation: the case of non-Gaussian gravitational waves. JCAP 07:034. https://doi.org/10.1088/1475-7516/2017/07/034. arXiv:1706.04627 [astro-ph.CO]

Bartolo N, Cannone D, Ricciardone A, Tasinato G (2016a) Distinctive signatures of space-time diffeomorphism breaking in EFT of inflation. JCAP 03:044. https://doi.org/10.1088/1475-7516/2016/03/044. arXiv:1511.07414 [astro-ph.CO]

Bartolo N, Domcke V, Figueroa DG, García-Bellido J, Peloso M, Pieroni M, Ricciardone A, Sakellariadou M, Sorbo L, Tasinato G (2018) Probing non-Gaussian stochastic gravitational wave backgrounds with LISA. JCAP 11:034. https://doi.org/10.1088/1475-7516/2018/11/034. arXiv:1806.02819 [astro-ph.CO]

Bartolo N, Bertacca D, Matarrese S, Peloso M, Ricciardone A, Riotto A, Tasinato G (2019a) Anisotropies and non-Gaussianity of the cosmological gravitational wave background. Phys Rev D 100(12):121501. https://doi.org/10.1103/PhysRevD.100.121501. arXiv:1908.00527 [astro-ph.CO]

Bartolo N, De Luca V, Franciolini G, Lewis A, Peloso M, Riotto A (2019b) Primordial black hole dark matter: LISA serendipity. Phys Rev Lett 122(21):211301. https://doi.org/10.1103/PhysRevLett.122.211301. arXiv:1810.12218 [astro-ph.CO]

Bartolo N, De Luca V, Franciolini G, Peloso M, Racco D, Riotto A (2019c) Testing primordial black holes as dark matter with LISA. Phys Rev D 99(10):103521. https://doi.org/10.1103/PhysRevD.99.103521. arXiv:1810.12224 [astro-ph.CO]

Bartolo N, Orlando G, Shiraishi M (2019d) Measuring chiral gravitational waves in Chern–Simons gravity with CMB bispectra. JCAP 01:050. https://doi.org/10.1088/1475-7516/2019/01/050. arXiv:1809.11170 [astro-ph.CO]

Bartolo N, Bertacca D, De Luca V, Franciolini G, Matarrese S, Peloso M, Ricciardone A, Riotto A, Tasinato G (2020a) Gravitational wave anisotropies from primordial black holes. JCAP 02:028. https://doi.org/10.1088/1475-7516/2020/02/028. arXiv:1909.12619 [astro-ph.CO]

Bartolo N, Bertacca D, Matarrese S, Peloso M, Ricciardone A, Riotto A, Tasinato G (2020b) Characterizing the cosmological gravitational wave background: anisotropies and non-Gaussianity. Phys Rev D 102(2):023527. https://doi.org/10.1103/PhysRevD.102.023527. arXiv:1912.09433 [astro-ph.CO]

Bartolo N, Caloni L, Orlando G, Ricciardone A (2021) Tensor non-Gaussianity in chiral scalar–tensor theories of gravity. JCAP 03:073. https://doi.org/10.1088/1475-7516/2021/03/073. arXiv:2008.01715 [astro-ph.CO]

Bartolo N et al (2016b) Science with the space-based interferometer LISA. IV: Probing inflation with gravitational waves. JCAP 12:026. https://doi.org/10.1088/1475-7516/2016/12/026. arXiv:1610.06481 [astro-ph.CO]

Bartolo N et al (2022) Probing anisotropies of the stochastic gravitational wave background with LISA. JCAP 11:009. https://doi.org/10.1088/1475-7516/2022/11/009. arXiv:2201.08782 [astro-ph.CO]

Bassett BA, Viniegra F (2000) Massless metric preheating. Phys Rev D 62:043507. https://doi.org/10.1103/PhysRevD.62.043507. arXiv:hep-ph/9909353

Bassett BA, Tamburini F, Kaiser DI, Maartens R (1999) Metric preheating and limitations of linearized gravity. 2. Nucl Phys B 561:188–240. https://doi.org/10.1016/S0550-3213(99)00495-2. arXiv:hep-ph/9901319

Battefeld D, Peter P (2015) A critical review of classical bouncing cosmologies. Phys Rep 571:1–66. https://doi.org/10.1016/j.physrep.2014.12.004. arXiv:1406.2790 [astro-ph.CO]

Battye RA, Shellard EPS (1994) Global string radiation. Nucl Phys B 423:260–304. https://doi.org/10.1016/0550-3213(94)90573-8. arXiv:astro-ph/9311017

Battye RA, Shellard EPS (1996) Radiative back reaction on global strings. Phys Rev D 53:1811–1826. https://doi.org/10.1103/PhysRevD.53.1811. arXiv:hep-ph/9508301

Battye RA, Pace F, Trinh D (2018) Gravitational wave constraints on dark sector models. Phys Rev D 98(2):023504. https://doi.org/10.1103/PhysRevD.98.023504. arXiv:1802.09447 [astro-ph.CO]

Baumann D (2011) Inflation. In: Theoretical advanced study institute in elementary particle physics: physics of the large and the small, pp 523–686. https://doi.org/10.1142/9789814327183_0010. arXiv:0907.5424 [hep-th]

Baumann D, Green D (2012) Signatures of supersymmetry from the early universe. Phys Rev D 85:103520. https://doi.org/10.1103/PhysRevD.85.103520. arXiv:1109.0292 [hep-th]

Baumann D, McAllister L (2015) Inflation and string theory. Cambridge Monographs on Mathematical Physics, Cambridge University Press. https://doi.org/10.1017/CBO9781316105733. arXiv:1404.2601 [hep-th]

Baumann D, Steinhardt PJ, Takahashi K, Ichiki K (2007) Gravitational wave spectrum induced by primordial scalar perturbations. Phys Rev D 76:084019. https://doi.org/10.1103/PhysRevD.76.084019. arXiv:hep-th/0703290

Bayle JB, Lilley M, Petiteau A, Halloin H (2019) Effect of filters on the time-delay interferometry residual laser noise for LISA. Phys Rev D 99(8):084023. https://doi.org/10.1103/PhysRevD.99.084023. arXiv:1811.01575 [astro-ph.IM]

Bea Y, Casalderrey-Solana J, Giannakopoulos T, Jansen A, Krippendorf S, Mateos D, Sanchez-Garitaonandia M, Zilhão M (2021a) Spinodal gravitational waves. arXiv e-prints arXiv:2112.15478 [hep-th]

Bea Y, Casalderrey-Solana J, Giannakopoulos T, Mateos D, Sanchez-Garitaonandia M, Zilhão M (2021b) Bubble wall velocity from holography. Phys Rev D 104(12):L121903. https://doi.org/10.1103/PhysRevD.104.L121903. arXiv:2104.05708 [hep-th]

Bea Y, Casalderrey-Solana J, Giannakopoulos T, Jansen A, Mateos D, Sanchez-Garitaonandia M, Zilhão M (2022) Holographic bubbles with Jecco: expanding, collapsing and critical. JHEP 09:008. https://doi.org/10.1007/JHEP09(2022)008, [Erratum: JHEP 03, 225 (2023)]. arXiv:2202.10503 [hep-th]

Belczynski K et al (2016) The effect of pair-instability mass loss on black hole mergers. Astron Astrophys 594:A97. https://doi.org/10.1051/0004-6361/201628980. arXiv:1607.03116 [astro-ph.HE]

Belgacem E, Dirian Y, Foffa S, Maggiore M (2018a) Gravitational-wave luminosity distance in modified gravity theories. Phys Rev D 97(10):104066. https://doi.org/10.1103/PhysRevD.97.104066. arXiv:1712.08108 [astro-ph.CO]

Belgacem E, Dirian Y, Foffa S, Maggiore M (2018b) Modified gravitational-wave propagation and standard sirens. Phys Rev D 98(2):023510. https://doi.org/10.1103/PhysRevD.98.023510. arXiv:1805.08731 [gr-qc]

Belgacem E, Dirian Y, Foffa S, Maggiore M (2018c) Nonlocal gravity. Conceptual aspects and cosmological predictions. JCAP 03:002. https://doi.org/10.1088/1475-7516/2018/03/002. arXiv:1712.07066 [hep-th]

Belgacem E, Dirian Y, Finke A, Foffa S, Maggiore M (2019a) Nonlocal gravity and gravitational-wave observations. JCAP 11:022. https://doi.org/10.1088/1475-7516/2019/11/022. arXiv:1907.02047 [astro-ph.CO]

Belgacem E, Dirian Y, Foffa S, Howell EJ, Maggiore M, Regimbau T (2019b) Cosmology and dark energy from joint gravitational wave-GRB observations. JCAP 08:015. https://doi.org/10.1088/1475-7516/2019/08/015. arXiv:1907.01487 [astro-ph.CO]

Belgacem E, Dirian Y, Finke A, Foffa S, Maggiore M (2020) Gravity in the infrared and effective nonlocal models. JCAP 04:010. https://doi.org/10.1088/1475-7516/2020/04/010. arXiv:2001.07619 [astro-ph.CO]

Belgacem E et al (2019c) Testing modified gravity at cosmological distances with LISA standard sirens. JCAP 07:024. https://doi.org/10.1088/1475-7516/2019/07/024. arXiv:1906.01593 [astro-ph.CO]

Bellini E, Sawicki I, Zumalacárregui M (2020) hi_class: background evolution, initial conditions and approximation schemes. JCAP 02:008. https://doi.org/10.1088/1475-7516/2020/02/008. arXiv:1909.01828 [astro-ph.CO]

Beltran Jimenez J, Heisenberg L (2017) Generalized multi-Proca fields. Phys Lett B 770:16–26. https://doi.org/10.1016/j.physletb.2017.03.002. arXiv:1610.08960 [hep-th]

Beltran Jimenez J, Piazza F, Velten H (2016) Evading the Vainshtein mechanism with anomalous gravitational wave speed: constraints on modified gravity from binary pulsars. Phys Rev Lett 116 (6):061101. https://doi.org/10.1103/PhysRevLett.116.061101. arXiv:1507.05047 [gr-qc]

Beltrán Jiménez J, Heisenberg L, Koivisto T (2018) Coincident general relativity. Phys Rev D 98 (4):044048. https://doi.org/10.1103/PhysRevD.98.044048. arXiv:1710.03116 [gr-qc]

Beltrán Jiménez J, Heisenberg L, Koivisto TS (2019) The geometrical trinity of gravity. Universe 5(7):173. https://doi.org/10.3390/universe5070173. arXiv:1903.06830 [hep-th]

Beltrán Jiménez J, Ezquiaga JM, Heisenberg L (2020a) Probing cosmological fields with gravitational wave oscillations. JCAP 04:027. https://doi.org/10.1088/1475-7516/2020/04/027. arXiv:1912.06104 [astro-ph.CO]

Beltrán Jiménez J, Heisenberg L, Koivisto TS, Pekar S (2020b) Cosmology in $f(Q)$ geometry. Phys Rev D 101(10):103507. https://doi.org/10.1103/PhysRevD.101.103507. arXiv:1906.10027 [gr-qc]

Ben Achour J, Crisostomi M, Koyama K, Langlois D, Noui K, Tasinato G (2016) Degenerate higher order scalar-tensor theories beyond Horndeski up to cubic order. JHEP 12:100. https://doi.org/10.1007/JHEP12(2016)100. arXiv:1608.08135 [hep-th]

Ben-Dayan I (2016) Gravitational waves in bouncing cosmologies from gauge field production. JCAP 09:017. https://doi.org/10.1088/1475-7516/2016/09/017. arXiv:1604.07899 [astro-ph.CO]

Ben-Dayan I, Kupferman J (2019) Sourced scalar fluctuations in bouncing cosmology. JCAP 07:050. https://doi.org/10.1088/1475-7516/2019/07/050, [Erratum: JCAP 12, E01 (2020)]. arXiv:1812.06970 [gr-qc]

Benakli K, Chen Y, Cheng P, Lafforgue-Marmet G (2019) Stochastic gravitational waves from spin- 3/2 fields. Phys Rev D 99(9):095032. https://doi.org/10.1103/PhysRevD.99.095032. arXiv:1811.11774 [hep-ph]

Beniwal A, Lewicki M, Wells JD, White M, Williams AG (2017) Gravitational wave, collider and dark matter signals from a scalar singlet electroweak baryogenesis. JHEP 08:108. https://doi.org/10.1007/JHEP08(2017)108. arXiv:1702.06124 [hep-ph]

Beniwal A, Lewicki M, White M, Williams AG (2019) Gravitational waves and electroweak baryogenesis in a global study of the extended scalar singlet model. JHEP 02:183. https://doi.org/10.1007/JHEP02(2019)183. arXiv:1810.02380 [hep-ph]

Bennett DP, Bouchet FR (1988) Evidence for a scaling solution in cosmic string evolution. Phys Rev Lett 60:257. https://doi.org/10.1103/PhysRevLett.60.257

Bennett DP, Bouchet FR (1991) Constraints on the gravity wave background generated by cosmic strings. Phys Rev D 43:2733–2735. https://doi.org/10.1103/PhysRevD.43.2733

Berges J, Tetradis N, Wetterich C (1997) Coarse graining and first order phase transitions. Phys Lett B 393:387–394. https://doi.org/10.1016/S0370-2693(96)01654-1. arXiv:hep-ph/9610354

Bernal JL, Raccanelli A, Verde L, Silk J (2018) Signatures of primordial black holes as seeds of supermassive black holes. JCAP 05:017. https://doi.org/10.1088/1475-7516/2018/05/017, [Erratum: JCAP 01, E01 (2020)]. arXiv:1712.01311 [astro-ph.CO]

Bernal N, Hajkarim F (2019) Primordial gravitational waves in nonstandard cosmologies. Phys Rev D 100(6):063502. https://doi.org/10.1103/PhysRevD.100.063502. arXiv:1905.10410 [astro-ph.CO]

Bertacca D, Raccanelli A, Bartolo N, Matarrese S (2018) Cosmological perturbation effects on gravitational-wave luminosity distance estimates. Phys Dark Universe 20:32–40. https://doi.org/10.1016/j.dark.2018.03.001. arXiv:1702.01750 [gr-qc]

Bertacca D, Ricciardone A, Bellomo N, Jenkins AC, Matarrese S, Raccanelli A, Regimbau T, Sakellariadou M (2020) Projection effects on the observed angular spectrum of the astrophysical stochastic gravitational wave background. Phys Rev D 101(10):103513. https://doi.org/10.1103/PhysRevD.101.103513. arXiv:1909.11627 [astro-ph.CO]

Bertone G et al (2020) Gravitational wave probes of dark matter: challenges and opportunities. SciPost Phys Core 3:007. https://doi.org/10.21468/SciPostPhysCore.3.2.007. arXiv:1907.10610 [astro-ph.CO]

Bethke L, Figueroa DG, Rajantie A (2013) Anisotropies in the gravitational wave background from preheating. Phys Rev Lett 111(1):011301. https://doi.org/10.1103/PhysRevLett.111.011301. arXiv:1304.2657 [astro-ph.CO]

Bethke L, Figueroa DG, Rajantie A (2014) On the anisotropy of the gravitational wave background from massless preheating. JCAP 06:047. https://doi.org/10.1088/1475-7516/2014/06/047. arXiv:1309.1148 [astro-ph.CO]

Bettoni D, Ezquiaga JM, Hinterbichler K, Zumalacárregui M (2017) Speed of gravitational waves and the fate of scalar–tensor gravity. Phys Rev D 95(8):084029. https://doi.org/10.1103/PhysRevD.95.084029. arXiv:1608.01982 [gr-qc]

Bettoni D, Domènech G, Rubio J (2019) Gravitational waves from global cosmic strings in quintessential inflation. JCAP 02:034. https://doi.org/10.1088/1475-7516/2019/02/034. arXiv:1810.11117 [astro-ph.CO]

Bezares M, ter Haar L, Crisostomi M, Barausse E, Palenzuela C (2021) Kinetic screening in nonlinear stellar oscillations and gravitational collapse. Phys Rev D 104(4):044022. https://doi.org/10.1103/PhysRevD.104.044022. arXiv:2105.13992 [gr-qc]

Bezares M, Aguilera-Miret R, ter Haar L, Crisostomi M, Palenzuela C, Barausse E (2022) No evidence of kinetic screening in simulations of merging binary neutron stars beyond general relativity. Phys Rev Lett 128(9):091103. https://doi.org/10.1103/PhysRevLett.128.091103. arXiv:2107.05648 [gr-qc]

Bhattacharjee P, Hill CT, Schramm DN (1992) Grand unified theories, topological defects and ultrahigh-energy cosmic rays. Phys Rev Lett 69:567–570. https://doi.org/10.1103/PhysRevLett.69.567

Biagetti M, Franciolini G, Kehagias A, Riotto A (2018) Primordial black holes from inflation and quantum diffusion. JCAP 07:032. https://doi.org/10.1088/1475-7516/2018/07/032. arXiv:1804.07124 [astro-ph.CO]

Bian L, Wu Y, Xie KP (2019) Electroweak phase transition with composite Higgs models: calculability, gravitational waves and collider searches. JHEP 12:028. https://doi.org/10.1007/JHEP12(2019)028. arXiv:1909.02014 [hep-ph]

Bian L, Guo HK, Wu Y, Zhou R (2020) Gravitational wave and collider searches for electroweak symmetry breaking patterns. Phys Rev D 101(3):035011. https://doi.org/10.1103/PhysRevD.101.035011. arXiv:1906.11664 [hep-ph]

Biekötter T, Heinemeyer S, No JM, Olea MO, Weiglein G (2021) Fate of electroweak symmetry in the early Universe: non-restoration and trapped vacua in the N2HDM. JCAP 06:018. https://doi.org/10.1088/1475-7516/2021/06/018. arXiv:2103.12707 [hep-ph]

Biesiada M, Ding X, Piórkowska A, Zhu ZH (2014) Strong gravitational lensing of gravitational waves from double compact binaries-perspectives for the Einstein Telescope. JCAP 2014(10):080–080. https://doi.org/10.1088/1475-7516/2014/10/080. arXiv:1409.8360 [astro-ph.HE]

Bigazzi F, Caddeo A, Canneti T, Cotrone AL (2021) Bubble wall velocity at strong coupling. JHEP 08:090. https://doi.org/10.1007/JHEP08(2021)090. arXiv:2104.12817 [hep-ph]

Binetruy P, Bohe A, Hertog T, Steer DA (2009) Gravitational wave bursts from cosmic superstrings with Y-junctions. Phys Rev D 80:123510. https://doi.org/10.1103/PhysRevD.80.123510. arXiv:0907.4522 [hep-th]

Binetruy P, Bohe A, Caprini C, Dufaux JF (2012) Cosmological backgrounds of gravitational waves and eLISA/NGO: phase transitions, cosmic strings and other sources. JCAP 06:027. https://doi.org/10.1088/1475-7516/2012/06/027. arXiv:1201.0983 [gr-qc]

Bird S, Cholis I, Muñoz JB, Ali-Haïmoud Y, Kamionkowski M, Kovetz ED, Raccanelli A, Riess AG (2016) Did LIGO detect dark matter? Phys Rev Lett 116(20):201301. https://doi.org/10.1103/PhysRevLett.116.201301. arXiv:1603.00464 [astro-ph.CO]

Birrell ND, Davies PCW (1984) Quantum fields in curved space. Cambridge Monographs on Mathematical Physics, Cambridge University Press, Cambridge. https://doi.org/10.1017/CBO9780511622632

Birrer S, Amara A (2018) lenstronomy: Multi-purpose gravitational lens modelling software package. Phys Dark Universe 22:189–201. https://doi.org/10.1016/j.dark.2018.11.002. arXiv:1803.09746 [astro-ph.CO]

Biscoveanu S, Talbot C, Thrane E, Smith R (2020) Measuring the primordial gravitational-wave background in the presence of astrophysical foregrounds. Phys Rev Lett 125:241101. https://doi.org/10.1103/PhysRevLett.125.241101. arXiv:2009.04418 [astro-ph.HE]

Biswas T, Mazumdar A, Siegel W (2006) Bouncing universes in string-inspired gravity. JCAP 03:009. https://doi.org/10.1088/1475-7516/2006/03/009. arXiv:hep-th/0508194

Biswas T, Brandenberger R, Mazumdar A, Siegel W (2007) Non-perturbative gravity, Hagedorn bounce & CMB. JCAP 12:011. https://doi.org/10.1088/1475-7516/2007/12/011. arXiv:hep-th/0610274

Biswas T, Koivisto T, Mazumdar A (2010) Towards a resolution of the cosmological singularity in non-local higher derivative theories of gravity. JCAP 11:008. https://doi.org/10.1088/1475-7516/2010/11/008. arXiv:1005.0590 [hep-th]

Biswas T, Gerwick E, Koivisto T, Mazumdar A (2012a) Towards singularity and ghost free theories of gravity. Phys Rev Lett 108:031101. https://doi.org/10.1103/PhysRevLett.108.031101. arXiv:1110.5249 [gr-qc]

Biswas T, Koshelev AS, Mazumdar A, Vernov SY (2012b) Stable bounce and inflation in non-local higher derivative cosmology. JCAP 08:024. https://doi.org/10.1088/1475-7516/2012/08/024. arXiv:1206.6374 [astro-ph.CO]

Biswas T, Koivisto T, Mazumdar A (2014) Atick-Witten Hagedorn conjecture, near scale-invariant matter and blue-tilted gravity power spectrum. JHEP 08:116. https://doi.org/10.1007/JHEP08(2014)116. arXiv:1403.7163 [hep-th]

Biswas T, Koshelev AS, Mazumdar A (2016) Gravitational theories with stable (anti-)de Sitter backgrounds. Fundam Theor Phys 183:97–114. https://doi.org/10.1007/978-3-319-31299-6_5. arXiv:1602.08475 [hep-th]

Biswas T, Koshelev AS, Mazumdar A (2017) Consistent higher derivative gravitational theories with stable de Sitter and anti-de Sitter backgrounds. Phys Rev D 95(4):043533. https://doi.org/10.1103/PhysRevD.95.043533. arXiv:1606.01250 [gr-qc]

Blanchard A et al (2020) Euclid preparation: VII. Forecast validation for Euclid cosmological probes. Astron Astrophys 642:A191. https://doi.org/10.1051/0004-6361/202038071. arXiv:1910.09273 [astro-ph.CO]

Blanco-Pillado JJ, Olum KD (2017) Stochastic gravitational wave background from smoothed cosmic string loops. Phys Rev D 96(10):104046. https://doi.org/10.1103/PhysRevD.96.104046. arXiv:1709.02693 [astro-ph.CO]

Blanco-Pillado JJ, Olum KD (2020) Direct determination of cosmic string loop density from simulations. Phys Rev D 101(10):103018. https://doi.org/10.1103/PhysRevD.101.103018. arXiv:1912.10017 [astro-ph.CO]

Blanco-Pillado JJ, Olum KD, Shlaer B (2011) Large parallel cosmic string simulations: new results on loop production. Phys Rev D 83:083514. https://doi.org/10.1103/PhysRevD.83.083514. arXiv:1101.5173 [astro-ph.CO]

Blanco-Pillado JJ, Olum KD, Shlaer B (2014) The number of cosmic string loops. Phys Rev D 89 (2):023512. https://doi.org/10.1103/PhysRevD.89.023512. arXiv:1309.6637 [astro-ph.CO]
Blanco-Pillado JJ, Olum KD, Shlaer B (2015) Cosmic string loop shapes. Phys Rev D 92(6):063528. https://doi.org/10.1103/PhysRevD.92.063528. arXiv:1508.02693 [astro-ph.CO]
Blanco-Pillado JJ, Olum KD, Siemens X (2018a) New limits on cosmic strings from gravitational wave observation. Phys Lett B 778:392–396. https://doi.org/10.1016/j.physletb.2018.01.050. arXiv:1709.02434 [astro-ph.CO]
Blanco-Pillado JJ, Olum KD, Wachter JM (2018b) Gravitational backreaction near cosmic string kinks and cusps. Phys Rev D 98(12):123507. https://doi.org/10.1103/PhysRevD.98.123507. arXiv:1808.08254 [gr-qc]
Blanco-Pillado JJ, Olum KD, Wachter JM (2019a) Energy-conservation constraints on cosmic string loop production and distribution functions. Phys Rev D 100(12):123526. https://doi.org/10.1103/PhysRevD.100.123526. arXiv:1907.09373 [astro-ph.CO]
Blanco-Pillado JJ, Olum KD, Wachter JM (2019b) Gravitational backreaction simulations of simple cosmic string loops. Phys Rev D 100(2):023535. https://doi.org/10.1103/PhysRevD.100.023535. arXiv:1903.06079 [gr-qc]
Blas D, Jenkins AC (2022a) Bridging the μHz gap in the gravitational-wave landscape with binary resonances. Phys Rev Lett 128(10):101103. https://doi.org/10.1103/PhysRevLett.128.101103. arXiv:2107.04601 [astro-ph.CO]
Blas D, Jenkins AC (2022b) Detecting stochastic gravitational waves with binary resonance. Phys Rev D 105(6):064021. https://doi.org/10.1103/PhysRevD.105.064021. arXiv:2107.04063 [gr-qc]
Blas D, Lesgourgues J, Tram T (2011) The cosmic linear anisotropy solving system (CLASS) II: approximation schemes. JCAP 07:034. https://doi.org/10.1088/1475-7516/2011/07/034. arXiv:1104.2933 [astro-ph.CO]
Blas D, Ivanov MM, Sawicki I, Sibiryakov S (2016) On constraining the speed of gravitational waves following GW150914. JETP Lett 103(10):624–626. https://doi.org/10.7868/S0370274X16100039. arXiv:1602.04188 [gr-qc]
Blasi S, Brdar V, Schmitz K (2020) Fingerprint of low-scale leptogenesis in the primordial gravitational-wave spectrum. Phys Rev Res 2(4):043321. https://doi.org/10.1103/PhysRevResearch.2.043321. arXiv:2004.02889 [hep-ph]
Bloomfield JK, Chernoff DF (2014) Cosmic string loop microlensing. Phys Rev D 89(12):124003. https://doi.org/10.1103/PhysRevD.89.124003. arXiv:1311.7132 [astro-ph.CO]
Bodeker D, Moore GD (2009) Can electroweak bubble walls run away? JCAP 05:009. https://doi.org/10.1088/1475-7516/2009/05/009. arXiv:0903.4099 [hep-ph]
Bodeker D, Moore GD (2017) Electroweak bubble wall speed limit. JCAP 05:025. https://doi.org/10.1088/1475-7516/2017/05/025. arXiv:1703.08215 [hep-ph]
Bodeker D, Buchmüller W, Fodor Z, Helbig T (1994) Aspects of the cosmological electroweak phase transition. Nucl Phys B 423:171–196. https://doi.org/10.1016/0550-3213(94)90569-X. arXiv:hep-ph/9311346
Boileau G, Christensen N, Meyer R, Cornish NJ (2021a) Spectral separation of the stochastic gravitational-wave background for LISA: observing both cosmological and astrophysical backgrounds. Phys Rev D 103(10):103529. https://doi.org/10.1103/PhysRevD.103.103529. arXiv:2011.05055 [gr-qc]
Boileau G, Lamberts A, Cornish NJ, Meyer R (2021b) Spectral separation of the stochastic gravitational-wave background for LISA in the context of a modulated Galactic foreground. Mon Not R Astron Soc 508(1):803–826. https://doi.org/10.1093/mnras/stab2575, [Erratum: Mon Not R Astron Soc 508, 5554–5555 (2021)]. arXiv:2105.04283 [gr-qc]
Boileau G, Jenkins AC, Sakellariadou M, Meyer R, Christensen N (2022) Ability of LISA to detect a gravitational-wave background of cosmological origin: the cosmic string case. Phys Rev D 105 (2):023510. https://doi.org/10.1103/PhysRevD.105.023510. arXiv:2109.06552 [gr-qc]
Bolliet B, Barrau A, Grain J, Schander S (2016) Observational exclusion of a consistent loop quantum cosmology scenario. Phys Rev D 93:124011. https://doi.org/10.1103/PhysRevD.93.124011. arXiv:1510.08766 [gr-qc]
Bond JR, Jaffe AH, Knox L (1998) Estimating the power spectrum of the cosmic microwave background. Phys Rev D 57:2117–2137. https://doi.org/10.1103/PhysRevD.57.2117. arXiv:astro-ph/9708203
Bonetti M, Sesana A, Haardt F, Barausse E, Colpi M (2019) Post-Newtonian evolution of massive black hole triplets in galactic nuclei—IV. Implications for LISA. Mon Not R Astron Soc 486(3):4044–4060. https://doi.org/10.1093/mnras/stz903. arXiv:1812.01011 [astro-ph.GA]

Bonilla A, D'Agostino R, Nunes RC, de Araujo JCN (2020) Forecasts on the speed of gravitational waves at high z. JCAP 03:015. https://doi.org/10.1088/1475-7516/2020/03/015. arXiv:1910.05631 [gr-qc]
Bonvin C, Durrer R (2011) What galaxy surveys really measure. Phys Rev D 84:063505. https://doi.org/10.1103/PhysRevD.84.063505. arXiv:1105.5280 [astro-ph.CO]
Bonvin C, Durrer R, Gasparini MA (2006a) Fluctuations of the luminosity distance. Phys Rev D 73:023523. https://doi.org/10.1103/PhysRevD.85.029901, [Erratum: Phys. Rev. D 85, 029901 (2012)]. arXiv:astro-ph/0511183
Bonvin C, Durrer R, Kunz M (2006b) The dipole of the luminosity distance: a direct measure of H(z). Phys Rev Lett 96:191302. https://doi.org/10.1103/PhysRevLett.96.191302. arXiv:astro-ph/0603240
Bonvin C, Caprini C, Sturani R, Tamanini N (2017) Effect of matter structure on the gravitational waveform. Phys Rev D 95(4):044029. https://doi.org/10.1103/PhysRevD.95.044029. arXiv:1609.08093 [astro-ph.CO]
Bordin L, Cabass G (2020) Graviton non-Gaussianities and parity violation in the EFT of inflation. JCAP 07:014. https://doi.org/10.1088/1475-7516/2020/07/014. arXiv:2004.00619 [astro-ph.CO]
Bordin L, Creminelli P, Khmelnitsky A, Senatore L (2018) Light particles with spin in inflation. JCAP 10:013. https://doi.org/10.1088/1475-7516/2018/10/013. arXiv:1806.10587 [hep-th]
Boyle LA, Buonanno A (2008) Relating gravitational wave constraints from primordial nucleosynthesis, pulsar timing, laser interferometers, and the CMB: Implications for the early Universe. Phys Rev D 78:043531. https://doi.org/10.1103/PhysRevD.78.043531. arXiv:0708.2279 [astro-ph]
Boyle LA, Steinhardt PJ (2008) Probing the early universe with inflationary gravitational waves. Phys Rev D 77:063504. https://doi.org/10.1103/PhysRevD.77.063504. arXiv:astro-ph/0512014
Boyle LA, Steinhardt PJ, Turok N (2004) The Cosmic gravitational wave background in a cyclic universe. Phys Rev D 69:127302. https://doi.org/10.1103/PhysRevD.69.127302. arXiv:hep-th/0307170
Braaten E, Nieto A (1995) Effective field theory approach to high temperature thermodynamics. Phys Rev D 51:6990–7006. https://doi.org/10.1103/PhysRevD.51.6990. arXiv:hep-ph/9501375
Braglia M, Kuroyanagi S (2021) Probing prerecombination physics by the cross-correlation of stochastic gravitational waves and CMB anisotropies. Phys Rev D 104(12):123547. https://doi.org/10.1103/PhysRevD.104.123547. arXiv:2106.03786 [astro-ph.CO]
Braglia M, Hazra DK, Finelli F, Smoot GF, Sriramkumar L, Starobinsky AA (2020) Generating PBHs and small-scale GWs in two-field models of inflation. JCAP 08:001. https://doi.org/10.1088/1475-7516/2020/08/001. arXiv:2005.02895 [astro-ph.CO]
Braglia M, Chen X, Hazra DK (2021) Probing primordial features with the stochastic gravitational wave background. JCAP 03:005. https://doi.org/10.1088/1475-7516/2021/03/005. arXiv:2012.05821 [astro-ph.CO]
Brahma S, Nelson E, Shandera S (2014) Fossilized gravitational wave relic and primordial clocks. Phys Rev D 89(2):023507. https://doi.org/10.1103/PhysRevD.89.023507. arXiv:1310.0471 [astro-ph.CO]
Brandenberger RH (1987) On the decay of cosmic string loops. Nucl Phys B 293:812–828. https://doi.org/10.1016/0550-3213(87)90092-7
Brandenburg A, Enqvist K, Olesen P (1996) Large scale magnetic fields from hydromagnetic turbulence in the very early universe. Phys Rev D 54:1291–1300. https://doi.org/10.1103/PhysRevD.54.1291. arXiv:astro-ph/9602031
Brandenburg A, Kahniashvili T, Mandal S, Roper Pol A, Tevzadze AG, Vachaspati T (2017) Evolution of hydromagnetic turbulence from the electroweak phase transition. Phys Rev D 96(12):123528. https://doi.org/10.1103/PhysRevD.96.123528. arXiv:1711.03804 [astro-ph.CO]
Brandenburg A, Kahniashvili T, Mandal S, Roper Pol A, Tevzadze AG, Vachaspati T (2019) The dynamo effect in decaying helical turbulence. Phys Rev Fluids 4:024608. https://doi.org/10.1103/PhysRevFluids.4.024608. arXiv:1710.01628 [physics.flu-dyn]
Brax P, Burrage C, Davis AC (2016) The speed of Galileon gravity. JCAP 03:004. https://doi.org/10.1088/1475-7516/2016/03/004. arXiv:1510.03701 [gr-qc]
Brax P, Heisenberg L, Kuntz A (2020) Unveiling the Galileon in a three-body system: scalar and gravitational wave production. JCAP 05:012. https://doi.org/10.1088/1475-7516/2020/05/012. arXiv:2002.12590 [gr-qc]
Brdar V, Graf L, Helmboldt AJ, Xu XJ (2019a) Gravitational waves as a probe of left-right symmetry breaking. JCAP 12:027. https://doi.org/10.1088/1475-7516/2019/12/027. arXiv:1909.02018 [hep-ph]
Brdar V, Helmboldt AJ, Kubo J (2019b) Gravitational waves from first-order phase transitions: LIGO as a window to unexplored seesaw scales. JCAP 02:021. https://doi.org/10.1088/1475-7516/2019/02/021. arXiv:1810.12306 [hep-ph]

Breitbach M, Kopp J, Madge E, Opferkuch T, Schwaller P (2019) Dark, cold, and noisy: constraining secluded hidden sectors with gravitational waves. JCAP 07:007. https://doi.org/10.1088/1475-7516/2019/07/007. arXiv:1811.11175 [hep-ph]

Brinckmann T, Lesgourgues J (2019) MontePython 3: boosted MCMC sampler and other features. Phys Dark Universe 24:100260. https://doi.org/10.1016/j.dark.2018.100260. arXiv:1804.07261 [astro-ph.CO]

Bruggisser S, Von Harling B, Matsedonskyi O, Servant G (2018a) Baryon asymmetry from a composite Higgs Boson. Phys Rev Lett 121(13):131801. https://doi.org/10.1103/PhysRevLett.121.131801. arXiv:1803.08546 [hep-ph]

Bruggisser S, Von Harling B, Matsedonskyi O, Servant G (2018b) Electroweak phase transition and baryogenesis in composite Higgs models. JHEP 12:099. https://doi.org/10.1007/JHEP12(2018)099. arXiv:1804.07314 [hep-ph]

Buchmüller W (2021) Metastable strings and dumbbells in supersymmetric hybrid inflation. JHEP 04:168. https://doi.org/10.1007/JHEP04(2021)168. arXiv:2102.08923 [hep-ph]

Buchmüller W, Domcke V, Kamada K, Schmitz K (2013) The gravitational wave spectrum from cosmological $B-L$ breaking. JCAP 10:003. https://doi.org/10.1088/1475-7516/2013/10/003. arXiv:1305.3392 [hep-ph]

Buchmüller W, Domcke V, Murayama H, Schmitz K (2020a) Probing the scale of grand unification with gravitational waves. Phys Lett B 809:135764. https://doi.org/10.1016/j.physletb.2020.135764. arXiv:1912.03695 [hep-ph]

Buchmüller W, Domcke V, Schmitz K (2020b) From NANOGrav to LIGO with metastable cosmic strings. Phys Lett B 811:135914. https://doi.org/10.1016/j.physletb.2020.135914. arXiv:2009.10649 [astro-ph.CO]

Bugaev E, Klimai P (2010) Induced gravitational wave background and primordial black holes. Phys Rev D 81:023517. https://doi.org/10.1103/PhysRevD.81.023517. arXiv:0908.0664 [astro-ph.CO]

Bugaev E, Klimai P (2014) Axion inflation with gauge field production and primordial black holes. Phys Rev D 90(10):103501. https://doi.org/10.1103/PhysRevD.90.103501. arXiv:1312.7435 [astro-ph.CO]

Bunk D, Hubisz J, Jain B (2018) A perturbative RS I cosmological phase transition. Eur Phys J C 78(1):78. https://doi.org/10.1140/epjc/s10052-018-5529-2. arXiv:1705.00001 [hep-ph]

Burden CJ (1985) Gravitational radiation from a particular class of cosmic strings. Phys Lett B 164:277–281. https://doi.org/10.1016/0370-2693(85)90326-0

Burke-Spolaor S et al (2019) The astrophysics of nanohertz gravitational waves. Astron Astrophys Rev 27(1):5. https://doi.org/10.1007/s00159-019-0115-7. arXiv:1811.08826 [astro-ph.HE]

Buschmann M, Foster JW, Safdi BR (2020) Early-universe simulations of the cosmological axion. Phys Rev Lett 124(16):161103. https://doi.org/10.1103/PhysRevLett.124.161103. arXiv:1906.00967 [astro-ph.CO]

Buscicchio R, Moore CJ, Pratten G, Schmidt P, Bianconi M, Vecchio A (2020) Constraining the lensing of binary black holes from their stochastic background. Phys Rev Lett 125(14):141102. https://doi.org/10.1103/PhysRevLett.125.141102. arXiv:2006.04516 [astro-ph.CO]

Byrnes CT, Copeland EJ, Green AM (2012) Primordial black holes as a tool for constraining non-Gaussianity. Phys Rev D 86:043512. https://doi.org/10.1103/PhysRevD.86.043512. arXiv:1206.4188 [astro-ph.CO]

Byrnes CT, Hindmarsh M, Young S, Hawkins MRS (2018) Primordial black holes with an accurate QCD equation of state. JCAP 08:041. https://doi.org/10.1088/1475-7516/2018/08/041. arXiv:1801.06138 [astro-ph.CO]

Byrnes CT, Cole PS, Patil SP (2019) Steepest growth of the power spectrum and primordial black holes. JCAP 06:028. https://doi.org/10.1088/1475-7516/2019/06/028. arXiv:1811.11158 [astro-ph.CO]

Cai RG, Yang T (2017) Estimating cosmological parameters by the simulated data of gravitational waves from the Einstein Telescope. Phys Rev D 95(4):044024. https://doi.org/10.1103/PhysRevD.95.044024. arXiv:1608.08008 [astro-ph.CO]

Cai RG, Tamanini N, Yang T (2017) Reconstructing the dark sector interaction with LISA. JCAP 05:031. https://doi.org/10.1088/1475-7516/2017/05/031. arXiv:1703.07323 [astro-ph.CO]

Cai RG, Liu TB, Liu XW, Wang SJ, Yang T (2018) Probing cosmic anisotropy with gravitational waves as standard sirens. Phys Rev D 97(10):103005. https://doi.org/10.1103/PhysRevD.97.103005. arXiv:1712.00952 [astro-ph.CO]

Cai RG, Pi S, Sasaki M (2019a) Gravitational waves induced by non-Gaussian scalar perturbations. Phys Rev Lett 122(20):201101. https://doi.org/10.1103/PhysRevLett.122.201101. arXiv:1810.11000 [astro-ph.CO]

Cai RG, Pi S, Wang SJ, Yang XY (2019b) Pulsar timing array constraints on the induced gravitational waves. JCAP 10:059. https://doi.org/10.1088/1475-7516/2019/10/059. arXiv:1907.06372 [astro-ph.CO]

Cai RG, Pi S, Wang SJ, Yang XY (2019c) Resonant multiple peaks in the induced gravitational waves. JCAP 05:013. https://doi.org/10.1088/1475-7516/2019/05/013. arXiv:1901.10152 [astro-ph.CO]

Cai RG, Pi S, Sasaki M (2020) Universal infrared scaling of gravitational wave background spectra. Phys Rev D 102(8):083528. https://doi.org/10.1103/PhysRevD.102.083528. arXiv:1909.13728 [astro-ph.CO]

Calcagni G (2020) Next step in gravity and cosmology: fundamental theory or data-driven models? Front Astron Space Sci 7:52. https://doi.org/10.3389/fspas.2020.00052. arXiv:2009.00846 [gr-qc]

Calcagni G, Kuroyanagi S (2021) Stochastic gravitational-wave background in quantum gravity. JCAP 03:019. https://doi.org/10.1088/1475-7516/2021/03/019. arXiv:2012.00170 [gr-qc]

Calcagni G, Kuroyanagi S, Marsat S, Sakellariadou M, Tamanini N, Tasinato G (2019a) Gravitational-wave luminosity distance in quantum gravity. Phys Lett B 798:135000. https://doi.org/10.1016/j.physletb.2019.135000. arXiv:1904.00384 [gr-qc]

Calcagni G, Kuroyanagi S, Marsat S, Sakellariadou M, Tamanini N, Tasinato G (2019b) Quantum gravity and gravitational-wave astronomy. JCAP 10:012. https://doi.org/10.1088/1475-7516/2019/10/012. arXiv:1907.02489 [gr-qc]

Calchi Novati S, Mirzoyan S, Jetzer P, Scarpetta G (2013) Microlensing towards the SMC: a new analysis of OGLE and EROS results. Mon Not R Astron Soc 435:1582. https://doi.org/10.1093/mnras/stt1402. arXiv:1308.4281 [astro-ph.GA]

Caldwell RR, Allen B (1992) Cosmological constraints on cosmic string gravitational radiation. Phys Rev D 45:3447–3468. https://doi.org/10.1103/PhysRevD.45.3447

Caldwell RR, Devulder C (2018) Axion Gauge field inflation and gravitational Leptogenesis: a lower bound on B modes from the matter–antimatter asymmetry of the universe. Phys Rev D 97(2):023532. https://doi.org/10.1103/PhysRevD.97.023532. arXiv:1706.03765 [astro-ph.CO]

Caldwell RR, Devulder C (2019) Gravitational wave opacity from Gauge field dark energy. Phys Rev D 100(10):103510. https://doi.org/10.1103/PhysRevD.100.103510. arXiv:1802.07371 [gr-qc]

Caldwell RR, Devulder C, Maksimova NA (2016) Gravitational wave-Gauge field oscillations. Phys Rev D 94(6):063005. https://doi.org/10.1103/PhysRevD.94.063005. arXiv:1604.08939 [gr-qc]

Caldwell RR, Smith TL, Walker DGE (2019) Using a primordial gravitational wave background to illuminate new physics. Phys Rev D 100(4):043513. https://doi.org/10.1103/PhysRevD.100.043513. arXiv:1812.07577 [astro-ph.CO]

Callister T, Fishbach M, Holz D, Farr W (2020) Shouts and murmurs: combining individual gravitational-wave sources with the stochastic background to measure the history of binary black hole mergers. Astrophys J Lett 896(2):L32. https://doi.org/10.3847/2041-8213/ab9743. arXiv:2003.12152 [astro-ph.HE]

Camera S, Nishizawa A (2013) Beyond concordance cosmology with magnification of gravitational-wave standard sirens. Phys Rev Lett 110(15):151103. https://doi.org/10.1103/PhysRevLett.110.151103. arXiv:1303.5446 [astro-ph.CO]

Campeti P, Komatsu E, Poletti D, Baccigalupi C (2021) Measuring the spectrum of primordial gravitational waves with CMB, PTA and laser interferometers. JCAP 01:012. https://doi.org/10.1088/1475-7516/2021/01/012. arXiv:2007.04241 [astro-ph.CO]

Cañas Herrera G, Contigiani O, Vardanyan V (2020) Cross-correlation of the astrophysical gravitational-wave background with galaxy clustering. Phys Rev D 102(4):043513. https://doi.org/10.1103/PhysRevD.102.043513. arXiv:1910.08353 [astro-ph.CO]

Cannone D, Gong JO, Tasinato G (2015a) Breaking discrete symmetries in the effective field theory of inflation. JCAP 08:003. https://doi.org/10.1088/1475-7516/2015/08/003. arXiv:1505.05773 [hep-th]

Cannone D, Tasinato G, Wands D (2015b) Generalised tensor fluctuations and inflation. JCAP 01:029. https://doi.org/10.1088/1475-7516/2015/01/029. arXiv:1409.6568 [astro-ph.CO]

Cao L, Lu Y, Zhao Y (2018) Host galaxy properties of mergers of stellar binary black holes and their implications for advanced LIGO gravitational wave sources. Mon Not R Astron Soc 474(4):4997–5007. https://doi.org/10.1093/mnras/stx3087. arXiv:1711.09190 [astro-ph.GA]

Caprini C, Durrer R (2006) Gravitational waves from stochastic relativistic sources: primordial turbulence and magnetic fields. Phys Rev D 74:063521. https://doi.org/10.1103/PhysRevD.74.063521. arXiv:astro-ph/0603476

Caprini C, Figueroa DG (2018) Cosmological backgrounds of gravitational waves. Class Quantum Grav 35(16):163001. https://doi.org/10.1088/1361-6382/aac608. arXiv:1801.04268 [astro-ph.CO]

Caprini C, Tamanini N (2016) Constraining early and interacting dark energy with gravitational wave standard sirens: the potential of the eLISA mission. JCAP 10:006. https://doi.org/10.1088/1475-7516/2016/10/006. arXiv:1607.08755 [astro-ph.CO]

Caprini C, Durrer R, Konstandin T, Servant G (2009a) General properties of the gravitational wave spectrum from phase transitions. Phys Rev D 79:083519. https://doi.org/10.1103/PhysRevD.79.083519. arXiv:0901.1661 [astro-ph.CO]

Caprini C, Durrer R, Servant G (2009b) The stochastic gravitational wave background from turbulence and magnetic fields generated by a first-order phase transition. JCAP 12:024. https://doi.org/10.1088/1475-7516/2009/12/024. arXiv:0909.0622 [astro-ph.CO]

Caprini C, Figueroa DG, Flauger R, Nardini G, Peloso M, Pieroni M, Ricciardone A, Tasinato G (2019) Reconstructing the spectral shape of a stochastic gravitational wave background with LISA. JCAP 11:017. https://doi.org/10.1088/1475-7516/2019/11/017. arXiv:1906.09244 [astro-ph.CO]

Caprini C et al (2016) Science with the space-based interferometer eLISA. II: Gravitational waves from cosmological phase transitions. JCAP 04:001. https://doi.org/10.1088/1475-7516/2016/04/001. arXiv:1512.06239 [astro-ph.CO]

Caprini C et al (2020) Detecting gravitational waves from cosmological phase transitions with LISA: an update. JCAP 03:024. https://doi.org/10.1088/1475-7516/2020/03/024. arXiv:1910.13125 [astro-ph.CO]

Cardoso V, Duque F, Khanna G (2021) Gravitational tuning forks and hierarchical triple systems. Phys Rev D 103(8):L081501. https://doi.org/10.1103/PhysRevD.103.L081501. arXiv:2101.01186 [gr-qc]

Carena M, Quirós M, Zhang Y (2019) Electroweak baryogenesis from dark-sector CP violation. Phys Rev Lett 122(20):201802. https://doi.org/10.1103/PhysRevLett.122.201802. arXiv:1811.09719 [hep-ph]

Carena M, Quirós M, Zhang Y (2020) Dark CP violation and gauged lepton or baryon number for electroweak baryogenesis. Phys Rev D 101(5):055014. https://doi.org/10.1103/PhysRevD.101.055014. arXiv:1908.04818 [hep-ph]

Carena M, Krause C, Liu Z, Wang Y (2021) New approach to electroweak symmetry nonrestoration. Phys Rev D 104(5):055016. https://doi.org/10.1103/PhysRevD.104.055016. arXiv:2104.00638 [hep-ph]

Carr B, Kuhnel F (2020) Primordial black holes as dark matter: recent developments. Annu Rev Nucl Part Sci 70:355–394. https://doi.org/10.1146/annurev-nucl-050520-125911. arXiv:2006.02838 [astro-ph.CO]

Carr B, Clesse S, García-Bellido J (2021a) Primordial black holes from the QCD epoch: linking dark matter, baryogenesis and anthropic selection. Mon Not R Astron Soc 501(1):1426–1439. https://doi.org/10.1093/mnras/staa3726. arXiv:1904.02129 [astro-ph.CO]

Carr B, Clesse S, García-Bellido J, Kühnel F (2021b) Cosmic conundra explained by thermal history and primordial black holes. Phys Dark Universe 31:100755. https://doi.org/10.1016/j.dark.2020.100755. arXiv:1906.08217 [astro-ph.CO]

Carr B, Kohri K, Sendouda Y, Yokoyama J (2021c) Constraints on primordial black holes. Rep Prog Phys 84(11):116902. https://doi.org/10.1088/1361-6633/ac1e31. arXiv:2002.12778 [astro-ph.CO]

Carr BJ (1975) The Primordial black hole mass spectrum. Astrophys J 201:1–19. https://doi.org/10.1086/153853

Carr BJ, Hawking SW (1974) Black holes in the early Universe. Mon Not R Astron Soc 168:399–415. https://doi.org/10.1093/mnras/168.2.399

Carr BJ, Gilbert JH, Lidsey JE (1994) Black hole relics and inflation: limits on blue perturbation spectra. Phys Rev D 50:4853–4867. https://doi.org/10.1103/PhysRevD.50.4853. arXiv:astro-ph/9405027

Caves CM (1980) Gravitational radiation and the ultimate speed in Rosen's bimetric theory of gravity. Ann Phys 125:35–52. https://doi.org/10.1016/0003-4916(80)90117-7

Celoria M, Comelli D, Pilo L (2017) Fluids, superfluids and supersolids: dynamics and cosmology of self gravitating media. JCAP 09:036. https://doi.org/10.1088/1475-7516/2017/09/036. arXiv:1704.00322 [gr-qc]

Celoria M, Comelli D, Pilo L (2018) Sixth mode in massive gravity. Phys Rev D 98(6):064016. https://doi.org/10.1103/PhysRevD.98.064016. arXiv:1711.10424 [hep-th]

Celoria M, Comelli D, Pilo L, Rollo R (2021) Boosting GWs in supersolid inflation. JHEP 01:185. https://doi.org/10.1007/JHEP01(2021)185. arXiv:2010.02023 [gr-qc]

Cervero J, Jacobs L (1978) Classical Yang–Mills Fields in a Robertson-walker universe. Phys Lett B 78:427–429. https://doi.org/10.1016/0370-2693(78)90477-X

Chala M, Nardini G, Sobolev I (2016) Unified explanation for dark matter and electroweak baryogenesis with direct detection and gravitational wave signatures. Phys Rev D 94(5):055006. https://doi.org/10.1103/PhysRevD.94.055006. arXiv:1605.08663 [hep-ph]

Chala M, Krause C, Nardini G (2018) Signals of the electroweak phase transition at colliders and gravitational wave observatories. JHEP 07:062. https://doi.org/10.1007/JHEP07(2018)062. arXiv:1802.02168 [hep-ph]

Chala M, Khoze VV, Spannowsky M, Waite P (2019) Mapping the shape of the scalar potential with gravitational waves. Int J Mod Phys A 34(33):1950223. https://doi.org/10.1142/S0217751X19502233. arXiv:1905.00911 [hep-ph]

Chang CF, Cui Y (2020) Stochastic gravitational wave background from global cosmic strings. Phys Dark Universe 29:100604. https://doi.org/10.1016/j.dark.2020.100604. arXiv:1910.04781 [hep-ph]

Chapline GF (1975) Cosmological effects of primordial black holes. Nature 253(5489):251–252. https://doi.org/10.1038/253251a0

Charnock T, Avgoustidis A, Copeland EJ, Moss A (2016) CMB constraints on cosmic strings and superstrings. Phys Rev D 93(12):123503. https://doi.org/10.1103/PhysRevD.93.123503. arXiv:1603.01275 [astro-ph.CO]

Chatterjee A, Mazumdar A (2018) Observable tensor-to-scalar ratio and secondary gravitational wave background. Phys Rev D 97(6):063517. https://doi.org/10.1103/PhysRevD.97.063517. arXiv:1708.07293 [astro-ph.CO]

Chen HY (2020) Systematic uncertainty of standard sirens from the viewing angle of binary neutron star inspirals. Phys Rev Lett 125(20):201301. https://doi.org/10.1103/PhysRevLett.125.201301. arXiv:2006.02779 [astro-ph.HE]

Chen HY, Fishbach M, Holz DE (2018) A two per cent Hubble constant measurement from standard sirens within five years. Nature 562(7728):545–547. https://doi.org/10.1038/s41586-018-0606-0. arXiv:1712.06531 [astro-ph.CO]

Chen HY, Cowperthwaite PS, Metzger BD, Berger E (2021a) A program for multimessenger standard siren cosmology in the Era of LIGO A+, Rubin observatory, and beyond. Astrophys J Lett 908(1):L4. https://doi.org/10.3847/2041-8213/abdab0. arXiv:2011.01211 [astro-ph.CO]

Chen S et al (2021b) Common-red-signal analysis with 24-yr high-precision timing of the European Pulsar Timing Array: inferences in the stochastic gravitational-wave background search. Mon Not R Astron Soc 508(4):4970–4993. https://doi.org/10.1093/mnras/stab2833. arXiv:2110.13184 [astro-ph.HE]

Chen W, Buckley JH, Ferrer F (2015) Search for GeV γ-ray pair halos around low redshift blazars. Phys Rev Lett 115:211103. https://doi.org/10.1103/PhysRevLett.115.211103. arXiv:1410.7717 [astro-ph.HE]

Chen X (2010) Primordial non-Gaussianities from inflation models. Adv Astron 2010:638979. https://doi.org/10.1155/2010/638979. arXiv:1002.1416 [astro-ph.CO]

Chen ZC, Huang F, Huang QG (2019) Stochastic gravitational-wave background from binary black holes and binary neutron stars and implications for LISA. Astrophys J 871(1):97. https://doi.org/10.3847/1538-4357/aaf581. arXiv:1809.10360 [gr-qc]

Chen ZC, Yuan C, Huang QG (2020) Pulsar timing array constraints on primordial black holes with NANOGrav 11-year dataset. Phys Rev Lett 124(25):251101. https://doi.org/10.1103/PhysRevLett.124.251101. arXiv:1910.12239 [astro-ph.CO]

Chernoff DF, Tye SHH (2018) Detection of low tension cosmic superstrings. JCAP 05:002. https://doi.org/10.1088/1475-7516/2018/05/002. arXiv:1712.05060 [astro-ph.CO]

Chernoff DF, Flanagan EE, Wardell B (2019) Gravitational backreaction on a cosmic string: formalism. Phys Rev D 99(8):084036. https://doi.org/10.1103/PhysRevD.99.084036. arXiv:1808.08631 [gr-qc]

Cheung MHY, Gais J, Hannuksela OA, Li TGF (2021) Stellar-mass microlensing of gravitational waves. Mon Not R Astron Soc 503(3):3326–3336. https://doi.org/10.1093/mnras/stab579. arXiv:2012.07800 [astro-ph.HE]

Chevallier M, Polarski D (2001) Accelerating universes with scaling dark matter. Int J Mod Phys D 10:213–224. https://doi.org/10.1142/S0218271801000822. arXiv:gr-qc/0009008

Chiang CW, Lu BQ (2020) First-order electroweak phase transition in a complex singlet model with $\mathbb{Z}_3$ symmetry. JHEP 07:082. https://doi.org/10.1007/JHEP07(2020)082. arXiv:1912.12634 [hep-ph]

Chiang CW, Senaha E (2017) On gauge dependence of gravitational waves from a first-order phase transition in classical scale-invariant $U(1)'$ models. Phys Lett B 774:489–493. https://doi.org/10.1016/j.physletb.2017.09.064. arXiv:1707.06765 [hep-ph]

Chluba J, Hamann J, Patil SP (2015) Features and new physical scales in primordial observables: theory and observation. Int J Mod Phys D 24(10):1530023. https://doi.org/10.1142/S0218271815300232. arXiv:1505.01834 [astro-ph.CO]

Choi HG, Park C, Jung S (2021) Small-scale shear: peeling off diffuse subhalos with gravitational waves. Phys Rev D 104(6):063001. https://doi.org/10.1103/PhysRevD.104.063001. arXiv:2103.08618 [astro-ph.CO]

Choudhury SR, Joshi GC, Mahajan S, McKellar BHJ (2004) Probing large distance higher dimensional gravity from lensing data. Astropart Phys 21:559–563. https://doi.org/10.1016/j.astropartphys.2004.04.001. arXiv:hep-ph/0204161

Christensen N (1997) Optimal detection strategies for measuring the stochastic gravitational radiation background with laser interferometric antennas. Phys Rev D 55:448–454. https://doi.org/10.1103/PhysRevD.55.448

Christensen N, Meyer R (1998) Markov chain Monte Carlo methods for Bayesian gravitational radiation data analysis. Phys Rev D 58:082001. https://doi.org/10.1103/PhysRevD.58.082001

Christensson M, Hindmarsh M, Brandenburg A (2001) Inverse cascade in decaying 3-D magnetohydrodynamic turbulence. Phys Rev E 64:056405. https://doi.org/10.1103/PhysRevE.64.056405. arXiv:astro-ph/0011321

Chruslinska M, Belczynski K, Klencki J, Benacquista M (2018) Double neutron stars: merger rates revisited. Mon Not R Astron Soc 474(3):2937–2958. https://doi.org/10.1093/mnras/stx2923. arXiv:1708.07885 [astro-ph.HE]

Clarke TJ, Copeland EJ, Moss A (2020) Constraints on primordial gravitational waves from the Cosmic Microwave Background. JCAP 10:002. https://doi.org/10.1088/1475-7516/2020/10/002. arXiv:2004.11396 [astro-ph.CO]

Clesse S, García-Bellido J (2015) Massive primordial black holes from hybrid inflation as dark matter and the seeds of galaxies. Phys Rev D 92(2):023524. https://doi.org/10.1103/PhysRevD.92.023524. arXiv:1501.07565 [astro-ph.CO]

Clesse S, García-Bellido J (2017a) Detecting the gravitational wave background from primordial black hole dark matter. Phys Dark Universe 18:105–114. https://doi.org/10.1016/j.dark.2017.10.001. arXiv:1610.08479 [astro-ph.CO]

Clesse S, García-Bellido J (2017b) The clustering of massive primordial black holes as dark matter: measuring their mass distribution with Advanced LIGO. Phys Dark Universe 15:142–147. https://doi.org/10.1016/j.dark.2016.10.002. arXiv:1603.05234 [astro-ph.CO]

Clesse S, García-Bellido J (2018) Seven Hints for primordial black hole dark matter. Phys Dark Universe 22:137–146. https://doi.org/10.1016/j.dark.2018.08.004. arXiv:1711.10458 [astro-ph.CO]

Clesse S, García-Bellido J (2022) GW190425, GW190521 and GW190814: three candidate mergers of primordial black holes from the QCD epoch. Phys Dark Univ 38:101111. https://doi.org/10.1016/j.dark.2022.101111. arXiv:2007.06481 [astro-ph.CO]

Clesse S, García-Bellido J, Orani S (2018) Detecting the stochastic gravitational wave background from primordial black hole formation. arXiv e-prints arXiv:1812.11011 [astro-ph.CO]

Cline JM, Kainulainen K (2013) Electroweak baryogenesis and dark matter from a singlet Higgs. JCAP 01:012. https://doi.org/10.1088/1475-7516/2013/01/012. arXiv:1210.4196 [hep-ph]

Cline JM, Kainulainen K (2020) Electroweak baryogenesis at high bubble wall velocities. Phys Rev D 101(6):063525. https://doi.org/10.1103/PhysRevD.101.063525. arXiv:2001.00568 [hep-ph]

Cline JM, Kainulainen K, Tucker-Smith D (2017) Electroweak baryogenesis from a dark sector. Phys Rev D 95(11):115006. https://doi.org/10.1103/PhysRevD.95.115006. arXiv:1702.08909 [hep-ph]

Cline JM, Friedlander A, He DM, Kainulainen K, Laurent B, Tucker-Smith D (2021) Baryogenesis and gravity waves from a UV-completed electroweak phase transition. Phys Rev D 103(12):123529. https://doi.org/10.1103/PhysRevD.103.123529. arXiv:2102.12490 [hep-ph]

Co RT, Dunsky D, Fernandez N, Ghalsasi A, Hall LJ, Harigaya K, Shelton J (2022) Gravitational wave and CMB probes of axion kination. JHEP 09:116. https://doi.org/10.1007/JHEP09(2022)116. arXiv:2108.09299 [hep-ph]

Cohen AG, Kaplan DB, Nelson AE (1991) Spontaneous baryogenesis at the weak phase transition. Phys Lett B 263:86–92. https://doi.org/10.1016/0370-2693(91)91711-4

Coleman J (2019) Matter-wave atomic gradiometer InterferometricSensor (MAGIS-100) at Fermilab. PoS ICHEP2018:021. https://doi.org/10.22323/1.340.0021. arXiv:1812.00482 [physics.ins-det]

Congedo G, Taylor A (2019) Joint cosmological inference of standard sirens and gravitational wave weak lensing. Phys Rev D 99(8):083526. https://doi.org/10.1103/PhysRevD.99.083526. arXiv:1812.02730 [astro-ph.CO]

Contaldi CR (2017) Anisotropies of gravitational wave backgrounds: a line of sight approach. Phys Lett B 771:9–12. https://doi.org/10.1016/j.physletb.2017.05.020. arXiv:1609.08168 [astro-ph.CO]

Contaldi CR, Pieroni M, Renzini AI, Cusin G, Karnesis N, Peloso M, Ricciardone A, Tasinato G (2020) Maximum likelihood map-making with the Laser Interferometer Space Antenna. Phys Rev D 102 (4):043502. https://doi.org/10.1103/PhysRevD.102.043502. arXiv:2006.03313 [astro-ph.CO]

Contigiani O (2020) Lensing efficiency for gravitational wave mergers. Mon Not R Astron Soc 492 (3):3359–3363. https://doi.org/10.1093/mnras/staa026. arXiv:2001.01135 [astro-ph.CO]

Cook JL, Sorbo L (2012) Particle production during inflation and gravitational waves detectable by ground-based interferometers. Phys Rev D 85:023534. https://doi.org/10.1103/PhysRevD.85.023534, [Erratum: Phys Rev D 86, 069901 (2012)]. arXiv:1109.0022 [astro-ph.CO]

Copeland EJ, Haws D, Hindmarsh M (1990) Classical theory of radiating strings. Phys Rev D 42:726–730. https://doi.org/10.1103/PhysRevD.42.726

Copeland EJ, Liddle AR, Lyth DH, Stewart ED, Wands D (1994) False vacuum inflation with Einstein gravity. Phys Rev D 49:6410–6433. https://doi.org/10.1103/PhysRevD.49.6410. arXiv:astro-ph/9401011

Copeland EJ, Myers RC, Polchinski J (2004) Cosmic F and D strings. JHEP 06:013. https://doi.org/10.1088/1126-6708/2004/06/013. arXiv:hep-th/0312067

Copeland EJ, Kibble TWB, Steer DA (2006a) Collisions of strings with Y junctions. Phys Rev Lett 97:021602. https://doi.org/10.1103/PhysRevLett.97.021602. arXiv:hep-th/0601153

Copeland EJ, Sami M, Tsujikawa S (2006b) Dynamics of dark energy. Int J Mod Phys D 15:1753–1936. https://doi.org/10.1142/S021827180600942X. arXiv:hep-th/0603057

Copeland EJ, Kibble TWB, Steer DA (2007) Constraints on string networks with junctions. Phys Rev D 75:065024. https://doi.org/10.1103/PhysRevD.75.065024. arXiv:hep-th/0611243

Copeland EJ, Firouzjahi H, Kibble TWB, Steer DA (2008) On the collision of cosmic superstrings. Phys Rev D 77:063521. https://doi.org/10.1103/PhysRevD.77.063521. arXiv:0712.0808 [hep-th]

Corianò C, Frampton PH, Tatullo A (2020) Conformal unification in a quiver theory and gravitational waves. Phys Lett B 811:135909. https://doi.org/10.1016/j.physletb.2020.135909. arXiv:2005.12216 [hep-ph]

Cornish N, Blas D, Nardini G (2017) Bounding the speed of gravity with gravitational wave observations. Phys Rev Lett 119(16):161102. https://doi.org/10.1103/PhysRevLett.119.161102. arXiv:1707.06101 [gr-qc]

Cornish NJ (2001) Mapping the gravitational wave background. Class Quantum Grav 18:4277–4292. https://doi.org/10.1088/0264-9381/18/20/307. arXiv:astro-ph/0105374

Cornish NJ, Littenberg TB (2007) Tests of Bayesian model selection techniques for gravitational wave astronomy. Phys Rev D 76:083006. https://doi.org/10.1103/PhysRevD.76.083006. arXiv:0704.1808 [gr-qc]

Cornwall JM (1997) Speculations on primordial magnetic helicity. Phys Rev D 56:6146–6154. https://doi.org/10.1103/PhysRevD.56.6146. arXiv:hep-th/9704022

Craig N, Englert C, McCullough M (2013) New probe of naturalness. Phys Rev Lett 111(12):121803. https://doi.org/10.1103/PhysRevLett.111.121803. arXiv:1305.5251 [hep-ph]

Craig N, Lou HK, McCullough M, Thalapillil A (2016) The Higgs portal above threshold. JHEP 02:127. https://doi.org/10.1007/JHEP02(2016)127. arXiv:1412.0258 [hep-ph]

Creminelli P, Vernizzi F (2017) Dark energy after GW170817 and GRB170817A. Phys Rev Lett 119 (25):251302. https://doi.org/10.1103/PhysRevLett.119.251302. arXiv:1710.05877 [astro-ph.CO]

Creminelli P, Nicolis A, Rattazzi R (2002) Holography and the electroweak phase transition. JHEP 03:051. https://doi.org/10.1088/1126-6708/2002/03/051. arXiv:hep-th/0107141

Creminelli P, Lewandowski M, Tambalo G, Vernizzi F (2018) Gravitational wave decay into dark energy. JCAP 12:025. https://doi.org/10.1088/1475-7516/2018/12/025. arXiv:1809.03484 [astro-ph.CO]

Creminelli P, Tambalo G, Vernizzi F, Yingcharoenrat V (2019) Resonant decay of gravitational waves into dark energy. JCAP 10:072. https://doi.org/10.1088/1475-7516/2019/10/072. arXiv:1906.07015 [gr-qc]

Creminelli P, Loayza N, Serra F, Trincherini E, Trombetta LG (2020a) Hairy black-holes in shift-symmetric theories. JHEP 08:045. https://doi.org/10.1007/JHEP08(2020)045. arXiv:2004.02893 [hep-th]

Creminelli P, Tambalo G, Vernizzi F, Yingcharoenrat V (2020b) Dark-energy instabilities induced by gravitational waves. JCAP 05:002. https://doi.org/10.1088/1475-7516/2020/05/002. arXiv:1910.14035 [gr-qc]

Crisostomi M, Koyama K, Tasinato G (2016) Extended scalar–tensor theories of gravity. JCAP 04:044. https://doi.org/10.1088/1475-7516/2016/04/044. arXiv:1602.03119 [hep-th]

Crisostomi M, Noui K, Charmousis C, Langlois D (2018) Beyond lovelock gravity: higher derivative metric theories. Phys Rev D 97(4):044034. https://doi.org/10.1103/PhysRevD.97.044034. arXiv:1710.04531 [hep-th]

Crocker K, Mandic V, Regimbau T, Belczynski K, Gladysz W, Olive K, Prestegard T, Vangioni E (2015) Model of the stochastic gravitational-wave background due to core collapse to black holes. Phys Rev D 92(6):063005. https://doi.org/10.1103/PhysRevD.92.063005. arXiv:1506.02631 [gr-qc]

Crocker K, Prestegard T, Mandic V, Regimbau T, Olive K, Vangioni E (2017) Systematic study of the stochastic gravitational-wave background due to stellar core collapse. Phys Rev D 95(6):063015. https://doi.org/10.1103/PhysRevD.95.063015. arXiv:1701.02638 [astro-ph.CO]

Croon D, Sanz V, White G (2018) Model discrimination in gravitational wave spectra from dark phase transitions. JHEP 08:203. https://doi.org/10.1007/JHEP08(2018)203. arXiv:1806.02332 [hep-ph]

Croon D, Gonzalo TE, White G (2019a) Gravitational waves from a Pati-Salam phase transition. JHEP 02:083. https://doi.org/10.1007/JHEP02(2019)083. arXiv:1812.02747 [hep-ph]

Croon D, Houtz R, Sanz V (2019b) Dynamical axions and gravitational waves. JHEP 07:146. https://doi.org/10.1007/JHEP07(2019)146. arXiv:1904.10967 [hep-ph]

Croon D, Kusenko A, Mazumdar A, White G (2020) Solitosynthesis and gravitational waves. Phys Rev D 101(8):085010. https://doi.org/10.1103/PhysRevD.101.085010. arXiv:1910.09562 [hep-ph]

Croon D, Gould O, Schicho P, Tenkanen TVI, White G (2021) Theoretical uncertainties for cosmological first-order phase transitions. JHEP 04:055. https://doi.org/10.1007/JHEP04(2021)055. arXiv:2009.10080 [hep-ph]

Crowder J, Cornish N (2007) A solution to the galactic foreground problem for LISA. Phys Rev D 75:043008. https://doi.org/10.1103/PhysRevD.75.043008. arXiv:astro-ph/0611546

Crowder J, Cornish NJ (2005) Beyond LISA: exploring future gravitational wave missions. Phys Rev D 72:083005. https://doi.org/10.1103/PhysRevD.72.083005. arXiv:gr-qc/0506015

Crowder SG, Namba R, Mandic V, Mukohyama S, Peloso M (2013) Measurement of parity violation in the early universe using gravitational-wave detectors. Phys Lett B 726:66–71. https://doi.org/10.1016/j.physletb.2013.08.077. arXiv:1212.4165 [astro-ph.CO]

Csikor F, Fodor Z, Heitger J (1999) Endpoint of the hot electroweak phase transition. Phys Rev Lett 82:21–24. https://doi.org/10.1103/PhysRevLett.82.21. arXiv:hep-ph/9809291

Cui Y, Lewicki M, Morrissey DE, Wells JD (2018) Cosmic archaeology with gravitational waves from cosmic strings. Phys Rev D 97(12):123505. https://doi.org/10.1103/PhysRevD.97.123505. arXiv:1711.03104 [hep-ph]

Cui Y, Lewicki M, Morrissey DE, Wells JD (2019) Probing the pre-BBN universe with gravitational waves from cosmic strings. JHEP 01:081. https://doi.org/10.1007/JHEP01(2019)081. arXiv:1808.08968 [hep-ph]

Cui Y, Lewicki M, Morrissey DE (2020) Gravitational wave bursts as harbingers of cosmic strings diluted by inflation. Phys Rev Lett 125(21):211302. https://doi.org/10.1103/PhysRevLett.125.211302. arXiv:1912.08832 [hep-ph]

Cuissa JRC, Figueroa DG (2019) Lattice formulation of axion inflation. Application to preheating. JCAP 06:002. https://doi.org/10.1088/1475-7516/2019/06/002. arXiv:1812.03132 [astro-ph.CO]

Cusin G, Lagos M (2020) Gravitational wave propagation beyond geometric optics. Phys Rev D 101(4):044041. https://doi.org/10.1103/PhysRevD.101.044041. arXiv:1910.13326 [gr-qc]

Cusin G, Tamanini N (2021) Characterization of lensing selection effects for LISA massive black hole binary mergers. Mon Not R Astron Soc 504(3):3610–3618. https://doi.org/10.1093/mnras/stab1130. arXiv:2011.15109 [astro-ph.CO]

Cusin G, Pitrou C, Uzan JP (2017) Anisotropy of the astrophysical gravitational wave background: analytic expression of the angular power spectrum and correlation with cosmological observations. Phys Rev D 96(10):103019. https://doi.org/10.1103/PhysRevD.96.103019. arXiv:1704.06184 [astro-ph.CO]

Cusin G, Dvorkin I, Pitrou C, Uzan JP (2018a) First predictions of the angular power spectrum of the astrophysical gravitational wave background. Phys Rev Lett 120:231101. https://doi.org/10.1103/PhysRevLett.120.231101. arXiv:1803.03236 [astro-ph.CO]

Cusin G, Pitrou C, Uzan JP (2018b) The signal of the gravitational wave background and the angular correlation of its energy density. Phys Rev D 97(12):123527. https://doi.org/10.1103/PhysRevD.97.123527. arXiv:1711.11345 [astro-ph.CO]

Cusin G, Durrer R, Ferreira PG (2019a) Polarization of a stochastic gravitational wave background through diffusion by massive structures. Phys Rev D 99(2):023534. https://doi.org/10.1103/PhysRevD.99.023534. arXiv:1807.10620 [astro-ph.CO]

Cusin G, Dvorkin I, Pitrou C, Uzan JP (2019b) Properties of the stochastic astrophysical gravitational wave background: astrophysical sources dependencies. Phys Rev D 100(6):063004. https://doi.org/10.1103/PhysRevD.100.063004. arXiv:1904.07797 [astro-ph.CO]

Cusin G, Dvorkin I, Pitrou C, Uzan JP (2020) Stochastic gravitational wave background anisotropies in the mHz band: astrophysical dependencies. Mon Not R Astron Soc 493(1):L1–L5. https://doi.org/10.1093/mnrasl/slz182. arXiv:1904.07757 [astro-ph.CO]

Cutler C, Harms J (2006) BBO and the neutron-star-binary subtraction problem. Phys Rev D 73:042001. https://doi.org/10.1103/PhysRevD.73.042001. arXiv:gr-qc/0511092

Cutler C, Holz DE (2009) Ultra-high precision cosmology from gravitational waves. Phys Rev D 80:104009. https://doi.org/10.1103/PhysRevD.80.104009. arXiv:0906.3752 [astro-ph.CO]

Cutting D, Hindmarsh M, Weir DJ (2018) Gravitational waves from vacuum first-order phase transitions: from the envelope to the lattice. Phys Rev D 97(12):123513. https://doi.org/10.1103/PhysRevD.97.123513. arXiv:1802.05712 [astro-ph.CO]

Cutting D, Hindmarsh M, Weir DJ (2020) Vorticity, kinetic energy, and suppressed gravitational wave production in strong first order phase transitions. Phys Rev Lett 125(2):021302. https://doi.org/10.1103/PhysRevLett.125.021302. arXiv:1906.00480 [hep-ph]

Cutting D, Escartin EG, Hindmarsh M, Weir DJ (2021) Gravitational waves from vacuum first order phase transitions II: from thin to thick walls. Phys Rev D 103(2):023531. https://doi.org/10.1103/PhysRevD.103.023531. arXiv:2005.13537 [astro-ph.CO]

Cyburt RH, Fields BD, Olive KA, Yeh TH (2016) Big Bang Nucleosynthesis: 2015. Rev Mod Phys 88:015004. https://doi.org/10.1103/RevModPhys.88.015004. arXiv:1505.01076 [astro-ph.CO]

Dabholkar A, Quashnock JM (1990) Pinning down the axion. Nucl Phys B 333:815–832. https://doi.org/10.1016/0550-3213(90)90140-9

Dai L, Venumadhav T (2017) On the waveforms of gravitationally lensed gravitational waves. arXiv e-prints arXiv:1702.04724 [gr-qc]

Dai L, Jeong D, Kamionkowski M (2013) Anisotropic imprint of long-wavelength tensor perturbations on cosmic structure. Phys Rev D 88(4):043507. https://doi.org/10.1103/PhysRevD.88.043507. arXiv:1306.3985 [astro-ph.CO]

Dai L, Venumadhav T, Sigurdson K (2017) Effect of lensing magnification on the apparent distribution of black hole mergers. Phys Rev D 95(4):044011. https://doi.org/10.1103/PhysRevD.95.044011. arXiv:1605.09398 [astro-ph.CO]

Dai L, Li SS, Zackay B, Mao S, Lu Y (2018) Detecting lensing-induced diffraction in astrophysical gravitational waves. Phys Rev D 98(10):104029. https://doi.org/10.1103/PhysRevD.98.104029. arXiv:1810.00003 [gr-qc]

Dal Canton T, Mangiagli A, Noble SC, Schnittman J, Ptak A, Klein A, Sesana A, Camp J (2019) Detectability of modulated X-rays from LISA's supermassive black hole mergers. Astrophys J 886:146. https://doi.org/10.3847/1538-4357/ab505a. arXiv:1902.01538 [astro-ph.HE]

Dalang C, Fleury P, Lombriser L (2020) Horndeski gravity and standard sirens. Phys Rev D 102(4):044036. https://doi.org/10.1103/PhysRevD.102.044036. arXiv:1912.06117 [gr-qc]

Dalang C, Fleury P, Lombriser L (2021) Scalar and tensor gravitational waves. Phys Rev D 103(6):064075. https://doi.org/10.1103/PhysRevD.103.064075. arXiv:2009.11827 [gr-qc]

Dall'Agata G (2018) Chromo-natural inflation in supergravity. Phys Lett B 782:139–142. https://doi.org/10.1016/j.physletb.2018.05.020. arXiv:1804.03104 [hep-th]

Damour T, Vilenkin A (1997) Cosmic strings and the string dilaton. Phys Rev Lett 78:2288–2291. https://doi.org/10.1103/PhysRevLett.78.2288. arXiv:gr-qc/9610005

Damour T, Vilenkin A (2000) Gravitational wave bursts from cosmic strings. Phys Rev Lett 85:3761–3764. https://doi.org/10.1103/PhysRevLett.85.3761. arXiv:gr-qc/0004075

Damour T, Vilenkin A (2001) Gravitational wave bursts from cusps and kinks on cosmic strings. Phys Rev D 64:064008. https://doi.org/10.1103/PhysRevD.64.064008. arXiv:gr-qc/0104026

Dapor A, Liegener K (2020) Modifications to gravitational wave equation from canonical quantum gravity. Eur Phys J C 80(8):741. https://doi.org/10.1140/epjc/s10052-020-8333-8. arXiv:2002.00834 [gr-qc]

Dar F, De Rham C, Deskins JT, Giblin JT, Tolley AJ (2019) Scalar gravitational radiation from binaries: vainshtein mechanism in time-dependent systems. Class Quantum Grav 36(2):025008. https://doi.org/10.1088/1361-6382/aaf5e8. arXiv:1808.02165 [hep-th]

Darian BK, Kunzle HP (1997) Cosmological Einstein Yang–Mills equations. J Math Phys 38:4696–4713. https://doi.org/10.1063/1.532116. arXiv:gr-qc/9610026

D'Ascoli S, Noble SC, Bowen DB, Campanelli M, Krolik JH, Mewes V (2018) Electromagnetic emission from supermassive binary black holes approaching merger. Astrophys J 865(2):140. https://doi.org/10.3847/1538-4357/aad8b4. arXiv:1806.05697 [astro-ph.HE]

Davelaar J, Haiman Z (2022a) Self-lensing flares from black hole binaries: general-relativistic ray tracing of black hole binaries. Phys Rev D 105(10):103010. https://doi.org/10.1103/PhysRevD.105.103010. arXiv:2112.05828 [astro-ph.HE]

Davelaar J, Haiman Z (2022b) Self-lensing flares from black hole binaries: observing black hole shadows via light curve tomography. Phys Rev Lett 128(19):191101. https://doi.org/10.1103/PhysRevLett.128.191101. arXiv:2112.05829 [astro-ph.HE]

Daverio D, Hindmarsh M, Kunz M, Lizarraga J, Urrestilla J (2016) Energy-momentum correlations for Abelian Higgs cosmic strings. Phys Rev D 93(8):085014. https://doi.org/10.1103/PhysRevD.95.049903, [Erratum: Phys.Rev.D 95, 049903 (2017)]. arXiv:1510.05006 [astro-ph.CO]

Davies AT, Froggatt CD, Moorhouse RG (1996) Electroweak baryogenesis in the next-to-minimal supersymmetric model. Phys Lett B 372:88–94. https://doi.org/10.1016/0370-2693(96)00076-7. arXiv:hep-ph/9603388

Davis RL, Shellard EPS (1989) Do axions need inflation? Nucl Phys B 324:167–186. https://doi.org/10.1016/0550-3213(89)90187-9

Davoudiasl H (2019) LIGO/Virgo black holes from a first order quark confinement phase transition. Phys Rev Lett 123(10):101102. https://doi.org/10.1103/PhysRevLett.123.101102. arXiv:1902.07805 [hep-ph]

De Curtis S, Delle Rose L, Panico G (2019) Composite dynamics in the early universe. JHEP 12:149. https://doi.org/10.1007/JHEP12(2019)149. arXiv:1909.07894 [hep-ph]

De Luca V, Desjacques V, Franciolini G, Malhotra A, Riotto A (2019) The initial spin probability distribution of primordial black holes. JCAP 05:018. https://doi.org/10.1088/1475-7516/2019/05/018. arXiv:1903.01179 [astro-ph.CO]

De Luca V, Franciolini G, Kehagias A, Peloso M, Riotto A, Ünal C (2019) The ineludible non-Gaussianity of the primordial black hole abundance. JCAP 07:048. https://doi.org/10.1088/1475-7516/2019/07/048. arXiv:1904.00970 [astro-ph.CO]

De Luca V, Desjacques V, Franciolini G, Riotto A (2020a) The clustering evolution of primordial black holes. JCAP 11:028. https://doi.org/10.1088/1475-7516/2020/11/028. arXiv:2009.04731 [astro-ph.CO]

De Luca V, Franciolini G, Pani P, Riotto A (2020b) Constraints on primordial black holes: the importance of accretion. Phys Rev D 102(4):043505. https://doi.org/10.1103/PhysRevD.102.043505. arXiv:2003.12589 [astro-ph.CO]

De Luca V, Franciolini G, Pani P, Riotto A (2020c) Primordial black holes confront LIGO/Virgo data: current situation. JCAP 06:044. https://doi.org/10.1088/1475-7516/2020/06/044. arXiv:2005.05641 [astro-ph.CO]

De Luca V, Franciolini G, Pani P, Riotto A (2020d) The evolution of primordial black holes and their final observable spins. JCAP 04:052. https://doi.org/10.1088/1475-7516/2020/04/052. arXiv:2003.02778 [astro-ph.CO]

De Luca V, Desjacques V, Franciolini G, Pani P, Riotto A (2021a) GW190521 mass gap event and the primordial black hole scenario. Phys Rev Lett 126(5):051101. https://doi.org/10.1103/PhysRevLett.126.051101. arXiv:2009.01728 [astro-ph.CO]

De Luca V, Franciolini G, Riotto A (2021b) NANOGrav data hints at primordial black holes as dark matter. Phys Rev Lett 126(4):041303. https://doi.org/10.1103/PhysRevLett.126.041303. arXiv:2009.08268 [astro-ph.CO]

Deffayet C, Pujolas O, Sawicki I, Vikman A (2010) Imperfect dark energy from kinetic gravity braiding. JCAP 10:026. https://doi.org/10.1088/1475-7516/2010/10/026. arXiv:1008.0048 [hep-th]

Deffayet C, Gao X, Steer DA, Zahariade G (2011) From k-essence to generalised Galileons. Phys Rev D 84:064039. https://doi.org/10.1103/PhysRevD.84.064039. arXiv:1103.3260 [hep-th]

Del Pozzo W, Sesana A, Klein A (2018) Stellar binary black holes in the LISA band: a new class of standard sirens. Mon Not R Astron Soc 475(3):3485–3492. https://doi.org/10.1093/mnras/sty057. arXiv:1703.01300 [astro-ph.CO]

Delaunay C, Grojean C, Wells JD (2008) Dynamics of non-renormalizable electroweak symmetry breaking. JHEP 04:029. https://doi.org/10.1088/1126-6708/2008/04/029. arXiv:0711.2511 [hep-ph]

Demidov SV, Gorbunov DS, Kirpichnikov DV (2018) Gravitational waves from phase transition in split NMSSM. Phys Lett B 779:191–194. https://doi.org/10.1016/j.physletb.2018.02.007. arXiv:1712.00087 [hep-ph]

Deng H, Vilenkin A (2017) Primordial black hole formation by vacuum bubbles. JCAP 12:044. https://doi.org/10.1088/1475-7516/2017/12/044. arXiv:1710.02865 [gr-qc]
Deng H, Garriga J, Vilenkin A (2017) Primordial black hole and wormhole formation by domain walls. JCAP 04:050. https://doi.org/10.1088/1475-7516/2017/04/050. arXiv:1612.03753 [gr-qc]
DePies MR, Hogan CJ (2007) Stochastic gravitational wave background from light cosmic strings. Phys Rev D 75:125006. https://doi.org/10.1103/PhysRevD.75.125006. arXiv:astro-ph/0702335
D'Eramo F, Schmitz K (2019) Imprint of a scalar era on the primordial spectrum of gravitational waves. Phys Rev Res 1:013010. https://doi.org/10.1103/PhysRevResearch.1.013010. arXiv:1904.07870 [hep-ph]
Deryagin DV, Grigoriev DY, Rubakov VA, Sazhin MV (1986) Possible anisotropic phases in the early universe and gravitational wave background. Mod Phys Lett A 1:593–600. https://doi.org/10.1142/S0217732386000750
de Rham C, Melville S (2018) Gravitational rainbows: LIGO and dark energy at its cutoff. Phys Rev Lett 121(22):221101. https://doi.org/10.1103/PhysRevLett.121.221101. arXiv:1806.09417 [hep-th]
de Rham C, Gabadadze G, Tolley AJ (2011) Resummation of massive gravity. Phys Rev Lett 106:231101. https://doi.org/10.1103/PhysRevLett.106.231101. arXiv:1011.1232 [hep-th]
Desjacques V, Riotto A (2018) Spatial clustering of primordial black holes. Phys Rev D 98(12):123533. https://doi.org/10.1103/PhysRevD.98.123533. arXiv:1806.10414 [astro-ph.CO]
Desvignes G et al (2016) High-precision timing of 42 millisecond pulsars with the European Pulsar Timing Array. Mon Not R Astron Soc 458(3):3341–3380. https://doi.org/10.1093/mnras/stw483. arXiv:1602.08511 [astro-ph.HE]
Dev PSB, Ferrer F, Zhang Y, Zhang Y (2019) Gravitational waves from first-order phase transition in a simple axion-like particle model. JCAP 11:006. https://doi.org/10.1088/1475-7516/2019/11/006. arXiv:1905.00891 [hep-ph]
Dewdney PE, Hall PJ, Schilizzi RT, Lazio TJLW (2009) The square kilometre array. Proc IEEE 97(8):1482–1496. https://doi.org/10.1109/JPROC.2009.2021005
Di Valentino E, Melchiorri A, Silk J (2016) Reconciling Planck with the local value of H_0 in extended parameter space. Phys Lett B 761:242–246. https://doi.org/10.1016/j.physletb.2016.08.043. arXiv:1606.00634 [astro-ph.CO]
Di Valentino E, Melchiorri A, Mena O (2017) Can interacting dark energy solve the H_0 tension? Phys Rev D 96(4):043503. https://doi.org/10.1103/PhysRevD.96.043503. arXiv:1704.08342 [astro-ph.CO]
Di Valentino E, Mena O, Pan S, Visinelli L, Yang W, Melchiorri A, Mota DF, Riess AG, Silk J (2021) In the realm of the Hubble tension—a review of solutions. Class Quantum Grav 38(15):153001. https://doi.org/10.1088/1361-6382/ac086d. arXiv:2103.01183 [astro-ph.CO]
Diego JM, Hannuksela OA, Kelly PL, Broadhurst T, Kim K, Li TGF, Smoot GF, Pagano G (2019) Observational signatures of microlensing in gravitational waves at LIGO/Virgo frequencies. Astron Astrophys 627:A130. https://doi.org/10.1051/0004-6361/201935490. arXiv:1903.04513 [astro-ph.CO]
Dimastrogiovanni E, Peloso M (2013) Stability analysis of chromo-natural inflation and possible evasion of Lyth's bound. Phys Rev D 87(10):103501. https://doi.org/10.1103/PhysRevD.87.103501. arXiv:1212.5184 [astro-ph.CO]
Dimastrogiovanni E, Fasiello M, Jeong D, Kamionkowski M (2014) Inflationary tensor fossils in large-scale structure. JCAP 12:050. https://doi.org/10.1088/1475-7516/2014/12/050. arXiv:1407.8204 [astro-ph.CO]
Dimastrogiovanni E, Fasiello M, Kamionkowski M (2016) Imprints of massive primordial fields on large-scale structure. JCAP 02:017. https://doi.org/10.1088/1475-7516/2016/02/017. arXiv:1504.05993 [astro-ph.CO]
Dimastrogiovanni E, Fasiello M, Fujita T (2017) Primordial gravitational waves from axion-gauge fields dynamics. JCAP 01:019. https://doi.org/10.1088/1475-7516/2017/01/019. arXiv:1608.04216 [astro-ph.CO]
Dimastrogiovanni E, Fasiello M, Hardwick RJ, Assadullahi H, Koyama K, Wands D (2018) Non-Gaussianity from axion-gauge fields interactions during inflation. JCAP 11:029. https://doi.org/10.1088/1475-7516/2018/11/029. arXiv:1806.05474 [astro-ph.CO]
Dimastrogiovanni E, Fasiello M, Tasinato G (2020) Searching for fossil fields in the gravity sector. Phys Rev Lett 124(6):061302. https://doi.org/10.1103/PhysRevLett.124.061302. arXiv:1906.07204 [astro-ph.CO]
Dimopoulos K, Markkanen T (2018) Non-minimal gravitational reheating during kination. JCAP 06:021. https://doi.org/10.1088/1475-7516/2018/06/021. arXiv:1803.07399 [gr-qc]

Dimopoulos K, Valle JWF (2002) Modeling quintessential inflation. Astropart Phys 18:287–306. https://doi.org/10.1016/S0927-6505(02)00115-9. arXiv:astro-ph/0111417

Dine M, Randall L, Thomas SD (1995) Supersymmetry breaking in the early universe. Phys Rev Lett 75:398–401. https://doi.org/10.1103/PhysRevLett.75.398. arXiv:hep-ph/9503303

Ding X, Biesiada M, Zhu ZH (2015) Strongly lensed gravitational waves from intrinsically faint double compact binaries-prediction for the Einstein Telescope. JCAP 2015(12):006–006. https://doi.org/10.1088/1475-7516/2015/12/006. arXiv:1508.05000 [astro-ph.HE]

Dolgov A, Silk J (1993) Baryon isocurvature fluctuations at small scales and baryonic dark matter. Phys Rev D 47:4244–4255. https://doi.org/10.1103/PhysRevD.47.4244

Domcke V, Mukaida K (2018) Gauge field and fermion production during axion inflation. JCAP 11:020. https://doi.org/10.1088/1475-7516/2018/11/020. arXiv:1806.08769 [hep-ph]

Domcke V, Pieroni M, Binétruy P (2016) Primordial gravitational waves for universality classes of pseudoscalar inflation. JCAP 06:031. https://doi.org/10.1088/1475-7516/2016/06/031. arXiv:1603.01287 [astro-ph.CO]

Domcke V, Muia F, Pieroni M, Witkowski LT (2017) PBH dark matter from axion inflation. JCAP 07:048. https://doi.org/10.1088/1475-7516/2017/07/048. arXiv:1704.03464 [astro-ph.CO]

Domcke V, Ema Y, Mukaida K (2020a) Chiral anomaly, Schwinger effect, Euler–Heisenberg Lagrangian, and application to axion inflation. JHEP 02:055. https://doi.org/10.1007/JHEP02(2020)055. arXiv:1910.01205 [hep-ph]

Domcke V, García-Bellido J, Peloso M, Pieroni M, Ricciardone A, Sorbo L, Tasinato G (2020b) Measuring the net circular polarization of the stochastic gravitational wave background with interferometers. JCAP 05:028. https://doi.org/10.1088/1475-7516/2020/05/028. arXiv:1910.08052 [astro-ph.CO]

Domcke V, Jinno R, Rubira H (2020c) Deformation of the gravitational wave spectrum by density perturbations. JCAP 06:046. https://doi.org/10.1088/1475-7516/2020/06/046. arXiv:2002.11083 [astro-ph.CO]

Domènech G (2020) Induced gravitational waves in a general cosmological background. Int J Mod Phys D 29(03):2050028. https://doi.org/10.1142/S0218271820500285. arXiv:1912.05583 [gr-qc]

Domènech G, Pi S, Sasaki M (2020) Induced gravitational waves as a probe of thermal history of the universe. JCAP 08:017. https://doi.org/10.1088/1475-7516/2020/08/017. arXiv:2005.12314 [gr-qc]

Dorsch GC, Huber SJ, No JM (2013) A strong electroweak phase transition in the 2HDM after LHC8. JHEP 10:029. https://doi.org/10.1007/JHEP10(2013)029. arXiv:1305.6610 [hep-ph]

Dorsch GC, Huber SJ, Mimasu K, No JM (2014) Echoes of the electroweak phase transition: discovering a second Higgs doublet through $A_0 \to ZH_0$. Phys Rev Lett 113(21):211802. https://doi.org/10.1103/PhysRevLett.113.211802. arXiv:1405.5537 [hep-ph]

Dorsch GC, Huber SJ, Konstandin T, No JM (2017) A second Higgs doublet in the early universe: baryogenesis and gravitational waves. JCAP 05:052. https://doi.org/10.1088/1475-7516/2017/05/052. arXiv:1611.05874 [hep-ph]

Dorsch GC, Huber SJ, Konstandin T (2021) On the wall velocity dependence of electroweak baryogenesis. JCAP 08:020. https://doi.org/10.1088/1475-7516/2021/08/020. arXiv:2106.06547 [hep-ph]

Dubath F, Polchinski J, Rocha JV (2008) Cosmic string loops, large and small. Phys Rev D 77:123528. https://doi.org/10.1103/PhysRevD.77.123528. arXiv:0711.0994 [astro-ph]

Duechting N (2004) Supermassive black holes from primordial black hole seeds. Phys Rev D 70:064015. https://doi.org/10.1103/PhysRevD.70.064015. arXiv:astro-ph/0406260

Dufaux JF, Bergman A, Felder GN, Kofman L, Uzan JP (2007) Theory and numerics of gravitational waves from preheating after inflation. Phys Rev D 76:123517. https://doi.org/10.1103/PhysRevD.76.123517. arXiv:0707.0875 [astro-ph]

Dufaux JF, Felder G, Kofman L, Navros O (2009) Gravity waves from tachyonic preheating after hybrid inflation. JCAP 03:001. https://doi.org/10.1088/1475-7516/2009/03/001. arXiv:0812.2917 [astro-ph]

Dufaux JF, Figueroa DG, García-Bellido J (2010) Gravitational waves from abelian gauge fields and cosmic strings at preheating. Phys Rev D 82:083518. https://doi.org/10.1103/PhysRevD.82.083518. arXiv:1006.0217 [astro-ph.CO]

Durrer R, Neronov A (2013) Cosmological magnetic fields: their generation, evolution and observation. Astron Astrophys Rev 21:62. https://doi.org/10.1007/s00159-013-0062-7. arXiv:1303.7121 [astro-ph.CO]

Dvali G, Vilenkin A (2004) Formation and evolution of cosmic D strings. JCAP 03:010. https://doi.org/10.1088/1475-7516/2004/03/010. arXiv:hep-th/0312007

Dvali G, Gruzinov A, Zaldarriaga M (2004) A new mechanism for generating density perturbations from inflation. Phys Rev D 69:023505. https://doi.org/10.1103/PhysRevD.69.023505. arXiv:astro-ph/0303591

Dvali GR, Shafi Q, Solganik S (2001) D-brane inflation. In: 4th European Meeting From the Planck Scale to the Electroweak Scale. arXiv:hep-th/0105203

Dvorkin I, Uzan JP, Vangioni E, Silk J (2016a) Synthetic model of the gravitational wave background from evolving binary compact objects. Phys Rev D 94(10):103011. https://doi.org/10.1103/PhysRevD.94.103011. arXiv:1607.06818 [astro-ph.HE]

Dvorkin I, Vangioni E, Silk J, Uzan JP, Olive KA (2016b) Metallicity-constrained merger rates of binary black holes and the stochastic gravitational wave background. Mon Not R Astron Soc 461(4):3877–3885. https://doi.org/10.1093/mnras/stw1477. arXiv:1604.04288 [astro-ph.HE]

Easther R, Lim EA (2006) Stochastic gravitational wave production after inflation. JCAP 04:010. https://doi.org/10.1088/1475-7516/2006/04/010. arXiv:astro-ph/0601617

Easther R, Giblin JT Jr, Lim EA (2007) Gravitational wave production at the end of inflation. Phys Rev Lett 99:221301. https://doi.org/10.1103/PhysRevLett.99.221301. arXiv:astro-ph/0612294

Easther R, Flauger R, Gilmore JB (2011) Delayed reheating and the breakdown of coherent oscillations. JCAP 04:027. https://doi.org/10.1088/1475-7516/2011/04/027. arXiv:1003.3011 [astro-ph.CO]

Ekstedt A, Löfgren J (2020) A critical look at the electroweak phase transition. JHEP 12:136. https://doi.org/10.1007/JHEP12(2020)136. arXiv:2006.12614 [hep-ph]

Ekstedt A, Schicho P, Tenkanen TVI (2023) DRalgo: a package for effective field theory approach for thermal phase transitions. Comput Phys Commun 288:108725. https://doi.org/10.1016/j.cpc.2023.108725. arXiv:2205.08815 [hep-ph]

El-Neaj YA et al (2020) AEDGE: atomic experiment for dark matter and gravity exploration in space. EPJ Quantum Technol 7:6. https://doi.org/10.1140/epjqt/s40507-020-0080-0. arXiv:1908.00802 [gr-qc]

Elghozi T, Nelson W, Sakellariadou M (2014) Cusps and pseudocusps in strings with Y-junctions. Phys Rev D 90(12):123517. https://doi.org/10.1103/PhysRevD.90.123517. arXiv:1403.3225 [hep-th]

Ellis J, Lewicki M (2021) Cosmic string interpretation of NANOGrav pulsar timing data. Phys Rev Lett 126(4):041304. https://doi.org/10.1103/PhysRevLett.126.041304. arXiv:2009.06555 [astro-ph.CO]

Ellis J, Fairbairn M, Lewicki M, Vaskonen V, Wickens A (2019a) Intergalactic magnetic fields from first-order phase transitions. JCAP 09:019. https://doi.org/10.1088/1475-7516/2019/09/019. arXiv:1907.04315 [astro-ph.CO]

Ellis J, Lewicki M, No JM (2019b) On the maximal strength of a first-order electroweak phase transition and its gravitational wave signal. JCAP 04:003. https://doi.org/10.1088/1475-7516/2019/04/003. arXiv:1809.08242 [hep-ph]

Ellis J, Lewicki M, No JM, Vaskonen V (2019c) Gravitational wave energy budget in strongly supercooled phase transitions. JCAP 06:024. https://doi.org/10.1088/1475-7516/2019/06/024. arXiv:1903.09642 [hep-ph]

Ellis J, Fairbairn M, Lewicki M, Vaskonen V, Wickens A (2020a) Detecting circular polarisation in the stochastic gravitational-wave background from a first-order cosmological phase transition. JCAP 10:032. https://doi.org/10.1088/1475-7516/2020/10/032. arXiv:2005.05278 [astro-ph.CO]

Ellis J, Lewicki M, No JM (2020b) Gravitational waves from first-order cosmological phase transitions: lifetime of the sound wave source. JCAP 07:050. https://doi.org/10.1088/1475-7516/2020/07/050. arXiv:2003.07360 [hep-ph]

Ellis J, Lewicki M, Vaskonen V (2020c) Updated predictions for gravitational waves produced in a strongly supercooled phase transition. JCAP 11:020. https://doi.org/10.1088/1475-7516/2020/11/020. arXiv:2007.15586 [astro-ph.CO]

Endlich S, Nicolis A, Wang J (2013) Solid inflation. JCAP 10:011. https://doi.org/10.1088/1475-7516/2013/10/011. arXiv:1210.0569 [hep-th]

Endlich S, Horn B, Nicolis A, Wang J (2014) Squeezed limit of the solid inflation three-point function. Phys Rev D 90(6):063506. https://doi.org/10.1103/PhysRevD.90.063506. arXiv:1307.8114 [hep-th]

Engel J, Ramsey-Musolf MJ, van Kolck U (2013) Electric dipole moments of nucleons, nuclei, and atoms: the standard model and beyond. Prog Part Nucl Phys 71:21–74. https://doi.org/10.1016/j.ppnp.2013.03.003. arXiv:1303.2371 [nucl-th]

Enqvist K, Sloth MS (2002) Adiabatic CMB perturbations in pre-big bang string cosmology. Nucl Phys B 626:395–409. https://doi.org/10.1016/S0550-3213(02)00043-3. arXiv:hep-ph/0109214

Enqvist K, Figueroa DG, Meriniemi T (2012) Stochastic background of gravitational waves from fermions. Phys Rev D 86:061301. https://doi.org/10.1103/PhysRevD.86.061301. arXiv:1203.4943 [astro-ph.CO]

Espinosa JR, Konstandin T, No JM, Quiros M (2008) Some cosmological implications of hidden sectors. Phys Rev D 78:123528. https://doi.org/10.1103/PhysRevD.78.123528. arXiv:0809.3215 [hep-ph]
Espinosa JR, Konstandin T, No JM, Servant G (2010) Energy budget of cosmological first-order phase transitions. JCAP 06:028. https://doi.org/10.1088/1475-7516/2010/06/028. arXiv:1004.4187 [hep-ph]
Espinosa JR, Gripaios B, Konstandin T, Riva F (2012) Electroweak baryogenesis in non-minimal composite Higgs models. JCAP 01:012. https://doi.org/10.1088/1475-7516/2012/01/012. arXiv:1110.2876 [hep-ph]
Espinosa JR, Racco D, Riotto A (2018) A cosmological signature of the SM Higgs instability: gravitational waves. JCAP 09:012. https://doi.org/10.1088/1475-7516/2018/09/012. arXiv:1804.07732 [hep-ph]
Essey W, Ando S, Kusenko A (2011) Determination of intergalactic magnetic fields from gamma ray data. Astropart Phys 35:135–139. https://doi.org/10.1016/j.astropartphys.2011.06.010. arXiv:1012.5313 [astro-ph.HE]
Estabrook FB, Tinto M, Armstrong JW (2000) Time delay analysis of LISA gravitational wave data: elimination of spacecraft motion effects. Phys Rev D 62:042002. https://doi.org/10.1103/PhysRevD.62.042002
Evangelista EFD, Araujo JCN (2014) The gravitational wave background from coalescing compact binaries: a new method. Braz J Phys 44(6):824–831. https://doi.org/10.1007/s13538-014-0272-0. arXiv:1504.06605 [astro-ph.CO]
Ezquiaga JM (2021) Hearing gravity from the cosmos: GWTC-2 probes general relativity at cosmological scales. Phys Lett B 822:136665. https://doi.org/10.1016/j.physletb.2021.136665. arXiv:2104.05139 [astro-ph.CO]
Ezquiaga JM, García-Bellido J (2018) Quantum diffusion beyond slow-roll: implications for primordial black-hole production. JCAP 08:018. https://doi.org/10.1088/1475-7516/2018/08/018. arXiv:1805.06731 [astro-ph.CO]
Ezquiaga JM, Holz DE (2021) Jumping the gap: searching for LIGO's biggest black holes. Astrophys J Lett 909(2):L23. https://doi.org/10.3847/2041-8213/abe638. arXiv:2006.02211 [astro-ph.HE]
Ezquiaga JM, Holz DE (2022) Spectral sirens: cosmology from the full mass distribution of compact binaries. Phys Rev Lett 129(6):061102. https://doi.org/10.1103/PhysRevLett.129.061102. arXiv:2202.08240 [astro-ph.CO]
Ezquiaga JM, Zumalacárregui M (2017) Dark energy after GW170817: dead ends and the road ahead. Phys Rev Lett 119(25):251304. https://doi.org/10.1103/PhysRevLett.119.251304. arXiv:1710.05901 [astro-ph.CO]
Ezquiaga JM, Zumalacárregui M (2018) Dark energy in light of multi-messenger gravitational-wave astronomy. Front Astron Space Sci 5:44. https://doi.org/10.3389/fspas.2018.00044. arXiv:1807.09241 [astro-ph.CO]
Ezquiaga JM, Zumalacárregui M (2020) Gravitational wave lensing beyond general relativity: birefringence, echoes and shadows. Phys Rev D 102(12):124048. https://doi.org/10.1103/PhysRevD.102.124048. arXiv:2009.12187 [gr-qc]
Ezquiaga JM, García-Bellido J, Ruiz Morales E (2018) Primordial black hole production in critical Higgs inflation. Phys Lett B 776:345–349. https://doi.org/10.1016/j.physletb.2017.11.039. arXiv:1705.04861 [astro-ph.CO]
Ezquiaga JM, García-Bellido J, Vennin V (2020a) The exponential tail of inflationary fluctuations: consequences for primordial black holes. JCAP 03:029. https://doi.org/10.1088/1475-7516/2020/03/029. arXiv:1912.05399 [astro-ph.CO]
Ezquiaga JM, Hu W, Lagos M (2020b) Apparent superluminality of lensed gravitational waves. Phys Rev D 102(2):023531. https://doi.org/10.1103/PhysRevD.102.023531. arXiv:2005.10702 [astro-ph.CO]
Ezquiaga JM, Holz DE, Hu W, Lagos M, Wald RM (2021) Phase effects from strong gravitational lensing of gravitational waves. Phys Rev D 103(6):064047. https://doi.org/10.1103/PhysRevD.103.064047. arXiv:2008.12814 [gr-qc]
Fabbri R, Pollock Md (1983) The effect of primordially produced gravitons upon the anisotropy of the cosmological microwave background radiation. Phys Lett B 125:445–448. https://doi.org/10.1016/0370-2693(83)91322-9
Fairbairn M, Hardy E, Wickens A (2019) Hearing without seeing: gravitational waves from hot and cold hidden sectors. JHEP 07:044. https://doi.org/10.1007/JHEP07(2019)044. arXiv:1901.11038 [hep-ph]
Farakos K, Kajantie K, Rummukainen K, Shaposhnikov ME (1994) 3-D physics and the electroweak phase transition: perturbation theory. Nucl Phys B 425:67–109. https://doi.org/10.1016/0550-3213(94)90173-2. arXiv:hep-ph/9404201

Farmer AJ, Phinney ES (2003) The gravitational wave background from cosmological compact binaries. Mon Not R Astron Soc 346:1197. https://doi.org/10.1111/j.1365-2966.2003.07176.x. arXiv:astro-ph/0304393

Farmer R, Renzo M, de Mink SE, Marchant P, Justham S (2019) Mind the gap: the location of the lower edge of the pair-instability supernova black hole mass gap. 887(1):53. https://doi.org/10.3847/1538-4357/ab518b. arXiv:1910.12874 [astro-ph.SR]

Farmer R, Renzo M, de Mink S, Fishbach M, Justham S (2020) Constraints from gravitational wave detections of binary black hole mergers on the ^{12} C $(\alpha, \gamma)^{16}$ O rate. Astrophys J Lett 902(2):L36. https://doi.org/10.3847/2041-8213/abbadd. arXiv:2006.06678 [astro-ph.HE]

Farr WM, Fishbach M, Ye J, Holz D (2019) A future percent-level measurement of the Hubble expansion at redshift 0.8 with advanced LIGO. Astrophys J Lett 883(2):L42. https://doi.org/10.3847/2041-8213/ab4284. arXiv:1908.09084 [astro-ph.CO]

Farris BD, Duffell P, MacFadyen AI, Haiman Z (2015) Binary black hole accretion during inspiral and merger. Mon Not R Astron Soc 447(1):L80–L84. https://doi.org/10.1093/mnrasl/slu184. arXiv:1409.5124 [astro-ph.HE]

Feldbrugge J, Pen UL, Turok N (2023) Oscillatory path integrals for radio astronomy. Ann Phys 451:169255. https://doi.org/10.1016/j.aop.2023.169255. arXiv:1909.04632 [astro-ph.HE]

Fenu E, Figueroa DG, Durrer R, García-Bellido J (2009) Gravitational waves from self-ordering scalar fields. JCAP 10:005. https://doi.org/10.1088/1475-7516/2009/10/005. arXiv:0908.0425 [astro-ph.CO]

Ferreira RZ, Notari A (2017) Thermalized axion inflation. JCAP 09:007. https://doi.org/10.1088/1475-7516/2017/09/007. arXiv:1706.00373 [astro-ph.CO]

Ferreira RZ, Ganc J, Noreña J, Sloth MS (2016) On the validity of the perturbative description of axions during inflation. JCAP 04:039. https://doi.org/10.1088/1475-7516/2016/04/039, [Erratum: JCAP 10, E01 (2016)]. arXiv:1512.06116 [astro-ph.CO]

Ferrer F, Masso E, Panico G, Pujolas O, Rompineve F (2019) Primordial black holes from the QCD axion. Phys Rev Lett 122(10):101301. https://doi.org/10.1103/PhysRevLett.122.101301. arXiv:1807.01707 [hep-ph]

Figueroa DG (2014) A gravitational wave background from the decay of the standard model Higgs after inflation. JHEP 11:145. https://doi.org/10.1007/JHEP11(2014)145. arXiv:1402.1345 [astro-ph.CO]

Figueroa DG, Byrnes CT (2017) The Standard Model Higgs as the origin of the hot Big Bang. Phys Lett B 767:272–277. https://doi.org/10.1016/j.physletb.2017.01.059. arXiv:1604.03905 [hep-ph]

Figueroa DG, Meriniemi T (2013) Stochastic background of gravitational waves from fermions—theory and applications. JHEP 10:101. https://doi.org/10.1007/JHEP10(2013)101. arXiv:1306.6911 [astro-ph.CO]

Figueroa DG, Tanin EH (2019a) Ability of LIGO and LISA to probe the equation of state of the early Universe. JCAP 08:011. https://doi.org/10.1088/1475-7516/2019/08/011. arXiv:1905.11960 [astro-ph.CO]

Figueroa DG, Tanin EH (2019b) Inconsistency of an inflationary sector coupled only to Einstein gravity. JCAP 10:050. https://doi.org/10.1088/1475-7516/2019/10/050. arXiv:1811.04093 [astro-ph.CO]

Figueroa DG, Torrenti F (2017a) Gravitational wave production from preheating: parameter dependence. JCAP 10:057. https://doi.org/10.1088/1475-7516/2017/10/057. arXiv:1707.04533 [astro-ph.CO]

Figueroa DG, Torrenti F (2017b) Parametric resonance in the early Universe—a fitting analysis. JCAP 02:001. https://doi.org/10.1088/1475-7516/2017/02/001. arXiv:1609.05197 [astro-ph.CO]

Figueroa DG, García-Bellido J, Rajantie A (2011) On the transverse-traceless projection in lattice simulations of gravitational wave production. JCAP 11:015. https://doi.org/10.1088/1475-7516/2011/11/015. arXiv:1110.0337 [astro-ph.CO]

Figueroa DG, Hindmarsh M, Urrestilla J (2013) Exact scale-invariant background of gravitational waves from cosmic defects. Phys Rev Lett 110(10):101302. https://doi.org/10.1103/PhysRevLett.110.101302. arXiv:1212.5458 [astro-ph.CO]

Figueroa DG, García-Bellido J, Torrentí F (2016) Gravitational wave production from the decay of the standard model Higgs field after inflation. Phys Rev D 93(10):103521. https://doi.org/10.1103/PhysRevD.93.103521. arXiv:1602.03085 [astro-ph.CO]

Figueroa DG, Megias E, Nardini G, Pieroni M, Quiros M, Ricciardone A, Tasinato G (2018) LISA as a probe for particle physics: electroweak scale tests in synergy with ground-based experiments. PoS GRASS2018:036. https://doi.org/10.22323/1.325.0036. arXiv:1806.06463 [astro-ph.CO]

Figueroa DG, Hindmarsh M, Lizarraga J, Urrestilla J (2020) Irreducible background of gravitational waves from a cosmic defect network: update and comparison of numerical techniques. Phys Rev D 102 (10):103516. https://doi.org/10.1103/PhysRevD.102.103516. arXiv:2007.03337 [astro-ph.CO]

Figueroa DG, Raatikainen S, Rasanen S, Tomberg E (2021) Non-Gaussian tail of the curvature perturbation in stochastic ultraslow-roll inflation: implications for primordial black hole production. Phys Rev Lett 127(10):101302. https://doi.org/10.1103/PhysRevLett.127.101302. arXiv:2012.06551 [astro-ph.CO]

Figueroa DG, Raatikainen S, Rasanen S, Tomberg E (2022) Implications of stochastic effects for primordial black hole production in ultra-slow-roll inflation. JCAP 05(05):027. https://doi.org/10.1088/1475-7516/2022/05/027. arXiv:2111.07437 [astro-ph.CO]

Finelli F, Brandenberger RH (1999) Parametric amplification of gravitational fluctuations during reheating. Phys Rev Lett 82:1362–1365. https://doi.org/10.1103/PhysRevLett.82.1362. arXiv:hep-ph/9809490

Finke A, Foffa S, Iacovelli F, Maggiore M, Mancarella M (2021) Cosmology with LIGO/Virgo dark sirens: Hubble parameter and modified gravitational wave propagation. JCAP 08:026. https://doi.org/10.1088/1475-7516/2021/08/026. arXiv:2101.12660 [astro-ph.CO]

Fishbach M, Holz DE, Farr WM (2018) Does the black hole merger rate evolve with redshift? Astrophys J Lett 863(2):L41. https://doi.org/10.3847/2041-8213/aad800. arXiv:1805.10270 [astro-ph.HE]

Fishbach M et al (2019) A standard siren measurement of the Hubble constant from GW170817 without the electromagnetic counterpart. Astrophys J Lett 871(1):L13. https://doi.org/10.3847/2041-8213/aaf96e. arXiv:1807.05667 [astro-ph.CO]

Flauger R, McAllister L, Pajer E, Westphal A, Xu G (2010) Oscillations in the CMB from axion monodromy inflation. JCAP 06:009. https://doi.org/10.1088/1475-7516/2010/06/009. arXiv:0907.2916 [hep-th]

Flauger R, Karnesis N, Nardini G, Pieroni M, Ricciardone A, Torrado J (2021) Improved reconstruction of a stochastic gravitational wave background with LISA. JCAP 01:059. https://doi.org/10.1088/1475-7516/2021/01/059. arXiv:2009.11845 [astro-ph.CO]

Ford LH (1987) Gravitational particle creation and inflation. Phys Rev D 35:2955. https://doi.org/10.1103/PhysRevD.35.2955

Fornal B (2021) Gravitational wave signatures of lepton universality violation. Phys Rev D 103(1):015018. https://doi.org/10.1103/PhysRevD.103.015018. arXiv:2006.08802 [hep-ph]

Fowler WA, Hoyle F (1964) Neutrino processes and pair formation in massive stars and supernovae. Astrophys J Suppl 9:201–319. https://doi.org/10.1086/190103

Franciolini G, Kehagias A, Matarrese S, Riotto A (2018) Primordial black holes from inflation and non-Gaussianity. JCAP 03:016. https://doi.org/10.1088/1475-7516/2018/03/016. arXiv:1801.09415 [astro-ph.CO]

Freedman WL et al (2019) The Carnegie-Chicago Hubble Program. VIII. An independent determination of the Hubble constant based on the tip of the red giant branch. Astrophys J 882:34. https://doi.org/10.3847/1538-4357/ab2f73. arXiv:1907.05922 [astro-ph.CO]

Freese K, Frieman JA, Olinto AV (1990) Natural inflation with pseudo Nambu-Goldstone bosons. Phys Rev Lett 65:3233–3236. https://doi.org/10.1103/PhysRevLett.65.3233

Fromme L, Huber SJ, Seniuch M (2006) Baryogenesis in the two-Higgs doublet model. JHEP 11:038. https://doi.org/10.1088/1126-6708/2006/11/038. arXiv:hep-ph/0605242

Frusciante N (2021) Signatures of $f(Q)$-gravity in cosmology. Phys Rev D 103(4):044021. https://doi.org/10.1103/PhysRevD.103.044021. arXiv:2101.09242 [astro-ph.CO]

Fryer CL, Woosley SE, Heger A (2001) Pair instability supernovae, gravity waves, and gamma-ray transients. Astrophys J 550:372–382. https://doi.org/10.1086/319719. arXiv:astro-ph/0007176

Fujikura K, Kamada K, Nakai Y, Yamaguchi M (2018) Phase transitions in twin Higgs models. JHEP 12:018. https://doi.org/10.1007/JHEP12(2018)018. arXiv:1810.00574 [hep-ph]

Fujita T, Kawasaki M, Tada Y, Takesako T (2013) A new algorithm for calculating the curvature perturbations in stochastic inflation. JCAP 12:036. https://doi.org/10.1088/1475-7516/2013/12/036. arXiv:1308.4754 [astro-ph.CO]

Fumagalli J, Renaux-Petel S, Witkowski LT (2021a) Oscillations in the stochastic gravitational wave background from sharp features and particle production during inflation. JCAP 08:030. https://doi.org/10.1088/1475-7516/2021/08/030. arXiv:2012.02761 [astro-ph.CO]

Fumagalli J, Se Renaux-Petel, Witkowski LT (2021b) Resonant features in the stochastic gravitational wave background. JCAP 08:059. https://doi.org/10.1088/1475-7516/2021/08/059. arXiv:2105.06481 [astro-ph.CO]

Fumagalli J, Renaux-Petel S, Ronayne JW, Witkowski LT (2023) Turning in the landscape: a new mechanism for generating primordial black holes. Phys Lett B 841:137921. https://doi.org/10.1016/j.physletb.2023.137921. arXiv:2004.08369 [hep-th]

Galtsov DV, Volkov MS (1991) Yang–Mills cosmology: cold matter for a hot universe. Phys Lett B 256:17–21. https://doi.org/10.1016/0370-2693(91)90211-8

Gao Z, Chen X, Hu YM, Zhang JD, Huang SJ (2022) A higher probability of detecting lensed supermassive black hole binaries by LISA. Mon Not R Astron Soc 512(1):1–10. https://doi.org/10.1093/mnras/stac365. arXiv:2102.10295 [astro-ph.CO]

Garbrecht B, Millington P (2015) Self-consistent solitons for vacuum decay in radiatively generated potentials. Phys Rev D 92:125022. https://doi.org/10.1103/PhysRevD.92.125022. arXiv:1509.08480 [hep-ph]

García-Bellido J, Figueroa DG (2007) A stochastic background of gravitational waves from hybrid preheating. Phys Rev Lett 98:061302. https://doi.org/10.1103/PhysRevLett.98.061302. arXiv:astro-ph/0701014

García-Bellido J, Nesseris S (2017) Gravitational wave bursts from Primordial Black Hole hyperbolic encounters. Phys Dark Universe 18:123–126. https://doi.org/10.1016/j.dark.2017.10.002. arXiv:1706.02111 [astro-ph.CO]

García-Bellido J, Nesseris S (2018) Gravitational wave energy emission and detection rates of Primordial Black Hole hyperbolic encounters. Phys Dark Universe 21:61–69. https://doi.org/10.1016/j.dark.2018.06.001. arXiv:1711.09702 [astro-ph.HE]

García-Bellido J, Ruiz Morales E (2017) Primordial black holes from single field models of inflation. Phys Dark Universe 18:47–54. https://doi.org/10.1016/j.dark.2017.09.007. arXiv:1702.03901 [astro-ph.CO]

García-Bellido J, Linde AD, Wands D (1996) Density perturbations and black hole formation in hybrid inflation. Phys Rev D 54:6040–6058. https://doi.org/10.1103/PhysRevD.54.6040. arXiv:astro-ph/9605094

García-Bellido J, García Pérez M, González-Arroyo A (2003) Symmetry breaking and false vacuum decay after hybrid inflation. Phys Rev D 67:103501. https://doi.org/10.1103/PhysRevD.67.103501. arXiv:hep-ph/0208228

García-Bellido J, Figueroa DG, Sastre A (2008) A gravitational wave background from reheating after hybrid inflation. Phys Rev D 77:043517. https://doi.org/10.1103/PhysRevD.77.043517. arXiv:0707.0839 [hep-ph]

García-Bellido J, Peloso M, Ünal C (2016) Gravitational waves at interferometer scales and primordial black holes in axion inflation. JCAP 12:031. https://doi.org/10.1088/1475-7516/2016/12/031. arXiv:1610.03763 [astro-ph.CO]

García-Bellido J, Peloso M, Ünal C (2017) Gravitational Wave signatures of inflationary models from Primordial Black Hole Dark Matter. JCAP 09:013. https://doi.org/10.1088/1475-7516/2017/09/013. arXiv:1707.02441 [astro-ph.CO]

Garfinkle D, Vachaspati T (1987) Radiation from kinky, cuspless cosmic loops. Phys Rev D 36:2229. https://doi.org/10.1103/PhysRevD.36.2229

Garoffolo A, Tasinato G, Carbone C, Bertacca D, Matarrese S (2020) Gravitational waves and geometrical optics in scalar–tensor theories. JCAP 11:040. https://doi.org/10.1088/1475-7516/2020/11/040. arXiv:1912.08093 [gr-qc]

Garoffolo A, Raveri M, Silvestri A, Tasinato G, Carbone C, Bertacca D, Matarrese S (2021) Detecting dark energy fluctuations with gravitational waves. Phys Rev D 103(8):083506. https://doi.org/10.1103/PhysRevD.103.083506. arXiv:2007.13722 [astro-ph.CO]

Garretson WD, Field GB, Carroll SM (1992) Primordial magnetic fields from pseudo Goldstone bosons. Phys Rev D 46:5346–5351. https://doi.org/10.1103/PhysRevD.46.5346. arXiv:hep-ph/9209238

Garriga J, Pomarol A (2003) A stable hierarchy from Casimir forces and the holographic interpretation. Phys Lett B 560:91–97. https://doi.org/10.1016/S0370-2693(03)00301-0. arXiv:hep-th/0212227

Garriga J, Vilenkin A, Zhang J (2016) Black holes and the multiverse. JCAP 02:064. https://doi.org/10.1088/1475-7516/2016/02/064. arXiv:1512.01819 [hep-th]

Gasperini M (2016) Observable gravitational waves in pre-big bang cosmology: an update. JCAP 12:010. https://doi.org/10.1088/1475-7516/2016/12/010. arXiv:1606.07889 [gr-qc]

Gasperini M, Veneziano G (1993) Pre-big bang in string cosmology. Astropart Phys 1:317–339. https://doi.org/10.1016/0927-6505(93)90017-8. arXiv:hep-th/9211021

Ge S (2020) Sublunar-mass primordial black holes from closed axion domain walls. Phys Dark Universe 27:100440. https://doi.org/10.1016/j.dark.2019.100440. arXiv:1905.12182 [hep-ph]

Geller M, Hook A, Sundrum R, Tsai Y (2018) Primordial anisotropies in the gravitational wave background from cosmological phase transitions. Phys Rev Lett 121(20):201303. https://doi.org/10.1103/PhysRevLett.121.201303. arXiv:1803.10780 [hep-ph]

Gerbino M, Gruppuso A, Natoli P, Shiraishi M, Melchiorri A (2016) Testing chirality of primordial gravitational waves with Planck and future CMB data: no hope from angular power spectra. JCAP 07:044. https://doi.org/10.1088/1475-7516/2016/07/044. arXiv:1605.09357 [astro-ph.CO]

Germani C, Musco I (2019) Abundance of primordial black holes depends on the shape of the inflationary power spectrum. Phys Rev Lett 122(14):141302. https://doi.org/10.1103/PhysRevLett.122.141302. arXiv:1805.04087 [astro-ph.CO]

Germani C, Prokopec T (2017) On primordial black holes from an inflection point. Phys Dark Universe 18:6–10. https://doi.org/10.1016/j.dark.2017.09.001. arXiv:1706.04226 [astro-ph.CO]

Gerosa D, Ma S, Wong KWK, Berti E, O'Shaughnessy R, Chen Y, Belczynski K (2019) Multiband gravitational-wave event rates and stellar physics. Phys Rev D 99(10):103004. https://doi.org/10.1103/PhysRevD.99.103004. arXiv:1902.00021 [astro-ph.HE]

Giacobbo N, Mapelli M (2019) The impact of electron-capture supernovae on merging double neutron stars. Mon Not R Astron Soc 482(2):2234–2243. https://doi.org/10.1093/mnras/sty2848. arXiv:1805.11100 [astro-ph.SR]

Giampieri G, Polnarev AG (1997) Detecting an anisotropic gravitational wave background with LISA. Class Quantum Grav 14:1521–1524. https://doi.org/10.1088/0264-9381/14/6/021

Giblin JT Jr, Price LR, Siemens X, Vlcek B (2012) Gravitational waves from global second order phase transitions. JCAP 11:006. https://doi.org/10.1088/1475-7516/2012/11/006. arXiv:1111.4014 [astro-ph.CO]

Giese F, Konstandin T, van de Vis J (2020) Model-independent energy budget of cosmological first-order phase transitions—a sound argument to go beyond the bag model. JCAP 07(07):057. https://doi.org/10.1088/1475-7516/2020/07/057. arXiv:2004.06995 [astro-ph.CO]

Giese F, Konstandin T, Schmitz K, van de Vis J (2021) Model-independent energy budget for LISA. JCAP 01:072. https://doi.org/10.1088/1475-7516/2021/01/072. arXiv:2010.09744 [astro-ph.CO]

Ginat YB, Desjacques V, Reischke R, Perets HB (2020) Probability distribution of astrophysical gravitational-wave background fluctuations. Phys Rev D 102(8):083501. https://doi.org/10.1103/PhysRevD.102.083501. arXiv:1910.04587 [astro-ph.CO]

Giovannini M (1998) Gravitational waves constraints on postinflationary phases stiffer than radiation. Phys Rev D 58:083504. https://doi.org/10.1103/PhysRevD.58.083504. arXiv:hep-ph/9806329

Giovannini M (1999) Production and detection of relic gravitons in quintessential inflationary models. Phys Rev D 60:123511. https://doi.org/10.1103/PhysRevD.60.123511. arXiv:astro-ph/9903004

Giovannini M (2008) Stochastic backgrounds of relic gravitons, TΛCDM paradigm and the stiff ages. Phys Lett B 668:44–50. https://doi.org/10.1016/j.physletb.2008.07.107. arXiv:0807.1914 [astro-ph]

Giovannini M (2009) Thermal history of the plasma and high-frequency gravitons. Class Quantum Grav 26:045004. https://doi.org/10.1088/0264-9381/26/4/045004. arXiv:0807.4317 [astro-ph]

Gleiser M, Marques GC, Ramos RO (1993) On the evaluation of thermal corrections to false vacuum decay rates. Phys Rev D 48:1571–1584. https://doi.org/10.1103/PhysRevD.48.1571. arXiv:hep-ph/9304234

Gleyzes J, Langlois D, Piazza F, Vernizzi F (2015a) Exploring gravitational theories beyond Horndeski. JCAP 02:018. https://doi.org/10.1088/1475-7516/2015/02/018. arXiv:1408.1952 [astro-ph.CO]

Gleyzes J, Langlois D, Piazza F, Vernizzi F (2015b) Healthy theories beyond Horndeski. Phys Rev Lett 114(21):211101. https://doi.org/10.1103/PhysRevLett.114.211101. arXiv:1404.6495 [hep-th]

Gleyzes J, Langlois D, Vernizzi F (2015c) A unifying description of dark energy. Int J Mod Phys D 23(13):1443010. https://doi.org/10.1142/S021827181443010X. arXiv:1411.3712 [hep-th]

Glioti A, Rattazzi R, Vecchi L (2019) Electroweak baryogenesis above the electroweak scale. JHEP 04:027. https://doi.org/10.1007/JHEP04(2019)027. arXiv:1811.11740 [hep-ph]

Gluscevic V, Kamionkowski M (2010) Testing parity-violating mechanisms with cosmic microwave background experiments. Phys Rev D 81:123529. https://doi.org/10.1103/PhysRevD.81.123529. arXiv:1002.1308 [astro-ph.CO]

Gogoberidze G, Kahniashvili T, Kosowsky A (2007) The spectrum of gravitational radiation from primordial turbulence. Phys Rev D 76:083002. https://doi.org/10.1103/PhysRevD.76.083002. arXiv:0705.1733 [astro-ph]

Goldberger WD, Wise MB (1999) Modulus stabilization with bulk fields. Phys Rev Lett 83:4922–4925. https://doi.org/10.1103/PhysRevLett.83.4922. arXiv:hep-ph/9907447

Goncharov B et al (2021) On the evidence for a common-spectrum process in the search for the nanohertz gravitational-wave background with the Parkes pulsar timing array. Astrophys J Lett 917(2):L19. https://doi.org/10.3847/2041-8213/ac17f4. arXiv:2107.12112 [astro-ph.HE]

Gordon C, Wands D, Bassett BA, Maartens R (2000) Adiabatic and entropy perturbations from inflation. Phys Rev D 63:023506. https://doi.org/10.1103/PhysRevD.63.023506. arXiv:astro-ph/0009131

Gorghetto M, Hardy E, Villadoro G (2018) Axions from strings: the attractive solution. JHEP 07:151. https://doi.org/10.1007/JHEP07(2018)151. arXiv:1806.04677 [hep-ph]

Gorghetto M, Hardy E, Nicolaescu H (2021) Observing invisible axions with gravitational waves. JCAP 06:034. https://doi.org/10.1088/1475-7516/2021/06/034. arXiv:2101.11007 [hep-ph]

Gould O (2021) Real scalar phase transitions: a nonperturbative analysis. JHEP 04:057. https://doi.org/10.1007/JHEP04(2021)057. arXiv:2101.05528 [hep-ph]

Gould O, Hirvonen J (2021) Effective field theory approach to thermal bubble nucleation. Phys Rev D 104 (9):096015. https://doi.org/10.1103/PhysRevD.104.096015. arXiv:2108.04377 [hep-ph]

Gould O, Kozaczuk J, Niemi L, Ramsey-Musolf MJ, Tenkanen TVI, Weir DJ (2019) Nonperturbative analysis of the gravitational waves from a first-order electroweak phase transition. Phys Rev D 100 (11):115024. https://doi.org/10.1103/PhysRevD.100.115024. arXiv:1903.11604 [hep-ph]

Gouttenoire Y, Servant G, Simakachorn P (2020a) Beyond the standard models with cosmic strings. JCAP 07:032. https://doi.org/10.1088/1475-7516/2020/07/032. arXiv:1912.02569 [hep-ph]

Gouttenoire Y, Servant G, Simakachorn P (2020b) BSM with cosmic strings: heavy, up to EeV mass, unstable particles. JCAP 07:016. https://doi.org/10.1088/1475-7516/2020/07/016. arXiv:1912.03245 [hep-ph]

Gouttenoire Y, Servant G, Simakachorn P (2021a) Kination cosmology from scalar fields and gravitational-wave signatures. arXiv e-prints arXiv:2111.01150 [hep-ph]

Gouttenoire Y, Servant G, Simakachorn P (2021b) Revealing the primordial irreducible inflationary gravitational-wave background with a spinning peccei-quinn axion. arXiv e-prints arXiv:2108.10328 [hep-ph]

Graham AW (2016) Galaxy bulges and their massive black holes: a review. Astrophys Space Sci Libr 418:263–313. https://doi.org/10.1007/978-3-319-19378-6_11. arXiv:1501.02937 [astro-ph.GA]

Graham MJ et al (2020) Candidate electromagnetic counterpart to the binary black hole merger gravitational wave event S190521g. Phys Rev Lett 124(25):251102. https://doi.org/10.1103/PhysRevLett.124.251102. arXiv:2006.14122 [astro-ph.HE]

Gray R et al (2020) Cosmological inference using gravitational wave standard sirens: a mock data analysis. Phys Rev D 101(12):122001. https://doi.org/10.1103/PhysRevD.101.122001. arXiv:1908.06050 [gr-qc]

Green AM, Liddle AR, Riotto A (1997) Primordial black hole constraints in cosmologies with early matter domination. Phys Rev D 56:7559–7565. https://doi.org/10.1103/PhysRevD.56.7559. arXiv:astro-ph/9705166

Greene JE, Strader J, Ho LC (2020) Intermediate-mass black holes. Annu Rev Astron Astrophys 58:257–312. https://doi.org/10.1146/annurev-astro-032620-021835. arXiv:1911.09678 [astro-ph.GA]

Greene PB, Kofman L, Linde AD, Starobinsky AA (1997) Structure of resonance in preheating after inflation. Phys Rev D 56:6175–6192. https://doi.org/10.1103/PhysRevD.56.6175. arXiv:hep-ph/9705347

Griest K, Kolb EW (1989) Solitosynthesis: cosmological evolution of nontopological solitons. Phys Rev D 40:3231. https://doi.org/10.1103/PhysRevD.40.3231

Grishchuk LP (1974) Amplification of gravitational waves in an istropic universe. Zh Eksp Teor Fiz 67:825–838

Grojean C, Servant G (2007) Gravitational waves from phase transitions at the electroweak scale and beyond. Phys Rev D 75:043507. https://doi.org/10.1103/PhysRevD.75.043507. arXiv:hep-ph/0607107

Grojean C, Servant G, Wells JD (2005) First-order electroweak phase transition in the standard model with a low cutoff. Phys Rev D 71:036001. https://doi.org/10.1103/PhysRevD.71.036001. arXiv:hep-ph/0407019

Groot Nibbelink S, van Tent BJW (2002) Scalar perturbations during multiple field slow-roll inflation. Class Quantum Grav 19:613–640. https://doi.org/10.1088/0264-9381/19/4/302. arXiv:hep-ph/0107272

Guedes GSF, Avelino PP, Sousa L (2018) Signature of inflation in the stochastic gravitational wave background generated by cosmic string networks. Phys Rev D 98(12):123505. https://doi.org/10.1103/PhysRevD.98.123505. arXiv:1809.10802 [astro-ph.CO]

Guo HK, Sinha K, Vagie D, White G (2021) Phase transitions in an expanding universe: stochastic gravitational waves in standard and non-standard histories. JCAP 01:001. https://doi.org/10.1088/1475-7516/2021/01/001. arXiv:2007.08537 [hep-ph]

Guth AH (1981) The inflationary universe: a possible solution to the horizon and flatness problems. Phys Rev D 23:347–356. https://doi.org/10.1103/PhysRevD.23.347

Guth AH, Pi SY (1982) Fluctuations in the new inflationary universe. Phys Rev Lett 49:1110–1113. https://doi.org/10.1103/PhysRevLett.49.1110

Haba N, Yamada T (2020) Gravitational waves from phase transition in minimal SUSY $U(1)_{B-L}$ model. Phys Rev D 101(7):075027. https://doi.org/10.1103/PhysRevD.101.075027. arXiv:1911.01292 [hep-ph]

Haiman Z (2017) Electromagnetic chirp of a compact binary black hole: a phase template for the gravitational wave inspiral. Phys Rev D 96(2):023004. https://doi.org/10.1103/PhysRevD.96.023004. arXiv:1705.06765 [astro-ph.HE]

Halverson J, Long C, Maiti A, Nelson B, Salinas G (2021) Gravitational waves from dark Yang–Mills sectors. JHEP 05:154. https://doi.org/10.1007/JHEP05(2021)154. arXiv:2012.04071 [hep-ph]

Hambye T, Strumia A (2013) Dynamical generation of the weak and Dark Matter scale. Phys Rev D 88:055022. https://doi.org/10.1103/PhysRevD.88.055022. arXiv:1306.2329 [hep-ph]

Hambye T, Strumia A, Teresi D (2018) Super-cool dark matter. JHEP 08:188. https://doi.org/10.1007/JHEP08(2018)188. arXiv:1805.01473 [hep-ph]

Handley WJ, Hobson MP, Lasenby AN (2015) polychord: next-generation nested sampling. Mon Not R Astron Soc 453(4):4385–4399. https://doi.org/10.1093/mnras/stv1911. arXiv:1506.00171 [astro-ph.IM]

Harada T, Yoo CM, Kohri K (2013) Threshold of primordial black hole formation. Phys Rev D 88 (8):084051. https://doi.org/10.1103/PhysRevD.88.084051, [Erratum: Phys. Rev. D 89, 029903 (2014)]. arXiv:1309.4201 [astro-ph.CO]

Haris K, Mehta AK, Kumar S, Venumadhav T, Ajith P (2018) Identifying strongly lensed gravitational wave signals from binary black hole mergers. arXiv e-prints arXiv:1807.07062 [gr-qc]

Harms J, Mahrdt C, Otto M, Priess M (2008) Subtraction-noise projection in gravitational-wave detector networks. Phys Rev D 77:123010. https://doi.org/10.1103/PhysRevD.77.123010. arXiv:0803.0226 [gr-qc]

Hasegawa T, Okada N, Seto O (2019) Gravitational waves from the minimal gauged $U(1)_{B-L}$ model. Phys Rev D 99(9):095039. https://doi.org/10.1103/PhysRevD.99.095039. arXiv:1904.03020 [hep-ph]

Hashino K, Kakizaki M, Kanemura S, Ko P, Matsui T (2017) Gravitational waves and Higgs boson couplings for exploring first order phase transition in the model with a singlet scalar field. Phys Lett B 766:49–54. https://doi.org/10.1016/j.physletb.2016.12.052. arXiv:1609.00297 [hep-ph]

Hashino K, Jinno R, Kakizaki M, Kanemura S, Takahashi T, Takimoto M (2019) Selecting models of first-order phase transitions using the synergy between collider and gravitational-wave experiments. Phys Rev D 99(7):075011. https://doi.org/10.1103/PhysRevD.99.075011. arXiv:1809.04994 [hep-ph]

Hassan SF, Rosen RA (2012) Bimetric gravity from ghost-free massive gravity. JHEP 02:126. https://doi.org/10.1007/JHEP02(2012)126. arXiv:1109.3515 [hep-th]

Hawking S (1971) Gravitationally collapsed objects of very low mass. Mon Not R Astron Soc 152:75

Hawking SW (1982) The development of irregularities in a single bubble inflationary universe. Phys Lett B 115:295. https://doi.org/10.1016/0370-2693(82)90373-2

Hazumi M et al (2012) IEEE proceedings. In: Clampin MC, et al. (eds) Space telescopes and instrumentation 2012: optical, infrared, and millimeter wave. SPIE Conference Series, vol 8442. Society of Photo-Optical Instrumentation Engineers, p 844219

Heger A, Woosley SE (2002) The nucleosynthetic signature of population III. Astrophys J 567:532–543. https://doi.org/10.1086/338487. arXiv:astro-ph/0107037

Heger A, Fryer CL, Woosley SE, Langer N, Hartmann DH (2003) How massive single stars end their life. Astrophys J 591:288–300. https://doi.org/10.1086/375341. arXiv:astro-ph/0212469

Helfer T, Aurrekoetxea JC, Lim EA (2019) Cosmic string loop collapse in full general relativity. Phys Rev D 99(10):104028. https://doi.org/10.1103/PhysRevD.99.104028. arXiv:1808.06678 [gr-qc]

Helmboldt AJ, Kubo J, van der Woude S (2019) Observational prospects for gravitational waves from hidden or dark chiral phase transitions. Phys Rev D 100(5):055025. https://doi.org/10.1103/PhysRevD.100.055025. arXiv:1904.07891 [hep-ph]

Henriques B, White S, Thomas P, Angulo R, Guo Q, Lemson G, Springel V (2013) Simulations of the galaxy population constrained by observations from z=3 to the present day: implications for galactic

winds and the fate of their ejecta. Mon Not R Astron Soc 431:3373. https://doi.org/10.1093/mnras/stt415. arXiv:1212.1717 [astro-ph.CO]
Heymans C et al (2021) KiDS-1000 cosmology: multi-probe weak gravitational lensing and spectroscopic galaxy clustering constraints. Astron Astrophys 646:A140. https://doi.org/10.1051/0004-6361/202039063. arXiv:2007.15632 [astro-ph.CO]
Hild S et al (2011) Sensitivity studies for third-generation gravitational wave observatories. Class Quantum Grav 28:094013. https://doi.org/10.1088/0264-9381/28/9/094013. arXiv:1012.0908 [gr-qc]
Hindmarsh M (1990) Gravitational radiation from kinky infinite strings. Phys Lett B 251:28–33. https://doi.org/10.1016/0370-2693(90)90226-V
Hindmarsh M (2018) Sound shell model for acoustic gravitational wave production at a first-order phase transition in the early Universe. Phys Rev Lett 120(7):071301. https://doi.org/10.1103/PhysRevLett.120.071301. arXiv:1608.04735 [astro-ph.CO]
Hindmarsh M, Hijazi M (2019) Gravitational waves from first order cosmological phase transitions in the Sound Shell Model. JCAP 12:062. https://doi.org/10.1088/1475-7516/2019/12/062. arXiv:1909.10040 [astro-ph.CO]
Hindmarsh M, Stuckey S, Bevis N (2009) Abelian Higgs cosmic strings: small scale structure and loops. Phys Rev D 79:123504. https://doi.org/10.1103/PhysRevD.79.123504. arXiv:0812.1929 [hep-th]
Hindmarsh M, Huber SJ, Rummukainen K, Weir DJ (2014) Gravitational waves from the sound of a first order phase transition. Phys Rev Lett 112:041301. https://doi.org/10.1103/PhysRevLett.112.041301. arXiv:1304.2433 [hep-ph]
Hindmarsh M, Huber SJ, Rummukainen K, Weir DJ (2015) Numerical simulations of acoustically generated gravitational waves at a first order phase transition. Phys Rev D 92(12):123009. https://doi.org/10.1103/PhysRevD.92.123009. arXiv:1504.03291 [astro-ph.CO]
Hindmarsh M, Huber SJ, Rummukainen K, Weir DJ (2017a) Shape of the acoustic gravitational wave power spectrum from a first order phase transition. Phys Rev D 96(10):103520. https://doi.org/10.1103/PhysRevD.96.103520, [Erratum: Phys. Rev. D 101, 089902 (2020)]. arXiv:1704.05871 [astro-ph.CO]
Hindmarsh M, Lizarraga J, Urrestilla J, Daverio D, Kunz M (2017b) Scaling from gauge and scalar radiation in Abelian Higgs string networks. Phys Rev D 96(2):023525. https://doi.org/10.1103/PhysRevD.96.023525. arXiv:1703.06696 [astro-ph.CO]
Hindmarsh M, Lizarraga J, Lopez-Eiguren A, Urrestilla J (2020) Scaling density of axion strings. Phys Rev Lett 124(2):021301. https://doi.org/10.1103/PhysRevLett.124.021301. arXiv:1908.03522 [astro-ph.CO]
Hindmarsh M, Lizarraga J, Urio A, Urrestilla J (2021) Loop decay in Abelian-Higgs string networks. Phys Rev D 104(4):043519. https://doi.org/10.1103/PhysRevD.104.043519. arXiv:2103.16248 [astro-ph.CO]
Hindmarsh MB, Kibble TWB (1995) Cosmic strings. Rep Prog Phys 58:477–562. https://doi.org/10.1088/0034-4885/58/5/001. arXiv:hep-ph/9411342
Hirata CM, Holz DE, Cutler C (2010) Reducing the weak lensing noise for the gravitational wave Hubble diagram using the non-Gaussianity of the magnification distribution. Phys Rev D 81:124046. https://doi.org/10.1103/PhysRevD.81.124046. arXiv:1004.3988 [astro-ph.CO]
Höche S, Kozaczuk J, Long AJ, Turner J, Wang Y (2021) Towards an all-orders calculation of the electroweak bubble wall velocity. JCAP 03:009. https://doi.org/10.1088/1475-7516/2021/03/009. arXiv:2007.10343 [hep-ph]
Hogan CJ (1986) Gravitational radiation from cosmological phase transitions. Mon Not R Astron Soc 218:629–636
Hogan CJ, Bender PL (2001) Estimating stochastic gravitational wave backgrounds with Sagnac calibration. Phys Rev D 64:062002. https://doi.org/10.1103/PhysRevD.64.062002. arXiv:astro-ph/0104266
Hogan CJ, Rees MJ (1984) Gravitational interactions of cosmic strings. Nature 311:109–113. https://doi.org/10.1038/311109a0
Holland J, Zavala I, Tasinato G (2020) On chromonatural inflation in string theory. JCAP 12:026. https://doi.org/10.1088/1475-7516/2020/12/026. arXiv:2009.00653 [hep-th]
Holz DE, Hughes SA (2005) Using gravitational-wave standard sirens. Astrophys J 629:15–22. https://doi.org/10.1086/431341. arXiv:astro-ph/0504616
Holz DE, Linder EV (2005) Safety in numbers: gravitational lensing degradation of the luminosity distance-redshift relation. Astrophys J 631:678–688. https://doi.org/10.1086/432085. arXiv:astro-ph/0412173

Hook A, Marques-Tavares G, Racco D (2021) Causal gravitational waves as a probe of free streaming particles and the expansion of the Universe. JHEP 02:117. https://doi.org/10.1007/JHEP02(2021)117. arXiv:2010.03568 [hep-ph]

Horava P (2009) Quantum gravity at a lifshitz point. Phys Rev D 79:084008. https://doi.org/10.1103/PhysRevD.79.084008. arXiv:0901.3775 [hep-th]

Horndeski GW (1974) Second-order scalar–tensor field equations in a four-dimensional space. Int J Theor Phys 10:363–384. https://doi.org/10.1007/BF01807638

Hossain MW, Myrzakulov R, Sami M, Saridakis EN (2014) Variable gravity: a suitable framework for quintessential inflation. Phys Rev D 90(2):023512. https://doi.org/10.1103/PhysRevD.90.023512. arXiv:1402.6661 [gr-qc]

Howlett C, Davis TM (2020) Standard siren speeds: improving velocities in gravitational-wave measurements of H_0. Mon Not R Astron Soc 492(3):3803–3815. https://doi.org/10.1093/mnras/staa049. arXiv:1909.00587 [astro-ph.CO]

Hu B, Raveri M, Frusciante N, Silvestri A (2014) Effective field theory of cosmic acceleration: an implementation in CAMB. Phys Rev D 89(10):103530. https://doi.org/10.1103/PhysRevD.89.103530. arXiv:1312.5742 [astro-ph.CO]

Huang FP, Li CS (2017) Probing the baryogenesis and dark matter relaxed in phase transition by gravitational waves and colliders. Phys Rev D 96(9):095028. https://doi.org/10.1103/PhysRevD.96.095028. arXiv:1709.09691 [hep-ph]

Huang FP, Zhang X (2019) Probing the gauge symmetry breaking of the early universe in 3-3-1 models and beyond by gravitational waves. Phys Lett B 788:288–294. https://doi.org/10.1016/j.physletb.2018.11.024. arXiv:1701.04338 [hep-ph]

Huang FP, Qian Z, Zhang M (2018) Exploring dynamical CP violation induced baryogenesis by gravitational waves and colliders. Phys Rev D 98(1):015014. https://doi.org/10.1103/PhysRevD.98.015014. arXiv:1804.06813 [hep-ph]

Huang W, Kang Z, Shu J, Wu P, Yang JM (2015) New insights in the electroweak phase transition in the NMSSM. Phys Rev D 91(2):025006. https://doi.org/10.1103/PhysRevD.91.025006. arXiv:1405.1152 [hep-ph]

Huang WC, Sannino F, Wang ZW (2020) Gravitational waves from Pati-Salam dynamics. Phys Rev D 102(9):095025. https://doi.org/10.1103/PhysRevD.102.095025. arXiv:2004.02332 [hep-ph]

Huang WC, Reichert M, Sannino F, Wang ZW (2021) Testing the dark SU(N) Yang–Mills theory confined landscape: from the lattice to gravitational waves. Phys Rev D 104(3):035005. https://doi.org/10.1103/PhysRevD.104.035005. arXiv:2012.11614 [hep-ph]

Huber SJ, Konstandin T (2008a) Gravitational wave production by collisions: more bubbles. JCAP 09:022. https://doi.org/10.1088/1475-7516/2008/09/022. arXiv:0806.1828 [hep-ph]

Huber SJ, Konstandin T (2008b) Production of gravitational waves in the nMSSM. JCAP 05:017. https://doi.org/10.1088/1475-7516/2008/05/017. arXiv:0709.2091 [hep-ph]

Huber SJ, Konstandin T, Nardini G, Rues I (2016) Detectable gravitational waves from very strong phase transitions in the general NMSSM. JCAP 03:036. https://doi.org/10.1088/1475-7516/2016/03/036. arXiv:1512.06357 [hep-ph]

Huey G, Lidsey JE (2001) Inflation, brane worlds and quintessence. Phys Lett B 514:217–225. https://doi.org/10.1016/S0370-2693(01)00808-5. arXiv:astro-ph/0104006

Hughes SA, Holz DE (2003) Cosmology with coalescing massive black holes. Class Quantum Grav 20:S65–S72. https://doi.org/10.1088/0264-9381/20/10/308. arXiv:astro-ph/0212218

Hui L, Nicolis A (2013) No-hair theorem for the Galileon. Phys Rev Lett 110:241104. https://doi.org/10.1103/PhysRevLett.110.241104. arXiv:1202.1296 [hep-th]

Hull M, Koyama K, Tasinato G (2015) A Higgs mechanism for vector Galileons. JHEP 03:154. https://doi.org/10.1007/JHEP03(2015)154. arXiv:1408.6871 [hep-th]

Huterer D, Shafer DL (2018) Dark energy two decades after: observables, probes, consistency tests. Rep Prog Phys 81(1):016901. https://doi.org/10.1088/1361-6633/aa997e. arXiv:1709.01091 [astro-ph.CO]

Huterer D, Starkman G (2003) Parameterization of dark-energy properties: a principal-component approach. Phys Rev Lett 90:031301. https://doi.org/10.1103/PhysRevLett.90.031301. arXiv:astro-ph/0207517

Iacconi L, Fasiello M, Assadullahi H, Dimastrogiovanni E, Wands D (2020a) Interferometer constraints on the inflationary field content. JCAP 03:031. https://doi.org/10.1088/1475-7516/2020/03/031. arXiv:1910.12921 [astro-ph.CO]

Iacconi L, Fasiello M, Assadullahi H, Wands D (2020b) Small-scale tests of inflation. JCAP 12:005. https://doi.org/10.1088/1475-7516/2020/12/005. arXiv:2008.00452 [astro-ph.CO]
Iacovelli F, Mancarella M, Foffa S, Maggiore M (2022) Forecasting the detection capabilities of third-generation gravitational-wave detectors using GWFAST. Astrophys J 941(2):208. https://doi.org/10.3847/1538-4357/ac9cd4. arXiv:2207.02771 [gr-qc]
Inayoshi K, Tamanini N, Caprini C, Haiman Z (2017) Probing stellar binary black hole formation in galactic nuclei via the imprint of their center of mass acceleration on their gravitational wave signal. Phys Rev D 96(6):063014. https://doi.org/10.1103/PhysRevD.96.063014. arXiv:1702.06529 [astro-ph.HE]
Inman D, Ali-Haïmoud Y (2019) Early structure formation in primordial black hole cosmologies. Phys Rev D 100(8):083528. https://doi.org/10.1103/PhysRevD.100.083528. arXiv:1907.08129 [astro-ph.CO]
Inomata K, Nakama T (2019) Gravitational waves induced by scalar perturbations as probes of the small-scale primordial spectrum. Phys Rev D 99(4):043511. https://doi.org/10.1103/PhysRevD.99.043511. arXiv:1812.00674 [astro-ph.CO]
Inoue S, Yokoyama J (2002) Curvature perturbation at the local extremum of the inflaton's potential. Phys Lett B 524:15–20. https://doi.org/10.1016/S0370-2693(01)01369-7. arXiv:hep-ph/0104083
Ishak M (2019) Testing general relativity in cosmology. Living Rev Relativ 22:1. https://doi.org/10.1007/s41114-018-0017-4. arXiv:1806.10122 [astro-ph.CO]
Iso S, Serpico PD, Shimada K (2017) QCD-electroweak first-order phase transition in a supercooled universe. Phys Rev Lett 119(14):141301. https://doi.org/10.1103/PhysRevLett.119.141301. arXiv:1704.04955 [hep-ph]
Iwasaki Y, Kanaya K, Sakai S, Yoshie T (1996) Chiral phase transition in lattice QCD with Wilson quarks. Z Phys C 71:337–342. https://doi.org/10.1007/s002880050179. arXiv:hep-lat/9504019
Jackiw R, Pi SY (2003) Chern–Simons modification of general relativity. Phys Rev D 68:104012. https://doi.org/10.1103/PhysRevD.68.104012. arXiv:gr-qc/0308071
Jackson MG, Jones NT, Polchinski J (2005) Collisions of cosmic F and D-strings. JHEP 10:013. https://doi.org/10.1088/1126-6708/2005/10/013. arXiv:hep-th/0405229
Jaeckel J, Khoze VV, Spannowsky M (2016) Hearing the signal of dark sectors with gravitational wave detectors. Phys Rev D 94(10):103519. https://doi.org/10.1103/PhysRevD.94.103519. arXiv:1602.03901 [hep-ph]
Jana S, Dalang C, Lombriser L (2021) Horndeski theories and beyond from higher dimensions. Class Quantum Grav 38(2):025003. https://doi.org/10.1088/1361-6382/abc272. arXiv:2007.06907 [gr-qc]
Jani K, Shoemaker D, Cutler C (2019) Detectability of intermediate-mass black holes in multiband gravitational wave astronomy. Nature Astron 4(3):260–265. https://doi.org/10.1038/s41550-019-0932-7. arXiv:1908.04985 [gr-qc]
Jedamzik J (n.d.) (to appear)
Jedamzik K (1997) Primordial black hole formation during the QCD epoch. Phys Rev D 55:5871–5875. https://doi.org/10.1103/PhysRevD.55.R5871. arXiv:astro-ph/9605152
Jedamzik K, Niemeyer JC (1999) Primordial black hole formation during first order phase transitions. Phys Rev D 59:124014. https://doi.org/10.1103/PhysRevD.59.124014. arXiv:astro-ph/9901293
Jedamzik K, Sigl G (2000) On metric preheating. Phys Rev D 61:023519. https://doi.org/10.1103/PhysRevD.61.023519. arXiv:hep-ph/9906287
Jedamzik K, Lemoine M, Martin J (2010) Collapse of small-scale density perturbations during preheating in single field inflation. JCAP 09:034. https://doi.org/10.1088/1475-7516/2010/09/034. arXiv:1002.3039 [astro-ph.CO]
Jenkins AC, Sakellariadou M (2018) Anisotropies in the stochastic gravitational-wave background: formalism and the cosmic string case. Phys Rev D 98(6):063509. https://doi.org/10.1103/PhysRevD.98.063509. arXiv:1802.06046 [astro-ph.CO]
Jenkins AC, Sakellariadou M (2019) Shot noise in the astrophysical gravitational-wave background. Phys Rev D 100(6):063508. https://doi.org/10.1103/PhysRevD.100.063508. arXiv:1902.07719 [astro-ph.CO]
Jenkins AC, Sakellariadou M (2020) Primordial black holes from cusp collapse on cosmic strings. arXiv e-prints arXiv:2006.16249 [astro-ph.CO]
Jenkins AC, Sakellariadou M (2021) Nonlinear gravitational-wave memory from cusps and kinks on cosmic strings. Class Quantum Grav 38(16):165004. https://doi.org/10.1088/1361-6382/ac1084. arXiv:2102.12487 [gr-qc]
Jenkins AC, Sakellariadou M, Regimbau T, Slezak E (2018) Anisotropies in the astrophysical gravitational-wave background: predictions for the detection of compact binaries by LIGO and

Virgo. Phys Rev D 98(6):063501. https://doi.org/10.1103/PhysRevD.98.063501. arXiv:1806.01718 [astro-ph.CO]
Jenkins AC, O'Shaughnessy R, Sakellariadou M, Wysocki D (2019a) Anisotropies in the astrophysical gravitational-wave background: the impact of black hole distributions. Phys Rev Lett 122 (11):111101. https://doi.org/10.1103/PhysRevLett.122.111101. arXiv:1810.13435 [astro-ph.CO]
Jenkins AC, Romano JD, Sakellariadou M (2019b) Estimating the angular power spectrum of the gravitational-wave background in the presence of shot noise. Phys Rev D 100(8):083501. https://doi.org/10.1103/PhysRevD.100.083501. arXiv:1907.06642 [astro-ph.CO]
Jeong D, Kamionkowski M (2012) Clustering Fossils from the Early Universe. Phys Rev Lett 108:251301. https://doi.org/10.1103/PhysRevLett.108.251301. arXiv:1203.0302 [astro-ph.CO]
Jin SJ, He DZ, Xu Y, Zhang JF, Zhang X (2020) Forecast for cosmological parameter estimation with gravitational-wave standard siren observation from the Cosmic Explorer. JCAP 03:051. https://doi.org/10.1088/1475-7516/2020/03/051. arXiv:2001.05393 [astro-ph.CO]
Jinno R, Takimoto M (2017a) Gravitational waves from bubble collisions: an analytic derivation. Phys Rev D 95(2):024009. https://doi.org/10.1103/PhysRevD.95.024009. arXiv:1605.01403 [astro-ph.CO]
Jinno R, Takimoto M (2017b) Probing a classically conformal B-L model with gravitational waves. Phys Rev D 95(1):015020. https://doi.org/10.1103/PhysRevD.95.015020. arXiv:1604.05035 [hep-ph]
Jinno R, Takimoto M (2019) Gravitational waves from bubble dynamics: beyond the envelope. JCAP 01:060. https://doi.org/10.1088/1475-7516/2019/01/060. arXiv:1707.03111 [hep-ph]
Jinno R, Nakayama K, Takimoto M (2016) Gravitational waves from the first order phase transition of the Higgs field at high energy scales. Phys Rev D 93(4):045024. https://doi.org/10.1103/PhysRevD.93.045024. arXiv:1510.02697 [hep-ph]
Jinno R, Lee S, Seong H, Takimoto M (2017) Gravitational waves from first-order phase transitions: towards model separation by bubble nucleation rate. JCAP 11:050. https://doi.org/10.1088/1475-7516/2017/11/050. arXiv:1708.01253 [hep-ph]
Jinno R, Konstandin T, Takimoto M (2019a) Relativistic bubble collisions—a closer look. JCAP 09:035. https://doi.org/10.1088/1475-7516/2019/09/035. arXiv:1906.02588 [hep-ph]
Jinno R, Seong H, Takimoto M, Um CM (2019b) Gravitational waves from first-order phase transitions: ultra-supercooled transitions and the fate of relativistic shocks. JCAP 10:033. https://doi.org/10.1088/1475-7516/2019/10/033. arXiv:1905.00899 [astro-ph.CO]
Jinno R, Konstandin T, Rubira H (2021) A hybrid simulation of gravitational wave production in first-order phase transitions. JCAP 04:014. https://doi.org/10.1088/1475-7516/2021/04/014. arXiv:2010.00971 [astro-ph.CO]
John P, Schmidt MG (2001) Do stops slow down electroweak bubble walls? Nucl Phys B 598:291–305. https://doi.org/10.1016/S0550-3213(00)00768-9, [Erratum: Nucl. Phys. B 648, 449–452 (2003)]. arXiv:hep-ph/0002050
Jones NT, Stoica H, Tye SHH (2003) The production, spectrum and evolution of cosmic strings in brane inflation. Phys Lett B 563:6–14. https://doi.org/10.1016/S0370-2693(03)00592-6. arXiv:hep-th/0303269
Jones-Smith K, Krauss LM, Mathur H (2008) A nearly scale invariant spectrum of gravitational radiation from global phase transitions. Phys Rev Lett 100:131302. https://doi.org/10.1103/PhysRevLett.100.131302. arXiv:0712.0778 [astro-ph]
Kahniashvili T, Vachaspati T (2006) On the detection of magnetic helicity. Phys Rev D 73:063507. https://doi.org/10.1103/PhysRevD.73.063507. arXiv:astro-ph/0511373
Kahniashvili T, Gogoberidze G, Ratra B (2005) Polarized cosmological gravitational waves from primordial helical turbulence. Phys Rev Lett 95:151301. https://doi.org/10.1103/PhysRevLett.95.151301. arXiv:astro-ph/0505628
Kahniashvili T, Campanelli L, Gogoberidze G, Maravin Y, Ratra B (2008) Gravitational radiation from primordial helical inverse cascade MHD turbulence. Phys Rev D 78:123006. https://doi.org/10.1103/PhysRevD.78.123006, [Erratum: Phys. Rev. D 79, 109901 (2009)]. arXiv:0809.1899 [astro-ph]
Kahniashvili T, Brandenburg A, Gogoberidze G, Mandal S, Roper Pol A (2021) Circular polarization of gravitational waves from early-Universe helical turbulence. Phys Rev Res 3(1):013193. https://doi.org/10.1103/PhysRevResearch.3.013193. arXiv:2011.05556 [astro-ph.CO]
Kainulainen K, Keus V, Niemi L, Rummukainen K, Tenkanen TVI, Vaskonen V (2019) On the validity of perturbative studies of the electroweak phase transition in the Two Higgs Doublet model. JHEP 06:075. https://doi.org/10.1007/JHEP06(2019)075. arXiv:1904.01329 [hep-ph]

Kaiser AR, McWilliams ST (2021) Sensitivity of present and future detectors across the black-hole binary gravitational wave spectrum. Class Quantum Grav 38(5):055009. https://doi.org/10.1088/1361-6382/abd4f6. arXiv:2010.02135 [gr-qc]
Kaiser DI (1996) Post inflation reheating in an expanding universe. Phys Rev D 53:1776–1783. https://doi.org/10.1103/PhysRevD.53.1776. arXiv:astro-ph/9507108
Kaiser DI (1997) Preheating in an expanding universe: analytic results for the massless case. Phys Rev D 56:706–716. https://doi.org/10.1103/PhysRevD.56.706. arXiv:hep-ph/9702244
Kaiser DI (1998) Resonance structure for preheating with massless fields. Phys Rev D 57:702–711. https://doi.org/10.1103/PhysRevD.57.702. arXiv:hep-ph/9707516
Kajantie K, Laine M, Rummukainen K, Shaposhnikov ME (1996a) Generic rules for high temperature dimensional reduction and their application to the standard model. Nucl Phys B 458:90–136. https://doi.org/10.1016/0550-3213(95)00549-8. arXiv:hep-ph/9508379
Kajantie K, Laine M, Rummukainen K, Shaposhnikov ME (1996b) The electroweak phase transition: a nonperturbative analysis. Nucl Phys B 466:189–258. https://doi.org/10.1016/0550-3213(96)00052-1. arXiv:hep-lat/9510020
Kajantie K, Laine M, Rummukainen K, Schroder Y (2003) The pressure of hot QCD up to g6 ln(1/g). Phys Rev D 67:105008. https://doi.org/10.1103/PhysRevD.67.105008. arXiv:hep-ph/0211321
Kamada A, Yamada M (2015a) Gravitational wave signals from short-lived topological defects in the MSSM. JCAP 10:021. https://doi.org/10.1088/1475-7516/2015/10/021. arXiv:1505.01167 [hep-ph]
Kamada A, Yamada M (2015b) Gravitational waves as a probe of the SUSY scale. Phys Rev D 91:063529. https://doi.org/10.1103/PhysRevD.91.063529. arXiv:1407.2882 [hep-ph]
Kamada K, Uchida F, Yokoyama J (2021) Baryon isocurvature constraints on the primordial hypermagnetic fields. JCAP 04:034. https://doi.org/10.1088/1475-7516/2021/04/034. arXiv:2012.14435 [astro-ph.CO]
Kamenshchik AY, Moschella U, Pasquier V (2001) An alternative to quintessence. Phys Lett B 511:265–268. https://doi.org/10.1016/S0370-2693(01)00571-8. arXiv:gr-qc/0103004
Kamionkowski M, Kovetz ED (2016) The quest for B modes from inflationary gravitational waves. Annu Rev Astron Astrophys 54:227–269. https://doi.org/10.1146/annurev-astro-081915-023433. arXiv:1510.06042 [astro-ph.CO]
Kang Z, Ko P, Matsui T (2018) Strong first order EWPT & strong gravitational waves in Z_3-symmetric singlet scalar extension. JHEP 02:115. https://doi.org/10.1007/JHEP02(2018)115. arXiv:1706.09721 [hep-ph]
Kapadia SJ, Pandey KL, Suyama T, Ajith P (2020) Prospects for probing ultralight primordial black holes using the stochastic gravitational-wave background induced by primordial curvature perturbations. Phys Rev D 101(12):123535. https://doi.org/10.1103/PhysRevD.101.123535. arXiv:2005.05693 [astro-ph.CO]
Karki S et al (2016) The advanced LIGO photon calibrators. Rev Sci Instrum 87(11):114503. https://doi.org/10.1063/1.4967303. arXiv:1608.05055 [astro-ph.IM]
Karnesis N, Lilley M, Petiteau A (2020) Assessing the detectability of a Stochastic Gravitational Wave Background with LISA, using an excess of power approach. Class Quantum Grav 37(21):215017. https://doi.org/10.1088/1361-6382/abb637. arXiv:1906.09027 [astro-ph.IM]
Karnesis N, Babak S, Pieroni M, Cornish N, Littenberg T (2021) Characterization of the stochastic signal originating from compact binary populations as measured by LISA. Phys Rev D 104(4):043019. https://doi.org/10.1103/PhysRevD.104.043019. arXiv:2103.14598 [astro-ph.IM]
Kashlinsky A et al (2019) Electromagnetic probes of primordial black holes as dark matter. arXiv e-prints arXiv:1903.04424 [astro-ph.CO]
Katz ML, Kelley LZ, Dosopoulou F, Berry S, Blecha L, Larson SL (2020) Probing massive black hole binary populations with LISA. Mon Not R Astron Soc 491(2):2301–2317. https://doi.org/10.1093/mnras/stz3102. arXiv:1908.05779 [astro-ph.HE]
Kawasaki M, Kusenko A, Yanagida TT (2012) Primordial seeds of supermassive black holes. Phys Lett B 711:1–5. https://doi.org/10.1016/j.physletb.2012.03.056. arXiv:1202.3848 [astro-ph.CO]
Kawasaki M, Kitajima N, Yanagida TT (2013) Primordial black hole formation from an axionlike curvaton model. Phys Rev D 87(6):063519. https://doi.org/10.1103/PhysRevD.87.063519. arXiv:1207.2550 [hep-ph]
Kawasaki M, Sekiguchi T, Yamaguchi M, Yokoyama J (2018) Long-term dynamics of cosmological axion strings. PTEP 2018(9):091E01. https://doi.org/10.1093/ptep/pty098. arXiv:1806.05566 [hep-ph]

Keeley RE, Joudaki S, Kaplinghat M, Kirkby D (2019) Implications of a transition in the dark energy equation of state for the H_0 and σ_8 tensions. JCAP 12:035. https://doi.org/10.1088/1475-7516/2019/12/035. arXiv:1905.10198 [astro-ph.CO]

Kehagias A, Musco I, Riotto A (2019) Non-Gaussian formation of primordial black holes: effects on the threshold. JCAP 12:029. https://doi.org/10.1088/1475-7516/2019/12/029. arXiv:1906.07135 [astro-ph.CO]

Kelley LZ, Blecha L, Hernquist L, Sesana A, Taylor SR (2017) The gravitational wave background from massive black hole binaries in illustris: spectral features and time to detection with pulsar timing arrays. Mon Not R Astron Soc 471(4):4508–4526. https://doi.org/10.1093/mnras/stx1638. arXiv:1702.02180 [astro-ph.HE]

Kerr M et al (2020) The Parkes pulsar timing array project: second data release. Publ Astron Soc Australia 37:e020. https://doi.org/10.1017/pasa.2020.11. arXiv:2003.09780 [astro-ph.IM]

Khan A, Paschalidis V, Ruiz M, Shapiro SL (2018) Disks around merging binary black holes: from GW150914 to supermassive black holes. Phys Rev D 97(4):044036. https://doi.org/10.1103/PhysRevD.97.044036. arXiv:1801.02624 [astro-ph.HE]

Khlebnikov SY, Tkachev II (1996) Classical decay of inflaton. Phys Rev Lett 77:219–222. https://doi.org/10.1103/PhysRevLett.77.219. arXiv:hep-ph/9603378

Khlebnikov SY, Tkachev II (1997) Relic gravitational waves produced after preheating. Phys Rev D 56:653–660. https://doi.org/10.1103/PhysRevD.56.653. arXiv:hep-ph/9701423

Kibble TWB (1985) Evolution of a system of cosmic strings. Nucl Phys B 252:227. https://doi.org/10.1016/0550-3213(85)90596-6, [Erratum: Nucl. Phys. B 261, 750 (1985)]

Kimura R, Yamamoto K (2012) Constraints on general second-order scalar-tensor models from gravitational Cherenkov radiation. JCAP 07:050. https://doi.org/10.1088/1475-7516/2012/07/050. arXiv:1112.4284 [astro-ph.CO]

Kinney WH (2005) Horizon crossing and inflation with large eta. Phys Rev D 72:023515. https://doi.org/10.1103/PhysRevD.72.023515. arXiv:gr-qc/0503017

Kisslinger L, Kahniashvili T (2015) Polarized gravitational waves from cosmological phase transitions. Phys Rev D 92(4):043006. https://doi.org/10.1103/PhysRevD.92.043006. arXiv:1505.03680 [astro-ph.CO]

Kite T, Ravenni A, Patil SP, Chluba J (2021) Bridging the gap: spectral distortions meet gravitational waves. Mon Not R Astron Soc 505(3):4396–4405. https://doi.org/10.1093/mnras/stab1558. arXiv:2010.00040 [astro-ph.CO]

Klaer VB, Moore GD (2017) The dark-matter axion mass. JCAP 11:049. https://doi.org/10.1088/1475-7516/2017/11/049. arXiv:1708.07521 [hep-ph]

Klein A et al (2016) Science with the space-based interferometer eLISA: supermassive black hole binaries. Phys Rev D 93(2):024003. https://doi.org/10.1103/PhysRevD.93.024003. arXiv:1511.05581 [gr-qc]

Knox L, Millea M (2020) Hubble constant hunter's guide. Phys Rev D 101(4):043533. https://doi.org/10.1103/PhysRevD.101.043533. arXiv:1908.03663 [astro-ph.CO]

Kobayashi T (2014) Primordial magnetic fields from the post-inflationary universe. JCAP 05:040. https://doi.org/10.1088/1475-7516/2014/05/040. arXiv:1403.5168 [astro-ph.CO]

Kocsis B, Frei Z, Haiman Z, Menou K (2006) Finding the electromagnetic counterparts of cosmological standard sirens. Astrophys J 637:27–37. https://doi.org/10.1086/498236. arXiv:astro-ph/0505394

Kocsis B, Suyama T, Tanaka T, Yokoyama S (2018) Hidden universality in the merger rate distribution in the primordial black hole scenario. Astrophys J 854(1):41. https://doi.org/10.3847/1538-4357/aaa7f4. arXiv:1709.09007 [astro-ph.CO]

Kofman L (2003) Probing string theory with modulated cosmological fluctuations. arXiv e-prints arXiv:astro-ph/0303614

Kofman L, Linde AD, Starobinsky AA (1994) Reheating after inflation. Phys Rev Lett 73:3195–3198. https://doi.org/10.1103/PhysRevLett.73.3195. arXiv:hep-th/9405187

Kofman L, Linde AD, Starobinsky AA (1997) Towards the theory of reheating after inflation. Phys Rev D 56:3258–3295. https://doi.org/10.1103/PhysRevD.56.3258. arXiv:hep-ph/9704452

Koh S, Kouwn S, Kwon OK, Oh P (2013) Cosmological perturbations of a quartet of scalar fields with a spatially constant gradient. Phys Rev D 88:043523. https://doi.org/10.1103/PhysRevD.88.043523. arXiv:1304.7924 [gr-qc]

Kohri K, Terada T (2018) Semianalytic calculation of gravitational wave spectrum nonlinearly induced from primordial curvature perturbations. Phys Rev D 97(12):123532. https://doi.org/10.1103/PhysRevD.97.123532. arXiv:1804.08577 [gr-qc]

Kohri K, Terada T (2021) Solar-mass primordial black holes explain NANOGrav hint of gravitational waves. Phys Lett B 813:136040. https://doi.org/10.1016/j.physletb.2020.136040. arXiv:2009.11853 [astro-ph.CO]

Konstandin T (2013) Quantum transport and electroweak baryogenesis. Phys Usp 56:747–771. https://doi.org/10.3367/UFNe.0183.201308a.0785. arXiv:1302.6713 [hep-ph]

Konstandin T (2018) Gravitational radiation from a bulk flow model. JCAP 03:047. https://doi.org/10.1088/1475-7516/2018/03/047. arXiv:1712.06869 [astro-ph.CO]

Konstandin T, No JM (2011) Hydrodynamic obstruction to bubble expansion. JCAP 02:008. https://doi.org/10.1088/1475-7516/2011/02/008. arXiv:1011.3735 [hep-ph]

Konstandin T, Servant G (2011a) Cosmological consequences of nearly conformal dynamics at the TeV scale. JCAP 12:009. https://doi.org/10.1088/1475-7516/2011/12/009. arXiv:1104.4791 [hep-ph]

Konstandin T, Servant G (2011b) Natural cold baryogenesis from strongly interacting electroweak symmetry breaking. JCAP 07:024. https://doi.org/10.1088/1475-7516/2011/07/024. arXiv:1104.4793 [hep-ph]

Konstandin T, Nardini G, Quiros M (2010) Gravitational backreaction effects on the holographic phase transition. Phys Rev D 82:083513. https://doi.org/10.1103/PhysRevD.82.083513. arXiv:1007.1468 [hep-ph]

Konstandin T, Nardini G, Rues I (2014) From Boltzmann equations to steady wall velocities. JCAP 09:028. https://doi.org/10.1088/1475-7516/2014/09/028. arXiv:1407.3132 [hep-ph]

Kopp M, Hofmann S, Weller J (2011) Separate universes do not constrain primordial black hole formation. Phys Rev D 83:124025. https://doi.org/10.1103/PhysRevD.83.124025. arXiv:1012.4369 [astro-ph.CO]

Kormendy J, Ho LC (2013) Coevolution (or not) of supermassive black holes and host galaxies. Annu Rev Astron Astrophys 51:511–653. https://doi.org/10.1146/annurev-astro-082708-101811. arXiv:1304.7762 [astro-ph.CO]

Koshelev AS, Sravan Kumar K, Starobinsky AA (2018) R^2 inflation to probe non-perturbative quantum gravity. JHEP 03:071. https://doi.org/10.1007/JHEP03(2018)071. arXiv:1711.08864 [hep-th]

Koshelev AS, Sravan Kumar K, Mazumdar A, Starobinsky AA (2020) Non-Gaussianities and tensor-to-scalar ratio in non-local R^2-like inflation. JHEP 06:152. https://doi.org/10.1007/JHEP06(2020)152. arXiv:2003.00629 [hep-th]

Kosowsky A, Turner MS (1993) Gravitational radiation from colliding vacuum bubbles: envelope approximation to many bubble collisions. Phys Rev D 47:4372–4391. https://doi.org/10.1103/PhysRevD.47.4372. arXiv:astro-ph/9211004

Kosowsky A, Turner MS, Watkins R (1992) Gravitational waves from first order cosmological phase transitions. Phys Rev Lett 69:2026–2029. https://doi.org/10.1103/PhysRevLett.69.2026

Kosowsky A, Mack A, Kahniashvili T (2002) Gravitational radiation from cosmological turbulence. Phys Rev D 66:024030. https://doi.org/10.1103/PhysRevD.66.024030. arXiv:astro-ph/0111483

Kowalska I, Bulik T, Belczynski K (2012) Gravitational wave background from population III binaries. Astron Astrophys 541:A120. https://doi.org/10.1051/0004-6361/201118604. arXiv:1202.3346 [astro-ph.CO]

Kozaczuk J (2015) Bubble expansion and the viability of singlet-driven electroweak baryogenesis. JHEP 10:135. https://doi.org/10.1007/JHEP10(2015)135. arXiv:1506.04741 [hep-ph]

Kozaczuk J, Profumo S, Haskins LS, Wainwright CL (2015) Cosmological phase transitions and their properties in the NMSSM. JHEP 01:144. https://doi.org/10.1007/JHEP01(2015)144. arXiv:1407.4134 [hep-ph]

Krauss LM (1992) Gravitational waves from global phase transitions. Phys Lett B 284:229–233. https://doi.org/10.1016/0370-2693(92)90425-4

Kudoh H, Taruya A (2005) Probing anisotropies of gravitational-wave backgrounds with a space-based interferometer: geometric properties of antenna patterns and their angular power. Phys Rev D 71:024025. https://doi.org/10.1103/PhysRevD.71.024025. arXiv:gr-qc/0411017

Kudoh H, Taruya A, Hiramatsu T, Himemoto Y (2006) Detecting a gravitational-wave background with next-generation space interferometers. Phys Rev D 73:064006. https://doi.org/10.1103/PhysRevD.73.064006. arXiv:gr-qc/0511145

Kumar S, Sundrum R, Tsai Y (2021) Non-Gaussian stochastic gravitational waves from phase transitions. JHEP 11:107. https://doi.org/10.1007/JHEP11(2021)107. arXiv:2102.05665 [astro-ph.CO]

Kuroyanagi S, Chiba T, Sugiyama N (2009) Precision calculations of the gravitational wave background spectrum from inflation. Phys Rev D 79:103501. https://doi.org/10.1103/PhysRevD.79.103501. arXiv:0804.3249 [astro-ph]

Kuroyanagi S, Chiba T, Sugiyama N (2011) Prospects for direct detection of inflationary gravitational waves by next generation interferometric detectors. Phys Rev D 83:043514. https://doi.org/10.1103/PhysRevD.83.043514. arXiv:1010.5246 [astro-ph.CO]

Kuroyanagi S, Miyamoto K, Sekiguchi T, Takahashi K, Silk J (2012) Forecast constraints on cosmic string parameters from gravitational wave direct detection experiments. Phys Rev D 86:023503. https://doi.org/10.1103/PhysRevD.86.023503. arXiv:1202.3032 [astro-ph.CO]

Kuroyanagi S, Miyamoto K, Sekiguchi T, Takahashi K, Silk J (2013) Forecast constraints on cosmic strings from future CMB, pulsar timing and gravitational wave direct detection experiments. Phys Rev D 87(2):023522. https://doi.org/10.1103/PhysRevD.87.023522, [Erratum: Phys. Rev. D 87, 069903 (2013)]. arXiv:1210.2829 [astro-ph.CO]

Kuroyanagi S, Nakayama K, Yokoyama J (2015) Prospects of determination of reheating temperature after inflation by DECIGO. PTEP 2015(1):013E02. https://doi.org/10.1093/ptep/ptu176. arXiv:1410.6618 [astro-ph.CO]

Kuroyanagi S, Takahashi K, Yonemaru N, Kumamoto H (2017) Anisotropies in the gravitational wave background as a probe of the cosmic string network. Phys Rev D 95(4):043531. https://doi.org/10.1103/PhysRevD.95.043531. arXiv:1604.00332 [astro-ph.CO]

Kuroyanagi S, Chiba T, Takahashi T (2018) Probing the universe through the stochastic gravitational wave background. JCAP 11:038. https://doi.org/10.1088/1475-7516/2018/11/038. arXiv:1807.00786 [astro-ph.CO]

Kusenko A (1997) Phase transitions precipitated by solitosynthesis. Phys Lett B 406:26–33. https://doi.org/10.1016/S0370-2693(97)00700-4. arXiv:hep-ph/9705361

Kusenko A, Mazumdar A (2008) Gravitational waves from fragmentation of a primordial scalar condensate into Q-balls. Phys Rev Lett 101:211301. https://doi.org/10.1103/PhysRevLett.101.211301. arXiv:0807.4554 [astro-ph]

Kusenko A, Mazumdar A, Multamaki T (2009) Gravitational waves from the fragmentation of a supersymmetric condensate. Phys Rev D 79:124034. https://doi.org/10.1103/PhysRevD.79.124034. arXiv:0902.2197 [astro-ph.CO]

Kusenko A, Sasaki M, Sugiyama S, Takada M, Takhistov V, Vitagliano E (2020) Exploring primordial black holes from the multiverse with optical telescopes. Phys Rev Lett 125:181304. https://doi.org/10.1103/PhysRevLett.125.181304. arXiv:2001.09160 [astro-ph.CO]

Kuzmin VA, Rubakov VA, Shaposhnikov ME (1985) On the anomalous electroweak baryon number nonconservation in the early universe. Phys Lett B 155:36. https://doi.org/10.1016/0370-2693(85)91028-7

Kyutoku K, Seto N (2016) Concise estimate of the expected number of detections for stellar-mass binary black holes by eLISA. Mon Not R Astron Soc 462(2):2177–2183. https://doi.org/10.1093/mnras/stw1767. arXiv:1606.02298 [astro-ph.HE]

Kyutoku K, Seto N (2017) Gravitational-wave cosmography with LISA and the Hubble tension. Phys Rev D 95(8):083525. https://doi.org/10.1103/PhysRevD.95.083525. arXiv:1609.07142 [astro-ph.CO]

Laghi D (2021) Gravitational wave cosmology with extreme mass-ratio inspirals. In: 55th Rencontres de Moriond on Gravitation. arXiv:2106.02053 [astro-ph.CO]

Laghi D, Tamanini N, Del Pozzo W, Sesana A, Gair J, Babak S, Izquierdo-Villalba D (2021) Gravitational-wave cosmology with extreme mass-ratio inspirals. Mon Not R Astron Soc 508(3):4512–4531. https://doi.org/10.1093/mnras/stab2741. arXiv:2102.01708 [astro-ph.CO]

Lagos M, Fishbach M, Landry P, Holz DE (2019) Standard sirens with a running Planck mass. Phys Rev D 99(8):083504. https://doi.org/10.1103/PhysRevD.99.083504. arXiv:1901.03321 [astro-ph.CO]

Laguna P, Larson SL, Spergel D, Yunes N (2010) Integrated Sachs-Wolfe effect for gravitational radiation. Astrophys J Lett 715:L12. https://doi.org/10.1088/2041-8205/715/1/L12. arXiv:0905.1908 [gr-qc]

Laine M, Meyer M, Nardini G (2017) Thermal phase transition with full 2-loop effective potential. Nucl Phys B 920:565–600. https://doi.org/10.1016/j.nuclphysb.2017.04.023. arXiv:1702.07479 [hep-ph]

Lamberts A, Garrison-Kimmel S, Clausen DR, Hopkins PF (2016) When and where did GW150914 form? Mon Not R Astron Soc 463(1):L31–L35. https://doi.org/10.1093/mnrasl/slw152. arXiv:1605.08783 [astro-ph.HE]

Lamberts A, Blunt S, Littenberg TB, Garrison-Kimmel S, Kupfer T, Sanderson RE (2019) Predicting the LISA white dwarf binary population in the Milky Way with cosmological simulations. Mon Not R

Astron Soc 490(4):5888–5903. https://doi.org/10.1093/mnras/stz2834. arXiv:1907.00014 [astro-ph.HE]

Langlois D, Noui K (2016) Degenerate higher derivative theories beyond Horndeski: evading the Ostrogradski instability. JCAP 02:034. https://doi.org/10.1088/1475-7516/2016/02/034. arXiv:1510.06930 [gr-qc]

Lasky PD, Bennett MF, Melatos A (2013) Stochastic gravitational wave background from hydrodynamic turbulence in differentially rotating neutron stars. Phys Rev D 87(6):063004. https://doi.org/10.1103/PhysRevD.87.063004. arXiv:1302.6033 [astro-ph.HE]

Laureijs R et al (2011) Euclid definition study report. arXiv e-prints arXiv:1110.3193 [astro-ph.CO]

Laurent B, Cline JM (2020) Fluid equations for fast-moving electroweak bubble walls. Phys Rev D 102(6):063516. https://doi.org/10.1103/PhysRevD.102.063516. arXiv:2007.10935 [hep-ph]

Leach SM, Liddle AR (2001) Inflationary perturbations near horizon crossing. Phys Rev D 63:043508. https://doi.org/10.1103/PhysRevD.63.043508. arXiv:astro-ph/0010082

Leach SM, Sasaki M, Wands D, Liddle AR (2001) Enhancement of superhorizon scale inflationary curvature perturbations. Phys Rev D 64:023512. https://doi.org/10.1103/PhysRevD.64.023512. arXiv:astro-ph/0101406

Leblond L, Shlaer B, Siemens X (2009) Gravitational waves from broken cosmic strings: the bursts and the beads. Phys Rev D 79:123519. https://doi.org/10.1103/PhysRevD.79.123519. arXiv:0903.4686 [astro-ph.CO]

Lehébel A, Babichev E, Charmousis C (2017) A no-hair theorem for stars in Horndeski theories. JCAP 07:037. https://doi.org/10.1088/1475-7516/2017/07/037. arXiv:1706.04989 [gr-qc]

Lehners JL (2010) Ekpyrotic non-Gaussianity: a review. Adv Astron 2010:903907. https://doi.org/10.1155/2010/903907. arXiv:1001.3125 [hep-th]

Lentati L et al (2015) European pulsar timing array limits on an isotropic stochastic gravitational-wave background. Mon Not R Astron Soc 453(3):2576–2598. https://doi.org/10.1093/mnras/stv1538. arXiv:1504.03692 [astro-ph.CO]

Lewicki M, Vaskonen V (2020a) Gravitational wave spectra from strongly supercooled phase transitions. Eur Phys J C 80(11):1003. https://doi.org/10.1140/epjc/s10052-020-08589-1. arXiv:2007.04967 [astro-ph.CO]

Lewicki M, Vaskonen V (2020b) On bubble collisions in strongly supercooled phase transitions. Phys Dark Universe 30:100672. https://doi.org/10.1016/j.dark.2020.100672. arXiv:1912.00997 [astro-ph.CO]

Lewicki M, Vaskonen V (2021) Gravitational waves from colliding vacuum bubbles in gauge theories. Eur Phys J C 81(5):437. https://doi.org/10.1140/epjc/s10052-021-09232-3, [Erratum: Eur. Phys. J. C 81, 1077 (2021)]. arXiv:2012.07826 [astro-ph.CO]

Lewicki M, Pujolàs O, Vaskonen V (2021) Escape from supercooling with or without bubbles: gravitational wave signatures. Eur Phys J C 81(9):857. https://doi.org/10.1140/epjc/s10052-021-09669-6. arXiv:2106.09706 [astro-ph.CO]

Lewicki M, Merchand M, Zych M (2022) Electroweak bubble wall expansion: gravitational waves and baryogenesis in Standard Model-like thermal plasma. JHEP 02:017. https://doi.org/10.1007/JHEP02(2022)017. arXiv:2111.02393 [astro-ph.CO]

Li B, Shapiro PR (2021) Precision cosmology and the stiff-amplified gravitational-wave background from inflation: NANOGrav, Advanced LIGO-Virgo and the Hubble tension. JCAP 10:024. https://doi.org/10.1088/1475-7516/2021/10/024. arXiv:2107.12229 [astro-ph.CO]

Li B, Rindler-Daller T, Shapiro PR (2014) Cosmological constraints on Bose–Einstein-condensed scalar field dark matter. Phys Rev D 89(8):083536. https://doi.org/10.1103/PhysRevD.89.083536. arXiv:1310.6061 [astro-ph.CO]

Li B, Shapiro PR, Rindler-Daller T (2017) Bose–Einstein-condensed scalar field dark matter and the gravitational wave background from inflation: new cosmological constraints and its detectability by LIGO. Phys Rev D 96(6):063505. https://doi.org/10.1103/PhysRevD.96.063505. arXiv:1611.07961 [astro-ph.CO]

Li M (2004) A model of holographic dark energy. Phys Lett B 603:1. https://doi.org/10.1016/j.physletb.2004.10.014. arXiv:hep-th/0403127

Li M, Li XD, Wang S, Wang Y (2011) Dark energy. Commun Theor Phys 56:525–604. https://doi.org/10.1088/0253-6102/56/3/24. arXiv:1103.5870 [astro-ph.CO]

Li TGF, Del Pozzo W, Vitale S, Van Den Broeck C, Agathos M, Veitch J, Grover K, Sidery T, Sturani R, Vecchio A (2012) Towards a generic test of the strong field dynamics of general relativity using

compact binary coalescence. Phys Rev D 85:082003. https://doi.org/10.1103/PhysRevD.85.082003. arXiv:1110.0530 [gr-qc]
Libanore S, Artale MC, Karagiannis D, Liguori M, Bartolo N, Bouffanais Y, Giacobbo N, Mapelli M, Matarrese S (2021) Gravitational wave mergers as tracers of large scale structures. JCAP 02:035. https://doi.org/10.1088/1475-7516/2021/02/035. arXiv:2007.06905 [astro-ph.CO]
Liddle AR, Lyth DH (2000) Cosmological inflation and large-scale structure. Cambridge University Press, Cambridge. https://doi.org/10.1017/CBO9781139175180
Liddle AR, Mazumdar A, Schunck FE (1998) Assisted inflation. Phys Rev D 58:061301. https://doi.org/10.1103/PhysRevD.58.061301. arXiv:astro-ph/9804177
Linde A, Mooij S, Pajer E (2013) Gauge field production in supergravity inflation: local non-Gaussianity and primordial black holes. Phys Rev D 87(10):103506. https://doi.org/10.1103/PhysRevD.87.103506. arXiv:1212.1693 [hep-th]
Linde AD (1980) Infrared problem in thermodynamics of the Yang–Mills gas. Phys Lett B 96:289–292. https://doi.org/10.1016/0370-2693(80)90769-8
Linde AD (1982) A new inflationary universe scenario: a possible solution of the horizon, flatness, homogeneity, isotropy and primordial monopole problems. Phys Lett B 108:389–393. https://doi.org/10.1016/0370-2693(82)91219-9
Linde AD (1994) Hybrid inflation. Phys Rev D 49:748–754. https://doi.org/10.1103/PhysRevD.49.748. arXiv:astro-ph/9307002
Linder EV (2003) Exploring the expansion history of the universe. Phys Rev Lett 90:091301. https://doi.org/10.1103/PhysRevLett.90.091301. arXiv:astro-ph/0208512
LISA (2023) LISA documentation. https://www.cosmos.esa.int/web/lisa/documents
LISA Data Challenge Working Group (n.d.) White paper (to appear)
LISA Science Study Team (2018) LISA Science Requirements Document. Tech. rep., LISA. https://www.cosmos.esa.int/web/lisa/documents
LISA Waveform Working Group (n.d.) White paper (to appear)
Littenberg T, Cornish N, Lackeos K, Robson T (2020) Global analysis of the gravitational wave signal from galactic binaries. Phys Rev D 101(12):123021. https://doi.org/10.1103/PhysRevD.101.123021. arXiv:2004.08464 [gr-qc]
Liu J, Guo ZK, Cai RG (2020) Primordial black holes from cosmic domain walls. Phys Rev D 101 (2):023513. https://doi.org/10.1103/PhysRevD.101.023513. arXiv:1908.02662 [astro-ph.CO]
Lizarraga J, Urrestilla J, Daverio D, Hindmarsh M, Kunz M (2016) New CMB constraints for Abelian Higgs cosmic strings. JCAP 10:042. https://doi.org/10.1088/1475-7516/2016/10/042. arXiv:1609.03386 [astro-ph.CO]
Loeb A (1998) Direct measurement of cosmological parameters from the cosmic deceleration of extragalactic objects. Astrophys J Lett 499:L111–L114. https://doi.org/10.1086/311375. arXiv:astro-ph/9802122
Lombriser L (2018) Parametrizations for tests of gravity. Int J Mod Phys D 27(15):1848002. https://doi.org/10.1142/S0218271818480024. arXiv:1908.07892 [astro-ph.CO]
Lombriser L, Lima NA (2017) Challenges to self-acceleration in modified gravity from gravitational waves and large-scale structure. Phys Lett B 765:382–385. https://doi.org/10.1016/j.physletb.2016.12.048. arXiv:1602.07670 [astro-ph.CO]
Lombriser L, Taylor A (2016) Breaking a dark degeneracy with gravitational waves. JCAP 03:031. https://doi.org/10.1088/1475-7516/2016/03/031. arXiv:1509.08458 [astro-ph.CO]
Long AJ, Hyde JM, Vachaspati T (2014) Cosmic strings in hidden sectors: 1. Radiation of standard model particles. JCAP 09:030. https://doi.org/10.1088/1475-7516/2014/09/030. arXiv:1405.7679 [hep-ph]
Lopez-Eiguren A, Lizarraga J, Hindmarsh M, Urrestilla J (2017) Cosmic microwave background constraints for global strings and global monopoles. JCAP 07:026. https://doi.org/10.1088/1475-7516/2017/07/026. arXiv:1705.04154 [astro-ph.CO]
Lorenz L, Ringeval C, Sakellariadou M (2010) Cosmic string loop distribution on all length scales and at any redshift. JCAP 10:003. https://doi.org/10.1088/1475-7516/2010/10/003. arXiv:1006.0931 [astro-ph.CO]
Lozanov KD (2019) Lectures on reheating after inflation. arXiv e-prints arXiv:1907.04402 [astro-ph.CO]
Lozanov KD, Amin MA (2017) Equation of state and duration to radiation domination after inflation. Phys Rev Lett 119(6):061301. https://doi.org/10.1103/PhysRevLett.119.061301. arXiv:1608.01213 [astro-ph.CO]
Lue A, Rajagopal K, Trodden M (1997) Semianalytical approaches to local electroweak baryogenesis. Phys Rev D 56:1250–1261. https://doi.org/10.1103/PhysRevD.56.1250. arXiv:hep-ph/9612282

Lue A, Wang LM, Kamionkowski M (1999) Cosmological signature of new parity violating interactions. Phys Rev Lett 83:1506–1509. https://doi.org/10.1103/PhysRevLett.83.1506. arXiv:astro-ph/9812088
Luty MA, Porrati M, Rattazzi R (2003) Strong interactions and stability in the DGP model. JHEP 09:029. https://doi.org/10.1088/1126-6708/2003/09/029. arXiv:hep-th/0303116
Lyth DH (2012) The hybrid inflation waterfall and the primordial curvature perturbation. JCAP 05:022. https://doi.org/10.1088/1475-7516/2012/05/022. arXiv:1201.4312 [astro-ph.CO]
Lyth DH, Riotto A (1999) Particle physics models of inflation and the cosmological density perturbation. Phys Rept 314:1–146. https://doi.org/10.1016/S0370-1573(98)00128-8. arXiv:hep-ph/9807278
Lyth DH, Wands D (2002) Generating the curvature perturbation without an inflaton. Phys Lett B 524:5–14. https://doi.org/10.1016/S0370-2693(01)01366-1. arXiv:hep-ph/0110002
MacLeod CL, Hogan CJ (2008) Precision of Hubble constant derived using black hole binary absolute distances and statistical redshift information. Phys Rev D 77:043512. https://doi.org/10.1103/PhysRevD.77.043512. arXiv:0712.0618 [astro-ph]
Madge E, Schwaller P (2019) Leptophilic dark matter from gauged lepton number: phenomenology and gravitational wave signatures. JHEP 02:048. https://doi.org/10.1007/JHEP02(2019)048. arXiv:1809.09110 [hep-ph]
Maggiore M (2007) Gravitational waves. Vol 1: Theory and experiments. Oxford University Press, Oxford. https://doi.org/10.1093/acprof:oso/9780198570745.001.0001
Maggiore M (2014) Phantom dark energy from nonlocal infrared modifications of general relativity. Phys Rev D 89(4):043008. https://doi.org/10.1103/PhysRevD.89.043008. arXiv:1307.3898 [hep-th]
Maggiore M (2018) Gravitational waves. Vol 2: Astrophysics and cosmology. Oxford University Press, Oxford
Maggiore M et al (2020) Science case for the Einstein telescope. JCAP 03:050. https://doi.org/10.1088/1475-7516/2020/03/050. arXiv:1912.02622 [astro-ph.CO]
Majumdar AS (2001) From brane assisted inflation to quintessence through a single scalar field. Phys Rev D 64:083503. https://doi.org/10.1103/PhysRevD.64.083503. arXiv:astro-ph/0105518
Maldacena JM (1998) The Large N limit of superconformal field theories and supergravity. Adv Theor Math Phys 2:231–252. https://doi.org/10.4310/ATMP.1998.v2.n2.a1. arXiv:hep-th/9711200
Maldacena JM (2003) Non-Gaussian features of primordial fluctuations in single field inflationary models. JHEP 05:013. https://doi.org/10.1088/1126-6708/2003/05/013. arXiv:astro-ph/0210603
Maleknejad A (2014) Chiral gravity waves and leptogenesis in inflationary models with non-Abelian gauge fields. Phys Rev D 90(2):023542. https://doi.org/10.1103/PhysRevD.90.023542. arXiv:1401.7628 [hep-th]
Maleknejad A, Komatsu E (2019) Production and backreaction of spin-2 particles of $SU(2)$ gauge field during inflation. JHEP 05:174. https://doi.org/10.1007/JHEP05(2019)174. arXiv:1808.09076 [hep-ph]
Maleknejad A, Sheikh-Jabbari MM (2011) Non-Abelian gauge field inflation. Phys Rev D 84:043515. https://doi.org/10.1103/PhysRevD.84.043515. arXiv:1102.1932 [hep-ph]
Maleknejad A, Sheikh-Jabbari MM (2013) Gauge-flation: inflation from non-Abelian gauge fields. Phys Lett B 723:224–228. https://doi.org/10.1016/j.physletb.2013.05.001. arXiv:1102.1513 [hep-ph]
Malhotra A, Dimastrogiovanni E, Fasiello M, Shiraishi M (2021) Cross-correlations as a diagnostic tool for primordial gravitational waves. JCAP 03:088. https://doi.org/10.1088/1475-7516/2021/03/088. arXiv:2012.03498 [astro-ph.CO]
Mandic V, Bird S, Cholis I (2016) Stochastic gravitational-wave background due to primordial binary black hole mergers. Phys Rev Lett 117(20):201102. https://doi.org/10.1103/PhysRevLett.117.201102. arXiv:1608.06699 [astro-ph.CO]
Mangiagli A, Bonetti M, Sesana A, Colpi M (2019) Merger rate of stellar black hole binaries above the pair instability mass gap. Astrophys J Lett 883(1):L27. https://doi.org/10.3847/2041-8213/ab3f33. arXiv:1907.12562 [astro-ph.HE]
Mangiagli A, Klein A, Bonetti M, Katz ML, Sesana A, Volonteri M, Colpi M, Marsat S, Babak S (2020) Observing the inspiral of coalescing massive black hole binaries with LISA in the era of Multi-Messenger Astrophysics. Phys Rev D 102:084056. https://doi.org/10.1103/PhysRevD.102.084056. arXiv:2006.12513 [astro-ph.HE]
Mapelli M, Giacobbo N, Toffano M, Ripamonti E, Bressan A, Spera M, Branchesi M (2018) The host galaxies of double compact objects merging in the local Universe. Mon Not R Astron Soc 481(4):5324–5330. https://doi.org/10.1093/mnras/sty2663. arXiv:1809.03521 [astro-ph.HE]

Margalit A, Contaldi CR, Pieroni M (2020) Phase decoherence of gravitational wave backgrounds. Phys Rev D 102(8):083506. https://doi.org/10.1103/PhysRevD.102.083506. arXiv:2004.01727 [astro-ph.CO]

Marsat S, Baker JG, Dal Canton T (2021) Exploring the Bayesian parameter estimation of binary black holes with LISA. Phys Rev D 103(8):083011. https://doi.org/10.1103/PhysRevD.103.083011. arXiv:2003.00357 [gr-qc]

Martin J, Yokoyama J (2008) Generation of large-scale magnetic fields in single-field inflation. JCAP 01:025. https://doi.org/10.1088/1475-7516/2008/01/025. arXiv:0711.4307 [astro-ph]

Martin J, Papanikolaou T, Vennin V (2020) Primordial black holes from the preheating instability in single-field inflation. JCAP 01:024. https://doi.org/10.1088/1475-7516/2020/01/024. arXiv:1907.04236 [astro-ph.CO]

Martin X, Vilenkin A (1996) Gravitational wave background from hybrid topological defects. Phys Rev Lett 77:2879–2882. https://doi.org/10.1103/PhysRevLett.77.2879. arXiv:astro-ph/9606022

Martin X, Vilenkin A (1997) Gravitational radiation from monopoles connected by strings. Phys Rev D 55:6054–6060. https://doi.org/10.1103/PhysRevD.55.6054. arXiv:gr-qc/9612008

Martinovic K, Meyers PM, Sakellariadou M, Christensen N (2021) Simultaneous estimation of astrophysical and cosmological stochastic gravitational-wave backgrounds with terrestrial detectors. Phys Rev D 103(4):043023. https://doi.org/10.1103/PhysRevD.103.043023. arXiv:2011.05697 [gr-qc]

Martins CJAP (2019) Scaling properties of cosmological axion strings. Phys Lett B 788:147–151. https://doi.org/10.1016/j.physletb.2018.11.031. arXiv:1811.12678 [astro-ph.CO]

Martins CJAP, Shellard EPS (1996) Quantitative string evolution. Phys Rev D 54:2535–2556. https://doi.org/10.1103/PhysRevD.54.2535. arXiv:hep-ph/9602271

Martins CJAP, Shellard EPS (2002) Extending the velocity dependent one scale string evolution model. Phys Rev D 65:043514. https://doi.org/10.1103/PhysRevD.65.043514. arXiv:hep-ph/0003298

Martins CJAP, Moore JN, Shellard EPS (2004) A Unified model for vortex string network evolution. Phys Rev Lett 92:251601. https://doi.org/10.1103/PhysRevLett.92.251601. arXiv:hep-ph/0310255

Marzo C, Marzola L, Vaskonen V (2019) Phase transition and vacuum stability in the classically conformal B-L model. Eur Phys J C 79(7):601. https://doi.org/10.1140/epjc/s10052-019-7076-x. arXiv:1811.11169 [hep-ph]

Marzola L, Racioppi A, Vaskonen V (2017) Phase transition and gravitational wave phenomenology of scalar conformal extensions of the Standard Model. Eur Phys J C 77(7):484. https://doi.org/10.1140/epjc/s10052-017-4996-1. arXiv:1704.01034 [hep-ph]

Mastrogiovanni S, Leyde K, Karathanasis C, Chassande-Mottin E, Steer DA, Gair J, Ghosh A, Gray R, Mukherjee S, Rinaldi S (2021) On the importance of source population models for gravitational-wave cosmology. Phys Rev D 104(6):062009. https://doi.org/10.1103/PhysRevD.104.062009. arXiv:2103.14663 [gr-qc]

Matsedonskyi O, Servant G (2020) High-temperature electroweak symmetry non-restoration from new fermions and implications for baryogenesis. JHEP 09:012. https://doi.org/10.1007/JHEP09(2020)012. arXiv:2002.05174 [hep-ph]

Matsui T (2018) Gravitational waves from the first order electroweak phase transition in the Z_3 symmetric singlet scalar model. EPJ Web Conf 168:05001. https://doi.org/10.1051/epjconf/201816805001. arXiv:1709.05900 [hep-ph]

Matsui Y, Kuroyanagi S (2019) Gravitational wave background from kink-kink collisions on infinite cosmic strings. Phys Rev D 100(12):123515. https://doi.org/10.1103/PhysRevD.100.123515. arXiv:1902.09120 [astro-ph.CO]

Matsunami D, Pogosian L, Saurabh A, Vachaspati T (2019) Decay of cosmic string loops due to particle radiation. Phys Rev Lett 122(20):201301. https://doi.org/10.1103/PhysRevLett.122.201301. arXiv:1903.05102 [hep-ph]

Max K, Platscher M, Smirnov J (2017) Gravitational wave oscillations in bigravity. Phys Rev Lett 119(11):111101. https://doi.org/10.1103/PhysRevLett.119.111101. arXiv:1703.07785 [gr-qc]

Max K, Platscher M, Smirnov J (2018) Decoherence of gravitational wave oscillations in bigravity. Phys Rev D 97(6):064009. https://doi.org/10.1103/PhysRevD.97.064009. arXiv:1712.06601 [gr-qc]

McDonough E, Alexander S (2018) Observable chiral gravitational waves from inflation in string theory. JCAP 11:030. https://doi.org/10.1088/1475-7516/2018/11/030. arXiv:1806.05684 [hep-th]

McManus R, Lombriser L, Peñarrubia J (2016) Finding Horndeski theories with Einstein gravity limits. JCAP 11:006. https://doi.org/10.1088/1475-7516/2016/11/006. arXiv:1606.03282 [gr-qc]

McManus R, Lombriser L, Peñarrubia J (2017) Parameterised post-Newtonian expansion in screened regions. JCAP 12:031. https://doi.org/10.1088/1475-7516/2017/12/031. arXiv:1705.05324 [gr-qc]

Mégevand A, Ramírez S (2018) Bubble nucleation and growth in slow cosmological phase transitions. Nucl Phys B 928:38–71. https://doi.org/10.1016/j.nuclphysb.2018.01.012. arXiv:1710.06279 [astro-ph.CO]

Megías E, Nardini G, Quirós M (2018a) Cosmological phase transitions in warped space: gravitational waves and collider signatures. JHEP 09:095. https://doi.org/10.1007/JHEP09(2018)095. arXiv:1806.04877 [hep-ph]

Megías E, Nardini G, Quirós M (2018b) Gravitational waves and collider signatures from holographic phase transitions in soft walls. PoS Confinement2018:227. https://doi.org/10.22323/1.336.0227. arXiv:1811.10891 [hep-ph]

Megias E, Nardini G, Quiros M (2020) Gravitational imprints from heavy Kaluza–Klein resonances. Phys Rev D 102(5):055004. https://doi.org/10.1103/PhysRevD.102.055004. arXiv:2005.04127 [hep-ph]

Merloni A et al (2012) eROSITA science book: mapping the structure of the energetic universe. arXiv e-prints arXiv:1209.3114 [astro-ph.HE]

Meyers PM, Martinovic K, Christensen N, Sakellariadou M (2020) Detecting a stochastic gravitational-wave background in the presence of correlated magnetic noise. Phys Rev D 102(10):102005. https://doi.org/10.1103/PhysRevD.102.102005. arXiv:2008.00789 [gr-qc]

Miller AL, Clesse S, De Lillo F, Bruno G, Depasse A, Tanasijczuk A (2021) Probing planetary-mass primordial black holes with continuous gravitational waves. Phys Dark Univ 32:100836. https://doi.org/10.1016/j.dark.2021.100836. arXiv:2012.12983 [astro-ph.HE]

Mirshekari S, Yunes N, Will CM (2012) Constraining generic Lorentz violation and the speed of the graviton with gravitational waves. Phys Rev D 85:024041. https://doi.org/10.1103/PhysRevD.85.024041. arXiv:1110.2720 [gr-qc]

Mirzagholi L, Komatsu E, Lozanov KD, Watanabe Y (2020a) Effects of gravitational Chern–Simons during axion-SU(2) inflation. JCAP 06:024. https://doi.org/10.1088/1475-7516/2020/06/024. arXiv:2003.05931 [gr-qc]

Mirzagholi L, Maleknejad A, Lozanov KD (2020b) Production and backreaction of fermions from axion-$SU(2)$ gauge fields during inflation. Phys Rev D 101(8):083528. https://doi.org/10.1103/PhysRevD.101.083528. arXiv:1905.09258 [hep-th]

Mishra A, Meena AK, More A, Bose S, Bagla JS (2021) Gravitational lensing of gravitational waves: effect of microlens population in lensing galaxies. Mon Not R Astron Soc 508(4):4869–4886. https://doi.org/10.1093/mnras/stab2875. arXiv:2102.03946 [astro-ph.CO]

Modesto L (2012) Super-renormalizable quantum gravity. Phys Rev D 86:044005. https://doi.org/10.1103/PhysRevD.86.044005. arXiv:1107.2403 [hep-th]

Mollerach S, Harari D, Matarrese S (2004) CMB polarization from secondary vector and tensor modes. Phys Rev D 69:063002. https://doi.org/10.1103/PhysRevD.69.063002. arXiv:astro-ph/0310711

Monin A, Voloshin MB (2008) The spontaneous breaking of a metastable string. Phys Rev D 78:065048. https://doi.org/10.1103/PhysRevD.78.065048. arXiv:0808.1693 [hep-th]

Moore CJ, Cole RH, Berry CPL (2015) Gravitational-wave sensitivity curves. Class Quantum Grav 32 (1):015014. https://doi.org/10.1088/0264-9381/32/1/015014. arXiv:1408.0740 [gr-qc]

Moore CJ, Gerosa D, Klein A (2019) Are stellar-mass black-hole binaries too quiet for LISA? Mon Not R Astron Soc 488(1):L94–L98. https://doi.org/10.1093/mnrasl/slz104. arXiv:1905.11998 [astro-ph.HE]

Moore GD, Nelson AE (2001) Lower bound on the propagation speed of gravity from gravitational Cherenkov radiation. JHEP 09:023. https://doi.org/10.1088/1126-6708/2001/09/023. arXiv:hep-ph/0106220

Moore GD, Prokopec T (1995) How fast can the wall move? A Study of the electroweak phase transition dynamics. Phys Rev D 52:7182–7204. https://doi.org/10.1103/PhysRevD.52.7182. arXiv:hep-ph/9506475

Moore GD, Rummukainen K (2001) Electroweak bubble nucleation, nonperturbatively. Phys Rev D 63:045002. https://doi.org/10.1103/PhysRevD.63.045002. arXiv:hep-ph/0009132

Moradinezhad Dizgah A, Franciolini G, Riotto A (2019) Primordial black holes from broad spectra: abundance and clustering. JCAP 11:001. https://doi.org/10.1088/1475-7516/2019/11/001. arXiv:1906.08978 [astro-ph.CO]

Morais AP, Pasechnik R (2020) Probing multi-step electroweak phase transition with multi-peaked primordial gravitational waves spectra. JCAP 04:036. https://doi.org/10.1088/1475-7516/2020/04/036. arXiv:1910.00717 [hep-ph]

Morais AP, Pasechnik R, Vieu T (2020) Multi-peaked signatures of primordial gravitational waves from multi-step electroweak phase transition. PoS EPS-HEP2019:054. https://doi.org/10.22323/1.364.0054. arXiv:1802.10109 [hep-ph]

Morita T, Soda J (2019) Arrival time differences of lensed massive gravitational waves. arXiv e-prints arXiv:1911.07435 [gr-qc]

Moroi T, Takahashi T (2001) Effects of cosmological moduli fields on cosmic microwave background. Phys Lett B 522:215–221. https://doi.org/10.1016/S0370-2693(01)01295-3, [Erratum: Phys.Lett.B 539, 303–303 (2002)]. arXiv:hep-ph/0110096

Morrás G, García-Bellido J, Nesseris S (2022) Search for black hole hyperbolic encounters with gravitational wave detectors. Phys Dark Universe 35:100932. https://doi.org/10.1016/j.dark.2021.100932. arXiv:2110.08000 [astro-ph.HE]

Morrissey DE, Ramsey-Musolf MJ (2012) Electroweak baryogenesis. New J Phys 14:125003. https://doi.org/10.1088/1367-2630/14/12/125003. arXiv:1206.2942 [hep-ph]

Mpetha CT, Congedo G, Taylor A (2023) Future prospects on testing extensions to ΛCDM through the weak lensing of gravitational waves. Phys Rev D 107(10):103518. https://doi.org/10.1103/PhysRevD.107.103518. arXiv:2208.05959 [astro-ph.CO]

Mukhanov VF, Chibisov GV (1981) Quantum fluctuations and a nonsingular universe. JETP Lett 33:532–535

Mukherjee S, Silk J (2020) Time-dependence of the astrophysical stochastic gravitational wave background. Mon Not R Astron Soc 491(4):4690–4701. https://doi.org/10.1093/mnras/stz3226. arXiv:1912.07657 [gr-qc]

Mukherjee S, Silk J (2021) Can we distinguish astrophysical from primordial black holes via the stochastic gravitational wave background? Mon Not R Astron Soc 506(3):3977–3985. https://doi.org/10.1093/mnras/stab1932. arXiv:2105.11139 [gr-qc]

Mukherjee S, Wandelt BD (2018) Beyond the classical distance-redshift test: cross-correlating redshift-free standard candles and sirens with redshift surveys. arXiv e-prints arXiv:1808.06615 [astro-ph.CO]

Mukherjee S, Wandelt BD, Silk J (2020a) Multimessenger tests of gravity with weakly lensed gravitational waves. Phys Rev D 101(10):103509. https://doi.org/10.1103/PhysRevD.101.103509. arXiv:1908.08950 [astro-ph.CO]

Mukherjee S, Wandelt BD, Silk J (2020b) Probing the theory of gravity with gravitational lensing of gravitational waves and galaxy surveys. Mon Not R Astron Soc 494(2):1956–1970. https://doi.org/10.1093/mnras/staa827. arXiv:1908.08951 [astro-ph.CO]

Mukherjee S, Broadhurst T, Diego JM, Silk J, Smoot GF (2021a) Impact of astrophysical binary coalescence time-scales on the rate of lensed gravitational wave events. Mon Not R Astron Soc 506(3):3751–3759. https://doi.org/10.1093/mnras/stab1980. arXiv:2106.00392 [gr-qc]

Mukherjee S, Broadhurst T, Diego JM, Silk J, Smoot GF (2021b) Inferring the lensing rate of LIGO-Virgo sources from the stochastic gravitational wave background. Mon Not R Astron Soc 501(2):2451–2466. https://doi.org/10.1093/mnras/staa3813. arXiv:2006.03064 [astro-ph.CO]

Mukherjee S, Lavaux G, Bouchet FR, Jasche J, Wandelt BD, Nissanke SM, Leclercq F, Hotokezaka K (2021c) Velocity correction for Hubble constant measurements from standard sirens. Astron Astrophys 646:A65. https://doi.org/10.1051/0004-6361/201936724. arXiv:1909.08627 [astro-ph.CO]

Mukherjee S, Wandelt BD, Nissanke SM, Silvestri A (2021d) Accurate precision Cosmology with redshift unknown gravitational wave sources. Phys Rev D 103(4):043520. https://doi.org/10.1103/PhysRevD.103.043520. arXiv:2007.02943 [astro-ph.CO]

Mukherjee S, Wandelt BD, Silk J (2021e) Testing the general theory of relativity using gravitational wave propagation from dark standard sirens. Mon Not R Astron Soc 502(1):1136–1144. https://doi.org/10.1093/mnras/stab001. arXiv:2012.15316 [astro-ph.CO]

Mukherjee S, Meinema MSP, Silk J (2022) Prospects of discovering subsolar primordial black holes using the stochastic gravitational wave background from third-generation detectors. Mon Not R Astron Soc 510(4):6218–6224. https://doi.org/10.1093/mnras/stab3756. arXiv:2107.02181 [astro-ph.CO]

Musco I (2019) Threshold for primordial black holes: dependence on the shape of the cosmological perturbations. Phys Rev D 100(12):123524. https://doi.org/10.1103/PhysRevD.100.123524. arXiv:1809.02127 [gr-qc]

Musco I, Miller JC, Rezzolla L (2005) Computations of primordial black hole formation. Class Quantum Grav 22:1405–1424. https://doi.org/10.1088/0264-9381/22/7/013. arXiv:gr-qc/0412063

Musco I, De Luca V, Franciolini G, Riotto A (2021) Threshold for primordial black holes. II. A simple analytic prescription. Phys Rev D 103(6):063538. https://doi.org/10.1103/PhysRevD.103.063538. arXiv:2011.03014 [astro-ph.CO]

Muttoni N, Mangiagli A, Sesana A, Laghi D, Del Pozzo W, Izquierdo-Villalba D, Rosati M (2022) Multiband gravitational wave cosmology with stellar origin black hole binaries. Phys Rev D 105 (4):043509. https://doi.org/10.1103/PhysRevD.105.043509. arXiv:2109.13934 [astro-ph.CO]

Mylova M, Özsoy O, Parameswaran S, Tasinato G, Zavala I (2018) A new mechanism to enhance primordial tensor fluctuations in single field inflation. JCAP 12:024. https://doi.org/10.1088/1475-7516/2018/12/024. arXiv:1808.10475 [gr-qc]

Nakama T, Silk J, Kamionkowski M (2017) Stochastic gravitational waves associated with the formation of primordial black holes. Phys Rev D 95(4):043511. https://doi.org/10.1103/PhysRevD.95.043511. arXiv:1612.06264 [astro-ph.CO]

Nakayama K, Saito S, Suwa Y, Yokoyama J (2008) Probing reheating temperature of the universe with gravitational wave background. JCAP 06:020. https://doi.org/10.1088/1475-7516/2008/06/020. arXiv:0804.1827 [astro-ph]

Nakazato K, Niino Y, Sago N (2016) Gravitational-wave background from binary mergers and metallicity evolution of galaxies. Astrophys J 832(2):146. https://doi.org/10.3847/0004-637X/832/2/146. arXiv:1605.02146 [astro-ph.HE]

Namba R, Peloso M, Shiraishi M, Sorbo L, Ünal C (2016) Scale-dependent gravitational waves from a rolling axion. JCAP 01:041. https://doi.org/10.1088/1475-7516/2016/01/041. arXiv:1509.07521 [astro-ph.CO]

Nambu Y (1977) String-like configurations in the Weinberg–Salam theory. Nucl Phys B 130:505. https://doi.org/10.1016/0550-3213(77)90252-8

Nambu Y, Taruya A (1997) Evolution of cosmological perturbation in reheating phase of the universe. Prog Theor Phys 97:83–89. https://doi.org/10.1143/PTP.97.83. arXiv:gr-qc/9609029

Namjoo MH, Firouzjahi H, Sasaki M (2013) Violation of non-Gaussianity consistency relation in a single field inflationary model. EPL 101(3):39001. https://doi.org/10.1209/0295-5075/101/39001. arXiv:1210.3692 [astro-ph.CO]

Nandra K et al (2013) The hot and energetic universe: a white paper presenting the science theme motivating the Athena+mission. arXiv e-prints arXiv:1306.2307 [astro-ph.HE]

Nardini G, Quiros M, Wulzer A (2007) A confining strong first-order electroweak phase transition. JHEP 09:077. https://doi.org/10.1088/1126-6708/2007/09/077. arXiv:0706.3388 [hep-ph]

Nayak B, Singh LP (2012) Brans–Dicke theory and primordial black holes in early matter-dominated era. Int J Theor Phys 51:1386–1395. https://doi.org/10.1007/s10773-011-1014-5. arXiv:0905.3657 [gr-qc]

Neronov A, Vovk I (2010) Evidence for strong extragalactic magnetic fields from Fermi observations of TeV blazars. Science 328:73–75. https://doi.org/10.1126/science.1184192. arXiv:1006.3504 [astro-ph.HE]

Neronov A, Roper Pol A, Caprini C, Semikoz D (2021) NANOGrav signal from magnetohydrodynamic turbulence at the QCD phase transition in the early Universe. Phys Rev D 103(4):041302. https://doi.org/10.1103/PhysRevD.103.L041302. arXiv:2009.14174 [astro-ph.CO]

Nester JM, Yo HJ (1999) Symmetric teleparallel general relativity. Chin J Phys 37:113 arXiv:gr-qc/9809049

Nicolaou C, Lahav O, Lemos P, Hartley W, Braden J (2020) The impact of peculiar velocities on the estimation of the Hubble constant from gravitational wave standard sirens. Mon Not R Astron Soc 495(1):90–97. https://doi.org/10.1093/mnras/staa1120. arXiv:1909.09609 [astro-ph.CO]

Nicolis A, Rattazzi R, Trincherini E (2009) The Galileon as a local modification of gravity. Phys Rev D 79:064036. https://doi.org/10.1103/PhysRevD.79.064036. arXiv:0811.2197 [hep-th]

Nielsen HB, Olesen P (1973) Vortex line models for dual strings. Nucl Phys B 61:45–61. https://doi.org/10.1016/0550-3213(73)90350-7

Niemi L, Ramsey-Musolf MJ, Tenkanen TVI, Weir DJ (2021) Thermodynamics of a two-step electroweak phase transition. Phys Rev Lett 126(17):171802. https://doi.org/10.1103/PhysRevLett.126.171802. arXiv:2005.11332 [hep-ph]

Niksa P, Schlederer M, Sigl G (2018) Gravitational waves produced by compressible MHD turbulence from cosmological phase transitions. Class Quantum Grav 35(14):144001. https://doi.org/10.1088/1361-6382/aac89c. arXiv:1803.02271 [astro-ph.CO]

Nishizawa A (2018) Generalized framework for testing gravity with gravitational-wave propagation. I. Formulation. Phys Rev D 97(10):104037. https://doi.org/10.1103/PhysRevD.97.104037. arXiv:1710.04825 [gr-qc]

Nishizawa A, Nakamura T (2014) Measuring speed of gravitational waves by observations of photons and neutrinos from compact binary mergers and supernovae. Phys Rev D 90(4):044048. https://doi.org/10.1103/PhysRevD.90.044048. arXiv:1406.5544 [gr-qc]

Nishizawa A, Taruya A, Saito S (2011) Tracing the redshift evolution of Hubble parameter with gravitational-wave standard sirens. Phys Rev D 83:084045. https://doi.org/10.1103/PhysRevD.83.084045. arXiv:1011.5000 [astro-ph.CO]

Nishizawa A, Yagi K, Taruya A, Tanaka T (2012) Cosmology with space-based gravitational-wave detectors—dark energy and primordial gravitational waves. Phys Rev D 85:044047. https://doi.org/10.1103/PhysRevD.85.044047. arXiv:1110.2865 [astro-ph.CO]

Nissanke S, Holz DE, Dalal N, Hughes SA, Sievers JL, Hirata CM (2013) Determining the Hubble constant from gravitational wave observations of merging compact binaries. arXiv e-prints arXiv:1307.2638 [astro-ph.CO]

Noller J, Nicola A (2019) Cosmological parameter constraints for Horndeski scalar–tensor gravity. Phys Rev D 99(10):103502. https://doi.org/10.1103/PhysRevD.99.103502. arXiv:1811.12928 [astro-ph.CO]

Noller J, Santoni L, Trincherini E, Trombetta LG (2020) Black hole ringdown as a probe for dark energy. Phys Rev D 101:084049. https://doi.org/10.1103/PhysRevD.101.084049. arXiv:1911.11671 [gr-qc]

Obata I, Soda J (2016) Chiral primordial Chiral primordial gravitational waves from Dilaton induced delayed chromonatural inflation. Phys Rev D 93(12):123502. https://doi.org/10.1103/PhysRevD.93.123502, [Addendum: Phys. Rev. D 95, 109903 (2017)]. arXiv:1602.06024 [hep-th]

Ogawa H, Kobayashi T, Koyama K (2020) Relativistic stars in a cubic Galileon Universe. Phys Rev D 101(2):024026. https://doi.org/10.1103/PhysRevD.101.024026. arXiv:1911.01669 [gr-qc]

Oguri M (2016) Measuring the distance-redshift relation with the cross-correlation of gravitational wave standard sirens and galaxies. Phys Rev D 93(8):083511. https://doi.org/10.1103/PhysRevD.93.083511. arXiv:1603.02356 [astro-ph.CO]

Oguri M (2018) Effect of gravitational lensing on the distribution of gravitational waves from distant binary black hole mergers. Mon Not R Astron Soc 480(3):3842–3855. https://doi.org/10.1093/mnras/sty2145. arXiv:1807.02584 [astro-ph.CO]

Oguri M (2019) Strong gravitational lensing of explosive transients. Rep Prog Phys 82(12):126901. https://doi.org/10.1088/1361-6633/ab4fc5. arXiv:1907.06830 [astro-ph.CO]

Oguri M, Takahashi R (2020) Probing dark low-mass halos and primordial black holes with frequency-dependent gravitational lensing dispersions of gravitational waves. Astrophys J 901(1):58. https://doi.org/10.3847/1538-4357/abafab. arXiv:2007.01936 [astro-ph.CO]

Okada N, Seto O, Uchida H (2021) Gravitational waves from breaking of an extra $U(1)$ in $SO(10)$ grand unification. PTEP 2021(3):033B01. https://doi.org/10.1093/ptep/ptab003. arXiv:2006.01406 [hep-ph]

Okounkova M, Farr WM, Isi M, Stein LC (2022) Constraining gravitational wave amplitude birefringence and Chern–Simons gravity with GWTC-2. Phys Rev D 106(4):044067. https://doi.org/10.1103/PhysRevD.106.044067. arXiv:2101.11153 [gr-qc]

Olmez S, Mandic V, Siemens X (2010) Gravitational-wave stochastic background from kinks and cusps on cosmic strings. Phys Rev D 81:104028. https://doi.org/10.1103/PhysRevD.81.104028. arXiv:1004.0890 [astro-ph.CO]

Olum KD, Blanco-Pillado JJ (1999) Field theory simulation of Abelian Higgs cosmic string cusps. Phys Rev D 60:023503. https://doi.org/10.1103/PhysRevD.60.023503. arXiv:gr-qc/9812040

Olum KD, Blanco-Pillado JJ (2000) Radiation from cosmic string standing waves. Phys Rev Lett 84:4288–4291. https://doi.org/10.1103/PhysRevLett.84.4288. arXiv:astro-ph/9910354

Opferkuch T, Schwaller P, Stefanek BA (2019) Ricci reheating. JCAP 07:016. https://doi.org/10.1088/1475-7516/2019/07/016. arXiv:1905.06823 [gr-qc]

Orlando G, Pieroni M, Ricciardone A (2021) Measuring parity violation in the stochastic gravitational wave background with the LISA-Taiji network. JCAP 03:069. https://doi.org/10.1088/1475-7516/2021/03/069. arXiv:2011.07059 [astro-ph.CO]

Osato K (2018) Exploring the distance-redshift relation with gravitational wave standard sirens and tomographic weak lensing. Phys Rev D 98(8):083524. https://doi.org/10.1103/PhysRevD.98.083524. arXiv:1807.00016 [astro-ph.CO]

Ostrogradksi M (1850) Mémoires sur les équations différentielles, relatives au problème des isopérimètres. Mem Acad St Petersbourg VI(4):385–517

Özsoy O (2021) Synthetic gravitational waves from a rolling axion monodromy. JCAP 04:040. https://doi.org/10.1088/1475-7516/2021/04/040. arXiv:2005.10280 [astro-ph.CO]

Özsoy O, Lalak Z (2021) Primordial black holes as dark matter and gravitational waves from bumpy axion inflation. JCAP 01:040. https://doi.org/10.1088/1475-7516/2021/01/040. arXiv:2008.07549 [astro-ph.CO]

Özsoy O, Parameswaran S, Tasinato G, Zavala I (2018) Mechanisms for primordial black hole production in string theory. JCAP 07:005. https://doi.org/10.1088/1475-7516/2018/07/005. arXiv:1803.07626 [hep-th]

Pagano G, Hannuksela OA, Li TGF (2020) lensingGW: a Python package for lensing of gravitational waves. Astron Astrophys 643:A167. https://doi.org/10.1051/0004-6361/202038730. arXiv:2006.12879 [astro-ph.CO]

Pajer E, Peloso M (2013) A review of axion inflation in the era of Planck. Class Quantum Grav 30:214002. https://doi.org/10.1088/0264-9381/30/21/214002. arXiv:1305.3557 [hep-th]

Pajer E, Schmidt F, Zaldarriaga M (2013) The observed squeezed limit of cosmological three-point functions. Phys Rev D 88(8):083502. https://doi.org/10.1103/PhysRevD.88.083502. arXiv:1305.0824 [astro-ph.CO]

Palenzuela C, Lehner L, Liebling SL (2010) Dual jets from binary black holes. Science 329:927. https://doi.org/10.1126/science.1191766. arXiv:1005.1067 [astro-ph.HE]

Palma GA, Sypsas S, Zenteno C (2020) Seeding primordial black holes in multifield inflation. Phys Rev Lett 125(12):121301. https://doi.org/10.1103/PhysRevLett.125.121301. arXiv:2004.06106 [astro-ph.CO]

Palmese A et al (2020) A statistical standard siren measurement of the Hubble constant from the LIGO/Virgo gravitational wave compact object merger GW190814 and Dark Energy Survey galaxies. Astrophys J Lett 900(2):L33. https://doi.org/10.3847/2041-8213/abaeff. arXiv:2006.14961 [astro-ph.CO]

Papageorgiou A, Peloso M, Ünal C (2018) Nonlinear perturbations from the coupling of the inflaton to a non-Abelian gauge field, with a focus on Chromo-Natural Inflation. JCAP 09:030. https://doi.org/10.1088/1475-7516/2018/09/030. arXiv:1806.08313 [astro-ph.CO]

Papageorgiou A, Peloso M, Ünal C (2019) Nonlinear perturbations from axion-gauge fields dynamics during inflation. JCAP 07:004. https://doi.org/10.1088/1475-7516/2019/07/004. arXiv:1904.01488 [astro-ph.CO]

Papanikolaou T, Vennin V, Langlois D (2021) Gravitational waves from a universe filled with primordial black holes. JCAP 03:053. https://doi.org/10.1088/1475-7516/2021/03/053. arXiv:2010.11573 [astro-ph.CO]

Parwani RR (1992) Resummation in a hot scalar field theory. Phys Rev D 45:4695. https://doi.org/10.1103/PhysRevD.45.4695, [Erratum: Phys. Rev. D 48, 5965 (1993)]. arXiv:hep-ph/9204216

Pattison C, Vennin V, Assadullahi H, Wands D (2017) Quantum diffusion during inflation and primordial black holes. JCAP 10:046. https://doi.org/10.1088/1475-7516/2017/10/046. arXiv:1707.00537 [hep-th]

Pearce L (2012) Solitosynthesis induced phase transitions. Phys Rev D 85:125022. https://doi.org/10.1103/PhysRevD.85.125022. arXiv:1202.0873 [hep-ph]

Peebles PJE, Vilenkin A (1999) Quintessential inflation. Phys Rev D 59:063505. https://doi.org/10.1103/PhysRevD.59.063505. arXiv:astro-ph/9810509

Peloso M, Rosati F (1999) On the construction of quintessential inflation models. JHEP 12:026. https://doi.org/10.1088/1126-6708/1999/12/026. arXiv:hep-ph/9908271

Peloso M, Sorbo L (2003) Moduli from cosmic strings. Nucl Phys B 649:88–100. https://doi.org/10.1016/S0550-3213(02)01020-9. arXiv:hep-ph/0205063

Peloso M, Sorbo L, Ünal C (2016) Rolling axions during inflation: perturbativity and signatures. JCAP 09:001. https://doi.org/10.1088/1475-7516/2016/09/001. arXiv:1606.00459 [astro-ph.CO]

Périgois C, Belczynski C, Bulik T, Regimbau T (2021) StarTrack predictions of the stochastic gravitational-wave background from compact binary mergers. Phys Rev D 103(4):043002. https://doi.org/10.1103/PhysRevD.103.043002. arXiv:2008.04890 [astro-ph.CO]

Pesce DW et al (2020) The Megamaser Cosmology Project. XIII. Combined Hubble constant constraints. Astrophys J Lett 891(1):L1. https://doi.org/10.3847/2041-8213/ab75f0. arXiv:2001.09213 [astro-ph.CO]

Pi S, Sasaki M (2020) Gravitational waves induced by scalar perturbations with a lognormal peak. JCAP 09:037. https://doi.org/10.1088/1475-7516/2020/09/037. arXiv:2005.12306 [gr-qc]

Piazza F, Pirtskhalava D, Rattazzi R, Simon O (2017) Gaugid inflation. JCAP 11:041. https://doi.org/10.1088/1475-7516/2017/11/041. arXiv:1706.03402 [hep-th]

Pieroni M, Barausse E (2020) Foreground cleaning and template-free stochastic background extraction for LISA. JCAP 07:021. https://doi.org/10.1088/1475-7516/2020/07/021, [Erratum: JCAP 09, E01 (2020)]. arXiv:2004.01135 [astro-ph.CO]
Piórkowska A, Biesiada M, Zhu ZH (2013) Strong gravitational lensing of gravitational waves in Einstein Telescope. JCAP 2013(10):022. https://doi.org/10.1088/1475-7516/2013/10/022. arXiv:1309.5731 [astro-ph.CO]
Pirtskhalava D, Santoni L, Trincherini E, Vernizzi F (2015) Weakly broken Galileon symmetry. JCAP 09:007. https://doi.org/10.1088/1475-7516/2015/09/007. arXiv:1505.00007 [hep-th]
Pisarski RD, Wilczek F (1984) Remarks on the chiral phase transition in chromodynamics. Phys Rev D 29:338–341. https://doi.org/10.1103/PhysRevD.29.338
Pitrou C, Cusin G, Uzan JP (2020) Unified view of anisotropies in the astrophysical gravitational-wave background. Phys Rev D 101(8):081301. https://doi.org/10.1103/PhysRevD.101.081301. arXiv:1910.04645 [astro-ph.CO]
Polarski D, Starobinsky AA (1996) Semiclassicality and decoherence of cosmological perturbations. Class Quantum Grav 13:377–392. https://doi.org/10.1088/0264-9381/13/3/006. arXiv:gr-qc/9504030
Polchinski J, Rocha JV (2006) Analytic study of small scale structure on cosmic strings. Phys Rev D 74:083504. https://doi.org/10.1103/PhysRevD.74.083504. arXiv:hep-ph/0606205
Polchinski J, Rocha JV (2007) Cosmic string structure at the gravitational radiation scale. Phys Rev D 75:123503. https://doi.org/10.1103/PhysRevD.75.123503. arXiv:gr-qc/0702055
Postma M (2002) Solitosynthesis of Q balls. Phys Rev D 65:085035. https://doi.org/10.1103/PhysRevD.65.085035. arXiv:hep-ph/0110199
Poulin V, Serpico PD, Calore F, Clesse S, Kohri K (2017) CMB bounds on disk-accreting massive primordial black holes. Phys Rev D 96(8):083524. https://doi.org/10.1103/PhysRevD.96.083524. arXiv:1707.04206 [astro-ph.CO]
Pourtsidou A, Avgoustidis A, Copeland EJ, Pogosian L, Steer DA (2011) Scaling configurations of cosmic superstring networks and their cosmological implications. Phys Rev D 83:063525. https://doi.org/10.1103/PhysRevD.83.063525. arXiv:1012.5014 [astro-ph.CO]
Preskill J, Vilenkin A (1993) Decay of metastable topological defects. Phys Rev D 47:2324–2342. https://doi.org/10.1103/PhysRevD.47.2324. arXiv:hep-ph/9209210
Profumo S, Ramsey-Musolf MJ, Wainwright CL, Winslow P (2015) Singlet-catalyzed electroweak phase transitions and precision Higgs boson studies. Phys Rev D 91(3):035018. https://doi.org/10.1103/PhysRevD.91.035018. arXiv:1407.5342 [hep-ph]
Prokopec T, Roos TG (1997) Lattice study of classical inflaton decay. Phys Rev D 55:3768–3775. https://doi.org/10.1103/PhysRevD.55.3768. arXiv:hep-ph/9610400
Prokopec T, Rezacek J, Świe B (2019) Gravitational waves from conformal symmetry breaking. JCAP 02:009. https://doi.org/10.1088/1475-7516/2019/02/009. arXiv:1809.11129 [hep-ph]
Pyne T, Gwinn CR, Birkinshaw M, Eubanks TM, Matsakis DN (1996) Gravitational radiation and very long baseline interferometry. Astrophys J 465:566–577. https://doi.org/10.1086/177443. arXiv:astro-ph/9507030
Qi JZ, Jin SJ, Fan XL, Zhang JF, Zhang X (2021) Using a multi-messenger and multi-wavelength observational strategy to probe the nature of dark energy through direct measurements of cosmic expansion history. JCAP 12(12):042. https://doi.org/10.1088/1475-7516/2021/12/042. arXiv:2102.01292 [astro-ph.CO]
Qiao J, Zhu T, Zhao W, Wang A (2020) Polarized primordial gravitational waves in the ghost-free parity-violating gravity. Phys Rev D 101(4):043528. https://doi.org/10.1103/PhysRevD.101.043528. arXiv:1911.01580 [astro-ph.CO]
Raccanelli A (2017) Gravitational wave astronomy with radio galaxy surveys. Mon Not R Astron Soc 469 (1):656–670. https://doi.org/10.1093/mnras/stx835. arXiv:1609.09377 [astro-ph.CO]
Raccanelli A, Kovetz ED, Bird S, Cholis I, Munoz JB (2016) Determining the progenitors of merging black-hole binaries. Phys Rev D 94(2):023516. https://doi.org/10.1103/PhysRevD.94.023516. arXiv:1605.01405 [astro-ph.CO]
Ragavendra HV, Saha P, Sriramkumar L, Silk J (2021) Primordial black holes and secondary gravitational waves from ultraslow roll and punctuated inflation. Phys Rev D 103(8):083510. https://doi.org/10.1103/PhysRevD.103.083510. arXiv:2008.12202 [astro-ph.CO]
Raidal M, Vaskonen V, Veermäe H (2017) Gravitational waves from primordial black hole mergers. JCAP 09:037. https://doi.org/10.1088/1475-7516/2017/09/037. arXiv:1707.01480 [astro-ph.CO]

Raidal M, Spethmann C, Vaskonen V, Veermäe H (2019) Formation and evolution of primordial black hole binaries in the early universe. JCAP 02:018. https://doi.org/10.1088/1475-7516/2019/02/018. arXiv:1812.01930 [astro-ph.CO]

Rajantie A, Sakellariadou M, Stoica H (2007) Numerical experiments with p F- and q D-strings: the formation of (p, q) bound states. JCAP 11:021. https://doi.org/10.1088/1475-7516/2007/11/021. arXiv:0706.3662 [hep-th]

Randall L, Servant G (2007) Gravitational waves from warped spacetime. JHEP 05:054. https://doi.org/10.1088/1126-6708/2007/05/054. arXiv:hep-ph/0607158

Randall L, Sundrum R (1999) A Large mass hierarchy from a small extra dimension. Phys Rev Lett 83:3370–3373. https://doi.org/10.1103/PhysRevLett.83.3370. arXiv:hep-ph/9905221

Ratra B (1992) Cosmological 'seed' magnetic field from inflation. Astrophys J Lett 391:L1–L4. https://doi.org/10.1086/186384

Rattazzi R, Zaffaroni A (2001) Comments on the holographic picture of the Randall–Sundrum model. JHEP 04:021. https://doi.org/10.1088/1126-6708/2001/04/021. arXiv:hep-th/0012248

Raveri M (2020) Reconstructing gravity on cosmological scales. Phys Rev D 101(8):083524. https://doi.org/10.1103/PhysRevD.101.083524. arXiv:1902.01366 [astro-ph.CO]

Raveri M, Hu B, Frusciante N, Silvestri A (2014) Effective field theory of cosmic acceleration: constraining dark energy with CMB data. Phys Rev D 90(4):043513. https://doi.org/10.1103/PhysRevD.90.043513. arXiv:1405.1022 [astro-ph.CO]

Raveri M, Baccigalupi C, Silvestri A, Zhou SY (2015) Measuring the speed of cosmological gravitational waves. Phys Rev D 91(6):061501. https://doi.org/10.1103/PhysRevD.91.061501. arXiv:1405.7974 [astro-ph.CO]

Regimbau T (2011) The astrophysical gravitational wave stochastic background. Res Astron Astrophys 11:369–390. https://doi.org/10.1088/1674-4527/11/4/001. arXiv:1101.2762 [astro-ph.CO]

Regimbau T, Hughes SA (2009) Gravitational-wave confusion background from cosmological compact binaries: implications for future terrestrial detectors. Phys Rev D 79:062002. https://doi.org/10.1103/PhysRevD.79.062002. arXiv:0901.2958 [gr-qc]

Regimbau T, Giampanis S, Siemens X, Mandic V (2012) The stochastic background from cosmic (super) strings: popcorn and (Gaussian) continuous regimes. Phys Rev D 85:066001. https://doi.org/10.1103/PhysRevD.85.066001. arXiv:1111.6638 [astro-ph.CO]

Regimbau T, Evans M, Christensen N, Katsavounidis E, Sathyaprakash B, Vitale S (2017) Digging deeper: observing primordial gravitational waves below the binary black hole produced stochastic background. Phys Rev Lett 118(15):151105. https://doi.org/10.1103/PhysRevLett.118.151105. arXiv:1611.08943 [astro-ph.CO]

Reitze D et al (2019) Cosmic explorer: the U.S. contribution to gravitational-wave astronomy beyond LIGO. Bull Am Astron Soc 51(7):035 arXiv:1907.04833 [astro-ph.IM]

Renaux-Petel S, Turzyński K (2016) Geometrical destabilization of inflation. Phys Rev Lett 117 (14):141301. https://doi.org/10.1103/PhysRevLett.117.141301. arXiv:1510.01281 [astro-ph.CO]

Renevey C, Kennedy J, Lombriser L (2020) Parameterised post-Newtonian formalism for the effective field theory of dark energy via screened reconstructed Horndeski theories. JCAP 12:032. https://doi.org/10.1088/1475-7516/2020/12/032. arXiv:2006.09910 [gr-qc]

Riazuelo A, Uzan JP (2000) Quintessence and gravitational waves. Phys Rev D 62:083506. https://doi.org/10.1103/PhysRevD.62.083506. arXiv:astro-ph/0004156

Ricarte A, Natarajan P (2018) The observational signatures of supermassive black hole seeds. Mon Not R Astron Soc 481(3):3278–3292. https://doi.org/10.1093/mnras/sty2448. arXiv:1809.01177 [astro-ph.GA]

Ricciardone A, Tasinato G (2017) Primordial gravitational waves in supersolid inflation. Phys Rev D 96 (2):023508. https://doi.org/10.1103/PhysRevD.96.023508. arXiv:1611.04516 [astro-ph.CO]

Ricciardone A, Dall'Armi LV, Bartolo N, Bertacca D, Liguori M, Matarrese S (2021) Cross-correlating astrophysical and cosmological gravitational wave backgrounds with the cosmic microwave background. Phys Rev Lett 127(27):271301. https://doi.org/10.1103/PhysRevLett.127.271301. arXiv:2106.02591 [astro-ph.CO]

Ricotti M, Ostriker JP, Mack KJ (2008) Effect of primordial black holes on the cosmic microwave background and cosmological parameter estimates. Astrophys J 680:829. https://doi.org/10.1086/587831. arXiv:0709.0524 [astro-ph]

Riess AG, Casertano S, Yuan W, Macri LM, Scolnic D (2019) Large magellanic cloud cepheid standards provide a 1% foundation for the determination of the Hubble constant and stronger evidence for

physics beyond ΛCDM. Astrophys J 876(1):85. https://doi.org/10.3847/1538-4357/ab1422. arXiv:1903.07603 [astro-ph.CO]
Riess AG et al (2022) A comprehensive measurement of the local value of the Hubble constant with 1 km s^{1} Mpc^{1} uncertainty from the Hubble space telescope and the SH0ES team. Astrophys J Lett 934(1):L7. https://doi.org/10.3847/2041-8213/ac5c5b. arXiv:2112.04510 [astro-ph.CO]
Rindler-Daller T, Shapiro PR (2014) Complex scalar field dark matter on galactic scales. Mod Phys Lett A 29(2):1430002. https://doi.org/10.1142/S021773231430002X. arXiv:1312.1734 [astro-ph.CO]
Ringeval C (2010) Cosmic strings and their induced non-Gaussianities in the cosmic microwave background. Adv Astron 2010:380507. https://doi.org/10.1155/2010/380507. arXiv:1005.4842 [astro-ph.CO]
Ringeval C, Suyama T (2017) Stochastic gravitational waves from cosmic string loops in scaling. JCAP 12:027. https://doi.org/10.1088/1475-7516/2017/12/027. arXiv:1709.03845 [astro-ph.CO]
Ringeval C, Sakellariadou M, Bouchet F (2007) Cosmological evolution of cosmic string loops. JCAP 02:023. https://doi.org/10.1088/1475-7516/2007/02/023. arXiv:astro-ph/0511646
Riotto A (2003) Inflation and the theory of cosmological perturbations. ICTP Lect Notes Ser 14:317–413 arXiv:hep-ph/0210162
Risaliti G, Lusso E (2019) Cosmological constraints from the Hubble diagram of quasars at high redshifts. Nature Astron 3(3):272–277. https://doi.org/10.1038/s41550-018-0657-z. arXiv:1811.02590 [astro-ph.CO]
Robbins KW, Olum KD (2019) Backreaction on an infinite helical cosmic string. Phys Rev D 100 (10):103512. https://doi.org/10.1103/PhysRevD.100.103512. arXiv:1908.09702 [astro-ph.CO]
Roberts D, Liddle AR, Lyth DH (1995) False vacuum inflation with a quartic potential. Phys Rev D 51:4122–4128. https://doi.org/10.1103/PhysRevD.51.4122. arXiv:astro-ph/9411104
Robson T, Cornish NJ (2019) Detecting gravitational wave bursts with LISA in the presence of Instrumental Glitches. Phys Rev D 99(2):024019. https://doi.org/10.1103/PhysRevD.99.024019. arXiv:1811.04490 [gr-qc]
Robson T, Cornish NJ, Liu C (2019) The construction and use of LISA sensitivity curves. Class Quantum Grav 36(10):105011. https://doi.org/10.1088/1361-6382/ab1101. arXiv:1803.01944 [astro-ph.HE]
Romano JD, Cornish NJ (2017) Detection methods for stochastic gravitational-wave backgrounds: a unified treatment. Living Rev Relativ 20:2. https://doi.org/10.1007/s41114-017-0004-1. arXiv:1608.06889 [gr-qc]
Roper Pol A, Mandal S, Brandenburg A, Kahniashvili T, Kosowsky A (2020) Numerical simulations of gravitational waves from early-universe turbulence. Phys Rev D 102(8):083512. https://doi.org/10.1103/PhysRevD.102.083512. arXiv:1903.08585 [astro-ph.CO]
Rossi EM, Lodato G, Armitage PJ, Pringle JE, King AR (2010) Black hole mergers: the first light. Mon Not R Astron Soc 401:2021. https://doi.org/10.1111/j.1365-2966.2009.15802.x. arXiv:0910.0002 [astro-ph.HE]
Ruan WH, Guo ZK, Cai RG, Zhang YZ (2020a) Taiji program: gravitational-wave sources. Int J Mod Phys A 35(17):2050075. https://doi.org/10.1142/S0217751X2050075X. arXiv:1807.09495 [gr-qc]
Ruan WH, Liu C, Guo ZK, Wu YL, Cai RG (2020b) The LISA-Taiji network. Nature Astron 4:108–109. https://doi.org/10.1038/s41550-019-1008-4. arXiv:2002.03603 [gr-qc]
Rubakov VA, Shaposhnikov ME (1996) Electroweak baryon number nonconservation in the early universe and in high-energy collisions. Usp Fiz Nauk 166:493–537. https://doi.org/10.1070/PU1996v039n05ABEH000145. arXiv:hep-ph/9603208
Rubakov VA, Sazhin MV, Veryaskin AV (1982) Graviton creation in the inflationary universe and the grand unification scale. Phys Lett B 115:189–192. https://doi.org/10.1016/0370-2693(82)90641-4
Rubin SG, Khlopov MY, Sakharov AS (2000) Primordial black holes from nonequilibrium second order phase transition. Grav Cosmol 6:51–58 arXiv:hep-ph/0005271
Rubio J, Wetterich C (2017) Emergent scale symmetry: connecting inflation and dark energy. Phys Rev D 96(6):063509. https://doi.org/10.1103/PhysRevD.96.063509. arXiv:1705.00552 [gr-qc]
Sabancilar E (2010) Cosmological constraints on strongly coupled moduli from cosmic strings. Phys Rev D 81:123502. https://doi.org/10.1103/PhysRevD.81.123502. arXiv:0910.5544 [hep-ph]
Sachdev S, Regimbau T, Sathyaprakash BS (2020) Subtracting compact binary foreground sources to reveal primordial gravitational-wave backgrounds. Phys Rev D 102(2):024051. https://doi.org/10.1103/PhysRevD.102.024051. arXiv:2002.05365 [gr-qc]

Saga S, Tashiro H, Yokoyama S (2020) Limits on primordial magnetic fields from primordial black hole abundance. JCAP 05:039. https://doi.org/10.1088/1475-7516/2020/05/039. arXiv:2002.01286 [astro-ph.CO]

Sahni V, Starobinsky A (2006) Reconstructing dark energy. Int J Mod Phys D 15:2105–2132. https://doi.org/10.1142/S0218271806009704. arXiv:astro-ph/0610026

Sahni V, Sami M, Souradeep T (2002) Relic gravity waves from brane world inflation. Phys Rev D 65:023518. https://doi.org/10.1103/PhysRevD.65.023518. arXiv:gr-qc/0105121

Saito R, Yokoyama J (2010) Gravitational-wave constraints on the abundance of primordial black holes. Prog Theor Phys 123:867–886. https://doi.org/10.1143/PTP.126.351, [Erratum: Prog. Theor. Phys. 126, 351–352 (2011)]. arXiv:0912.5317 [astro-ph.CO]

Sakellariadou M (1990) Gravitational waves emitted from infinite strings. Phys Rev D 42:354–360. https://doi.org/10.1103/PhysRevD.42.354, [Erratum: Phys. Rev. D 43, 4150 (1991)]

Sakellariadou M (2005) A Note on the evolution of cosmic string/superstring networks. JCAP 04:003. https://doi.org/10.1088/1475-7516/2005/04/003. arXiv:hep-th/0410234

Sakellariadou M (2007) Cosmic strings. In: Unruh WG, Schützhold R (eds) Quantum analogues: from phase transitions to black holes and cosmology. Lecture notes in physics, vol 718. Springer, Berlin, Heidelberg, pp 247–288. https://doi.org/10.1007/3-540-70859-6_10. arXiv:hep-th/0602276

Sakellariadou M, Stoica H (2008) Dynamics of F/D networks: the role of bound states. JCAP 08:038. https://doi.org/10.1088/1475-7516/2008/08/038. arXiv:0806.3219 [hep-th]

Sakellariadou M, Vilenkin A (1990) Cosmic-string evolution in flat space-time. Phys Rev D 42:349–353. https://doi.org/10.1103/PhysRevD.42.349

Sakstein J, Jain B (2017) Implications of the neutron star merger GW170817 for cosmological scalar–tensor theories. Phys Rev Lett 119(25):251303. https://doi.org/10.1103/PhysRevLett.119.251303. arXiv:1710.05893 [astro-ph.CO]

Sakstein J, Babichev E, Koyama K, Langlois D, Saito R (2017) Towards strong field tests of beyond Horndeski gravity theories. Phys Rev D 95(6):064013. https://doi.org/10.1103/PhysRevD.95.064013. arXiv:1612.04263 [gr-qc]

Salcido J, Bower RG, Theuns T, McAlpine S, Schaller M, Crain RA, Schaye J, Regan J (2016) Music from the heavens—gravitational waves from supermassive black hole mergers in the EAGLE simulations. Mon Not R Astron Soc 463(1):870–885. https://doi.org/10.1093/mnras/stw2048. arXiv:1601.06156 [astro-ph.GA]

Saltas ID, Sawicki I, Amendola L, Kunz M (2014) Anisotropic stress as a signature of nonstandard propagation of gravitational waves. Phys Rev Lett 113(19):191101. https://doi.org/10.1103/PhysRevLett.113.191101. arXiv:1406.7139 [astro-ph.CO]

Sanidas SA, Battye RA, Stappers BW (2012) Constraints on cosmic string tension imposed by the limit on the stochastic gravitational wave background from the European Pulsar Timing Array. Phys Rev D 85:122003. https://doi.org/10.1103/PhysRevD.85.122003. arXiv:1201.2419 [astro-ph.CO]

Sanidas SA, Battye RA, Stappers BW (2013) Projected constraints on the cosmic (super)string tension with future gravitational wave detection experiments. Astrophys J 764:108. https://doi.org/10.1088/0004-637X/764/1/108. arXiv:1211.5042 [astro-ph.CO]

Sasaki M, Suyama T, Tanaka T, Yokoyama S (2016) Primordial black hole scenario for the gravitational-wave event GW150914. Phys Rev Lett 117(6):061101. https://doi.org/10.1103/PhysRevLett.117.061101, [Erratum: Phys. Rev. Lett. 121, 059901 (2018)]. arXiv:1603.08338 [astro-ph.CO]

Sasaki M, Suyama T, Tanaka T, Yokoyama S (2018) Primordial black holes–perspectives in gravitational wave astronomy. Class Quantum Grav 35(6):063001. https://doi.org/10.1088/1361-6382/aaa7b4. arXiv:1801.05235 [astro-ph.CO]

Sathyaprakash BS, Schutz BF, Van Den Broeck C (2010) Cosmography with the Einstein telescope. Class Quantum Grav 27:215006. https://doi.org/10.1088/0264-9381/27/21/215006. arXiv:0906.4151 [astro-ph.CO]

Sato S et al (2017) The status of DECIGO. J Phys Conf Ser 840(1):012010. https://doi.org/10.1088/1742-6596/840/1/012010

Satoh M (2010) Slow-roll inflation with the Gauss–Bonnet and Chern–Simons corrections. JCAP 11:024. https://doi.org/10.1088/1475-7516/2010/11/024. arXiv:1008.2724 [astro-ph.CO]

Saurabh A, Vachaspati T, Pogosian L (2020) Decay of cosmic global string loops. Phys Rev D 101 (8):083522. https://doi.org/10.1103/PhysRevD.101.083522. arXiv:2001.01030 [hep-ph]

Scelfo G, Bellomo N, Raccanelli A, Matarrese S, Verde L (2018) GW×LSS: chasing the progenitors of merging binary black holes. JCAP 09:039. https://doi.org/10.1088/1475-7516/2018/09/039. arXiv:1809.03528 [astro-ph.CO]

Scelfo G, Boco L, Lapi A, Viel M (2020) Exploring galaxies-gravitational waves cross-correlations as an astrophysical probe. JCAP 10:045. https://doi.org/10.1088/1475-7516/2020/10/045. arXiv:2007.08534 [astro-ph.CO]
Scharre PD, Will CM (2002) Testing scalar tensor gravity using space gravitational wave interferometers. Phys Rev D 65:042002. https://doi.org/10.1103/PhysRevD.65.042002. arXiv:gr-qc/0109044
Schmidt SJ et al (2020) Evaluation of probabilistic photometric redshift estimation approaches for LSST. Mon Not R Astron Soc 499(2):1587–1606. https://doi.org/10.1093/mnras/staa2799. arXiv:2001.03621 [astro-ph.CO]
Schneider P, Ehlers J, Falco EE (1992) Gravitational lenses. Springer, Berlin. https://doi.org/10.1007/978-3-662-03758-4
Schnittman JD, Krolik JH (2008) The infrared afterglow of supermassive black hole mergers. Astrophys J 684:835–844. https://doi.org/10.1086/590363. arXiv:0802.3556 [astro-ph]
Schutz BF (1986) Determining the Hubble constant from gravitational wave observations. Nature 323:310–311. https://doi.org/10.1038/323310a0
Schwaller P (2015) Gravitational waves from a dark phase transition. Phys Rev Lett 115(18):181101. https://doi.org/10.1103/PhysRevLett.115.181101. arXiv:1504.07263 [hep-ph]
Scolnic DM et al (2018) The complete light-curve sample of spectroscopically confirmed SNe Ia from Pan-STARRS1 and cosmological constraints from the combined pantheon sample. Astrophys J 859 (2):101. https://doi.org/10.3847/1538-4357/aab9bb. arXiv:1710.00845 [astro-ph.CO]
Sedda MA et al (2020) The missing link in gravitational-wave astronomy: discoveries waiting in the decihertz range. Class Quantum Grav 37(21):215011. https://doi.org/10.1088/1361-6382/abb5c1. arXiv:1908.11375 [gr-qc]
Sendra I, Smith TL (2012) Improved limits on short-wavelength gravitational waves from the cosmic microwave background. Phys Rev D 85:123002. https://doi.org/10.1103/PhysRevD.85.123002. arXiv:1203.4232 [astro-ph.CO]
Sereno M, Sesana A, Bleuler A, Jetzer P, Volonteri M, Begelman MC (2010) Strong lensing of gravitational waves as seen by LISA. Phys Rev Lett 105:251101. https://doi.org/10.1103/PhysRevLett.105.251101. arXiv:1011.5238 [astro-ph.CO]
Sereno M, Jetzer P, Sesana A, Volonteri M (2011) Cosmography with strong lensing of LISA gravitational wave sources. Mon Not R Astron Soc 415:2773. https://doi.org/10.1111/j.1365-2966.2011.18895.x. arXiv:1104.1977 [astro-ph.CO]
Serpico PD, Poulin V, Inman D, Kohri K (2020) Cosmic microwave background bounds on primordial black holes including dark matter halo accretion. Phys Rev Res 2(2):023204. https://doi.org/10.1103/PhysRevResearch.2.023204. arXiv:2002.10771 [astro-ph.CO]
Servant G (2014) Baryogenesis from strong *CP* violation and the QCD axion. Phys Rev Lett 113 (17):171803. https://doi.org/10.1103/PhysRevLett.113.171803. arXiv:1407.0030 [hep-ph]
Sesana A (2016) Prospects for multiband gravitational-wave astronomy after GW150914. Phys Rev Lett 116(23):231102. https://doi.org/10.1103/PhysRevLett.116.231102. arXiv:1602.06951 [gr-qc]
Sesana A, Gair J, Berti E, Volonteri M (2011) Reconstructing the massive black hole cosmic history through gravitational waves. Phys Rev D 83:044036. https://doi.org/10.1103/PhysRevD.83.044036. arXiv:1011.5893 [astro-ph.CO]
Seto N (2004) Annual modulation of the galactic binary confusion noise background and LISA data analysis. Phys Rev D 69:123005. https://doi.org/10.1103/PhysRevD.69.123005. arXiv:gr-qc/0403014
Seto N (2006) Prospects for direct detection of circular polarization of gravitational-wave background. Phys Rev Lett 97:151101. https://doi.org/10.1103/PhysRevLett.97.151101. arXiv:astro-ph/0609504
Seto N, Taruya A (2007) Measuring a parity violation signature in the early universe via ground-based laser interferometers. Phys Rev Lett 99:121101. https://doi.org/10.1103/PhysRevLett.99.121101. arXiv:0707.0535 [astro-ph]
Seto N, Taruya A (2008) Polarization analysis of gravitational-wave backgrounds from the correlation signals of ground-based interferometers: Measuring a circular-polarization mode. Phys Rev D 77:103001. https://doi.org/10.1103/PhysRevD.77.103001. arXiv:0801.4185 [astro-ph]
Seto N, Kawamura S, Nakamura T (2001) Possibility of direct measurement of the acceleration of the universe using 0.1-Hz band laser interferometer gravitational wave antenna in space. Phys Rev Lett 87:221103. https://doi.org/10.1103/PhysRevLett.87.221103. arXiv:astro-ph/0108011
Shajiee VR, Tofighi A (2019) Electroweak phase transition, gravitational waves and dark matter in two scalar singlet extension of the standard model. Eur Phys J C 79(4):360. https://doi.org/10.1140/epjc/s10052-019-6881-6. arXiv:1811.09807 [hep-ph]

Shannon RM et al (2015) Gravitational waves from binary supermassive black holes missing in pulsar observations. Science 349(6255):1522–1525. https://doi.org/10.1126/science.aab1910. arXiv:1509.07320 [astro-ph.CO]

Sharma A, Harms J (2020) Searching for cosmological gravitational-wave backgrounds with third-generation detectors in the presence of an astrophysical foreground. Phys Rev D 102(6):063009. https://doi.org/10.1103/PhysRevD.102.063009. arXiv:2006.16116 [gr-qc]

Shellard EPS (1987) Cosmic string interactions. Nucl Phys B 283:624–656. https://doi.org/10.1016/0550-3213(87)90290-2

Shtanov Y, Traschen JH, Brandenberger RH (1995) Universe reheating after inflation. Phys Rev D 51:5438–5455. https://doi.org/10.1103/PhysRevD.51.5438. arXiv:hep-ph/9407247

Siemens X, Creighton J, Maor I, Ray Majumder S, Cannon K, Read J (2006) Gravitational wave bursts from cosmic (super)strings: quantitative analysis and constraints. Phys Rev D 73:105001. https://doi.org/10.1103/PhysRevD.73.105001. arXiv:gr-qc/0603115

Siemens X, Mandic V, Creighton J (2007) Gravitational wave stochastic background from cosmic (super) strings. Phys Rev Lett 98:111101. https://doi.org/10.1103/PhysRevLett.98.111101. arXiv:astro-ph/0610920

Sigl G, Olinto AV, Jedamzik K (1997) Primordial magnetic fields from cosmological first order phase transitions. Phys Rev D 55:4582–4590. https://doi.org/10.1103/PhysRevD.55.4582. arXiv:astro-ph/9610201

Silverstein E, Westphal A (2008) Monodromy in the CMB: gravity waves and string inflation. Phys Rev D 78:106003. https://doi.org/10.1103/PhysRevD.78.106003. arXiv:0803.3085 [hep-th]

Slosar A et al (2019) Scratches from the past: inflationary archaeology through features in the power spectrum of primordial fluctuations. Bull Am Astron Soc 51(3):98 arXiv:1903.09883 [astro-ph.CO]

Smith R, Thrane E (2018) Optimal search for an astrophysical gravitational-wave background. Phys Rev X 8(2):021019. https://doi.org/10.1103/PhysRevX.8.021019. arXiv:1712.00688 [gr-qc]

Smith TL, Caldwell R (2017) Sensitivity to a frequency-dependent circular polarization in an isotropic stochastic gravitational wave background. Phys Rev D 95(4):044036. https://doi.org/10.1103/PhysRevD.95.044036. arXiv:1609.05901 [gr-qc]

Smith TL, Pierpaoli E, Kamionkowski M (2006) A new cosmic microwave background constraint to primordial gravitational waves. Phys Rev Lett 97:021301. https://doi.org/10.1103/PhysRevLett.97.021301. arXiv:astro-ph/0603144

Smith TL, Smith TL, Caldwell RR, Caldwell R (2019) LISA for cosmologists: calculating the signal-to-noise ratio for stochastic and deterministic sources. Phys Rev D 100(10):104055. https://doi.org/10.1103/PhysRevD.100.104055, [Erratum: Phys. Rev. D 105, 029902 (2022)]. arXiv:1908.00546 [astro-ph.CO]

Soares-Santos M et al (2019) First measurement of the Hubble constant from a dark standard siren using the dark energy survey galaxies and the LIGO/Virgo binary-black-hole merger GW170814. Astrophys J Lett 876(1):L7. https://doi.org/10.3847/2041-8213/ab14f1. arXiv:1901.01540 [astro-ph.CO]

Son DT (2005) Effective Lagrangian and topological interactions in supersolids. Phys Rev Lett 94:175301. https://doi.org/10.1103/PhysRevLett.94.175301. arXiv:cond-mat/0501658

Sorbo L (2011) Parity violation in the cosmic microwave background from a pseudoscalar inflaton. JCAP 06:003. https://doi.org/10.1088/1475-7516/2011/06/003. arXiv:1101.1525 [astro-ph.CO]

Sotiriou TP, Zhou SY (2014) Black hole hair in generalized scalar–tensor gravity. Phys Rev Lett 112:251102. https://doi.org/10.1103/PhysRevLett.112.251102. arXiv:1312.3622 [gr-qc]

Sousa L, Avelino PP (2013) Stochastic gravitational wave background generated by cosmic string networks: velocity-dependent one-scale model versus scale-invariant evolution. Phys Rev D 88(2):023516. https://doi.org/10.1103/PhysRevD.88.023516. arXiv:1304.2445 [astro-ph.CO]

Sousa L, Avelino PP (2014) Stochastic gravitational wave background generated by cosmic string networks: The small-loop regime. Phys Rev D 89(8):083503. https://doi.org/10.1103/PhysRevD.89.083503. arXiv:1403.2621 [astro-ph.CO]

Sousa L, Avelino PP (2016) Probing cosmic superstrings with gravitational waves. Phys Rev D 94(6):063529. https://doi.org/10.1103/PhysRevD.94.063529. arXiv:1606.05585 [astro-ph.CO]

Sousa L, Avelino PP, Guedes GSF (2020) Full analytical approximation to the stochastic gravitational wave background generated by cosmic string networks. Phys Rev D 101(10):103508. https://doi.org/10.1103/PhysRevD.101.103508. arXiv:2002.01079 [astro-ph.CO]

Spergel D et al (2015) Wide-field infrarred survey telescope-astrophysics focused telescope assets WFIRST-AFTA 2015 report. arXiv e-prints arXiv:1503.03757 [astro-ph.IM]

Speri L, Tamanini N, Caldwell RR, Gair JR, Wang B (2021) Testing the quasar Hubble diagram with LISA standard sirens. Phys Rev D 103(8):083526. https://doi.org/10.1103/PhysRevD.103.083526. arXiv:2010.09049 [astro-ph.CO]

Spokoiny B (1993) Deflationary universe scenario. Phys Lett B 315:40–45. https://doi.org/10.1016/0370-2693(93)90155-B. arXiv:gr-qc/9306008

Spurio Mancini A, Köhlinger F, Joachimi B, Pettorino V, Schäfer BM, Reischke R, van Uitert E, Brieden S, Archidiacono M, Lesgourgues J (2019) KiDS+GAMA: constraints on Horndeski gravity from combined large-scale structure probes. Mon Not R Astron Soc 490(2):2155–2177. https://doi.org/10.1093/mnras/stz2581. arXiv:1901.03686 [astro-ph.CO]

Srednicki M, Theisen S (1987) Nongravitational decay of cosmic strings. Phys Lett B 189:397. https://doi.org/10.1016/0370-2693(87)90648-4

Starobinsky AA (1979) Spectrum of relict gravitational radiation and the early state of the universe. JETP Lett 30:682–685

Starobinsky AA (1980) A new type of isotropic cosmological models without singularity. Phys Lett B 91:99–102. https://doi.org/10.1016/0370-2693(80)90670-X

Starobinsky AA (1982) Dynamics of phase transition in the new inflationary universe scenario and generation of perturbations. Phys Lett B 117:175–178. https://doi.org/10.1016/0370-2693(82)90541-X

Starobinsky AA (1983) The perturbation spectrum evolving from a nonsingular initially De-Sitter cosmology and the microwave background anisotropy. Sov Astron Lett 9:302

Starobinsky AA (1992) Spectrum of adiabatic perturbations in the universe when there are singularities in the inflation potential. JETP Lett 55:489–494

Stephanov MA (2006) QCD phase diagram: an overview. PoS LAT2006:024. https://doi.org/10.22323/1.032.0024. arXiv:hep-lat/0701002

Stevens T, Johnson MB, Kisslinger LS, Henley EM, Hwang WYP, Burkardt M (2008) Role of charged gauge fields in generating magnetic seed fields in bubble collisions during the cosmological electroweak phase transition. Phys Rev D 77:023501. https://doi.org/10.1103/PhysRevD.77.023501. arXiv:0707.1346 [astro-ph]

Strumia A, Tetradis N (1999) A consistent calculation of bubble nucleation rates. Nucl Phys B 542:719–741. https://doi.org/10.1016/S0550-3213(98)00804-9. arXiv:hep-ph/9806453

Sun L et al (2020) Characterization of systematic error in Advanced LIGO calibration. Class Quantum Grav 37(22):225008. https://doi.org/10.1088/1361-6382/abb14e. arXiv:2005.02531 [astro-ph.IM]

Surace M, Kokkotas KD, Pnigouras P (2016) The stochastic background of gravitational waves due to the f-mode instability in neutron stars. Astron Astrophys 586:A86. https://doi.org/10.1051/0004-6361/201527197. arXiv:1512.02502 [astro-ph.CO]

Surig A (1998) Selfconsistent treatment of bubble nucleation at the electroweak phase transition. Phys Rev D 57:5049–5063. https://doi.org/10.1103/PhysRevD.57.5049. arXiv:hep-ph/9706259

Suyama T (2020) On arrival time difference between lensed gravitational waves and light. Astrophys J 896 (1):46. https://doi.org/10.3847/1538-4357/ab8d3f. arXiv:2003.11748 [gr-qc]

Takahashi R (2004) Quasigeometrical optics approximation in gravitational lensing. Astron Astrophys 423:787–792. https://doi.org/10.1051/0004-6361:20040212. arXiv:astro-ph/0402165

Takahashi R (2017) Arrival time differences between gravitational waves and electromagnetic signals due to gravitational lensing. Astrophys J 835(1):103. https://doi.org/10.3847/1538-4357/835/1/103. arXiv:1606.00458 [astro-ph.CO]

Takahashi R, Nakamura T (2003) Wave effects in gravitational lensing of gravitational waves from chirping binaries. Astrophys J 595:1039–1051. https://doi.org/10.1086/377430. arXiv:astro-ph/0305055

Takahashi T, Soda J (2009) Chiral primordial gravitational waves from a Lifshitz point. Phys Rev Lett 102:231301. https://doi.org/10.1103/PhysRevLett.102.231301. arXiv:0904.0554 [hep-th]

Talukder D, Thrane E, Bose S, Regimbau T (2014) Measuring neutron-star ellipticity with measurements of the stochastic gravitational-wave background. Phys Rev D 89(12):123008. https://doi.org/10.1103/PhysRevD.89.123008. arXiv:1404.4025 [gr-qc]

Tamanini N (2017) Late time cosmology with LISA: probing the cosmic expansion with massive black hole binary mergers as standard sirens. J Phys Conf Ser 840(1):012029. https://doi.org/10.1088/1742-6596/840/1/012029. arXiv:1612.02634 [astro-ph.CO]

Tamanini N, Caprini C, Barausse E, Sesana A, Klein A, Petiteau A (2016) Science with the space-based interferometer eLISA. III: probing the expansion of the Universe using gravitational wave standard

sirens. JCAP 04:002. https://doi.org/10.1088/1475-7516/2016/04/002. arXiv:1601.07112 [astro-ph.CO]

Tamanini N, Klein A, Bonvin C, Barausse E, Caprini C (2020) Peculiar acceleration of stellar-origin black hole binaries: measurement and biases with LISA. Phys Rev D 101(6):063002. https://doi.org/10.1103/PhysRevD.101.063002. arXiv:1907.02018 [astro-ph.IM]

Tanaka T, Urakawa Y (2011) Dominance of gauge artifact in the consistency relation for the primordial bispectrum. JCAP 05:014. https://doi.org/10.1088/1475-7516/2011/05/014. arXiv:1103.1251 [astro-ph.CO]

Tang Y, Haiman Z, Macfadyen A (2018) The late inspiral of supermassive black hole binaries with circumbinary gas discs in the LISA band. Mon Not R Astron Soc 476(2):2249–2257. https://doi.org/10.1093/mnras/sty423. arXiv:1801.02266 [astro-ph.HE]

Tashiro H, Vachaspati T (2015) Parity-odd correlators of diffuse gamma rays and intergalactic magnetic fields. Mon Not R Astron Soc 448(1):299–306. https://doi.org/10.1093/mnras/stu2736. arXiv:1409.3627 [astro-ph.CO]

Tashiro H, Chiba T, Sasaki M (2004) Reheating after quintessential inflation and gravitational waves. Class Quantum Grav 21:1761–1772. https://doi.org/10.1088/0264-9381/21/7/004. arXiv:gr-qc/0307068

Tasinato G (2021) An analytic approach to non-slow-roll inflation. Phys Rev D 103(2):023535. https://doi.org/10.1103/PhysRevD.103.023535. arXiv:2012.02518 [hep-th]

Tattersall OJ, Ferreira PG, Lagos M (2018) General theories of linear gravitational perturbations to a Schwarzschild Black Hole. Phys Rev D 97(4):044021. https://doi.org/10.1103/PhysRevD.97.044021. arXiv:1711.01992 [gr-qc]

Tavecchio F, Ghisellini G, Foschini L, Bonnoli G, Ghirlanda G, Coppi P (2010) The intergalactic magnetic field constrained by Fermi/LAT observations of the TeV blazar 1ES 0229+200. Mon Not R Astron Soc 406:L70–L74. https://doi.org/10.1111/j.1745-3933.2010.00884.x. arXiv:1004.1329 [astro-ph.CO]

ter Haar L, Bezares M, Crisostomi M, Barausse E, Palenzuela C (2021) Dynamics of screening in modified gravity. Phys Rev Lett 126:091102. https://doi.org/10.1103/PhysRevLett.126.091102. arXiv:2009.03354 [gr-qc]

Teukolsky SA, Vallisneri M (2019) The architecture of the LISA science analysis. Tech. rep., Caltech. https://kiss.caltech.edu/final_reports/LISA_Final_Report.pdf

Tevzadze AG, Kisslinger L, Brandenburg A, Kahniashvili T (2012) Magnetic fields from QCD phase transitions. Astrophys J 759:54. https://doi.org/10.1088/0004-637X/759/1/54. arXiv:1207.0751 [astro-ph.CO]

Thorne B, Fujita T, Hazumi M, Katayama N, Komatsu E, Shiraishi M (2018) Finding the chiral gravitational wave background of an axion-SU(2) inflationary model using CMB observations and laser interferometers. Phys Rev D 97(4):043506. https://doi.org/10.1103/PhysRevD.97.043506. arXiv:1707.03240 [astro-ph.CO]

Thrane E (2013) Measuring the non-Gaussian stochastic gravitational-wave background: a method for realistic interferometer data. Phys Rev D 87(4):043009. https://doi.org/10.1103/PhysRevD.87.043009. arXiv:1301.0263 [astro-ph.IM]

Thrane E, Romano JD (2013) Sensitivity curves for searches for gravitational-wave backgrounds. Phys Rev D 88(12):124032. https://doi.org/10.1103/PhysRevD.88.124032. arXiv:1310.5300 [astro-ph.IM]

Timpano SE, Rubbo LJ, Cornish NJ (2006) Characterizing the galactic gravitational wave background with LISA. Phys Rev D 73:122001. https://doi.org/10.1103/PhysRevD.73.122001. arXiv:gr-qc/0504071

Tinto M, Armstrong JW (1999) Cancellation of laser noise in an unequal-arm interferometer detector of gravitational radiation. Phys Rev D 59:102003. https://doi.org/10.1103/PhysRevD.59.102003

Tinto M, Dhurandhar SV (2021) Time-delay interferometry. Living Rev Relativ 24:1. https://doi.org/10.1007/s41114-020-00029-6

Tinto M, Estabrook FB, Armstrong JW (2002) Time delay interferometry for LISA. Phys Rev D 65:082003. https://doi.org/10.1103/PhysRevD.65.082003

Tinto M, Estabrook FB, Armstrong JW (2004) Time delay interferometry with moving spacecraft arrays. Phys Rev D 69:082001. https://doi.org/10.1103/PhysRevD.69.082001. arXiv:gr-qc/0310017

Tisserand P et al (2007) Limits on the Macho content of the galactic halo from the EROS-2 survey of the magellanic clouds. Astron Astrophys 469:387–404. https://doi.org/10.1051/0004-6361:20066017. arXiv:astro-ph/0607207

Torrado J, Lewis A (2021) Cobaya: code for Bayesian analysis of hierarchical physical models. JCAP 05:057. https://doi.org/10.1088/1475-7516/2021/05/057. arXiv:2005.05290 [astro-ph.IM]

Toubiana A et al (2021) Detectable environmental effects in GW190521-like black-hole binaries with LISA. Phys Rev Lett 126(10):101105. https://doi.org/10.1103/PhysRevLett.126.101105. arXiv:2010.06056 [astro-ph.HE]
Tranberg A (2011) Standard model CP-violation and cold electroweak baryogenesis. Phys Rev D 84:083516. https://doi.org/10.1103/PhysRevD.84.083516. arXiv:1009.2358 [hep-ph]
Tranberg A, Tähtinen S, Weir DJ (2018) Gravitational waves from non-Abelian gauge fields at a tachyonic transition. JCAP 04:012. https://doi.org/10.1088/1475-7516/2018/04/012. arXiv:1706.02365 [hep-ph]
Traschen JH, Brandenberger RH (1990) Particle production during out-of-equilibrium phase transitions. Phys Rev D 42:2491–2504. https://doi.org/10.1103/PhysRevD.42.2491
Trinca A, Schneider R, Valiante R, Graziani L, Zappacosta L, Shankar F (2022) The low-end of the black hole mass function at cosmic dawn. Mon Not R Astron Soc 511(1):616–640. https://doi.org/10.1093/mnras/stac062. arXiv:2201.02630 [astro-ph.GA]
Tristram M et al (2021) Planck constraints on the tensor-to-scalar ratio. Astron Astrophys 647:A128. https://doi.org/10.1051/0004-6361/202039585. arXiv:2010.01139 [astro-ph.CO]
Troxel MA et al (2018) Dark energy survey year 1 results: cosmological constraints from cosmic shear. Phys Rev D 98(4):043528. https://doi.org/10.1103/PhysRevD.98.043528. arXiv:1708.01538 [astro-ph.CO]
Turner MS (1983) Coherent scalar field oscillations in an expanding universe. Phys Rev D 28:1243. https://doi.org/10.1103/PhysRevD.28.1243
Turner MS, Widrow LM (1988) Inflation produced, large scale magnetic fields. Phys Rev D 37:2743. https://doi.org/10.1103/PhysRevD.37.2743
Turok N (1984) Grand unified strings and galaxy formation. Nucl Phys B 242:520–541. https://doi.org/10.1016/0550-3213(84)90407-3
Ulmer A, Goodman J (1995) Femtolensing: beyond the semiclassical approximation. Astrophys J 442:67. https://doi.org/10.1086/175422. arXiv:astro-ph/9406042
Ünal C (2019) Imprints of primordial non-Gaussianity on gravitational wave spectrum. Phys Rev D 99(4):041301. https://doi.org/10.1103/PhysRevD.99.041301. arXiv:1811.09151 [astro-ph.CO]
Ünal C, Kovetz ED, Patil SP (2021) Multimessenger probes of inflationary fluctuations and primordial black holes. Phys Rev D 103(6):063519. https://doi.org/10.1103/PhysRevD.103.063519. arXiv:2008.11184 [astro-ph.CO]
Ungarelli C, Vecchio A (2001) Studying the anisotropy of the gravitational wave stochastic background with LISA. Phys Rev D 64:121501. https://doi.org/10.1103/PhysRevD.64.121501. arXiv:astro-ph/0106538
Vachaspati T (1991) Magnetic fields from cosmological phase transitions. Phys Lett B 265:258–261. https://doi.org/10.1016/0370-2693(91)90051-Q
Vachaspati T (2010) Cosmic rays from cosmic strings with condensates. Phys Rev D 81:043531. https://doi.org/10.1103/PhysRevD.81.043531. arXiv:0911.2655 [astro-ph.CO]
Vachaspati T (2021) Progress on cosmological magnetic fields. Rep Prog Phys 84(7):074901. https://doi.org/10.1088/1361-6633/ac03a9. arXiv:2010.10525 [astro-ph.CO]
Vachaspati T, Vilenkin A (1985) Gravitational radiation from cosmic strings. Phys Rev D 31:3052. https://doi.org/10.1103/PhysRevD.31.3052
Vachaspati T, Pogosian L, Steer D (2015) Cosmic strings. Scholarpedia 10(2):31682. https://doi.org/10.4249/scholarpedia.31682. arXiv:1506.04039 [astro-ph.CO]
Vainshtein AI (1972) To the problem of nonvanishing gravitation mass. Phys Lett B 39:393–394. https://doi.org/10.1016/0370-2693(72)90147-5
Valbusa Dall'Armi L, Ricciardone A, Bartolo N, Bertacca D, Matarrese S (2021) Imprint of relativistic particles on the anisotropies of the stochastic gravitational-wave background. Phys Rev D 103(2):023522. https://doi.org/10.1103/PhysRevD.103.023522. arXiv:2007.01215 [astro-ph.CO]
Valbusa Dall'Armi L, Ricciardone A, Bertacca D (2022) The dipole of the astrophysical gravitational-wave background. JCAP 11:040. https://doi.org/10.1088/1475-7516/2022/11/040. arXiv:2206.02747 [astro-ph.CO]
Valiante R, Schneider R, Graziani L, Zappacosta L (2018) Chasing the observational signatures of seed black holes at $z > 7$: candidate statistics. Mon Not R Astron Soc 474(3):3825–3834. https://doi.org/10.1093/mnras/stx3028. arXiv:1801.08165 [astro-ph.GA]
Vallisneri M, Bayle JB, Babak S, Petiteau A (2021) Time-delay interferometry without delays. Phys Rev D 103(8):082001. https://doi.org/10.1103/PhysRevD.103.082001. arXiv:2008.12343 [gr-qc]

Van Den Broeck C, Trias M, Sathyaprakash BS, Sintes AM (2010) Weak lensing effects in the measurement of the dark energy equation of state with LISA. Phys Rev D 81:124031. https://doi.org/10.1103/PhysRevD.81.124031. arXiv:1001.3099 [gr-qc]

Vaskonen V (2017) Electroweak baryogenesis and gravitational waves from a real scalar singlet. Phys Rev D 95(12):123515. https://doi.org/10.1103/PhysRevD.95.123515. arXiv:1611.02073 [hep-ph]

Vaskonen V, Veermäe H (2020) Lower bound on the primordial black hole merger rate. Phys Rev D 101 (4):043015. https://doi.org/10.1103/PhysRevD.101.043015. arXiv:1908.09752 [astro-ph.CO]

Vecchio A (2002) LISA and gravitational-wave stochastic backgrounds. Class Quantum Grav 19:1449–1455. https://doi.org/10.1088/0264-9381/19/7/329

Velten H, Gomes S (2020) Is the Hubble diagram of quasars in tension with concordance cosmology? Phys Rev D 101(4):043502. https://doi.org/10.1103/PhysRevD.101.043502. arXiv:1911.11848 [astro-ph.CO]

Vennin V, Starobinsky AA (2015) Correlation Functions in Stochastic Inflation. Eur Phys J C 75:413. https://doi.org/10.1140/epjc/s10052-015-3643-y. arXiv:1506.04732 [hep-th]

Verbiest GJ, Achucarro A (2011) High speed collision and reconnection of Abelian Higgs strings in the deep type-II regime. Phys Rev D 84:105036. https://doi.org/10.1103/PhysRevD.84.105036. arXiv:1106.4666 [hep-th]

Verde L, Treu T, Riess AG (2019) Tensions between the Early and the Late Universe. Nature Astron 3:891. https://doi.org/10.1038/s41550-019-0902-0. arXiv:1907.10625 [astro-ph.CO]

Vilenkin A (1981) Gravitational radiation from cosmic strings. Phys Lett B 107:47–50. https://doi.org/10.1016/0370-2693(81)91144-8

Vilenkin A (1982) Cosmological evolution of monopoles connected by strings. Nucl Phys B 196:240–258. https://doi.org/10.1016/0550-3213(82)90037-2

Vilenkin A (1984) Cosmic strings as gravitational lenses. Astrophys J Lett 282:L51–L53. https://doi.org/10.1086/184303

Vilenkin A, Shellard EPS (2000) Cosmic strings and other topological defects. Cambridge University Press, Cambridge

Vilenkin A, Vachaspati T (1987) Radiation of goldstone bosons from cosmic strings. Phys Rev D 35:1138. https://doi.org/10.1103/PhysRevD.35.1138

Vincent G, Antunes ND, Hindmarsh M (1998) Numerical simulations of string networks in the Abelian Higgs model. Phys Rev Lett 80:2277–2280. https://doi.org/10.1103/PhysRevLett.80.2277. arXiv:hep-ph/9708427

Volonteri M, Haardt F, Madau P (2003) The assembly and merging history of supermassive black holes in hierarchical models of galaxy formation. Astrophys J 582:559–573. https://doi.org/10.1086/344675. arXiv:astro-ph/0207276

Volonteri M et al (2020) Black hole mergers from dwarf to massive galaxies with the NewHorizon and Horizon-AGN simulations. Mon Not R Astron Soc 498(2):2219–2238. https://doi.org/10.1093/mnras/staa2384. arXiv:2005.04902 [astro-ph.GA]

von Harling B, Servant G (2018) QCD-induced electroweak phase transition. JHEP 01:159. https://doi.org/10.1007/JHEP01(2018)159. arXiv:1711.11554 [hep-ph]

Wachter JM, Olum KD (2017) Gravitational backreaction on piecewise linear cosmic string loops. Phys Rev D 95(2):023519. https://doi.org/10.1103/PhysRevD.95.023519. arXiv:1609.01685 [gr-qc]

Wands D, Bartolo N, Matarrese S, Riotto A (2002) An observational test of two-field inflation. Phys Rev D 66:043520. https://doi.org/10.1103/PhysRevD.66.043520. arXiv:astro-ph/0205253

Wang LF, Zhao ZW, Zhang JF, Zhang X (2020a) A preliminary forecast for cosmological parameter estimation with gravitational-wave standard sirens from TianQin. JCAP 11:012. https://doi.org/10.1088/1475-7516/2020/11/012. arXiv:1907.01838 [astro-ph.CO]

Wang LF, Jin SJ, Zhang JF, Zhang X (2022a) Forecast for cosmological parameter estimation with gravitational-wave standard sirens from the LISA-Taiji network. Sci China Phys Mech Astron 65 (1):210411. https://doi.org/10.1007/s11433-021-1736-6. arXiv:2101.11882 [gr-qc]

Wang R, Ruan WH, Yang Q, Guo ZK, Cai RG, Hu B (2022b) Hubble parameter estimation via dark sirens with the LISA-Taiji network. Natl Sci Rev 9(2):nwab054. https://doi.org/10.1093/nsr/nwab054. arXiv:2010.14732 [astro-ph.CO]

Wang S, Wang YF, Huang QG, Li TGF (2018) Constraints on the primordial black hole abundance from the first advanced LIGO observation run using the stochastic gravitational-wave background. Phys Rev Lett 120(19):191102. https://doi.org/10.1103/PhysRevLett.120.191102. arXiv:1610.08725 [astro-ph.CO]

Wang S, Terada T, Kohri K (2019) Prospective constraints on the primordial black hole abundance from the stochastic gravitational-wave backgrounds produced by coalescing events and curvature perturbations. Phys Rev D 99(10):103531. https://doi.org/10.1103/PhysRevD.99.103531, [Erratum: Phys.Rev.D 101, 069901 (2020)]. arXiv:1903.05924 [astro-ph.CO]

Wang X, Huang FP, Zhang X (2020b) Gravitational wave and collider signals in complex two-Higgs doublet model with dynamical CP-violation at finite temperature. Phys Rev D 101(1):015015. https://doi.org/10.1103/PhysRevD.101.015015. arXiv:1909.02978 [hep-ph]

Wang X, Huang FP, Zhang X (2021a) Energy budget and the gravitational wave spectra beyond the bag model. Phys Rev D 103(10):103520. https://doi.org/10.1103/PhysRevD.103.103520. arXiv:2010.13770 [astro-ph.CO]

Wang Y, Stebbins A, Turner EL (1996) Gravitational lensing of gravitational waves from merging neutron star binaries. Phys Rev Lett 77:2875–2878. https://doi.org/10.1103/PhysRevLett.77.2875. arXiv:astro-ph/9605140

Wang Y, Lo RKL, Li AKY, Chen Y (2021b) Identifying type II strongly lensed gravitational-wave images in third-generation gravitational-wave detectors. Phys Rev D 103(10):104055. https://doi.org/10.1103/PhysRevD.103.104055. arXiv:2101.08264 [gr-qc]

Watanabe Y, Komatsu E (2006) Improved calculation of the primordial gravitational wave spectrum in the standard model. Phys Rev D 73:123515. https://doi.org/10.1103/PhysRevD.73.123515. arXiv:astro-ph/0604176

Weir DJ (2016) Revisiting the envelope approximation: gravitational waves from bubble collisions. Phys Rev D 93(12):124037. https://doi.org/10.1103/PhysRevD.93.124037. arXiv:1604.08429 [astro-ph.CO]

Wetterich C (1988) Cosmology and the fate of dilatation symmetry. Nucl Phys B 302:668–696. https://doi.org/10.1016/0550-3213(88)90193-9. arXiv:1711.03844 [hep-th]

Wetterich C (1995) The Cosmon model for an asymptotically vanishing time dependent cosmological 'constant'. Astron Astrophys 301:321–328 arXiv:hep-th/9408025

Wetterich C (2014) Variable gravity Universe. Phys Rev D 89(2):024005. https://doi.org/10.1103/PhysRevD.89.024005. arXiv:1308.1019 [astro-ph.CO]

Wetterich C (2015) Inflation, quintessence, and the origin of mass. Nucl Phys B 897:111–178. https://doi.org/10.1016/j.nuclphysb.2015.05.019. arXiv:1408.0156 [hep-th]

Wichoski UF, MacGibbon JH, Brandenberger RH (2002) High-energy neutrinos, photons and cosmic ray fluxes from VHS cosmic strings. Phys Rev D 65:063005. https://doi.org/10.1103/PhysRevD.65.063005. arXiv:hep-ph/9805419

Witten E (1984) Cosmic separation of phases. Phys Rev D 30:272–285. https://doi.org/10.1103/PhysRevD.30.272

Wong KC et al (2020) H0LiCOW—XIII. A 2.4 per cent measurement of H0 from lensed quasars: 5.3 tension between early- and late-Universe probes. Mon Not R Astron Soc 498(1):1420–1439. https://doi.org/10.1093/mnras/stz3094. arXiv:1907.04869 [astro-ph.CO]

Wren AJ, Fuentes JL, Malik KA (2017) Gravitational waves in a flat radiation-matter universe including anisotropic stress. arXiv e-prints arXiv:1712.10012 [gr-qc]

Wyrzykowski L et al (2010) The OGLE view of microlensing towards the Magellanic Clouds – II. OGLE-II Small Magellanic Cloud data. Mon Not R Astron Soc 407:189–200. https://doi.org/10.1111/j.1365-2966.2010.16936.x. arXiv:1004.5247 [astro-ph.GA]

Wyrzykowski L et al (2011a) The OGLE view of microlensing towards the Magellanic Clouds – III. Ruling out subsolar MACHOs with the OGLE-III LMC data. Mon Not R Astron Soc 413:493. https://doi.org/10.1111/j.1365-2966.2010.18150.x. arXiv:1012.1154 [astro-ph.GA]

Wyrzykowski L et al (2011b) The OGLE view of microlensing towards the Magellanic Clouds – IV. OGLE-III SMC data and final conclusions on MACHOs. Mon Not R Astron Soc 416:2949. https://doi.org/10.1111/j.1365-2966.2011.19243.x. arXiv:1106.2925 [astro-ph.GA]

Xie KP, Bian L, Wu Y (2020) Electroweak baryogenesis and gravitational waves in a composite Higgs model with high dimensional fermion representations. JHEP 12:047. https://doi.org/10.1007/JHEP12(2020)047. arXiv:2005.13552 [hep-ph]

Yagi K, Seto N (2011) Detector configuration of DECIGO/BBO and identification of cosmological neutron-star binaries. Phys Rev D 83:044011. https://doi.org/10.1103/PhysRevD.83.044011, [Erratum: Phys. Rev. D 95, 109901 (2017)]. arXiv:1101.3940 [astro-ph.CO]

Yamada K, Tanaka T (2020) Parametrized test of parity-violating gravity using GWTC-1 events. PTEP 2020(9):093E01. https://doi.org/10.1093/ptep/ptaa103. arXiv:2006.11086 [gr-qc]

Yamamoto N (2018) Spin Hall effect of gravitational waves. Phys Rev D 98(6):061701. https://doi.org/10.1103/PhysRevD.98.061701. arXiv:1708.03113 [hep-th]

Yang J, Bian L (2022) Magnetic field generation from bubble collisions during first-order phase transition. Phys Rev D 106(2):023510. https://doi.org/10.1103/PhysRevD.106.023510. arXiv:2102.01398 [astro-ph.CO]

Yang KZ, Mandic V, Scarlata C, Banagiri S (2020a) Searching for cross-correlation between stochastic gravitational wave background and galaxy number counts. Mon Not R Astron Soc 500(2):1666–1672. https://doi.org/10.1093/mnras/staa3159. arXiv:2007.10456 [astro-ph.CO]

Yang T, Banerjee A, Colgáin EO (2020b) Cosmography and flat ΛCDM tensions at high redshift. Phys Rev D 102(12):123532. https://doi.org/10.1103/PhysRevD.102.123532. arXiv:1911.01681 [astro-ph.CO]

Yoo CM, Harada T, Garriga J, Kohri K (2018) Primordial black hole abundance from random Gaussian curvature perturbations and a local density threshold. PTEP 2018(12):123E01. https://doi.org/10.1093/ptep/pty120. arXiv:1805.03946 [astro-ph.CO]

Young S, Byrnes CT (2015) Signatures of non-Gaussianity in the isocurvature modes of primordial black hole dark matter. JCAP 04:034. https://doi.org/10.1088/1475-7516/2015/04/034. arXiv:1503.01505 [astro-ph.CO]

Young S, Byrnes CT (2020) Initial clustering and the primordial black hole merger rate. JCAP 03:004. https://doi.org/10.1088/1475-7516/2020/03/004. arXiv:1910.06077 [astro-ph.CO]

Young S, Byrnes CT, Sasaki M (2014) Calculating the mass fraction of primordial black holes. JCAP 07:045. https://doi.org/10.1088/1475-7516/2014/07/045. arXiv:1405.7023 [gr-qc]

Young S, Musco I, Byrnes CT (2019) Primordial black hole formation and abundance: contribution from the non-linear relation between the density and curvature perturbation. JCAP 11:012. https://doi.org/10.1088/1475-7516/2019/11/012. arXiv:1904.00984 [astro-ph.CO]

Yuan C, Murase K, Zhang BT, Kimura SS, Mészáros P (2021) Post-merger jets from supermassive black hole coalescences as electromagnetic counterparts of gravitational wave emission. Astrophys J Lett 911(1):L15. https://doi.org/10.3847/2041-8213/abee24. arXiv:2101.05788 [astro-ph.HE]

Yunes N, Pretorius F (2009) Fundamental theoretical bias in gravitational wave astrophysics and the parameterized post-Einsteinian framework. Phys Rev D 80:122003. https://doi.org/10.1103/PhysRevD.80.122003. arXiv:0909.3328 [gr-qc]

Zel'dovich YB, Novikov ID (1967) The hypothesis of cores retarded during expansion and the hot cosmological model. Sov Astron 10:602

Zhan H, Tyson JA (2018) Cosmology with the large synoptic survey telescope: an overview. Rept Prog Phys 81(6):066901. https://doi.org/10.1088/1361-6633/aab1bd. arXiv:1707.06948 [astro-ph.CO]

Zhang X (1993) Operators analysis for Higgs potential and cosmological bound on Higgs mass. Phys Rev D 47:3065–3067. https://doi.org/10.1103/PhysRevD.47.3065. arXiv:hep-ph/9301277

Zhang Y, Vachaspati T, Ferrer F (2019) Magnetic field production at a first-order electroweak phase transition. Phys Rev D 100(8):083006. https://doi.org/10.1103/PhysRevD.100.083006. arXiv:1902.02751 [hep-ph]

Zhao W, Van Den Broeck C, Baskaran D, Li TGF (2011) Determination of dark energy by the Einstein telescope: comparing with CMB, BAO and SNIa observations. Phys Rev D 83:023005. https://doi.org/10.1103/PhysRevD.83.023005. arXiv:1009.0206 [astro-ph.CO]

Zhao W, Zhang Y, You XP, Zhu ZH (2013) Constraints of relic gravitational waves by pulsar timing arrays: forecasts for the FAST and SKA projects. Phys Rev D 87(12):124012. https://doi.org/10.1103/PhysRevD.87.124012. arXiv:1303.6718 [astro-ph.CO]

Zhao ZW, Wang LF, Zhang JF, Zhang X (2020) Prospects for improving cosmological parameter estimation with gravitational-wave standard sirens from Taiji. Sci Bull 65(16):1340–1348. https://doi.org/10.1016/j.scib.2020.04.032. arXiv:1912.11629 [astro-ph.CO]

Zhou R, Bian L (2022) Gravitational wave and electroweak baryogenesis with two Higgs doublet models. Phys Lett B 829:137105. https://doi.org/10.1016/j.physletb.2022.137105. arXiv:2001.01237 [hep-ph]

Zhou Z, Jiang J, Cai YF, Sasaki M, Pi S (2020) Primordial black holes and gravitational waves from resonant amplification during inflation. Phys Rev D 102(10):103527. https://doi.org/10.1103/PhysRevD.102.103527. arXiv:2010.03537 [astro-ph.CO]

Zlatev I, Wang LM, Steinhardt PJ (1999) Quintessence, cosmic coincidence, and the cosmological constant. Phys Rev Lett 82:896–899. https://doi.org/10.1103/PhysRevLett.82.896. arXiv:astro-ph/9807002

Zumalacárregui M, García-Bellido J (2014) Transforming gravity: from derivative couplings to matter to second-order scalar–tensor theories beyond the Horndeski Lagrangian. Phys Rev D 89:064046. https://doi.org/10.1103/PhysRevD.89.064046. arXiv:1308.4685 [gr-qc]

Zumalacárregui M, Bellini E, Sawicki I, Lesgourgues J, Ferreira PG (2017) hi_class: Horndeski in the cosmic linear anisotropy solving system. JCAP 08:019. https://doi.org/10.1088/1475-7516/2017/08/019. arXiv:1605.06102 [astro-ph.CO]

Zuntz J, Paterno M, Jennings E, Rudd D, Manzotti A, Dodelson S, Bridle S, Sehrish S, Kowalkowski J (2015) CosmoSIS: modular cosmological parameter estimation. Astron Comput 12:45–59. https://doi.org/10.1016/j.ascom.2015.05.005. arXiv:1409.3409 [astro-ph.CO]

Publisher's Note Springer Nature remains neutral with regard to jurisdictional claims in published maps and institutional affiliations.

Authors and Affiliations

Pierre Auclair[1] · David Bacon[2] · Tessa Baker[2,3] · Tiago Barreiro[4] · Nicola Bartolo[5,6,7] · Enis Belgacem[8] · Nicola Bellomo[9] · Ido Ben-Dayan[10,11,12] · Daniele Bertacca[5,6,7] · Marc Besancon[13] · Jose J. Blanco-Pillado[14,15] · Diego Blas[16,17] · Guillaume Boileau[18] · Gianluca Calcagni[19] · Robert Caldwell[20] · Chiara Caprini[1,21,22] · Carmelita Carbone[23] · Chia-Feng Chang[24] · Hsin-Yu Chen[25] · Nelson Christensen[18] · Sebastien Clesse[26] · Denis Comelli[27] · Giuseppe Congedo[28] · Carlo Contaldi[29] · Marco Crisostomi[30,31,32] · Djuna Croon[33,34] · Yanou Cui[24] · Giulia Cusin[21] · Daniel Cutting[35] · Charles Dalang[21] · Valerio De Luca[21] · Walter Del Pozzo[36,37] · Vincent Desjacques[38] · Emanuela Dimastrogiovanni[39,40] · Glauber C. Dorsch[41] · Jose Maria Ezquiaga[42,43] · Matteo Fasiello[2,44] · Daniel G. Figueroa[45] · Raphael Flauger[46] · Gabriele Franciolini[21] · Noemi Frusciante[47] · Jacopo Fumagalli[44,48] · Juan García-Bellido[44] · Oliver Gould[49] · Daniel Holz[42] · Laura Iacconi[2] · Rajeev Kumar Jain[50] · Alexander C. Jenkins[51,52] · Ryusuke Jinno[44,53] · Cristian Joana[54] · Nikolaos Karnesis[55] · Thomas Konstandin[53] · Kazuya Koyama[2] · Jonathan Kozaczuk[46] · Sachiko Kuroyanagi[44] · Danny Laghi[56] · Marek Lewicki[57] · Lucas Lombriser[21] · Eric Madge[58] · Michele Maggiore[21] · Ameek Malhotra[39] · Michele Mancarella[21] · Vuk Mandic[59] · Alberto Mangiagli[1] · Sabino Matarrese[5,6,7] · Anupam Mazumdar[40] · Suvodip Mukherjee[60,61,62] · Ilia Musco[63,64] · Germano Nardini[65] · Jose Miguel No[44] · Theodoros Papanikolaou[1,66] · Marco Peloso[5,6] · Mauro Pieroni[29] · Luigi Pilo[67,68] · Alvise Raccanelli[5,6,7,22] · Sébastien Renaux-Petel[47] · Arianna I. Renzini[69,70] · Angelo Ricciardone[5,6] · Antonio Riotto[21] · Joseph D. Romano[71] · Rocco Rollo[72] · Alberto Roper Pol[1,73] · Ester Ruiz Morales[74] · Mairi Sakellariadou[52] · Ippocratis D. Saltas[75] · Marco Scalisi[76] · Kai Schmitz[22] · Pedro Schwaller[77] · Olga Sergijenko[78,79] · Geraldine Servant[53,80] · Peera Simakachorn[53,80] · Lorenzo Sorbo[81] · Lara Sousa[82,83,84] · Lorenzo Speri[85] · Danièle A. Steer[1] · Nicola Tamanini[56] · Gianmassimo Tasinato[86] · Jesús Torrado[87] · Caner Unal[75,88] · Vincent Vennin[1] · Daniele Vernieri[89] · Filippo Vernizzi[90] · Marta Volonteri[48] ·

Jeremy M. Wachter[91] · David Wands[2] · Lukas T. Witkowski[48] · Miguel Zumalacárregui[85] · James Annis[92] · Fëanor Reuben Ares[33,93] · Pedro P. Avelino[83,84] · Anastasios Avgoustidis[49] · Enrico Barausse[30,31,32] · Alexander Bonilla[94] · Camille Bonvin[21] · Pasquale Bosso[95] · Matteo Calabrese[96,97] · Mesut Çalışkan[98] · Jose A. R. Cembranos[99] · Mikael Chala[100] · David Chernoff[101] · Katy Clough[102] · Alexander Criswell[59] · Saurya Das[95] · Antonio da Silva[47,103] · Pratika Dayal[104] · Valerie Domcke[22,105] · Ruth Durrer[21] · Richard Easther[106] · Stephanie Escoffier[107] · Sandrine Ferrans[108] · Chris Fryer[109] · Jonathan Gair[85] · Chris Gordon[110] · Martin Hendry[111] · Mark Hindmarsh[35] · Deanna C. Hooper[35] · Eric Kajfasz[107] · Joachim Kopp[22,77] · Savvas M. Koushiappas[112,113] · Utkarsh Kumar[10] · Martin Kunz[21] · Macarena Lagos[114] · Marc Lilley[115] · Joanes Lizarraga[17] · Francisco S. N. Lobo[47,103] · Azadeh Maleknejad[22] · C. J. A. P. Martins[82,83] · P. Daniel Meerburg[40] · Renate Meyer[116] · José Pedro Mimoso[46,103] · Savvas Nesseris[44] · Nelson Nunes[47] · Vasilis Oikonomou[55] · Giorgio Orlando[40] · Ogan Özsoy[75] · Fabio Pacucci[117,118] · Antonella Palmese[11] · Antoine Petiteau[1,13] · Lucas Pinol[44] · Simon Portegies Zwart[119] · Geraint Pratten[120] · Tomislav Prokopec[8] · John Quenby[121] · Saeed Rastgoo[122] · Diederik Roest[40] · Kari Rummukainen[35] · Carlo Schimd[123] · Aurélia Secroun[107] · Alberto Sesana[124] · Carlos F. Sopuerta[125,126] · Ismael Tereno[47] · Andrew Tolley[29] · Jon Urrestilla[15] · Elias C. Vagenas[127] · Jorinde van de Vis[52] · Rien van de Weygaert[11] · Barry Wardell[128] · David J. Weir[35] · Graham White[129] · Bogumiła Świeżewska[57] · Valery I. Zhdanov[130] · The LISA Cosmology Working Group

✉ Germano Nardini
chairscoswg@gmail.com

1 Laboratoire Astroparticule et Cosmologie, Université de Paris, CNRS, 75013 Paris, France

2 Institute of Cosmology & Gravitation, University of Portsmouth, Portsmouth PO1 3FX, UK

3 Department of Physics and Astronomy, Queen Mary University of London, Mile End Road, London E1 4NS, UK

4 Universidade Lusófona de Humanidades e Tecnologias Campo Grande, 376, 1749-024 Lisbon, Portugal

5 Dipartimento di Fisica e Astronomia "G. Galilei", Università degli Studi di Padova, Via Marzolo 8, 35131 Padua, Italy

6 INFN, Sezione di Padova, Via Marzolo 8, 35131 Padua, Italy

7 INAF - Osservatorio Astronomico di Padova, Vicolo dell'Osservatorio 5, 35122 Padua, Italy

8 Institute for Theoretical Physics, Faculty of Science, Utrecht University, Princetonplein 5, 3584 CC Utrecht, The Netherlands

9 Theory Group, Department of Physics, The University of Texas at Austin, Austin, TX 78712, USA

10 Department of Physics, Ariel University, POB 3, 4070000 Ariel, Israel

11 Berkeley Center for Cosmological Physics, University of California, Berkeley, CA 94720, USA

[12] Department of Physics, University of California, Berkeley, CA 94720, USA

[13] CEA Paris-Saclay, Irfu/DPhP, Bat.141, 91191 Gif-sur-Yvette, France

[14] IKERBASQUE, Basque Foundation for Science, 48011 Bilbao, Spain

[15] Department of Physics, UPV/EHU, 48080 Bilbao, Spain

[16] Grup de Física Teòrica, Departament de Física, Universitat Autònoma de Barcelona, Bellaterra, 08193 Barcelona, Spain

[17] Institut de Fisica d'Altes Energies (IFAE), The Barcelona Institute of Science and Technology, Campus UAB, 08193 Bellaterra, Barcelona, Spain

[18] Artemis, Observatoire de la Côte d'Azur, Université Côte d'Azur, CNRS, CS 34229, 06304 Nice Cedex 4, France

[19] Instituto de Estructura de la Materia, CSIC, Serrano 121, 28006 Madrid, Spain

[20] Department of Physics and Astronomy, Dartmouth College, 6127 Wilder Laboratory, Hanover, NH 03755, USA

[21] Department of Theoretical Physics, University of Geneva, 24 Quai Ernest-Ansermet, Geneva, Switzerland

[22] Theoretical Physics Department, CERN, 1211 Geneva 23, Switzerland

[23] INAF - Istituto di Astrofisica Spaziale e Fisica cosmica di Milano (IASF-MI), Via Alfonso Corti 12, 20133 Milan, Italy

[24] Department of Physics and Astronomy, University of California, Riverside, CA 92521, USA

[25] Department of Physics and Kavli Institute for Astrophysics and Space Research, Massachusetts Institute of Technology, Cambridge, USA

[26] Service de Physique Théorique, Université Libre de Bruxelles, CP225, Campus de la Plaine, Boulevard du Triomphe, 1050 Brussels, Belgium

[27] INFN, Sezione di Ferrara, 44122 Ferrara, Italy

[28] Institute for Astronomy, University of Edinburgh, Royal Observatory, Blackford Hill, Edinburgh EH9 3HJ, UK

[29] Theoretical Physics Group, Blackett Laboratory, Imperial College London, London SW7 2AZ, UK

[30] SISSA, Via Bonomea 265, 34136 Trieste, Italy

[31] INFN Sezione di Trieste, Trieste, Italy

[32] IFPU - Institute for Fundamental Physics of the Universe, Via Beirut 2, 34014 Trieste, Italy

[33] TRIUMF Theory Group, 4004 Wesbrook Mall, Vancouver, BC V6T2A3, Canada

[34] Department of Physics, Institute for Particle Physics Phenomenology, Durham University, Durham DH1 3LE, UK

[35] Department of Physics and Helsinki Institute of Physics, PL 64, University of Helsinki, 00014 Helsinki, Finland

[36] Dipartimento di Fisica "E. Fermi", Università di Pisa, 56127 Pisa, Italy

[37] INFN, Sezione di Pisa, 56127 Pisa, Italy

[38] Physics Department, Technion, 3200003 Haifa, Israel

[39] Sydney Consortium for Particle Physics and Cosmology, School of Physics, The University of New South Wales, Sydney, NSW 2052, Australia

[40] Van Swinderen Institute for Particle Physics and Gravity, University of Groningen, 9747 AG Groningen, The Netherlands

[41] Departamento de Física, Universidade Federal de Minas Gerais, Belo Horizonte, MG 31270-901, Brazil

[42] Kavli Institute for Cosmological Physics and Enrico Fermi Institute, The University of Chicago, Chicago, IL 60637, USA

[43] Niels Bohr International Academy, Niels Bohr Institute, Blegdamsvej 17, 2100 Copenhagen, Denmark

[44] Instituto de Física Teórica UAM/CSIC, Universidad Autónoma de Madrid, Cantoblanco, 28049 Madrid, Spain

[45] Instituto de Fisica Corpuscular (IFIC), University of Valencia-CSIC, 46980 Valencia, Spain

[46] UC San Diego, 9500 Gilman Dr, La Jolla, CA 92093, USA

[47] Instituto de Astrofisíca e Ciências do Espaço, Faculdade de Ciências da Universidade de Lisboa, Edificio C8, Campo Grande, 1749016 Lisbon, Portugal

[48] Institut d'Astrophysique de Paris, GReCO, UMR 7095 du CNRS et de Sorbonne Université, 98bis boulevard Arago, 75014 Paris, France

[49] School of Physics and Astronomy, University Park, University of Nottingham, Nottingham NG7 2RD, UK

[50] Department of Physics, Indian Institute of Science, Bangalore 560012, India

[51] Department of Physics and Astronomy, University College London, London WC1E 6BT, UK

[52] Theoretical Particle Physics and Cosmology Group, Physics Department, King's College London, University of London, Strand, London WC2R 2LS, UK

[53] Deutsches Elektronen-Synchrotron DESY, Notkestr. 85, 22607 Hamburg, Germany

[54] CAS Key Laboratory of Theoretical Physics, Institute of Theoretical Physics, Chinese Academy of Sciences, Beijing 100190, China

[55] Department of Physics, Aristotle University of Thessaloniki, Thessaloniki 54124, Greece

[56] Laboratoire des 2 Infinis - Toulouse (L2IT-IN2P3), Université de Toulouse, CNRS, UPS, 31062 Toulouse Cedex 9, France

[57] Faculty of Physics, University of Warsaw ul. Pasteura 5, 02-093 Warsaw, Poland

[58] Department of Particle Physics and Astrophysics, Weizmann Institute of Science, 7610001 Rehovot, Israel

[59] School of Physics and Astronomy, University of Minnesota Twin Cities, Minneapolis, MN 55455, USA

[60] Perimeter Institute for Theoretical Physics, 31 Caroline Street N., Waterloo, ON N2L 2Y5, Canada

[61] Gravitation Astroparticle Physics Amsterdam, Anton Pannekoek Institute for Astronomy and Institute for High-Energy Physics, University of Amsterdam, Science Park 904, 1090 GL Amsterdam, The Netherlands

[62] Institute Lorentz, Leiden University, PO Box 9506, 2300 RA Leiden, The Netherlands

[63] Dipartimento di Fisica, Sapienza Università di Roma, Piazzale Aldo Moro 5, 00185 Rome, Italy

[64] INFN, Sezione di Roma, Piazzale Aldo Moro 2, 00185 Rome, Italy

[65] Faculty of Science and Technology, University of Stavanger, 4036 Stavanger, Norway

[66] National Observatory of Athens, Lofos Nymfon, 11852 Athens, Greece

[67] Dipartimento di Scienze Fisiche e Chimiche, Università degli Studi dell'Aquila, Via Vetoio, 67100 L'Aquila, Italy

[68] INFN, Laboratori Nazionali del Gran Sasso, 67010 Assergi, Italy

[69] LIGO Laboratory, California Institute of Technology, Pasadena, CA 91125, USA

[70] Department of Physics, California Institute of Technology, Pasadena, CA 91125, USA

[71] Department of Physics and Astronomy, Texas Tech University, Box 41051, Lubbock, TX 79409-1051, USA

[72] Centro Nazionale INFN di Studi Avanzati GGI, Largo Enrico Fermi 2, 50125 Florence, Italy

[73] School of Natural Sciences and Medicine, Ilia State University, 3-5 Cholokashvili Ave, Tbilisi 0194, Georgia

[74] Departamento de Física, ETSIDI, Universidad Politécnica de Madrid, 28012 Madrid, Spain

[75] CEICO, FZU – Institute of Physics of the Czech Academy of Sciences, Na Slovance 2, 182 21 Prague, Czech Republic

[76] Max-Planck-Institut für Physik (Werner-Heisenberg-Institut), Föhringer Ring 6, 80805 Munchen, Germany

[77] PRISMA+ Cluster of Excellence & Mainz Institute for Theoretical Physics, Johannes Gutenberg-Universität Mainz, 55099 Mainz, Germany

[78] Main Astronomical Observatory of the National Academy of Sciences of Ukraine, Zabolotnoho str., 27, Kyiv 03143, Ukraine

[79] AGH University of Science and Technology, Aleja Mickiewicza, 30, 30-059 Krakow, Poland

[80] II. Institute of Theoretical Physics, Universität Hamburg, 22761 Hamburg, Germany

[81] Amherst Center for Fundamental Interactions, Department of Physics, University of Massachusetts, Amherst, MA 01003, USA

[82] Centro de Astrofísica da Universidade do Porto, Rua das Estrelas, 4150-762 Porto, Portugal

[83] Instituto de Astrofisica e Ciências do Espaço, CAUP, Rua das Estrelas, 4150-762 Porto, Portugal

[84] Departamento de Física e Astronomia, Faculdade de Ciências, Universidade do Porto, Rua do Campo Alegre 687, 4169-007 Porto, Portugal

[85] Max Planck Institute for Gravitational Physics (Albert Einstein Institute), Am Mühlenberg 1, Potsdam 14476, Germany

[86] Department of Physics, Swansea University, Swansea SA2 8PP, UK

[87] Institute for Theoretical Particle Physics and Cosmology (TTK), RWTH Aachen University, 52056 Aachen, Germany

[88] Department of Physics, Ben-Gurion University, 84105 Be'er Sheva, Israel

[89] Dipartimento di Fisica "E. Pancini", Università di Napoli "Federico II" and INFN, Sezione di Napoli, Compl. Univ. di Monte S. Angelo, Edificio G, Via Cinthia, 80126 Napoli, Italy

[90] Institut de physique théorique, Université Paris Saclay CEA, CNRS, 91191 Gif-sur-Yvette, France

[91] Department of Physics, Skidmore College, 815 N. Broadway, Saratoga Springs, NY 12866, USA

[92] Fermi National Accelerator Laboratory, Pine and Kirk, Batavia, IL, USA

[93] Department of Physics and Astronomy, University of Sussex, Falmer, East Sussex BN1 9QH, UK

[94] Departamento de Física, Universidade Federal de Juiz de Fora, 36036-330 Juiz de Fora, MG, Brazil

[95] University of Lethbridge, 4401 University Drive, Lethbridge, AB T1K 3M4, Canada

[96] INAF - Osservatorio Astronomico di Torino, Via Osservatorio 20, 10025 Pino Torinese, TO, Italy

[97] OAVdA - Astronomical Observatory of the Autonomous Region Valle d'Aosta, Loc. Lignan 39, 11020 Nus, AO, Italy

[98] The William H. Miller III Department of Physics and Astronomy, Johns Hopkins University, Baltimore, MD 21218, USA

[99] Departamento de Fisica Teorica and IPARCOS, Facultad de Ciencias Fisicas, Universidad Complutense de Madrid, Plaza de Ciencias, n 1, 28040 Madrid, Spain

[100] Departamento de Física Teórica y del Cosmos, Universidad de Granada, Campus de Fuentenueva, 18071 Granada, Spain

[101] Deptartment of Astronomy, Ithaca, NY 14853, USA

[102] School of Mathematical Sciences, Queen Mary University of London, Mile End Road, London E1 4NS, UK

[103] Departamento de Física, Faculdade de Ciências, Universidade de Lisboa, 1749-016 Lisbon, Portugal

[104] Kapteyn Astronomical Institute, University of Groningen, P.O. Box 800, 9700 AV Groningen, The Netherlands

[105] Institute of Physics, École Polytechnique Fédérale de Lausanne (EPFL), 1015 Lausanne, Switzerland

[106] Department of Physics, University of Auckland, Private Bag 92019, Auckland, New Zealand

[107] Aix Marseille Univ, CNRS/IN2P3, CPPM, IPhU, Marseille, France

[108] Center for Relativistic Astrophysics, Georgia Institute of Technology, Atlanta, GA 30332, USA

[109] Center for Theoretical Astrophysics, Los Alamos National Laboratory, Los Alamos, NM 87545, USA

[110] School of Physical and Chemical Sciences, University of Canterbury, Private Bag 4800, Christchurch 8140, New Zealand

[111] Institute for Gravitational Research & School of Physics and Astronomy, University of Glasgow, Glasgow G12 8QQ, UK

[112] Department of Physics, Brown University, Providence, RI, USA

[113] Brown Theoretical Physics Centner, Brown University, Providence, RI, USA

[114] Department of Physics and Astronomy, Columbia University, New York, NY 10027, USA

[115] SYRTE, Observatoire de Paris, Université PSL, CNRS, Sorbonne Université, LNE, 61 avenue de l'Observatoire, 75014 Paris, France

[116] Department of Statistics, University of Auckland, Auckland, New Zealand

[117] Center for Astrophysics | Harvard & Smithsonian, Cambridge, MA 02138, USA

[118] Black Hole Initiative, Harvard University, Cambridge, MA 02138, USA

[119] Leiden Observatory, Leiden University, PO Box 9513, 2300 RA Leiden, The Netherlands

[120] Institute for Gravitational Wave Astronomy & School of Physics and Astronomy, University of Birmingham, Birmingham B15 2TT, UK

[121] High Energy Physics Group Blackett Laboratory, London SW72BZ, UK

[122] Department of Physics, University of Alberta, Edmonton, Alberta T6G 2G1, Canada

[123] Aix Marseille Univ, CNRS, CNES, LAM, Marseille, France

[124] Dipartimento di Fisica "G. Occhialini", Universitá degli Studi di Milano-Bicocca, 20126 Milan, Italy

[125] Institut de Ciències de l'Espai (ICE, CSIC), Campus UAB, Carrer de Can Magrans s/n, 08193 Cerdanyola del Vallès, Spain

[126] Institut d'Estudis Espacials de Catalunya (IEEC), Carrer del Gran Capità 2-4, Edifici Nexus, Despatx 201, 08034 Barcelona, Spain

[127] Department of Physics, Kuwait University, P.O. Box 5969, 13060 Safat, Kuwait

[128] School of Mathematics and Statistics, University College Dublin, Belfield, Dublin 4 D04 V1W8, Ireland

[129] Kavli IPMU (WPI), UTIAS, The University of Tokyo, Kashiwa, Chiba 277-8583, Japan

[130] Taras Shevchenko National University of Kyiv, Astronomical Observatory, Observatorna str., 3, Kyiv 04053, Ukraine